Volume 202, 1998

DEVELOPMENTAL BIOLOGY

Editor-in-Chief
Eric N. Olson

Editors
Marianne Bronner-Fraser
Eric H. Davidson
Scott Fraser
Richard Harland
Philip Ingham
Laurinda A. Jaffe
Robb Krumlauf
Gail Martin
Gary Ruvkun
Matthew P. Scott

Reviews Editor
Gary M. Wessel

ACADEMIC PRESS

Cover photo. Integrin $\alpha 4$ mRNA was detected in cranial regions of 8- to 15-somite chick embryos as seen in sections through embryos after *in situ* hybridization with integrin $\alpha 4$ mRNA.

DEVELOPMENTAL BIOLOGY

(ISSN 0012-1606)

Published semimonthly by Academic Press, 6277 Sea Harbor Drive, Orlando, FL 32887-4900

1998: Volumes 193–204. Price: $2632.00 U.S.A. and Canada; $3158.00 all other countries.
All prices include postage and handling.

Information concerning personal subscription rates may be obtained by writing to the Publishers. All correspondence and subscription orders should be addressed to the office of the Publishers at 6277 Sea Harbor Drive, Orlando, FL 32887-4900. Send notices of change of address to the office of the Publishers at least 6 to 8 weeks in advance. Please include both old and new addresses. POSTMASTER: Send changes of address to *Developmental Biology*, 6277 Sea Harbor Drive, Orlando, FL 32887-4900.
Periodicals postage paid at Orlando, FL, and at additional mailing offices.

COPYRIGHT © 1998 BY ACADEMIC PRESS

DEVELOPMENTAL BIOLOGY is a registered trademark
of Academic Press (a division of Harcourt Brace & Company)

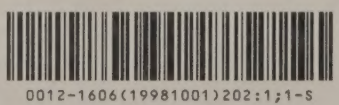

DEVELOPMENTAL BIOLOGY

Editor-in-Chief **Eric N. Olson**

Editors
Marianne Bronner-Fraser (Pasadena, CA)
Eric H. Davidson (Pasadena, CA)
Scott Fraser (Pasadena, CA)
Richard Harland (Berkeley, CA)
Philip Ingham (Sheffield, U.K.)
Laurinda Jaffe (Farmington, CT)
Robb Krumlauf (London, U.K.)
Gail Martin (San Francisco, CA)
Gary Ruvkun (Boston, MA)
Matthew P. Scott (Stanford, CA)

Reviews Editor
Gary M. Wessel (Providence, RI)

Editorial Board
Kathryn Anderson (New York, NY)
Michael Bate (Cambridge, U.K.)
Richard R. Behringer (Houston, TX)
Allan Bradley (Houston, TX)
Peter J. Bryant (Irvine, CA)
Susan V. Bryant (Irvine, CA)
Margaret Buckingham (Paris, France)
Jose A. Campos-Ortega (Köln, Germany)
Mario R. Capecchi (Salt Lake City, UT)
Sean Carroll (Madison, WI)
Pierre Chambon (Strasbourg, France)
Bodo Christ (Freiburg, Germany)
Nam-Hai Chua (New York, NY)
Stephen Cohen (Heidelberg, Germany)
Ann Cowan (Farmington, CT)
Igor B. Dawid (Bethesda, MD)
Edward M. De Robertis (Los Angeles, CA)
Wolfgang Driever (Freiburg, Germany)
Gregor Eichele (Houston, TX)
Anne Ephrussi (Heidelberg, Germany)
Richard A. Firtel (La Jolla, CA)
John Peter Gergen (Stony Brook, NY)
Iva Greenwald (New York, NY)
Ernst Hafen (Zurich, Switzerland)
Peter W. H. Holland (Reading, U.K.)
Yuh Nung Jan (San Francisco, CA)
Lawrence C. Katz (Durham, NC)
Rolf Kemler (Freiburg, Germany)
Daniel P. Kiehart (Durham, NC)
William H. Klein (Houston, TX)
William J. Lennarz (Stony Brook, NY)
Maria Leptin (Köln, Germany)
Sharon R. Long (Palo Alto, CA)
David R. McClay (Durham, NC)
Barbara J. Meyer (Berkeley, CA)
Diana G. Myles (Davis, CA)
Bradley B. Olwin (Boulder, CO)
Charles P. Ordahl (San Francisco, CA)
Stuart Orkin (Boston, MA)
Luis Parada (Dallas, TX)
Norbert Perrimon (Boston, MA)
James W. Posakony (La Jolla, CA)
Nadia Rosenthal (Charlestown, MA)
Josh R. Sanes (St. Louis, MO)
Robert Schwartz (Houston, TX)
Barry D. Shur (Atlanta, GA)
Didier Stainier (San Francisco, CA)
Hermann Steller (Cambridge, MA)
Paul W. Sternberg (Pasadena, CA)
Clifford J. Tabin (Boston, MA)
Masatoshi Takeichi (Kyoto, Japan)
Patrick Tam (Westworthville, Australia)
Steve Wasserman (La Jolla, CA)
David Wilkinson (London, U.K.)
Debra J. Wolgemuth (New York, NY)
William B. Wood (Boulder, CO)
Christopher V. E. Wright (Nashville, TN)
Martin Yanofsky (La Jolla, CA)
H. Joseph Yost (Salt Lake City, UT)

Published under the Auspices of the Society for Developmental Biology

DEVELOPMENTAL BIOLOGY

Volume 202, Number 1, October 1, 1998

Copyright © 1998 by Academic Press. All Rights Reserved

No part of this publication may be reproduced or transmitted in any form, or by any means, electronic or mechanical, including photocopy, recording, or any information storage and retrieval system, without permission in writing from the Publisher. *Exceptions:* It is the policy of Academic Press that authors need not obtain permission in the following cases only: (1) to use their original figures or tables in their future works; (2) to make copies of their papers for use in their classroom teaching; and (3) to include their papers as part of their dissertations.

The appearance of the code at the bottom of the first page of an article in this journal indicates the Publisher's consent that copies of the article may be made for personal or internal use, or for the personal or internal use of specific clients. This consent is given on the condition, however, that the copier pay the stated per copy fee through the Copyright Clearance Center, Inc. (222 Rosewood Drive, Danvers, Massachusetts 01923), for copying beyond that permitted by Sections 107 or 108 of the U.S. Copyright Law. This consent does not extend to other kinds of copying, such as copying for general distribution, for advertising or promotional purposes, for creating new collective works, or for resale. Copy fees for pre-1998 articles are as shown on the article title pages; if no fee code appears on the title page, the copy fee is the same as for current articles.

0012-1606/98 $25.00

MADE IN THE UNITED STATES OF AMERICA

This journal is printed on acid-free paper. ♾

DEVELOPMENTAL BIOLOGY is a registered trademark
of Academic Press (a division of Harcourt Brace & Company)

DEVELOPMENTAL BIOLOGY

Volume 202, Number 1, October 1, 1998

Contents

MAP Kinase Inactivation Is Required Only for G2–M Phase Transition in Early Embryogenesis Cell Cycles of the Starfishes *Marthasterias glacialis* and *Astropecten aranciacus*	**Daniel Fisher, Ariane Abrieu, Marie-Noëlle Simon, Stephen Keyse, Valérie Vergé, Marcel Dorée, and André Picard**	**1**
The Relationship between Rhombomeres and Vestibular Neuron Populations as Assessed in Quail–Chicken Chimeras	**Carmen Díaz, Luis Puelles, Faustino Marín, and Joel C. Glover**	**14**
The α_4 Subunit of Integrin Is Important for Neural Crest Cell Migration	**Sung H. Kil, Catherine E. Krull, Gordon Cann, Dennis Clegg, and Marianne Bronner-Fraser**	**29**
Roles of Transforming Growth Factor-α and Epidermal Growth Factor in Chick Limb Development	**Caroline N. Dealy, Victoria Scranton, and Hsu-Chen Cheng**	**43**
The *Cspg2* Gene, Disrupted in the *hdf* Mutant, Is Required for Right Cardiac Chamber and Endocardial Cushion Formation	**C. H. Mjaatvedt, H. Yamamura, A. A. Capehart, D. Turner, and R. R. Markwald**	**56**
A Single Rostrocaudal Colonization of the Rodent Intestine by Enteric Neuron Precursors Is Revealed by the Expression of Phox2b, Ret, and p75 and by Explants Grown under the Kidney Capsule or in Organ Culture	**H. M. Young, C. J. Hearn, D. Ciampoli, B. R. Southwell, J.-F. Brunet, and D. F. Newgreen**	**67**
N-Cadherin/Catenin-Mediated Morphoregulation of Somite Formation	**Kersti K. Linask, Cheryl Ludwig, Ming-Da Han, Xiao Liu, Glenn L. Radice, and Karen A. Knudsen**	**85**
Precocious Expression of the Wilms' Tumor Gene *xWT1* Inhibits Embryonic Kidney Development in *Xenopus laevis*	**John B. Wallingford, Thomas J. Carroll, and Peter D. Vize**	**103**
Voltage-Dependent Activation of Frog Eggs by a Sperm Surface Disintegrin Peptide	**Fraser M. Shilling, Craig R. Magie, and Richard Nuccitelli**	**113**
A Novel Alternative Spliced Variant of the Transcription Factor AP2α Is Expressed in the Murine Ocular Lens	**Chiaki Ohtaka-Maruyama, Fumio Hanaoka, and Ana B. Chepelinsky**	**125**
Identification of Gametophytic Mutations Affecting Female Gametophyte Development in *Arabidopsis*	**Cory A. Christensen, Santhi Subramanian, and Gary N. Drews**	**136**

Erratum

Volume **192,** Number 2 (1997): in Article No. DB978773, "Localized Maternal Proteins in *Xenopus* Revealed by Subtractive Immunization," by James M. Denegre, Erich R. Ludwig, and Kimberly L. Mowry, pages 446–454 **152**

DEVELOPMENTAL BIOLOGY 202, 1–13 (1998)
ARTICLE NO. DB988981

MAP Kinase Inactivation Is Required Only for G2–M Phase Transition in Early Embryogenesis Cell Cycles of the Starfishes *Marthasterias glacialis* and *Astropecten aranciacus*

Daniel Fisher,* Ariane Abrieu,* Marie-Noëlle Simon,† Stephen Keyse,‡ Valérie Vergé,† Marcel Dorée,* and André Picard†,[1]

**CRBM CNRS ERS 155, 1919 route de mende, 34293 Montpellier cedex 5, France; †Laboratoire Arago, UMR 7628, BP 44, F 66651 Banyuls sur mer cedex, France; and ‡ICRF, Molecular Pharmacology Unit, Biomedical Research Center, Level J., Ninewells Hospital, Dundee DD1 9SY, United Kingdom*

Downregulation of MAP kinase is a universal consequence of fertilization in the animal kingdom. Here we show that oocytes of the starfishes *Astropecten aranciacus* and *Marthasterias glacialis* complete meiotic maturation and form a pronucleus when treated with 1-methyladenine and then complete DNA replication and arrest at G2 if not fertilized. Release of G2 by fertilization or a variety of parthenogenetic treatments is associated with inactivation of MAP kinase. Prevention of MAP kinase inactivation by microinjection of Ste11-ΔN, a constitutively active budding yeast MAP kinase kinase kinase, arrests fertilized eggs at G2 in either the first or the second mitotic cell cycle, in a dose-dependent manner. G1 arrest is never observed. Conversely, inactivation of MAP kinase by microinjection of the MAP kinase-specific phosphatase Pyst-1 releases mature starfish oocytes from G2 arrest. The role of MAP kinase in arresting cell cycle at various stages in oocytes of different animal species is discussed. © 1998 Academic Press

INTRODUCTION

MAP kinases (MAPKs) have been shown to play an essential role in progression of somatic cells from G1 to S phase through transcriptional activation of early genes involved in the control of cell proliferation (reviewed in Karin and Hunter, 1995). Paradoxically, no oncogenic form of either MAPK or MAPKK are known, however (for review, see Hunter, 1997). This may indicate that constitutive activation of MAPK may exert some negative effect on cell proliferation in higher organisms. Indeed, MAPK is reported to drop before the G2 to M phase transition (Kohno, 1985; Meloche *et al.*, 1995), and there is no report of somatic cells maintaining high MAPK activity throughout the cell cycle under physiological conditions.

Downregulation of MAPK is also a universal consequence of fertilization in the animal kingdom (Ferrell *et al.*, 1991; Shibuya *et al.*, 1992; Verlhac *et al.*, 1994; Picard *et al.*, 1996) and is absolutely required for embryos, both vertebrate and invertebrate, to enter first mitosis (Abrieu *et al.*, 1997b; Walter *et al.*, 1997; Tachibana *et al.*, 1997).

Recently, MAPK was proposed to link the fertilization signal transduction pathway to the G1/S phase transition in eggs of the starfish *Asterina pectinifera* (Tachibana *et al.*, 1997). Specifically, it was shown in this species that unfertilized eggs are arrested at G1 with high MAPK activity, and either fertilization or inactivation of MAPK by microinjection of a specific MAPK phosphatase causes initiation of DNA replication. In contrast, we previously reported that unfertilized eggs of the starfishes *Marthasterias glacialis* and *Astropecten aranciacus* synthesize DNA and arrest at what seems to be a G2 state with high MAPK activity (Picard *et al.*, 1996). DNA synthesis in unfertilized eggs was not due to repair, as it was sup-

[1] To whom correspondence should be addressed. Fax: (33) 4 68 88 73 98. E-mail: picard@arago.obs-banyuls.fr.

0012-1606/98 $25.00
Copyright © 1998 by Academic Press
All rights of reproduction in any form reserved.

pressed by aphidicolin. However, an alternative interpretation could be that oocytes enter, but perhaps do not complete, S phase in unfertilized eggs of these two starfish species. In this case, failure to complete DNA replication could have activated a checkpoint, preventing oocytes from progressing into mitosis.

The aim of the present work was to examine this possibility, in order to elucidate the apparent discrepancy between results obtained in various starfish species. We show that fully mature oocytes of the starfishes *A. aranciacus* and *M. glacialis* actually complete DNA replication and arrest at G2 if not fertilized, and that MAPK inactivation, a physiological consequence of fertilization, is required to release them from G2 arrest. Thus prolongation or inappropriate reactivation of MAPK activity may arrest progression of the first mitotic cell cycle at different stages, including entry into mitosis (Abrieu *et al.*, 1997b) or exit from mitosis (reviewed in Sagata, 1997), depending on species.

MATERIAL AND METHODS

Starfish oocytes. The starfishes *A. aranciacus* and *M. glacialis* were collected by diving during the breeding season near the marine biological station of Banyuls sur mer (Banyuls, France). Fully grown oocytes were used throughout this work. Oocytes were prepared free of follicle cells by rinsing them three times in calcium-free sea water (0.5 M NaCl, 10 mM KCl, 50 mM $MgCl_2$, 10 mM Hepes, pH 8.2) and then three times in filtered natural sea water. Meiosis reinitiation was induced usually with 1 μM 1-methyladenine (1-MeAde). Oocytes could be fertilized before (Germinal Vesicle stage) or after hormone application, with 10^5-fold diluted dry sperm.

Artificial activation of mature oocytes could be obtained by various treatments:

- Microinjection of human centrosomes (Picard *et al.*, 1987). Human centrosomes from KE37 lymphoid cells were prepared according to Gosti-Testu *et al.* (1986) and were a gift from Michel Bornens.
- Microinjection of Calcium buffer. Calcium buffer was a 1/1 mixture of 0.2 M Ca-EGTA with 0.2 M EGTA-KOH in 10 mM Pipes-KOH, pH 7.0.
- Two steps 1-MeAde treatment. Follicle cell free oocytes were treated with a threshold level (0.1 μM) of 1-MeAde and extensively rinsed after GVBD. A second treatment (10 μM) after second polar body emission triggered fertilization membrane elevation and parthenogenetic development (Picard and Dorée, 1983).

Recombinant proteins and mRNAs. The plasmid encoding Pyst1 was isolated as described in Groom *et al.* (1996). Construction of the sea urchin GST-cyclin B has been described previously (Abrieu *et al.*, 1996).

The DNA fragment encoding residues 370–717 of Ste 11 was amplified by PCR using budding yeast genomic DNA as template and the two oligonucleotides GGATCCCATATGGCCCTATTACAAGGA and CGCGGATCCTCAAATTATGTGTGCATCC as primers. ThePCR product was cloned in PBluescript (PBS), checked by sequencing, and subcloned as a *Bam*H1 fragment in the yeast expression vector YcpGAL STE11ΔN and as a *Nde*I–*Bam*HI fragment in pET3a. Galactose-induced overexpression in yeast YcpGAL STE11ΔN was lethal, as described (Cairns *et al.*, 1992), showing that the expressed protein is functional.

Recombinant proteins and mRNAs were prepared according to standard procedures.

Immunological procedures. The polyclonal antibody directed against phosphotyrosine has been described previously (Abrieu *et al.*, 1997a). Immunoblots were analyzed by alkaline phosphatase detection.

Bromodeoxyuridine (BrdU) was incorporated by addition of 0.1 mg/ml BrdU to the oocyte suspension. Then oocytes were fixed at the appropriate times directly in 4 N HCl (2 h), followed by one rinse in methanol (1 h) and one rinse in TBS–0.1% Tween 20. Then samples were treated with first antibody (monoclonal anti-BrdU, Amersham) overnight and second antibody (sheep anti-mouse Texas red, Amersham) for 1 h.

Microinjections. Microinjections were performed according to the procedure described by Hiramoto (1974).

Kinase assays. MBP kinase assays were performed on oocytes of *A. aranciacus:* 10 oocytes were taken in 5 μl sea water, homogenized in 15 μl EB (60 mM Na glycerophosphate, 15 mM EGTA, 1 mM $MgCl_2$, pH 7.4) and frozen in liquid nitrogen. After thawing, homogenates were centrifuged (13,000*g*, 15 min, 4°C) and 15 μl of the supernatant was fixed with 5 μl of 4× Laemmli sample buffer and boiled. In gel MBP-kinase activities were assayed exactly as described by Shibuya *et al.* (1992).

[^{3}H]Thymidine incorporation. We showed previously that DNA replication can occur in polar bodies, in a very asynchronous fashion (Picard *et al.*, 1996). In order to measure only thymidine incorporation in pronuclei, we eliminated polar bodies just after 1st polar body emission by a 20-min digestion by pronase (0.5 mg/ml) of vitelline or fertilization membrane and egg jelly, followed by two rinses in sea water containing 0.1% bovine serum albumin, and two rinses more after second polar body emission. The eggs were then resuspended in the same medium containing 300 μCi/ml [^{3}H]thymidine. Samples of eggs were fixed and extracted overnight at 4°C with 5% TCA. After two additional TCA washes, eggs were solubilized and incorporated radioactivity was measured in a liquid scintillation counter.

RESULTS

Fully Mature Oocytes of the Starfishes Astropecten aranciacus and Marthasterias glacialis Complete DNA Replication and Arrest at G2 If Not Fertilized or Parthenogenetically Activated

In contrast to amphibian oocytes, hormone-stimulated starfish oocytes complete meiotic maturation even if not fertilized. In a typical experiment at 18°C, *M. glacialis* oocytes emitted the first polar body at 80 min post-hormone addition (pha) and the second polar body at 120 min pha. Procaryons reformed as soon as second meiosis was achieved and fused together within minutes after second polar body emission. Later on, the female pronucleus usually migrated and became central within about 1 h after second polar body emission (Fig. 1). This is at variance with sea urchin eggs, which arrest in G1 with a peripheric pronucleus. Cytolysis of unfertilized eggs usually occurred 5 to 6 h later.

Copyright © 1998 by Academic Press. All rights of reproduction in any form reserved.

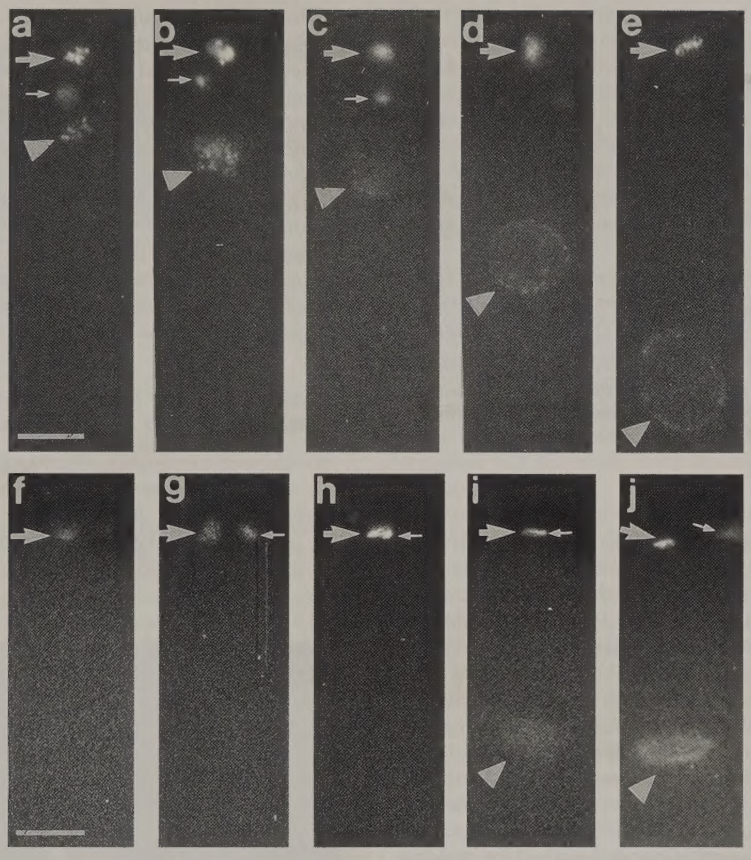

FIG. 1. Unfertilized fully mature oocytes replicate DNA. Oocytes of the starfish *M. glacialis* were fixed at various times after second polar body emission (a and f, 5 min; b and g, 20 min; c and h, 40 min; d and i, 60 min; e and j, 80 min) and processed for Hoechst DNA staining (a–e) or DNA-incorporated BrdU (f–j in oocytes incubated in 0.1 mg/ml BrdU since hormone addition). The pronucleus reforms (arrowhead) at the animal pole (a–c) and then usually migrates toward the center (d and e). DNA replication, which is always observed in both polar bodies (pb1, large arrow; pb2, tiny arrow), begins in the female pronucleus with a poor synchronism, 40 to 60 min after second polar body emission (i and j, arrowhead). Bar: a–e, 15 μM; f–j, 23 μM. The difference in size of oocytes is due to the fixation procedures: methanol–glycerol for a–e and 4 N HCl for f–j.

BrdU incorporation experiments showed that replication of DNA began after centration of the pronucleus, at about 180 min pha (Fig. 1), as previously described (Picard *et al.*, 1996). Our previous experiments could not exclude that fully mature oocytes enter S phase but fail to complete genome duplication; Thus, the activation of the DNA replication checkpoint mechanisms could account for the arrest of cell cycle progression. A careful study of [^{3}H]thymidine incorporation showed that, despite a delay and a noteworthy lack of synchronism of unfertilized eggs compared to fertilized eggs in initiating DNA replication, unfertilized eggs incorporated finally half the amount of [^{3}H]thymidine that was incorporated in the DNA of fertilized eggs (Fig. 2), showing that DNA replication was complete in the majority of the unfertilized, thus haploid, eggs. We reinforced this conclusion by showing that activation of fully mature eggs triggered M phase entry without finishing DNA replication. Oocytes were induced to complete meiotic maturation with 1-MeAde and, after arresting, they were activated in the presence of BrdU with ionophore A23187 (Schuetz, 1975), which is well known to mimic fertilization and induce DNA replication in G1-arrested sea urchin eggs (Steinhart and Epel, 1974; Steinhart *et al.*, 1974). The use of ionophore A23187 circumvented the difficulty of discrimination between authentic DNA replication in the male pronucleus and putative DNA replication in the female pronucleus. As shown in Fig. 3, activated oocytes readily exited interphase and entered mitosis, as judged by Nomarski observation of nuclear envelope breakdown (Figs. 3a and 3b) and chromosome condensation

Copyright © 1998 by Academic Press. All rights of reproduction in any form reserved.

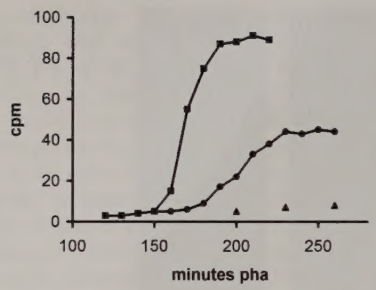

FIG. 2. Unfertilized fully mature oocytes complete DNA replication. [^{3}H]Thymidine incorporation into DNA was measured (see Materials and Methods) in control fertilized eggs (squares), unfertilized oocytes (circles), or aphidicolin-treated unfertilized oocytes (triangles), as a function of time after second polar body emission (which was completed at 120 min pha in this experiment).

(DNA Hoechst staining, Fig. 3c), but no incorporation of BrdU was detected between the time of activation and the time of entry into mitosis (Fig. 3d). Moreover, we found that aphidicolin, which blocks DNA replication by inhibiting DNA polymerase α, does not inhibit, nor even delay, cleavage in schedule (not shown), demonstrating that checkpoint mechanisms are repressed in starfish early embryos; thus, even if DNA replication had been uncomplete, this could not account for a cell cycle arrest.

These results show that uncompletion of DNA replication is not the cause of cell cycle arrest and suggest that the fully mature oocytes are arrested in G2 of the cell cycle. In order to strengthen this conclusion we searched for molecular and physiological analogies between cell cycle arrest after completion of meiosis and genuine and undisputed G2 arrest of full-grown immature oocytes. In G2-arrested oocytes, cyclin B-cdc2 dimeres are stocked as an inactive pre-MPF, phosphorylated on the cdc2-tyrosine 15. Western blot analysis of p13-suc1-purified material revealed that cyclin B was mostly destroyed at second polar body emission and then continuously synthesized and accumulated in association with cdc2 (Fig. 4A). The cdc2 subunit was phosphorylated on tyrosine during S phase and kept tyrosine-phosphorylated after cell cycle arrest (Fig. 4A). H1 kinase activity remained low for a long time after second polar body emission (Fig. 4B), confirming that oocytes were arrested in G2.

Another peculiarity of G2-arrested immature oocytes is the ability to amplify MPF activity: microinjection of a small volume (usually 1/20 of the cell volume) of cytoplasm containing MPF activity (for example taken from M-phase maturing oocytes) triggers MPF activation and M-phase entry of the recipient G2-arrested oocyte. MPF amplification is demonstrated by the conserved high efficiency of serial transferts (Kishimoto and Kanatani, 1976). As expected, fully mature starfish oocytes readily exited cell cycle arrest, supported MPF amplification, and entered mitosis when microinjected with cytoplasm taken after GVBD from maturing oocytes (Table 1) or with highly purified cyclin B-cdc2 kinase (not shown).

Finally, we found that other treatments (microinjection of 1 mM okadaic Acid, of 1 μM cyclin A, or 1 mM PSTAIR peptide), which specifically induce activation of the G2 inactive MPF dimeres, also induce NEBD and MPF activation in fully mature starfish oocytes (not shown, see Discussion).

Taken together, the above experiments show that hormone-stimulated oocytes of *M. glacialis* and *A. aranciacus* complete DNA replication and arrest at G2 after meiotic maturation.

Release of Mature Starfish Oocytes from G2 Arrest Is Associated with Inactivation of MAP Kinase

We showed previously that MAPK activity drops at the time of second polar body emission in fertilized but not unfertilized eggs of *A. aranciacus* and does not reappear later (Picard *et al.*, 1996). As shown in Fig. 5, a variety of

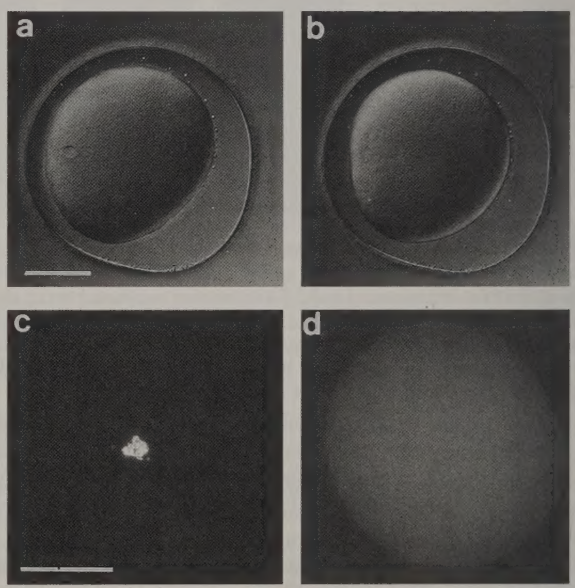

FIG. 3. Calcium-ionophore-activated fully mature oocytes of *M. glacialis* do not incorporate BrdU before M-phase entry. Upon ionophore activation, fully mature oocytes elevated fertilization membrane (a, 10 min after ionophore addition, 200 min pha) and then entered M phase, as judged by nuclear envelope breakdown and monoaster formation (b, 60 min). Accordingly, chromosomes condensed (c, DNA Hoechst staining; compare with Fig. 1e for a control). However, when BrdU (0.1 mg/ml) was added 10 min before ionophore activation, it was not incorporated into DNA at the time of M phase (d). Bar (in a for upper panels, in c for lower panels) = 100 μm.

Copyright © 1998 by Academic Press. All rights of reproduction in any form reserved.

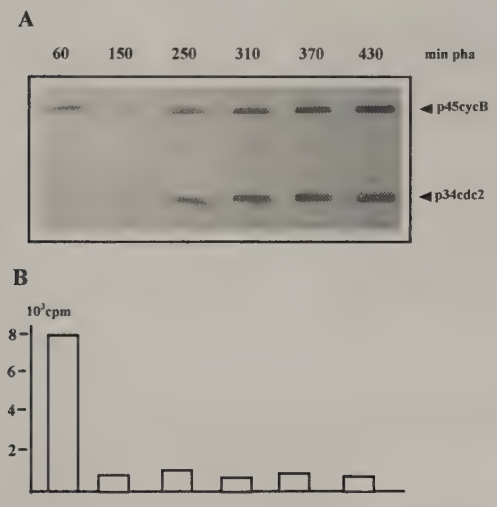

FIG. 4. Fully mature oocytes of the starfish *A. aranciacus* contain an inactive cyclin B–cdc2 kinase complex comprising partially dephosphorylated cyclin B and tyrosine-phosphorylated cdc2. (A) 1000 oocytes were homogenized at various times after hormone addition (min pha), and the material recovered on p13-suc1 beads was analyzed using Western blots with anti-cyclin B (revealing p45cycB) and anti-phosphotyrosine antibodies (revealing tyrosine-phosphorylated p34cdc2). Cyclin B is destroyed after second polar body emission (150 min: pb2 emission occurred at 130 min in this experiment) and then accumulated again at a level higher than the M-phase level (compare 430 min to 60 min). The lower band of dephosphorylated cyclin B is predominant. cdc2 tyrosine 15 remained dephosphorylated at least until 150 min pha and then rephosphorylated gradually. (B) Accordingly, whole histone H1 kinase activity (^{32}P incorporation on histone H1, measured on a single egg each time) remained low in fully mature oocytes, compared to M-phase oocytes, showing the cdc2–cyclin B complex is inactive.

treatments that release mature starfish oocytes from arrest at the pronucleus stage and induce cell cycling were all found to inactivate MAPK, even when applied after oocytes had completed meiotic maturation and were arrested at G2. These treatments, besides fertilization and ionophore A23187, include microinjection of a Ca-EGTA buffer to raise intracellular Ca^{2+} to the micromolar level (Picard and Dorée, 1983a), two-step application of 1-MeAde (Picard and Dorée, 1983b), or microinjection of purified human centrosomes (Picard *et al.*, 1987). We observed occasionally that a small and variable proportion of *A. aranciacus* oocytes can escape arrest at the pronucleus stage upon prolonged incubation in natural sea water. This also was systematically associated with inactivation of MAPK, as illustrated in Fig. 5 (compare lanes 7 and 8). Finally, MPF or cyclin A microinjection triggered MPF amplification only after MAPK inactivation, at variance with OA microinjection which triggered GVBD while keeping high MAPK activity (not shown).

In previous experiments we showed that the time of MAPK inactivation during meiotic maturation was dependent on the time of fertilization of maturing oocytes: In *A. aranciacus* oocytes fertilized early in first meiotic prometaphase (20 min pha), MAPK was inactivated after second polar body emission (125 min pha), while in oocytes fertilized late in first metaphase (75 min pha) MAPK activity dropped as early as 105 min pha, before second polar body emission (Abrieu *et al.*, 1997b). In the present work we examined the effects of premature fertilization on cell cycle resumption and MAP kinase inactivation. Starfish prophase-blocked oocytes can be inseminated, although several sperms succeed in penetrating because the block to polyspermy is not yet well established at that stage (Fig. 6Aa). Upon hormone addition, prematurely inseminated oocytes reinitiate meiosis in schedule with controls as judged by nuclear envelope breakdown and multiple furrowing. We found that even when insemination occurred 30

TABLE 1

Fully Mature Oocytes of the Starfish *Astropecten aranciacus* Exit G2 Arrest, Support MPF Amplification, and Enter First Mitosis When Microinjected with Cytoplasm Taken after GVBD from Maturing Oocytes

Experiment	Donor	Recipient	Ratio (injection/oocyte volume)	NEBD[a]
A	Maturing oocyte (first metaphase)	Mature oocytes (pronucleus stage)	1/50	9/10
B	Recipients of Expt A	Mature oocytes (pronucleus stage)	1/50	10/10
C	Recipients of Expt B	Mature oocytes (pronucleus stage)	1/50	10/10
D	Recipients of Expt C	Immatures oocytes (GV stage)	1/20 1/50	5/5 0/5
E	Maturing oocyte (first metaphase)	Immatures oocytes (GV stage)	1/20 1/50	10/10 0/10

[a] Number of oocytes undergoing nuclear envelope breakdown and chromosome condensation/total number of injected oocytes.

Copyright © 1998 by Academic Press. All rights of reproduction in any form reserved

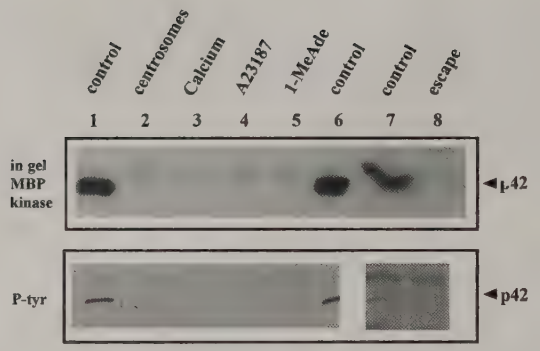

FIG. 5. A variety of treatments that release mature starfish oocytes from arrest at the pronucleus stage also induce inactivation of the p42 MAP kinase. Samples of 10 oocytes (*A. aranciacus*) were taken in duplicates after arrest at the pronucleus stage (controls; lane 1, 150 min pha; lane 6, TBS microinjected oocytes, 300 min pha) or at the time of nuclear envelope breakdown after different parthenogenetic treatments (lane 2, microinjection of human centrosomes; lane 3, microinjection of 50 pl of a mixture of 0.2 M Ca-EGTA with 0.2 M EGTA in 10 mM Pipes–KOH, pH 7.0; lane 4, treatment with 1 μM ionophore A23187; lane 5, treatment with 1 μM 1-MeAde) and processed for determination of in-gel MBP kinase activities (top) or immunoblotting for phosphotyrosine detection (bottom). In another experiment, samples of eggs spontaneously escaping the pronucleus arrest were selected, as judged by disappearance of the nuclear envelope and analyzed for in-gel MBP kinase activity and phosphotyrosine content (lane 8, spontaneously cycling unfertilized eggs, 340 min pha; lane 7, control eggs, 340 min pha).

min before hormonal stimulation, eggs entered mitosis roughly in schedule with controls. However, when inseminated 2 h before hormone addition, eggs failed to enter first mitosis after completion of meiosis: Multiple pronuclei reformed, occasionally migrated, and fused together, but nuclear envelope breakdown was never observed (Fig. 6Ab), even as late as 6 h pha. Hormone addition at various times between 30 min and 2 h after insemination resulted in corresponding varying ratios of definitely G2-arrested eggs (Fig. 6B). BrdU added after pronuclei reformation was incorporated into DNA (not shown), showing these prematurely inseminated eggs arrested in G2, like the unfertilized ones. In-gel MBP kinase activity revealed that eggs inseminated 2 h before hormone addition failed to inactivate MAPK even a long time after second polar body emission (Fig. 6C). Thus, eggs inseminated too prematurely before meiosis reinitiation behave like unfertilized eggs: They lose memory of fertilization signal and arrest at G2 with high MAPK activity after completion of meiosis.

A major immediate consequence of fertilization is a large release of calcium in the egg cortex, which is sufficient to induce most of the consequences of fertilization, including cell cycling after completion of meiosis and MAPK inactivation, and can be mimicked by calcium microinjection or calcium ionophore application. Prior microinjection of EGTA or BAPTA (1 mM final concentration) before fertilization of starfish oocytes was found to inhibit mitotic entry after meiosis (see Fig. 10) as previously reported (Picard and Dorée, 1983a); EGTA-microinjected and fertilized eggs arrested after DNA replication, as inferred from BrdU incorporation (not shown). Accordingly, MAPK failed to drop after second polar body emission in these eggs, while it normally dropped in eggs microinjected with EGTA soon (2 to 3 min) after fertilization (Fig. 7).

Taken together, these experiments highlight a strong correlation between MAPK inactivation at meiosis completion and entry into mitosis of fully mature eggs.

Prevention of MAPK Inactivation Arrests Fertilized Eggs at G2 in a Dose-Dependent Manner

In order to prevent MAPK inactivation after second polar body emission in fertilized eggs, we microinjected the budding yeast MAPKKK Ste11, rendered constitutively active by a N-terminal truncation (see Materials and Methods). When Ste11-ΔN (50 μg/ml final concentration) was microinjected during the second meiotic cell cycle, it maintained MAPK active and prevented fertilized eggs of *A. aranciacus* and *M. glacialis* from proceeding into embryogenesis and arrested them at G2 (Picard *et al.*, 1996). In the present work, we confirmed this result and further found that Ste11-ΔN-microinjected eggs arrest at G2, either in the first mitotic cell cycle, only in the second mitotic cell cycle, or not at all, depending on the amount of microinjected protein and the resulting level of MAPK activity: 50 μg/ml Ste11-ΔN maintained a high level of MAPK activity, which was correlated with arrest at G2 in the first mitotic cell cycle; 30 μg/ml Ste11-ΔN maintained a medium level of MAPK activity, which was correlated with arrest at G2 in the second mitotic cell cycle only; and 3 μg/ml Ste11-ΔN maintained only a low level of MAPK activity and failed to arrest eggs (Fig. 8). We never observed arrest at G1 in *A. aranciacus* or *M. glacialis*.

Inactivation of MAPK by Microinjection of a MAPK-Specific Phosphatase Releases Mature Starfish Oocytes from G2 Arrest

To directly assess the role of MAPK in the G2 arrest of mature starfish oocytes, it was necessary to inactivate it in situations when it should be active. Activity of the MAP kinase ERK2 is dependent on the phosphorylation of conserved T and Y residues: Dephosphorylation of these residues by the dual-specificity phosphatase Pyst1 inactivates the kinase (Groom *et al.*, 1996). We found that microinjection of Pyst 1 mRNAs before hormonal stimulation, or after completion of meiotic maturation and G2 arrest, caused MAPK inactivation (not shown, see Fig. 10). Then, we followed individually Pyst 1-microinjected oocytes in the three situations described above, where G2 arrest was correlated with high MAPK activity:

Copyright © 1998 by Academic Press. All rights of reproduction in any form reserved.

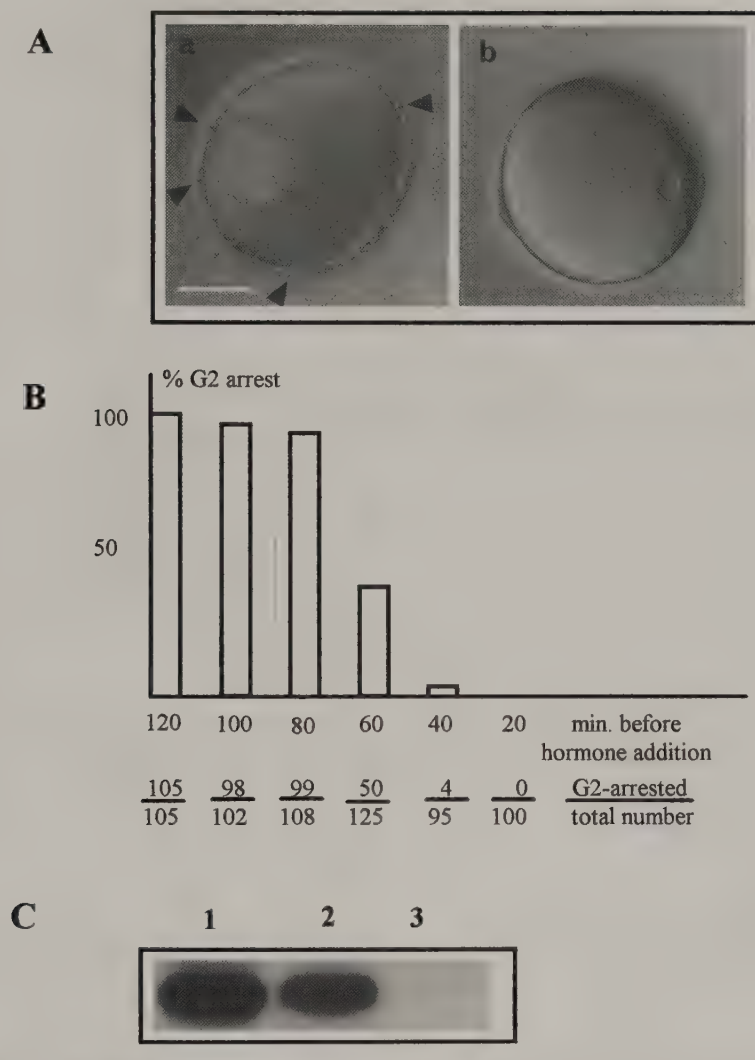

FIG. 6. Eggs inseminated too long before hormone addition fail to enter mitotic cycles after meiosis and to inactivate MAP kinase after second polar body emission. (A) Prophase oocytes could be inseminated. (a) Several sperms penetrated (arrowheads) and fertilization membrane elevated only locally around the sperm entry. After completion of meiosis, several pronuclei reformed, but the eggs did not enter M phase if hormone had been added 2 h after insemination (b, 360 min pha). (B) The ratio of oocytes that arrested in G2 after meiosis completion (ordinate) increased when the time elapsed between insemination and hormone addition increased (abscissa). Fractions represent the number of G2-arrested eggs, as judged by the presence of nuclear envelope, relative to the total number of eggs checked in each sample. Status of eggs was recorded at 360 min pha. Results did not change significantly later, until egg cytolysis. (C) Oocytes inseminated 2 h before hormone addition failed to inactivate efficiently MAPK after second polar body emission. In each lane, 10 oocytes (lane 1, unfertilized mature oocytes, 200 min pha; lane 2, oocytes inseminated 2 h before hormone, fixed at 360 min pha; lane 3, oocytes fertilized 1 h after hormone, fixed at 150 min pha) were processed for determination of in-gel MBP kinase activity. Bar, 100 μm.

• In unfertilized fully mature oocytes, MAPK inactivation resulted in resumption of mitotic cycles, as judged by cycles of nuclear envelope breakdown and reassembly, cycles of monaster formation (not shown), and chromosome condensation (compare Figs. 9a and 9b). After several cycles, DNA accumulated in eggs (Fig. 9c).

• This holds true when eggs inseminated 2 h before hormone addition (which should arrest at G2 with several

Copyright © 1998 by Academic Press. All rights of reproduction in any form reserved.

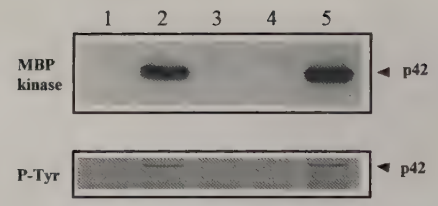

FIG. 7. Oocytes microinjected with 1 mM EGTA and then fertilized fail to inactivate MAPK after completion of meiosis. In each lane, 10 *A. aranciacus* oocytes were processed for determination of in-gel MBP kinase activity (top) or Western blot analysis of phosphotyrosine in p42 MAPK (bottom). Lane 1, prophase-arrested oocytes; lane 2, maturing oocytes (70 min pha); lane 3, fertilized mature oocytes (130 min pha); lane 4, fertilized mature eggs, microinjected with EGTA (1 mM final concentration) 10 min after fertilization (130 min pha); lane 5, fertilized mature eggs, microinjected with EGTA 10 min before fertilization (fixed at 240 min pha).

permanent pronuclei, see above) were microinjected with Pyst 1 mRNAs (Figs. 9d–9f).

• Finally, Pyst 1 translation also released from G2 arrest eggs fertilized in the presence of 1 mM intracellular EGTA. Figure 10 depicts one such oocyte at three different times: in Figs. 10c and 10d (200 min pha) the nuclear envelope was clearly seen, showing this egg was in interphase at that time. Ten minutes later (Figs. 10e and 10f) the nuclear envelope has broken down and entered M phase. Finally, at 235 min pha the nuclear envelope reassembled around individual chromosomes, giving rise to small procaryons, indicating the egg was in interphase again (Figs. 10g and 10h). During the same time, control uninjected oocytes remained arrested with prominent pronuclei (Figs. 10a and 10b). Accordingly, release from G2 arrest in Pyst1-microinjected eggs was correlated with MAPK inactivation (Fig. 10, bottom). All three kinds of observations were repeated three times on at least 10 oocytes.

DISCUSSION

In the present work we have shown that, if not fertilized or if the signal generated by fertilization is repressed (by prior EGTA microinjection) or lost (by too late hormone addition to inseminated immature oocytes), mature oocytes of the starfishes *A. aranciacus* and *M. glacialis* arrest at G2 after completion of DNA replication. G2 arrest was demonstrated by cytological and physiological observations:

• First, DNA replication occurred and was completed, as shown in Figs. 1 and 2.

• Second, fully mature oocytes were able to amplify MPF activity, which is a peculiarity of G2-arrested cells. This ability is accounted for by the presence of a sufficient amount of inactive cyclin B–cdc2 complex, whose activation can be obtained by ways specific for G2-arrested cells: Microinjection of MPF-containing cytoplasm or purified active MPF. Entry into M phase and MPF amplification induced by microinjection of 1 mM okadaic acid (OA), a potent inhibitor of phosphatases 1 and 2A, are also restricted to G2 cells (Picard *et al.*, 1989). Particularly, OA microinjection is unable to trigger resumption of the cell cycle in unfertilized sea urchin eggs, which are arrested in G1 (Picard *et al.*, 1989), although it triggers premature entry into mitosis after S phase in fertilized sea urchin eggs (Patel and Whitaker, 1991). We confirmed in fully mature *M. glacialis* and *A. aranciacus* oocytes that OA microinjection triggered rapid entry into mitosis and MPF amplification (not shown; see Picard *et al.*, 1989). Similarly, recombinant cyclin A microinjection (1 μM final concentration) induces MPF activation in prophase-arrested starfish oocytes (our unpublished results); this holds true in fully mature pronucleus-arrested oocytes (not shown). Finally, we also showed that microinjection of PSTAIR synthetic peptide, a sequence conserved in cdc2 homologs, was able to trigger MPF amplification and NEBD in fully mature starfish oocytes, as already described in prophase-blocked immature oocytes (Labbé *et al.*, 1989), even in the presence of 0.25 mM EGTA, which inhibits PSTAIR-induced calcium increase and fertilization membrane elevation (Picard *et al.*, 1990).

Moreover we show that this arrest at G2/M is due to and requires MAPK activity. Fertilization downregulates MAPK and allows eggs to escape G2 arrest, but, if MAPK is artificially reactivated, embryos will again arrest at G2, either in the first or the second cell cycle, depending on the activity of MAPK generated by microinjecting constitutively active MAPKKK. We showed previously that inappropriate reactivation of MAPK also induces G2 arrest in cycling *Xenopus* egg extracts (Abrieu *et al.*, 1997b). G1 arrest was never observed. In contrast, MAPK is responsible for arrest at G1 of fully mature, unfertilized oocytes of the starfish *Asterina pectinifera*, and suppression of MAPK inactivation at fertilization arrests eggs predominantly at G1 (Tachibana *et al.*, 1997). Thus, MAP kinase is responsible for arrest at different stages of the first mitotic cell cycle in fully mature and unfertilized eggs of different starfish species.

The difference between the two groups of starfish species may, however, not be as sharp as it appears at first sight. Indeed, about 30% of *A. pectinifera* eggs were reported to escape G1 arrest due to ectopic activation of MAPK, and in this case they arrested at G2 (T. Kishimoto, personnal communication). Conversely, MAPK may slow down the first round of DNA replication in *M. glacialis*, as it is completed much more rapidly in fertilized eggs, which inactivate MAPK, than in fully mature, unfertilized eggs, which maintain a high level of MAPK activity. A likely interpretation of the difference between the two groups of starfish species is thus that the threshold level of MAPK activity for arrest at G1/S is higher than that for arrest at

Copyright © 1998 by Academic Press. All rights of reproduction in any form reserved.

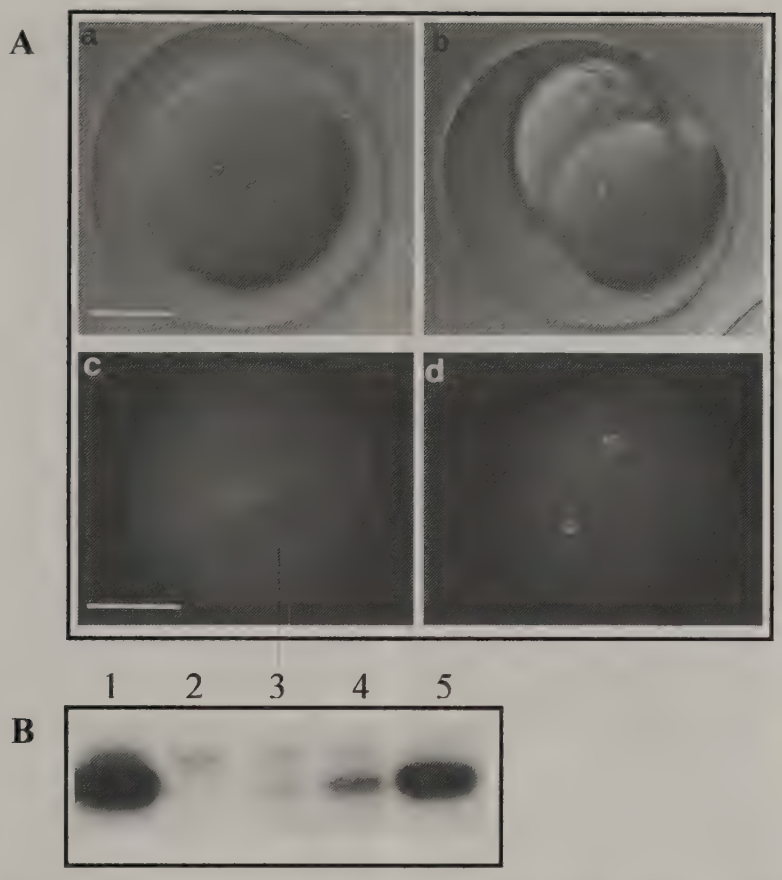

FIG. 8. The time of arrest in G2 depends on the level of MAP kinase activity maintained through microinjection of the recombinant MAPKKK Ste11-ΔN in fertilized eggs of the starfish *A. aranciacus*. In a first experiment (left column), oocytes were fertilized at 75 min pha in the presence of BrdU. Eggs injected with 50 μg/ml Ste11-ΔN after first polar body emission (120 min pha), which did not cleave (Aa), were taken at 420 min pha and processed for BrdU detection in the zygote pronucleus (Ac) or in-gel MBP kinase activity (B, lane 5). In a second experiment using the same batch of oocytes (right column), a lesser amount of Ste11-ΔN was microinjected (about 30 μg/ml) at 120 min pha. This did not prevent first cleavage, but oocytes arrested at the two-cell stage (Ab, micrograph taken at 420 min pha); in this experiment BrdU was added when the eggs initiated the first cleavage and embryos arrested at the two-cell stage at 420 min pha were processed for BrdU detection (Ad) or in-gel MBP kinase activity (B, lane 4). In addition, B further shows in-gel MBP kinase activities of (1) control unfertilized eggs at 420 min pha, (2) control embryos at the eight-cell stage; and (3) embryos microinjected with only 3 μg/ml Ste11-ΔN, taken at the eight-cell stage at 470 min pha. In each lane, total proteins from 10 eggs were loaded for determination of MBP kinase activities. Bar (in a for upper panel, in c for lower panel), 100 μm.

G2/M. Mature oocytes may either contain a higher level of MAPK activity or be more sensitive to MAPK, in *A. pectinifera*, which arrest predominantly in G1, than in other starfish species, which arrest in G2/M and never in G1. Indeed, a careful examination of Fig. 7 shows that the MAPK activity artificially maintained by microinjection of constitutive Ste11 kinase in *A. aranciacus* oocytes is lesser than the meiotic level, indicating that there is a strong MAPK inhibitory activity in the cell after completion of meiosis. In contrast to the constitutive Ste11 kinase, the microinjection of the no-constitutive mos-pMAL MAPKKK was found unefficient in reactivating MAPK in fertilized eggs (unpublished results), suggesting that inactivation of MAPK in fertilized eggs is at least partially due to a downregulation of MAPKKK.

MAPK has been shown to prevent parthenogenetic activation and arrest vertebrate oocytes at the second meiotic metaphase by preventing activation of the cyclin degradation pathway (reviewed in Sagata, 1997). The mechanism responsible for MAPK-dependent inhibition of the G1/S and

Copyright © 1998 by Academic Press. All rights of reproduction in any form reserved.

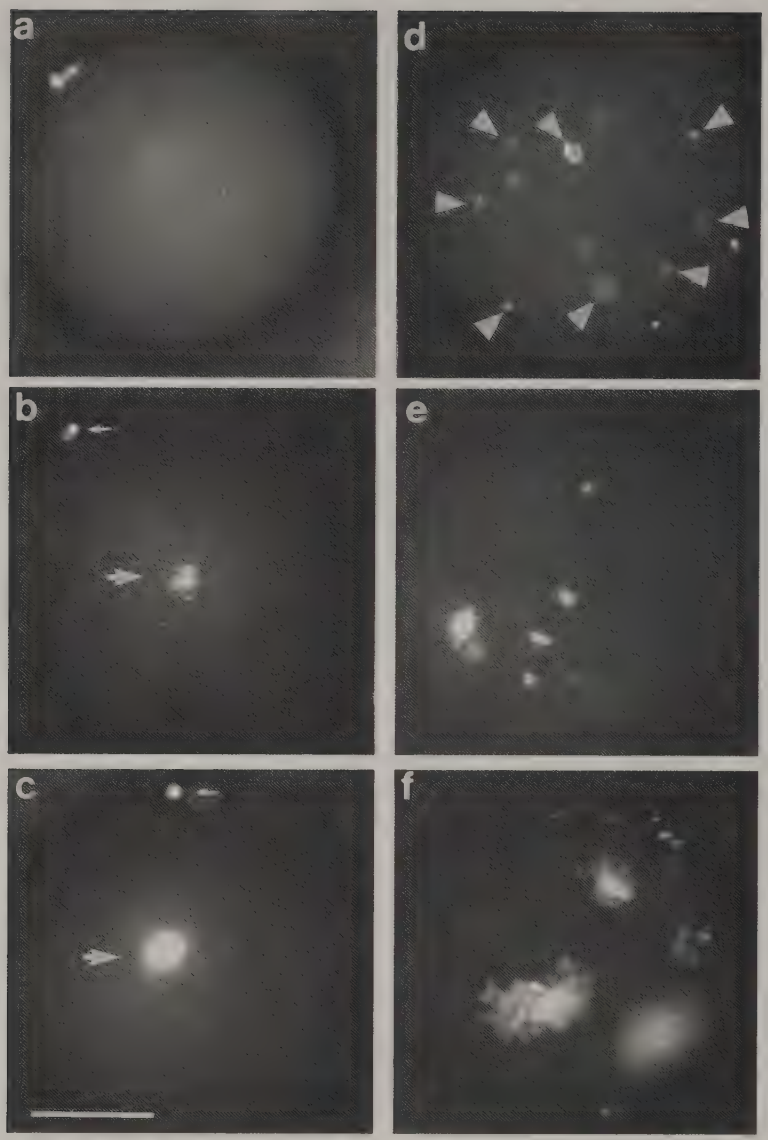

FIG. 9. Expression of the MAPK-specific phosphatase Pyst1 induces entry into mitosis in fully mature oocytes. (Left) Unfertilized *Marthasterias glacialis* fully mature oocytes. (Right) Fully mature oocytes that were inseminated 2 h before hormone addition. In the latter case, several sperms entered the oocytes, giving rise to several separate nuclei after completion of meiosis as shown by Hoechst DNA staining (arrowheads point to some pronuclei in d; in each picture a single egg is shown). (a and d) Controls (360 min pha). (Middle and bottom panels) Pyst 1 mRNAs were microinjected after the time of second polar body emission (125 min pha), and eggs were processed for Hoechst DNA staining at various times. (b and e) M-phase eggs, fixed 90 min after Pyst 1 microinjection (thus about 220 min pha). Chromatin has condensed. In polyspermic eggs, several pronuclei in a cell occasionally fused to give rise to a reduced number of mitotic figures (e). In unfertilized oocytes the condensed chromosomes remained clustered (b) and a single nucleus reformed in interphase at the center of the egg (small arrow in b and c, polar bodies; large arrow, egg nucleus). (c and f) Eggs fixed 210 min after Pyst1 microinjection (thus about 340 min pha). Several cell cycles occurred (not shown), and the nuclear DNA content increased as shown by the bright Hoechst fluorescence in the chromatine of both unfertilized (c) and polyspermic eggs (f). Bar, 60 μm.

Copyright © 1998 by Academic Press. All rights of reproduction in any form reserved.

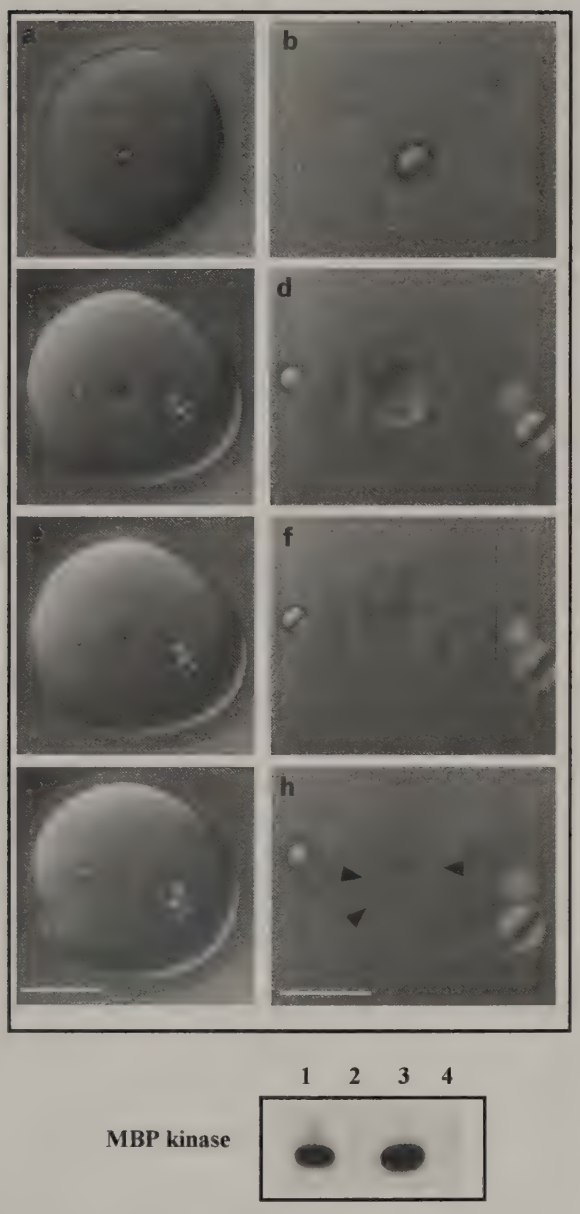

FIG. 10. Inactivation of MAPK by Pyst1 rescues from G2 arrest *A. aranciacus* eggs microinjected with EGTA before fertilization. (Top) Oocytes fertilized in the presence of 1 mM intracellular EGTA. Pictures in the right column are 2.3× magnifications of the nuclear area in the corresponding picture in left column. (a and b) Control, 500 min pha; in the absence of Pyst1 the egg is definitively arrested at G2 with multiple pronuclei dispersed in the cytoplasm. (c–h) An EGTA-injected and fertilized egg was microinjected with Pyst1 mRNAs after fertilization. (c and d) 200 min pha, all pronuclei have fused together. (e and f) 210 min pha, NEBD has occurred. (g and h) 235 min pha, multiple small procaryons (arrow heads) have reformed in the egg after exit from first mitosis, in the absence of cleavage. (Bottom) In-gel MBP kinase activities of (1) control unfertilized eggs arrested at the pronucleus stage (500 min pha), (2) control fertilized embryos at the eight-cell stage (500 min pha), (3) eggs injected with EGTA prior to fertilization (500 min pha), (4) eggs injected with EGTA prior to fertilization and then further injected with Pyst1 mRNAs (200 min pha). Bar, 100 μm (left column); 50 μm (right column).

the G2/M transitions and prevention of parthenogenetic development in starfish species remains elusive. Even though arrest of mature oocytes at G2/M is associated with tyrosine phosphorylation of cdc2 in *Astropecten* and *Marthasterias*, how MAPK mediates MPF inactivation at completion of maturation, while it rather appears to prevent MPF inactivation at initiation of maturation (Abrieu *et al.*, 1997a) is open for further investigation.

The fact that prolongation or inappropriate reactivation of MAPK induces cell cycle arrest at different stages of the cell cycle, including the G1/S transition (*A. pectinifera*), the G2/M transition (*A. aranciacus, M. glacialis, Xenopus*), or exit from mitosis (*Xenopus*) is reminiscent of checkpoint mechanisms, which arrest cell cycle progression if a defect that would compromise genetic stability is detected, either in G1/S, G2/M, or metaphase/anaphase. We proposed previously that MAPK may mimic a constitutive activation of checkpoint mechanisms, not only in metaphase as it was already demonstrated (Minshull *et al.*, 1994; Murray, 1995; Takenaka *et al.*, 1997; Wang *et al.*, 1997), but also in G1 and G2 (Abrieu *et al.* 1997b). This hypothesis is supported by the fact that MAPK is strongly repressed during early embryogenesis (Ferrell *et al.*, 1991; our unpublished results in starfish and sea urchin) and, correlatively that checkpoint mechanisms are downregulated during this period.

The mechanism responsible for the universal drop of MAPK activity that occurs after fertilization in both vertebrates and invertebrates is not understood. MAPK inactivation, suppressed by microinjection of EGTA prior to fertilization, appears to be triggered by the calcium transient associated with both fertilization and parthenogenetic activation. It is not, however, a direct consequence of the calcium transient, as the drop of MAPK activity is delayed with respect to fertilization in starfish as in many other animals. In *Spisula*, for example, oocytes are still arrested at G2/prophase of the first meiotic cell cycle when fertilized, yet MAPK does not undergo inactivation before first polar body emission (Shibuya *et al.*, 1992). In starfish, oocytes inseminated before GVBD do not inactivate MAPK earlier than the second polar body emission, at least 2 h later. Moreover, MAPK inactivation is suppressed if EGTA is microinjected before, but not shortly after (2–3 min), fertilization. Finally, MAPK inactivation is also suppressed when

Copyright © 1998 by Academic Press. All rights of reproduction in any form reserved

the memory of fertilization has been lost, due to a too long gap between insemination of G2-arrested oocytes and meiosis reinitiation. At least in *Xenopus*, the sequence of events from the calcium transient to MAPK inactivation involves downregulation of the whole MAPK cascade, including Mos, Raf, and MAPKK, as the activity of each of these upstream kinases has been shown to drop following fertilization (Sagata *et al.*, 1989; McNicol *et al.*, 1995). Interestingly, the requirement for a calcium transient for MAPK inactivation can be bypassed if MPF is microinjected in oocytes arrested at G2 after completion of meiotic maturation. In contrast, microinjection of MPF in oocytes arrested at G2 before meiotic maturation allows them to complete meiotic maturation. Then they arrest again at G2 with high MAPK activity. This suggests that the mechanism responsible for inactivation of the MAPK cascade is set up late during meiotic maturation.

ACKNOWLEDGMENTS

We are thankful for financial support donations from ARC, the Ligue Nationale contre le Cancer, and the Ligues Départementales de l'Ardèche, du Gard et des Pyrénées Orientales. V.V. was supported by grants from ARC and the Singer-Polignac Foundation.

REFERENCES

Abrieu, A., Lorca T., Labbé, J. C., Morin, N., Keyse, S., and Dorée, M. (1996). MAP kinase does not inactivate, but rather prevents the cyclin degradation pathway from being turned on in Xenopus egg extracts. *J. Cell Sci.* **109,** 239–246.

Abrieu, A., Dorée, M., and Picard, A. (1997a). Mitogen-activated protein-kinase activation down-regulates a mechanism that inactivates cyclin B-cdc2 kinase in G2-arrested oocytes. *Mol. Biol. Cell* **8,** 249–261.

Abrieu, A., Fisher, D., Simon, M. N., Dorée, M., and Picard, A. (1997b). MAPK inactivation is required for the G2 to M-phase transition of the first mitotic cell cycle. *EMBO J.* **16,** 6407–6413.

Cairns, B. R., Ramer, S. W., and Kornberg, R. D. (1992). Order of action of components in the yeast pheromone response pathway revealed with a dominant allele of the STE11 kinase and the multiple phosphorylation of the STE7 kinase. *Genes Dev.* **6,** 1305–1318.

Ferrell, J. E., Jr., Wu, M., Gerhart, J. C., and Martin, G. S. (1991). Cell cycle tyrosine phosphorylation of p34cdc2 and a microtubule-associated protein kinase homolog in Xenopus oocytes and eggs. *Mol. Cell Biol.* **11,** 1965–1971.

Gosti-Testu, F., Marty, M. C., Berges, J., Maunoury, R., and Bornens, M. (1986). Identification of centrosomal proteins in a human lymphoblastic cell line. *EMBO J.* **5,** 2545–2550.

Groom, L. A., Sneddon, A. A., Alessi, D. R., Dowd, S., and Keyse, S. M. (1996). Differential regulation of the MAP, SAP and RK/p38 kinases by Pyst1, an novel cytosolic dual specificity phosphatase. *EMBO J.* **15,** 3621–3632.

Hiramoto, Y. (1974). A method of microinjection. *Exp. Cell Res.* **87,** 403–406.

Hunter, T. (1997). Oncoprotein networks. *Cell* **88,** 333–346.

Karin, M., and Hunter, T. (1995). Transcriptional control by protein phosphorylation: signal transmission from the cell surface to the nucleus. *Curr. Biol.* **5,** 747–757.

Kishimoto, T., and Kanatani, H. (1976). Cytoplasmic factor responsible for germinal vesicle breakdown and meiotic maturation in starfish oocyte. *Nature* **260,** 321–322.

Kohno, M. (1985). Diverse mitogenic agents induce rapid phosphorylation of a common set of cellular proteins at tyrosine in quiescent mammalian cells. *J. Biol. Chem.* **260,** 1771–1779.

Labbé, J. C., Picard, A., Peaucellier, G., Cavadore, J. C., Nurse, P., and Dorée, M. (1989). Purification of MPF from starfish: Identification as the H1 histone kinase p34cdc2 and a possible mechanism for its periodic activation. *Cell* **57,** 253–263.

MacNicol, A. M., Muslin, A. J., Howard, E. L., Kikuchi, A., Mac Nicol, M. C., and Williams, L. T. (1995). Regulation of Raf1-dependent signaling during early *Xenopus* development. *Mol. Cell. Biol.* **15,** 6686–6693.

Meloche, S. (1995). Cell cycle reentry of mammalian fibroblasts is accompanied by the sustained activation of p44MAPK and p42MAPK isoforms in the G1 phase and their inactivation at the G1–S transition. *J. Cell Physiol.* **163,** 577–588.

Minshull, J. H., Sun, H., Tonks, N. K. and Murray, A. W. (1994). A MAP kinase-dependent spindle assembly checkpoint in *Xenopus* egg extracts. *Cell* **79,** 475–486.

Murray, A. W. (1995). The genetics of cell cycle checkpoints. *Curr. Opin. Cell Biol.* **6,** 872–876.

Patel, R., and Whitaker, M. (1991). Okadaic acid suppress calcium regulation of mitosis onset in sea urchin embryos. *Cell Regul.* **2,** 391–402.

Picard, A., and Dorée, M. (1983a). Is calcium the second messenger of 1-methyladenine in meiosis reinitiation of starfish oocytes? *Exp. Cell Res.* **145,** 325–337.

Picard, A., and Dorée, M. (1983b). Hormone-induced parthenogenetic activation of mature starfish oocytes. *Exp. Cell Res.* **145,** 315–323.

Picard, A., Galas, S., and Dorée, M. (1996). Newly assembled cyclin B-cdc2 kinase is required to suppress DNA replication between meiosis I and meiosis II in starfish oocytes. *EMBO J.* **15,** 3590–3598.

Picard, A., Karsenti, E., Dabauvalle, M. C., and Dorée, M. (1987). Release of mature starfish oocytes from interphase arrest by microinjection of human centrosomes. *Nature* **327,** 170–172.

Picard, A., Capony, J. P., Brautigan, D. L., and Dorée, M. (1989). Involvement of protein phosphatases 1 and 2A in the control of M phase promoting factor activity in starfish. *J. Cell Biol.* **109,** 3347–3354.

Picard, A., Cavadore, J. C., Lory, P., Bernengo, J. C., Ojeda, C., and Dorée, M. (1990). A peptide sequence conserved in p34cdc2 homologs induces a transient increase of free Calcium in starfish and amphibian oocytes. *Science* **247,** 327–329.

Sagata, N. (1997). What does Mos do in oocytes and somatic cells? *BioEssays* **19,** 13–21.

Sagata, N., Watanabe, N., Vande Woude, W. G., and Ikawa, Y. (1989). The c-mos protooncogene product is a cytostatic factor responsible for meiotic arrest in vertebrate eggs. *Nature* **342,** 512–518.

Schuetz, A. W. (1975). Cytoplasmic activation of starfish oocytes by sperm and divalent ionophore A-23187. *J. Cell Biol.* **66,** 86–94.

Copyright © 1998 by Academic Press. All rights of reproduction in any form reserved.

Shibuya, E. K., Boulton, T. G., Cobb, M. H., and Rudermen, J. V. (1992). Activation of p42 MAP kinase and the release of oocytes from cell cycle arrest. *EMBO J.* **11,** 3963–3975.

Steinhart, R. A., and Epel, D. (1974). Activation of sea urchin eggs by a calcium ionophore. *Proc. Natl. Acad. Sci. USA* **71,** 1915–1919.

Steinhart, R. A., Epel, D., and Carrol, E. J. (1974). Is calcium ionophore a universal activator for unfertilized eggs? *Nature* **25,** 41–43.

Strausfeld, U., Labbé, J. C., Fesquet, D., Cavadore, J. C., Picard, A., Sadhu, K., Russell, P., and Dorée, M. (1991). Dephosphorylation and activation of a p34cdc2/cyclin B complex in vitro by human cdc25 protein. *Nature* **351,** 242–245.

Tachibana, K., Machida, T., Nomura, Y., and Kishimoto, T. (1997). MAP kinase links the fertilization signal transduction pathway to the G1/S phase transition in starfish eggs. *EMBO J.* **16,** 4333–4339.

Takenaka, K., Gotoh, Y., and Nishida, E. (1997). MAP kinase is required for the spindle assembly checkpoint but is dispensable for the normal M-phase entry and exit in *Xenopus* egg cell cycle extracts. *J. Cell Biol.* **136,** 1091–1098.

Thibier, C., de Smedt, V., Poulhe, R., Huchon, D., Jessus, C., and Ozon, R. (1997). *In vivo* regulation of cytostatic activity in *Xenopus* metaphase II arrested oocytes. *Dev. Biol.* **185,** 55–66.

Verlhac, M. H., Kubiak, J. Z., Clarke, H. J., and Maro, B. (1994). Microtubule and chromatin behavior follow MAP kinase activity but not MPF activity during meiosis in mouse oocytes. *Development* **120,** 1017–1025.

Walter, S. A., Guadagno, T. M., and Ferrell, J. E. Jr. (1997). Induction of a G2 phase arrest in *Xenopus* egg extracts by activation of p42 MAP kinase. *Mol. Biol. Cell* **8,** 2157–2169.

Wang, X. M., Zhai, Y., and Ferrell, J. E. Jr. (1997). A role for mitogen activated protein kinase in the spindle assembly checkpoint in XTC cells. *J. Cell Biol.* **137,** 433–443.

Received for publication January 21, 1998
Revised May 22, 1998
Accepted June 12, 1998

Copyright © 1998 by Academic Press. All rights of reproduction in any form reserved.

DEVELOPMENTAL BIOLOGY 202, 14–28 (1998)
ARTICLE NO. DB988986

The Relationship between Rhombomeres and Vestibular Neuron Populations as Assessed in Quail–Chicken Chimeras

Carmen Díaz,* Luis Puelles,* Faustino Marín,* and Joel C. Glover†,[1]

**Department of Morphological Sciences, Faculty of Medicine, University of Murcia, E 30071 Murcia, Spain; and †Department of Anatomy, Institute of Basic Medical Science, University of Oslo, PB 1105 Blindern, 0317 Oslo, Norway*

The aim of this study was to evaluate the role segmentation plays in the determination of neuronal identity in the hindbrain. We focused on two specific sets of hindbrain neurons, namely, the vestibulospinal and vestibulo-ocular neurons, which comprise distinct groups that can be identified and distinguished by virtue of their axonal projection pathways. The relationship between rhombomeres and the vestibular neuron groups was assessed by a combination of quail–chicken chimeric grafting and selective retrograde axonal tracing. Individual quail hemirhombomeres were transplanted homotopically and isochronically into a chicken embryo host. Subsequently, vestibulospinal and vestibulo-ocular neurons with specific axon trajectories were labeled retrogradely with biotin-conjugated dextran-amines. The relationship between the spatial domains of the vestibular neuron groups and rhombomere-derived domains had the following features: (1) some groups were derived from single rhombomeres; (2) some groups were derived from multiple contiguous rhombomeres; (3) two groups occupied domains that could not be defined in terms of whole rhombomere lengths; (4) some groups spanning multiple rhombomeres exhibited an internal cytoarchitectonic organization that related to individual rhombomeres; and (5) some groups exhibited limited boundary violation. These results support the notion that positional information within defined domains of the neural tube provides a groundplan for the regional determination of neuronal identity and axon pathfinding, and that hindbrain segmentation contributes to this process. But they also indicate that segmentation is not the only mechanism that defines the rostrocaudal domains of neuron types. Moreover, they emphasize that the relationship between rhombomeres and neuronal determination cannot be couched simply in terms of segmental iteration or of bimeric (paired rule) specification. © 1998 Academic Press

INTRODUCTION

The generation of diverse yet regionally specific neuronal phenotypes in the central nervous system implies the existence of positional determinants with stereotyped distributions within the neural tube. In the hindbrain region, the neural tube is partitioned into a series of neuromeres, called rhombomeres (Lumsden, 1990; Vaage, 1969). Each rhombomere expresses a unique combination of transcription factors, thus endowing the rhombomeric domains with distinct molecular cues that could in principle establish rhombomere-specific patterns of neuronal differentiation (Keynes and Krumlauf, 1994). Indeed, several functionally identified neuronal populations have been found to correlate to rhombomeric domains at the early stages when rhombomere boundaries are visible. These include the motoneurons and parasympathetic neurons of the cranial nerve nuclei (Auclair *et al.*, 1996; Gilland and Baker, 1993; Lumsden, 1990), the cochlear efferent neurons (Fritzsch *et al.*, 1993; Simon and Lumsden, 1993), and certain populations of vestibular neurons (Glover, 1989, 1994, 1996).

In the classical anatomical description of the vestibular system, the vestibular neurons in the hindbrain are grouped into nuclei on the basis of cytoarchitectonic features (cell size, shape, and distribution). More recently, the vestibular neurons have been shown in the chicken embryo to be organized in coherent clusters with characteristic patterns of axon trajectory and termination among motoneuron targets (Fig. 1; see Glover, 1994; Glover and Petursdottir,

[1] To whom correspondence should be addressed. Fax: +47-22851278. E-mail: joel@pons.uio.no.

0012-1606/98 $25.00
Copyright © 1998 by Academic Press
All rights of reproduction in any form reserved.

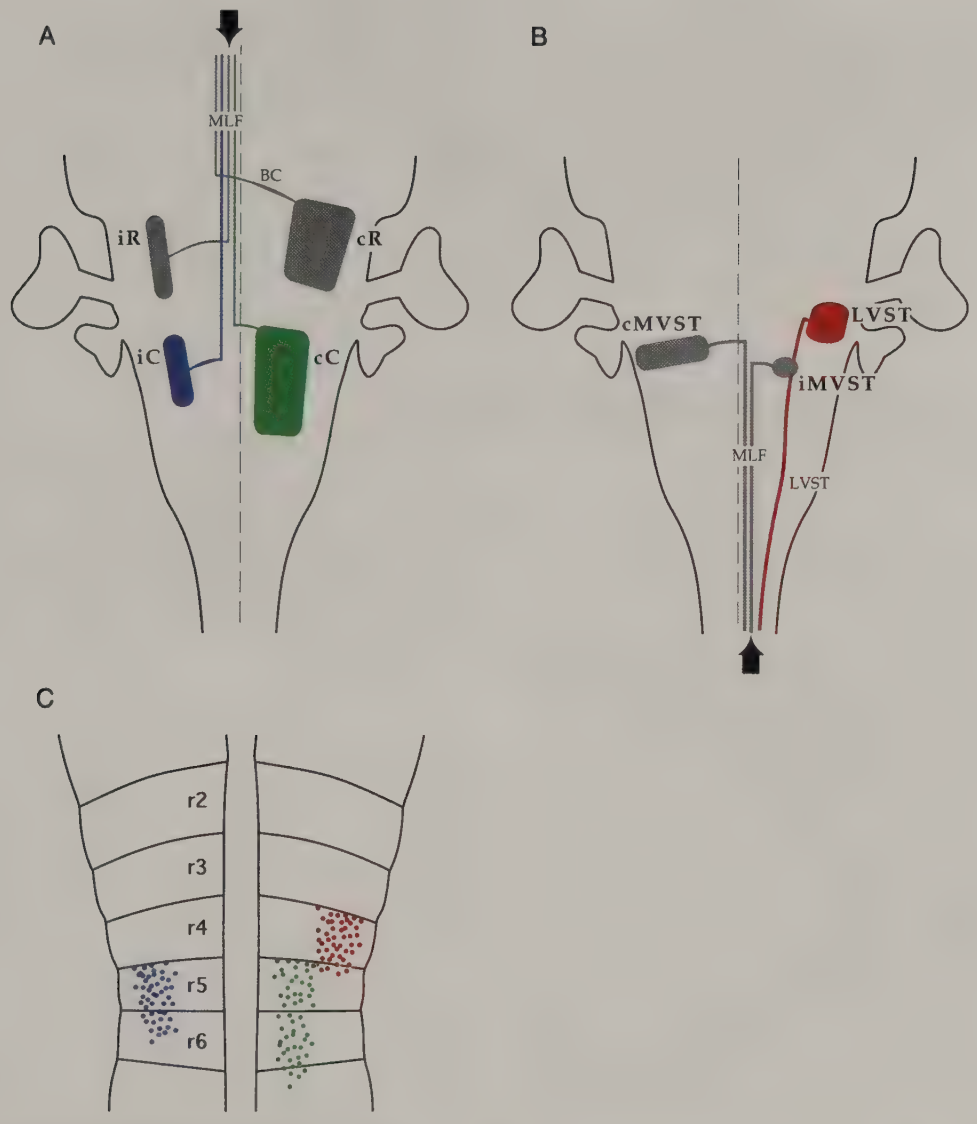

FIG. 1. Vestibular projection neuron groups can be defined on the basis of hodology and occupy specific rhombomeric domains at early stages. (A) The rough locations and axon trajectories of the four hodologically defined groups of vestibulo-ocular neurons in horizontal projection at d11. The groups are named according to the side on which their axons project and their rostrocaudal location (iR, ipsilateral rostral; cR, contralateral rostral; iC, ipsilateral caudal; cC, contralateral caudal). The major axon tracts of projection are the medial longitudinal fascicle (MLF) and the brachium conjuctivum (BC). The arrow indicates the approximate site of tracer application that gives retrograde labeling of these groups. (B) The rough locations and axon trajectories of the three hodologically defined groups of vestibulospinal neurons in horizontal projection at d11. The groups are named according to a nomenclature used in vestibular physiology wherein the vestibulospinal projections are separated into a medial and a lateral vestibulospinal tract (MVST and LVST). The MVST projection originates from two groups, one projecting ipsilaterally (iMVST), the other contralaterally (cMVST). The major axon tracts of projection are the MLF and the LVST. The arrow indicates the approximate site of tracer application that gives retrograde labeling of these groups. (C) The locations of the iC, cC, and LVST groups at earlier stages (about stages 22–25) when rhombomeres (r) are still visible. The individual groups are color-coded as in A and B. The iR, cR, iMVST, and cMVST groups are not shown because they cannot be identified unambiguously at these stages.

Copyright © 1998 by Academic Press. All rights of reproduction in any form reserved.

TABLE 1
Summary of Preparations by Labeled Vestibular Group and Grafted Rhombomere

Projection	Side	Labeled groups	r3	r4	r5
v-spinal	Ipsi	LVST, iMVST	—	3 (2)	5 (1)
	Contra	cMVST	—	1 (1)	—
v-ocular	Ipsi	iR, iC	(1)	2 (2)	—
	Contra	cR, cC	(2)	3 (1)	2

Note. The number of completely normal preparations is followed in parentheses by the number of preparations with minimal defects in the basal or floor plates.

1998). The relationship between neurons and their axon trajectories is called "hodology" (from "hodos", the Greek word for "path"). On the basis of this concept, the organization of the vestibular system has been described as a "hodological mosaic," wherein vestibular neurons with specific axonal projection phenotypes are localized to specific, segregated domains of the hindbrain neural tube (Fig. 1; see Glover, 1989, 1994; Glover and Petursdottir, 1998). Recent studies in the zebrafish indicate that hodology as an organizational feature of the vestibular system is likely to be conserved phylogenetically (Baker *et al.*, 1996). Since hodological patterns are the end result of complex molecular interactions between growing axons and potential pathways and targets, a stereotyped hodological organization is likely to be related to regionally specific patterns of gene expression.

At early stages of neural tube development, when rhombomeres are visible, some of the vestibular neuron groups are strikingly correlated with rhombomeric domains (Fig. 1C; see Glover, 1989, 1996). Because of the link between rhombomeric domains and transcription factor expression (Keynes and Krumlauf, 1994), the vestibular hodological mosaic has been proposed as a genetically predetermined pattern of connections from which species-specific variants might be sculpted (Glover, 1994; Glover and Petursdottir, 1998). To test this notion, it is necessary to elucidate the relationship between vestibular neuron clusters and the spatiotemporal pattern of gene expression within the hindbrain. As a first step, we are trying to assess completely the relationship between vestibular neuron groups and rhombomeric domains.

Unfortunately, the mature pattern of vestibular neurons is not fully evident at the stages when rhombomeres are visible (compare Figs. 1A and 1B to Fig. 1C). Some groups are insuffiently populated to allow for reliable demarcation at early stages, and certain groups cannot be identified unambiguously until later stages because of delayed differentiation (Glover and Petursdottir, 1991). Indeed, the overt morphological boundaries between rhombomeres disappear well before all hindbrain neurons have been born and migrated to their definitive positions (Hemond and Glover, 1993). Thus, fate-mapping techniques that indelibly mark individual rhombomeres are required to assess the relationship between neuronal populations and rhombomeric domains in the mature hindbrain. The main goal of the present report was to use the quail–chicken chimera technique to render specific hemirhombomeres visible at late stages of development when all the vestibular groups can be labeled, thus permitting a direct assessment of this relationship.

In a general survey of rhombomeric domains using the quail–chicken chimera technique, Marín and Puelles (1995) found that many mature hindbrain nuclei occupied either single or multiple rhombomere-derived domains. For those stretching over multiple rhombomeres, cytoarchitectonic subdivisions were often correlated to single rhombomeres. In particular, the set of classically defined vestibular nuclei spanned all the rhombomeres, and some of the nuclear subdivisions were roughly in register with rhombomere boundaries. Here, we combine the quail–chicken chimera technique with retrograde labeling of the vestibular neuron groups identified by axon trajectory. This has allowed us to identify how rhombomere boundaries relate to the vestibular hodological mosaic. Our study also provides new information relevant to the question of what kind of "segmentation rules," if any, are at play in the regional determination of neuronal identity in the hindbrain.

MATERIALS AND METHODS

Fertilized chicken and quail eggs were obtained from the animal facility at the University of Murcia or from local suppliers and incubated at 38°C. Homotopic, isochronic grafting of single hemirhombomeres (r3, r4, or r5) was performed as previously described (Marín and Puelles, 1995) on the second day of incubation. The developmental timepoint of the operation was assessed by stage (Hamburger and Hamilton, 1951) and the number of fully formed somites and ranged from stages 10^{+} to 12, corresponding to 11–14 somites. The chimeras were then reincubated for 9 to 10 days, reaching stages 36–38, at which time they were removed from the egg into ice-cold chicken physiological saline (137 mM NaCl, 5 mM KCl, 2 mM $CaCl_2$, 1 mM $MgCl_2$, 1 mM Na phosphate, 5 mM Hepes, 11 mM glucose, pH 7.4) and decapitated. The brain was dissected free and maintained *in vitro* for retrograde axonal labeling with biotin dextran amine (BDA), as previously described (Glover *et al.*, 1986; Glover, 1995). Following labeling, the tissue was fixed in buffered 4% paraformaldehyde or a periodic acid–lysine–paraformaldehyde mixture (McLean and Nakane, 1974) for 6 h and cryoprotected overnight in 20% sucrose in phosphate buffer (pH 7.4, 4°C) containing 0.1–0.2% hydrogen peroxide to quench endogenous peroxidases. Sections were cut on a cryostat at 20–30 μm in the sagittal or horizontal plane and collected onto glass slides. Quail cells were detected by immunohistochemistry. The sections were incubated overnight at room temperature with the QCPN antibody (Developmental Studies Hybridoma Bank, University of Iowa), diluted 1:5 in 0.1% sodium azide, 0.05% Triton X-100 in 0.1M PBS, or for 2 days at 4°C in the same antibody diluted 1:10. Biotinylated secondary antibody treatment and visualization with a Vectastain ABC kit (Burlingame, CA) were standard, leading to nuclear labeling with the antibody and cytoplasmic labeling with

Copyright © 1998 by Academic Press. All rights of reproduction in any form reserved.

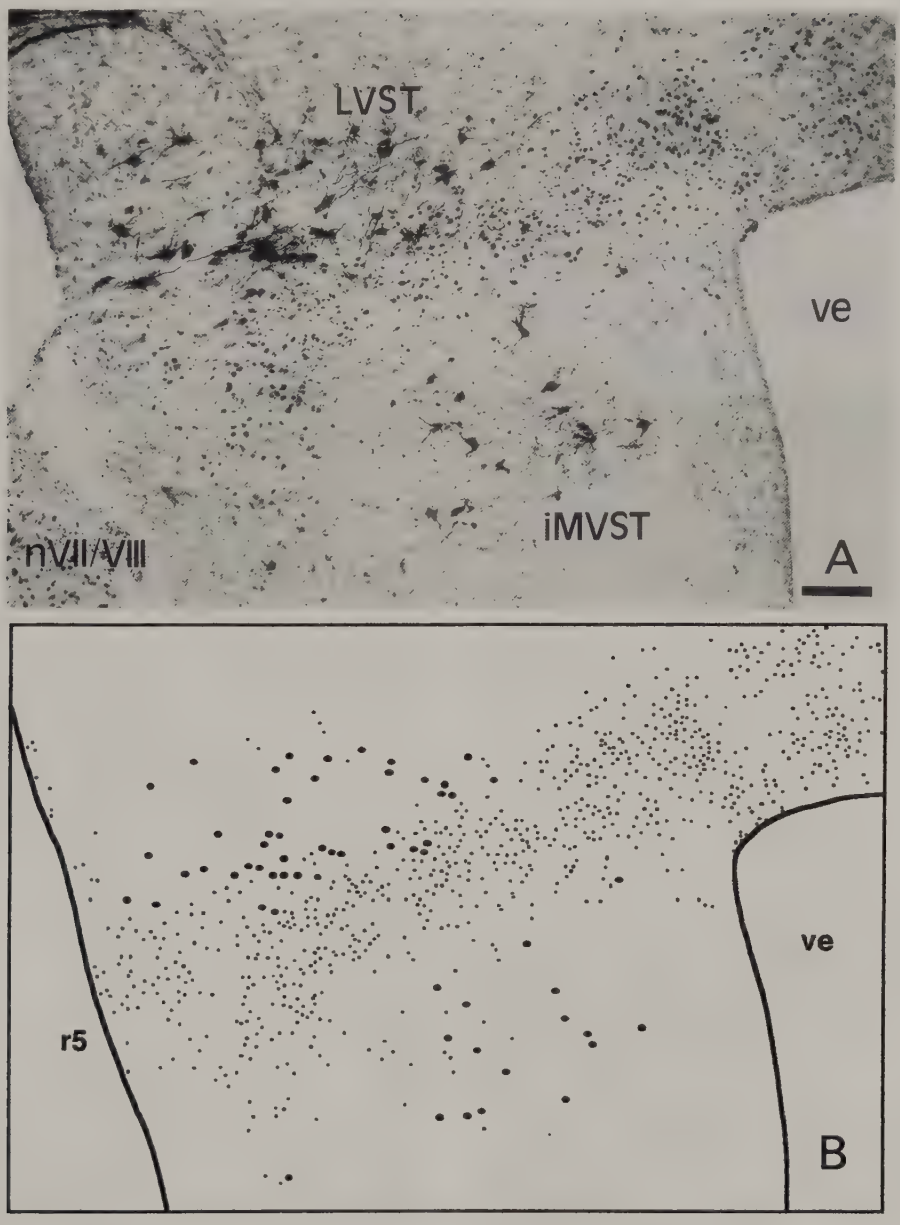

FIG. 2. Combined quail–chick chimeric grafting and retrograde axonal tracing with BDA allows for comparison of projection neuron groups and rhombomeric domains. (A) Horizontal section from a chicken embryo with a graft of a quail hemirhombomere 5 and with BDA injected into the upper cervical spinal cord ipsilateral to the graft. BDA-labeled vestibulospinal interneurons are recognizable by their dark cytoplasmic staining that reveals dendrites and axons. Two identified vestibulospinal groups can be seen: the LVST and the iMVST. Quail cells are recognizable by their immunostained nuclei. (B) Drawing of the same photograph with large dots indicating vestibulospinal neurons and small dots indicating quail nuclei. The quail graft occupies a wedge of the hindbrain, but with some intermingling with adjacent chicken tissue. Scale bar, 250 μm.

Copyright © 1998 by Academic Press. All rights of reproduction in any form reserved.

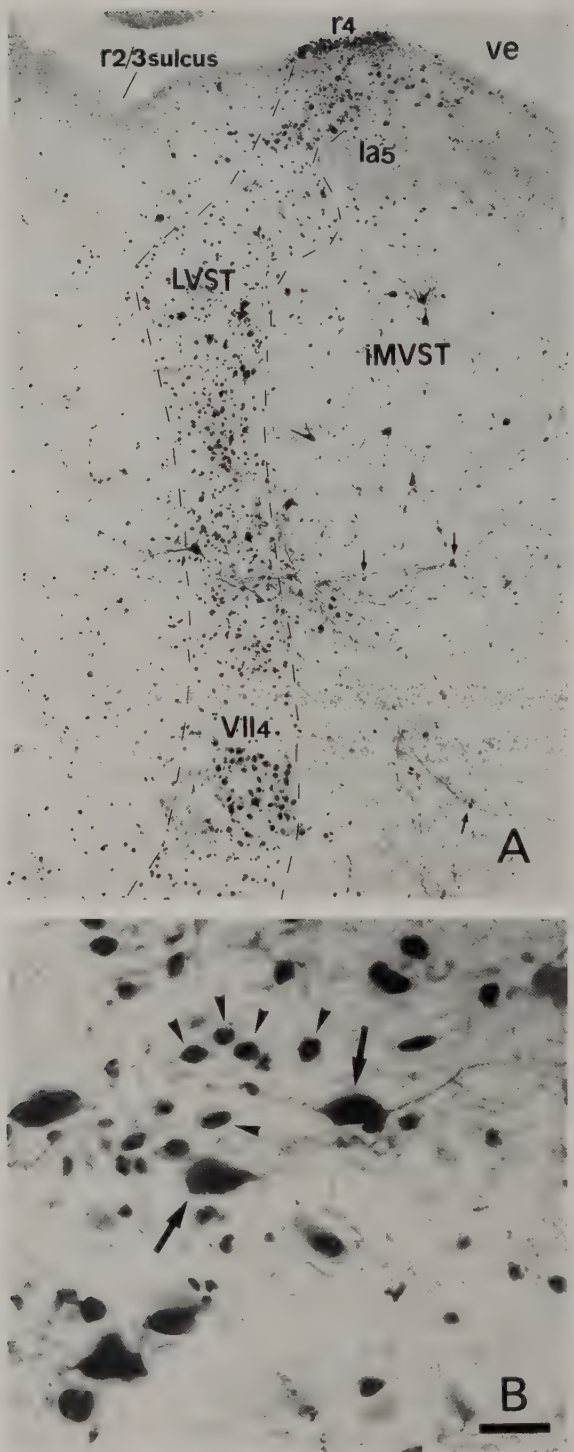

BDA. Some sections did not receive antibody to show BDA-labeled cells only.

Vestibulospinal and vestibulo-ocular neuron groups were identified using criteria defined by Glover and Petursdottir (1991, 1998). Vestibulospinal groups were labeled retrogradely and unilaterally from approximately the first cervical spinal segment, whereas vestibulo-ocular groups were labeled retrogradely and unilaterally from the medial longitudinal fascicle just caudal to the trochlear nucleus (see Figs. 1A and 1B). Based on their axon trajectories and positions, the retrogradely labeled neurons could be assigned to one of three vestibulospinal or four vestibulo-ocular groups.

The overall survival of embryos following the grafting procedure was 55%. In 34 of 38 surviving embryos that developed to stages 36–38, the graft had visibly integrated into the host neural tube, and 26 of these embryos were judged to be either completely normal ($n = 16$) or had only minimal defects in the basal plate or floor plate at the site of the graft ($n = 10$). As the vestibular groups of interest lie predominantly in the alar plate, we analyzed all of these preparations but based our interpretations primarily on those that were completely normal (Table 1).

Digital images of sections containing BDA-labeled interneurons and donor quail cells were imported into Photoshop (Microsoft) format using a Leaf Lumina camera. Plots of cell positions were generated in a digital overlay constructed in the Canvas (Deneba) drawing program (Fig. 2). Horizontal or sagittal projections of individual preparations were constructed by aligning the rostral and caudal limits of the grafted rhombomere. Since these limits are skewed with respect to the horizontal and sagittal planes of the head, the projections do not provide a true representation of the position of the groups with respect to the projection outline, but do indicate reliably the topological relationship between group position and rhombomeric domain. To obtain quantitative estimates of the proportions of neurons lying in neighboring rhombomeres, retrogradely labeled neuron profiles were counted directly from the sections in the microscope. Only BDA-labeled neurons lying clearly to either side of the graft–host interface received definitive rhombomere assignments in this analysis; those lying within the boundary zone (see below) were deliberately left ambiguous.

FIG. 3. The boundary between graft and host rhombomeres is defined as the zone of intermingled graft and host cells. (A) Sagittal section of a hindbrain with r4 quail graft and BDA-labeled vestibulospinal neurons ipsilateral to the graft. Rostral is to the left. Quail cells are tightly contiguous at the ventricular surface, but are more spread toward the ventral brain surface. The dashed lines indicate the approximate location of the boundary zone of intermingling between graft and host tissue. Arrows indicate a few of the quail cells (probably oligodendrocytes) that have penetrated further into the host tissue along fiber tracts. At such sites of more extensive graft cell dispersal, the boundary is assumed to follow the generally straight ventricular-to-pial trajectory, thus cutting across the area of dispersal. (B) Most BDA-labeled neurons can be identified as graft- versus host-derived, irrespective of location, by virtue of the quail nucleus-specific marker. Higher magnification view showing the appearance of BDA+/quail+ cells (LVST neurons, arrows) and BDA−/quail+ cells (arrowheads). Scale bar, 260 μm (A) and 50 μm (B).

Copyright © 1998 by Academic Press. All rights of reproduction in any form reserved.

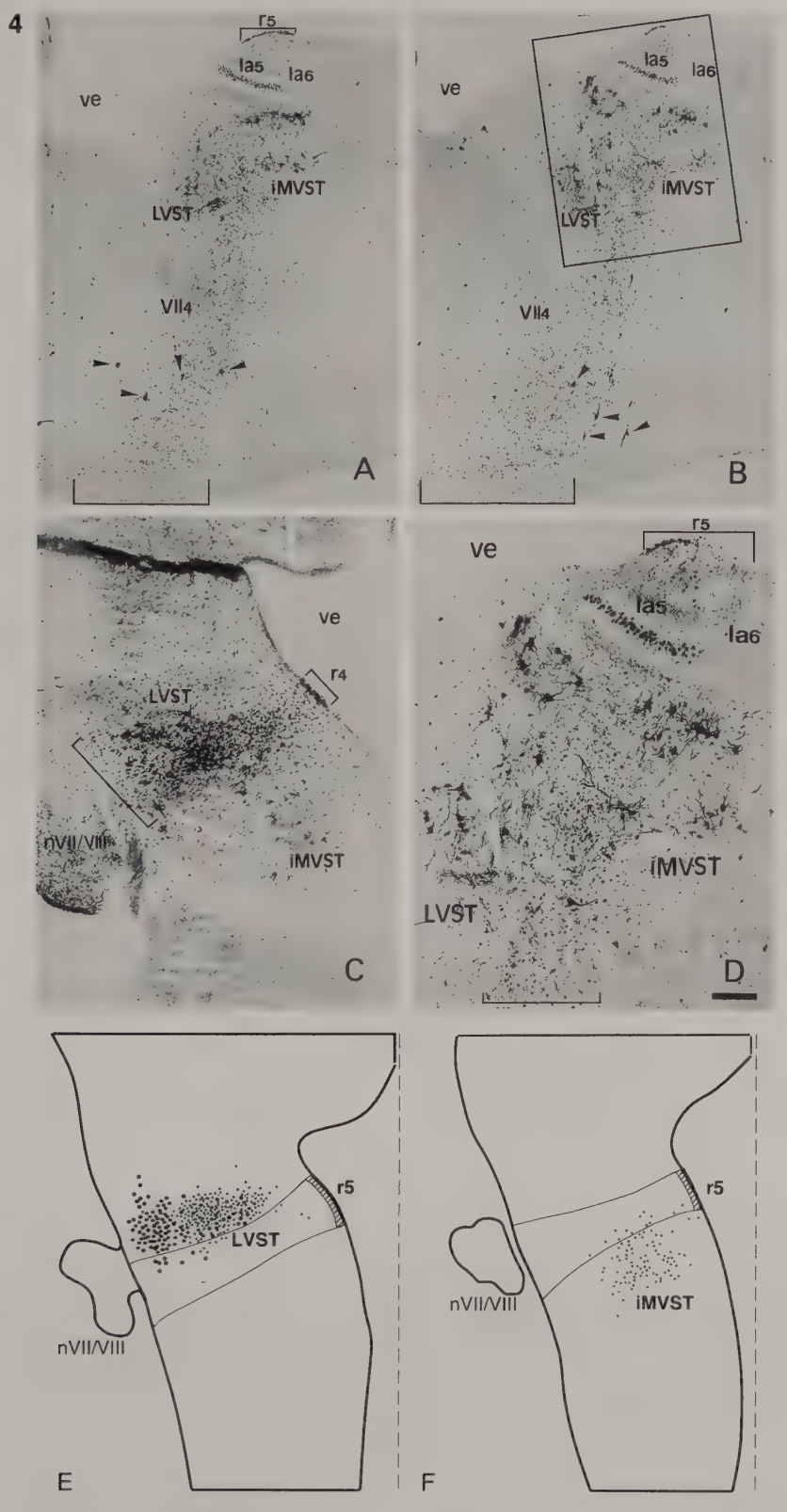
4
r5
la5
la6
ve
iMVST
LVST
VII4
A
B
r4
nVII/VIII
C
D
E
F

RESULTS

There are three hodologically defined vestibulospinal groups: the LVST, iMVST, and cMVST groups, each of which projects along a specific pathway to the spinal cord (Fig. 1B; see also Glover and Petursdottir, 1991). There are four hodologically defined vestibulo-ocular groups: the iR, cR, iC, and cC groups, each of which projects along a specific pathway to their target motoneurons in the oculomotor nucleus (Fig. 1A; see also Glover, 1994; Glover and Petursdottir, 1998). To assess the relationships of these groups to individual rhombomeres, we grafted a quail r3, r4, or r5 into a chicken host, and subsequently labeled the vestibulospinal or vestibulo-ocular neurons with BDA.

As previously observed (Marín and Puelles, 1995; Wingate and Lumsden, 1996), the domain derived from a single rhombomere occupied at stages 36–38 a wedge of the hindbrain, narrowest at the ventricular surface and widening toward the pial surface (Figs. 2 and 3A). At the ventricular surface, graft cells were packed tightly, providing a sharp transition from graft to host tissue (Fig. 3A). The transition was less sharp deep to the ventricular surface, however, with intermingling of graft and host cells up to several cell diameters. At specific sites, especially near fiber tracts, graft cells dispersed much more extensively into host territory, up to 1 or 2 rhombomeres distant (Figs. 2 and 3A; see also Marín and Puelles, 1995). Preliminary results using cell type-specific antibodies suggest that many of these cells are oligodendrocytes (S. Martínez, personal communication). Irrespective of location, most BDA-labeled neurons could be distinguished as graft- versus host-derived (Fig. 3B). The definition of rhombomere boundaries at the graft–host interfaces is described in the legend to Fig. 3.

The Vestibulospinal Groups Relate Principally to Single Rhombomeres

The LVST group was contained systematically within r4 grafts (Fig. 4C) and roughly bounded caudally by r5 grafts (Figs. 4A, 4B, 4D, and 4E). A few LVST neurons (about 5%) lay in some preparations just within r3 ($n = 1$) or r5 ($n = 8$). On the basis of the quail-specific nuclear marker, at least half of these were derived from r4, evidently having migrated or dispersed to the proximate regions of r3 and r5.

The iMVST group lay almost entirely caudal to r5 grafts in two well-labeled cases (Figs. 4A, 4B, 4D, and 4E), with only 2 and 7% of the labeled cells lying in r5. At least some of the iMVST cells in r5 were quail-negative and thus not derived from r5 (presumably derived from r6). In four other cases the iMVST group was not labeled completely and it was difficult to delineate its domain, but the majority of cells lay clearly within r6.

The cMVST group lay largely caudal to r4 grafts (Fig. 5), but about 15–20% of the cMVST neurons were located well within the lateral part of r4 (Figs. 5A, 5B, and 5E). Similarly, most of the commissural axons of the cMVST neurons, easily identified at the midline, lay clearly within r5, but a smaller proportion could be seen in r4 (Fig. 5C). Some of the cMVST neurons in r4 were quail-positive and thus r4-derived. By comparison with r5- and r6-specific landmarks identified by Marín and Puelles (1995), the caudal boundary lay at about the r5/6 border. For example, the cMVST group lay beneath only the r5 portion of the auditory nucleus laminaris, and its commissural axons traversed the r5 portion, but not the r6 portion, of the abducens motor nucleus (Fig. 5D). Similar comparison with established segmental landmarks allowed us to place the caudal boundary of the iMVST group at about the r6/7 border.

In summary (see Figs. 9 and 10), the LVST group is localized to r4 (r4-derived), with a minor spillover into r3 or r5 (at least partly r4-derived), the cMVST group is localized largely to r5 (r5-derived) but with a substantial component in the lateral portion of r4 (at least partly r4-derived), and the iMVST is localized to r6 (presumably r6-derived), with a minor spillover into r5 (also presumably r6-derived). Thus, each of these groups relates principally to a single rhombomere, and r4, r5, and r6 each contain a unique set of vestibulospinal axon projection phenotypes.

The Vestibulo-Ocular Groups Relate to Single or Multiple Rhombomeres

The cR group lay rostral to r3 grafts with virtually no constituent neurons located within r3 in either of two preparations (Figs. 6A, 6C, and 6E).

The cC group as a whole stretched from the caudal part of r4 to the rostral part of r7. At its medial aspect it lay almost entirely caudal to the r4/5 boundary (Figs. 6B and 6D). Laterally, however, a substantial number of cC neurons lay within the caudal part of r4 (Figs. 6B, 6C, and 6F). Due to

FIG. 4. The relationship of the LVST and iMVST vestibulospinal groups to r4 and r5. Sagittal sections of a hindbrain with an r5 graft (A, B, and D; rostral to left) and horizontal section of a hindbrain with r4 graft (C; rostral at top). D is a higher magnification view of the outlined field in B. Note that the iMVST group lies below the r6 portion of nucleus laminaris. Domains of the grafted hemirhombomeres are indicated by brackets at the pial and ventricular surfaces. Arrowheads in A and B indicate isolated BDA-labeled reticulospinal neurons. E and F show dot plots of the LVST and iMVST groups in horizontal projection (which can be compared directly to C and to Fig. 2A), generated from photographs as described under Materials and Methods. The domains of the grafted rhombomeres are marked by hatching in the ventricular zone and by boundary lines. The sizes of the dots roughly represent the relative sizes of the neurons. Abbreviations: ve, ventricle; la5 and la6, r5 and r6 portions of nucleus laminaris, respectively; VII4, r4 portion of facial motor nucleus; nVII/VIII, facial and vestibuloacoustic nerves. Scale bar, 525 μm (A and B), 400 μm (C), and 260 μm (D).

Copyright © 1998 by Academic Press. All rights of reproduction in any form reserved.

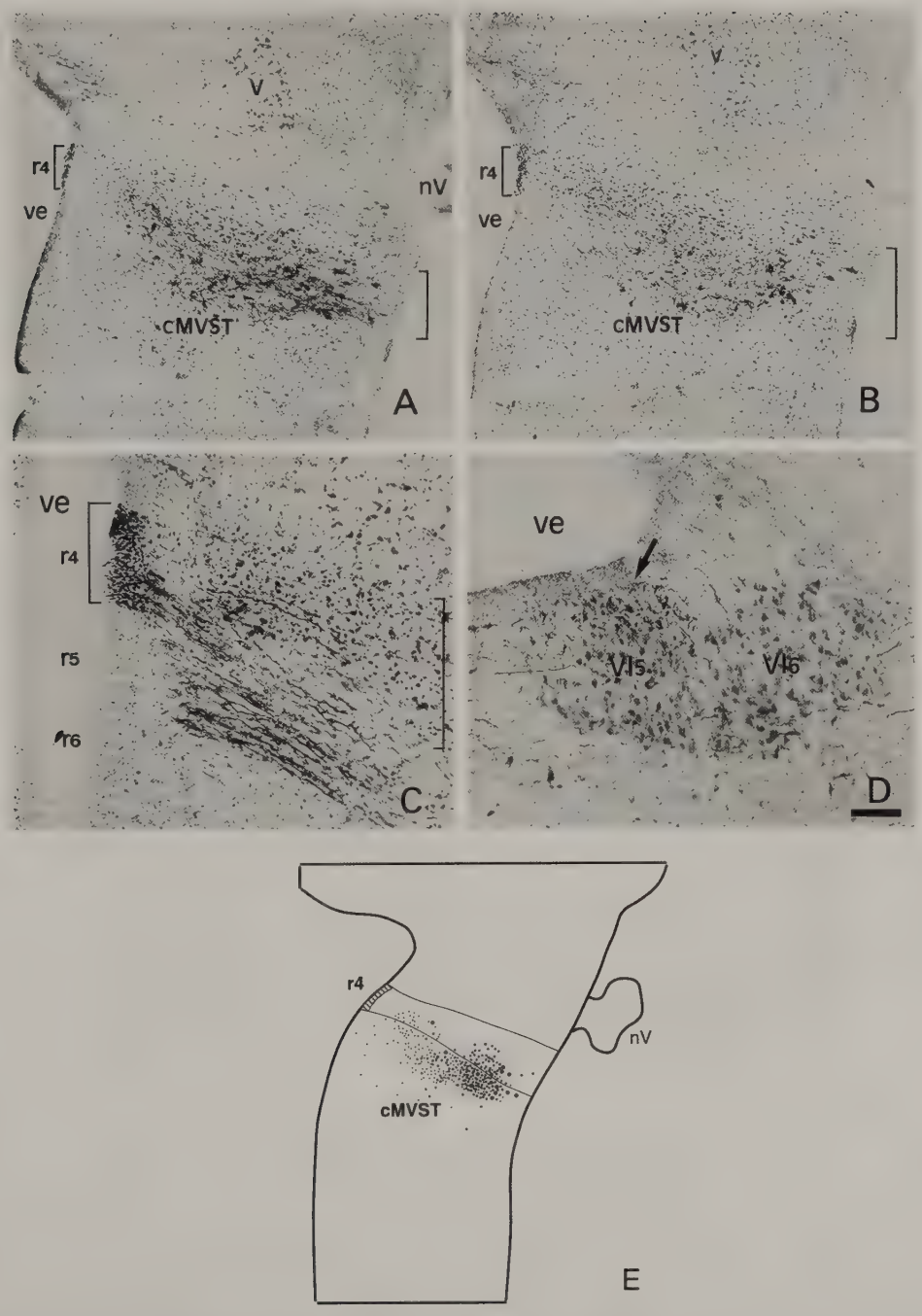

FIG. 5. The relationship of the cMVST vestibulospinal group to r4. Horizontal (A, B, C; rostral at top) and sagittal (D; rostral to left) sections of hindbrains with r4 graft. Domains of the grafted hemirhombomeres are indicated by brackets at the pial and ventricular surfaces. C and D show the location of cMVST commissural axons as they course toward the midline. Note that cMVST axons coursing through the abducens nucleus relate only to its rostral, r5-derived part (arrow in D). E shows a dot plot of the cMVST group in horizontal projection (which can be compared directly to A and B), generated as described in the legend to Fig. 3. Abbreviations: ve, ventricle; V, trigeminal motor nucleus; nV, trigeminal nerve; VI5 and VI6, r5 and r6 portions of abducens motor nucleus, respectively. Scale bar, 400 μm (A and B) and 200 μm (C and D).

Copyright © 1998 by Academic Press. All rights of reproduction in any form reserved.

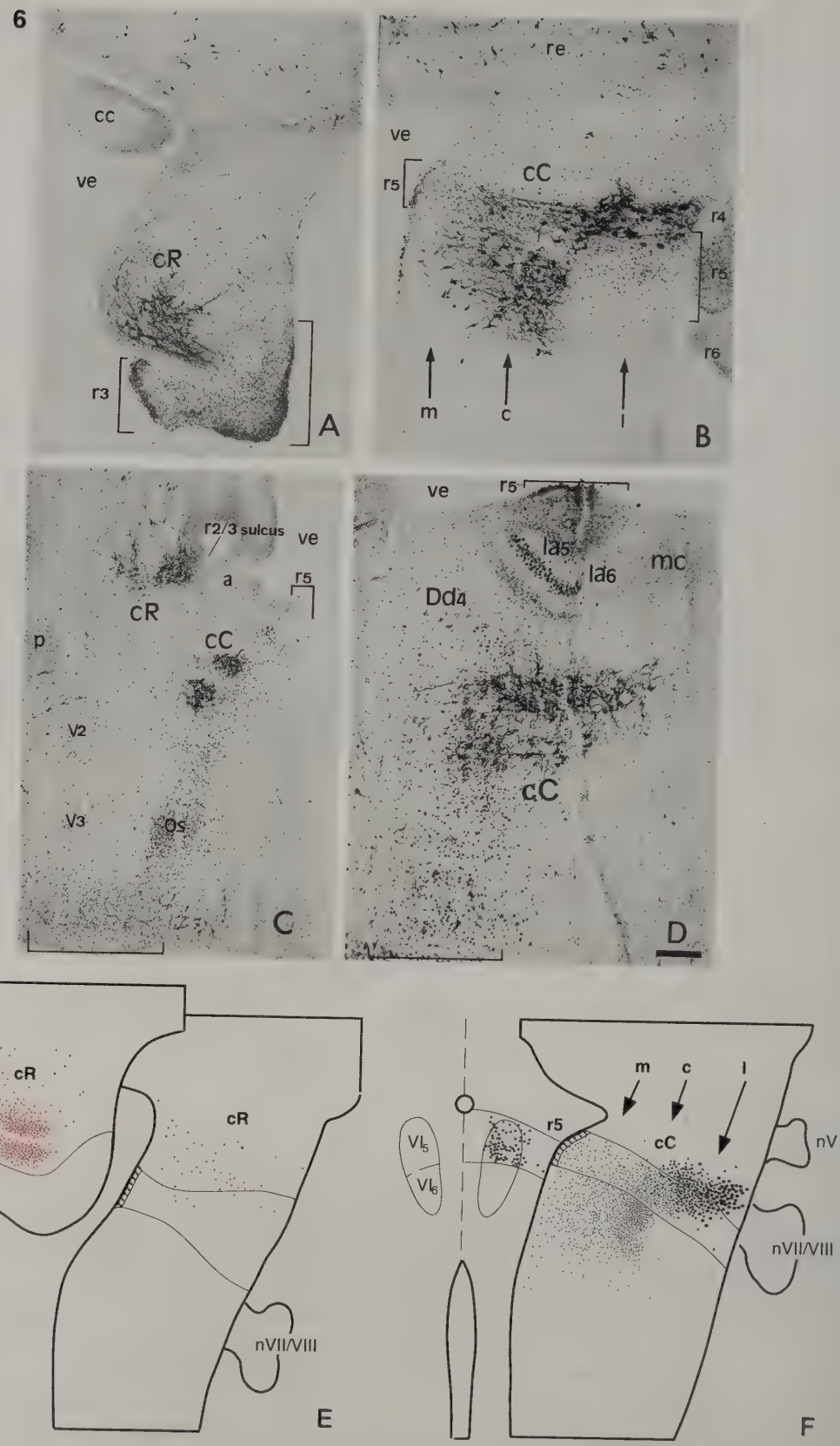
6
cc
ve
cR
r3
A
re
ve
r5
cC
r4
r5
r6
m
c
B
r2/3 sulcus
ve
a
r5
cR
p
cC
V2
V3
Os
C
ve
r5
la5
la6
mc
Dd4
cC
D
cR
cR
r3
nVII/VIII
E
m
c
l
r5
cC
nV
Vl_5
Vl_6
nVII/VIII
F

heavy BDA labeling that obscured the quail-specific nuclear marker, it was unclear whether these were derived from r4 or r5.

Though spanning several rhombomeres, the cC group had subdivisions that were partly in register with the individual rhombomeric domains. In horizontal projection, four components could be distinguished on the basis of position and cytoarchitecture (Fig. 6F). The first, lying most medially and ventrally, was composed of projection neurons within the r5 portion of the abducens motor nucleus (Figs. 6F and 7). The second (medial) and third (central) components were both related to the alar plate of r5 and r6 and the rostral part of r7 (Figs. 6B, 6D, and 6F). The fourth (lateral) component lay in the rostral region of r5 and the caudal region of r4 (Figs. 6B, 6C, and 6F).

The bulk of the iC group was clearly localized to r5, and the bulk of the iR group was clearly located in r2 and r3 (Fig. 8). There were, however, a few labeled neurons (<10%) in r4 that could be assigned only arbitrarily to either iC or iR (Figs. 8A, 8E, and 8F).

Comparison with established segmental landmarks (Marín and Puelles, 1995) allowed us to estimate the locations of the rostral boundaries of the iR and cR groups and the caudal boundary of the cC group (Figs. 6 and 8).

To summarize (see Figs. 9 and 10), the cR group lies in r2 and extends into r1. The cC group spans r4 through r7, with four characteristic subcomponents localized to specific rhombomeric and mediolateral domains. The iR group lies largely within r2 and r3, and the iC group lies largely within r5. Thus, these groups relate to one, two, or more rhombomeres, and each rhombomere contains a unique set of vestibulo-ocular axon projection phenotypes.

DISCUSSION

Hindbrain segmentation certainly appears to make an important contribution to demarcating axon projection phenotypes within the vestibular complex. Our principal finding, however, is that the axon projection phenotypes of the vestibular neurons have a complex relationship to the rhombomeres. Some of the hodologically defined groups of vestibular projection neurons relate to single rhombomeres, whereas others relate to multiple contiguous rhombomeres. Different rhombomeres thus contain different sets of projection phenotypes.

A secondary finding is that the correlation to rhombomeric domains is not absolutely strict. All the groups exhibit minor boundary transgressions by a few percent of the total number of constituent neurons. Two groups, though, have substantial portions that extend well into adjacent rhombomeres, such that their domains cannot be defined in terms of whole rhombomere lengths. Before discussing the significance of the rhombomeric pattern, it is instructive to examine the possible causes of boundary transgression.

Potential Causes of Boundary Transgression

In principle, technical artifacts such as imprecision in resecting the host and donor rhombomeres, damage to the rhombomere boundaries during surgery or implantation, or aberrant intermingling of the heterospecific quail and chicken cells following graft integration could lead to a contamination of one rhombomeric domain by cells from an adjacent rhombomere. On the other hand, a natural source of boundary violation by active cell migration has also been reported in the chicken embryo, with as many as 15% of cells in single labeled neuroepithelial cell clones penetrating from their rhombomere of origin into a neighboring rhombomere while boundaries are still visible (Birgbauer and Fraser, 1994). The LVST group epitomizes this phenomenon: a few of its constituent cells derive from r4 but wind up in r3 and r5 (see Fig. 10). In this case, the transgression is clearly not a technical artifact, as a similar degree of spillover is seen at earlier stages in the absence of any experimental disruption of the rhombomere boundaries (Fig. 1C; J. C. Glover, unpublished results). In the case of the

FIG. 6. Relationship of the cR and cC vestibulo-ocular groups to r3 (A) and r5 (B–D). (A) Horizontal section (rostral at top) showing the cR group, which lies rostral to r3. (B) Horizontal section showing the cC group with its distinct medial, central, and lateral components (m, c, l); the medial and central components lie in r5, r6 and the rostral part of r7, and the lateral component straddles the r4/5 boundary. Note that dispersed reticular neurons (re) in r2 are also labeled with BDA. (C) Sagittal section (rostral to left) showing the cR neurons at the base of the cerebellum and also the lateral component of cC. (D) Detail of a sagittal section (rostral to left) across the central component of cC, illustrating its r5 and r6 portions as they relate to nucleus laminaris. Boundaries of the grafted hemirhombomeres are indicated by brackets at the pial and ventricular surfaces. The boundary between r2 and r3 is also visible as a marked sulcus at the ventricular surface in C (see Marín and Puelles, 1995). E and F show dot plots of the cR and cC groups, respectively, generated as described in the legend to Fig. 3. These can be compared directly to A and B. In each of E and F, two partial projections are shown for clarity. In E, they show differentially the dorsal (left) and ventral (right) cells of the cR group. In F, they show differentially the ventral cC neurons within the abducens motor nucleus (left) and the more dorsal cC neurons (medial, central, and lateral components, right). Abbreviations: ve, ventricle; cc, cerebellar cortex; a, nucleus angularis; p, principal trigeminal sensory nucleus; V2 and V3, r2 and r3 portions of principal trigeminal motor nucleus; Os, nucleus olivaris superior; Dd4, r4 portion of dorsal Deiter's nucleus; la5 and la6, r5 and r6 portions of nucleus laminaris; mc, nucleus magnocellularis; nV, trigeminal nerve; nVII/VIII, facial and vestibuloacoustic nerve complex; VI5 and VI6, r5 and r6 portions of abducens motor nucleus; m, c, and l, medial, central, and lateral subdivisions, respectively. Scale bar, 200 μm (A), 525 μm (B), 400 μm (C), and 260 μm (D).

Copyright © 1998 by Academic Press. All rights of reproduction in any form reserved.

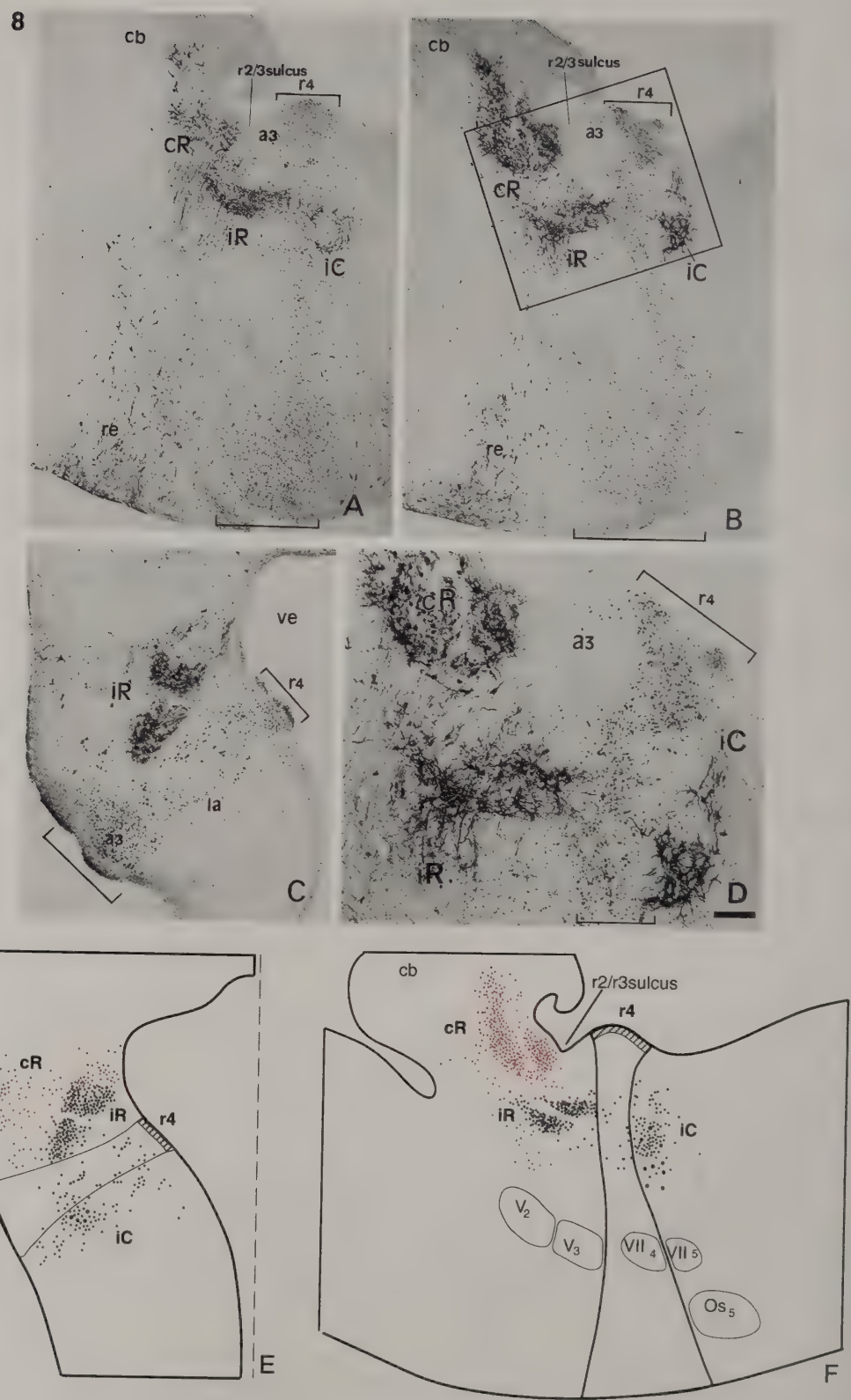
8
cb
r2/3sulcus
r4
a3
cR
iR
iC
re
A
B
ve
la
C
D
nV
E
r2/r3sulcus
V2
V3
VII 4
VII 5
Os5
F

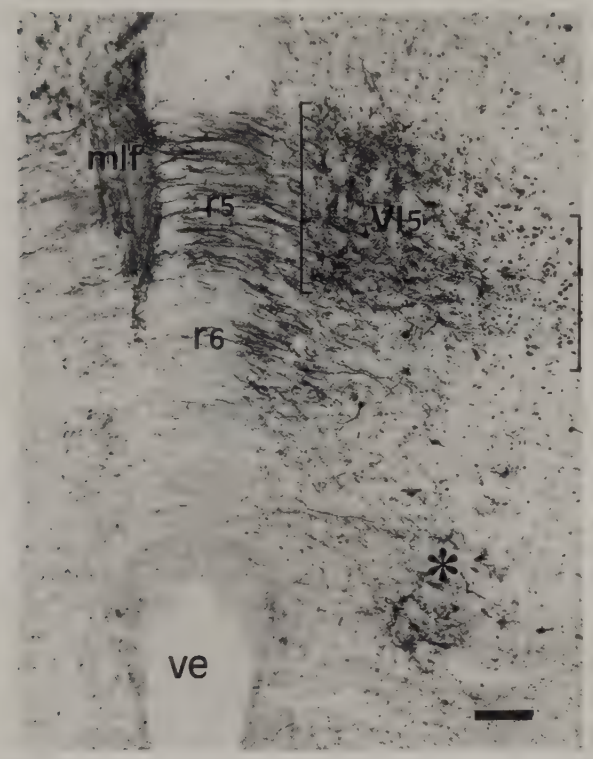

FIG. 7. Horizontal section (rostral at top) showing the ventral cC neurons and their commissural axons in r5 and r6 in an embryo with an r5 graft (boundaries indicated by brackets). Note that some neurons in the more caudal nucleus prepositus hypoglossi are also labeled with BDA (asterisk). Abbreviations: ve, ventricle; VI5, r5 portion of abducens motor nucleus. Scale bar, 200 μm.

other groups, it is not yet clear whether the boundary transgressions occur as a result of technical artifact or normal cell movement.

Alternatively, some examples of noncoincidence we have observed might not represent transgressions at all, but rather arise because the regional specification of vestibular neuron identity is not slavishly in register with the rhombomeres. Perhaps some gene products responsible for specifying neuronal identity have a "sloppy" distribution with respect to the rhombomere boundaries. This could result, for example, from a gradual spatial restriction of gene expression from larger domains down to single rhombomeric domains (as is the case for HoxB1 and r4; see Sundin and Eichele, 1990). If determination occurred before the gene expression domain had retreated to its definitive rhombomeric territory, then the resultant neuron type would not be neatly delimited by a rhombomere boundary.

Another important feature is that, aside from the minor boundary transgressions, whole rhombomere lengths are not obligatory units of specific neuron types. The cMVST and cC groups provide clear examples, where a substantial portion of each group is localized to a fraction of a rhombomere length (r4 in both cases). In the case of the cMVST group, at least some of the r4 component indeed derives from r4 instead of having migrated from r5 (see Fig. 10). In the case of the cC group the origin of the r4 component is not clear. Importantly, the relevant component of the cC group (the lateral component) straddles the r4/5 boundary but does not extend into the caudal half of r5 and is thus almost exactly anti-correlated to the rhombomeric periodicity (see Fig. 6F). Marín and Puelles (1995) describe additional examples of this phenomenon. For example, the r3 portion of the trigeminal motor nucleus lies only in the rostral part of r3, the r4 and r5 portions of the central motor nucleus of the facial nerve are aggregated at the r4/5 boundary, and the r6 portion of the glossopharyngeal motor nucleus lies only in the caudal part of r6. Further research is required to determine how these examples of noncoincidence between rhombomeric domains and neuronal phenotypes arise.

How Do Specific Axon Trajectory Features Relate to the Rhombomeres?

Vestibulospinal neurons differentiate in three contiguous rhombomeres (r4–r6), whereas vestibulo-ocular neurons differentiate in seven rhombomeres (r1–r7, but evidently sparsely in r4). Thus, whether the axon of a vestibular neuron ascends or descends in the hindbrain is not patterned at single rhombomere resolution. What about whether the axon of a vestibular neuron crosses the midline before ascending or descending? Ipsilaterally projecting ves-

FIG. 8. Relationship of the iR and iC vestibulo-ocular groups to r4. (A and B) Sagittal sections (rostral to left) showing the iR, iC, and cR groups. The cR group (also labeled here because the cR commissural axons passed through the injection site) lies dorsal to and extends further rostral than the iR group. (C) Horizontal section (rostral at top) showing the iR group. (D) Detail of B. Boundaries of the r4 graft are indicated by brackets at the pial and ventricular surfaces. The boundary between r2 and r3 is also visible as a marked sulcus at the ventricular surface in A and B. E and F show dot plots of the cR (red dots), iR, and iC groups in horizontal and sagittal projections, respectively, generated as described in the legend to Fig. 3. E and F can be compared directly to C and B, respectively. Abbreviations: cb, cerebellum; a3, r3 portion of nucleus angularis; re, reticular neurons; 1a, nucleus laminaris; nV, trigeminal nerve; V2 and V3, r2 and r3 portions of principal trigeminal motor nucleus; VII4 and VII5, r4 and r5 portions of facial motor nucleus; Os5, r5 portion of superior olivary nucleus. Scale bar, 525 μm (A and B), 400 μm (C), and 260 μm (D).

Copyright © 1998 by Academic Press. All rights of reproduction in any form reserved.

9

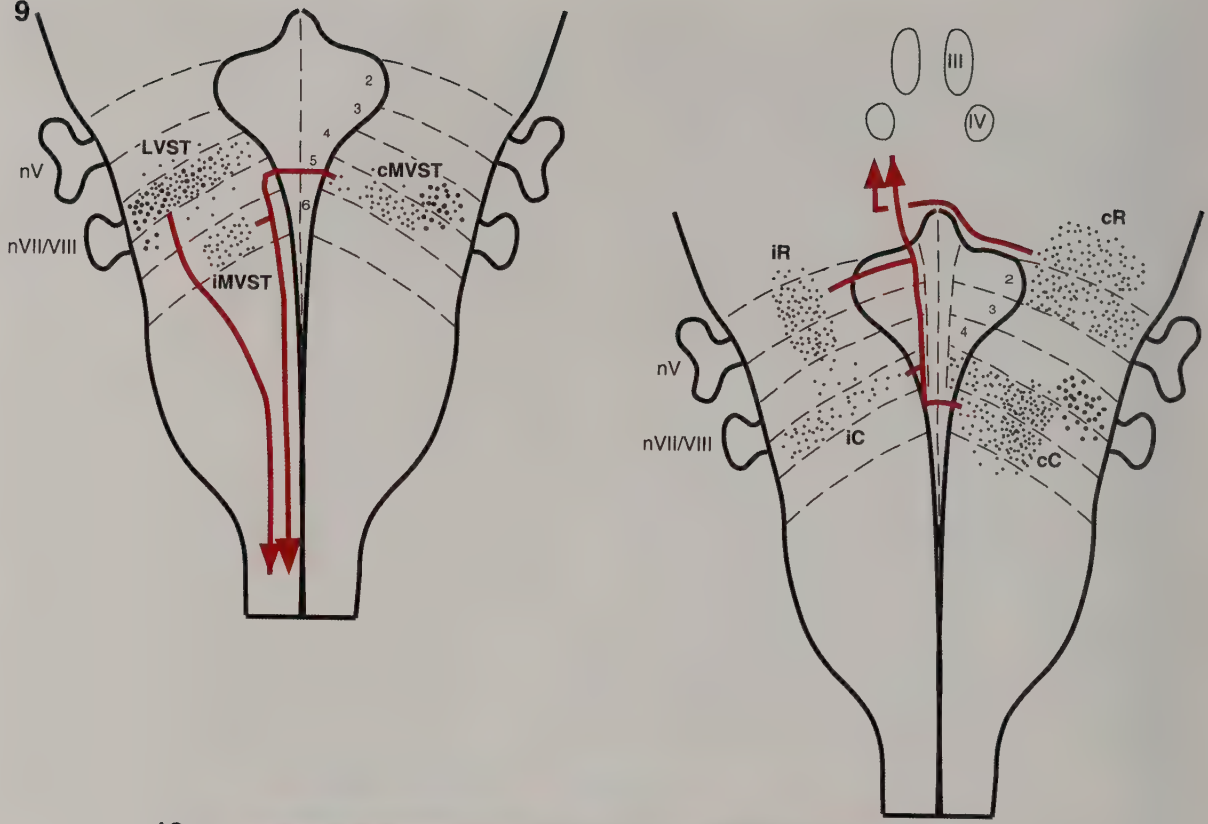
LVST
cMVST
iMVST
nV
nVII/VIII
2
3
4
5
6
III
IV
iR
cR
iC
cC

10

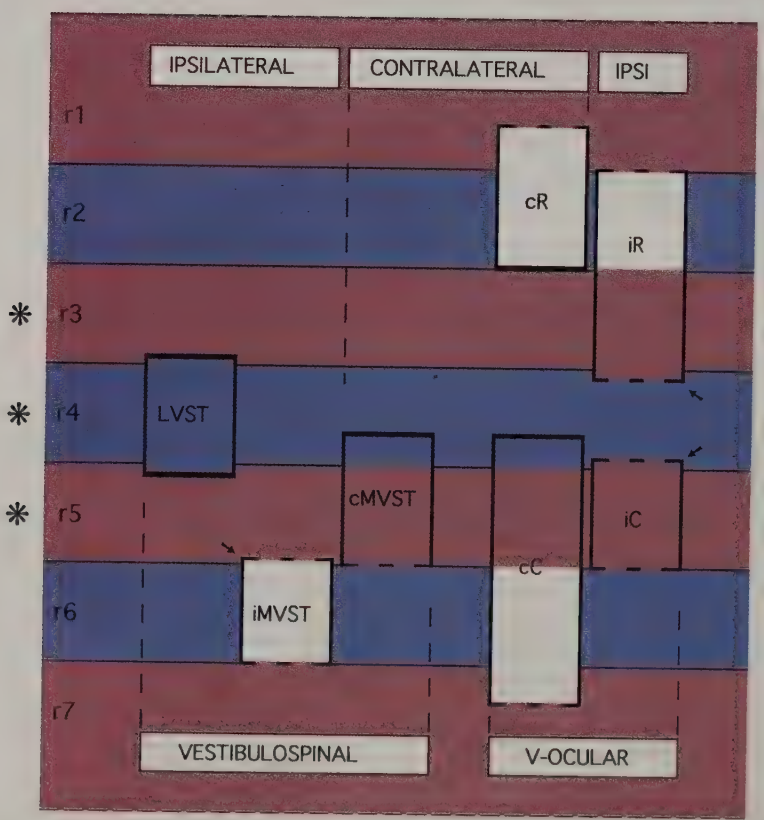
IPSILATERAL
CONTRALATERAL
IPSI
r1
r2
r3
r4
r5
r6
r7
cR
iR
LVST
cMVST
iC
cC
iMVST
VESTIBULOSPINAL
V-OCULAR

tibulospinal and vestibulo-ocular neurons differentiate in r2–r6, whereas their commissural counterparts differentiate in r1, r2, and r4–r7 (evidently rarely in most of r4). Again, single rhombomeres are not the spatial units of determination. If these two trajectory features (direction and laterality) are combined, in only three cases is there a strong correlation between a single rhombomere and a specific neuron type: (1) the LVST group, which is the only group whose axons descend ipsilaterally in the lateral vestibulospinal tract, is largely restricted to r4; (2) the iMVST group, which is the only group whose axons descend ipsilaterally in the MLF, is largely restricted to r6; and (3) the iC group, whose axons ascend ipsilaterally in the MLF, is largely restricted to r5. All other combinations of axon trajectory features arise in multimeric units (Fig. 10).

Among the multimeric groups, there are some indications that specific combinations of axon trajectory features may relate to pairs of adjacent rhombomeres, although such rhombomere pairs are not mutually exclusive. For example, the cR group (contralateral, ascending in brachium conjunctivum and MLF) lies largely in r1 and r2, and the iR group (ipsilateral, ascending in MLF) lies largely in r2 and r3. The cMVST group (contralateral, descending in MLF) lies largely in r5 but also has a substantial number of cells in the caudal part of r4. The cC group (contralateral, ascending in MLF) is more extensive from this point of view (r4–r7), but its medial and central components lie largely in r5 and r6, and its lateral component straddles the boundary between r4 and r5 and is, therefore, related to both of these rhombomeres.

Multimeric organization may have functional significance. It has been argued previously, on the basis of termination patterns on the different oculomotor neuron pools, that the cC group may be expected to comprise functional subdivisions (Glover, 1996). This brings up the possibility that the individual rhombomeric compartments of a multimeric group might specify functional differences within a population of neurons of uniform axon trajectory. This notion is supported by the correlation of specific cytoarchitectonic subdivisions of the cC group to specific rhombomeres. Elucidation of the relationship between rhombomeres and functional features such as termination pattern, afferent input, neurotransmitter content, and electrophysiological properties will be required to resolve this issue.

Relationship to Proposed Models of Segmental Organization

Is the rhombomeric distribution of the hodologically defined vestibular neuron groups consistent with proposed models of the segmental organization of hindbrain neuron populations? One model proposes that neurons of all axon projection phenotypes are segmentally iterated (Clarke and Lumsden, 1993). This is clearly not the case for the mature pattern of the vestibular neurons (although these are only a fraction of the neurons in any given rhombomere and the differences we report here may have gone undetected in the general population analyzed by Clarke and Lumsden (1993)). To account for reported discrepancies with their model (see Glover and Petursdottir, 1991), Clarke and Lumsden (1993) proposed that an initial segmental iteration is modulated by regressive events such as cell death or axon retraction. However, studies of the early patterning of vestibular and reticular projection neurons (Glover, unpublished) rather support the view that rhombomeric domains exhibit striking differences in their content of projection phenotypes from the same early stages analyzed by Clarke and Lumsden (1993).

Another model, based on the distribution of cranial nerve motoneurons and the expression patterns of certain Hox genes, proposes that the rhombomeres imbue the hindbrain with a paired rule system for neuronal determination. That is, neurons of a given phenotype arise in two-rhombomere units (Lumsden, 1990; McKay *et al.*, 1994). This clearly does not hold for all the vestibular groups studied here (see Fig. 10).

The "segmental plan" of the vestibular hodological mosaic thus does not fit systematically either of these two models. There is no clear evidence of a general segmental iteration nor of a consistent bimeric organization. These models, which are derived from studies of the segmental organization of invertebrates and anamniote vertebrates, are insufficient to account for the specification of axon pathfinding by hindbrain projection neurons in an amniote vertebrate.

FIG. 9. Overview of the different vestibular projection neuron groups and their relationships to the rhombomeres in horizontal projection. Red arrows indicate axon trajectories and tracts.

FIG. 10. A schematic semiquantitative representation of the rhombomeric domains of the different vestibular projection neuron groups. The groups are arranged by hodological classification (vestibulospinal (descending axons) versus vestibulo-ocular (ascending axons) and ipsilaterally versus contralaterally projecting). The rhombomeres that were subjected to transplantation are indicated by asterisks. The rostral and caudal limits of each group are shown in relation to rhombomere boundaries. Limits denoted by solid lines were determined directly by transplantation. Most of the limits denoted by broken lines were estimated through comparison with rhombomere-specific landmarks. Those indicated by arrows were tested directly by transplantation, but remain uncertain because of ambiguity in defining the identity of neurons (see text). The color of each group indicates which rhombomere it was derived from; the origin of white groups or regions was either not tested or remains unclear.

Copyright © 1998 by Academic Press. All rights of reproduction in any form reserved.

REFERENCES

Auclair, F., Valdés, N., and Marchand, R. (1996). Rhombomere-specific origin of branchial and visceral motoneurons of the facial nerve in the rat embryo. *J. Comp. Neurol.* **369,** 451–461.

Baker, R., Suwa, H., Marsh, E., and Gilland, E. (1996). Segmental arrangement of vestibuloocular neurons in the hindbrain of adult zebrafish and closely related cyprinids. *Soc. Neurosci. Abstr.* **22,** 1833.

Birgbauer, E., and Fraser, S. E. (1994). Violation of cell lineage restriction compartments in the chick hindbrain. *Development* **120,** 1347–1356.

Clarke, J. D., and Lumsden, A. (1993). Segmental repetition of neuronal phenotype sets in the chick embryo hindbrain. *Development* **118,** 151–162.

Fritzsch, B., Christensen, M. A., and Nichols, D. H. (1993). Fiber pathways and positional changes in efferent perikarya of 2.5- to 7-day chick embryos as revealed with DiI and dextran amines. *J. Neurobiol.* **24,** 1481–1499.

Gilland, E., and Baker, R. (1993). Conservation of neuroepithelial and mesodermal segments in the embryonic vertebrate head. *Acta Anat.* **148,** 110–123.

Glover, J. C., Petursdottir, G., and Jansen, J. K. S. (1986). Fluorescent dextran-amines used as axonal tracers in the nervous system of the chicken embryo. *J. Neurosci. Methods* **18,** 243–254.

Glover, J. C. (1989). Rhombomeres and longitudinal boundaries in the chicken embryo subdivide vestibular neurons according to axonal pathway. *Soc. Neurosci. Abstr.* **15,** 959.

Glover, J. C. (1994). The organization of vestibulo-ocular and vestibulospinal projections in the chicken embryo. *Eur. J. Morphol.* **32,** 193–200.

Glover, J. C. (1995). Retrograde and anterograde axonal tracing with fluorescent dextran-amines in the embryonic nervous system. *Neurosci. Protocols* **30,** 1–13.

Glover, J. C. (1996). Development of second-order vestibular projections in the chicken embryo. *Ann. N. Y. Acad. Sci.* **781,** 13–20.

Glover, J. C. (1998). The development of vestibulo-ocular and vestibulospinal projections in the chicken embryo. In "Reviews of Oculomotor Research," Vol. 5, "Ontogeny and Phylogeny." W. Graf (Ed.), Elsevier.

Glover, J. C., and Petursdottir, G. (1991). Regional specificity of developing reticulospinal, vestibulospinal, and vestibulo-ocular projections in the chicken embryo. *J. Neurobiol.* **22,** 353–376.

Glover, J. C., and Petursdottir, G. (1998). The functional neuroanatomy of the vestibulo-ocular projections of the chicken embryo. In "Reviews of Oculomotor Research," Vol. 5, "Ontogeny and Phylogeny." W. Graf (Ed.), Elsevier.

Hamburger, V., and Hamilton, H. (1951). A series of normal stages in the development of the chick embryo. *J. Morphol.* **88,** 49–92.

Hemond, S. G., and Glover, J. C. (1993). Clonal patterns of cell proliferation, migration, and dispersal in the brainstem of the chicken embryo. *J. Neurosci.* **13,** 1387–1402.

Jansen, J. K. (1991). A note on the development of the vestibulo-ocular pathway in the chicken. *Anat. Embryol.* **184,** 305–311.

Keynes, R., and Krumlauf, R. (1994). Hox genes and regionalization of the nervous system. *Annu. Rev. Neurosci.* **17,** 109–132.

Lumsden, A. (1990). The cellular basis of segmentation in the developing hindbrain. *Trends Neurosci.* **13,** 329–335.

Marín, F., and Puelles, L. (1995). Morphological fate of rhombomeres in quail/chick chimeras: A segmental analysis of hindbrain nuclei. *Eur. J. Neurosci.* **7,** 1714–1738.

McKay, I. J., Muchamore, I., Krumlauf, R., Maden, M., Lumsden, A., and Lewis, J. (1994). The kreisler mouse: A hindbrain segmentation mutant that lacks two rhombomeres. *Development* **120,** 2199–2211.

McLean, I. W., and Nakane, P. K. (1974). Periodate–lysine–paraformaldehyde fixative: A new fixation for immunoelectron microscopy. *J. Histochem. Cytochem.* **22,** 1077–1083.

Petursdottir, G. (1990). Vestibulo-ocular projections in the 11-day chicken embryo: Pathway specificity. *J. Comp. Neurol.* **297,** 283–297.

Simon, H., and Lumsden, A. (1993). Rhombomere-specific origin of the contralateral vestibulo-acoustic efferent neurons and their migration across the embryonic midline. *Neuron* **11,** 209–220.

Sundin, O. H., and Eichele, G. (1990). A homeo domain protein reveals the metameric nature of the developing chick hindbrain. *Genes Dev.* **4,** 1267–1276.

Vaage, S. (1969). The segmentation of the primitive neural tube in chick embryos (Gallus domesticus). *Adv. Anat. Embryol. Cell Biol.* **41,** 1–88.

Wingate, R. J., and Lumsden, A. (1996). Persistence of rhombomeric organisation in the postsegmental hindbrain. *Development* **122,** 2143–2152.

Received for publication December 3, 1997
Revised June 16, 1998
Accepted June 16, 1998

Copyright © 1998 by Academic Press. All rights of reproduction in any form reserved.

DEVELOPMENTAL BIOLOGY 202, 29–42 (1998)
ARTICLE NO. DB988985

The α_4 Subunit of Integrin Is Important for Neural Crest Cell Migration

Sung H. Kil,* Catherine E. Krull,* Gordon Cann,†,‡ Dennis Clegg,‡ and Marianne Bronner-Fraser*,[1]

**Division of Biology 139-74, California Institute of Technology, Pasadena, California 91125;*
†*Division of Oncology, Stanford University Medical Center, Stanford, California 94305; and*
‡*Neuroscience Research Institute, Department of Molecular, Cellular, and Developmental Biology, University of California at Santa Barbara, Santa Barbara, California 93106*

We identify the α_4 subunit of integrin as a predominant integrin expressed by neural crest cells in both avian and murine embryos. Using degenerate primers, we obtained a PCR fragment of the chick integrin α_4 subunit that was subsequently used to clone the full-length subunit with a predicted amino acid sequence 60% identical to human and mouse α_4 subunits. *In situ* hybridization demonstrates that chick integrin α_4 mRNA is expressed at high levels by migrating neural crest cells and neural crest-derived ganglia at both cranial and trunk levels. An antibody against the murine α_4 subunit revealed similar distribution patterns in mouse to chick. In addition to neural crest cells, the integrin α_4 subunit was later observed on the muscle masses of the limb, the apical ectodermal ridge, and the developing liver. To examine the functional role of the integrin α_4 subunit in neural crest cell migration, we used an explant preparation that allows visualization of neural crest cells in their normal environment with or without perturbing reagents. In the presence of a blocking antibody against the mouse integrin α_4 subunit, there was a profound abrogation of neural crest cell migration at trunk and hindbrain levels. Both the numbers of migrating neural crest cells and the total distance traversed were markedly reduced. Similarly, avian embryos injected with synthetic peptides that contain the integrin α_4 binding site in fibronectin displayed abnormal neural crest cell migration. Our results suggest that the integrin α_4 subunit is important for normal neural crest cell migration and may be one of the primary α subunits used for neural crest cell migration *in vivo*. Furthermore, the integrin α_4 subunit represents a useful neural crest marker in the mouse. © 1998 Academic Press

INTRODUCTION

Interactions between cells and their surrounding extracellular environment are involved in many aspects of normal development, including gastrulation, neurulation, neurite outgrowth, and organogenesis. The extracellular matrix (ECM) is an organized network composed of glycoproteins including fibronectin and laminin, proteoglycans, and glycosaminoglycans that are secreted locally by cells (Hay, 1989). In addition to serving as a structural support, the ECM plays an important role in several developmental processes, including cell differentiation, cell migration, and axon guidance (Adams and Watt, 1989; Sanes, 1989; Neugebauer, 1991; Chiquet, 1989; Adams, 1989; West, 1979; Spiegelman, 1983; Bronner-Fraser, 1986b; Gong, 1996). For example, fibronectin is involved in gastrulation (Boucaut *et al.*, 1984) and neural crest cell migration (Bronner-Fraser, 1986b; Olsson, 1996), whereas tenascin and laminin play a role in chondrocyte differentiation (Mackie, 1987) and muscle development (Umbhauer, 1994; von der Mark, 1989; Gu, 1994).

Neural crest cells are highly motile cells that interact with the extracellular matrix as they emanate from the neural tube and migrate extensively to their final destinations. Neural crest cells at different axial levels of the embryo follow distinct migratory pathways (Le Douarin, 1982). Cranial neural crest cells migrate ventrally underneath the ectoderm to give rise to cranial sensory ganglia, the ciliary ganglion of the eye, and cartilaginous components of the face (Le Douarin, 1982; Noden, 1983; Nichols, 1986). Trunk neural crest cells migrate dorsolaterally underneath the ectoderm and ventromedially through the rostral half of the somitic sclerotome. The ventromedial

[1] To whom correspondence should be addressed. Fax: (626) 395-7717. E-mail: mbronner@caltech.edu.

0012-1606/98 $25.00
Copyright © 1998 by Academic Press
All rights of reproduction in any form reserved

stream gives rise to the dorsal root ganglia, sympathetic ganglia, cells of the adrenal medulla, and aortic plexuses whereas the dorsolaterally migrating cells give rise to melanocytes (Le Douarin, 1982; Rickman *et al.*, 1985; Bronner-Fraser, 1986a; Loring and Erickson, 1987; Serbedzija *et al.*, 1989; Serbedzija *et al.*, 1992). The ECM lining neural crest pathways has been well-characterized and contains fibronectin, laminin, collagen, and vitronectin (reviewed by Erickson and Perris, 1993). A number of these molecules are important for neural crest cell migration both *in vitro* and *in vivo* (Rovasio *et al.*, 1983; Bronner-Fraser and Lallier, 1988; Bronner-Fraser, 1988; Delannet *et al.*, 1994; Perris *et al.*, 1991b; Poole and Thiery, 1986).

Integrins comprise a family of glycoprotein receptors that mediate the adhesion of numerous cell types, including neural crest cells, to ECM molecules (reviewed by Hynes, 1987, 1992). Integrins are composed of α and β subunits that are noncovalently linked. The association of a particular α and β subunits determines the receptor's specificity for a given ligand (Hynes, 1992). Integrins have been shown to be required for normal development. Mice null for integrin α_5 and α_4 are early embryonic lethals, due to defects in mesodermal derivatives, epicardium and coronary vessel development, and failure of chorioallontoic fusion (Yang *et al.*, 1993, 1995). Perturbation experiments using antibodies against the β_1 subunit have demonstrated an important role for β_1 integrins in avian somite development (Jaffredo *et al.*, 1988) and cranial neural crest cell migration *in vivo* and *in vitro* (Bronner-Fraser, 1985, Bronner-Fraser, 1986b; Lallier *et al.*, 1992). Cultured trunk neural crest cells possess several integrin receptors for vitronectin ($\alpha_v\beta_1$, $\alpha_v\beta_3$, and $\alpha_v\beta_5$; Delannet *et al.*, 1994) and laminin ($\alpha_1\beta_1$; Duband *et al.*, 1992; Lallier and Bronner-Fraser, 1992). Migrating trunk neural crest cells express low levels the α_1 subunit *in vivo* (Duband *et al.*, 1992). Antibodies against the integrin β_1 subunit block trunk neural crest attachment to fibronectin and laminin *in vitro* and perturb cranial neural crest cell migration *in vivo* (Lallier and Bronner-Fraser, 1992; Bronner-Fraser, 1986b). In addition, antisense perturbation experiments show that integrin α subunits are important for neural crest cell migration (Lallier and Bronner-Fraser, 1993; Kil *et al.*, 1996b). However, these studies were unable to identify specific integrin α subunits that are expressed by neural crest cells and play an important role in neural crest cell migration.

Although a subpopulation of neural crest cells (Stepp *et al.*, 1994) and neural crest derivatives (Sheppard *et al.*, 1994) have been shown to express the α_4 subunit of integrin (Stepp *et al.*, 1994; Sheppard, 1994), no function in neural crest cell migration or differentiation has been described. The integrin α_4 subunit heterodimerizes with integrin β_1 and β_7 subunits to form a receptor for fibronectin through a non-RGD site, an EILDV sequence within the type III connecting segment region (CS-1) of the molecule (Mould, 1990). *In vitro* studies showed that a synthetic peptide to CS-1 region of fibronectin promotes neural crest attachment and migration (Dufour *et al.*, 1988). It also binds to a counterreceptor for VCAM-1, a member of the immunoglobulin superfamily (Guan and Hynes, 1990) through an LDV-like sequence (May, 1993). In addition, integrin $\alpha_4\beta_1$ has been shown to be a receptor for thrombospondin-1 (Yabkowitz, 1993).

In the present study, we examined the role of the integrin α_4 subunit in neural crest cell migration in chicken and mouse embryos. Whole mount *in situ* hybridization with an avian α_4 subunit probe and staining with a mouse anti-integrin α_4 antibody revealed similar patterns of expression in avian and mouse neural crest cells. To test the functional importance of the α_4 subunit in neural crest cell migration, we perturbed binding of the α_4 subunits using a blocking mouse antibody in mouse hindbrain and trunk explants. We noted a significant decrease in the numbers of neural crest cells that emigrated from the neural tube in the anti-α_4 antibody-treated versus control preparations. Furthermore, those neural crest cells that left the neural tube traveled a short distance compared to neural crest cells under control conditions. Our results suggest that the α_4 subunit of integrin is important for normal neural crest cell migration *in vivo*. In addition, it represents a useful neural crest marker in the mouse.

EXPERIMENTAL METHODS

Cloning and sequencing of the avian integrin α_4 subunit. To clone the chicken integrin α_4 subunit, we used integrin α subunit degenerate primers (described by Erle, 1991) and reverse transcription–polymerase chain reaction (RT–PCR) to amplify multiple integrin α subunit cDNAs from Embryonic Day 6 chick retina. Using this approach, we obtained partial PCR clones encoding integrin α_2, α_v, α_4, α_6, and α_8 subunits that were approximately 290 bp long. The PCR fragment of integrin α_4 subunit was then subcloned into the Bluescript KS+ vector (Stratagene) and used to screen a chicken stage 12–15 (Hamburger, 1951) cDNA library (kindly provided by Drs. D. Wilkinson and A. Nieto). Using a conventional screening protocol (Sambrook, 1989), we obtained a 3.9-kb integrin α_4 subunit clone. For sequencing, we used both a chain-termination sequencing kit (Sequence version 2.0 DNA kit from Amersham) and an automated PCR sequencing kit (ABI Prism Dye Terminator Cycle Sequencing Ready Reaction Kit from ABI). Sequencing reactions were separated on a polyacrylamide gel or an automated sequencing gel apparatus from ABI at the Caltech sequencing facility. Sequence analysis was accomplished with the aid of Macvector, the AssemblyLGN, the Genework program (Oxford Molecular Group), and the GCG software package from the Wisconsin Genetic Group.

In situ hybridization and HNK-1 antibody immunohistochemistry. Fertile White Leghorn chick eggs (HY-line International) were incubated at 38°C for 1.5 to 4 days, collected, rinsed in Howard Ringer's solution and fixed with 4% paraformaldehyde overnight. Embryos were then dehydrated through a series of methanol/phosphate-buffered saline (PBS) with 0.1% Tween 20 solutions (Pwt). To synthesize the integrin α_4 subunit RNA probe, we followed the protocol described by Wilkinson (Wilkinson, 1992). For most *in situs*, we used a 500-bp RNA probe encompassing portion of extracellular domain of integrin α_4 subunit. In other experiments, the entire gene and 700 bp that correspond to another

Copyright © 1998 by Academic Press. All rights of reproduction in any form reserved.

region of the extracelluar domain were used as probes. All probes gave identical results. The method of Henrique *et al.* (Henrique *et al.*, 1995) was used to perform *in situ* hybridization. After color development, embryos were cleared in 70% methanol at 4°C and photographed. Prior to sectioning, embryos were incubated in 5 and 15% sucrose in PBS for 2 h and overnight, respectively, and embedded in gelatin for 4 h. Embryos were frozen in liquid nitrogen and cryosectioned at 25–30 μm. Sections were affixed to slides precoated with polylysine (Fisher) and coverslipped with Gel Mount (Biomeda). Some embryos were dehydrated in an ethanol series, embedded in paraplast (Oxford Labware), and microsectioned at 20–25 μm. Sections were affixed to slides precoated with polylysine in the presence of 0.2% gelatin in water. Sections were then deparaffinized in a series of histosol and ethanol solutions. For colocalization studies with HNK-1 antibody, the sections (after deparaffinization) were incubated with HNK-1 antibody supernatant overnight at 4°C. After washing, secondary antibody (goat anti-mouse IgM) conjugated to fluorescein was added for 1 h at room temperature. Following washes with PBS, sections were coverslipped with Gel Mount (Biomeda). Sense probe was used as controls and results were negative.

Microinjection of CS-1 peptide into avian embryos. To test the function of the CS-1 region of fibronectin in avian neural crest cell migration, 10 mM CS-1 peptide (DELPQLVTLPHPNLHGPEILDVPST) or scrambled CS-1 peptide (DELPQLVTLPHPNLHGPPVISELID) was injected into the mesenchyme lateral to the mesencephalon on the left side of chicken embryos at stage 8–9 (Hamburger, 1951) using a micromanipulator. The peptides were synthesized by the UCSB Advanced Instrumentation Center and HPLC purified. After the injection, embryos were incubated at 37°C for 18–24 h. Embryos were fixed with Carnoy's fixative and embedded in paraplast.

Immunocytohistochemistry with HNK-1 antibody was performed as described above.

PS-2 antibody preparation. The antibodies PS-2 (anti-mouse integrin α_4 antibody ascites from SCID mice prepared by TSD Services of Germantown, NY) and MAB 1997 (non-function-blocking integrin β_1 antibody, Chemicon) were dialyzed extensively in PBS at 4°C for 1 h and once overnight. Dialysis membrane (molecular cutoff of 12,000–14,000 Da, Spectrapor) was boiled in 5 mM EDTA/200 mM sodium bicarbonate for 5 min, rinsed twice, and autoclaved for 10 min in a large volume of deionized water. After dialysis, the antibody was sterilized using a 0.4-μm microcentrifuge filter unit (Fisher) and stored at 4°C.

Immunohistochemistry with PS/2 antibody. E7.5–E10.5 mouse embryos (Kaufman, 1992) from BDF-1 female mice (Caltech) were removed from the mother and placed in sterile PBS. After removal of extraembryonic membranes, the embryos were placed in DMEM–F12 medium (Gibco) containing 10% fetal bovine serum (FBS) and 0.1% penstrep (Gibco). Subsequently, embryos were fixed in 2% paraformaldehyde for 2 h at 4°C, incubated in 5 and 15% sucrose overnight, and embedded in gelatin for 4 h to overnight. Embryos were frozen in liquid nitrogen and cryosectioned at 14 μm. Sections were postfixed with methanol for 5 min at −20°C. After fixation, sections were washed with 0.1 % BSA–PBS, blocked with 10% rabbit serum in PBS/0.1% BSA for 30 min, and incubated with primary antibody, PS/2 (anti-integrin α_4 antibody), overnight. The sections were washed three times with PBS for 5 min and incubated with a biotinylated secondary antibody (anti rat IgG) for three hours at room temperature. Sections were then fixed in methanol containing 0.3% H_2O_2 for 30 min and washed three times for 5 min in PBS. After methanol fixation, sections were incubated with ABC reagent mix (Vector) for 30 min, incubated in DAB substrate (Vector) for 40 min, dehydrated in ethanol and histosol, and mounted with Permount (Fisher). Control experiments were done and the results were negative.

Mouse hindbrain explants. Mouse explants were prepared as described previously (Krull *et al.*, 1995, 1997). To label premigratory neural crest cells, the lumen of the neural tube in E8.5 mouse embryos was injected with DiI (stock concentration of 5 mg/ml diluted 1:10 in 3 M sucrose; Serbedzija *et al.*, 1992). After DiI injection, the region including the hindbrain was excised from the embryo by making two transverse cuts caudal to the forebrain and rostral to the third somite. Tissues ventral to the notochord were removed with fine tungsten needles. These hindbrain explants, including ectoderm, neural tube, and notochord, were then incubated in DMEM–F12 medium containing 10 μg/ml of PS/2 (anti-integrin α_4 subunit antibody). As controls, explants were either incubated with DMEM–F12 medium alone or medium containing 10 μg/ml of MAB 1997 (a non-function-blocking β_1 antibody, Chemicon). Explants were placed on 0.4-μm culture inserts (Millipore) precoated with 20 μg/ml of fibronectin for 1 h at room temperature. One milliliter of medium (DMEM–F12, with 10% FBS, 0.1% penstrep, with or without antibodies) was added to the bottom of the insert. Explants then were incubated at 37°C for 24–48 h and photographed using a Zeiss Axiovert microscope equipped with fluorescence optics or a confocal microscope (Bio-Rad).

Mouse trunk explants. Mouse trunk regions of E9.5 mouse embryos containing the last six somites were prepared in a manner similar to that for the hindbrain explants described above. Premigratory neural crest cells were labeled by filling the lumen of the neural tube with DiI as described previously (Serbedzija *et al.*, 1992). Following antibody treatment as described above, the extent of neural crest cell migration in the explants was analyzed using a confocal microscope (Bio-Rad).

Measurement of neural crest cell migration and distance traveled. To quantify neural crest cell migration, fixed hindbrain and trunk neural crest explants were visualized with a confocal microscope equipped with a 10× objective and images were collected using Comos software. The migration distance (μm) was measured as a straight-line distance between the lateral edge of the neural tube to a given labeled cell using the measurement tool of Photoshop 4.0 software. For the hindbrain explants, the straight-line distance traversed by neural crest cells migrating caudal to the otic vesicle was measured between the lateral edge of the neural tube near the otic vesicle and the cells' endopoint (three explants for a given condition). For trunk explants, the distance from the neural tube of neural crest cells within a 10-somite region were measured (five explants for a given condition). Statistical analyses were done using the χ^2 test for independence between two or more samples.

RESULTS

Cloning of Chicken Integrin α_4 Subunit

Degenerate primers for integrin α subunits (Erle, 1991) were employed to screen the E6 chick retina cDNA library, from which we obtained a 500-bp PCR fragment with a sequence corresponding to the integrin α_4 subunit. The PCR fragment was subcloned into the Bluescript KS+ vector and used as a probe to screen a stage 13–15 avian cDNA library. A 3.9-bp gene was cloned, sequenced, and

Copyright © 1998 by Academic Press. All rights of reproduction in any form reserved.

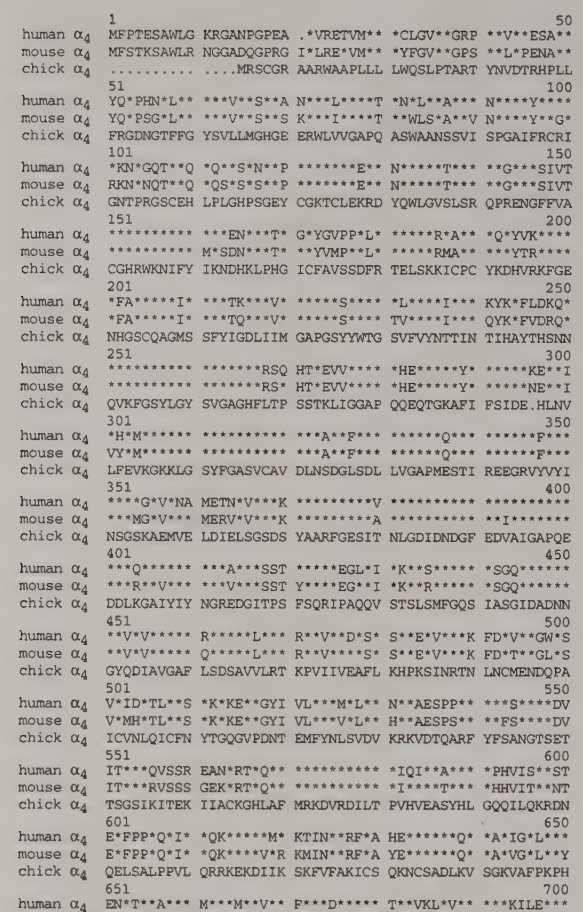
1 50
human α4 MFPTESAWLG KRGANPGPEA .*VRETVM** *CLGV**GRP **V**ESA**
mouse α4 MFSTKSAWLR NGGADQGPRG I*LRE*VM** *YFGV**GPS **L*PENA**
chick α4 ....MRSCGR AARWAAPLLL LWQSLPTART YNVDTRHPLL
51 100
human α4 YQ*PHN*L** ***V**S**A N***L****T *N*L**A*** N****V****
mouse α4 YQ*PSG*L** ***V**S**S K***I****T **WLS*A**V N****Y**G*
chick α4 FRGDNGTFFG YSVLLMGHGE ERWLVVGAPQ ASWAANSSVI SPGAIFRCRI
101 150
human α4 *KN*GQT**Q *Q**S*N**P *******E** N*****T*** **G***SIVT
mouse α4 RKN*NQT**Q *QS*S*S**P *******E** N*****T*** **G***SIVT
chick α4 GNTPRGSCEH LPLGHPSGEY CGKTCLEKRD YQWLGVSLSR QPRENGFFVA
151 200
human α4 ********** ***EN***T* G*YGVPP*L* *****R*A** *Q*YVK****
mouse α4 ********** M*SDN***T* **YVMP**L* *****RMA** ***YTR****
chick α4 CGHRWKNIFY IKNDHKLPHG ICFAVSSDFR TELSKKICPC YKDHVRKFGE
201 250
human α4 *FA*****I* ***TK***V* *****S**** *L****I*** KYK*FLDKQ*
mouse α4 *FA*****I* ***TQ***V* *****S**** TV****I*** QYK*FVDRQ*
chick α4 NHGSCQAGMS SFYIGDLIIM GAPGSYYWTG SVFVYNTTIN TIHAYTHSNN
251 300
human α4 ********** *******RSQ HT*EVV**** *HE*****Y* *****KE**I
mouse α4 ********** *******RS* HT*EVV**** *HE*****Y* *****NE**I
chick α4 QVKFGSYLGY SVGAGHFLTP SSTKLIGGAP QQEQTGKAFI FSIDE.HLNV
301 350
human α4 *H*M****** ********** ***A**F*** ******Q*** ******F***
mouse α4 VY*M****** ********** ***A**F*** ******Q*** ******F***
chick α4 LFEVKGKKLG SYFGASVCAV DLNSDGLSDL LVGAPMESTI REEGRVYVYI
351 400
human α4 ****G*V*NA METN*V***K *********V ********** **********
mouse α4 ***MG*V*** MERV*V***K ********A ********** **I*******
chick α4 NSGSKAEMVE LDIELSGSDS YAARFGESIT NLGDIDNDGF EDVAIGAPQE
401 450
human α4 ***Q****** ***A***SST *****EGL*I *K**S***** *SGQ******
mouse α4 ***R**V*** ***V***SST Y****EG**I *K**R***** *SGQ******
chick α4 DDLKGAIYIY NGREDGITPS FSQRIPAQQV STSLSMFGQS IASGIDADNN
451 500
human α4 **V*V***** R*****L*** R**V**D*S* S**E*V***K FD*V**GW*S
mouse α4 **V*V***** Q*****L*** R**V****S* S**E*V***K FD*T**GL*S
chick α4 GYQDIAVGAF LSDSAVVLRT KPVIIVEAFL KHPKSINRTN LNCMENDQPA
501 550
human α4 V*ID*TL**S *K*KE**GYI VL***M*L** N**AESPP** ***S****DV
mouse α4 V*MH*TL**S *K*KE**GYI VL***V*L** H**AESPS** **FS****DV
chick α4 ICVNLQICFN YTGQGVPDNT EMFYNLSVDV KRKVDTQARF YFSANGTSET
551 600
human α4 IT***QVSSR EAN*RT*Q** ********** *IQI**A*** *PHVIS**ST
mouse α4 IT***RVSSS GEK*RT*Q** ********** *I****T*** *HHVIT**NT
chick α4 TSGSIKITEK IIACKGHLAF MRKDVRDILT PVHVEASYHL GQQILQKRDN
601 650
human α4 E*FPP*Q*I* *QK*****M* KTIN**RF*A HE******Q* *A*IG*L***
mouse α4 E*FPP*Q*I* *QK****V*R KMIN**RF*A YE******Q* *A*VG*L**Y
chick α4 QELSALPPVL QRRKEKDIIK SKFVFAKICS QKNCSADLKV SGKVAFPKPH
651 700
human α4 EN*T**A*** M***M**V** F***D***** T**VKL*V** ***KILE***
mouse α4 EN*T**A*** M**IM**V** F***D***** T*NV*L*T** ***KIL****
chick α4 DKKMYLVVGS TKTLLLNISL HNAGNDAYET VLHIQFPKGL YFIRVPDLEE
701 750
human α4 ***N***T*N SGVVQLDC*I **I**DHL*R *DISF*L*V* *LS***E**S
mouse α4 ***N***TES SGIVKLAC*L **I**DRL*R *DISF*L*V* *LS**HE**S
chick α4 KQIHCEVLDK DIHAVKLISV GYLYVQIQSW ISVS.LWDTS SFTRAEDDLN
751 800
human α4 *TVHAT*E** E*MDN*KHSR **V*I***** VK*TV****N *T*****SND
mouse α4 *SVHA**E** G*LDQVR**R **LTI**R** VM*TV**L*N *T*****SS*
chick α4 IIINVSCKNE NE.NLLLDNM VTVAVPLKYE TELITHGFVT PPSFVYGTNE
801 850
human α4 ENEPET**V* KM*L****** T*N*****VS V*I*V**S*S *QTD****IL
mouse α4 ENEPET**A* KL*L****** T*I*****VS VKI*V**S*L *Q*D*****L
chick α4 NEASVMCMEE NINFTFHVIN AGPSMAPNIN LELMIPNAFP PHDFKLFNVM
851 900
human α4 *VQ**T***H FEN*Q*V*AL EQQKSAMQT* *GI*R*L**T D**LL**I*A
mouse α4 *VQ**T*Q*H FKH*G*E*TF AQQKGIAGT* T*I*K*L**T D**LL**M*A
chick α4 DIKTTVGECS YNEYPRNCNA PEKTE..NIL KDVVTFFSKP AKRQMYCMKN
901 950
human α4 *PH**NFL*N F*K**S**** SVHIQ**GR* SI****ET*A ****I***GF
mouse α4 *QH**DFL*N F*K**S**** SVHIQ**GR* SI****ET*S ****IK**AF
chick α4 DSLCLQIHCK LGNMENGKEA TIQLHLEATP ALLEMDDAST LKFEVRATAS
951 1000
human α4 **P*PR**** N**EN**H*L ***L***R** RYF*IV**SS S*LL*LIVL*
mouse α4 **PHP***** N**EN**H*F ***L***R** R*F*II**TI S*LL*LIVL*
chick α4 PEKNAKVIEL QKDKQVAYVY LEGVHHQKPK YHVTVLIIGI GLIAGITLFL
1001 1039
human α4 *I*YVM**A* *******S*L *EE**RD*** YINSKSN**
mouse α4 *I*CVM**A* *******S*L *EE**RD*** YVNSKSN**
chick α4 LLSLLLWKIG FFKRQYKPIP QDMNRKESWS FTSGNK.DD

FIG. 1. Comparison of avian integrin α_4 subunit to human and mouse integrin α_4 proteins. A 3.9-bp cDNA was cloned that encodes a protein that is 60% identical to the human and mouse analyzed. The cDNA of the integrin α_4 subunit encodes a protein that is 60% identical to the human (Takada, 1989) and mouse (Neuhaus, 1991) integrin α_4 subunit (Fig. 1) but is 19 and 20 amino acids shorter at the N-terminus than human and mouse integrin α_4 proteins. At the nucleotide level, the avian integrin α_4 subunit is 69 and 68% identical to the human and mouse genes, respectively. The protein contains a long extracellular domain, a transmembrane domain, and a short cytoplasmic domain (30 amino acids) that is characteristic of most integrin α subunits (reviewed by Hynes, 1987). In addition, the integrin α_4 protein contains the GFFKR (Fig. 1) sequence in the cytoplasmic domain that is conserved in other integrin α subunits and is thought to play a role in inside-out signaling (reviewed by Schwartz *et al.*, 1995). Importantly, the GKEA sequence (Fig. 1), unique to the α_4 subunit (Takada, 1989; Neuhaus, 1991), is present in the chick gene. These results suggest that this integrin corresponds to the avian homolog of the α_4 subunit.

Integrin α_4 Subunit mRNA Expression in Avian Neural Crest Cells

Whole mount *in situ* hybridization with a digoxygenin-labeled 500-bp integrin α_4 subunit RNA probe was performed on chicken embryos ranging from stage 5 to stage 17 (Hamburger, 1951). Prior to initiation of cranial neural crest cell migration at the eight-somite stage, strong expression was observed in premigratory cranial neural crest cells situated within the dorsal midbrain (Figs. 2A and 2B). Subsequently, integrin α_4 mRNA was expressed by cranial neural crest cells during their migratory phase both at midbrain (Figs. 2D and 2E) and hindbrain (Figs. 2G and 2H) levels. In addition to expression in presumptive neural crest cells, there was intense expression in Hensen's node and in the mesoderm at the level of the open neural plate (Fig. 2C). Integrin α_4 subunit expression was also noted in the nasal and optic placode, the otic vesicle, and the trigeminal ganglia in the cranial region.

In the trunk region, prominent integrin α_4 expression was observed in migrating trunk neural crest cells (Figs. 3A–3D). The myotome and lateral mesoderm displayed high levels of integrin α_4 mRNA expression, as did the developing musculature and apical ectodermal ridge of the limb (data not shown).

To verify that cells expressing the α_4 subunit mRNA were indeed neural crest cells, embryos were processed by *in situ* hybridization with the integrin α_4 probe and subse-

integrin α_4 subunit. The avian integrin α_4 protein contains the GFFKR (in bold) sequence in the cytoplasmic domain of all integrin α subunits and the GKEA (in bold) sequence that is unique to the α_4 subunits. The putative transmembrane domain is underlined. Astericks and periods denote conserved amino acids and missing amino acids, respectively.

Copyright © 1998 by Academic Press. All rights of reproduction in any form reserved.

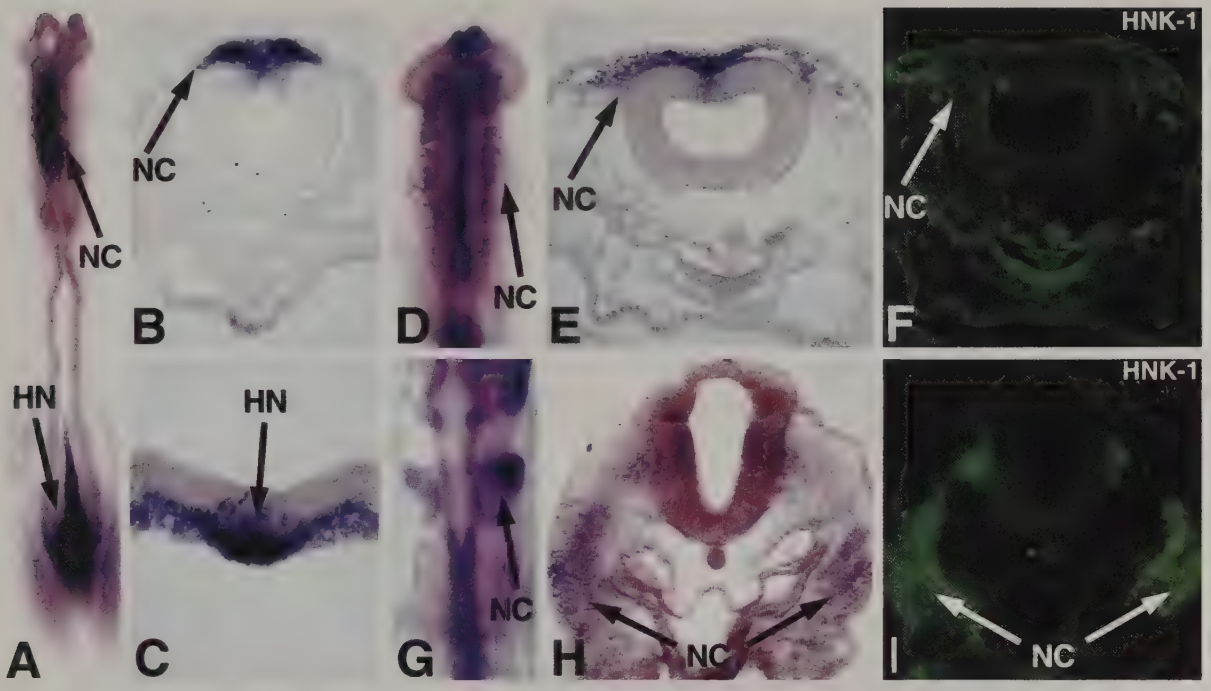

FIG. 2. Integrin α_4 mRNA was detected in cranial regions of 8- to 15-somite chick embryos as seen in sections through embryos after *in situ* hybridization with integrin α_4 mRNA. At the 8-somite stage, strong expression was observed in premigratory cranial neural crest cells (NC) situated within the dorsal midbrain neural tube (A and B). Integrin α_4 mRNA was expressed by cranial neural crest cells during their migratory phase both at midbrain (D and E) and hindbrain (G and H) levels. In addition, there was strong expression in Hensen's node (HN) and in the mesoderm at the level of the open neural plate (A and C). Colocalization of HNK-1 immunoreactivity and integrin α_4 mRNA expression was observed in migrating neural cells between the epidermis and cranial mesenchyme (E and F, H and I). The HNK-1 antibody does not recognize premigratory and early migrating neural crest cells.

quently stained with the HNK-1 antibody, which recognizes a carbohydrate epitope on most migrating neural crest cells (Vincent, 1984; Tucker *et al.*, 1984). In cranial regions, colocalization of HNK-1 immunoreactivity and integrin α_4 mRNA expression was observed in migrating neural cells in the cranial mesenchyme (Fig. 2H and 2I). In contrast, premigratory and early migrating neural crest cells within and above the dorsal neural tube expressed the α_4 subunit (Fig. 2E), but did not yet express the HNK-1 epitope (Fig. 2F), which only becomes detectable following their departure from the neural tube (Teillet, 1987). Trunk neural crest cells migrating ventrally through the rostral portion of the somitic sclerotome also coexpressed the HNK-1 epitope and integrin α_4 mRNA (Figs. 3C and 3D).

Integrin α_4 Subunit Protein Expression in Murine Neural Crest Cells

In the mouse, the PS/2 antibody recognizes the integrin α_4 subunit and has been used to functionally inhibit lymphocyte adhesion to fibronectin (Miyake, 1991). We used this antibody to compare integrin α_4 expression in the chick and mouse. In E8.5 mouse embryos, we noted that cranial neural crest cells displayed strong α_4 integrin immunoreactivity (Figs. 4A–4C) at the level of the forebrain, midbrain, and hindbrain. Migrating neural crest cells that have entered the first branchial arch demonstrated strong α_4 protein expression. At later stages, α_4 immunoreactivity was prevalent in neural crest-derived cranial ganglia including the trigeminal ganglia (Fig. 4D).

In the trunk region of E9.5 embryos, neural crest cells displayed integrin α_4 immunoreactivity both during their migration as well as during condensation into dorsal root ganglia (DRG) and other derivatives (Figs. 4D–4F). In addition to the expression in the neural crest cells and their derivatives, integrin α_4 immunoreactivity was noted in the gut (Fig. 4E) and myotome (Fig. 4F). The expression in the DRG and myotome increased with developmental age and was pronounced by E11.0 (Fig. 4G). In addition, the apical epidermal ridge of the forelimb (Fig. 4H) and the hindlimb (data not shown), the myoblasts of the forelimb (Fig. 4H),

Copyright © 1998 by Academic Press. All rights of reproduction in any form reserved.

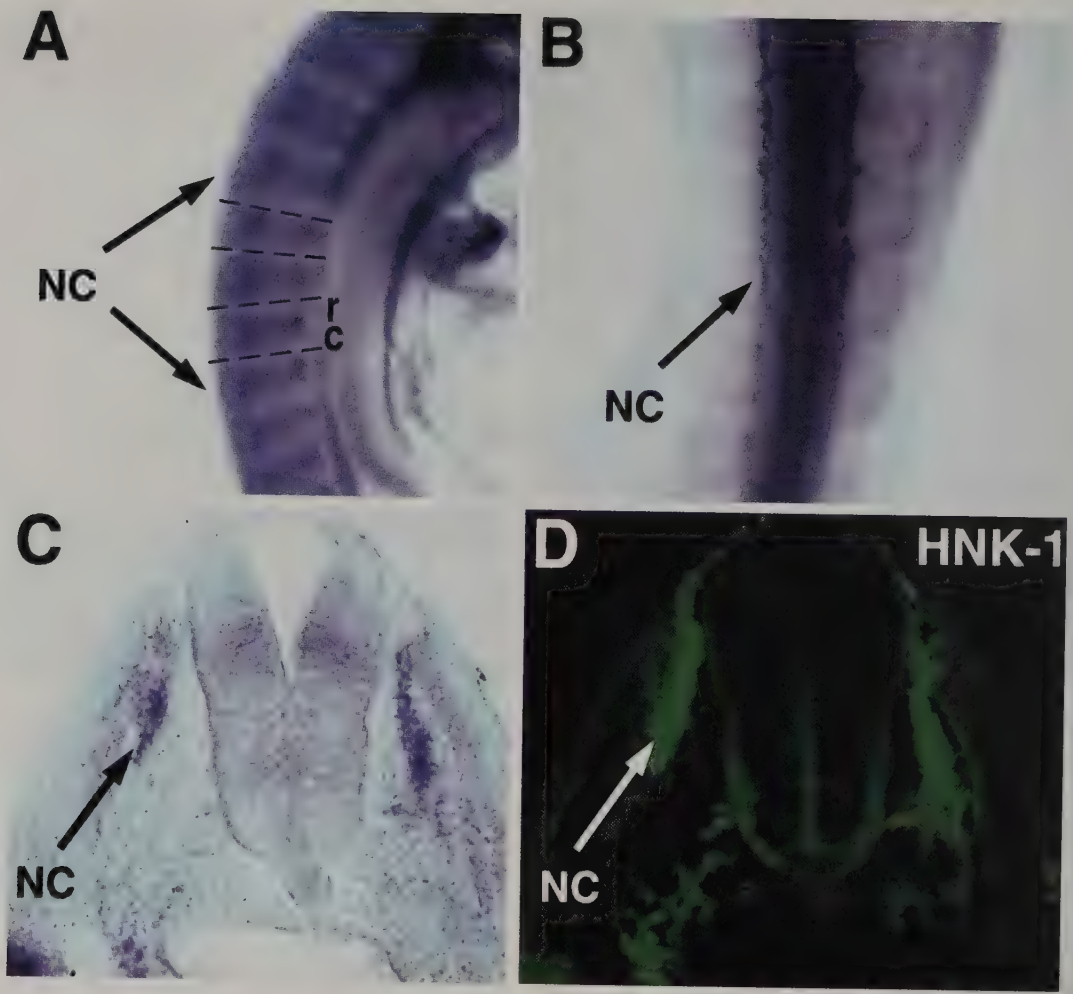

FIG. 3. Integrin α_4 subunit mRNA was detected in trunk regions of 27- to 30-somite chick embryos. Neural crest cells (NC) of a 27-somite-stage embryo express integrin α_4 mRNA as they migrate through the rostral half of the somite (A). Premigratory trunk neural crest cells stain intensely for integrin α_4 mRNA expression in the caudal region of a 30-somite-stage embryo (B). Trunk neural crest cells migrating ventrally through the rostral (r) portion of the somitic sclerotome also coexpress the HNK-1 epitope and integrin α_4 mRNA (C and D). The HNK-1 antibody does not recognize premigratory and early migrating neural crest cells. The dashed lines represent borders of somites. c denotes the caudal portion of the somitic sclerotome.

the liver (Fig. 4I), and the heart (data not shown) showed prominent integrin α_4 immunoreactivity.

Some differences were noted between the expression patterns of avian integrin α_4 mRNA and mouse integrin α_4 protein. For example, there was little or no integrin α_4 immunoreactivity localized to premigratory mouse neural crest cells whereas high levels of α_4 mRNA were noted in premigratory avian neural crest cells in the cranial region. Similarly, in avian embryos, the dorsal half of the neural tube displayed low levels of α_4 expression, whereas no protein expression was noted in the mouse neural tube. It is unclear whether these represent species differences or reflect differences between mRNA and protein expression. With the exception of these differences, the avian and murine patterns overlapped.

Anti-α_4 Antibody Blocks Neural Crest Cell Migration in Mouse Hindbrain and Trunk Explants

We recently developed a novel explant preparation that allows direct visualization of neural crest cell migration in normal living tissue (Krull *et al.*, 1995, 1997) Advantages of

Copyright © 1998 by Academic Press. All rights of reproduction in any form reserved.

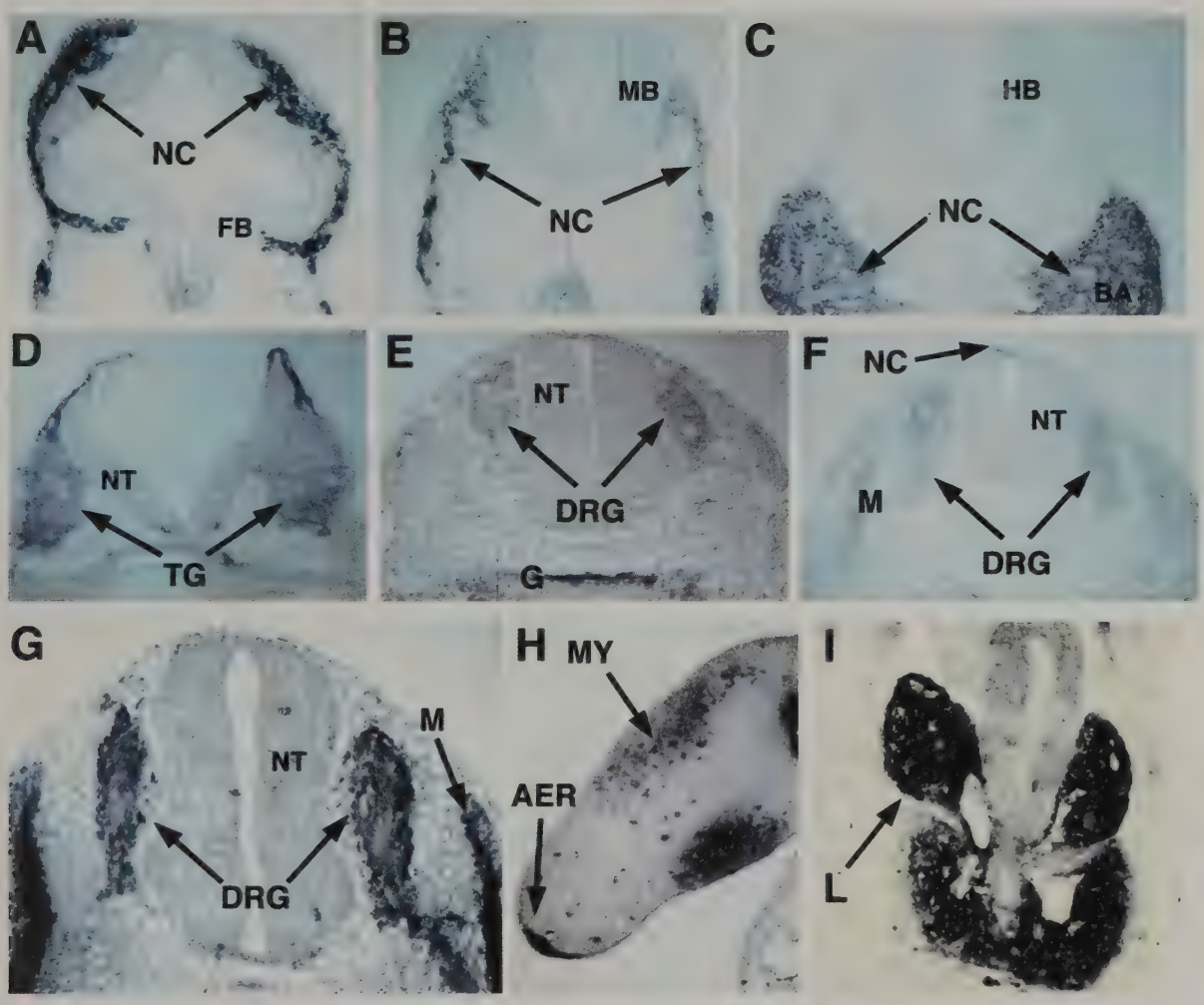

FIG. 4. Integrin α_4 subunit protein was detected in early mouse embryos. In E8.5 mouse embryos, cranial neural crest cells displayed strong PS/2 immunoreactivity (A–C) at the level of the forebrain (FB), the midbrain (MB), and the hindbrain (HB). Migrating neural crest cells that entered the first branchial arch (BA) had strong integrin α_4 protein expression (C). In the trunk region of E9.5 embryos, neural crest cells displayed prominent integrin α_4 immunoreactivity both during their migration as well as during condensation into dorsal root ganglia (DRG) and trigeminal ganglia (TG; see D–F). In addition to expression in neural crest cells and their derivatives, integrin α_4 immunoreactivity was noted on the myotome (M; see F). Expression in the DRG and myotome increased with developmental age and were pronounced by E11.0 (G). In addition, the apical epidermal ridge (AER) and myoblasts (MY) of the forelimb (H), liver (L; see I), and gut (G; see E) showed prominent integrin α_4 immunoreactivity.

these preparations are that they offer high accessibility to perturbing reagents, easy visualization of migrating neural crest cells, and applicability to avian or murine systems. To examine the role of the integrin α_4 subunit in cranial and trunk neural crest cell migration, we added function-blocking PS/2 antibody against the α_4 subunit of integrin as a perturbing reagent to explants removed from the mouse hindbrain and trunk.

The neural tube at hindbrain levels in E8.5 mouse embryos was labeled with DiI to mark premigratory neural crest cells (Serbedzija *et al.*, 1992). Hindbrains plus adjacent tissue (including the otic placode and three rostral-most somites) were excised from labeled mouse embryos and incubated for three hours in (1) control medium without antibody (n = 10; Fig. 5A), (2) control medium with a non-function-blocking antibody to integrin β_1 subunit (n = 5, Fig. 5B), or (3) medium containing a function-blocking anti-integrin α_4 antibody (n = 11 at 1 μg/ml and n = 14 at

Copyright © 1998 by Academic Press. All rights of reproduction in any form reserved.

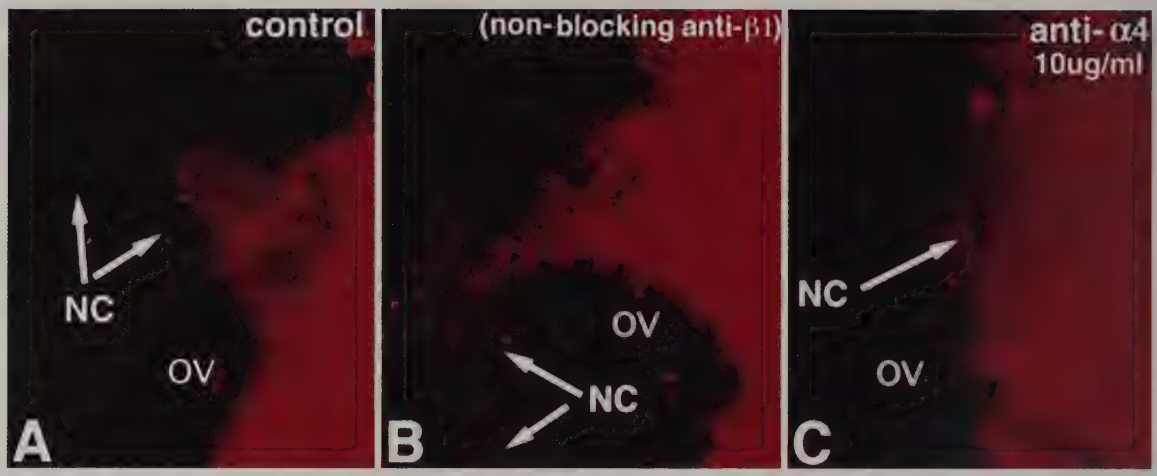

FIG. 5. To test the function of the integrin α_4 subunit in cranial neural crest cell migration, hindbrain explants were treated with anti-integrin α_4 (PS/2) antibody. The neural tube at hindbrain levels in E8.5 mouse embryos was labeled with DiI to mark premigratory neural crest cells. Labeled hindbrains plus adjacent tissue (including the otic placode and three rostral-most somites) were incubated for 3 h in (A) control medium without antibody, (B) control medium with a non-function-blocking antibody to integrin, or (C) medium containing a function-blocking anti-integrin α_4 antibody. Numerous migrating neural crest cells (NC) were observed in characteristic streams around the otic vesicle (OV) in all control explants. In the presence of 10 μg/ml of PS/2 antibody, hindbrain neural crest cell migration was markedly reduced.

10 μg/ml; Fig. 5C). The explants were positioned on Millicell inserts and incubated for an additional 24–48 h.

In the presence of 10 μg/ml of anti-integrin α_4 antibody, hindbrain neural crest cell migration was markedly reduced. Only three explants (n = 14) exhibited detectable neural crest cell migration (Fig. 7A). There was a 57% reduction in number of neural crest cells (n = 23) that emigrated from the neural tube when compared to the number of cells emigrated in control explants (n = 77 with medium alone and n = 81 with control antibody). Neural crest cells in the anti-integrin α_4 antibody-treated explants were not found at distances greater than 200 μm away from the neural tube, whereas 30–35% neural crest cells in the control antibody-treated and nontreated explants migrated distances greater than 200 μm. Numerous migrating neural crest cells were observed in characteristic streams around the otic vesicle in all control explants. For hindbrain explants, the P value for explants treated with the control anti-β_1 antibody compared with no antibody was >0.25. The P value for explants in the presence of the PS/2 anti-α_4 antibody compared with controls was ≤0.05.

To examine the potential function of the integrin α_4 in trunk neural crest cell migration, the neural tubes of E9.5 mouse embryos were prelabeled with DiI. Trunk regions containing the last 6 somites plus the neural tube of 20- to 25-somite-stage embryos were explanted as described (Krull *et al.*, 1997; Studer, 1996). In control explants treated without antibody (n = 16; Fig. 6A) and in the presence of the non-function-blocking anti-integrin β1 antibody (n = 13; Fig. 6B), neural crest cells migrate in their typical metameric pattern through the rostral but not caudal half of each somitic sclerotome. In presence of the anti-integrin α_4 antibody (n = 15; Fig. 6C), we observed that 7 of 15 explants showed nearly complete inhibition of neural crest cell emigration. Analysis of explants showed a 70% reduction in the numbers of neural crest cells (n = 98) that emigrated from the neural tube compared with control explants (n = 323 with medium alone and n = 262 with control antibody). Furthermore, those neural crest cells in treated explants that left the neural tube only traveled a short distance compared to neural crest cells under control conditions. Neural crest cells in the anti-integrin α_4 antibody-treated explants were not found at distances greater than 150 μm from the neural tube, whereas 10–17% of the neural crest cells in the control antibody-treated and nontreated explants migrated to distances greater than 150 μm (Fig. 7B). For trunk explants, the P values were ≤0.005 for explants treated with the control anti-β_1 compared with blocking anti-α_4 antibodies. However, the segmental pattern of migration was unaffected by addition of the anti-α_4 antibody. These results indicate that the integrin α_4 subunit is required for neural crest cell emigration and migration in both the head and trunk.

CS Peptide Injections into Avian Embryos

Integrin α_4 subunit is a receptor for fibronectin and VCAM-1 (Mould, 1990; Guan and Hynes, 1990). The CS-1

Copyright © 1998 by Academic Press. All rights of reproduction in any form reserved.

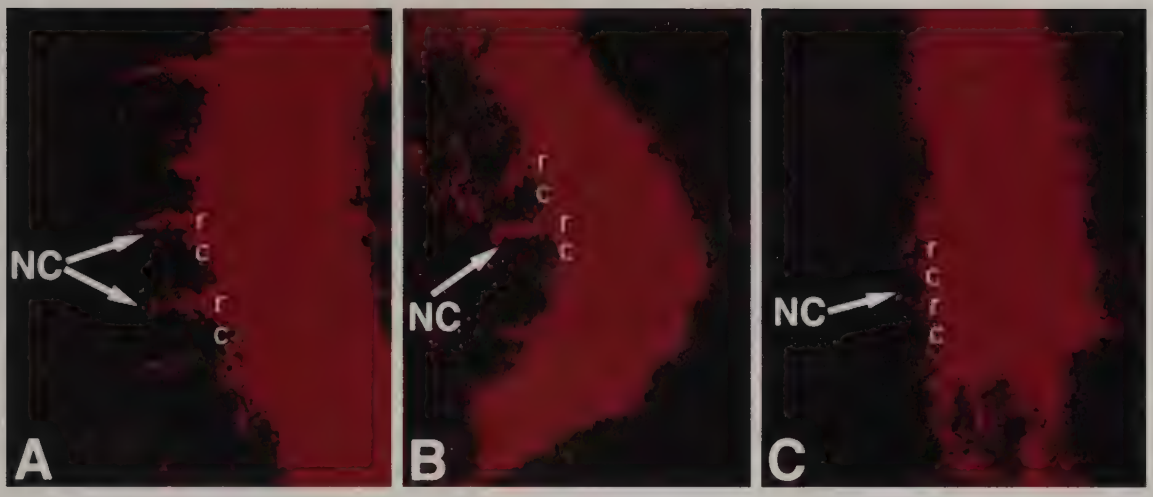

FIG. 6. To test the function of the integrin α_4 subunit in trunk neural crest cell migration, trunk explants were treated with anti-α_4 integrin (PS/2) antibody. The neural tubes of E9.5 mouse embryos were prelabeled with DiI and trunk regions containing the last six somites plus the neural tube were treated with antibodies. In control explants in the absence of antibody (A) or in the presence of the non-function-blocking anti-integrin β_1 antibody (B), neural crest cells (NC) migrate in their typical metameric pattern through the rostral (r) but not caudal (c) half of each somitic sclerotome. In the presence of the anti-integrin α_4 antibody (C), there was a nearly complete inhibition of neural crest cell emigration in 7of 15 explants tested.

peptide contains the LDV sequence of fibronectin that represents one of the binding sites for the integrin α_4 subunit (Wayner *et al.*, 1989; Guan and Hynes, 1990; Mould, 1990; Ruegg, 1992). CS-1 also inhbits adhesion to VCAM-1 (May, 1993), which contains an LDV-like sequence. To competitively inhibit cell interactions with the CS-1 domain, we injected CS-1 peptide into the mesenchyme adjacent to the mesencephalon of chick embryos. In injected embryos, we noted both neural tube defects and neural crest cells in ectopic locations (17 of a total of 23 embryos). Some neural crest cells were found in the lumen of the neural tube or situated on the dorsal portion of the neural tube (Fig. 8B), atypical of migratory neural crest. In addition, some neural tube cells detached from each other, appearing rounded rather than as columnar epithelial cells (data not shown). The control embryos injected with a scrambled version of CS-1 appeared normal with respect to cranial neural crest cell migration and neural tube morphology (7 of a total of 8 embryos; Fig. 8A). These results suggest that a molecule containing an LDV-like sequence is necessary for cranial neural crest cell migration.

DISCUSSION

We have taken advantages of both chick and mouse systems to show that the integrin α_4 subunit plays a functionally important role in neural crest cell migration. Both cranial and trunk neural crest cells display high levels of integrin α_4 subunit expression. Based on the finding that a blocking antibody significantly abrogates neural crest cell migration *in vivo*, we propose that the α_4 subunit is an important integrin α receptor on neural crest cells and is likely to be the major receptor utilized by the neural crest cell to emigrate from the neural tube. At the immunocytochemical level, its expression appears higher than that of other α subunits (α_v and α_1; Kil *et al.*, 1996a; Lallier and Bronner-Fraser, 1992), although no direct quantitation has been performed. Thus, this subunit can serve as a useful marker for migrating neural crest cells in both species. This may be particularly useful in mice, where few good markers for neural crest cells have been described.

Sequence Analysis of Avian Integrin α_4 Subunit

Sequence comparison of avian integrin α_4 subunit with human and mouse integrins α_4 subunits reveals some unusual properties. At the nucleotide level, avian integrin α_4 subunit is 69 and 68% identical to the human and mouse genes, respectively. However, the avian integrin α_4 shows lower amino acid identity to human and mouse integrin α_4 protein (60% to human and mouse) but a high nucleotide identity (69%; data not shown). The avian integrin α_4 is 19 and 20 amino acids shorter at the N-terminus than human and mouse integrin α_4 proteins, respectively. We believe the methionine indicates the N-terminus since the AUG is embedded in a consensus initiation sequence ((GC-C)GCCA/GCC**AUG**G; Kozak, 1987). The predicted protein

Copyright © 1998 by Academic Press. All rights of reproduction in any form reserved.

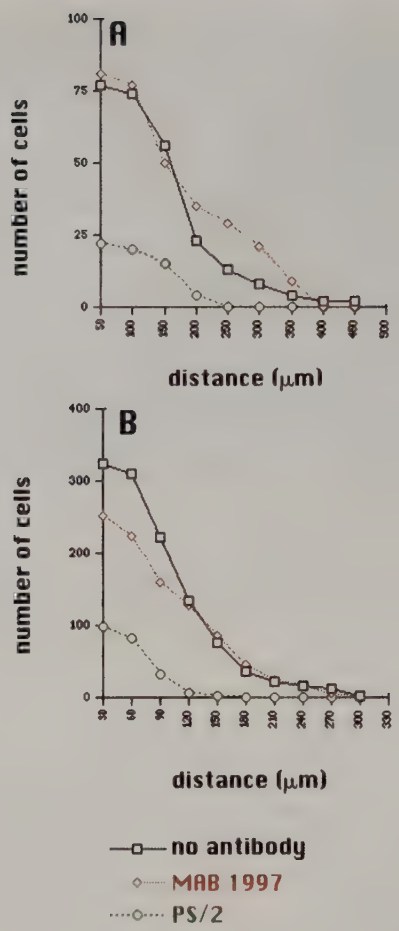

FIG. 7. To quantify neural crest cell migration observed in hindbrain and trunk explants treated with anti-α_4 integrin antibody, the migration distance (μm) was measured as a straightline distance from the lateral edge of the neural tube to a given cell's final position. For the hindbrain explants (A), the cell number and distance traversed by neural crest cells of the caudal stream around the otic vesicle were measured (three explants for a given condition). For trunk explants (B), the cell number and distance traversed of neural crest cells within 10-somite explants were measured (three explants for a given condition). The number of cells (y-axis) was plotted against distance migrated (x-axis). Statistical analyses were done using χ^2 test for independence between two or more samples. For hindbrain explants, the P value for explants treated with the control anti-β_1 antibody was >0.25. The P value for explants in the presence of the anti-α_4 integrin antibody was ≤ 0.05. For trunk explants, the P values were ≤ 0.005 for explants treated with the anti-β_1 and anti-α_4 antibodies.

sequence of our chick cDNA clone is 98% identical to a C-terminal fragment of ~100 amino acids in length previously reported by Stepp *et al.* (1994).

The Integrin α_4 Subunit is Expressed by Neural Crest Cells

Colocalization studies using the HNK-1 antibody, which recognizes migrating avian neural crest cells, and integrin α_4 mRNA show that many HNK-1-immunoreactive neural crest cells are also positive for integrin α_4 mRNA expression. The integrin α_4 subunit is expressed in premigratory cranial neural crest cells within the dorsal neural tube and, therefore, precedes both their emigration and the onset of HNK-1 epitope production. At the level of the trunk, we noted many neural crest cells that were positive for integrin α_4 mRNA during their migratory phase. Our colocalization study shows that many, but not all HNK-1-immunoreactive neural crest cells express the integrin α_4 subunit. Since not all HNK-1-positive cells express the α_4 subunit, we cannot rule out the possibility that there are other α subunits expressed by some of the migrating avian neural crest cell population.

Previous studies have alluded to the expression of the integrin α_4 subunit on neural crest cells and their derivatives. Our results concur with those of Sheppard *et al.* (1994), who reported the presence of the α_4 subunit on neural crest-derived dorsal root ganglia. However, our results differ markedly from those reported by Stepp *et al.* (1994), who noted a complex pattern of integrin α_4 mRNA and protein expression in the mesenchyme, somites, neural tube, ectoderm, and a subpopulation of trunk neural crest cells. In contrast, we find that the integrin α_4 subunit is expressed predominantly on neural crest cells, with little or no expression in the ectoderm and early somites, although there is later expression in the dermomyotome. Although the reasons for these differences are unclear, these previous authors used, for immunolabeling, an antibody against the human integrin α_4 cytoplasmic domain whose specificity is unknown in chick. We used several different RNA probes encompassing the entire coding region of integrin α_4 subunit for whole-mount *in situ* hybridization which gave identical results. In contrast, they performed radioactive *in situs* on sections using a different probe. Therefore, it is likely that the apparent differences are technical and that recent advances in *in situ* hybridization and antibody labeling technology have greatly increased the resolution and decreased the signal to noise problems associated with detection of mRNA.

Role of Integrin α_4 Subunit in Neural Crest Cell Migration

In the presence of a function-blocking integrin α_4 antibody, there was a significant reduction (57–70%) in the number of neural crest cells that migrated. Importantly, more than half of the explants tested did not show any neural crest cell emigration from the neural tube. In contrast, explants treated with a nonblocking integrin antibody were unaffected. These results suggest that integrin α_4 subunit is involved in both emigration and migration of neural crest cells. Our colocalization studies with HNK-1

Copyright © 1998 by Academic Press. All rights of reproduction in any form reserved.

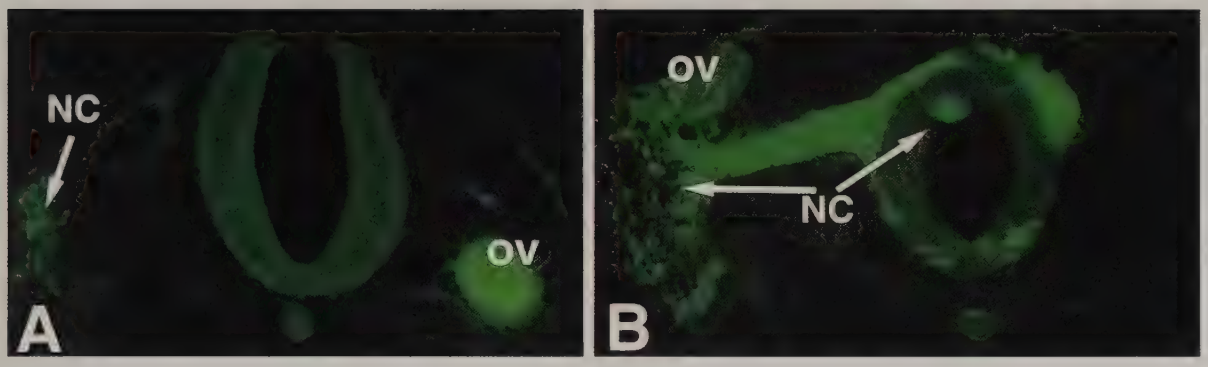

FIG. 8. Fluorescence photomicrographs of transverse paraffin sections showing the effects of the CS-1 peptide on cranial neural crest cell migration in embryos fixed 18–24 h after injection as observed by HNK-1 staining. Embryos injected with scrambled CS-1 peptides (A) have normal cranial neural crest (NC) migration at the level of the otic vesicle (OV) and neural tube; neural crest cells emigrate from the dorsal neural tube and migrate ventrally underneath the ectoderm. Embryos injected with CS-1 peptides (B) have neural crest cells (NC) in the lumen of the neural tube and on top of the neural tube.

antibody and integrin mRNA probe show that many but not all HNK-1-positive neural crest cells express integrin α_4 mRNA. HNK-1-positive/integrin α_4-negative neural crest cells may account for the neural crest cell migration observed in some treated explants. However, it is possible that some of the apparently nonexpressing cells express sufficient levels of α_4 to be functionally active without being detectable by *in situ* hybridization. It should be noted that the colocalization experiments were done in the chick, where a good neural crest marker is available, whereas the perturbation experiments were done in mice and the two systems may not be entirely equivalent.

Our transient perturbation experiments demonstrate a functional role for the integrin α_4 subunit at both cranial and trunk levels. However, disruption of the integrin α_4 subunit by homologous recombination in mice (Hynes *et al.*, 1995) did not produce an obvious neural crest phenotype. In homozygous α_4-null mice, neural crest-derived tissues such as the dorsal root and trigeminal ganglia are present. One possibility is that the subpopulation of neural crest cells that normally lack α_4 subunits contributes to the formation of dorsal root ganglia in integrin α_4-deficient mice. Alternatively, it is possible that other integrin subunits may functionally compensate in neural crest cells after inactivation of the α_4 subunit, accounting for the relatively normal ganglion formation. For example, Yang *et al.* showed that α_v integrin subunit can replace fibronectin receptor function in embryonic cells deficient in $\alpha_5\beta_1$ integrin (Yang *et al.*, 1996). Caution must be used, however, in interpreting apparently negative results from a genetic loss-of-function analysis. More thorough characterization of the null mice may reveal subtle defects in the numbers of emigrating neural crest cells and their distances of migration. In addition, targeted disruptions of the integrin α_4 subunit at the time of neural crest cell migration may yield results different than those obtained in mice that are α_4-null from conception. Thus, further experiments are necessary to compare and contrast the phenotypes of antibody perturbation and genetic loss-of-function of the integrin α_4 subunit.

In some cases, integrin antibodies have been shown to induce signaling through integrin receptors; for example, in the immune system, an antibody against $\alpha_4\beta_7$ can trigger T-cell blastogenesis (Teague *et al.*, 1994). Similarly, the TASC antibody against β_1 integrin has been shown to induce signal transduction in retinal neurons binding responding to laminin (Neugebauer and Reichardt, 1991). Although there is no evidence that the PS/2 antibody used in this study can induce cell signaling, we cannot formally rule out the possibility that addition of this antibody may influence neural crest cell behavior by activating an intracellular signaling cascade.

What Types of Neural Crest Cell–ECM Interactions Are Mediated by Integrin α_4?

Integrin α_4 associate with integrin β_1 and β_7 subunits. Both integrins $\alpha_4\beta_1$ and $\alpha_4\beta_7$ bind to an LDV-like sequence found in the CS-1 region of fibronectin (Wayner *et al.*, 1989; Guan and Hynes, 1990; Mould, 1990; Ruegg, 1992) and VCAM-1, a member of the immunoglobulin superfamily (Elices *et al.*, 1990). Neural crest cells have been shown to express the integrin β_1 subunit (Krotoski *et al.*, 1986). In addition, fibronectin is abundant along neural crest cell pathways (Newgreen and Theiry, 1980; Thiery *et al.*, 1982; Krotoski *et al.*, 1986). Therefore, integrin α_4 likely associates with the β_1 subunit to form a receptor that mediates neural crest cell interaction with fibronectin. Results of our perturbation experiments using the CS-1 peptide, containing the LDV sequence (Mould *et al.*, 1990), suggest that the

Copyright © 1998 by Academic Press. All rights of reproduction in any form reserved.

CS-1 region of fibronectin may be important for neural crest cell migration. *In vitro* studies by Dufour *et al.* (1988) have shown that both the RGD and the CS-1 regions of the fibronectin molecule are required for neural crest cell migration. Some differences in peptide effects were observed: whereas the RGD region supported both attachment and spreading of neural crest cells, the CS-1 region only supported cell attachment (Dufour *et al.*, 1988). However, it is formally possible that CS-1 peptides inhibit interactions with unknown molecules. Although the integrin β_7 subunit has not yet been shown to be expressed by neural crest cells, $\alpha_4\beta_7$ may also be present on neural crest cells. VCAM-1 has been shown to be expressed on the neural crest-derived outflow tract of the embryonic heart, where it was colocalized with integrin α_4 in mouse (Sheppard, 1994) but was not detectable along the migratory pathways of mouse neural crest cells (Kwee, 1995). Hence, neural crest cell interaction with VCAM-1 by integrin α_4 subunit may not be relevant to neural crest cell migration. These findings suggest that integrin α_4 coupled with integrin β_1 may mediate the interaction of neural crest cells with fibronectin.

In summary, our findings show that the integrin α_4 subunit displays high levels of expression on both cranial and trunk neural crest cells in birds and mice. Furthermore, the α_4 subunit of integrin is functionally important for neural crest cell migration, such that blocking its function significantly abrogates neural crest cell migration *in vivo*. The results suggest that the α_4 subunit may be a predominant integrin α receptor on neural crest cells. It may play a particularly important role in neural crest cell emigration from the neural tube.

ACKNOWLEDGMENTS

We thank Drs. Arthur Lander, Diane O'Dowd, Ben Murray, and Martin Garcia-Castro for critical comments on the manuscript and constructive discussion during the course of this work. This study was supported by USPHS HD15527 and a grant from the Muscular Dystrophy Foundation to M.B.F.

REFERENCES

Adams, J. C., and Watt, F. M. (1989). Fibronectin inhibits the terminal differentiation of human keratinocytes. *Nature* **340,** 307–309.

Boucaut, J. C., Darribere, T., Boulekbache, H., and Thiery, J. P. (1984). Prevention of gastrulation but not neurulation by antibodies to fibronectin in amphibian embryos. *Nature* **307,** 364–367.

Bronner-Fraser, M. (1985). Alterations in neural crest migration by a monoclonal antibody that affects cell adhesion. *J. Cell Biol.* **101,** 610–617.

Bronner-Fraser, M. (1986a). Analysis of the early stages of trunk neural crest migration in avian embryos using monoclonal antibody HNK-1. *Dev. Biol.* **115,** 44–55.

Bronner-Fraser, M. (1986b). An antibody to a receptor for fibronectin and laminin perturbs cranial neural crest development. *Dev. Biol.* **117,** 528–536.

Bronner-Fraser, M. (1988). Distribution and function of tenascin during cranial neural crest development in the chick. *J. Neurosci. Res.* **21,** 135–147.

Bronner-Fraser, M., and Lallier, T. (1988). A monoclonal antibody against a laminin–heparan sulfate proteoglycan complex perturbs cranial neural crest migration *in vivo*. *J. Cell Biol.* **106,** 1321–1330.

Chiquet, M. (1989). Tenascin/J1/cytotactin: The potential function of hexabrachion proteins in neural development. *Dev. Neurosci.* **11,** 266–275.

Delannet, M., Martin, F., Bossy, B., Cheresh, D. A., Reichardt, L. F., and Duband, J. L. (1994). Specific roles of the $\alpha V\beta 1$, $\alpha V\beta 3$ and $\alpha V\beta 5$ integrins in avian neural crest cell adhesion and migration on vitronectin. *Development* **120,** 2687–2702.

Duband, J.-L., Belkin, A. M., Syfrig, J., Thiery, J. P., and Koteliansky, V. E. (1992). Expression of alpha 1 integrin, a laminin–collagen receptor, during myogenesis and neurogenesis in the avian embryo. *Development* **116,** 585–600.

Dufour, S., Duband, J. L., Humphries, M. J., Obara, M., Yamada, K. M., and Thiery, J. P. (1988). Attachment, spreading and locomotion of avian neural crest cells are mediated by multiple adhesion sites on fibronectin molecules. *EMBO J.* **7,** 2661–2671.

Elices, M. J., Osborn, Y., Takada, C., Crouse, S., Luhowsky, M., Helmer, E., and Lobb, R. R. (1990). VCAM-1 on activated endothelium interacts with the leukocyte integrin VLA-4 at a site distinct from the VLA-4/fibronectin binding site. *Cell* **60,** 577–584.

Erickson, C. A., and Perris, R. (1993). The role of cell–cell and cell–matrix interactions in the morphogenesis of the neural crest. *Dev. Biol.* **159,** 60–74.

Erle, D. J., Sheppard, D., Breuss, J., Ruegg, C., and Pytela, R. (1991). Novel integrin alpha and beta subunit cDNAs identified in airway epithelial cells and lung leukocytes using the polymerase chain reaction. *Am. J. Respir. Cell Mol. Biol.* **5,** 170–177.

Gong, Q., and Shipley, M. T. (1996). Expression of extracellular matrix molecules and cell surface molecules in the olfactory nerve pathway during early development. *Comp. Neurol.* **26,** 1–14.

Gu, M., Wang, W., Song, W. K., Cooper D. N., and Kaufman, S. J. (1994). Selective modulation of the interaction of alpha 7 beta 1 integrin with fibronectin and laminin by L-14 lectin during skeletal muscle differentiation. *J. Cell Sci.* **107,** 175–181.

Guan, J.-L., and Hynes, R. O. (1990). Lymphoid cells recognise an alternatively spliced segment of fibronectin via the integrin receptor $\alpha 4\beta 1$. *Cell* **60,** 53–61.

Hamburger, V., and Hamilton, H. L. (1951). A series of normal stages in the development of the chick embryo. *J. Morphol.* **88,** 49–92.

Hay, E. D. (1989). Extracellular matrix, cell skeletons, and embryonic development. *Am. J. Med. Genet.* **34,** 14–29.

Henrique, D., Adam, J., Myat, A., Chitnis, A., Lewis, J., and Ish-Horowicz, D. (1995). Expression of a Delta homologue in prospective neurons in the chick. *Nature* **375,** 787–790.

Hynes, R. O. (1987). Integrins: A family of cell surface receptors. *Cell* **4,** 549–554.

Hynes, R. O. (1992). Integrins: Versatility, modulation, and signaling in cell adhesion. *Cell* **69,** 11–25.

Jaffredo, T., Horwitz, A. F., Buck, C. A., Rong, P. M., and Dieterlen-Lievre, F. (1988). Myoblast migration specifically inhibited in the chick embryo by grafted CSAT hybridoma cells secreting an anti-integrin antibody. *Development* **103,** 431–446.

Copyright © 1998 by Academic Press. All rights of reproduction in any form reserved.

Kaufman, M. H. (1992). "The Atlas of Mouse Development." Academic Press, San Diego, CA.

Kil, S. H., and Bronner-Fraser, M. (1996a). Expression of the avian a7-integrin in developing nervous system and myotome. *Int. J. Dev. Neurosci.* **14,** 181–190.

Kil, S. H., Lallier, T., Bronner-Fraser, M. (1996b). Inhibition of cranial neural crest adhesion *in vitro* and migration *in vivo* using integrin antisense oligonucleotides. *Dev. Biol.* **179,** 91–101.

Kozak, M. (1987). At least six nucleotides preceding the AUG initiator codon enhance translation in mammalian cells. *J. Mol. Biol.* **196,** 947–950.

Krotoski, D., Domingo, C., and Bronner-Fraser, M. (1986). Distribution of a putative cell surface receptor for fibronectin and laminin in the avian embryo. *J. Cell Biol.* **103,** 1061–1072.

Krull, C. E., Collazo, A., Fraser, S. E., and Bronner-Fraser, M. (1995). Segmental migration of trunk neural crest: Time-lapse analysis reveals a role for PNA-binding molecules. *Development* **121,** 3733–3743.

Krull, C. E., Lansford, R., Gale, N. W., Collazo, A., Marcelle, C., Yancopoulos, G., Fraser, S. E., and Bronner-Fraser, M. (1997). Interactions of Eph-related receptors and ligands confer rostrocaudal pattern to trunk neural crest migration. *Curr. Biol.* **7,** 571–580.

Kwee, L., Baldwin, H. S., Shen, H. M., Stewart, C. L., Buck, C., Buck, C. A., and Labow, M. A. (1995). Defective development of the embryonic and extraembryonic circulatory systems in vascular cell adhesion molecule (VCAM-1) deficient mice. *Development* **121,** 489–503.

Lallier, T., and Bronner-Fraser, M. (1992). $\alpha 1\beta 1$ integrin on neural crest cells recognizes some laminin substrata in a Ca^{2+}-dependent manner. *J. Cell Biol.* **119,** 1335–1345.

Lallier, T., and Bronner-Fraser, M. (1993). Inhibition of neural crest cell attachment by integrin antisense oligonucleotides. *Science* **259,** 692–695.

Lallier, T., Leblanc, G., Artinger, K. B., and Bronner-Fraser, M. (1992). Cranial and trunk neural crest cells use different mechanisms for attachment to extracellular matrices. *Development* **116,** 531–541.

Le Douarin, N. (1982). "The Neural Crest." Cambridge Univ. Press, Cambridge.

Loring, J. F., and Erickson, C. A. (1987). Neural crest cell migratory pathways in the trunk of the chick embryo. *Dev. Biol.* **121,** 220–236.

Mackie, E. J., Thesleff, I., and Chiquet-Ehrismann, R. (1987). Tenascin is associated with chondrogenic and osteogenic differentiation *in vivo* and promotes chondrogenesis *in vitro*. *J. Cell Biol* **105,** 2569–2579.

May, M. J., Entwistle, G., Humphries, M. J., and Ager, A. (1993). VCAM-1 is a CS1 peptide-inhibitable adhesion molecule expressed by lymph node high endothelium. *J. Cell Sci.* **106,** 109–119.

Miyake, K., Weissman, I. L., Greenberger, J. S., and Kincade, P. W. (1991). Evidence for a role of the integrin VLA-4 in lymphohemopoiesis. *J. Exp. Med.* **173,** 599–607.

Mould, A. P., Wheldon, L. A., Komoriya, A., Wayner, E. A., Yamada, K. M., and Humphries, M. J. (1990). Affinity chromatographic isolation of the melanoma adhesion receptor for the IIICS region of fibronectin and its identification as the integrin alpha 4 beta 1. *J. Biol. Chem.* **265,** 4020–4024.

Neugebauer, K. M., Emmett, C. J., Venstrom, K. A., and Reichardt, L. F. (1991a). Vitronectin and thrombospondin promote retinal neurite outgrowth: Developmental regulation and role of integrins. *Neuron* **6,** 345–358.

Neugebauer, K. M., and Reichardt, L. F. (1991b). Cell-surface regulation of β_1-integrin activity on developing retinal neurons. *Nature* **350,** 68–71.

Neuhaus, H., Hu, M. C., Hemler, M. E., Takada, Y., Holzmann, B., and Weissman, I. L. (1991). Cloning and expression of cDNAs for the alpha subunit of the murine lymphocyte–Peyer's patch adhesion molecule. *J. Cell Biol.* **115,** 1149–1158.

Newgreen, D. F., and Theiry, J. P. (1980). Fibronectin in early avian embryos: Synthesis and distribution along the migration pathways of neural crest cells. *Cell Tissue Res.* **211,** 269–291.

Nichols, D. H. (1986). Formation and distribution of neural crest mesenchyme to the first pharyngeal arch region of the mouse embryo. *Am. J. Anat.* **176,** 221–231.

Noden, D. M. (1983). The role of the neural crest in patterning of avian cranial skeletal, connective, and muscle tissues. *Dev. Biol.* **96,** 144–165.

Olsson, L., Svensson, K., and Perris, R. (1996). Effects of extracellular matrix molecules on subepidermal neural crest cell migration in wild type and white mutant (dd) axolotl embryos. *Pigment Cell Res.* **9,** 18–27.

Perris, R., Krotoski, D., and Bronner-Fraser, M. (1991b). Collagens in avian neural crest development: Distribution *in vivo* and migration-promoting ability *in vitro*. *Development* **113,** 969–984.

Poole, T. J., and Thiery, J. P. (1986). Antibodies and synthetic peptides that block cell–fibronectin adhesion arrest neural crest migration in vivo. *In* "Progress in Developmental Biology." Al. R. Liss, New York.

Rickman, T. P., Le Douarin, N. M., and Keynes, R. J. (1985). The migration of neural crest cells and the growth cones of motor axons through the rostral half of the chick somite. *J. Embryol. Exp. Morphol.* **90,** 437–455.

Rovasio, R., Delouvee, A., Timpl, R., Yamada, K., and Thiery, J. P. (1983). In vitro avian neural crest cell adhesion and migration: Requirement for fibronectin in the extracellular matrix. *J. Cell Biol.* **96,** 462–473.

Ruegg, C., Postigo, A. A., Sikorsk, E. E., Butcher, E. C., Pytela, R., and Erle, D. J. (1992). Role of integrin alpha 4 beta 7/alpha 4 beta P in lymphocyte adherence to fibronectin and VCAM-1 and in homotypic cell clustering. *J. Cell Biol* **117,** 179–189.

Sambrook, J., Fritsch, E. F., and Maniatis, T. (1989). Molecular Cloning, 2nd ed. Cold Spring Harbor Laboratory Press, Cold Spring Harbor, NY.

Sanes, J. R. (1989). Extracellular matrix molecules that influence neural development. *Annu. Rev. Neurosci.* **12,** 491–516.

Schwartz, M. A., Schaller, M. D., and Ginsberg, M. H. (1995). INTEGRINS: Emerging paradigms of signal transduction. *Annu. Rev. Cell Dev. Biol.* **11,** 549–599.

Serbedzija, G. N., Bronner-Fraser, M., and Fraser, S. E. (1992). Vital dye analysis of cranial neural crest cell migration in the mouse embryo. *Development* **116,** 297–307.

Serbedzija, G. N., Fraser, S. E., and Bronner-Fraser, M. (1989). A vital dye analysis of the timing and pathways of avian trunk neural crest cell migration. *Development* **106,** 809–816.

Sheppard, A. M., Onken, M. D., Rosen, G. D., Noakes, P. G., and Dean, D. C. (1994). Expanding roles for alpha 4 integrin and its ligands in development. *Cell Adhes. Commun.* **2,** 27–43.

Spiegelman, B. M., and Ginty, C. A. (1983). Fibronectin modulation of cell shape and lipogenic gene expression in 3T3-adipocytes. *Cell* **35,** 657–666.

Copyright © 1998 by Academic Press. All rights of reproduction in any form reserved.

Stepp, M. A., Urry, L. A., and Hynes, R. O. (1994). Expression of alpha 4 integrin mRNA and protein and fibronectin in the early chicken embryo. *Cell Adhes. Commun.* **2,** 359–375.

Studer, M., Lumsden, A., Ariza-McNaughton, L., Bradley, A., and Krumlauf, R. (1996). Altered segmental identity and abnormal migration of motor neurons in mice lacking Hoxb-1. *Nature* 630–634.

Takada, Y., Elices, M. J., Crouse, C., and Hemler, M. E. (1989). The primary structure of the alpha 4 subunit of VLA-4: Homology to other integrins and a possible cell–cell adhesion function. *EMBO J.* **8,** 1361–1368.

Teague, T. K., Lazarovits, A. T., and Mcintyre, B. W. (1994). Integrin $\alpha_4\beta_7$ co-stimulation of human peripheral blood T cell proliferation. *Cell Adhes. Commun.* **2,** 539–547.

Teillet, M. A., Kalcheim, C., and Le Douarin, N. M. (1987). Formation of the dorsal root ganglia in the avian embryo: Segmental origin and migratory behavior of neural crest progenitor cells. *Dev. Biol.* **120,** 329–347.

Thiery, J. P., Duband, J. L., Rutishauser, U., and Edelman, G. M. (1982). Cell adhesion molecules in early chicken embryogenesis. *Proc. Natl. Acad. Sci. USA* **79,** 6737–6741.

Tucker, G. C., Aoyama, H., Lipinski, M., Turz, T., and Thiery, J. P. (1984). Identical reactivity of monoclonal antibodies HNK-1 and NC-1: Conservation in vertebrates on cells derived from neural primordium and on some leukocytes. *Cell Differ.* **14,** 223–230.

Umbhauer, M., Riou, J. F., Smith, J., C., and Boucaut, J. C. (1994). Control of somitic expression of tenascin in *Xenopus* embryos by myogenic factors and Brachyury. *Dev. Dyn.* **200,** 269–277.

Vincent, M., and Thiery, J. P. (1984). A cell surface marker for neural crest and placodal cells: Further evolution in peripheral and central nervous system. *Dev. Biol.* **103,** 468–481.

von der Mark, K., and Ocalan, M. (1989). Antagonistic effects of laminin and fibronectin on the expression of the myogenic phenotype. *Differentiation* 150–157.

Wayner, E. A., Garcia-Pardo, A., Humphries, M. J., McDonald, J. A., and Carter, W. G. (1989). Identification and characterization of the T lymphocyte adhesion receptor for an alternative cell attachment domain (CS-1) in plasma fibronectin. *J. Cell Biol.* **109,** 1321–30.

West, C. M., Lanza, R., Rosenbloom, J., Lowe, M., Holtzer, H., and Avdalovic, N. (1979). Fibronectin alters the phenotypic properties of cultured chick embryo chondroblasts. *Cell* **17,** 491–501.

Wilkinson, D. (Ed.) (1992). "In Situ Hybridisation: A Practical Approach." IRL Press, Oxford.

Yabkowitz, R., Dixit, V. M., Guo, N., Roberts, D. D., and Shimizu, Y. (1993). Activated T-cell adhesion to thrombospondin is mediated by the alpha 4 beta 1 (VLA-4) and alpha 5 beta 1 (VLA-5) integrins. *J. Immunol.* **151,** 1–14.

Yang, J. T., Rayburn, H., and Hynes, R. O. (1993). Embryonic mesodermal defects in α5 integrin-deficient mice. *Development* **119,** 1093–1105.

Yang, J. T., Rayburn, H., and Hynes, R. O. (1995). Cell adhesion events mediated by α4 integrins are essential in placental and cardiac development. *Development* **121,** 549–560.

Yang J. T., Cardarelli, P. M., Lehnert, K., Rowland, S., and Krissansen, G. W. (1996) Fibronectin receptor functions in embryonic cells deficient in alpha 5 beta 1 integrin can be replaced by alpha V integrins. *Mol. Biol. Cell.* **7,** 1737–1748.

Received for publication April 20, 1998
Revised June 11, 1998
Accepted June 12, 1998

Copyright © 1998 by Academic Press. All rights of reproduction in any form reserved.

DEVELOPMENTAL BIOLOGY 202, 43–55 (1998)
ARTICLE NO. DB988988

Roles of Transforming Growth Factor-α and Epidermal Growth Factor in Chick Limb Development

Caroline N. Dealy, Victoria Scranton, and Hsu-Chen Cheng

Department of Anatomy, University of Connecticut Health Center, Farmington, Connecticut 06030

We have examined the distribution of transforming growth factor-α (TGF-α), epidermal growth factor (EGF), and the chicken EGF receptor (c-*erbB*), in embryonic chick limbs. Prior to limb budding, TGF-α is present in prospective limb-forming mesoderm and in prospective apical ectodermal ridge (AER)-forming ectoderm, but is not detected in non-limb-forming flank mesoderm or ectoderm, nor in presumptive non-AER-forming limb ectoderm, suggesting possible roles in initial limb formation and AER induction. Consistent with this possibility, TGF-α is present in the mesoderm of the wing buds of the amelic chick mutants *limbless* and *wingless*, which form and bud normally, but is absent from *limbless* and *wingless* ectoderm, which fails to form an AER. TGF-α and EGF are present in the AER of the developing limb, and TGF-α, EGF, and c-*erbB* are present in the underlying subridge mesoderm, suggesting possible roles in reciprocal AER/subridge mesoderm interactions required for limb outgrowth. We found that exogenous TGF-α and EGF can promote the outgrowth of limb mesoderm in the absence of the AER *in vitro* and can also promote the outgrowth of *limbless* and *wingless* wing bud explants. EGF is present in ventral but not dorsal limb ectoderm, suggesting a role for EGF in specification of ventral ectoderm. TGF-α and EGF are not detected in the differentiating cartilaginous elements or muscle primordia of the limb, suggesting that cessation of TGF-α and EGF expression may be required for cartilage and muscle formation. We have found that exogenous TGF-α and EGF inhibit chondrogenesis and myogenesis of limb mesenchyme *in vitro*. Together these results indicate that signaling through the EGF receptor via endogenous TGF-α and EGF may be important for initial limb formation, AER induction, outgrowth of limb mesoderm, and regulation of limb chondrogenic and myogenic differentiation. © 1998 Academic Press

Key Words: limb formation; limb development; TGF-α; EGF.

INTRODUCTION

The developing chick limb bud provides a readily manipulable system for studying the roles of molecules potentially involved in inductive tissue interactions, as well as factors important in the regulation of the differentiation of various cell types. The vertebrate limb initially forms as a consequence of a series of inductive interactions between the medial and lateral tissues of the embryo (Stephens *et al.*, 1991), leading to local proliferation and subsequent outgrowth of limb mesoderm from discrete regions of the lateral plate. Early limb mesoderm induces the overlying limb epithelium to form a specialized thickened structure, the apical ectodermal ridge (AER) (Zwilling, 1961; Saunders, 1977), which maintains the subridge mesoderm in a labile, undifferentiated, and proliferative state (Kosher *et al.*, 1979) while promoting proximodistal limb outgrowth (Saunders, 1948). As the cells of the subridge mesoderm leave the influence of the AER, they differentiate to form the various structures of the limb, including the cartilaginous skeletal elements and muscle masses.

The epidermal growth factor (EGF) family of signaling molecules includes epidermal growth factor (EGF; reviewed in Carpenter and Cohen, 1990) and transforming growth factor-α (TGF-α; reviewed in Derynck, 1992), which are ligands for the tyrosine kinase EGF receptor encoded by the *erbB*1 gene (Olofsson *et al.*, 1986). EGF family members are widely expressed in a variety of species and have been suggested to have roles not only in cell proliferation but also in cell determination and survival. In *Drosophila*, there is a single EGF receptor (EGFR; Price *et al.*, 1989), for which three EGF-like ligands (*gurken*, Neuman-Silberberg and

0012-1606/98 $25.00
Copyright © 1998 by Academic Press
All rights of reproduction in any form reserved.

Schüpbach, 1993; *spitz*, Rutledge *et al.*, 1992; and *vein*, Schnepp *et al.*, 1996) have been identified. The *Drosophila* EGFR has a remarkable number of roles in fly development (Simcox, 1997) and is required for the growth of wing imaginal discs and differentiation of wing cell types (Clifford and Schüpbach, 1989; Díaz-Benjumea and García-Bellido, 1990). During vertebrate development, the EGFR, EGF, and TGF-α are expressed in the embryo at sites of epithelial mesenchymal interactions, such as in the developing otic vesicle, craniofacial primordia, lung, kidney, and limbs (Kronmiller *et al.*, 1991a; Salido *et al.*, 1991; Canoun *et al.*, 1993; Díaz-Ruiz *et al.*, 1993; Huang *et al.*, 1996), and functional studies have implicated the EGFR and its ligands in inductive tissue interactions during lung branching, tooth formation, mandibular morphogenesis, and differentiation of palatal shelf epithelia (Partanen, 1990; Kronmiller *et al.*, 1991b; Dixon and Ferguson, 1992; Warburton *et al.*, 1992; Barros *et al.*, 1995). In the present study we describe the patterns of expression of the EGFR, and of its ligands EGF and TGF-α, in the developing chick limb bud and report effects of exogenous application of TGF-α and EGF on limb morphogenesis and mesenchymal cell differentiation *in vitro*. Our results suggest TGF-α and EGF may play important roles in limb formation, outgrowth, and cytodifferentiation.

MATERIALS AND METHODS

Immunohistochemistry. For TGF-α immunostaining, tissues were fixed either in Bouin's fixative or in 95% ethanol/10% formaldehyde/5% acetic acid, embedded in paraffin, and sectioned at 10 μm. Sections were deparaffinized in xylene and hydrated through graded alcohols, followed by blocking with 0.1% BSA, 5% horse serum and 0.05% Triton X-100 for 30 min. Sections were then incubated for 1 h with 1 μg/ml of monoclonal anti-human TGF-α (Calbiochem No. GF10) as a primary antibody. This antibody has been previously shown to recognize chick, rat, and human TGF-α (Díaz Ruiz *et al.*, 1993; Chia *et al.*, 1995) and does not exhibit any cross-reactivity with human or mouse EGF. Sections were incubated with biotinylated secondary antibody for 1 h, followed by a 1-h incubation with avidin/alkaline phosphatase (ABC-AP) enzyme complex. TGF-α-positive staining was revealed using BCIP/NBT substrate (Boehringer-Mannheim). Positive control sections of Day 11 embryonic chick mesonephros showed specific staining in alternate cells of the distal tubules, while proximal tubules and glomeruli were negative (not shown) as previously described (Díaz Ruiz *et al.*, 1993). Negative control sections of chick limbs treated with mock-primary antibody or incubated with normal rabbit serum (diluted 1:100) instead of primary antibody (not shown) showed no positive staining.

The procedure for EGF immunostaining was the same except tissues were fixed in 4% paraformaldehyde instead of Bouin's. Following quenching in 2% hydrogen peroxide, sections were incubated for 30 min in blocking solution (0.1% BSA, 1.5% goat serum, and 0.05% Triton X-100) and then for 1 h in 10 μg/ml primary antibody (rabbit polyclonal anti-mouse EGF; Upstate Biotechnology No. 06102), which has been shown to recognize rat EGF without cross-reactivity to TGF-α. Following a 1-h incubation with biotinylated secondary antibody, sections were incubated for 1 h with avidin/horseradish peroxidase (ABC Elite) enzyme complex. EGF-positive staining was revealed using DAB substrate (Vector). Negative control sections showed no positive staining (not shown).

In situ hybridization. *In situ* hybridization on Bouin's-fixed tissue sections was performed as described (Coelho *et al.*, 1991). Chicken c-*erbB* cDNA (Lax *et al.*, 1988), which corresponds to the chicken EGFR gene (Olofsson *et al.*, 1986), was generously provided by Dr. Bjorn Vennstrom. A cDNA probe for hybridization was prepared by digesting the c-*erbB* clone with *Sst*I and *Eco*RI, releasing the 3.4-kb insert. Hybridization probes for chicken *FGF8*, *FGF4*, *BMP4*, and *sonic hedgehog* cDNAs were obtained and prepared as described (Dealy, 1997). Chicken *BMP2* cDNA (Francis *et al.*, 1994) was generously provided by Dr. Phillipa Francis-West, and a specific cDNA probe for hybridization was prepared using *Hin*dIII digestion of chick *BMP2* cDNA to release the 947-bp insert. The chick *Msx2* and *Wnt7a* cDNA probes were prepared as described (Coelho *et al.*, 1991; Dealy *et al.*, 1993). Probes were labeled with [^{33}P]dCTP by random primer procedure.

Organ culture. Organ culture of stage 25 distal wing tips and stage 20/21 whole *limbless* and *wingless* wing buds on serum-free nutrient agar substrates was performed as described (Dealy and Kosher, 1995, 1996a). Cultures were either unsupplemented or supplemented with 50 ng/ml (8×10^{-7} M) of recombinant human EGF (R&D) or 50 ng/ml (1×10^{-8} M) of recombinant human TGF-α (R&D). Cell proliferation in cultured explants was examined as described (Dealy and Kosher, 1995) by immunohistochemical analysis of the incorporation of 5-bromodeoxyuridine (BrdU) into nuclei engaged in DNA synthesis during a 1 hour labeling period.

Micromass cultures. High-density micromass cultures were prepared from the mesenchymal cells composing the distal subridge region of stage 25 wing buds or from whole stage 23 wing buds as previously described (Gay and Kosher, 1984). Cultures were maintained in a 4:1 dilution of Ham's F12 medium containing 5% FBS and conditioned medium from NS1 cells (Developmental Studies Hybridoma Bank) and were either unsupplemented or supplemented with 5 ng/ml (8×10^{-8} M) EGF or 5 ng/ml TGF-α (1×10^{-9} M). The culture medium was changed daily. Micromass cultures from stage 25 wing tips, which contain a homogeneous population of chondrogenic precursors (Gay and Kosher, 1984), were assayed for differentiation into cartilage using Alcian blue (pH 1.0) staining on Day 4 as described (Yamada, 1970). Micromass cultures from stage 23 whole wing buds, which contain a heterogeneous cell population, were stained with a muscle-specific antibody against myosin protein (mouse monoclonal anti-chick fast myosin light chain, F310; kindly provided by Dr. Frank Stockdale) on Day 3 to reveal myogenic cells as described (Crow *et al.*, 1983; Kosher and Rodgers, 1987).

RESULTS

Distribution of TGF-α, EGF, and c-erbB during Limb Initiation

At stage 16, just prior to initial limb budding and before AER formation, TGF-α immunoreactive material is present in high amounts in the mesoderm of the prospective wing (not shown) and leg (Fig. 1A) forming regions of the lateral plate. Intense TGF-α immunoreactivity is also found in the ectoderm overlying the prospective limb mesoderm that will subsequently give rise to the AER (Michaud *et al.*, 1997). Relatively little TGF-α is detected in prospective

Copyright © 1998 by Academic Press. All rights of reproduction in any form reserved.

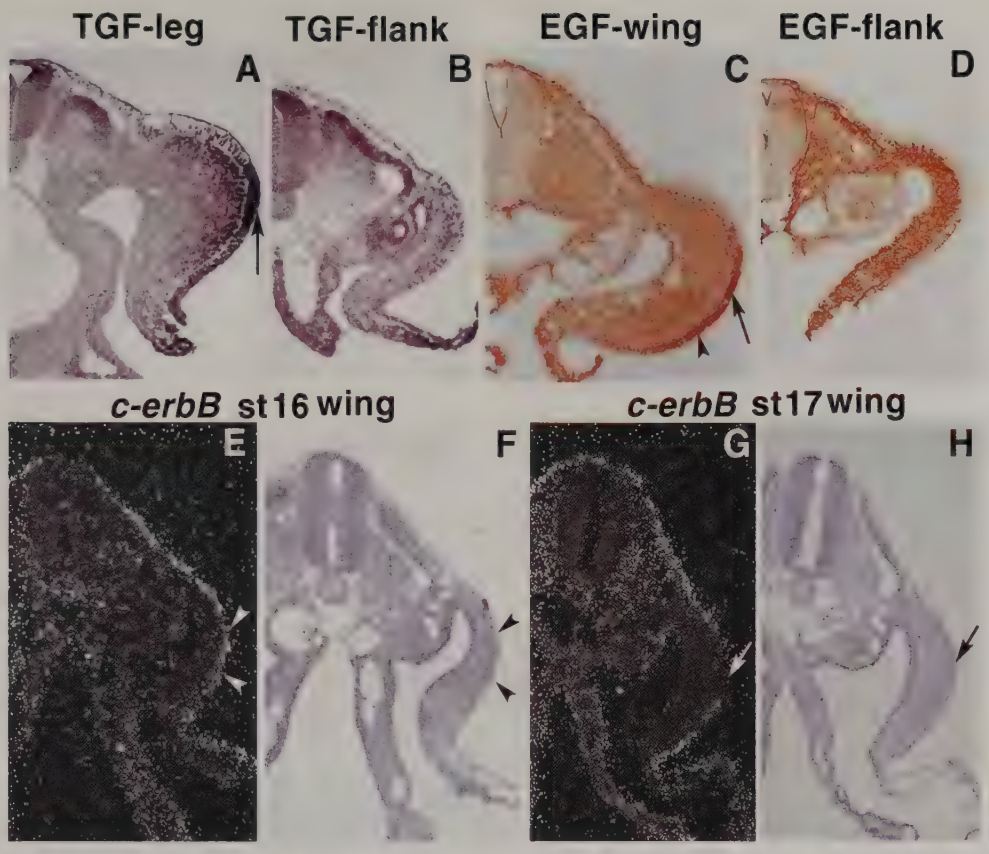

FIG. 1. (A–D) TGF-α (A,B) and EGF (C,D) immunostaining in sections of stage 16 presumptive leg-forming (A), wing-forming (C), and flank-forming (B,D) regions of the embryonic lateral plate. Note the presence of abundant TGF-α in the mesoderm of the prospective leg-forming (A) regions but not in the prospective non-limb-forming flank (B). Note also the intense TGF-α immunoreactivity in the prospective AER-forming ectoderm overlying the prospective leg-forming (A) mesoderm (arrow in A), while relatively little TGF-α is detected in the prospective non-ridge dorsal or ventral limb ectoderm. Little TGF-α is observed in the mesoderm or ectoderm of the non-limb-forming flank (B). In contrast to TGF-α, EGF immunoreactive material is fairly uniformly distributed throughout the mesoderm of the prospective wing-forming (C) and flank-forming (D) regions. Note the presence of EGF immunostaining in the lateral plate ectoderm overlying the prospective wing-forming (C) regions, particularly in the portions of the ectoderm that will become AER (arrow in C) and ventral limb ectoderm (arrowhead in C). Little EGF immunoreactivity is present in the ectoderm overlying the non-limb-forming flank (D). (E–H) *In situ* hybridization analysis of the expression of c-*erbB* mRNA in sections of stage 16 (E,F) and stage 17 (G,H) prospective wing-forming regions of the embryonic lateral plate (dark field, E,G; bright field, F,H). At stage 16, note the expression of high amounts of c-*erbB* mRNA by the entire ectoderm overlying the prospective wing-forming region (arrowheads in E and F). However, at stage 17 c-*erbB* expression attenuates in the portion of the overlying the early budding limbs that will form the AER (arrows in G and H). In other regions of the stage 16 embryonic trunk, TGF-α and EGF are present in the dorsal neural tube/neural crest and dermomyotome. TGF-α is also present in rostral mesonephros, while EGF is abundant in sclerotome. Neither TGF-α nor EGF are detectable in the notochord. c-*erbB* mRNA is expressed by trunk surface ectoderm, dermomyotome and sclerotome, and splanchnic mesoderm. Note that c-*erbB* mRNA is also expressed by the notochord despite the absence of either TGF-α or EGF protein; while little or no c-*erbB* mRNA is detectable in dorsal neural tube although both ligands are present.

nonridge limb ectoderm. Little TGF-α is observed in the mesoderm or ectoderm of the non-limb-forming flank regions of the lateral plate (Fig. 1B). In contrast to TGF-α, EGF-immunoreactive material is fairly uniformly distributed throughout the mesoderm of the prospective wing (Fig. 1C), leg (not shown), and flank (Fig. 1D) regions of the stage 16 lateral plate. EGF is also present in the lateral plate ectoderm overlying the prospective wing- and leg-forming regions, particularly in the portions of the ectoderm that will become AER and ventral limb ectoderm (Fig. 1C). Little

Copyright © 1998 by Academic Press. All rights of reproduction in any form reserved.

EGF is present in flank ectoderm (Fig. 1D). c-*erbB*, which encodes the chicken EGF receptor (Olofsson *et al.*, 1986) is expressed in high amounts by the ectoderm and in low amounts by the mesoderm of the entire embryonic trunk lateral plate at stage 16, including both prospective limb-forming (Fig. 1E,F) and non-limb-forming regions (not shown). At stage 17, c-*erbB* expression attenuates in the nascent AER overlying the early budding limbs (Figs. 1G and 1H), but continues to be expressed by dorsal and ventral limb ectoderm (Figs. 1G and 1H) and throughout the non-limb-forming flank ectoderm (not shown).

In other regions of the stage 16 embryonic trunk (Fig. 1), TGF-α and EGF are present in the dorsal neural tube/neural crest and dermomyotome (but not differentiated myotome). TGF-α is present in rostral mesonephros, while EGF is abundant in sclerotome. Neither TGF-α nor EGF are detectable in the notochord. c-*erbB* mRNA is expressed in the surface ectoderm of the trunk, dermomyotome and sclerotome, and splanchnic mesoderm. c-*erbB* mRNA is also expressed by the notochord despite the absence of either TGF-α or EGF protein and is not detectable in dorsal neural tube although both ligands are present.

Distribution of TGF-α, EGF, and c-erbB during Normal Limb Outgrowth

TGF-α (Figs. 2A and 2B) and EGF (Figs. 2C–2E) are present in the AER and the mesoderm directly subjacent to the AER between stage 18 and 25 when the AER is directing the proliferation and outgrowth of the limb. Little TGF-α is present in the dorsal or ventral nonridge limb ectoderm (Figs. 2A and 2B). In contrast, EGF protein is abundant in ventral but not dorsal ectoderm up to about stage 22 (Fig. 2C). EGF becomes restricted to the apical portion of the AER cells after stage 20, when the AER becomes pseudostratified (Todt and Fallon, 1984) (Figs. 2D and 2E). An apical localization of EGF has also been noted in kidney epithelial cells (Dempsey *et al.*, 1997). TGF-α (Fig. 2B) and EGF (Fig. 2D) are absent from the proximal central core of the limb coincident with the onset of chondrogenic differentiation, and from the most proximal dorsal and ventral myogenic regions where overt muscle differentiation is occurring. TGF-α and EGF protein are not detected in differentiated cartilage and muscle at stage 31 (not shown). c-*erbB* is expressed at low levels throughout the limb mesoderm at stages 18–25 (Figs. 2F–2H). c-*erbB* is also expressed in higher amounts by nonridge dorsal and ventral limb ectoderm but is not expressed by the mature AER (Figs. 2F and 2H). Little c-*erbB* is detected in the proximal central chondrogenic region of the limb at stage 25, but c-*erbB* is expressed in dorsal and ventral regions that are undergoing myogenesis (Fig. 2H). At stage 31 (not shown), c-*erbB* is expressed in limb mesoderm and ectoderm but is excluded from differentiated cartilage elements.

Distribution of TGF-α, c-erbB in Limbless and Wingless Limb buds

In contrast to normal limb buds in which TGF-α is present in the AER (Figs. 3A and 3C), little detectable TGF-α is present in the ectoderm of *limbless* (Figs. 3B and 3D) or *wingless* (not shown) mutant limb buds. However, TGF-α is present in the mesoderm of *limbless* (Fig. 3B) and *wingless* (not shown) limb buds at levels comparable to those in normal limb buds (Fig. 3A) during initial limb budding. In contrast to TGF-α, EGF is present in both ectoderm and mesoderm of *limbless* (Fig. 3F) and *wingless* (not shown) wing buds in amounts comparable to those in normal limb buds (Fig. 3E) during their formation. However, by stage 21, EGF staining is considerably reduced in the mesoderm of *wingless* (Fig. 3H) and *limbless* (not shown) wing buds compared to normal mesoderm (Fig. 3G), although EGF persists in stage 21 *wingless* (Fig. 3H) and *limbless* (not shown) ectoderm. However, unlike the ventral ectoderm distribution of EGF observed in normal limb buds (Fig. 3G), EGF is found throughout the ectoderm of *wingless* (Fig. 3H) and *limbless* (not shown) buds. In normal wing buds (Fig. 3I,K), c-*erbB* is expressed by nonridge ectoderm but is excluded from the AER. In *limbless* (Figs. 3J and 3L) and *wingless* (not shown) wing buds, c-*erbB* is expressed in high amounts throughout the entire ectoderm, including the apical ectoderm that fails to form an AER. c-*erbB* is also expressed throughout both *limbless* (Figs. 3J and 3L), *wingless* (not shown), and normal (Figs. 3I and 3K) limb mesoderm.

Effects of Exogenous TGF-α and EGF on Limb Explants in Organ Culture

To examine the effects of TGF-α and EGF on proliferation and outgrowth of limb mesoderm in the absence of the AER, explants of the posterior two-thirds of the distal portion of stage 25 wing buds (Fig. 4), from which all ectoderm including the AER had been removed, were maintained in organ culture in a serum-free defined medium with and without TGF-α or EGF supplementation. Control explants cultured on unsupplemented medium for 2 days undergo little outgrowth and exhibit little cell proliferation (Fig. 4A). However, in the presence of TGF-α (Fig. 4B) or EGF (Fig. 4C) these explants are larger and possess localized groups of proliferating cells. By Day 4 of culture, control explants have failed to grow out, forming compact rounded masses (Fig. 4D) which have uniformly differentiated into cartilage, as revealed by Alcian blue (pH 1.0) staining (not shown). However, explants of posterior mesoderm minus all ectoderm cultured in the presence of TGF-α (Fig. 4E) or EGF (Fig. 4F) possess obvious mesodermal cell outgrowths, which fail to stain with Alcian blue (not shown) and are thus likely undifferentiated.

To explore further the possible roles of TGF-α and EGF in limb outgrowth and AER/subridge mesoderm interactions, we examined the effects of exogenous TGF-α and EGF on explants of the wing buds of the amelic chick mutants

Copyright © 1998 by Academic Press. All rights of reproduction in any form reserved.

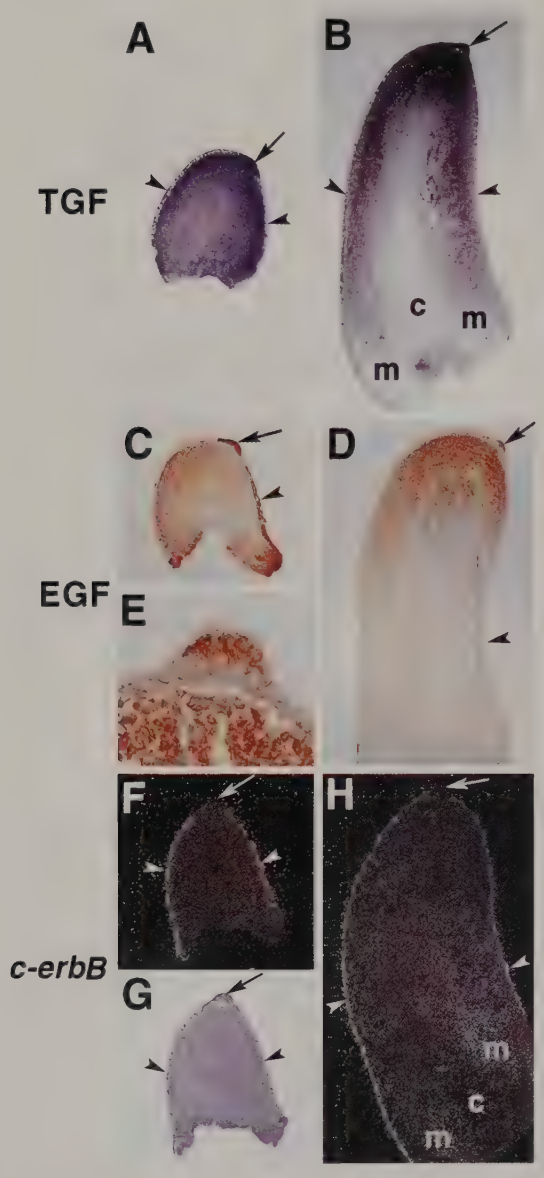

FIG. 2. (A–E) TGF-α (A,B) and EGF (C–E) immunostaining in sagittal sections of stage 19 (A,C) and stage 25 (B–E) limb buds. High amounts of TGF-α are present throughout the AER (arrows in A and B) and the mesoderm directly subjacent to the AER. Little TGF-α is present in the dorsal or ventral nonridge limb ectoderm (arrowheads in A and B). Little TGF-α is detected in the proximal central chondrogenic core (c) and proximal dorsoventral myogenic regions (m) of the limb at stage 25 (B). EGF is also abundant in limb subridge mesoderm (C–E). At stage 19, EGF immunostaining is present throughout the AER (arrow in C) and in ventral ectoderm (arrowhead in C). At stage 25, EGF is restricted to the very distal edge of the AER (E, high magnification) and is no longer abundant in ventral ectoderm (arrowhead in D). Note also the absence of abundant EGF in the chondrogenic central core and dorsoventral myogenic regions of the limb at stage 25 (D). (F–H) *In situ* hybridization analysis of the expression of c-*erbB* mRNA in sections of sagittal stage 20 wing (F,G) and stage 25 leg (H) buds (dark field, F,H; bright field, G). c-*erbB* mRNA is expressed in low levels throughout limb mesoderm and in higher levels by the dorsal and ventral ectoderm (arrowheads) but is excluded from the AER (arrows). At stage 25 (H), little c-*erbB* mRNA is expressed in the proximal chondrogenic central core (c) of the limb, whereas c-*erbB* mRNA is expressed by the proximal dorsoventral myogenic regions (m).

limbless and *wingless*, which fail to grow out *in ovo* (Zwilling 1961; Carrington and Fallon, 1984, 1988) or *in vitro* (Dealy and Kosher, 1996a). *limbless* (Fig. 4G) and *wingless* (Fig. 4I) wing bud explants undergo little outgrowth and form small necrotic masses after 2 days of culture on control serum-free defined medium. However, contralateral *limbless* (Fig. 4H) and *wingless* (Fig. 4J) wing bud explants cultured in the presence of EGF (Figs. 4H and 4J) or TGF-α (not shown) undergo dramatic outgrowth, and the formerly thin apical ectoderms of the mutant wing bud explants thicken considerably. The overall morphology of mutant wing buds cultured in the presence of EGF (and TGF-α, not shown) resembles that of normal wing buds cultured on control medium (Fig. 4K).

To determine if the mutant wing bud explants cultured in the presence of TGF-α or EGF possess molecular characteristics of normal wing buds, we examined by in situ hybridization their expression of *Msx2, BMP2, BMP4, FGF8,* and *FGF4,* which are not expressed by the ectoderm of *limbless* (Coelho *et al.*, 1991; Grieshammer *et al.*, 1996; Noramly *et al.*, 1996; Ros *et al.*, 1996; Fig. 5A) and *wingless* (not shown and Fig. 5D) wing buds, and of *sonic hedgehog,* which is not expressed by the mesoderm of *limbless* (Grieshammer *et al.*, 1996; Noramly *et al.*, 1996; Ros *et al.*, 1996) or *wingless* (not shown) wing buds. We found that the thickened apical ectoderms of EGF-treated and TGF-α-treated (not shown) *limbless* and *wingless* wing bud explants express *Msx2* (Fig. 5B) and *BMP2* (Fig. 5E), similar to the expression of *Msx2* and *BMP2* by the AERs of normal wing bud explants cultured on control media (Figs. 5C and 5F). The AERs of normal control wing bud explants express *FGF8, FGF4,* and *BMP4,* and the mesoderm of normal control wing bud explants expresses *sonic hedgehog* (not shown). However, exogenous TGF-α and EGF were unable to induce expression of *FGF8, FGF4, BMP4,* and *sonic hedgehog* by *limbless* or *wingless* wing bud explants (not shown). Furthermore, *Wnt7a,* which is restricted to the dorsal ectoderm of normal stage 21 limb buds (Dealy *et al.*, 1993; Parr *et al.*, 1993), but which is expressed throughout the bidorsal ectoderm of stage 21 *limbless* (Grieshammer *et al.*, 1996; Ros *et al.*, 1996) and *wingless* (not shown) wing buds, continues to be expressed throughout the ectoderm of *wingless* and *limbless* wing bud explants cultured in the presence of TGF-α and EGF, including the thickened distal ectoderm (not

Copyright © 1998 by Academic Press. All rights of reproduction in any form reserved.

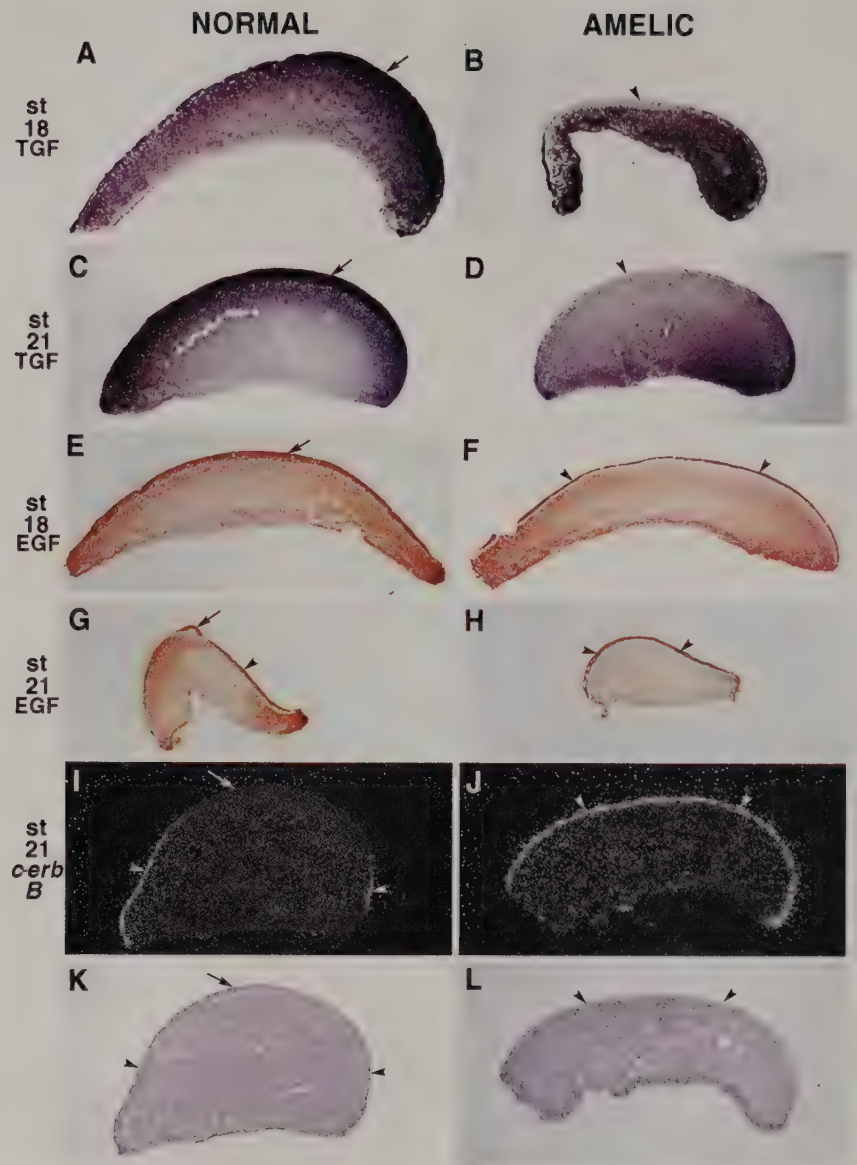

FIG. 3. (A–D) TGF-α immunostaining in frontal sections of normal (A,C) and *limbless* (B,D) wing (A,B) and leg (C,D) buds at stage 18 (A,B) and stage 21 (C,D). In contrast to normal limb buds (A,C) in which TGF-α is present in the AER (arrows in A and C), little or no TGF-α is detected in the distal apical ectoderm of *limbless* wing (B) and leg (D) buds (arrowheads in B and D) at stage 18 (B) or stage 21 (D). However, note that at stage 18, TGF-α is present in the mesoderm of *limbless* wing buds (B) at levels comparable to those in normal limb buds (A). By stage 21, the level of TGF-α is dramatically reduced in *limbless* mesoderm (D) compared to those in normal mesoderm (C). (E–H) EGF immunostaining in sections of normal (frontal, E; sagittal, G), *limbless* (frontal, F), and *wingless* (sagittal, G) wing buds at stage 19 (E,F) and stage 21 (G,H). EGF is present in the distal apical ectoderm of both *limbless* (F) and *wingless* (H) wing buds (arrowheads in F and H) in amounts comparable to those observed in the AER of normal wing buds (arrows in E and G) at both stage 19 (E,F) and stage 21 (G,H). However, unlike the ventral ectoderm distribution of EGF observed in normal wing buds (arrowhead in G), EGF is found throughout the ectoderm of *wingless* (H) and *limbless* (not shown) wing buds (arrowheads in H). EGF is also present in the mesoderm of *limbless* (F) and *wingless* (not shown) wing buds in amounts comparable to those in normal wing buds (E) at stage 19 (E,F), but is attenuated at stage 21 (H) compared to normal wing buds (G). (I–L) *In situ* hybridization analysis of expression of c-*erbB* mRNA in frontal sections of stage 20 normal (I,K) and *limbless* (J,L) wing buds (dark field, I,J; bright field, K,L). In normal wing buds (I,K), c-*erbB* mRNA is expressed by nonridge ectoderm (arrowheads) but is excluded from the AER (arrow). In *limbless* wing buds (J,L), c-*erbB* mRNA is expressed in high amounts throughout the entire nonridge ectoderm (arrowheads). c-*erbB* mRNA is also expressed at low levels throughout both *limbless* (J) and normal (I) mesoderm.

Copyright © 1998 by Academic Press. All rights of reproduction in any form reserved.

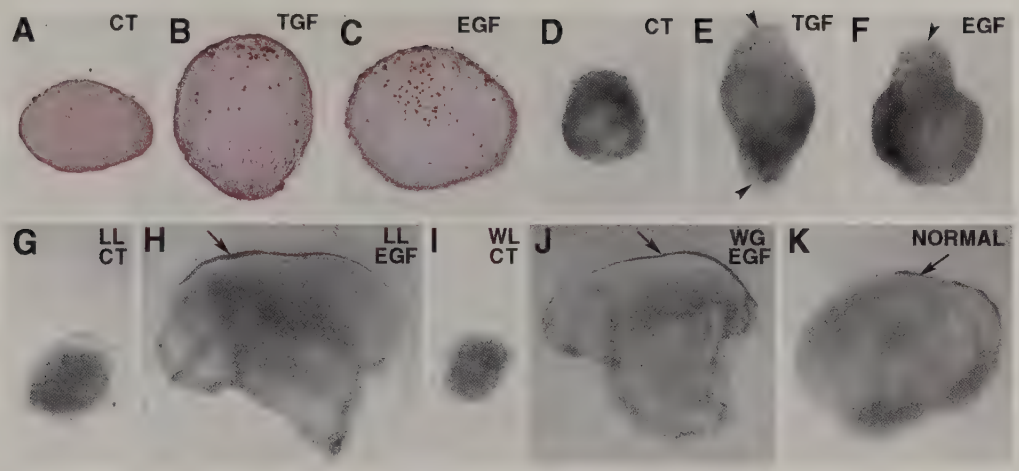

FIG. 4. (A–F) Explants of stage 25 posterior mesoderm minus all ectoderm cultured on control medium (A,D) or medium supplemented with 50 ng/ml TGF-α (B,E) or EGF (C,F) after 2 days (A–C) or 4 days (D–F). (A–C) Incorporation of immunohistochemically detectable BrdU into dividing cells. Control explants (A) undergo little outgrowth and possess few dividing cells, while TGF-α-treated (B) and EGF-treated (C) explants grow out and possess localized groups of proliferating cells. (D–F) Living explants. Control explants (D) form small compact masses, while explants treated with TGF-α (E) or EGF (F) are larger and possess outgrowths of mesodermal cells growing out from the central explant mass (arrowheads in E and F). (G–K) Living explants of stage 20/21 *limbless* (G,H), *wingless* (I,J), and normal (K) wing buds after 2 days of culture on control (G,I,K) medium or medium supplemented with 50 ng/ml EGF. Control *limbless* (G) and *wingless* (I) wing buds fail to grow out and form compact masses containing degenerative cells. In contrast, contralateral *limbless* (H) and *wingless* (J) wing buds cultured in the presence of EGF undergo considerable outgrowth, and their thin distal apical ectoderm thickens (arrows in H and J). The overall morphology of mutant buds cultured in the presence of EGF resembles that of normal wing buds cultured on control medium (K), which grow out and possess a thickened AER (arrow in K).

shown). We also found that the entire ectoderm, including the thickened distal ectoderm, of control and TGF-α- and EGF-treated *limbless* and *wingless* mutant explants continues to express c-*erbB* (not shown).

Effects of TGF-α and EGF on Chondrogenesis and Myogenesis in Vitro

The exclusion of TGF-α and EGF from regions of the limb undergoing chrondrogenesis and myogenesis suggests that cessation of EGF or TGF-α activity may be necessary for chondrogenesis and myogenesis to occur. To examine this possibility, the effects of TGF-α and EGF on chondrogenesis and myogenesis were examined in micromass cultures (Fig. 6) prepared from the mesodermal cells contained in the distal tip of stage 25 limb buds, which comprise a uniform population of chondrogenic precursors, or from whole stage 23 wing bud mesoderm, which contains a heterogenous mixture of cell types including myogenic precursors. After 4 days, control stage 25 micromass cultures uniformly differentiate into cartilage, as shown by staining with Alcian blue (Fig. 6A). However, cultures treated with TGF-α (Fig. 6B) and to a lesser extent with EGF (not shown) show little Alcian blue-positive staining. Similarly, after 3 days, control stage 23 micromass cultures contain abundant differentiated myocytes (Fig. 6D), as demonstrated by staining with a muscle specific monoclonal antibody F310 (Crow *et al.*, 1983), whereas cultures treated with TGF-α (Fig. 6E) and less dramatically with EGF (not shown) contain few positively stained myogenic cells.

DISCUSSION

Role of TGF-α in Limb Initiation

The presence of TGF-α in presumptive wing- and leg-forming regions of the lateral plate, but not in the non-limb-forming flank, suggests TGF-α may play a role in initial limb formation. Our studies on TGF-α expression in *limbless* and *wingless* mutant limb buds are also consistent with this possibility. Limb initiation occurs normally in *limbless* and *wingless* mutant embryos (Zwilling 1961; Carrington and Fallon, 1984, 1988), although *limbless* and *wingless* limb buds subsequently fail to develop an AER (Sawyer 1982; Carrington and Fallon, 1984, 1988). Thus molecules that may be involved in limb initiation would be expected to be expressed normally in *limbless* and *wingless* limb buds. Indeed, TGF-α is present in levels comparable to normal levels in the mesoderm of *limbless* and *wingless* limb buds during their initial formation, although it declines dramatically in the mutant distal mesoderm following budding.

Copyright © 1998 by Academic Press. All rights of reproduction in any form reserved.

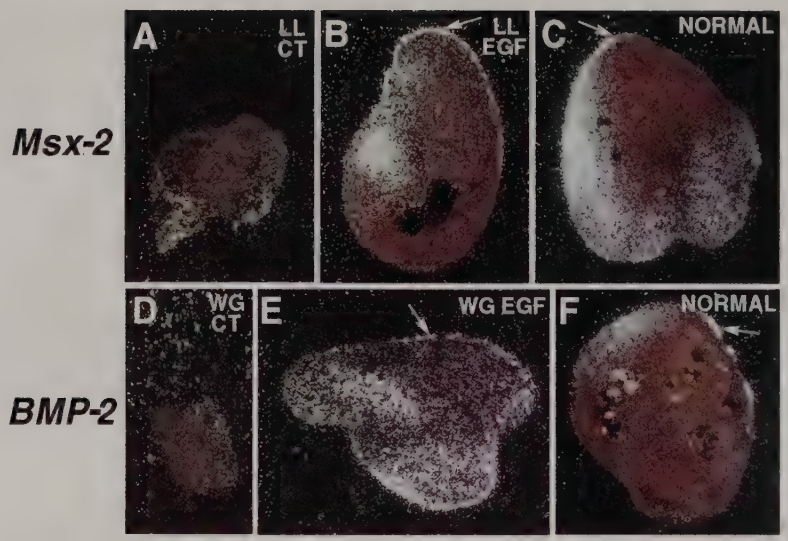

FIG. 5. *In situ* hybridization analysis of expression of *Msx2* (A–C) and *BMP2* (D–F) mRNA in frontal sections of explants of stage 20/21 *limbless* (A,B), *wingless* (D,E), and normal (C,F) wing buds cultured for 2 days on control medium (A,C,D,F) or medium supplemented with 50 ng/ml EGF (B,E). Control mutant wing bud explants undergo little outgrowth and their thin ectoderms do not express *Msx2* (A) or *BMP2* (D). In contrast, mutant wing bud explants cultured in the presence of EGF undergo considerable outgrowth and their thickened ectoderms express *Msx2* (arrow in B) and *BMP2* (arrow in E), similar to the expression of *Msx2* and *BMP2* by the AERs of normal wing bud explants cultured on control medium (arrows in C and F).

Recent studies have focused on FGF8 and FGF10 as endogenous limb inducing signals, based on their ability to induce ectopic limbs from the flank of chick embryos and on their pattern of expression in limb-forming but not non-limb-forming lateral plate (Crossley *et al.*, 1996; Vogel *et al.*, 1996; Ohuchi *et al.*, 1997). However, in transgenic mice in which FGF8/FGF10 signaling is disrupted by loss of FGFR2 binding, rudimentary limb buds are nonetheless observed to form (Xu *et al.*, 1998). That these rudimentary limb buds subsequently fail to grow out provides strong support for roles for FGF8/FGF10 in the reciprocal AER/subridge mesoderm interactions required for limb outgrowth. However, that even rudimentary limb buds form in the absence of FGF8/FGF10 signaling suggests the existence of other signals, possibly emanating from more axial tissues (Stephens *et al.*, 1991; Dealy, 1997; Fernandez-Teran *et al.*, 1997), that are sufficient to initiate limb bud formation. In this regard, IGF-I, which is expressed by axial tissues as well as by the limb-forming but not non-limb-forming lateral plate (Geduspan *et al.*, 1992; Streck *et al.*, 1992), can induce the formation of rudimentary limb buds from early limb-forming lateral plate prior to its acquisition of limb-forming ability and can also induce the formation of rudimentary limbs from the non-limb-forming flank (Dealy and Kosher, 1996b). The mitogenic response to EGF has been shown to depend on signaling through the receptor for IGF-I (Coppola *et al.*, 1994), and intracellular transactivation of the IGF-I receptor through the EGF receptor has been demonstrated *in vitro* (Burgaud and Baserga, 1996). EGF, TGF-α, FGFs, and IGF-I can act synergistically to promote cell proliferation (Krane *et al.*, 1991; Han *et al.*, 1992; Rosselot *et al.*, 1994; Onagbesan and Peddie, 1995; Simmons *et al.*, 1995) and can cross-induce each other's expression (Clemmons, 1984; Krane *et al.*, 1991; Baserga, 1993; Hana and Murphy, 1994; Simmons *et al.*, 1995; Vardy *et al.*, 1995). IGF-I activity is required for FGFs to promote limb outgrowth (Dealy *et al.*, 1996). Thus, perhaps TGF-α may act in concert with IGF-I or FGFs to promote initial limb formation.

Role of TGF-α and EGF in AER Formation and Patterning

Just prior to and during the initial formation of the limb bud, TGF-α is expressed in the portion of the ectoderm overlying the prospective limb-forming regions of the lateral plate that will specifically give rise to the AER (Michaud *et al.*, 1997). This suggests that TGF-α may have a role in determining specific regions of the limb-forming ectoderm that will become the AER. The presence of TGF-α in the presumptive and nascent AER is similar to that of *FGF8*, which has also been suggested to be a marker for acquisition of AER competence (Kuhlman and Niswander, 1997). The lack of abundant TGF-α protein in the distal apical ectoderm of *limbless* and *wingless* limb buds, which fail to form an AER (Sawyer, 1982; Carrington and Fallon,

Copyright © 1998 by Academic Press. All rights of reproduction in any form reserved.

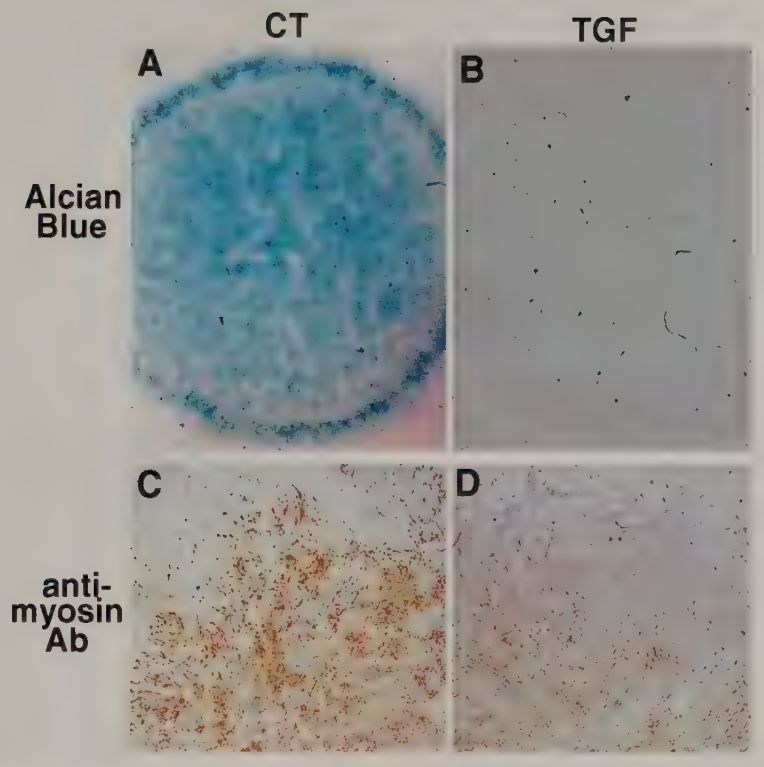

FIG. 6. Micromass cultures prepared from the mesodermal cells contained in the distal tip of stage 25 (A,B) or stage 23 (C,D) wing buds cultured in control medium (A,C) or medium supplemented with 5 ng/ml TGF-α (B,D) stained with Alcian blue (pH 1.0) after 4 days of culture (A,B) or with an anti-myosin antibody after 3 days of culture (C,D). Note that control stage 25 micromass cultures uniformly differentiate into cartilage, as revealed by intense Alcian blue staining (A), while cultures treated with TGF-α (B) show little Alcian blue-positive staining. Similarly, control stage 23 micromass cultures contain abundant differentiated myocytes, as demonstrated by staining with an anti-myosin antibody (C) whereas TGF-α-treated cultures (D) contain few positively stained myogenic cells.

1984, 1988) also supports a role for TGF-α in AER competence and formation.

Studies have suggested that positioning of the normal chick AER occurs along a dorsoventral ectodermal boundary (Altabef *et al.*, 1997), and that *limbless* limb buds, which fail to form an AER, lack this dorsoventral ectodermal boundary (Grieshammer *et al.*, 1996; Ros *et al.*, 1996). In the present study, we found that the dorsal ectoderm marker *Wnt7a* continues to be expressed throughout the ectoderm of *limbless* and *wingless* wing bud explants cultured in the presence of TGF-α and EGF. However, despite the continued absence of a dorsoventral ectodermal boundary, the distal apical ectoderms of the TGF-α- and EGF-treated *limbless* and *wingless* wing bud explants thicken considerably and express *Msx2* and *BMP2*, genes characteristically expressed by normal AERs which are not expressed by *limbless* or *wingless* ectoderms (Coelho *et al.*, 1991; Grieshammer *et al.*, 1996; Noramly *et al.*, 1996; Ros *et al.*, 1996; and not shown). Thus, at least some characteristics of normal AERs are restored to *limbless* and *wingless* mutant ectoderms by exogenous TGF-α and EGF.

TGF-α and EGF are present in the AER of the developing limb, and TGF-α, EGF, and c-*erbB* are present in the underlying subridge mesoderm, suggesting roles in the reciprocal interactions between the AER and the subridge mesoderm that are required for limb outgrowth. Since c-*erbB* is not expressed in the mature AER, it is likely that TGF-α and EGF do not act in an autocrine fashion on the AER itself, but rather act in a paracrine fashion on the underlying distal mesoderm. Consistent with this hypothesis, we found that exogenous TGF-α and EGF promote outgrowth of limb mesoderm in the absence of the AER *in vitro* and also promote outgrowth of *limbless* and *wingless* wing bud explants. In the present study, we found that the TGF-α and EGF initially present in the distal mesoderm of stage 18 *limbless* and *wingless* limb buds, which subsequently fail to form an AER, is dramatically attenuated by stage 21, indicating that maintenance of TGF-α and EGF in

Copyright © 1998 by Academic Press. All rights of reproduction in any form reserved.

the subridge mesoderm is AER-dependent. The low level of TGF-α and EGF protein present in stage 21 *limbless* and *wingless* distal mesoderm is apparently insufficient for mutant limb morphogenesis, since we found that exogenous TGF-α and EGF were required to promote outgrowth of *limbless* and *wingless* wing buds. Consistent with a role for TGF-α in AER activity, we found that TGF-α is absent from the distal ectoderm of *limbless* and *wingless* limb buds, which fail to grow out. However, unlike TGF-α, EGF is present in *limbless* and *wingless* ectoderm. The inability of endogenous EGF to promote outgrowth of mutant mesoderm and to induce expression of *Msx2* and *BMP2* in mutant ectoderm (see above) suggests that these activities may be mediated through the mesoderm. Alternately, it is possible that factors downstream of EGFR signaling are defective in *limbless* and *wingless* ectoderms.

Role of EGF in Limb Ventralization

The information that specifies limb dorsoventrality initially resides in presumptive limb mesoderm but is transferred to presumptive limb ectoderm by stage 16 (Geduspan and MacCabe, 1989). We have found that EGF is abundant in presumptive ventral but not dorsal limb ectoderm at stage 16 and in ventral but not dorsal limb ectoderm until stage 22, at which stage studies have demonstrated that limb ectoderm is no longer able to control the dorsoventral axis of the underlying limb mesoderm (MacCabe *et al.*, 1974). These observations suggest that EGF may play a role in specification of ventral limb ectoderm and possibly limb dorsoventrality. EGFR signaling has also been implicated in ventralization of *Drosophila* embryonic ectoderm (Raz and Shilo, 1993; Schweitzer *et al.*, 1995; Golembo *et al.*, 1996). The presence of EGF in *limbless* and *wingless* ectoderm, which is bidorsal (Abbott and Pisenti, 1993; Grieshammer *et al.*, 1996; Noramly *et al.*, 1996; Ros *et al.*, 1996), is consistent with our suggestion that *limbless* and *wingless* ectoderms may be defective in factors downstream of EGFR signaling.

TGF-α and EGF Inhibit Chondrogenesis and Myogenesis in Vitro

The AER maintains the mesoderm of the limb in a labile undifferentiated condition. When, as a result of proximodistal outgrowth, cells leave the influence of the AER, those cells located in the central core of the limb differentiate into cartilage, while those located along the dorsal and ventral periphery of the limb become muscle (Kosher *et al.*, 1979; Kosher and Rodgers, 1987). In the present study, we found that TGF-α, EGF, and c-*erbB* mRNA are present in the undifferentiated precursors located at the distal tip of the limb. However, TGF-α and EGF are absent from the central core of the limb where the cells are undergoing chondrogenic differentiation, and c-*erbB* mRNA is not expressed by the differentiated cartilage elements of the limb, suggesting that one of the functions of endogenous TGF-α and EGF present in limb subridge mesoderm may be to suppress the chondrogenic differentiation of these cells. In the present study we found that exogenous TGF-α and, to a lesser extent, EGF inhibit cartilage formation by limb mesenchymal cells in micromass culture. This hypothesis is further supported by other studies in which exogenous TGF-α and EGF were found to inhibit chondrogenesis of mandibular (Coffin-Collins and Hall, 1989) and hindlimb (Huang *et al.*, 1996) mesenchyme.

We have also found that TGF-α and EGF protein are no longer detected in regions of the limb that have undergone myogenic differentiation, and c-*erbB* mRNA becomes localized to the dorsal and ventral limb muscle masses coincident with their formation. Other studies have also reported a colocalization of the EGF receptor in developing embryonic muscle (Yamane *et al.*, 1997). In the present study, we found that exogenous TGF-α and, less dramatically, EGF inhibit myogenic differentiation of limb mesenchymal cells *in vitro*. These observations suggest that TGF-α and EGF may be negative regulators of myogenesis in the developing limb.

Possible Mechanisms and Functions of EGF Receptor Signaling

The distinct expression patterns of TGF-α and EGF in the limb suggest that endogenous TGF-α and EGF have different roles in limb development, despite their shared signaling through the same *erbB*1 EGF receptor. Specification of biological response to the EGFR may be regulated by differential ligand binding affinities (Lax *et al.*, 1988; Lipeski *et al.*, 1996), alternate intracellular routing and processing of ligand/receptor complexes (Korc *et al.*, 1987; Decker, 1990; Ebner and Derynck, 1991), and *erbB* receptor heterodimer formation (Olofsson *et al.*, 1986; Beerli and Hynes, 1996; Riese *et al.*, 1996; Lim *et al.*, 1997). Signaling through the EGF receptor can antagonize signaling through the receptor for members of the BMP family of signaling molecules (Kretzschmar *et al.*, 1997). BMPs are involved in many aspects of limb development and patterning (reviewed in Hogan, 1996) and can stimulate chondrogenic and myogenic differentiation (Asahina *et al.*, 1993; Schultheiss *et al.*, 1997). It is possible that one of the functions of EGF or TGF-α in the limb may be to oppose the activities of BMPs during limb outgrowth, patterning, or cytodifferentiation.

ACKNOWLEDGMENT

Supported by NIH Grant HD22610 to C.N.D.

REFERENCES

Abbott, U. K., and Pisenti, J. M. (1993). Making the connection: exploring classical concepts in normal and abnormal limb development using contemporary approaches. *Prog. Clin. Biol. Res.* **383A**, 99–112.

Copyright © 1998 by Academic Press. All rights of reproduction in any form reserved.

Altabef, M., Clarke, J. D. W., and Tickle, C. (1997). Dorso-ventral ectodermal compartments and origin of apical ectodermal ridge in developing chick limb. *Development* **124,** 4547–4556.

Asahina, I., Sampath, T. K., Nishimura, I., and Hauschka, P. V. (1993). Human osteogenic protein-1 induces both chondroblastic and osteoblastic differentiation of osteoprogenitor cells derived from newborn rat calvaria. *J. Cell Biol.* **123,** 921–933.

Barros, E. J. G., Santos, O. F. P., Matsumoto, K., Nakamura, T., and Nigam, S. K. (1995). Differential tubulogenic and branching morphogenetic activities of growth factors: Implications for epithelial tissue development. *Proc. Natl. Acad. Sci. USA* **92,** 4412–4416.

Baserga, R. (1993). Gene regulation by IGF-I. *Mol. Reprod. Dev.* **35,** 353–357.

Beerli, R. R., and Hynes, N. E. (1996). Epidermal growth factor-related peptides activate distinct subsets of ErbB receptors and differ in their biological activities. *J. Biol. Chem.* **271,** 6071–6076.

Burgaud, J-L., and Baserga, R. (1996). Intracellular transactivation of the insulin-like growth factor I receptor by an epidermal growth factor receptor. *Exp. Cell Res.* **223,** 412–419.

Canoun, C., Ma, C., Halpren, D., Shum, L., Bringas, P., Sank, A., and Slavkin, H. C. (1993). Endogenous epidermal growth factor regulates limb development. *J. Surg. Res.* **54,** 638–647.

Carrington, J. L., and Fallon, J. F. (1984). Evidence that the ectoderm is the affected germ layer in the *wingless* mutant chick embryo. *J. Exp. Zool.* **232,** 297–308.

Carrington, J. L., and Fallon, J. F. (1988). Initial limb budding is independent of apical ectodermal ridge activity: Evidence from a *limbless* mutant. *Development* **104,** 361–367.

Carpenter, G., and Cohen, S. (1990). Epidermal growth factor. *J. Biol. Chem.* **265,** 7709–7712.

Chia, C. M., Winston, R. M. L., and Handyside, A. H. (1995). EGF, TGF-α and EGFR expression in human preimplantation embryos. *Development* **121,** 299–307.

Clemmons, D. R. (1984). Multiple hormones stimulate the production of somatomedin by cultured human fibroblasts. *J. Clin. Endocrinol. Metab.* **58,** 850–856.

Clifford, R. T., and Schüpbach, T. (1989). Coordinately and differentially mutable activities of *torpedo*, the *Drosophila melanogaster* homolog of the vertebrate EGF receptor gene. *Genetics* **122,** 771–787.

Coelho, C. N. D., Krabbenhoft, K., Upholt, W. B., Fallon, J. F., and Kosher, R. A. (1991). Altered expression of the chicken homeobox-containing genes Ghox-7 and Ghox-8 in the limb buds of *limbless* mutant chick embryos. *Development* **113,** 1487–1493.

Coffin-Collins, P. A., and Hall, B. K. (1989). Chondrogenesis of mandibular mesenchyme from the embryonic chick is inhibited by mandibular epithelium and by epidermal growth factor. *Int. J. Dev. Biol.* **33,** 297–311.

Coppola, D., Ferber, A., Miura, M., Sell, C., D'Ambrosio, C., Rubin, R., and Baserga, R. (1994). A functional insulin-like growth factor I receptor is required for the mitogenic and transforming activities of the epidermal growth factor receptor. *Mol. Cell Bio.* **14,** 4588–4595.

Crossley, P. H., Minowada, G., MacArthur, C. A., and Martin, G. R. (1996). Roles for FGF8 in the induction, initiation, and maintenance of chick limb development. *Cell* **84,** 127–136.

Crow, M. T., Olson, P. S., and Stockdale, R. E. (1983). Myosin light chain expression during avian muscle development. *J. Cell Biol.* **96,** 736–744.

Dealy, C. N. (1997). Hensen's node provides an endogenous limb-forming signal. *Dev. Biol.* **188,** 216–223.

Dealy, C. N., and Kosher, R. A. (1995). Studies on insulin-like growth factor-I and insulin in chick limb morphogenesis. *Dev. Dyn.* **202,** 67–79.

Dealy, C. N., and Kosher, R. A. (1996a). IGF-I, insulin and FGFs induce outgrowth of the limb buds of amelic mutant chick embryos. *Development* **122,** 1323–1330.

Dealy, C. N., and Kosher, R. A. (1996b). IGF-I and insulin in the acquisition of limb-forming ability by the embryonic lateral plate. *Dev. Biol.* **177,** 291–299.

Dealy, C. N., Clarke, K., and Scranton, V. (1996). Ability of FGFs to promote the outgrowth and proliferation of limb mesoderm is dependent on IGF-I activity. *Dev. Dyn.* **206,** 463–469.

Dealy, C. N., Roth, A., Ferrari, D., Brown, A. M. C., and Kosher, R. A. (1993). *Wnt-5a* and *Wnt-7a* are expressed in the developing chick limb bud in a manner suggesting roles in pattern formation along the proximodistal and dorsoventral axes. *Mech. Dev.* **43,** 175–186.

Decker, S. J. (1990). Epidermal growth factor and transforming growth factor-α induce differential processing of the epidermal growth factor receptor. *Biochem. Biophys. Res. Comm.* **166,** 615–621.

Dempsey, P. J., Meise, K. S., Yoshitake, Y., Nishikawa, K., and Coffey, R. J. (1997). Apical enrichment of human EGF precurser in Madin-Darby canine kidney cells involves preferential basolateral ectodomain cleavage sensitive to a metalloproteinase inhibitor. *J. Cell Biol.* **138,** 747–758.

Derynck, R. (1992). The physiology of transforming growth factor-α. *Adv. Cancer Res.* **58,** 27–52.

Díaz-Benjumea, F. J., and García-Bellido, A. (1990). Behavior of cells mutant for an EGF receptor homolog of *Drosophila* in genetic mosaics. *Proc. R. Soc. Lond.* **242,** 36–44.

Díaz-Ruiz, C., Perez-Tomás, R., Cullere, X., and Domingo, J. (1993). Immunohistochemical localization of transforming growth factor-α and epidermal growth factor-receptor in the mesonephros and metanephros of the chicken. *Cell Tissue Res.* **271,** 3–8.

Dixon, M. J., and Ferguson, M. W. J. (1992). The effects of epidermal growth factor, transforming growth factors-alpha and -beta and platelet-derived growth factor on murine palatal shelves in organ culture. *Arch. Oral Biol.* **37,** 395–410.

Ebner, R., and Derynck, R. (1991). Epidermal growth factor and transforming growth factor-α: Differential intracellular routing and processing of ligand-receptor complexes. *Cell Regul.* **2,** 599–612.

Fernandez-Teran, M., Piedra, M. E., Simandl, B. K., Fallon, J. F., and Ros, M. A. (1997). Limb initiation and development is normal in the absence of the mesonephros. *Dev. Biol.* **189,** 246–255.

Francis, P. H., Richardson, M. K., Brickell, P. M., and Tickle, C. (1994). Bone morphogenetic proteins and a signalling pathway that controls patterning in the developing chick limb. *Development* **20,** 209–218.

Gay, S, W., and Kosher, R. A. (1984). Uniform cartilage differentiation in micromass cultures prepared from a relatively homogenous population of chondrogenic progenitor cells of the chick limb bud: Effects of prostoglandins. *J. Exp. Zool.* **232,** 317–326.

Grieshammer, U., Minowada, G., Pisenti, J. M., Abbott, U. K., and Martin, G. R. (1996). The chick *limbless* mutation causes abnormalities in limb bud dorsal–ventral patterning: Implications for the mechanism of apical ridge formation. *Development* **122,** 3851–3861.

Copyright © 1998 by Academic Press. All rights of reproduction in any form reserved.

Geduspan, J. S., and MacCabe, J. A. (1989). Transfer of dorsoventral information from mesoderm to ectoderm at the onset of limb development. *Anat. Rec.* **224,** 79–87.

Geduspan, J. S., Padanilam, B. J., and Solursh, M. (1992). Coordinate expression of IGF-I and its receptor during limb outgrowth. *Dev. Dyn.* **195,** 67–73.

Golembo, M., Raz, E., and Shilo, B-Z. (1996). The *Drosophila* embryonic midline is the site of Spitz processing, and induces activation of the EGF receptor in the ventral ectoderm. *Development* **122,** 3363–3370.

Han, V. K. M., Smith, A., Myint, W., Nygard, K., and Bradshaw, S. (1992). Mitogenic activity of epidermal growth factor on newborn rat astroglia: Interaction with insulin-like growth factors. *Endocrinology* **131,** 1134–1142.

Hana, V., and Murphy, L. J. (1994). Interdependence of epidermal growth factor and insulin- like growth factor-I expression in the mouse uterus. *Endocrinology* **135,** 107–112.

Hogan, B. L. M. (1996). Bone morphogenetic proteins: Multifunctional regulators of vertebrate development. *Genes Dev.* **10,** 1580–1594.

Huang, L., Solursh, M., and Sandra, A. (1996). The role of transforming growth factor alpha in rat craniofacial development and chondrogenesis. *J. Anat.* **189,** 73–86.

Korc, M., Haussler, C. A., and Trookman, N. S. (1987). Divergent effects of epidermal growth factor and transforming growth factors on a human endometrial carcinoma cell line. *Cancer Res.* **47,** 4909–4914.

Kosher, R. A., and Rodgers, B. J. (1987). Separation of the myogenic and chondrogenic progenitor cells of undifferentiated limb mesenchyme. *Dev. Biol.* **121,** 376–388.

Kosher, R. A., Savage, M. P., and Chan, S.-C. (1979). *In vitro* studies on the morphogenesis and differentiation of the mesoderm subjacent to the apical ectodermal ridge of the embryonic chick limb bud. *J. Embryol. Exp. Morph.* **50,** 75–97.

Krane, J. F., Murphy, D. P., Carter, D. M., and Krueger, J. G. (1991). Synergistic effects of epidermal growth factor (EGF) and insulin-like growth factor I/ somatomedin C (IGF-I) on keratinocyte proliferation may be mediated by IGF-I transmodulation of the EGF receptor. *J. Invest. Dermatol.* **96,** 419–424.

Kretzschmar, M., Doody, J., and Massague, J. (1997). Opposing BMP and EGF signaling pathways converge on TGF- family mediator Smad1. *Nature* **389,** 618–622.

Kronmiller, J. E., Upholt, W. B., and Kollar, E. J. (1991a). Expression of epidermal growth factor mRNA in the developing mouse mandibular process. *Arch. Oral Biol.* **36,** 405–410.

Kronmiller, J. E., Upholt, W. B., and Kollar, E. J. (1991b). EGF antisense oligo deoxynucleotides block murine odontogenesis *in vitro*. *Dev. Biol.* **147,** 485–488.

Kuhlman, J., and Niswander L. (1997). Limb deformity proteins: role in mesodermal induction of the apical ectodermal ridge. *Development* **124,** 133–139.

Lax, I., Johnson, A., Howk, R., Sap, J., Bellot, F., Winkler, M., Ullrich, A., Vennstrom, B., Schlessinger, J., and Givol, D. (1988). Chicken epidermal growth factor (EGF) receptor: cDNA cloning, expression in mouse cells, and differential binding of EGF and transforming growth factor-alpha. *Mol. Cell Biol.* **8,** 1970–1978.

Lim, H., Dey, S. K., and Das, S. K. (1997). Differential expression of the *erb*B2 gene in the periimplantation mouse uterus: Potential mediator of signaling by epidermal growth factor-like growth factors. *Endocrinology* **138,** 1328–1337.

Lipeski, L. E., Boylan, J. M., and Gruppuso, P. A. (1996). A comparison of epidermal growth factor receptor mediated mitogenic signaling in response to transforming growth factor-α and epidermal growth factor in cultured fetal rat hepatocytes. *Biochem. Mol. Biol. Int.* **39,** 975–983.

MacCabe, J. A., Errick, J., and Saunders, J. W., Jr. (1974). Ectodermal control of the dorso ventral axis in the leg bud of the chick embryo. *Dev. Biol.* **39,** 69–82.

Michaud, J. L., Lapointe, F., and LeDouarin, N. M. (1997). The dorsoventral polarity of the presumptive limb is determined by signals produced by the somites and by the lateral somatopleure. *Development* **124,** 1453–1463.

Neuman-Silberberg, F. S., and Schüpbach, T. (1993). The *Drosophila* dorsoventral patterning gene *gurken* produces a dorsally localized RNA and encodes a TGF-α-like protein. *Cell* **75,** 165–174.

Noramly, S., Pisenti, J., Abbott, U., and Morgan, B. (1996). Gene expression in the *limbless* mutant: Polarized gene expression in the absence of *shh* and an AER. *Dev. Biol.* **179,** 339–346.

Ohuchi, H., Nakagawa, T., Yamamoto, A., Araga, A., Ohata, T., Ishimaru, Y., Yoshioka, H., Kuwana, T., Nohno, T., Yamasaki, M., Itoh, N., and Noji, S. (1997). The mesenchymal factor, FGF10, initiates and maintains the outgrowth of the chick limb bud through interaction with FGF8, an apical ectodermal factor. *Development* **124,** 2235–2244.

Olofsson, B., Pizon, V., Zahraoui, A., Tavitian, A., and Therwath, A. (1986). Structure and expression of the chicken epidermal growth factor receptor gene locus. *Eur. J. Biochem.* **160,** 261–266.

Onagbesan, O. M., and Peddie, M. J. (1995). Effects of insulin-like growth factor I and interactions with transforming growth factor-α and LH on proliferation of chicken granulosa cells and projection of progesterone in culture. *J. Reprod. Fertil.* **104,** 259–265.

Partanen, A. M. (1990). Epidermal growth factor and transforming growth factor-alpha in the development of epithelial-mesenchymal organs of the mouse. In "Growth Factors and Development" (M. Nilsen-Hamilton, Ed.), pp. 31–53, Academic Press, New York.

Parr, B. A., Shea, M. J., Vassilera, G., and McMahon, A. P. (1993). Mouse *Wnt* genes exhibit discrete domains of expression in the early embryonic CNS and limb buds. *Development* **119,** 247–261.

Price, J. V., Clifford, R. J., and Schübach, T. (1989). The maternal ventralizing locus *torpedo* is allelic to *faint little ball,* an embryonic lethal, and encodes the *Drosophila* EGF receptor homolog. *Cell* **56,** 1085–1092.

Raz, E., and Shilo, B-Z. (1993). Establishment of ventral cell fates in the *Drosophila* embryonic ectoderm requires DER, the EGF receptor homolog. *Genes Dev.* **7,** 1937–1948.

Riese, D. J., II., Kim, E. D., Elenius, K., Buckley, S., Klagsbrun, M., Plowman, G. D., and Stern, D. F. (1996). The epidermal growth factor receptor couples transforming growth factor-α, heparin-binding epidermal growth factor-like factor, and amphiregulin to Neu, ErbB-3, and ErbB-4. *J. Biol. Chem.* **271,** 20047–20052.

Ros, M. A., López-Martínez, A., Simandl, B. K., Rodriguez, C., Izpisúa-Belmonte, J. C., Dahn, R., and Fallon, J. F. (1996). The limb field mesoderm determines initial limb bud anteroposterior asymmetry and budding independent of *sonic hedgehog* or apical ectodermal gene expressions. *Development* **122,** 2319–2330.

Rosselot, G., Vasilatos-Younken, R., and Leach, R. M. (1994). Effect of growth hormone, insulin-like growth factor I, basic fibroblast growth factor, and transforming growth factor-β on cell proliferation and proteoglycan synthesis by avian postembryonic growth plate chondrocytes. *J. Bone Miner. Res.* **9,** 431–439.

Copyright © 1998 by Academic Press. All rights of reproduction in any form reserved.

Rutledge, B. J., Zhang, K., Bier, E., Jan, Y. N., and Perrimon, N. (1992). The *Drosophila spitz* gene encodes a putative EGF-like growth factor involved in dorsal–ventral axis formation and neurogenesis. *Genes Dev.* **6,** 1503–1517.

Salido, E. C., Lakshmanan, J., Fisher, D. A., Shapiro, L. J., and Barajas, L. (1991). Expression of epidermal growth factor in the rat kidney. *Histochemistry* **96,** 65–72.

Saunders, J. W., Jr. (1948). The proximo-distal sequence of origin of parts of the chick wing and the role of the ectoderm. *J. Exp. Zool.* **108,** 363–404.

Saunders, J. W., Jr. (1977). The experimental analysis of chick limb development. In "Vertebrate Limb and Somite Morphogenesis" (D. A. Ede, J. R. Hinchcliffe, and M. Balls, Eds.), pp. 1–24. Cambridge Univ. Press, Cambridge.

Sawyer. L. (1982). Fine structural analysis of limb development in the wingless mutant chick embryo. *J. Embryol. Exp. Morph.* **68,** 69–86.

Schnepp, B., Grumbling, G., Donaldson, T., and Simcox, A. (1996). Vein is a novel component in the *Drosophila* epidermal growth factor receptor pathway with similarity to the neuregulins. *Genes Dev.* **10,** 2302–2313.

Schultheiss, T. M., Burch, J. B., and Lassar, A. B. (1997). A role for bone morphogenetic proteins in the induction of cardiac myogenesis. *Dev. Dyn.* **11,** 451–462.

Schweitzer, R., Shaharabany, M., Seger, R., and Shilo, B-Z. (1995). Secreted *spitz* triggers the DER signaling pathway and is a limiting component in embryonic ventral ectoderm determination. *Genes Dev.* **9,** 1518–1529.

Simcox, A. (1997). Differential requirement for EGF-like ligands in *Drosophila* wing development. *Mech. Dev.* **62,** 41–50.

Simmons, J. G., Hoyt, E. C., Westwick, J. K., Brenner, D. A., Pucilowska, J. B., and Lund, P. K. (1995). Insulin-like growth factor-I and epidermal growth factor interact to regulate growth and gene expression in IEC-6 intestinal epithelial cells. *Mol. Endocrinol.* **9,** 1157–1165

Stephens, T. D., Spall, R., Baker, W. C., Hiatt, S. R., Pugmire, D. E., Shaker, M. R., Willis, H. J., and Winger, K. P. (1991). Axial and paraxial influences on limb morphogenesis. *J. Morphol.* **208,** 367–379.

Streck, R. D., Wood, T. L., Hsu, M.-S., and Pintar, J. E. (1992). Insulin-like growth factor-I and -II and insulin-like grow factor binding protein-2 RNA are expressed in adjacent tissues within rat embryonic and fetal limbs. *Dev. Biol.* **151,** 586–596.

Todt, W. L., and Fallon, J. F. (1984). Development of the apical ectodermal ridge in the chick wing bud. *J. Embryol. Exp. Morph.* **80,** 21–41.

Vardy, D. A., Kari, C., Lazarus, G. S., Jensen, P. J., Zilberstein, A., Plowman, G. D., and Rodeck, U. (1995). Induction of autocrine epidermal growth factor receptor ligands in human keratinocytes by insulin/insulin-like growth factor-I. *J. Cell Physol.* **163,** 257–265.

Vogel, A., Rodriguez, C., and Izpisúa-Belmonte, J.-C. (1996). Involvement of FGF8 in initiation, outgrowth and patterning of the vertebrate limb. *Development* **122,** 1737–1750.

Warburton, D., Seth, R., Shum, L., Horcher, P. G., Hall, F. L., Werb, Z., and Slavkin, H. C. (1992). Epigenetic role of epidermal growth factor expression and signalling in embryonic mouse lung morphogenesis. *Dev. Biol.* **149,** 123–133.

Xu, X., Weinstein, M., Li, C., Naski, M., Cohen, R. I., Ornitz, D. M., Leder, P., and Deng, C. (1998). Fibroblast growth factor receptor-2 (FGFR2)-mediated reciprocal regulation loop between FGF8 and FGF10 is essential for limb induction. *Development* **125,** 753–765.

Yamada, K. (1970). Dual staining of some sulfated mucopolysaccharides with Alcian Blue (pH 1.0) and ruthenium red (pH 2.5). *Histochemie* **23,** 13–20.

Yamane, A., Mayo, M. L., Bringas, P., Jr., Chen, L., Huynh, M., Thai, K., Shum, L., and Slavkin, H. C. (1997). TGF-alpha, EGF, and their cognate EGF receptor are co-expressed with desmin during embryonic, fetal, and neonatal myogenesis in mouse tongue development. *Dev. Dyn.* **209,** 353–366.

Zwilling, E. (1961). Limb morphogenesis. *Adv. Morphogenesis* **1,** 301–330.

Received for publication March 10, 1998
Accepted June 17, 1998

Copyright © 1998 by Academic Press. All rights of reproduction in any form reserved.

DEVELOPMENTAL BIOLOGY 202, 56–66 (1998)
ARTICLE NO. DB989001

The *Cspg2* Gene, Disrupted in the *hdf* Mutant, Is Required for Right Cardiac Chamber and Endocardial Cushion Formation

C. H. Mjaatvedt,*,[1] H. Yamamura,† A. A. Capehart,* D. Turner,* and R. R. Markwald*

**Department of Cell Biology and Anatomy, Medical University of South Carolina, 171 Ashley Avenue, Charleston, South Carolina 29425; and †Tokyo Women's Medical College, The Heart Institute of Japan, 8-1, Kawada-cho, Shinjuku-ku, Tokyo, Japan*

The heart defect (*hdf*) mouse is a recessive lethal that arose from a transgene insertional mutation on chromosome 13. Embryos homozygous for the transgene die *in utero* by embryonic day 10.5 postcoitus and exhibit specific defects along the anterior–posterior cardiac axis. The future right ventricle and conus/truncus of the single heart tube fail to form and the endocardial cushions in the atrioventricular and conus/truncus regions are absent. Because the *hdf* mouse mutation provided the opportunity to identify a gene required for endocardial cushion formation and for specification or maintenance of the anterior most segments of the heart, we initiated studies to further characterize the phenotype, clone the insertion site, and identify the gene disrupted. Chromosome mapping studies first identified the gene, *Cspg2* (versican), as a candidate *hdf* gene. In addition, an antibody recognizing a glycosaminoglycan epitope on versican was found to be positive by immunohistochemistry in the extracellular matrix of normal wild-type embryonic hearts, but absent in homozygous hearts. Expression analysis of the *Cspg2* gene showed that the 6/8, 6/9, and 7/9 *Cspg2* exon boundaries were present in mRNA of normal wild-type embryonic hearts but absent in the homozygous mutant embryos. DNA sequence flanking the transgene was used to isolate from a normal mouse library overlapping genomic DNA segments that span the transgene insertion site. The contiguous genomic DNA segment was found to contain exon 7 of the *Cspg2* in a position 3′ to the transgene insertion site. These four separate lines of evidence support the hypothesis that *Cspg2* is the gene disrupted by the transgene insertion in the *hdf* mouse line. The findings of this study and our previous studies of the *hdf* insertional mutant mouse have shown that normal expression of the *Cspg2* gene is required for the successful development of the endocardial cushion swellings and the embryonic heart segments that give rise to the right ventricle and conus/truncus in the outlet of the looped heart. **© 1998 Academic Press**

INTRODUCTION

The formation of the vertebrate heart tube is a progressive event that occurs along the anterior/posterior embryonic axis by the sequential addition of primitive segments (De la Cruz *et al.*, 1989). The first segment to form from the mesodermal heart fields is the primitive right ventricle. This is followed by the formation of the primitive left ventricle. These two segments comprise the initial straight heart tube. As the tube begins bending to the right between the two segments, the atrioventricular (AV) canal and the sinoatrial segments are sequentially added to the posterior end of the tube. The last segment to form is the conal/truncal segment of the heart outlet. This segment is unlike the earlier formed segments in that it forms at the anterior, rather than the posterior, end of the heart tube. The conal/truncal segment, therefore, does not appear to be derived directly from the mesoderm of the heart-forming region, but may arise indirectly from the primitive right ventricle or from anterior splanchnic mesoderm associated with the dorsal mesentary of the aortic sac and recruited into the forming heart tube.

Although each of the segments possess unique characteristics, they all possess underlying phenotypic similarities typical of a modular unit. All of the segments consist of an

[1] To whom correspondence should be addressed. Fax: (803) 792-0664. E-mail: mjaatvch@musc.edu.

0012-1606/98 $25.00
Copyright © 1998 by Academic Press
All rights of reproduction in any form reserved.

outer developing myocardium that is separated from an inner endothelial cell monolayer called the endocardium. Between these two epithelia, in all segments, is a thick intervening layer of extracellular matrix containing basement membrane components derived from both the myocardium and the endothelium. As development proceeds each of the segments differentiate in a regionally specific manner, but they also integrate with each other to remodel the single-looped heart into a mature four-chambered structure. The failure of any one segment to develop properly can result in structural malformations associated with more than one chamber.

Recently, we described the identification of an insertional mutant mouse called heart defect (*hdf*; Yamamura *et al.*, 1997). The *hdf* mouse is a homozygous recessive lethal that arose from the insertion of a lacZ reporter containing transgene into a single site within the central region of mouse chromosome 13. Homozygous embryos die at approximately embryonic day 10.5 postcoitum (dpc) and exhibit a defective heart morphology. In all homozygous embryos, the primitive right ventricle (first segment) of the looped heart fails to grow or develop normally and does not acquire an outlet (conus/truncus) segment. While the primitive left ventricle, AV, and atrium become abnormally distended. The initial matrix swellings of the endocardial cushions are absent in both the conus/truncus and the AV segments of the *hdf* homozygous heart tube. The formation of endocardial cushions within discrete regions of the embryonic heart tube is a required step in the developmental program of vertebrate heart morphogenesis (Markwald *et al.*, 1977). The endocardial cushions are initially found in only two segments (the atrioventricular and conus/truncus) of the primitive heart tube and can be observed initially as acellular expansions of matrix located between the myocardial and endocardial cell layers. The cushion swellings arise in pairs on either side of the lumen and functionally serve as one way valves of the blood flow during relatively early stages. With further development, some the endothelial cells lining the cushions undergo a transdifferentiation and form a population of mesenchymal cells that invade the expanded matrix. This transdifferentiation is in response to an inductive signal secreted by the myocardium into the extracellular matrix in only the AV and outlet segments of the heart (Eisenberg and Markwald, 1995; Krug *et al.*, 1987; Mjaatvedt *et al.*, 1991; Potts and Runyan, 1989; Rezaee *et al.*, 1993).

Because the *hdf* mouse mutation provided the opportunity to identify a gene required for regulation of the initial endocardial cushion formation and for initiating or maintaining segmental identity in the heart we have cloned the locus and identified the gene disrupted. We report here our data that the *Cspg2* gene is disrupted by the transgene insertion resulting in a loss of expression of versican in the developing *hdf* mouse heart. These results suggest that the *Cspg2* gene has a functional role in normal right heart chamber specification and initial development of the endocardial cushion swellings.

MATERIALS AND METHODS

Chromosome Mapping by Interspecific Backcross Analysis

A suitable polymorphism was used for chromosome mapping by interspecific backcross analysis as previously described (Yamamura *et al.*, 1997). The linkage analysis was performed using the Jackson Laboratory mapping panel of 94 DNA samples from a panel (BSS) of the backcross (C57BL/6JEi × SPRET/Ei) × SPRET/Ei (Rowe *et al.*, 1994).

Southern Blotting

Genomic DNA was isolated from mice as previously described (Mjaatvedt *et al.*, 1993). Five micrograms of wild-type or transgenic DNA was digested with an appropriate restriction enzyme, electrophoresed in a 0.8% agarose gel, transferred to nylon membrane (MSI), and hybridized with the lacZ portion of the transgene radiolabeled with [^{32}P]dCTP (Feinberg and Vogelstein, 1984). Membranes were washed under high stringency conditions and autoradiographs were made as previously reported (Mjaatvedt *et al.*, 1993).

Genomic Library Screens

A normal mouse genomic library (129/Sv; Stratagene) was screened using radiolabeled probes (Feinberg and Vogelstein, 1984) generated from a 322-bp portion of sequence flanking the transgene insertion (Yamamura *et al.*, 1997). Positive genomic clones were identified and isolated. The insert DNA was purified, cut with restriction enzymes, and subcloned into plasmid vectors using standard techniques (Ausubel *et al.*, 1995; Sambrook *et al.*, 1989).

Immunofluorescent Staining of Embryos

Specimens were stained immunohistochemically as previously described with some modifications (Mjaatvedt *et al.*, 1991). Specimens were fixed with Dent's fixative (80% methanol/20% DMSO), dehydrated through an ethanol series, infiltrated with xylene, embedded in paraffin, and sectioned. Selected sections were rehydrated with an ethanol series to water and then equilibrated in phosphate-buffered saline (PBS; 10 mM phosphate/140 mM NaCl, pH 7.2). Hydrated sections were blocked with 10% whole goat serum in 1% bovine serum albumin in PBS prior to incubation with primary antibody. The primary antibody to myosin light-chain 2v (MLC2v) and myosin light-chain 2a (MLC2a) were kindly provided by Dr. S. W. Kubalak (Medical University of South Carolina). The MLC2v and the MLC2a antibodies localize to the ventricular and atrial embryonic heart chambers, respectively. Secondary antibody to fluorochrome-labeled goat anti-rabbit IgG (Jackson ImmunoResearch Laboratories, Inc., No. 111-015-003) was diluted 1:100. For whole-mount immunostaining, embryos were fixed with Dent's fixative, rehydrated through a decreasing methanol series to water, equilibrated with phosphate-buffered saline, and blocked with 1% bovine serum albumin in PBS (overnight; 4°C). Undiluted primary TC2 antibody containing cell culture supernatant (or non-antibody-containing supernatant; control) was incubated (4°C) with the embryos overnight. The embryos were then extensively rinsed with PBS and incubated with a diluted (1/100 in PBS) fluorescein-labeled anti-mouse IgM secondary antibody (Cappel Research Products, Durham, NC) overnight (4°C) and rinsed again

Copyright © 1998 by Academic Press. All rights of reproduction in any form reserved.

extensively. The monoclonal TC2 antibody recognizes a native chondroitin sulfate glycosaminoglycan epitope on *Cspg2* and was produced by an *in vitro* immunization protocol (Capehart *et al.*, 1998, manuscript in preparation; Capehart *et al.*, 1997). The stained sections and whole-mount stained embryos were observed by epifluorescent microscopy.

LacZ Staining Methods

Histochemical staining of the mouse embryos for β-galactosidase was conducted as described (Yamamura *et al.*, 1997). Embryos were fixed in 0.2% glutaraldehyde in PBS with 2 mM $MgCl_2$ and 5 mM EGTA and then rinsed three times in PBS with 2 mM $MgCl_2$, 0.02% NP-40, and 0.01% sodium deoxycholate. Embryos were incubated in 0.1% X-gal (Sigma) in PBS with 2 mM $MgCl_2$, 0.02% NP-40, and 0.01% sodium deoxycholate, 20 mM $K_3Fe(CN)_6$, 20 mM $K_4Fe(CN)_6$ at 37°C for 12 h and washed in PBS containing 10 mM EDTA. Some β-galactosidase-reacted specimens were dehydrated through an ethanol series, embedded into paraplast, and sectioned. Sections were counterstained with nuclear fast red and examined with a Zeiss Photomicroscope.

Reverse Transcription/Polymerase Chain Reaction (RT-PCR)

Total RNA from heart or whole embryo was isolated from normal wild-type, hemizygous *hdf* or homozygous *hdf* embryos using standard procedures (mRNA STAT-30; Tel-Test "B," Inc.). The total RNA was pretreated with RNase-free DNase (BRL, Bethesda, MD) to remove any contaminating genomic DNA and 2 μg was used for first-strand cDNA synthesis using random hexamers and reverse transcriptase (Superscript; BRL). Aliquots of the cDNA from each genotype were added to separate tubes containing a PCR reaction mixture according to manufacturer's suggestions (Qiagen) and primers specific for *Cspg2* exon boundaries were used as follows (forward and reverse, respectively): *Cspg2* exon 2/3, 5′-AGGCATCTTATGGATGTGCTCAAC-3′, 5′-TGACAAGGTAGGACCACTTTTCCAG-3′; *Cspg2* exon 4/5, 5′-ACCAGCAGGTACACTCTGAACTTTG-3′, 5′-ACACATCATAGGTTTCCTGGGGAG-3′; *Cspg2* exon 5/6, 5′-GCTGTTACGGAGACATGATGGG-3′, 5′-TGCTATCAGGGAGAGGGAAGCATG-3′; *Cspg2* exon 6/8, 5′-GCGACTGTTGGAGAACTTCAGG-3′, 5′-TTCAAATGAGTCTGGTAACTCGGG-3′; *Cspg2* exon 6/9, 5′-GCAGCTTGGAGAAATGGCTTTG-3′, 5′-TCCGTTGAGGCATGGGTTTG-3′; *Cspg2* exon 7/8, 5′-CAACGTGTCTTTGAGGAAGAGTCC-3′, 5′-TTAGGCACTGTGGTAACGAGCTG-3′; *Cspg2* exon 7/9, 5′-CCATCGACAGCCTTCACAGAAC-3′, 5′-TGCACACATAGGAAGTCTCGGTAG-3′; *Cspg2* exon 8/9, 5′-CGTGGAAGGCACAGCAGTTTAC-3′, 5′-AAGTTCACACTGGTCTCCGCTG-3′; *Cspg2* exon 9/10, 5′-CACCTGTTATCCTACCGAGACTTCC-3′, 5′-GCACCATTCCGACAAGGGTTAG-3′; *Cspg2* exon 11/12, 5′-GCACAAATTCCAAGGACAGTGCTAC-3′, 5′-CAGTCCAGCGGAAGTCATGTTC-3′; *Cspg2* exon 10/11/12/13 (10/13), 5′-GAATGTCACTCTAACCCTTGTCGG-3′, 5′-GCAAGTGTAGGTGAGGTGGTAATTG-3′; *Cspg2* exon 13/14/15 (13/15), 5′-TGAGAACTGGAGACCCAACCAG-3′, 5′-CCAGCGATGCTCATGTTTTGATG-3′; mef2C, 5′-AACGAATGCAGGGATTTGGG-3′, 5′-ATCTCACAGTCACACAGCACGCTC-3′. Each reaction mixture was heated to 95°C (5 min.), and then the temperature was lowered to 80°C and *Taq* polymerase was added (2.5 units; Qiagen). The cDNA was amplified using an automatic DNA thermal cycler (Termolyne Amplitron II) and 40 cycles of the following conditions: 95°C 30-s denaturation, 55°C 30-s annealing, 72°C 1-min extension. A final extension was performed at 72°C for 3 min. Equal volumes of the amplification product were separated on 2% agarose gels (SeaKem LE) and stained with ethidium bromide.

RESULTS

Mapping Analysis of the hdf Locus

We previously reported the location of the *hdf* transgene insertion site to be in the central region of chromosome 13, four crossovers proximal to D13Mit30 (Yamamura *et al.*, 1997). To potentially identify other DNA markers or genes mapping closer to the *hdf* insertion site, we mapped the insertion using another mapping panel (BSS) of DNA samples from progeny of a (C57BL/6J X *Mus spretus*) F1 × *M. spretus* backcross (Rowe *et al.*, 1994). Results from these experiments not only confirmed the position of transgene insertion to a central site on chromosome 13 (Yamamura *et al.*, 1997), but also showed that the insertion site was linked with the D13Mit27 locus. Recently, the D13Mit27 marker was mapped to approximately 0.6 cM of the *Cspg2* gene (Seymour *et al.*, 1996). The *hdf* locus in the BSS panel is approximately 2.1 cM from D13Bir16, 2.1 cM from the dihydrofolate reductase (*Dhfr*) gene, and 4 cM proximal to the D13Xrf249 locus (Bassett *et al.*, 1997) (Fig. 1). The D13Xrf249 gene has homology with the MEF2 open reading frame (locus SCYJL102w) of *Saccharomyces cerevisiae.*

Immunohistochemical Analysis

We have previously shown that the β-galactosidase staining patterns in the *hdf* homozygous and hemizygous mice showed a similar distribution of expression along the anterior–posterior axis of the heart tube. In both homozygous and hemizygous mice, the lacZ transgene expression was most intense in the anterior portions of the looped heart that at 9.5 dpc consist of the developing conus/truncus and future right ventricle (Yamamura *et al.*, 1997) (Fig. 2). LacZ transgene expression appeared much lower in the left ventricle and was nearly undetectable in regions of the atrium in hemizygous mouse hearts, suggesting that the *hdf* gene was unevenly expressed throughout the heart tube. However, in the homozygous mutant embryos, lacZ expression extended more posteriorly through the left ventricle and into the primitive atrium of the looped heart. This extended expression into more posterior segments suggested the possibility that disruption of the *hdf* gene in the homozygotes affects the establishment or maintenance of normal segmental boundaries in the looped heart. To explore this possibility further, we immunostained homozygous embryonic hearts using antibodies previously shown to localize within specific segmental domains of the embryonic mouse heart. Using an antibody specific for ventricular isoform of myosin light-chain-2 (MLC2v) as a probe for the ventricular segment of the looped heart, we immunostained sections of normal wild-type and *hdf* ho-

Copyright © 1998 by Academic Press. All rights of reproduction in any form reserved.

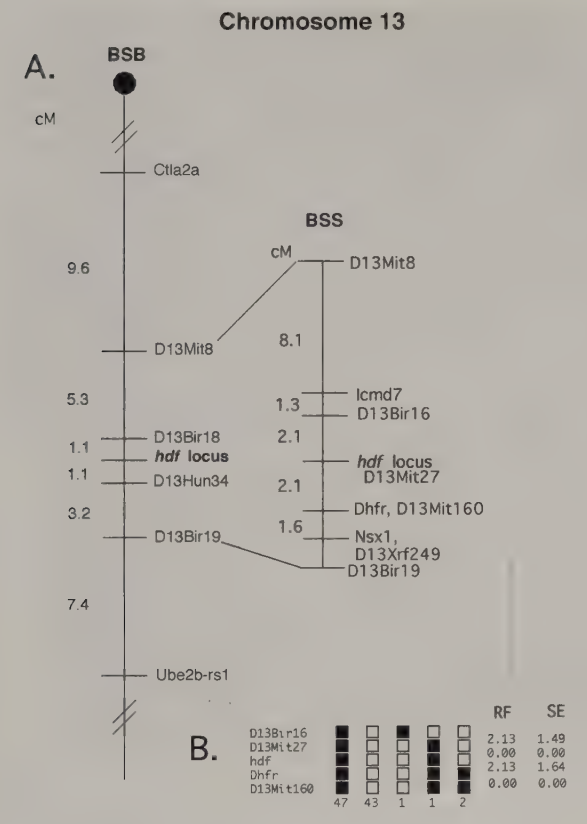

FIG. 1. (A) Linkage map of the *hdf* locus on mouse chromosome 13 by two different interspecific backcross mapping panels. The location of the *hdf* locus is shown in relation to flanking markers mapped in the (C57BL/6J × *Mus spretus*) F1 × C57BL/6J backcross (BSB) and the (C57BL/6J × *M. spretus*) F1 × *M. spretus* (BSS) panel (shown in the expanded region between D13Mit8 and D13Bir19). The *hdf* locus on the BSS map showed tight linkage to marker D13Mit27. (B) Haplotype diagram of anonymous markers and genes located near the *hdf* locus for the 94 animals in the BSS backcross. Solid black boxes represent the C57BL/6J genotype and open boxes represent the *M. spretus* genotype. The number of animals within each haplotype are shown along the bottom of the diagram. RF, percentage recombination frequency; and SE, standard error.

mozygous embryos. The MLC2v antibody localized specifically to the myocardium of the heart ventricular segment in the wild-type (Fig. 3A) embryos (10.5 dpc). Similar results were seen in the *hdf* homozygous embryos except that the myocardial staining of the primitive ventricle appeared closer to the aortic sac than observed in the wild-type hearts (Fig. 3B). This may be due to the underdeveloped right ventricle and truncated conus/truncus development found in the mutants. Both wild-type normal and *hdf* homozygous embryos were also immunostained with antibody specific for the MLC-2a protein. Observations of wild-type embryo hearts immunostained with this antibody showed positive staining in both the atrium and the ventricle of the myocardium at this stage of development (Fig. 3C). Sections of the similarly staged *hdf* homozygous embryos also showed no segmental compartmentalization of the MLC-2a immunostaining pattern (Fig. 3D).

A striking phenotypic feature of the *hdf* homozygous hearts is the absence of the acellular cushion swellings normally found in both the atrioventricular and the outlet (conus/truncus) segments of the heart tube. Normally, the endocardial cushions in these two regions of the heart exhibit an expanded region of extracellular matrix (cardiac jelly) consisting of a number of basement membrane molecules such as fibronectin and collagen (Kitten *et al.*, 1987, 1986). Proteoglycans are also highly enriched in these segments and together with hyaluronan may contribute significantly to cushion expansion before the invasion of cells. To analyze the *hdf* homozygous hearts further, we immunostained cardiac matrix with an anti-chondroitin sulfate proteoglycan antibody called TC2. Wild-type normal mouse embryos whole-mount immunostained with TC2 showed a positive staining pattern throughout the early embryonic heart tube. In contrast, the TC2 antibody showed no detectable localization of immunostaining within the heart of homozygous *hdf* embryos (Fig. 4).

Identification of Genomic Sequence Flanking the Transgene

A genomic library was constructed from the DNA of hemizygous transgenic mice and screened using probes derived from the lacZ portion of the inserted transgene (Yamamura *et al.*, 1997). One of the clones, named *hdf* 3.3, contained 1780 bp of unidentified mouse sequence flanking the start of transgene sequence. Comparison of this flank-

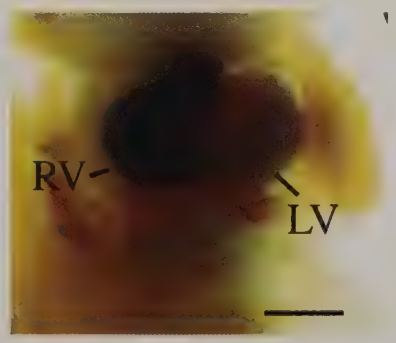

FIG. 2. Expression of β-galactosidase in a embryonic 11 dpc mouse heart hemizygous for the transgene insertion. β-Galactosidase shows a strong expression pattern on the right side (ventricle) of the looped heart tube and outlet (conus/truncus) segment. In contrast the left ventricle (inlet) of the looped heart shows only weak expression of β-galactosidase. Bar, 500 μm.

Copyright © 1998 by Academic Press. All rights of reproduction in any form reserved.

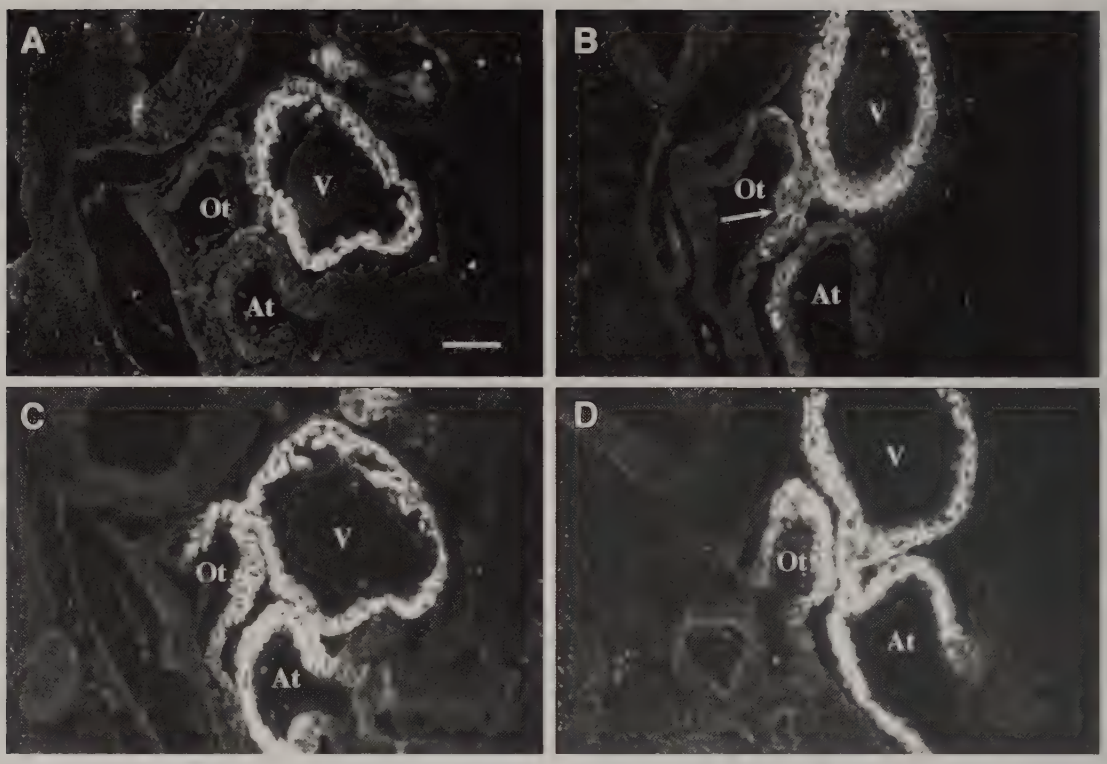

FIG. 3. Immunolocalization of the MLC2v and MLC2a in embryonic hearts. Embryonic 9.5 dpc heart sections from *hdf* homozygous (B, D) and normal wild-type (A, C) embryos. Immmunofluorescent images obtained using antibodies specific for either myosin light-chain 2v (A, B) or myosin light-chain 2a (C, D). Staining patterns for MLC2v was confined to the primitive ventricular segment in both the wild-type and *hdf* homozygous mutant hearts. However, the myocardial staining of the primitive ventricle (V) appeared closer (arrow) to the aortic sac in the homozygous mutant than observed in the wild-type hearts. Staining patterns for MLC2a showed immunostaining in all segments of the looped heart tube in both the wild-type normal and *hdf* homozygous mutant hearts. A, atrium; V, primitive ventricle; Ot, outlet. Bar, 100 μm.

ing sequence with those deposited in the EMBL/GenBank DNA and protein databases showed no significant homology with known genes. The sequence information was used to design PCR primers for a 322-bp region of the flanking sequence. To help confirm the authenticity of the flanking sequence, radiolabeled probe made from the 322-bp region was used in Southern blot analysis (Mjaatvedt *et al.*, 1993) of genomic DNA from normal and transgenic animals (see Fig. 5A). The probe hybridized to a 2.2-kb band in *Eco*RI digested DNA from wild-type littermates. Hybridization to DNA derived from transgenic hemizygous animals localized to the 2.2-kb band and to another band that migrated at 5.5 kb. To confirm that the shift from 2.2 to 5.5 kb was not the result of a polymorphism present in parental background of the *hdf* mice, *Eco*RI-digested DNA from the CBA and C57/B6 mouse parental strains was also included on the blot. In both these strains, the probe hybridized only to the 2.2-kb band.

Genomic Analysis of the Insertion Site

To characterize the normal genomic organization at the transgene insertion site, 322 bp of a flanking sequence (Yamamura *et al.*, 1997) was used as template to synthesize a radiolabeled probe for screening a wild-type mouse genomic library (129/Sv; Stratagene). Six lambda clones were identified and isolated in subsequent screens that contained different sized DNA inserts. The genomic DNA insert was isolated from each clone, analyzed for restriction endonuclease sites, and aligned into a contiguous sequence of approximately 20 kb (Fig. 6). *Hin*dIII restriction endonuclease fragments of 1.8, 2.5, and 3.6 kb (Fig. 5C) surrounding the flanking sequence 322-bp site were then subcloned. Sequence analysis of the subcloned inserts showed that one end of the 2.5-kb *Hin*dIII fragment contained approximately 400 bp of sequence identical to that obtained from sequencing the flanking clone, *hdf* 3.3, up to the genomic DNA/transgene transition at 1780 bp.

Copyright © 1998 by Academic Press. All rights of reproduction in any form reserved

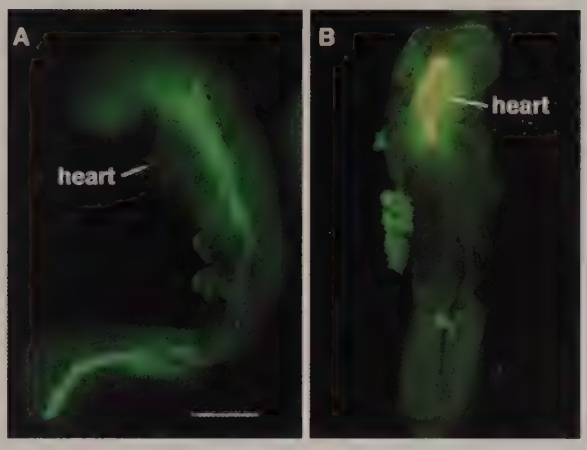

FIG. 4. Immunolocalization of the TC2 monoclonal antibody in the *hdf* embryonic heart. Whole-embryo immunofluorescent images of *hdf* homozygous embryo viewed from one side (A) and an enface view of a normal wild-type (B) embryos (8.5–9.0 dpc) using the TC-2 monoclonal antibody shows strong localization in the wild-type heart but not in the *hdf* homozygous heart tube. Green fluorescence in the midline of the embryo was variably observed in all embryos including control embryos. Bar, 500 μm.

Each of the inserts from the *Hin*dIII subclones was used separately as probes in Southern blots of normal and transgenic genomic DNA. Probe synthesized from the 1.8-kb *Hin*dIII fragment hybridized to a band at approximately 13.5 kb in wild-type DNA (Fig. 5B, lane 1). In animals hemizygous for the transgene an additional band at 10.5 kb was recognized by the 1.8-kb probe (Fig. 5B, lane 2). The 322-bp flanking sequence probe hybridized to a 2.2-kb band in normal wild-type DNA and a 5.5-kb band in transgenic derived DNA (Fig. 5A). The 2.5- and 3.6-kb probes also hybridized to an additional band at 5.5 kb in DNA derived from hemizygous animals (data not shown). The 5.5-kb band recognized by the 322-bp flanking sequence probe and the 10.5-kb band recognized by the 1.8-kb probe both correspond to the sizes previously identified as flanking sequence bands using the transgene as probe template (Yamamura *et al.*, 1997), suggesting that these fragments span the transgene insertion site.

Analysis of Cspg2 Gene in the hdf Mutant Mouse

Expression of the *Cspg2* gene was evaluated in wild-type and homozygous mutant embryos and isolated hearts by RT-PCR using primers for the *Cspg2* mRNA that spanned single and multiple exon boundaries. These results (summarized in Fig. 7) showed that mRNA derived from the *Cspg2* gene was expressed in both the wild-type and the mutant hearts. All four known potential alternative splice forms of the *Cspg2* gene (Shinomura *et al.*, 1995) were found to be expressed in cDNA of wild-type whole embryos (data not shown) and isolated heart cDNA. However, cDNA from the homozygous mutant embryos and isolated hearts was shown to lack the 6/8, 6/9, 7/8, and 7/9 exon boundaries (Fig. 7). All of the other exon boundary combinations tested in the 5′ and 3′ end of the *Cspg2* message were found to be present in both normal wild-type and homozygous hearts. In addition to *Cspg2*, primers for mef2C and an expressed sequence tag named D13Sut1e, both of which map in the general vicinity of *hdf*, were also evaluated by RT-PCR using normal and mutant mRNA. Both the mef2C and the D13Sut1e messages were detected in normal hearts and in the *hdf* mutant hearts (Fig. 7).

PCR analysis with exon specific primers was used to determine if any *Cspg2* gene sequence could be detected within the 17-kb genomic contig that spans the transgene insertion. Analysis using each of the six genomic clones

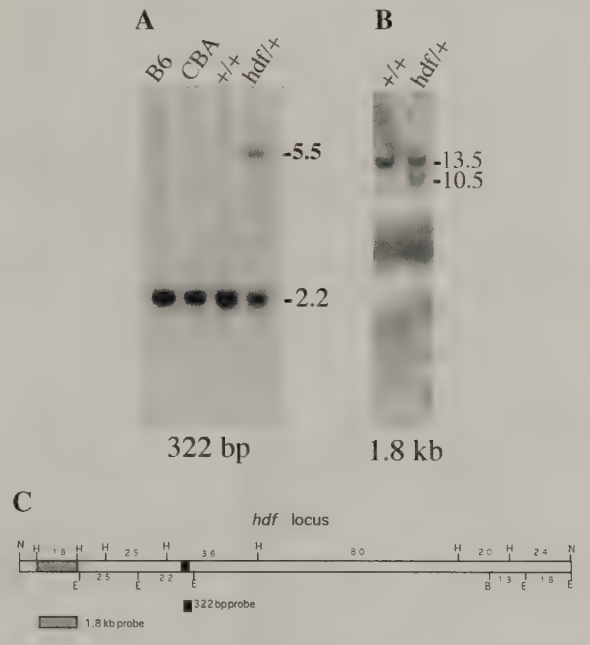

FIG. 5. Southern blot analysis of the genomic region surrounding the *hdf* insertion site. Autoradiographs shown in the panels above were probed with either the 322-bp sequence immediately flanking the transgene (A) or the 1.8-kb genomic fragment (B). The location of these probes relative to the genomic physical map near the transgene insertion site is shown in C. The 322-bp probe hybridized to a 2.2-kb band in *Eco*RI digests of both the C57BL/6 (B6) and the CBA parental background mouse strains and in the *hdf* wild-type (+/+) normal littermates, but in the *hdf* mutant (*hdf*/+) mouse DNA an additional 5.5-kb band was detected (A). The 1.8-kb probe hybridized to a 13.5-kb band in *Eco*RI digests of normal wild-type DNA, but also recognized a 10.5-kb band in the *hdf* mutant DNA, suggesting that this sequence was located on the opposite side to the transgene insertion site.

Copyright © 1998 by Academic Press. All rights of reproduction in any form reserved.

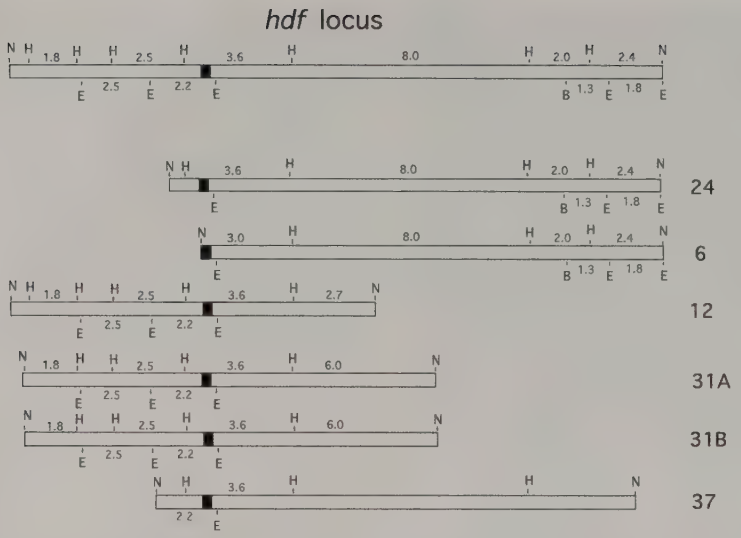

FIG. 6. Genomic restriction site map constructed from overlapping clones surrounding the *hdf* insertion site on chromosome 13. Inserts from six different lambda clones (designations shown to the right of each insert) were analyzed with selected restriction endonucleases (N, *Not*I; H, *Hin*dIII; E, *Eco*RI; B, *Bam*HI) and aligned to form the *hdf* locus map shown at the top. The black box indicates the location of the 322-bp flanking sequence used as probe to screen the normal mouse genomic library.

isolated showed that all of them were positive for *Cspg2* exon 7. In order to establish the orientation of exon 7 with respect to the transgene insertion, further analysis of each lambda clone was performed using two separate sets of primers derived from the 5′ end and from the 3′ region of exon 7. All six genomic clones were positive for the 3′ end, and all but the clone 12 were positive for the 5′ end. These results suggested that the transgene inserted within a region just 3′ to exon 7.

Southern blot analysis of DNA from wild-type and *hdf* heterozygous mice was performed using probes to the 5′ exon 1, central exon 7, and 3′ exon 15 of the *Cspg2* gene. The results of the Southern blot analysis with these probes and several different restriction enzyme DNA digestions did not reveal informative differences (data not shown) in banding patterns between wild-type normal or mutant derived DNA.

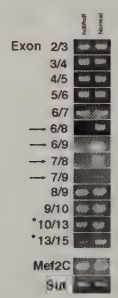

FIG. 7. Analysis of *Cspg2* alternative mRNA expression in normal and the *hdf* mutant embryonic hearts. Specific primers for *Cspg2* mRNA that span single exon boundaries or multiple boundaries (*) were used to evaluate by RT-PCR expression in hearts at embryonic day 9.5 pc. All exon boundaries corresponding to the known four alternative splice forms of *Cspg2* were detected in the cDNAs from wild-type (normal) embryonic hearts. In contrast, homozygous *hdf* mutant hearts (*hdf*/*hdf*) lacked the 6/8, 6/9, 7/8, and 7/9 exon splice forms (arrows). Mef2C and an expressed sequence tag named D13Sut1e were both shown to be easily detectable in both wild-type (normal) and heart homozygous for the transgene.

DISCUSSION

The results of this study show that the *hdf* recessive lethal mutant mouse line arose as the result of a transgene insertion into the middle *Cspg2* gene locus located on chromosome 13. The *Cspg2* gene encodes the core protein for a large chondroitin sulfate proteoglycan (versican/PG-M) that consists of 15 exons and spans a region of approximately 100 kb in the mouse genome (Shinomura *et al.*, 1995). The exons encode modular protein domains found in the proteoglycan whose presence in the protein core is regulated by transcription of alternatively spliced forms of the gene (Ito *et al.*, 1995). These functional protein

Copyright © 1998 by Academic Press. All rights of reproduction in any form reserved.

domains include a hyaluronan-binding domain, two chondroitin sulfate side chain attachment domains (α and β), two epidermal growth factor like domains, a lectin-like domain, and a complement regulatory domain. At least four different mRNA species forms (V0, V1, V2, and V3 (Shinomura *et al.*, 1995) have been identified in adult tissue that are produced by the alternative splicing out of the chondroitin sulfate attachment domains.

Four separate lines of evidence support the hypothesis that *Cspg2* is the gene disrupted by the transgene insertion in the *hdf* mutant. The first data to indicate that *Cspg2* was a candidate for the disrupted gene came from our chromosome mapping studies, presented here, that linked the *hdf* locus with the anonymous sequence tagged site marker D13Mit27 by interspecific backcross analysis of the Jackson Laboratory's BSS interspecific backcross mouse mapping panel (Rowe *et al.*, 1994). Mapping of the *hdf* locus onto the BSS mouse mapping panel confirmed our previous mapping data that placed *hdf* onto mouse chromosome 13 using the BSB (C57BL/6J × *M. spretus*)F1 female × C57BL/6J male) interspecific backcross mapping panel (Yamamura *et al.*, 1997). Although the *Cspg2* gene had not been placed onto either the BSS or the BSB mouse mapping panel, the D13Mit27 marker found to map with the *hdf* locus in the BSS panel proved to be useful for identification of *Cspg2* as a candidate gene target of the *hdf* insertional mutation. A survey of the linkage data from other mouse mapping panels showed that the D13Mit27 marker had been placed within 0.6 cM of *Cspg2* in a high-resolution linkage map of chromosome 13 near the *pearl* mutant mouse locus (Seymour *et al.*, 1996). Subsequently, we identified a suitable polymorphism in the 5′ region of the *Cspg2* gene and confirmed the linkage of *Cspg2* with the *hdf* locus (data deposited www.jax.org/resources/documents/cmdata/bkmap/BSB13data.html). Our mapping data placed the *hdf* locus centromeric to the *Dhfr* gene locus and is in agreement with the placement of the *Cspg2* gene on the high resolution map (Seymour *et al.*, 1996), but disagrees with the published consensus map for chromosome 13 in which *Cspg2* is located telomeric to the *Dhfr* locus approximately 13 cM from D13Mit27 and the *hdf* locus (Justice and Stephenson, 1997). Although this mapping data revealed *Cspg2* as a candidate *hdf* gene, two other potential candidates, a *mef2* gene (D13Xrf249) and an expressed sequence tag called D13Sut1e were also identified as potential candidates in our mapping study. In the BSS mapping panel, D13Xrf249 had been mapped approximately 4 cM telomeric to the *hdf* locus. The D13Xrf249 gene was mapped using a dbEST (GenBank R02242) probe that has homology with the MEF2 open reading frame (locus SCYJL102w) of *S. cerevisiae* chromosome X (Bassett *et al.*, 1997). The expressed sequence tag designated D13Sut1e had been placed onto the BSB mapping panel in the vicinity of the *hdf* locus; however, its exact linkage relative to *hdf* could not be determined since some of the animals in the panel were not genotyped for the EST. We considered the MEF2 gene an interesting *hdf* candidate since the promoter elements found in several cardiac genes that drive lacZ in a right-sided pattern of expression in the developing mouse heart contain MEF2 consensus sequences (Kuisk *et al.*, 1996; Li *et al.*, 1996; Moessler *et al.*, 1996; Ross *et al.*, 1996). However, analysis of MEF2 and the D13Sut1e mRNA expression showed that both were expressed in the wild-type normal and the homozygous mutant embryos and were eliminated as a candidates. The second line of evidence that supported the hypothesis that *Cspg2* was disrupted in the *hdf* mutant came from expression studies of the *Cspg2* mRNA in normal and mutant embryos. Results of RT-PCR analysis using specific primers that spanned *Cspg2* exon boundaries showed that mRNA derived from the *Cspg2* gene was present in the homozygous embryos and hearts; however, the message was truncated. The disrupted mRNA encodes the GAG attachment domains but does not appear to produce functional protein that can be recognized by the TC2 antibody. Intact messages for *Cspg2* were always detected in the wild-type normal embryos. In cDNA derived from wild-type normal isolated hearts each of the exon boundaries between 6/8, 6/9, 7/8, and 7/9 were found to be present suggesting that the developing embryonic mouse heart normally synthesizes all four splice variants of the *Cspg2* gene. Homozygous embryos were missing all the critical exon junctions between 6/8, 6/9, 7/8, and 7/9. Therefore, none of the *Cspg2* alternative splice forms are intact in the defective hearts, suggesting that the *hdf* insertional mutation created a null for mature *Cspg2* protein in the transgenic mouse. A third line of supporting evidence came from immunostaining with the TC2 antibodies. The TC2 epitope was found to be abundant throughout the normal mouse heart at embryonic day 8.5–9.0 pc, but was undetectable in the hearts of the homozygous mutant embryos. The TC2 antibody recognizes a glycosaminoglycan epitope on the *Cspg2* proteoglycan and immunostaining of both mouse and in chick embryos show that the epitope is expressed at sites (e.g., heart, chondrogenic sites) consistent with the lacZ expression patterns of the transgene observed in both homozygous and heterozygous *hdf* embryos (Capehart *et al.*, 1998, manuscript in preparation). In addition the *hdf*/lacZ transgene expression pattern during development is consistent with the pattern of expression for the *Cspg2* gene (versican) in the chick (unpublished results).

The fourth line of data that supports the hypothetical loss of *Cspg2* in *hdf* comes from genomic analysis of the transgene insertion site. A probe synthesized from a region flanking the transgene insertion was used to isolate from a normal mouse genomic library several overlapping lambda clones that spanned a region of approximately 17 kb. The validity for these clones to represent the site disrupted by the transgene depended on the authenticity of the 322-bp probe as flanking sequence. Therefore, several criteria were used to confirm that the flanking sequence used was authentic including mapping of the sequence back to chromosome 13 and Southern blots of transgenic derived DNA (Fig. 5) showing a band shift from 2.2 to 5.5 kb. This band

Copyright © 1998 by Academic Press. All rights of reproduction in any form reserved.

shift corresponds with a band identified on previously reported transgenic DNA blots probed with only the lacZ portion of the transgene as probe (Yamamura *et al.*, 1997). Cloned *Hin*dIII fragments from the isolated genomic lambda clones were also used to probe Southern blots of transgenic DNA. Again band shifts to 5.5 and 10.5 kb were observed (Fig. 5) that corresponded to the two bands previously observed (Yamamura *et al.*, 1997). These data, collectively, suggests that the contiguous region of genomic DNA spanned by the lambda clones encompasses the transgene insertion site. The detection of the *Cspg2* exon 7 sequences within each of the cloned genomic inserts confirmed the hypothesis that the transgene had inserted into middle region the *Cspg2* gene. These data that only the 3′ region of exon 7 was detectable in the genomic clone 12 and that both exons 7 and 8 appeared by genomic Southern blot analysis and PCR to be undisturbed by the transgene insertion confirmed that the site of the transgene insertion was within the 9-kb intron that separates the two condroitin binding domains (exon 7 and 8; Ito *et al.*, 1995).

The conclusion that the *hdf* mouse represents a null mutation for the *Cspg2* gene is consistent with our previous experimental data and descriptions of the *hdf* phenotypic characteristics. Although the *hdf* homozygous embryos die prior to the formation of limb buds, the *hdf*/lacZ expression patterns observed in the hemizygous embryos in chrondrogenic forming regions are consistent with versican expression (du Cros *et al.*, 1995; Kimata *et al.*, 1986; Roth *et al.*, 1997; Shinomura *et al.*, 1990, 1993). We had predicted (Yamamura *et al.*, 1997) based on the lack of cushion swellings in the atrioventricular and conus/truncus region of the heart in the *hdf* homozygous embryos that the *hdf* insertion had disrupted the normal expression of extracellular matrix either indirectly by interfering with a regulatory pathway or directly by physical disruption of an extracellular matrix gene. *In vitro* bioassays showed that *hdf* homozygous AV cushion explants, consisting of myocardium, endothelium, and associated matrix (cardiac jelly), could be rescued in their ability to form cushion mesenchyme. These results suggested that the failure to form mesenchyme *in vivo* was not intrinsic to the inductive competence of the myocardium or endocardium and that an extracellular factor(s) present in the culture system could compensate functionally, possibly providing the three-dimensional space required for migration. We do not know, as yet, if *Cspg2* is present within the *in vitro* type I collagen gel matrix preparations or if another molecule present can substitute for *Cspg2* proteoglycan. The absence of endocardial cushions in the *hdf* mutant null for *Cspg2* is also consistent with previously published data suggesting that chrondroitin sulfate proteoglycans are a functional component of developing heart cushions. The developing heart cushions have been shown to consist of several extracellular matrix components including chondroitin sulfate proteoglycans (Funderburg *et al.*, 1991; Funderburg and Markwald, 1986). Also, versican core protein has been localized by immunohistochemistry in the extracellular matrix of developing avian heart (unpublished results). The *Cspg2* proteoglycan may function in association with hyaluronan, another cushion matrix component found abundantly in the endocardial cushions, to increase local hydration at the site of cushion swellings and create space for mesenchyme migration. Hyaluronidase treatment of cultured rat embryos also results in the absence of endocardial cushions (Baldwin *et al.*, 1994). Another potential function for *Cspg2* proteoglycan in the cushion may be to interact with growth factors/cytokines and sequester or facilitate their biological function on nearby cardiac cells.

The *hdf* mouse is the first *in vivo* demonstration of the functional importance of *Cspg2* gene for the specific development of the endocardial cushions and the two segments that form the entire right limb (right ventricle and associated conus/truncus region) of the developing heart. The failed formation of the right limb of the looped heart in the *hdf* homozygous embryos, now known to lack *Cspg2*, suggests a functional role for the proteoglycan in the initiation or maintenance of the specification process that forms the right ventricle and conus/truncus regions. Results using antibody markers for myocardial segmental identity showed that the mutant homozygous hearts, at day 9.5 pc, express MLC-2a, MLC-2v, and α and β heavy-chain myosins within the myocardial cell layer of the heart tube. Both the MLC-2a and the MLC-2v showed a relatively normal pattern of expression for a day 9.5 pc embryonic heart within the posterior limb and the proximal part of the anterior limb (future right ventricle). This suggests that the establishment of the earliest segmental boundaries in the heart tube can occur in the absence of normal *Cspg2* gene expression. Our data suggest that expression of one or more of the four *Cspg2* alternative splice forms in the embryonic heart may not be obligatory for establishment of the first primitive heart segments, but is required for the sustained differentiation of the right ventricle and future development of the conus/truncus segment, the final segment formed within the looped heart and the only one to form from the anterior end of the heart tube (De la Cruz *et al.*, 1977).

The basic helix–loop–helix gene dHAND is also expressed within the right side of the looped heart tube (Srivastava *et al.*, 1997) and dHAND null embryonic hearts appear morphologically similar to *hdf* homozygous hearts suggesting that dHAND and *Cspg2* may function within a common pathway during chamber specification or differentiation in the heart. However, the AV endocardial cushion swellings, absent in the *hdf* homozygotes, are present within the dHAND null hearts suggesting that the *Cspg2* gene is expressed in the atrioventricular junction. Thus dHAND may not function to upregulate *Cspg2* within the AV endocardial cushions, but could potentially regulate expression, directly or indirectly, of the *Cspg2* gene within the right ventricle and conus/truncus. The transcription factor Pax3, defective in the *splotch* mouse (Epstein *et al.*, 1991), may also regulate versican since *splotch* mutants exhibit an increased versican expression within neural crest pathways (Henderson and Copp, 1997). However, it should be noted that Pax3 normally is not detectable by RT-PCR or

Copyright © 1998 by Academic Press. All rights of reproduction in any form reserved.

in situ hybridization in heart tissue prior to neural crest invasion and the cardiac neural crest express strong levels of Pax3 message (Conway *et al.*, 1997). This indicates that the mutant Pax3 in *splotch* neural crest could only have an indirect effect on *Cspg2* expression in the right outlet myocardium.

The findings of this study and our earlier phenotypic studies of the *hdf* insertional mutant mouse (Yamamura *et al.*, 1997) have shown that normal expression of the *Cspg2* gene is required for the successful development of the embryonic mouse heart. *Cspg2* gene expression appears to play an especially important role during morphogenesis of looped heart tube between embryonic day 8.5 and 10.5 pc. Specifically, observations of defects found in the *hdf* homozygous hearts show that *Cspg2* gene expression is required for the differentiation of the right side (ventricle) of the looped heart tube, its outlet (conus/truncus) and formation of cushion swellings in the AV and conal segments.

ACKNOWLEDGMENTS

We thank Drs. E. Krug, A. Mjaatvedt, and M. Kern for their critical comments and valuable discussions of this work. This research was funded by NIH Grants HL33756 and HL52813.

REFERENCES

Ausubel, F. M., Brent, R., Kingston, R. E., Morre, D. D., Seidman, J. G., Smith, J. A., and Struhl, K. (1995). Current protocols in molecular biology. *In* "Current Protocols in Molecular Biology" (J. Kaaren, Ed.). Wiley, New York.

Baldwin, H. S., Lloyd, T. R., and Solursh, M. (1994). Hyaluronate degradation affects ventricular function of the early postlooped embryonic rat heart in situ. *Circ. Res.* **74,** 244–252.

Bassett, D. E., Jr., Boguski, M. S., Spencer, F., Reeves, R., Kim, S., Weaver, T., and Hieter, P. (1997). Genome cross-referencing and XREFdb: Implications for the identification and analysis of genes mutated in human disease. *Nature Genet.* **15,** 339–44.

Capehart, A., Wienecke, M., Kitten, G., Solursh, M., and Krug, E. (1997). Production of a monoclonal antibody by in vitro immunization that recognizes a native chondroitin sulfate epitope in the embryonic chick limb and heart. *J. Histochem. Cytochem.* **45,** 1567–1581.

Conway, S. J., Henderson, D. J., and Copp, A. J. (1997). Pax3 is required for cardiac neural crest migration in the mouse: evidence from the splotch (Sp2H) mutant. *Development* **124,** 505–514.

De la Cruz, M. V., Sanchez Gomez, C., Arteaga, M. M., and Arguello, C. (1977). Experimental study of the development of the truncus and the conus in the chick embryo. *J Anat* **123,** 661–686.

De la Cruz, M. V., Sanchez-Gomez, C., and Palomino, M. A. (1989). The primitive cardiac regions in the straight tube heart (stage 9-) and their antomical expression in the mature heat: an experimental study in the chick heart. *J. Anat.* **165,** 121–131.

du Cros, D., LeBaron, R., and Couchman, J. (1995). Association of versican with dermal matrices and its potential role in hair follicle development and cycling. *J. Invest. Dermatol.* **105,** 426–431.

Eisenberg, L. M., and Markwald, R. R. (1995). Molecular regulation of atrioventricular valvuloseptal morphogenesis. *Circ. Res.* **77,** 1–6.

Epstein, D. J., Vekemans, M., and Gros, P. (1991). Splotch (Sp2H), a mutation affecting development of the mouse neural tube, shows a deletion within the paired homeodomain of Pax-3. *Cell* **67,** 767–774.

Feinberg, A. P., and Vogelstein, B. (1984). A technique for radiolabeling DNA restriction endonuclease fragments to high specific activity: Addendum. *Anal. Biochem.* **137,** 266–27.

Funderburg, F. M., Langford, J. K., and Hiltgen, G. G. (1991). Chondroitin sulfate proteoglycans: Do they play a role during cardiac morphogenesis? *Prog. Clin. Biol. Res.* **373,** 227–243.

Funderburg, F. M., and Markwald, R. R. (1986). Conditioning of native substrates by chondroitin sulfate proteoglycans during cardiac mesenchymal cell migration. *J. Cell Biol.* **103,** 2475–2487.

Henderson, D., and Copp, A. (1997). Over-expression of chrondroitin sulphate proteoglycan versican is associated with defective neural crest migration in the Pax3 mutant mouse (splotch). *Mech. Dev.* **69,** 39–51.

Ito, K., Shinomura, T., Zako, M., Ujita, M., and Kimata, K. (1995). Multiple forms of mouse PG-M, a large chondroitin sulfate proteoglycan generated by alternative splicing. *J. Biol. Chem.* **270,** 958–965.

Justice, M., and Stephenson, D. (1997). Mouse chromosome 13. *Mamm Genome* 7 Spec No, S223–37.

Kimata, K., Oike, Y., Tani, K., Shinomura, T., Yamagata, M., Uritani, M., and Suzuki, S. (1986). A large chondroitin sulfate proteoglycan (PG-M) synthesized before chondrogenesis in the limb bud of chick embryo. *J. Biol. Chem.* **261,** 13517–13525.

Kitten, G. T., Kolker, S. J., Krob, S. L., and Klewer, S. E. (1996). Type VI collagen in the cardiac valves and connective tissue septa during heart development. *Braz. J. Med. Biol. Res.* **29,** 1189–1193.

Kitten, G. T., Markwald, R. R., and Bolender, D. L. (1987). Distribution of basement membrane antigens in cryopreserved early embryonic hearts. *Anat. Rec.* **217,** 379–90.

Krug, E., Mjaatvedt, C., and Markwald, R. (1987). Extracellular matrix from embryonic myocardium elicits an early morphogenetic event in cardiac endothelial differentiation. *Dev. Biol.* **120,** 348–55.

Kuisk, I. R., Li, H. D. T., and Capetanaki, Y. (1996). A single MEF2 site governs desmin transcription in both heart and skeletal muscle during mouse embryoenesis. *Dev.. Biol..* **174,** 1–13.

Li, L., Miano, J. M., Mercer, B., and Olson, E. N. (1996). Expression of the SM22alpha promoter in transgenic mice provides evidence for distinct transcriptional regulatory programs in vascular and visceral smooth muscle cells. *J. Cell Biol.* **132,** 849–89.

Markwald, R. R., Fitzharris, T. P., and Manasek, F. J. (1977). Structural development of endocardial cushions. *Am. J. Anat.* **148,** 85–119.

Mjaatvedt, A. E., Citron, M. P., and Reeves, R. H. (1993). High-resolution mapping of D16led-1, Gart, Gas-4, Cbr, Pcp-4, and Erg on distal mouse chromosome 16. *Genomics* **17,** 382–36.

Mjaatvedt, C. H., Krug, E. L., and Markwald, R. R. (1991). An antiserum (ES1) against a particulate form of extracellular matrix blocks the transition of cardiac endothelium into mesenchyme in culture. *Dev. Biol.* **145,** 219–230.

Moessler, H., Mericskay, M., Li, Z., Nagl, S., Paulin, D., and Small, J. V. (1996). The SM 22 promoter directs tissue-specific expression in arterial but not in venous or visceral smooth muscle cells in transgenic mice. *Development* **122,** 2415–2425.

Copyright © 1998 by Academic Press. All rights of reproduction in any form reserved.

Potts, J. D., and Runyan, R. B. (1989). Epithelial–mesenchymal cell transformation in the embryonic heart can be mediated, in part, by transforming growth factor-β. *Dev. Biol.* **134,** 392–401.

Rezaee, M., Isokawa, K., Halligan, N., Markwald, R. R., and Krug, E. L. (1993). Identification of an extracellular 130-kDa protein involved in early cardiac morphogenesis. *J. Biol. Chem.* **268,** 14404–14411.

Ross, R., Navankasattusas, S., Harvey, R., and Chien, K. (1996). An HF-1a/HF-1b/MEF-2 combinatorial element confers cardiac ventricular specificity and established an anterior-posterior gradient of expression. *Development* **122,** 1799–1809.

Roth, S., Muller, K., Fischer, D., and Dannhauer, K. (1997). Specific properties of the extracellular chondroitin sulphate proteoglycans in the mandibular condylar growth centre in pigs. *Arch. Oral Biol.* **42,** 63–76.

Rowe, L. B., Nadeau, J. H., Turner, R., Frankel, W. N., Letts, V. A., Eppig, J. T., Ko, M. S., Thurston, S. J., and Birkenmeier, E. H. (1994). Maps from two interspecific backcross DNA panels available as a community genetic mapping resource. *Mamm. Genome* **5,** 253–274. [published erratum appears in *Mamm. Genome* **5**(7), 463, 1994.]

Sambrook, J., Fritsch, E., and Maniatis, T. (1989). "Molecular Cloning: A Laboratory Manual." Cold Spring Harbor Laboratory Press, Cold Spring Harbor, NY.

Seymour, A., Yanak, B., OqBrien, E., Rusiniak, M., Novak, E., Pinto, L., Swank, R., and Gorin, M. (1996). An integrated genetic map of the pearl locus of mouse chromosome 13. *Genome Res.* **6,** 538–544.

Shinomura, T., Jensen, K., Yamagata, M., Kimata, K., and Solursh, M. (1990). The distribution of mesenchyme proteoglycan (PG-M) during wing bud outgrowth. *Anat. Embryol. (Berl.)* **181,** 227–233.

Shinomura, T., Nishida, Y., Ito, K., and Kimata, K. (1993). cDNA cloning of PG-M, a large chondroitin sulfate proteoglycan expressed during chondrogenesis in chick limb buds: Alternative spliced multiforms of PG-M and their relationships to versican. *J. Biol. Chem.* **268,** 14461–14469.

Shinomura, T., Zako, M., Ito, K., Ujita, M., and Kimata, K. (1995). The gene structure and organization of mouse PG-M, a large chondroitin sulfate proteoglycan: Genomic background for the generation of multiple PG-M transcripts. *J. Biol. Chem.* **270,** 10328–10333.

Srivastava, D., Thomas, T., Lin, Q., Kirby, M. L., Brown, D., and Olson, E. N. (1997). Regulation of cardiac mesodermal and neural crest development by the bHLH transcription factor, dHAND. *Nature Genet.* **16,** 154–160.

Yamamura, H., Zhang, M., Markwald, R., and Mjaatvedt, C. (1997). A heart segmental defect in the anterior-posterior axis of a transgenic mutant mouse. *Dev. Biol.* **186,** 58–72.

Received for publication May 14, 1998
Revised June 30, 1998
Accepted June 30, 1998

Copyright © 1998 by Academic Press. All rights of reproduction in any form reserved.

DEVELOPMENTAL BIOLOGY 202, 67–84 (1998)
ARTICLE NO. DB988987

A Single Rostrocaudal Colonization of the Rodent Intestine by Enteric Neuron Precursors Is Revealed by the Expression of Phox2b, Ret, and p75 and by Explants Grown under the Kidney Capsule or in Organ Culture

H. M. Young,* C. J. Hearn,† D. Ciampoli,* B. R. Southwell,* J.-F. Brunet,‡ and D. F. Newgreen†

**Department of Anatomy & Cell Biology, University of Melbourne, Parkville 3052, Victoria, Australia; †The Murdoch Institute, Royal Children's Hospital, Parkville 3052, Victoria, Australia; and ‡Laboratoire de Génétique et de Physiologie du Développement, IBDM, CNRS/INSERM/ Université de la Méditerraneé, Luminy Case 907, 13288 Marseille Cedex 9, France*

The colonization of the rodent gastrointestinal tract by enteric neuron precursors is controversial due to the lack of specific cellular markers at early stages. The transcription factor, Phox2b, is expressed by enteric neuron precursors (Pattyn *et al. Development* 124, 4065–4075, 1997). In this study, we have used an antiserum to Phox2b to characterize in detail the spatiotemporal expression of Phox2b in the gastrointestinal tract of adult mice and embryonic mice and rats. In adult mice, all enteric neurons (labeled with neuron-specific enolase antibodies), and a subpopulation of glial cells (labeled with GFAP antibodies), showed immunoreactivity to Phox2b. In embryonic mice, the appearance of Phox2b-immunoreactive cells was mapped during development of the gastrointestinal tract. At Embryonic Days 9.5–10 (E9.5–10), Phox2b-labeled cells were present only in the stomach, and during subsequent development, labeled cells appeared as a single rostrocaudal wave along the gastrointestinal tract; at E14 Phox2b-labeled cells were present along the entire length of the gastrointestinal tract. Ret and p75 have also been reported to label migratory-stage enteric neuron precursors. A unidirectional, rostral-to-caudal colonization of the gastrointestinal tract of embryonic mice by Ret- and p75-immunoreactive cells was also observed, and the locations of Ret- and p75-positive cells within the gut were very similar to that of Phox2b-positive cells. To verify the location of enteric neuron precursors within the gut, explants from spatiotemporally defined regions of embryonic intestine, 0.3–3 mm long, were grown in the kidney subcapsular space, or in catenary organ culture, and examined for the presence of neurons. The location and sequence of appearance of enteric neuron precursors deduced from the explants grown under the kidney capsule or in organ culture was very similar to that seen with the Phox2b, Ret, and p75 antisera. Previous studies have mapped the rostrocaudal colonization of the rat intestine by enteric neuron precursors using HNK-1 as a marker. In the current study, all HNK-1-labeled cells in the gastrointestinal tract of rat embryos showed immunoreactivity to Phox2b, but HNK-1 cells comprised only a small subpopulation of the Phox2b-labeled cells. In addition, in rats, Phox2b-labeled cells were present in advance of (more caudal to) the most caudal HNK-1-labeled cells by 600–700 μm in the hindgut at E15. We conclude that the neural crest cell population that arises from the vagal level of the neural axis and that populates the stomach, midgut, and hindgut expresses Phox2b, Ret, and p75. In contrast, the sacral-level neural crest cells that populate the hindgut either do not express, or show a delayed expression of, all of the known markers of vagal- and trunk-level neural crest cells. © 1998 Academic Press

Key Words: neural crest; mouse; intestine; Phox2b; p75, Ret.

INTRODUCTION

The neurons and glial cells of the enteric nervous system are derived from the neural crest. In both birds and mammals, the vast majority of enteric neurons in the stomach and intestine arise from vagal-level (somites 1–7) neural crest, particularly from the level of somites 2–6 (Yntema and Hammond, 1954; Le Douarin and Teillet, 1973; Epstein *et al.*, 1994; Durbec *et al.*, 1996). Most of the enteric neurons in the esophagus do not arise from vagal-level neural crest (Epstein *et al.*, 1994), and recent evidence suggests that they arise from anterior trunk-level neural crest, which also gives rise to the

0012-1606/98 $25.00
Copyright © 1998 by Academic Press
All rights of reproduction in any form reserved.

superior cervical ganglion (Durbec *et al.*, 1996). Although most of the enteric neurons in the hindgut arise from vagal-level neural crest, studies using chick–quail chimeras and studies in which premigratory cells had been labeled with DiI or retroviruses have shown that some cells that populate the hindgut arise from sacral-level neural crest, which lies caudal to somite 28 in birds and somite 24 in mice (Le Douarin and Teillet, 1973; Pomeranz *et al.*, 1991; Serbedzija *et al.*, 1991). These cells colonize the hindgut well before the arrival of vagal-level-derived neural crest cells (Serbedzija *et al.*, 1991, Kapur *et al.*, 1992). In both mouse and chicken embryos, the vagal-level neural crest cells colonize the gastrointestinal tract rostrocaudally, and if segments of hindgut are removed prior to the arrival of the vagal neural crest cells but after the time the sacral neural crest cells are reported to have reached the hindgut, enteric neurons do not develop in the hindgut explants (Allan and Newgreen, 1980; Nishijima *et al.*, 1990; Kapur *et al.*, 1992). Moreover, following transection of the midgut prior to the arrival of the vagal neural crest cells, enteric neurons do not develop in the hindgut of chick embryos (Meijers *et al.*, 1989). Thus the contribution of the sacral neural crest to the formation of the enteric nervous system is controversial, and it appears that either the sacral neural crest cells do not give rise to enteric neurons or that they differentiate into enteric neurons only when vagal crest cells are present (see Allan and Newgreen, 1980; Gershon *et al.*, 1992).

While they are migrating, the precursor cells of the enteric nervous system do not express a neuronal or glial cell phenotype. In rodents, the expression of neurofilaments (Baetge *et al.*, 1990; Newgreen and Hartley, 1995), glial fibrillary acidic protein (GFAP, Rothman and Gershon, 1986), esterases (Webster, 1973), catecholaminergic markers (Cochard *et al.*, 1978; Teitelman *et al.*, 1978, 1981; Baetge and Gershon, 1989; Baetge *et al.*, 1990), and a variety of neurotransmitters (Rothman and Gershon, 1982; Rothman *et al.*, 1984; Branchek and Gershon, 1989) does not commence in a gut region until several hours to many days after the region has been first colonized. A major difficulty in determining in detail how the gastrointestinal tract is colonized by precursors of the enteric nervous system has been the deficiency of good markers of migratory-stage neural crest cells that recognize all enteric neuron precursors. In birds, the colonization of the gut by migrating neural crest cells has been studied using chick–quail chimeras (LeDouarin and Teillet, 1973) and the equivalent monoclonal antibodies, HNK-1 and NC-1 (Tucker *et al.*, 1986; Pomeranz and Gershon, 1990; Epstein *et al.*, 1991, Newgreen *et al.*, 1996). However, HNK-1 appears to recognize only a small subpopulation of migrating crest cells in the developing intestine of rats and has not been used successfully in mice. The colonization of the mouse gut by enteric neuron precursors has been studied using *DβH-nlacZ* mice (Kapur *et al.*, 1992) and by the expression of c-*ret* (Pachnis *et al.*, 1993). The *DβH-nlacZ* transgene is expressed by a subpopulation of enteric neurons (Kapur *et al.*, 1991). Using wholemount preparations of E9.5–E13 mouse gut, Kapur *et al.* (1992) demonstrated that there is a unidirectional, rostrocaudal wave of expression of the transgene during development, and this was inferred to represent the colonisation of the gut by vagal-level enteric neuron precursors. However, since DBH is only expressed by a subpopulation of enteric neurons, it is possible that the sacral-level enteric neuron precursors do not express this gene (Kapur *et al.*, 1992). The expression of c-*ret* also shows a rostrocaudal progression during mouse embryonic development (Pachnis *et al.*, 1993). c-*ret* encodes the receptor tyrosine kinase, Ret, which is a component of the receptor complex for glial-derived neurotrophic factor (GDNF; Jing *et al.*, 1996; Treanor *et al.*, 1996), and it is critical for the development of the enteric nervous system (Schuchardt *et al.*, 1994, Moore *et al.*, 1996, Pichel *et al.*, 1996, Sánchez *et al.*, 1996; see also Gershon, 1997, for review). Within the developing enteric nervous system, Ret is expressed by cells with neuronal and nonneuronal potential (Lo and Anderson, 1995), consistent with it being a neural stem cell marker, but it is unknown whether c-*ret* is expressed by all enteric neuron precursors. Since the expression of c-*ret* by cells in the embryonic mouse gut was only monitored in sections by Pachnis *et al.* (1993), expression of c-*ret* by a small number of cells in the caudal hindgut during early development could have been overlooked. p75 is the low-affinity nerve growth factor receptor, and like Ret, has been reported to be expressed by migratory-stage enteric neuron precursors (Lo and Anderson, 1995). However, the spatiotemporal pattern of expression of p75 has not been examined in the gastrointestinal tract of any species.

An ideal molecule to follow the migration and colonization of the gastrointestinal tract by enteric neuron precursors would be one that is expressed by migrating enteric neuron precursors and continues to be expressed by differentiated enteric neurons, so that it could be determined whether it is expressed by all, or a subpopulation, of enteric neurons. Transcription factors are often expressed before neuronal precursors begin to differentiate and can therefore be useful for monitoring the development of particular parts of the nervous system. For example, the transcription factor, Islet-1, is expressed by migrating, undifferentiated cholinergic amacrine cells in the retina; the development of the orderly spacing of cholinergic amacrine cells seen in mature animals has recently been examined by using an antibody to Islet-1 to map the behaviour of immature cholinergic amacrine cells (Galli-Resta *et al.*, 1997). The homeodomain transcription factors, Phox2a and Phox2b, are coexpressed in many parts of the peripheral autonomic nervous system, including the enteric nervous system, and in discrete parts of the central nervous system (Tiveron *et al.*, 1996; Morin *et al.*, 1997; Pattyn *et al.*, 1997). However, the two genes show some differences in onset and duration of expression, and while both *Phox2a* and *Phox2b* are expressed by developing enteric neurons, only *Phox2b* is expressed by migrating enteric neuron precursors (Pattyn *et al.*, 1997).

The aims of the current study were (i) to determine whether all, or only a subpopulation, of differentiated

Copyright © 1998 by Academic Press. All rights of reproduction in any form reserved.

TABLE 1
Primary Antisera Used

Antiserum	Concentration	Source of reference
Calretin (goat)	1:50	SWANT, Belinzona, Switzerland
Glial fibrillary acidic protein (GFAP) (rabbit)	1:1000	Dako, Botany, NSW, Australia; Code 20334
HNK-1 (mouse)	1:10	Hybridoma maintained at the Murdoch Institute, Royal Children's Hospital, Parkville, VIC, Australia
Neuron-specific enolase (NSE) (rabbit)	1:1000	Dako
Nitric oxide synthase (NOS) (sheep)	1:1000	Kind gift of Drs. P. Emson and I. Charles
p75 (rabbit)	1:250	Promega Corporation, Annandale, NSW, Australia
Phox2b (rabbit)	1:700 (or 1:7000 or 1:14,000 for tyramine signal amplification)	Pattyn *et al.*, 1997
Ret (rabbit)	1:50	Immuno-biological laboratories Co. Ltd., Tokyo, Japan

enteric neurons show immunoreactivity to Phox2b protein; (ii) to establish a detailed spatiotemporal timetable of the appearance of Phox2b-, Ret-, and p75-labeled cells within the gut of embryonic mice; and (iii) to examine the location of enteric neuron precursors by (a) explanting spatiotemporally defined regions of embryonic mouse intestine to the kidney subcapsular space of adult host mice for 2–3 weeks, and (b) growing spatiotemporally defined regions of embryonic mouse intestine in organ culture for 10 days. The explants grown under the kidney capsule and in organ culture were then processed, using immunohistochemical or histological techniques, to deduce if enteric neuron precursors were present at the time of explantation.

MATERIALS AND METHODS

Adult, neonatal, and embryonic BALB/c mice from an inbred colony and embryonic Sprague–Dawley rats were used. Embryos were obtained from timed, pregnant mice or rats; the date at which a copulatory plug was observed was designated E0, and the date of birth, P0. Embryonic mice were then staged precisely using the staging system of Theiler (1989; denoted by T) and rats with the staging system of Christie (1964; denoted by C). Segments of the gastrointestinal tract were fixed overnight in 4% formaldehyde in 0.1 M phosphate buffer, pH 7.0, at 4°C. After washing, whole-mount preparations or frozen sections were processed for single or double-label fluorescence immunohistochemistry as described previously (Newgreen and Hartley, 1995; Young *et al.*, 1996). In some preparations, the primary antiserum was revealed using avidin–biotin–horseradish peroxidase and diaminobenzidine. The preparations were then embedded in resin and sectioned at 1 μm, and the sections were stained with a mixture of toluidine blue and methylene blue. The primary and secondary antisera used are shown in Tables 1 and 2. To perform double-label immunohistochemistry with two primary antisera raised in the same species [rabbit anti-Phox2b plus rabbit anti-neuron-specific enolase (NSE) or rabbit anti-Phox2b plus rabbit anti-glial fibrillary acidic protein (GFAP)], the tyramine signal amplification kit (NEN Life Science Products, Boston, MA) was used. Whole-mount preparations of fixed gut were preincubated in 0.5% blocking powder (from the kit) in 0.1 M Tris–HCl containing 0.15 M NaCl for 30 min at room temperature and then incubated in 1:7000 or 1:14,000 anti-Phox2b for 48 h. The tissue was then washed in 0.1 M Tris–HCl containing 0.15 M NaCl plus 0.05% Triton X-100 (TNT) and incubated in

TABLE 2
Secondary Antisera Used

Species in which primary antisera were raised	Seconary antisera	Concentration	Source
Rabbit	Donkey anti-rabbit Cy3	1:1000	Jackson Immunoresearch Inc., West Grove, Pa
Rabbit plus sheep (or goat)	Biotinylated donkey anti-rabbit followed	1:100	Jackson Immunoresearch Inc.
	by streptavidin–Texas red and donkey	1:100	Amersham
	anti-sheep FITC	1:50	Jackson Immunoresearch
Rabbit plus mouse	Biotinylated horse antimouse followed	1:200	Vector
	by streptavidin–Texas red and donkey	1:100	Amersham
	anti-rabbit FITC	1:25	Amersham

Copyright © 1998 by Academic Press. All rights of reproduction in any form reserved

biotinylated donkey anti-rabbit (1:100; Jackson Immuno-research Inc., West Grove, PA) for 2 h. After washing in TNT, the tissue was incubated in streptavidin–HRP (from kit; 1:100 in phosphate-buffered saline, PBS) for 30 min in the dark, washed in TNT, incubated in biotinyl tyramine (1:100 in amplification diluent, both from kit), washed in TNT, and then incubated in streptavidin–Texas red (1:50, Amersham, Melbourne, VIC, Australia) for 1 h. After washing in PBS, the tissue was incubated in the second primary antiserum (rabbit anti-NSE or rabbit anti-GFAP, see Table 1) for 48 h and then in donkey anti-rabbit FITC (1:25; Amersham) for 90 min. Control pieces of tissue that had been incubated in anti-Phox2b (1:7000 or 1:14,000) for 48 h and then in donkey anti-rabbit FITC showed no staining. Control experiments in which whole-mount preparations of adult and embryonic myenteric plexus were exposed to secondary antisera only revealed no staining.

Explants to the kidney subcapsular space of mice. Pregnant mice with embryos at E9.5–E14 gestational age were killed by cervical dislocation, and the embryos were removed, placed in sterile tissue culture medium, and precisely staged (see above). Intestinal segments 0.3–3 mm long from carefully defined regions of the gastrointestinal tract were explanted to the subcapsular space of the kidney of adult host mice and allowed to grow for 2–3 weeks as described previously (Young *et al.*, 1996). The host animals were then killed and the explants removed. Some explants were fixed overnight in 4% formaldehyde in 0.1 M phosphate buffer, and then frozen sections were cut on a cryostat and processed for Phox2b, neuron-specific enolase (NSE), or nitric oxide synthase (NOS) immunohistochemistry. Other explants were fixed in 2.5% formaldehyde plus 3.5% glutaraldehyde in 0.1 M phosphate buffer, pH 7.3, for 1 h prior to dehydration through alcohol and embedding in glycol methacrylate. Sections, 4 μm thick, were cut and stained with Lee's methylene blue–basic fuchsin (Bennett *et al.*, 1976).

Organ culture. All of the organ culture experiments were performed using two regions of the gastrointestinal tract of E10.5–late E11.5 (T17–T19+) embryos: (a) midgut, which was defined as the region of gut rostral to the caecal swelling; and (b) hindgut, which included the entire gut caudal to the cecal swelling. The gut segments were 0.3–0.7 mm long and were dissected out in Dulbecco's modified eagle medium (DME). The ends of each segment were attached to the two sides of a V-shape notch which had been cut into small squares (about 3 mm^2) of black Millipore paper (type HA; Millipore, North Ryde, NSW, Australia). The filter paper had been sterilized using ethanol. The pieces of filter paper, with the gut segments suspended catenary-fashion from the sides of the V-shaped notch, were then laid across the top of Terasaki wells (60-well plate; Disposable Products, Technology Park, SA, Australia), containing 14 μl of culture medium. The culture medium consisted of DME containing 20 mM glutamine, 6 mg/ml penicillin, 10 mg/ml streptomycin, and 10% heat-inactivated fetal calf serum. The cultures were maintained in a 5% CO_2 environment at 37°C and cultured for 10 days before being fixed in 4% formaldehyde and processed as whole-mounts for immunohistochemistry as described above.

Microscopy. Preparations were viewed on a Zeiss Axioskop or Axioplan microscope, and video images were recorded using an ImagePoint cooled CCD camera (Photometrics Ltd., Tucson, AZ) and V for Windows imaging software (Digital Optics Ltd., Auckland, New Zealand). Each image was processed using a sharpen filter and contrast adjustment. Plates were made using Corel PhotoPaint and Corel Draw (Corel Corp., Dublin, Ireland). Some preparations were scanned on a Bio-Rad MRC 1024 confocal laser scanning microscope installed on an Axioplan fluorescence microscope with a krypton/argon laser. The images were processed using Confocal Assistant and Corel PhotoPaint and Corel Draw software.

RESULTS

Identification of Phox2b-Stained Cells in the Gastrointestinal Tract of the Late Embryonic, Neonatal, and Adult Mice

In the small and large intestine of adult mice, strong Phox2b immunoreactivity was shown by the nuclei of cells within the myenteric (Fig. 1A) and submucosal plexuses (Fig. 1B). Stained nuclei were found only within the ganglia and along the internodal strands. The interstitial cells of Cajal, which form a plexus between the myenteric ganglia (Torihashi *et al.*, 1995), and muscle cells were not stained. Many of the Phox2b-immunoreactive nuclei were round in shape with prominent, unstained nucleoli; other stained nuclei were oval in shape, without prominent nucleoli and were less strongly stained than the round nuclei (Fig. 1B). In preparations that had been processed for double-label immunohistochemistry using antisera to NSE and Phox2b, almost all of the NSE-stained cells showed Phox2b immunoreactivity (Figs. 1C and 1C′); of 1000 NSE-positive cells from two preparations of myenteric plexus from the large intestine, 999 were Phox2b positive. Some of the Phox2b-stained cells did not show immunoreactivity to NSE. These cells appeared to have only a small amount of cytoplasm and hence may have been glial cells (Figs. 1C and 1C′). All of the NOS- (Fig. 1D) and calretinin-immunoreactive neurons, which together constitute over 70% of all myenteric neurons in the mouse small intestine (Sang and Young, 1996), also showed Phox2b staining. In preparations that had been double-stained to reveal GFAP and Phox2b immunoreactivities, some, but not all, of the GFAP-stained cells showed Phox2b immunostaining (Figs. 1E and 1E′). The intensity of the Phox2b immunostaining exhibited by the GFAP-positive cells was usually lower than that of neuronal nuclei. Whole-mount preparations of the external muscle from the esophagus (Fig. 1F) and intestine from late embryonic (E16, T24) and neonatal mice were also processed to reveal Phox2b immunoreactivity, and the pattern of staining observed was identical to that seen in the intestine of adult mice.

Identification of Ret- and p75-Stained Cells in the Gastrointestinal Tract of Adult Mice

In the enteric nervous system of adult mice, no specific Ret immunostaining was observed. A reticular pattern of p75 immunostaining was observed, but it was not possible, even using a confocal microscope, to determine if the stained structures were the cell membranes of nerve cell bodies or of neuronal and glial cell processes that were passing around the nerve cell bodies (Fig. 1G). We were therefore unable to determine if individual enteric neurons were p75 immunoreactive.

Copyright © 1998 by Academic Press. All rights of reproduction in any form reserved.

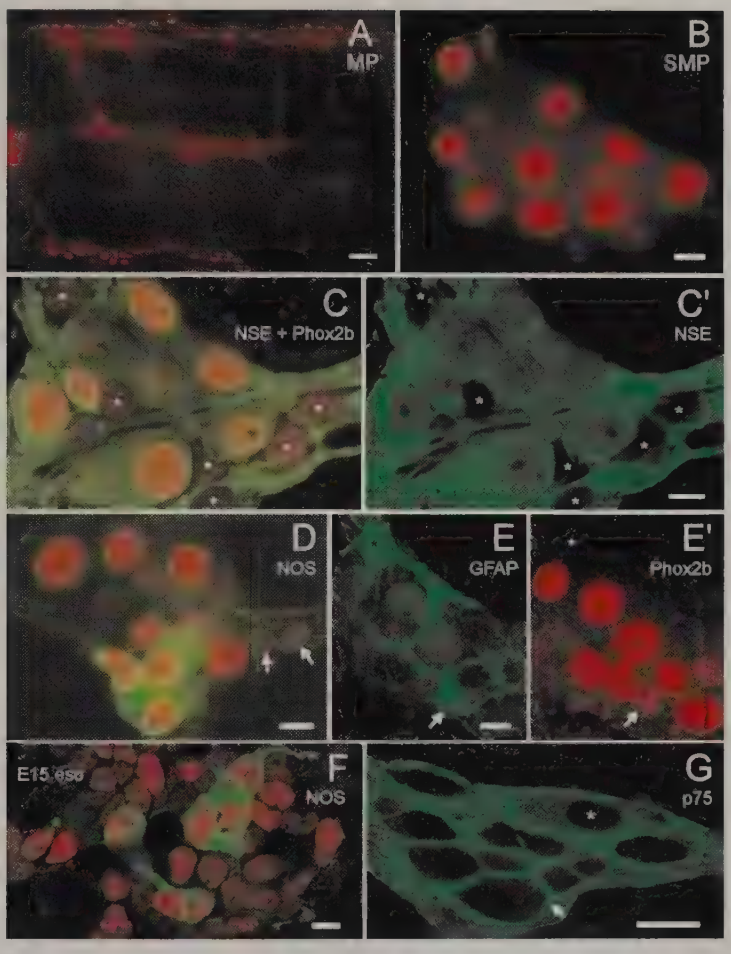

FIG. 1. Low-power micrograph of a whole-mount preparation of longitudinal muscle/myenteric plexus (*MP*) from the small intestine of an adult mouse showing the pattern of Phox2b immunoreactivity. Stained nuclei are present only in the ganglia and internodal strands. Scale bar, 50 μm. (B) Whole-mount preparation of a submucosal ganglion (*SMP*) from the small intestine of an adult mouse showing Phox2b-stained nuclei. Many of the strongly stained nuclei are round with prominent nucleoli. There are also oval nuclei present that are less intensely stained; these may be the nuclei of glial cells. Scale bar, 10 μm. (C and C′) Confocal microscope images (single optical sections) of a whole-mount preparation of the myenteric plexus of the large intestine of an adult mouse following processing for Phox2b-specific (red) and neuron-specific enolase immunoreactivity (green). C is an overlay of the NSE and Phox2b immunostaining, and C′ shows the pattern of NSE staining only. All of the NSE-immunostained cells have Phox2b-stained nuclei, but some Phox2b-stained cells (*asterisks*) do not show NSE immunostaining; most of the Phox2b-stained cells that are NSE-negative (*asterisks*) have very little cytoplasm and are likely to be glial cells. Scale bar, 10 μm. (D) Whole-mount preparation of the myenteric plexus of the small intestine of an adult mouse following processing for Phox2b (red) and nitric oxide synthase immunoreactivity (*NOS*, green). All of the NOS-immunostained cells show Phox2b staining, but some Phox2b-stained cells do not show NOS immunostaining. Some of the Phox2b-stained cells that are NOS-negative (*arrows*) have very little cytoplasm and are located along the internodal strands. Scale bar, 10 μm. (E and E′) Confocal microscope images (projections of 15 optical sections, 0.5 μm z steps) of a whole-mount preparation of myenteric plexus from the small intestine of an adult mouse showing GFAP (E) and Phox2b (E′) immunostaining. There are two GFAP-immunostained cells in the field of view, one of which shows Phox2b immunostaining (*arrow*), and the other (*asterisk*) is Phox2b-negative. Scale bar, 10 μm. (F) Confocal microscope image (single optical section) of a whole-mount preparation of esophagus from an E15 mouse showing Phox2b (red) and NOS (green) immunoreactivities. All of the NOS cells have Phox2b-stained nuclei, but NOS cells comprise only a small proportion of all of the Phox2b-positive cells. Scale bar, 10 μm. (G) Confocal micrograph of a myenteric ganglion from an adult mouse showing the reticular pattern of p75 immunoreactivity. There are rims of staining outlining the cells (*arrow*). There is also weak cytoplasmic staining in one of the neurons (*asterisk*). Scale bar, 20 μm.

Copyright © 1998 by Academic Press. All rights of reproduction in any form reserved.

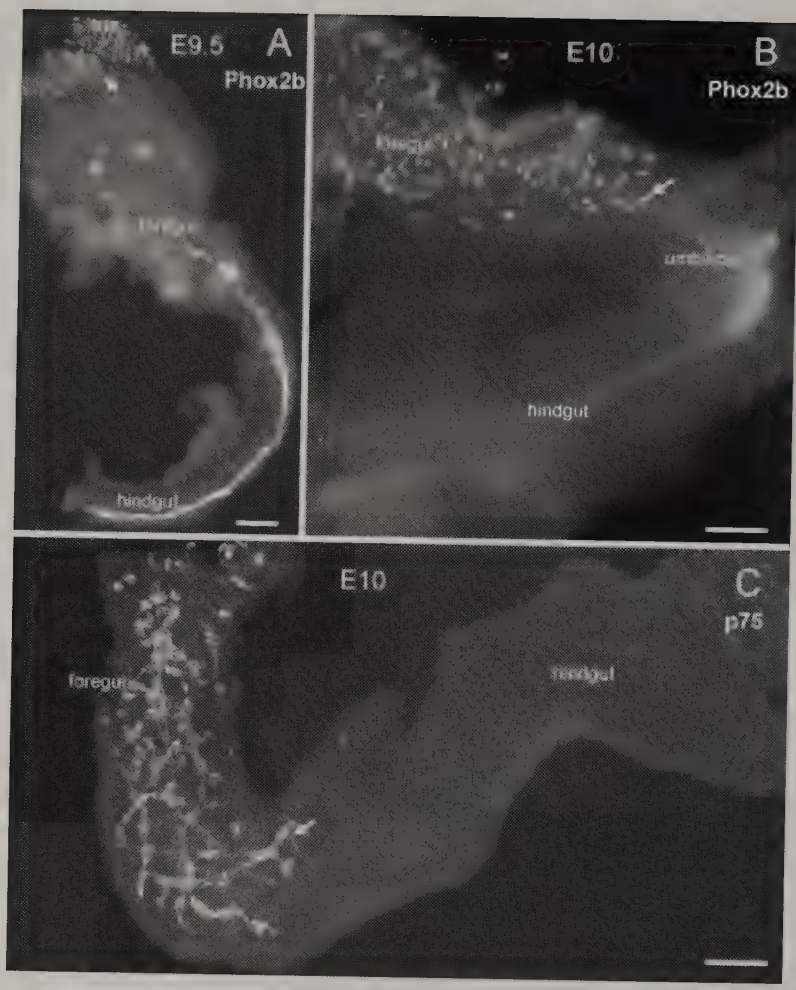

FIG. 2. Whole-mount preparations of gastrointestinal tract from E9.5 and E10 mice showing the pattern of Phox2b or p75 immunoreactivity. (A) Mid- and hindgut plus tissue attached to the foregut from an E9.5 (T15, 27 somite) mouse. Phox2b-stained cells (*arrow*) are present adjacent to the foregut. Scale bar, 100 μm. The line of fluorescence down the middle of the preparation is nonspecific staining in the gut lumen. (B) At E10 (T16), Phox2b-stained cells extend throughout the foregut. The most caudal Phox2b-stained cell (*arrow*) is rostral to the umbilicus. There are no stained cells present in the hindgut. Scale bar, 100 μm. (C) At E10 (T16), p75-stained cells also extend throughout the foregut, but there are no stained cells present in the hindgut. The most caudal p75-stained cell (*arrow*) is in the midgut. Scale bar, 100 μm.

Spatiotemporal Pattern of Appearance of Phox2b-Immunoreactive Cells in the Early Developing Gastrointestinal Tract

In E9.5 mice [Thieler stage 15 (T15), 25–27 somites] Phox2b-stained cells were present in the mesenchyme adjacent to the foregut (Fig. 2A). By E10 (T16), Phox2b-stained cells were present in the mesenchyme of the foregut and rostral midgut and extended to within 100–200 μm of the umbilicus (Fig. 2B), but stained cells were not observed within the mesenchyme of the hindgut. At E11 (T18), the most caudal Phox2b-stained cells were at the level of the umbilicus (Fig. 9A). By E11.5 (T19), the most caudal stained cells were at the level of, and sometimes just caudal to, the caecal swelling. By E12 (T20) the cecum had been colonized and stained cells were also present in the rostral one-third of the hindgut (Fig. 3A). By E13 (T21) the wavefront of stained cells was in the caudal half of the hindgut. By E14 (T22) mice Phox2b-stained cells were present along the entire gut. In E9.5–E13 (T15–21) mice, we did not observe any Phox2b-stained cells within the mesenchyme of the hindgut prior to (i.e., caudal to) the wave of labeled cells spreading rostrocaudally from the foregut. However, in

Copyright © 1998 by Academic Press. All rights of reproduction in any form reserved.

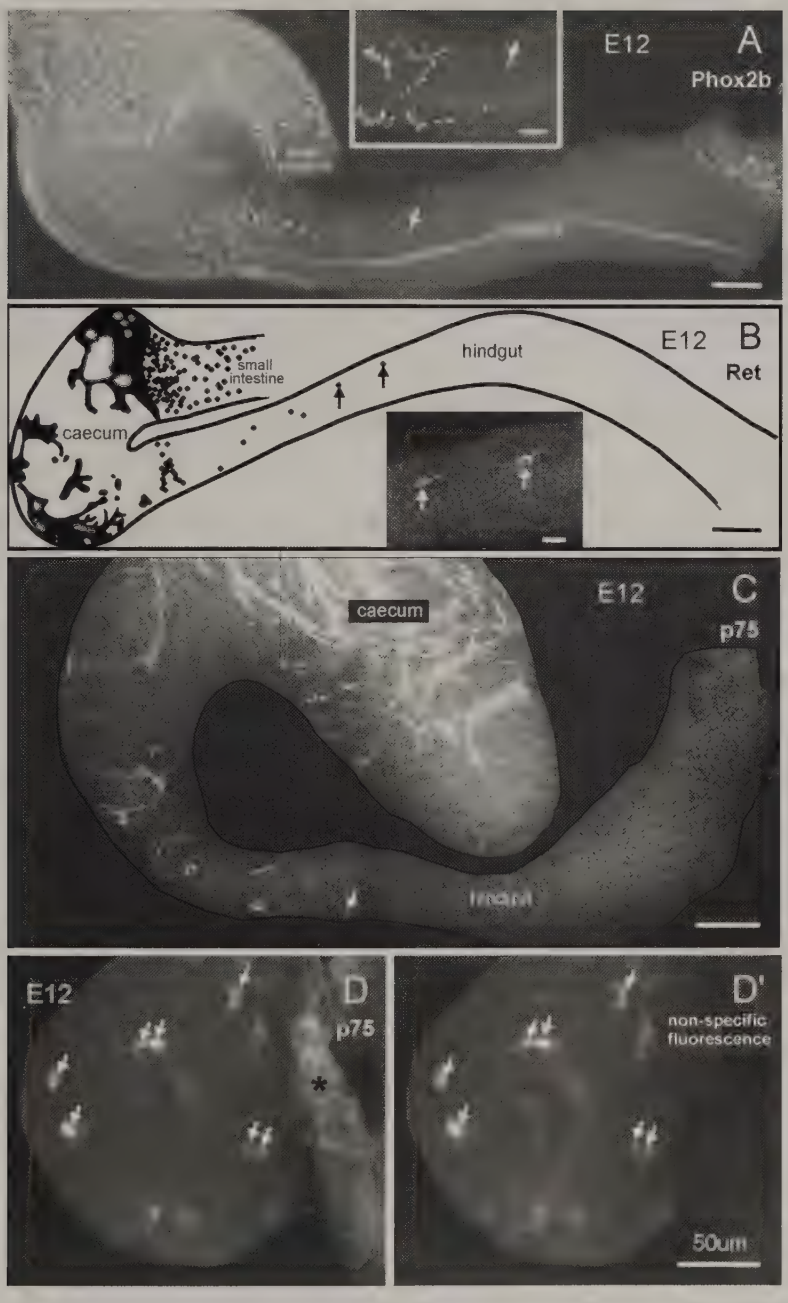

FIG. 3. (A–C) Whole-mount preparations of cecum and hindgut from E12 (T20) mice stained for Phox2b (A), Ret (B), and p75 (C). (A) Phox2b cells are present in the caecum, and extend into the hindgut. The most caudal Phox2b-stained cell within the gut mesenchyme (*arrow*) is in the rostral half of the hindgut. A group of stained cells (*asterisk*) is present external to the mesenchyme of the caudal hindgut. (Inset) Higher magnification of the most caudal Phox2b-stained cells. Note that Phox2b-stained cells near the wavefront are often aligned in rows that spiral, or run longitudinally, along the gut. Scale bars, 100 and 50 μm (inset). (B) Tracing of the most caudal part of the hindgut of an E12 (T20) mouse that had been processed for Ret immunohistochemistry. The Ret immunostaining was too weak to be illustrated in a low-power fluorescence micrograph, and thus this drawing was obtained by photographing the entire hindgut using a ×40 objective, making a montage, and then plotting the location of the Ret-positive cells on an overlay. The locations of Ret-positive cells are indicated

Copyright © 1998 by Academic Press. All rights of reproduction in any form reserved.

some preparations from E10–12 (T16–20) mice, groups of Phox2b-stained cells were present adjacent to, but clearly outside of, the mesenchyme of the caudal hindgut (Fig. 3A). These groups of cells were probably the primordia of the pelvic plexus. Within the mesenchyme of the gut wall, some fluorescent cells were present. However, these cells were identified as nucleated embryonic blood cells because they showed nonspecific fluorescence (the fluorescence was visible through the FITC, Texas red, and UV filters, while the fluorescence of the Phox2b-stained cells was only visible through a single filter).

Spatiotemporal Pattern of Appearance of Ret- and p75-Immunoreactive Cells in the Early Developing Gastrointestinal Tract

Since at least some enteric neuron precursors express c-*ret* (Pachnis *et al.*, 1993) and p75 (Lo and Anderson, 1995; Lo *et al.*, 1997), the spatiotemporal appearance of the Phox2b-positive cells was compared to that of Ret- and p75-immunoreactive cells. At E10 (T16), E10.5 (T17), and E11 (T18), the location of p75-positive cells was very similar to that of Phox2b-positive cells in that p75-stained cells were present in the gut rostral to the umbilicus, but not in the hindgut (Figs. 2C and 9B); no immunoreactivity to Ret could be detected in the gut at these stages. At E12 (T20), Ret- and p75-immunostained cells were present throughout the foregut and cecum; the most caudal Ret- and p75-positive cells were in the rostral half of the hindgut (Figs. 3B and 3C), which was very similar to the location of the most caudal Phox2b-stained cells at this stage (Fig. 3A). No Ret- or p75-positive cells were observed within the mesenchyme of the caudal end of the hindgut at E12, although groups of p75-stained cells were observed adjacent to, and clearly outside of, the caudal hindgut in some specimens (Figs. 3D and 3D′). At E13 (T21), Ret- and p75-stained cells extended down to the caudal third of the hindgut, and at E14 (T22), Ret- and p75-stained cells were present throughout the entire gastrointestinal tract. Thus, Ret- and p75-positive cells were found at the same rostrocaudal locations as the Phox 2b-positive cells.

Arrangement of Cells at or near the Wavefront

The arrangement of Phox2b-, Ret-, and p75-stained cells at the wavefront was similar. In E10 (T16) preparations, Phox2b- and p75-stained cells appeared randomly and densely distributed with no obvious differences between the density and arrangement of cells at the "front" and those behind (i.e., rostral to) them (Figs. 2B and 2C); this gave a sharp cutoff of the labeling. In E10.5 (T17) and older embryos, the density of stained cells at the wavefront was always considerably lower than that 500 μm or more rostral, giving a graded decline of density of labeled cells. At these stages, many of the most caudal Phox2b-, Ret-, and p75-stained cells were arranged in chains that ran longitudinally down the gut, or that spiralled around the gut (Figs. 3A (inset), 4A, and 4B). The Phox2b-positive nuclei forming these chains were separated by less than 10 μm from each other (Fig. 4A). Ret and p75 immunostaining revealed that the processes of neighboring cells forming the chains were in contact with each other (Fig. 4B). Rostral to the wavefront, Phox2b-, Ret-, and p75-positive cells all appeared to be evenly distributed (Figs. 4C–4E), and there appeared to be less Ret-stained cells than Phox2b- or p75-stained cells.

Formation of Enteric Ganglia and the Location of Enteric Neuron Precursors within the Mesenchyme of the Gut

The first indication of the formation of groups of cells that form ganglia was observed in the small intestine of E13 (T21) mice, where groups of Phox2b-labeled cells and areas lacking such cells could be identified (Figs. 4F and 4G). Subsequently, the proportion of Phox2b-stained cells that were present in groups increased, and by birth the vast majority of stained cells were present in groups aligned circumferentially around the gut that were similar in shape and arrangement to myenteric ganglia present in adult mice.

In sections through the embryonic gut, Phox2b- and p75-stained cells formed a layer, one to two cells thick in the outer mesenchyme, with usually only a single layer of unstained cells present external to the stained cells (Figs. 4H, 4I, and 5A). Since the longitudinal muscle layer does not form until E18 in mice (Torihashi *et al.*, 1997), the cells external to the Phox2b-stained cells are likely to be serosal cells.

Presence of Neurons in Explants of Embryonic Mouse Intestine Grafted to the Kidney Subcapsular Space and in Explants of E11 Mid- and Hindgut Grown in Organ Culture

Segments of embryonic intestine explanted to the kidney subcapsular space grew and differentiated (Fig. 6)

---

with black dots or black regions. The most caudal Ret-stained cells (*arrows*) are in the rostral half of the hindgut. (Inset) Micrograph of the two most caudal Ret-stained cells indicated in the drawing. Scale bars, 100 μm and 20 μm (inset). (C) p75-stained cells are present in the cecum, and the most caudal stained cell (*arrow*) is in the rostral hindgut. There are no stained cells in the caudal hindgut. Scale bar, 100 μm. (D and D′) Frozen section through the hindgut of an E12 mouse after processing for p75 immunohistochemistry using a secondary antibody conjugated to Cy-3 and viewed through a rhodamine/Texas red/Cy-3 filter (D) and a FITC filter (D′). Cells that are p75-positive are present outside of the mesenchyme of the hindgut (*asterisk* in D), but the only fluorescent cells within the mesenchyme of the hindgut are blood cells (*arrows*) that can be seen through both filters. Scale bar, 50 μm.

Copyright © 1998 by Academic Press. All rights of reproduction in any form reserved.

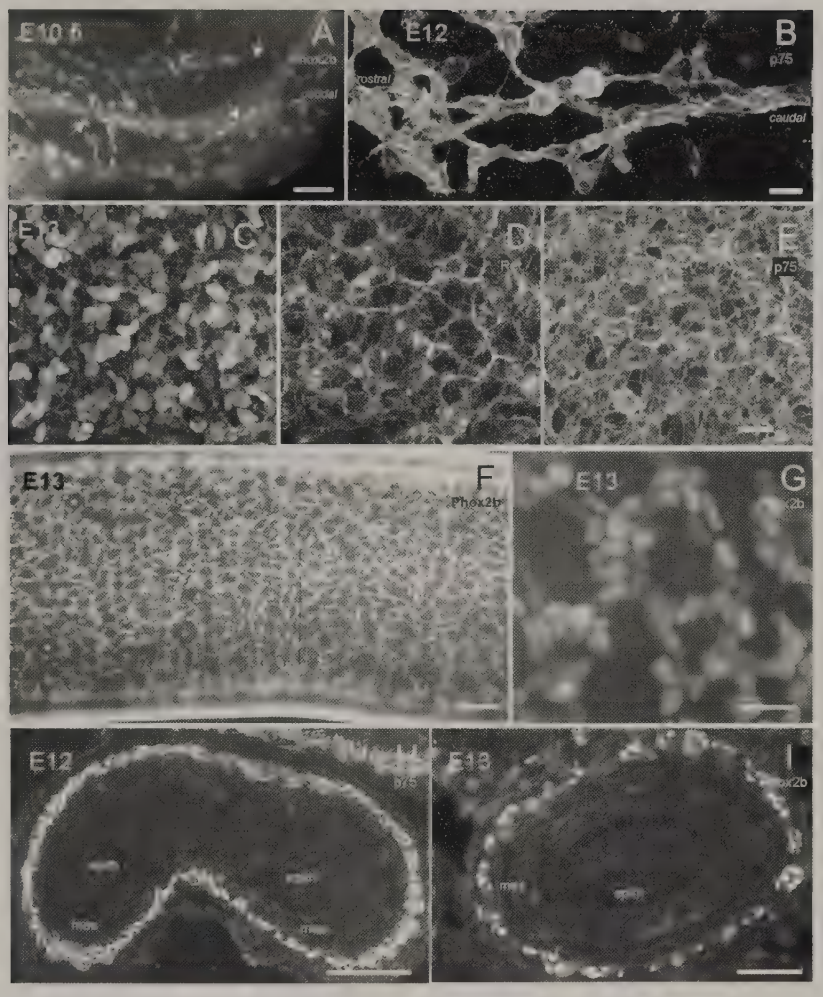

FIG. 4. Phox2b-stained cells close to the wavefront (which is close to the umbilicus) in a whole-mount preparation of E10.5 (T17) mouse gut. The Phox 2b-stained cells often occur in chains (*arrows*) that run longitudinally down, or spiral around, the gut. Scale bar, 50 μm. (B) Chain of p75-stained cells near the wavefront in the rostral hindgut of an E12 (T20) mouse. Scale bar, 20 μm. (C–E) Fluorescence micrographs of whole-mount preparations of gut from E13 (T 21) embryos to show the distribution of Phox2b-, and Ret-, and p75-immunoreactive cells just behind the wavefront, in the rostral hindgut (just caudal to the cecum). At this stage, the most caudal Phox2b-, and Ret-, and p75-stained cells are in the caudal half of the hindgut (see Fig. 8). Scale bar, 20 μm. (F and G) Low-power (F) and high-power (G) micrographs of Phox2b-stained cells in whole-mount preparations of the small intestine from an E13 mouse (T21). Some of the cells are clustered into groups and cell-free areas can be identified (*asterisks*). Scale bars: 100 μm (F) and 20 μm (G). (H) Frozen section of an E12 mouse embryo showing the distribution of p75-stained cells, which are present in the outer mesenchyme (*mes*). *epith*, epithelium lining the lumen. Scale bar, 10 μm. (I) Phox2b-stained cells in a frozen section of an E13 mouse. Stained cells are present in the outer part of the mesenchyme (*mes*). *epith*, epithelium lining the lumen. Scale bar, 50 μm.

and were very similar histologically to tissue from mice at an equivalent developmental age. Explants from spatiotemporally defined regions of intestine from E9.5–E14 mice (Fig. 7) were grown in the subcapsular space for 2–3 weeks. To determine if the explants contained neurons, antisera to NSE (Figs. 6A and 6B), Phox2b (Figs. 6D and 6E), or NOS (Fig. 6C) or conventional histology (Fig. 6F) was used. The regions from where the explants were taken and the presence or absence of neurons in the explants are shown in Fig. 7. Nine of the explants of foregut or midgut from E10–E12 mice, and six of the explants of hindgut from E10–E12 mice were processed

Copyright © 1998 by Academic Press. All rights of reproduction in any form reserved.

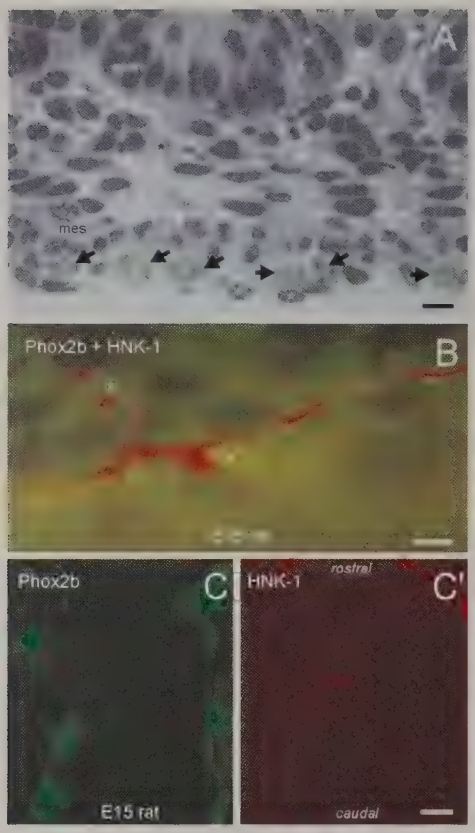

FIG. 5. Transverse, 1-μm section of resin-embedded small intestine from an E15 mouse in which the Phox2b antiserum had been revealed using avidin–biotin–horseradish peroxidase and DAB. The stained cells (*arrows*) are in the outer mesenchyme (*mes*), with only a single layer of cells (*white asterisks*) external to the stained cells. The brown cell (*black asterisk*) in the mucosa is a blood cell that shows endogenous peroxidase activity. *epith*, epithelium. Scale bar, 10 μm. (B, C and C') Whole-mount preparations of intestine from embryonic rats following processing for Phox2b (green) and HNK-1 (red) immunoreactivities. (B) Hindgut from an E16 rat. Both of the HNK-1-stained cells (*asterisks*) in this field of view show Phox2b staining, but HNK-1-stained cells compose only a small proportion of the Phox2b-stained cells. Scale bar, 10 μm. (C and C') Hindgut from an E15 rat. Paired confocal micrograph images of the region of hindgut caudal to the cecum where the most caudal HNK-1-positive cell was observed (C'). Phox2b-stained cells were found caudal to this point (C). Scale bar, 10 μm.

for both Phox2b and NSE or NOS and NSE immunohistochemistry. In every case, the results obtained with the different neuronal markers were identical; that is, if neurons could be detected with one marker, then they were also detected with the other and vice versa. The presence of neurons in the explants suggested a single rostrocaudal wave of colonization of the gastrointestinal tract by enteric neuron precursors. As shown in Fig. 8, the locations of enteric neuron precursors at different embryonic stages revealed by Phox2b immunostaining and by explants grafted to the subcapsular space were similar. Both techniques suggested a single rostrocaudal wave of colonization of the gastrointestinal tract by enteric neuron precursors, and neither technique revealed a caudal–rostral wave of colonisation of the gastrointestinal tract.

Segments from two different regions of gut from E10.5–late E11.5 (T17-T19+) mice were grown in organ culture for 10 days. The two regions were (i) midgut, which was defined as the region of gut rostral to the caecal swelling; and (ii) the hindgut, caudal to the cecal swelling (Figs. 9A and 9B). Experiments with *DBH-LacZ* transgenic mice (Kapur *et al.*, 1992) and Phox2b (Fig. 9A) and p75 (Fig. 9B) antisera have shown that enteric neuron precursors derived from the vagal-level neural crest would be present in segments of E11 midgut, but not in the hindgut, and cells derived from the sacral-level neural crest would be present in E11 hindgut (Serbedzija *et al.*, 1991). The catenary organ culture system developed for these experiments preserves the linear tubular gut morphology while allowing for growth and elongation. After 10 days in culture, the explants had grown in diameter and length (Figs. 9C, 9E, 9G, and 9H) and were up to 3 mm long. To determine if the organ-cultured explants contained neurons, antisera to NSE (Figs. 9C, 9D, and 9G) and NOS (Figs. 9E, 9F, and 9H) were used. Most of the explants were processed for double-label immunohistochemistry, but some were processed for NOS alone. The results obtained using the two antisera were identical, that is, if NOS-immunoreactive neurons were present, NSE-immunoreactive neurons were also present and vice versa. The results are shown in Table 3. After 10 days in organ culture, NSE- and NOS-immunoreactive nerve cell bodies and nerve fibers were present in all (n = 46) of the explants of midgut (Figs. 9C–9F; Table 3). In addition, all of the midgut explants had NSE- and NOS-immunoreactive nerve fibers extending from the ends of the explants onto the filter paper (Figs. 9D and 9E). Groups of immunostained neurons, which had migrated out of the explant, were also present on the filter paper (Fig. 9D). None of the 15 hindgut explants from E10.5 (T17) or E11 (T18) mice had any NSE- or NOS-stained cells within the explant or nerve fibers extending from the explant onto the filter paper (Table 3). The gut of E11.5 (T19) and late E11.5 (T19+) mice could be differentiated by changes in the shape of the caecum. Of 23 hindgut explants from E11.5 (T19) mice processed for NOS/NSE double staining or NOS alone, 22 did not possess any stained neurons or exhibit nerve fiber outgrowth (Figs. 9E and 9G). However, in one of the E11.5 hindgut explants, neurons were present along only about 25% of the length of the explant. Of the 10 explants of hindgut from late E11.5 (T19+) mice, 3 also had NSE- and NOS-stained cells within the explants and fibers growing from the explants (Table 3). For comparison, when the same regions of E11.5 mid- or hindgut that were used for the organ culture experiments were grown under the kidney

Copyright © 1998 by Academic Press. All rights of reproduction in any form reserved.

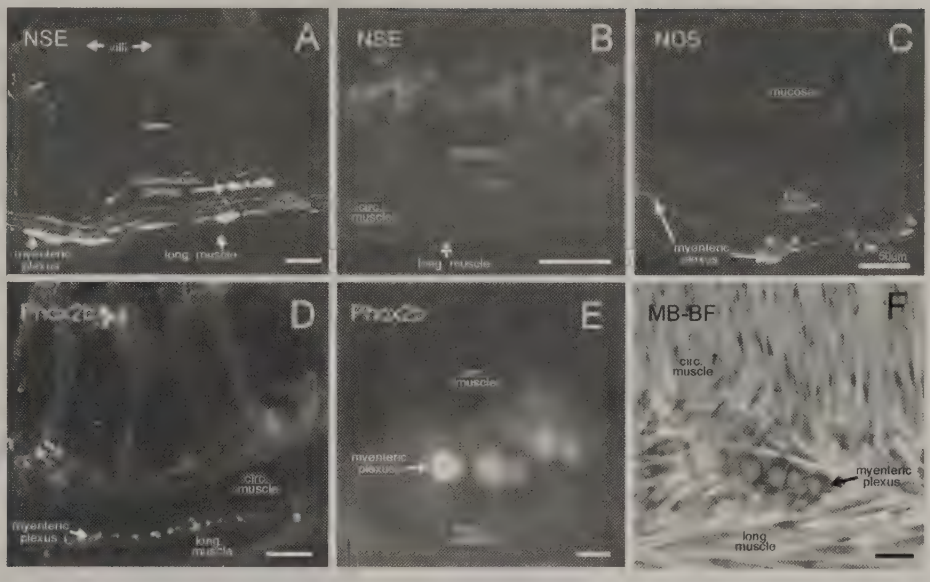

FIG. 6. Explants of embryonic mouse intestine following growth in the renal subcapsular space of host adult mice for 2–3 weeks. The explants illustrated in A, and C–F possessed neurons, whereas the explant illustrated in B did not possess neurons. (A) NSE immunostaining in an explant of E10 mouse foregut after growing in the subcapsular space for 2.5 weeks. NSE-stained cell bodies are present in the myenteric and submucosal plexuses and stained fibers (*open arrows*) are present in the circular muscle layer (*circ. muscle*) and mucosa. Scale bar, 50 μm. (B) NSE-immunostaining in an explant of E10 mouse hindgut after growing in the subcapsular space for two weeks. No NSE-immunoreactive structures are present. Scale bar, 50 μm. (C) NOS immunostaining in an explant of E10 mouse foregut after growing in the subcapsular space for three weeks. NOS-stained cell bodies are present in the myenteric plexus and stained fibers are present in the circular muscle layer (*circ. muscle*), but not the mucosa. Scale bar, 50 μm. (D and E) Low-power (D) and high-power (E) micrographs of an explant of E10 mouse foregut after growing in the renal subcapsular space for 2 weeks. Phox2b-stained cells are present in the myenteric plexus. There is some staining of the lamina propria (*asterisk* in D) which is possibly cross-reactivity with a component of the extracellular matrix. *circ. muscle*, circular muscle layer; *long. muscle*, longitudinal muscle layer. Scale bars, 50 μm (D) and 10 μm (E). (F) Explant of a segment of hindgut taken from just caudal to the caecum of an E13 mouse, cultured in the renal subcapsular space for 2 weeks, and then stained for methylene blue/basic fuchsin (*MB-BF*). Stained neurons are present in the myenteric plexus. Scale bar, 20 μm.

capsule, neurons were present in the explants of midgut ($n = 2$), but not in the explants of hindgut ($n = 4$; Fig. 7).

Comparison Between Phox2b- and HNK-1 Immunostaining in the Embryonic Rat Gut

The pattern of Phox2b immunoreactivity observed in the gut of embryonic rats was very similar to that observed in embryonic mice. In preparations of embryonic rat gut that had been stained to reveal both Phox2b and HNK-1 immunolabeling, all of the HNK-1-stained cells possessed Phox2b-positive nuclei, but HNK-1-positive cells comprised only a small proportion of all Phox2b-stained cells (Fig. 5B). In E14.75 (C26) rats, Phox2b-stained cells were present in the rostral but not caudal hindgut. HNK-1-stained cells were also present in the rostral but not caudal hindgut. However, the most caudal Phox2b-stained cells were 600–700 μm in advance of (i.e., caudal to) the most caudal HNK-1-stained cell processes (Figs. 5C and 5C′).

DISCUSSION

This study used a variety of methods to examine the colonization of the mouse gastrointestinal tract by enteric neuron precursors: (i) Antisera to the homeodomain transcription factor, Phox2b, the receptor tyrosine kinase, Ret, and the low-affinity nerve growth factor receptor, p75, were used on whole-mount preparations of embryonic mouse gut to map in detail the spatiotemporal appearance of Phox2b-, Ret-, and p75-positive cells. (ii) Explants from spatiotemporally defined regions of embryonic intestine were grown in the kidney subcapsular space for 2–3 weeks and then examined for the presence of differentiated neurons. (iii) Segments of E10.5–E11 midgut (which previous studies had shown contain vagal-level neural crest cells) and E10.5–E11 hindgut (which previous studies had shown would contain sacral-level, but not vagal-level, neural crest cells) were grown in organ culture for 10 days, before they were examined for the presence of neurons.

All of the methods revealed a progressive, unidirectional,

Copyright © 1998 by Academic Press. All rights of reproduction in any form reserved.

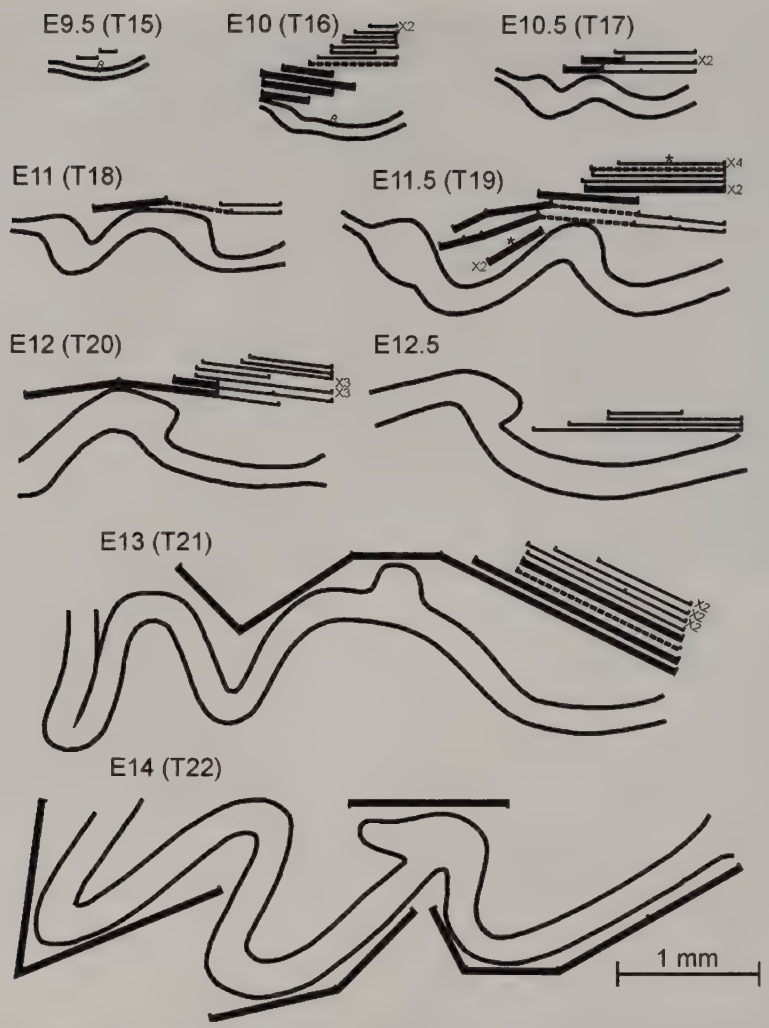

FIG. 7. Locations from where segments of embryonic mouse intestine were taken and then explanted to the kidney subcapsular space. The presence of neurons forming well-developed ganglia in the explants is indicated with the thick black line, and an absence of neurons is indicated with a thin line. Some explants, indicated with a dotted line, possessed only sparse neurons. The E11.5 explants indicated with asterisks correspond to the regions of mid- and hindgut used in the organ culture experiments.

rostrocaudal colonization of the gastrointestinal tract by enteric neuron precursors which was very similar to that described using the transgene, *DβH-nlacZ*, as a marker of vagal-level enteric neuron precursors (Kapur *et al.*, 1992). Phox2b-, Ret-, and p75 staining and the explants grown under the kidney capsule or in organ culture also showed similar locations for the most caudal enteric neuron precursors at each embryonic stage in the mouse. The colonization of the embryonic rat gastrointestinal tract by Phox2b-stained cells also occurred rostrocaudally. Since Phox2b, Ret, and p75 are expressed by migratory-stage or immediate post-migratory-stage enteric neuron precursor cells, the rostrocaudal appearance of Phox2b-, Ret-, and p75-stained cells in the embryonic gut of rodents represents the colonization of the gut by vagal neural crest cells. No Phox2b, Ret, or p75 staining was observed in the hindgut prior to the arrival of vagal neural crest cells. When segments of hindgut were removed prior to the arrival of vagal neural crest cells, but after the reported arrival of sacral neural crest cells (Serbedzija *et al.*, 1991), and grown either in the renal subcapsular space or in organ culture, no enteric neurons were observed in the explants.

Copyright © 1998 by Academic Press. All rights of reproduction in any form reserved.

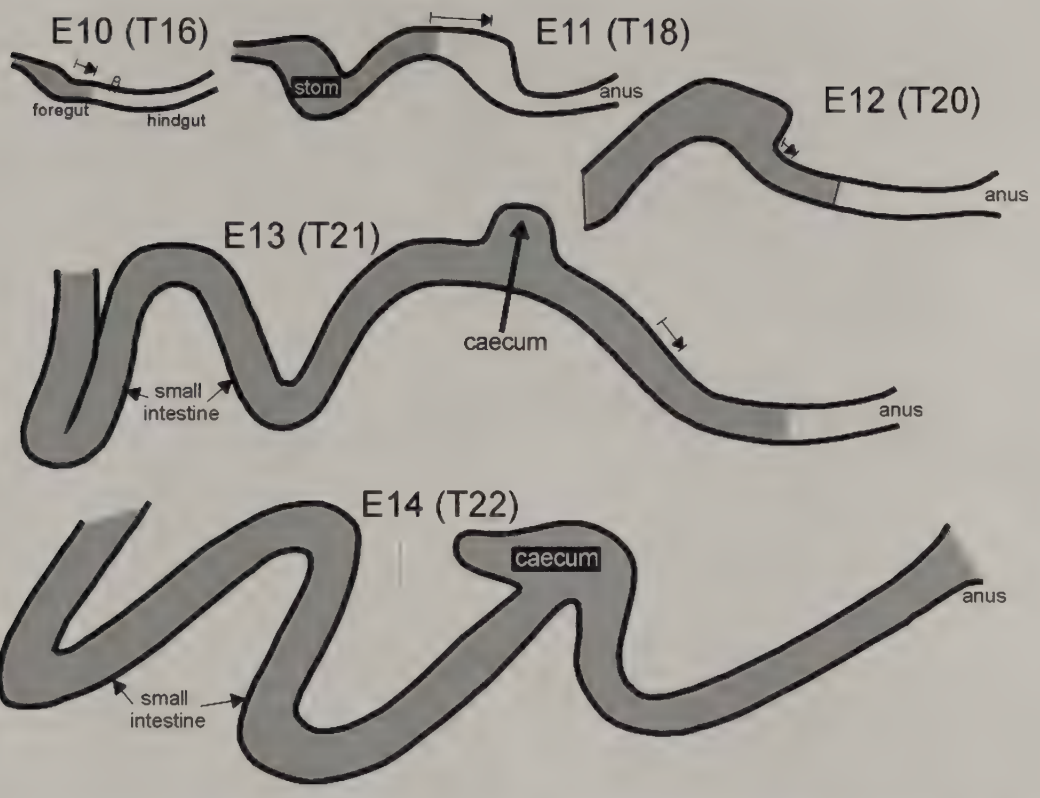

FIG. 8. Summary of location of Phox2b-stained cells (*grey*) and that of enteric neuron precursors deduced from renal subcapsular grafts (*arrows*). The left-hand limits of the arrows indicate regions where enteric neurons were always found in the explants, and the right-hand limits indicate regions where enteric neurons were never found. The wavefront is therefore within the limits of the arrows.

Phox2b as a Marker of Enteric Neurons and Their Precursors

This study has shown that an important feature of the homeodomain transcription factor, Phox2b, is that, unlike other markers of enteric neuron progenitors such as *DβH-nlacZ* in mice (Kapur *et al.*, 1992) and HNK-1 in rats (D. F. Newgreen, personal observations), Phox2b is expressed by essentially all differentiated enteric neurons and also a subpopulation of glial cells. The Phox2b antiserum appears to stain migratory-stage, or immediate post-migratory-stage, enteric neuron precursors, because Phox2b-stained cells were observed adjacent to the foregut in E9.5 mice. Furthermore, the location of neuron precursors in the embryonic mouse gut determined using Phox2b immunostaining on whole-mount preparations of gut was very similar to that observed using antisera to Ret and p75 and to that deduced from the kidney subcapsular graft (see Fig. 8) and organ culture experiments.

Since Phox2b is expressed by all differentiated enteric neurons, it would therefore seem possible that Phox2b is expressed by all enteric neuron precursors. It appeared that there were considerably more Phox2b-labeled cells than Ret-labeled cells in the gut mesenchyme of embryonic mice. Thus, like *DβH-nlacZ* and HNK-1, Ret appears to be a marker of only a subpopulation of neural crest cells and their progenitors in the embryonic gut (Lo and Anderson, 1995). We were unable to determine whether the p75 antiserum stains as many enteric nervous system precursors as the Phox2b antiserum, or if all differentiated enteric neurons express p75.

Elsewhere in the nervous system, Phox2b is also expressed by early neuron precursors (Pattyn *et al.*, 1997). For example, in the rhombencephalon, Phox2b is expressed in the proliferative neuroepithelium (Pattyn *et al.*, 1997). The expression of Phox2b by both differentiated neurons and a subpopulation of glial cells suggests that the onset of Phox2b expression by neural crest cells is prior to the formation of separate enteric neuron and glial cell lineages. Studies using postmigratory neural crest cells isolated from the gut of E14.5 rat embryos have shown that although some neural crest cells at this stage

Copyright © 1998 by Academic Press. All rights of reproduction in any form reserved.

TABLE 3
Presence of Neurons in Segments of Mid- or Hindgut from Embryonic Mice Grown in Organ Culture for 10 Days

Neuronal marker	Embryonic stage	No. of explants with stained neurons/total No. of explants examined	
		Midgut	Hindgut
NOS	E10.5 (T17)	4/4	0/4
	E11 (T18)	11/11	0/11
	E11.5 (T19)	21/21	1[a]/23
	Late E11.5	10/10	3/10
NSE	E10.5 (T17)	4/4	0/4
	E11 (T18)	11/11	0/11
	E11.5 (T19)	18/18	1[a]/19
	Late E11.5	9/9	3/9

[a] Neurons were present only along 25% of the length of the explant.

are committed to becoming either neurons or glial cells, others are multipotent and have the potential to give rise to both neurons and glial cells (Lo and Anderson, 1995). Thus, for different neural crest cells, the formation of distinct neuron and glial cell lineages appears to occur at different developmental stages.

The spatiotemporal colonization of the rat gut by enteric neuron precursors has been examined previously using an antiserum to the cell surface antigen, HNK-1, which appears to be expressed by enteric neuron precursors, but not glial cell precursors (Newgreen and Hartley, 1995). Using Phox2b immunostaining, we observed rostrocaudal colonization of the embryonic rat gut similar to that reported previously. However, Phox2b appears to be expressed earlier than HNK-1, because the most caudal HNK-1-stained cell was rostral to the most caudal Phox2b-stained cell. Thus, while Phox2b appears to be expressed by migrating, undifferentiated enteric neuron precursors, HNK-1 is a marker of a subpopulation of early differentiating neurons in the rat gut.

Characteristics of Sacral Neural Crest Cells That Migrate into the Hindgut

Studies in mice and avian embryos using a variety of labeling techniques have shown that neural crest cells arising from sacral levels of the neural tube give rise to cells in the hindgut. When the neural axis posterior to somite 28 of quails is grafted into chicken embryos, quail cells are subsequently found within the enteric plexuses of the hindgut of the chimeras (Le Douarin and Teillet, 1973, 1974). Similarly, when a vital dye or a retrovirus is introduced into or near the premigratory sacral-level neural crest cells (Pomeranz *et al.*, 1991; Serbedzija *et al.*, 1991), labeled cells are observed later in the gut mesenchyme and within the gut epithelium. The fate of the sacral-level neural crest cells in the hindgut has never been established. As no enteric neurons develop in the hindgut following removal of the vagal neural crest (Yntema and Hammond, 1954), transection of the midgut prior to the arrival of vagal neural crest cells (Meijers *et al.*, 1989), or removal and culture of the hindgut prior to the arrival of vagal neural crest cells (Allan and Newgreen, 1980; Nishijima *et al.*, 1990; Kapur *et al.*, 1992; Young *et al.*, 1996), it appears either that sacral neural crest cells do not give rise to enteric neurons or that they only differentiate into enteric neurons in the presence of the vagal-level neural crest (see Allan and Newgreen, 1980; Gershon *et al.*, 1992; Kapur, 1993).

Using DiI to label premigratory neural crest cells in embryonic mice, Serbedzija *et al.* (1991) reported that the sacral neural crest cells leave the neural tube between E9 and E9.5 and arrive in the hindgut approximately 12 h later; the fate of the DiI-labeled cells could not be determined. However, in the current study, Phox2b-, Ret-, or p75-positive-cells were not observed in the hindgut until the rostrocaudal wave at E12–E14, which represented the migration of vagal neural crest cells. Double-label studies in mature mice also showed that all neurons, including those in the large intestine, that could be labeled with antisera to neuron-specific markers also showed Phox2b staining; thus, the sacral neural crest cells do not differentiate into Phox2b-negative enteric neurons. There are two possible explanations for the absence of Phox2b-labeled cells in the embryonic hindgut prior to the vagal wave. First, the sacral-level neural crest cells that colonize the gut do not normally become enteric neurons. It is already apparent that not all of the cells that populate the hindgut from the sacral level of the neural axis are destined to become neurons, as following the labeling of premigratory cells with DiI, some of the labeled cells are found in the epithelium lining the gut (Serbedzija *et al.*, 1991). The fate of these cells is unknown. Likewise, it is feasible that the cells in the mesenchyme of the mouse hindgut that arise from the sacral neural crest are not normally enteric neuron precursors. In the present study, only a subpopulation of the enteric glial cells showed Phox2b staining, and it is conceivable that the sacral neural crest cells give rise to the Phox2b-negative enteric glial cells in the hindgut. The second possible explanation for the absence of Phox2b-stained cells in the hindgut prior to the arrival of vagal neural crest cells is that the sacral neural crest cells that colonize the hindgut show a delayed expression of Phox2b. This would seem unlikely because, like the enteric neuron precursors of vagal neural crest origin, the precursors of sympathetic ganglion cells in embryonic mice express Phox2b at E9.5 (Pattyn *et al.*, 1997). Moreover, in the current study, groups of Phox2b- and p75-stained cells were observed in close association with, but clearly outside of, the hindgut of embryonic mice prior to the arrival of vagal enteric neuron progenitors. These groups of Phox2b- and p75-stained cells are probably the primordia of the pelvic plexus, which arises from the sacral neural crest (Yntema and Hammond, 1955). Hence, if the sacral neural crest cells

Copyright © 1998 by Academic Press. All rights of reproduction in any form reserved.

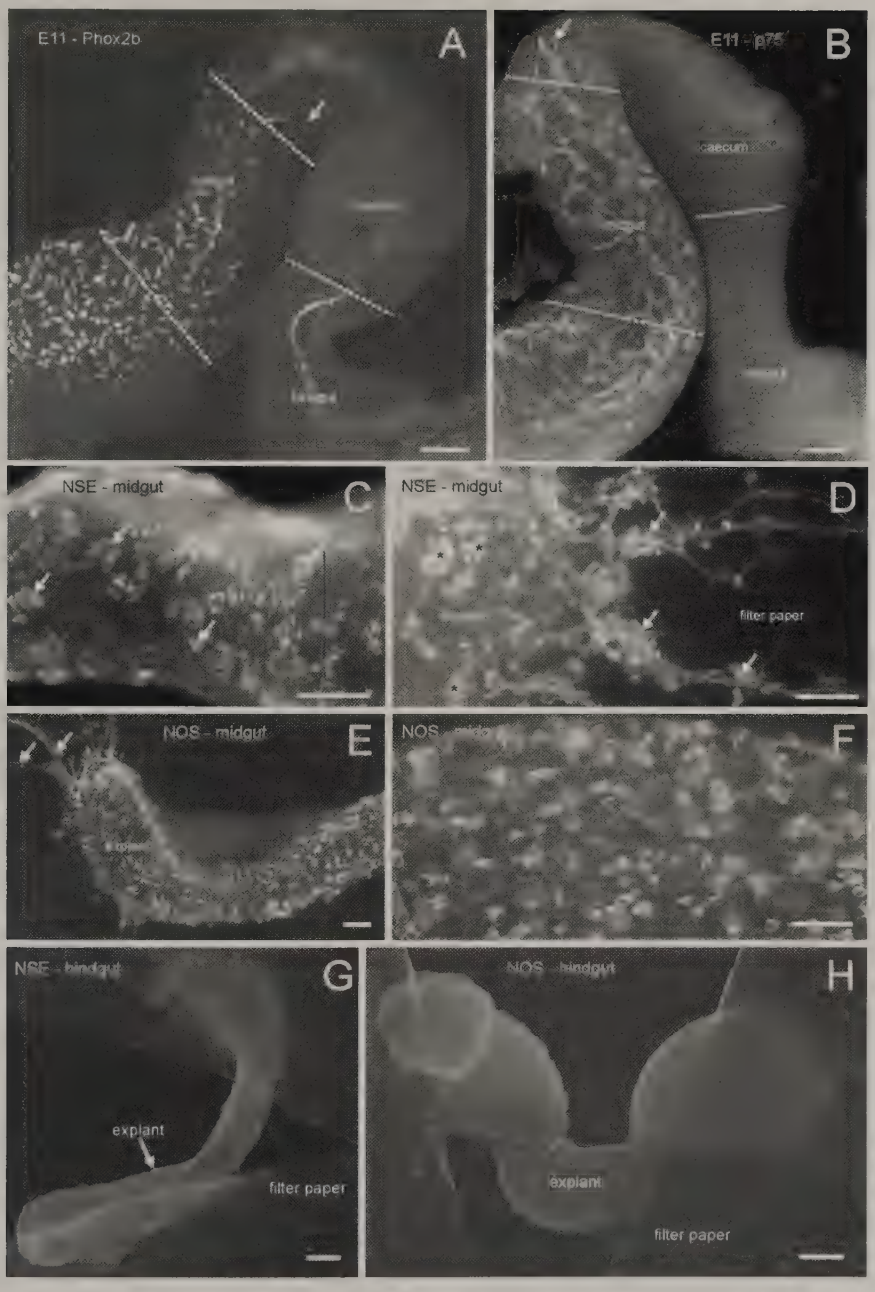

FIG. 9. (A and B) Mid- and hindgut from E11 mice that had been processed for Phox2b (A) or p75 (B) immunohistochemistry. The most caudal stained cells (*arrows*) are located rostral to the cecum. The midgut (between the stippled lines) and hindgut (caudal to the cecum) were the regions that were used for the organ culture experiments. The line of fluorescence down the middle of the preparation stained with the Phox2b antiserum is nonspecific staining of the lumenal contents. Scale bars, 100 μm. (C–H) Explants of midgut (C–F) and hindgut (G and H) from E11.5 mice following growth in organ culture for 10 days and processing for NSE (C, D, and G) or NOS (E, F, and H) immunohistochemistry. (C) Groups of NSE-immunostained nerve cell bodies (*arrows*) within an explant of midgut. Scale bar, 100 μm. (D) The edge of a midgut explant showing NSE-positive neurons within the explant (*asterisks*) and NSE-positive cell bodies (*arrows*) and nerve fibers outside of the explant. Scale bar, 100 μm. (E) Low-power micrograph of an explant of midgut processed for NOS immunohistochem-

Copyright © 1998 by Academic Press. All rights of reproduction in any form reserved.

that colonize the hindgut do show a delayed expression of Phox2b or p75, they differ not only from the vagal-level neural crest cells that give rise to enteric neurons and the trunk neural crest cells that give rise to sympathetic ganglia and enteric ganglia in the esophagus but also from the sacral-level neural crest cells that give rise to the pelvic plexus, all of which show Phox2b and p75 staining from very early stages.

The sacral-level neural crest cells that colonize the gut either do not express, or show a delayed expression, of many other markers expressed by the vagal- and anterior trunk-level enteric neuron progenitors. Studies using markers of vagal-level enteric neuron progenitors such as c-*ret* (Pachnis *et al.*, 1993, Tsuzuki *et al.*, 1995, Watanabe *et al.*, 1997; current study), *DβH-nlacZ* (Kapur *et al.*, 1992), HNK-1 (Newgreen and Hartley, 1995), p75 and Phox2b (current study) during mouse and rat embryonic development have all shown a progressive, unidirectional, rostrocaudal expression of these markers along the gut, with no reports of expression of the markers in the hindgut prior to the arrival of vagal-level neural crest cells. Unfortunately, the spatiotemporal pattern of expression of the transcription factor, *MASH1*, which is also expressed by enteric neuron precursors (Lo *et al.*, 1991, 1997; Lo and Anderson, 1995), has not been examined in the gastrointestinal tract of any species. Anterior trunk-level neural crest cells that give rise to enteric neurons in the esophagus (Durbec *et al.*, 1996) also express c-*ret* (Tsuzuki *et al.*, 1995) and Phox2b (current study). Thus, the sacral-level neural crest cells that migrate into the hindgut differ from both vagal and anterior trunk enteric neuron precursors in that they either do not express c-*ret*, *DβH-nlacZ*, HNK-1, p75, or Phox2b at all, or they do not express them until 3–4 days after arriving within the gut mesenchyme.

A number of studies have shown that when segments of hindgut are removed from E10–E11 mice and grown in the kidney subcapsular space, neurons do not appear in the explants (Nishijima *et al.*, 1990; Kapur *et al.*, 1992; Young *et al.*, 1996; current study). Similarly, in the current study we also showed that neurons were not found in explants of hindgut from E10.5–E11 mice grown in organ culture for 10 days. Neurons were observed in 1 (of 23) of the E11.5 hindgut explants and in 3 of 10 of the hindgut explants taken from late E11.5 mice, and it is likely that these neurons arose from the most rostral of the vagally derived neural crest cells. In the E11.5 hindgut explant that possessed neurons, the neurons were only present at one end of the explant. Given that neural crest cell migration through the gastrointestinal tract appears to be driven by cell numbers (Yntema and Hammond, 1954; Newgreen *et al.*, 1996), it is likely that, when removed from the embryo, the explant contained only a very small number of enteric neuron precursors which were insufficient in number to populate the entire explant. In contrast to the results of the current study, Rothman and Gershon (1982) found neurons in explants of caudal foregut and hindgut from E9 and E10 mice that had been grown *in vitro* for 2 weeks. The differences between the results from the two *in vitro* studies may be due to different organ culture techniques, and it is possible that, under some environmental conditions, the sacral neural crest cells will differentiate into enteric neurons. There is no doubt that sacral neural crest cells normally provide nonenteric neurons, including those of the pelvic plexus, adjacent to the distal hindgut (Yntema and Hammond, 1955). The results of the current study indicate that either the sacral-level neural crest cells are not normally enteric neuron precursors, or if they are enteric neuron precursors, they are very unusual in that not only do they not express, or show delayed expression of, many of the markers shown by other autonomic neuron precursors, but they also require the presence of vagal level neural crest cells to differentiate into neurons.

Role of Phox2b in Enteric Neuron Precursors

The role of Phox2b in many early neural precursor cells is unknown. Phox2b is a closely related protein to Phox2a, and they show similar distribution patterns in the central and peripheral nervous systems (Tiveron *et al.*, 1996; Pattyn *et al.*, 1997). Although the role of Phox2b is still unknown, recent studies have started to reveal the role of Phox2a. Mice in which the *Phox2a* gene is knocked out die at birth (Morin *et al.*, 1997). They show abnormalities in some regions of the CNS and in the most rostral sympathetic and parasympathetic ganglia, but there are no obvious abnormalities in the enteric nervous system. There is also a reduced expression of Ret in cranial ganglia in the *Phox2a−/−* mice, indicating that Phox2a regulates Ret expression in these ganglia (Morin *et al.*, 1977). Subsequent studies have shown that the expression of Phox2a is itself regulated by another transcription factor, MASH1, and in *Mash1−/−* mice there is little or no expression of Phox2a (Hirsch *et al.*, 1998; Lo *et al.*, 1998). Thus it has been postulated that there is a cascade in which MASH1 induces Phox2a, which in turn activates Ret (Lo *et al.*, 1998). Phox2b is expressed normally in *Mash1−/−* mice (Hirsch *et al.*, 1998), and the genes regulating its expression and which are regulated by Phox2b have yet to be identified.

istry. Stained cells are present within the explant, and fibers have grown from the explant onto the filter paper (*arrows*). Scale bar, 100 μm. (F) Higher power micrograph showing NOS-immunoreactive nerve cell bodies in an explant of midgut. Scale bar, 50 μm. (G and H) No immunoreactive structures were present in explants of hindgut grown in organ culture and then processed for NSE (G) or NOS (H) immunohistochemistry. Scale bars, 100 μm.

Copyright © 1998 by Academic Press. All rights of reproduction in any form reserved.

CONCLUSIONS

The nuclear regulatory protein, Phox2b, was shown to be the most useful marker to date with which to study the colonization of the developing gut by enteric neuron precursors because it is expressed by all differentiated enteric neurons and because the onset of its expression is very early, in migratory-stage neural crest cells. The colonization of the gastrointestinal tract of embryonic mice and rats by Phox2b-stained cells occurred as a progressive, unidirectional, rostrocaudal wave representing the migration of vagal neural crest cells. A similar colonization of the gut was observed using antisera to Ret and p75 to label migrating neural crest cells and by examining explants grown in the renal subcapsular space or in organ culture. Enteric neurons did not develop in segments of embryonic mouse hindgut that were removed after the arrival of sacral neural crest cells, but prior to the arrival of vagal neural crest cells, and transplanted to the kidney subcapsular space or grown in organ culture. However, despite Phox2b, Ret, and p75 being expressed by migrating, undifferentiated enteric neuron precursors from the vagal neural crest and by the precursors of the pelvic plexus that arise from the sacral neural crest, the cells that populate the hindgut from the sacral level neural axis do not express Phox2b, Ret, or p75.

ACKNOWLEDGMENTS

This work was supported by the National Health and Medical Research Council of Australia (H.M.Y., C.J.H., D.C., B.R.S., D.F.N.) and CNRS and ARC (J.F.B.).

REFERENCES

Allan, I. J., and Newgreen, D. F. (1980). The origin and differentiation of enteric neurons of the intestine of the fowl embryo. *Am. J. Anat.* **157,** 137–154.

Baetge, G., and Gershon, M. D. (1989). Transient catecholaminergic (TC) cells in the vagus nerves and bowel of fetal mice: relationship to the development of enteric neurons. *Dev. Biol.* **132,** 189–211.

Baetge, G., Pintar, J. E., and Gershon, M. D. (1990). Transiently catecholaminergic (TC) cells in the bowel of fetal rats and mice: Precursors of non-catecholaminergic enteric neurons. *Dev. Biol.* **141,** 353–380.

Bennett, H. S., Wyrick, A. D., Lee, S. W., and McNeil, J. H. (1976). Science and art in preparing tissues embedded in plastic for light microscopy with special reference to glycol methacrylate, glass knives and simple stains. *Stain Technol.* **51,** 71.

Branchek, T. A., and Gershon, M. D. (1989). Time course of expression of neuropeptide Y, calcitonin gene-related peptide, and NADPH diaphorase activity in neurons of the developing murine bowel and the appearance of 5-hydroxytryptamine in mucosal enterochromaffin cells. *J. Comp. Neurol.* **285,** 262–273.

Christie, G. A. (1964). Developmental stages in somite and postsomite rat embryos, based on external appearance, and including some features of the macroscopic development of the oral cavity. *J. Morphol.* **114,** 263–286.

Cochard, P., Goldstein, M., and Black, I. B. (1978). Ontogenetic appearance and disappearance of tyrosine hydroxylase and catecholamines. *Proc. Nat. Acad. Sci. USA* **75,** 2986–2990.

Durbec P. L., Larsson-Blomberg, L. B., Schuchardt, A., Costantini, F., and Pachnis, V. (1996). Common origin and developmental dependence on c-*ret* of subsets of enteric and sympathetic neuroblasts. *Development* **122,** 349–358.

Epstein, M. L., Poulsen, K. T., and Thiboldeaux, R. (1991). Formation of ganglia in the gut of the chick embryo. *J. Comp. Neurol.* **307,** 189–199.

Epstein, M. L., Mikawa, T., Brown, A. M. C., and McFarlin, D. R. (1994). Mapping the origin of the avian enteric nervous system with a retroviral marker. *Dev. Dyn.* **201,** 236–244.

Galli-Resta, L., Resta, G., Tan, S.-S., and Reece, B. E. (1997). Mosaics of Islet-1 expressing amacrine cells assembled by short-range cellular interactions. *J. Neurosci.* **17,** 7831–7838.

Gershon, M. D. (1997). Genes and lineages in the formation of the enteric nervous system. *Curr. Opin. Neurobiol.* **7,** 101–109.

Gershon, M. D., Chalazonitis, A., and Rothman, T. P. (1992). From neural crest to bowel: Development of the enteric nervous system. *J. Neurobiol.* **24,** 199–214.

Hirsch, M.-R., Tiveron, M-C., Guillemot, F., Brunet, J.-F., and Goridis, C. (1998). Control of noradrenergic differentiation and Phox2a expression by MASH1 in the central and peripheral nervous system. *Development* **125,** 599–608.

Jing, S., Wen, D., Yu, Y., Holst, P. L., Luo, Y., Fang, M., Tamir, R., Antonio, L., Hu, Z., Cupples, R., Louis, J.-C., Hu, S., Altrock, B. W., and Fox, G. M. (1996) GDNF-induced activation of the Ret protein tyrosine kinase is mediated by GDNF-α, a novel receptor for GDNF. *Cell* **85,** 1113–1124.

Kapur, R. P. (1993). Contemporary approaches toward understanding the pathogenesis of Hirschsprung disease. *Pediatr. Pathol.* **13,** 83–100.

Kapur, R. P., Hoyle, G. W., Mercer, E. H., Brinster, R. L., and Palmiter, R. D. (1991). Some neuronal cell populations express human dopamine β-hydroxylase-*lacZ* transgenes transiently during embryonic development. *Neuron* **7,** 717–727.

Kapur, R. P., Yost, C., and Palmiter, R. D. (1992). A transgenic model for studying development of the enteric nervous system in normal and aganglionic mice. *Development* **116,** 167–175.

Le Douarin, N. M., and Teillet, M. A. (1973). The migration of neural crest cells to the wall of the digestive tract in avian embryo. *J. Embryol. Exp. Morphol.* **30,** 31–48.

Le Douarin, N. M., and Teillet, M.-A. M. (1974). Experimental analysis of the migration and differentiation of neuroblasts of the autonomic nervous system and of neuroectodermal mesenchymal derivatives, using a biological cell marking technique. *Dev. Biol.* **41,** 162–184.

Lo, L.-C., Johnson, J. E., Wuenschell, C. W., Saito, T., and Anderson, D. J. (1991). Mammalian achaete-scute homolog 1 is transiently expressed by spatially restricted subsets of early neuroepithelial and neural crest cells. *Genes Dev.* **5,** 1524–1537.

Lo, L., and Anderson, D. J. (1995). Postmigratory neural crest cells expressing c-RET display restricted developmental and proliferative capacities. *Neuron* **15,** 527–539.

Lo, L., Sommer, L., and Anderson, D. J. (1997). MASH1 maintains competence for BMP2-induced neuronal differentiation in post-migratory neural crest cells. *Curr. Biol.* **7,** 440–450.

Lo, L., Tiveron, M.-C., and Anderon, D. J. (1998). MASH1 activates expression of the paired homeodomain transcription factor Phox2a, and couples pan-neuronal and subtype-specific compo-

Copyright © 1998 by Academic Press. All rights of reproduction in any form reserved.

nents of autonomic neuronal identity. *Development,* **125,** 609–620.

Meijers, J. H. C., Tibboel, D., van der Kamp, A. W. M., van Haperen-Heuts, I. C. C. M., and Molenaar, J. C. (1989). A model for aganglionosis in the chicken embryo. *J. Pediatr. Surg.* **24,** 557–561.

Moore, M. W., Klein, R. D., Farias, I., Sauer, H., Armanini, M., Phillips, H., Reichardt, L. F., Ryan, A. M., Carver-Moore-K., and Rosenthal, A. (1996). Renal and neuronal abnormalities in mice lacking GDNF. *Nature* **382,** 76–79.

Morin, X., Cremer, H., Hirsch, M.-R., Kapur, R. P., Goridis, C., and Brunet, J.-F. (1997). Defects in sensory and autonomic ganglia and absence of locus coeruleus in mice deficient for the homeobox gene *Phox2a. Neuron* **18,** 411–423.

Newgreen, D. F., and Hartley, L. (1995). Extracellular matrix and adhesive molecules in the early development of the gut and its innervation in normal and spotting lethal rat embryos. *Acta Anat.* **154,** 243–260.

Newgreen, D. F., Southwell, B., Hartley, L., and Allan, I. J. (1996). Migration of enteric neural crest cells in relation to growth of the gut in avian embryos. *Acta Anat.* **157,** 105–115.

Nishijima, E., Meijers, H., Tibboel, D., Luider, T. M., Peters-van der Sanden, M. M. J., and van der Kamp, A. W. M., and Molenaar, J. C. (1990). Formation and malformation of the enteric nervous system. *J. Pediatr. Surg.* **25,** 627–631.

Pachnis, V., Mankoo, B., and Costantini, F. (1993). Expression of the c-ret proto-oncogene during mouse embryogenesis. *Development* **119,** 1005–1017.

Pattyn A., Morin, X., Cremer, H., Goridis, C., and Brunet, J.-F. (1997). Expression and interactions of the two closely related homeobox genes *Phox2a* and *Phox2b* during neurogenesis. *Development* **124,** 4065–4075.

Pichel, J. G., Shen, L., Sheng, H. Z., Granholm, A.-C., Drago, J., Grinberg, A., Lee, E. J., Huang, S. B., Saarma, M., Hoffer, B. J., Sariola, H., and Westphal, H. (1996). Defects in enteric innervation and kidney development in mice lacking GDNF. *Nature* **382,** 73–76.

Pomeranz, H. D., and Gershon, M. D. (1990). Colonization of the avian hindgut by cells derived from the sacral neural crest. *Dev. Biol.* **137,** 378–394.

Pomeranz, H. D., Rothman, T. P., and Gershon, M. D. (1991). Colonization of the post-umbilical bowel by cells derived from the sacral neural crest: Direct tracing of cell migration using an intercalated probe and a replication-deficient retrovirus. *Development* **111,** 647–655.

Rothman, T. P., and Gershon, M. D. (1982). Phenotypic expression in the developing murine enteric nervous system. *J. Neurosci.* **2,** 381–393.

Rothman, T. P., and Gershon, M. D. (1986). Colonization of the bowel by the precursors of enteric glia: Studies of normal and congenitally aganglionic mutant mice. *J. Comp. Neurol.* **252,** 493–506.

Rothman, T. P., Nilaver, G., and Gershon, M. D. (1984). Colonization of the developing murine enteric nervous system and subsequent phenotypic expression by the precursors of peptidergic neurons. *J. Comp. Neurol.* **225,** 13–23.

Sánchez, M. P., Silos-Santiago, I., Frisén, J., He, B., Lira, S. A., and Barbacid, M. (1996). Renal agenesis and the absence of enteric neurons in mice lacking GDNF. *Nature* **382,** 70–73.

Sang, Q., and Young, H. M. (1996). Chemical coding of neurons in the myenteric plexus and external muscle of the small and large intestine of the mouse. *Cell Tissue Res.* **284,** 39–53.

Schuchardt, A., D'Agati, V., Larsson-Blomberg, L., Costantini, F., and Pachnis, V. (1994). Defects in the kidney and enteric nervous system of mice lacking the tyrosine kinase receptor Ret. *Nature* **367,** 380–383.

Serbedzija, G. N., Burgan, S., Fraser, S. E., and Bronner-Fraser, M. (1991). Vital dye labelling demonstrates a sacral neural crest contribution to the enteric nervous system of chick and mouse embryos. *Development* **111,** 857–866.

Teitelman, G., Joh, T. H., and Reis, D. J. (1978). Transient expression of a noradrenergic phenotype in cells of the rat embryonic gut. *Brain Res.* **158,** 229–234.

Teitelman, G., Gershon, M. D., Rothman, T. P., Joh, T. H., and Reis, D. J. (1981). Proliferation and distribution of cells that transiently express a catecholaminergic phenotype during development in mice and rats. *Dev. Biol.* **86,** 348–355.

Thieler, K. (1989). "The House Mouse: Atlas of Embryonic Development." Springer-Verlag, New York.

Tiveron, M.-C., Hirsch, M.-R. and Brunet, J.-F. (1996). The expression pattern of the transcription factor Phox2a delineates synaptic pathways of the autonomic nervous system. *Development* **16,** 7649–7660.

Torihashi, S., Ward, S. M., Nishikawa, S. I., Nishi, K., Kobayashi, S., and Sanders, K. M. (1995). *c-kit* Dependent development of interstitial cells and electrical activity in the murine gastrointestinal tract. *Cell Tissue Res.* **280,** 97–111.

Torihashi, S., Ward, S. M., and Sanders, K. M. (1997). Development of c-Kit-positive cells and the onset of electrical rhythmicity in murine small intestine. *Gastroenterology* **112,** 144–155.

Treanor, J. J. S., Goodman, L., De Sauvage, F., Stone, D. M., Poulsen, K. T., Beck, C. D., Gray, C., Armanini, M. P., Pollack, R. A., Hefti, F., Phillips, H. S., Goddard, A., Moore, M. W., Buj-Bello, A., Davies, A. M., Asai, N., Takahashi, M., Vandlen, R., Henderson, C. E., and Rosenthal, A. (1996). Characterization of a multicomponent receptor for GDNF. *Nature* **382,** 80–83.

Tsuzuki, T., Takahashi, M., Asai, N., Iwashita, T., Matsuyama, M., and Asai, J. (1995). Spatial and temporal expression of the *ret* proto-oncogene product in embryonic, infant and adult rat tissues. *Oncogene* **10,** 191–198.

Tucker, G. C., Ciment, G., and Thiery, J. P. (1986). Pathways of avian neural crest cell migration in the developing gut. *Dev. Biol.* **116,** 439–450.

Watanabe, Y., Harada, T., Ito, T., Ishiguro, Y., Ando, H., Seo, T., Kobayashi, S., Takahashi, M., and Nimura, Y. (1997). *ret* Proto-oncogene product is a useful marker of lineage determination in the development of the enteric nervous system in rats. *J. Pediatr. Surg.* **32,** 28–33.

Webster, W. (1973). Embryogenesis of the enteric ganglia in normal mice and in mice that develop congenital aganglionic megacolon. *J. Embryol. Exp. Morphol.* **30,** 573–585.

Yntema, C. L., and Hammond, W. S. (1954). The origin of intrinsic ganglia of trunk viscera from vagal neural crest in the chick embryo. *J. Comp. Neurol.* **101,** 515–541.

Yntema, C. L., and Hammond, W. S. (1955). Experiments on the origin and development of sacral autonomic nerves in the chick embryo. *J. Exp. Zool.* **129,** 375–414.

Young, H. M., Ciampoli, D., Southwell, B. R., and Newgreen, D. F. (1996). Origin of interstitial cells of Cajal in the mouse intestine. *Dev. Biol.* **180,** 97–107.

Received for publication January 8, 1998
Revised May 28, 1998
Accepted June 15, 1998

Copyright © 1998 by Academic Press. All rights of reproduction in any form reserved.

DEVELOPMENTAL BIOLOGY 202, 85–102 (1998)
ARTICLE NO. DB989025

N-Cadherin/Catenin-Mediated Morphoregulation of Somite Formation

Kersti K. Linask,*,[1] Cheryl Ludwig,* Ming-Da Han,* Xiao Liu,* Glenn L. Radice,† and Karen A. Knudsen‡

**Department of Cell Biology, University of Medicine and Dentistry of New Jersey, Stratford, New Jersey; †Center for Research on Reproduction and Women's Health, University of Pennsylvania, Philadelphia, Pennsylvania; and ‡Lankenau Medical Research Center, Wynnewood, Pennsylvania*

Somitogenesis during early stages in the chick and mouse embryo was examined in relation to N-cadherin-mediated adhesion. Previous studies indicated that N-cadherin localizes to the somite regions during their formation. Those observations were extended to include a spatiotemporal immunohistochemical analyses of β-catenin and α-catenin, as well as a more detailed study of N-cadherin, during segmentation, compaction, and compartmentalization of the somite. N-cadherin and the catenins appear early within the segmental plate and are expressed as small patch-like foci throughout this tissue. The small foci of immunostaining coalesce into larger clusters of N-cadherin/catenin-expressing regions. The clusters subsequently coalesce into a region of centrally localized cells that express N-cadherin/catenins at their apical surfaces. The multiple clusters are spaced wide apart in the anterior segmental plates that form the first 6 somite pairs, as contrasted to segmental plates that form somites 7 and beyond. To examine the functional significance of N-cadherin, segmental plates were exposed to antibodies that perturb N-cadherin-mediated adhesion in the chick embryo. The multiple, anomalous somites that result in these experiments indicate that each N-cadherin/catenin-expressing cluster can give rise to a somitic structure. β-Catenin involvement in somitogenesis suggests a role for Wnt-mediated signaling. Embryos treated with LiCl also show induction of similar anomalous somites indicating further the possibility that Wnt-mediated signaling may be involved in the clustering event. It is suggested that β-catenin serves to initiate the adhesion process which is spread then by N-cadherin. Later during compartmentalization, N-cadherin/catenins remain expressed by the myotome compartment. Taken together, these results suggest that the Ca^{2+}-dependent cell adhesion molecule N-cadherin and the intracellular catenins are important in segmentation and formation of the somite and myotome compartment. It is proposed that the N-cadherin-mediated adhesion process may serve as a common, evolutionarily conserved, link in the differentiation pathways of skeletal and cardiac muscle. © 1998 Academic Press

INTRODUCTION

Somites form in an anterior to posterior manner as paired structures arising from the segmental plate located on either side of the developing neural tube in the vertebrate embryo. The segmental plates are formed during the process of gastrulation and are organized as loose paraxial mesoderm. Every 60–90 min, new pairs of somites form by sequential epithelialization of the segmental plates. The essential elements of cell behavior during somite formation are similar in most vertebrates (Keynes and Stern, 1988).

Each somite arises when a group of cells within the most rostral end of the segmental plate undergoes a change in organization from mesenchyme to a rosette, concomitantly displaying cell–cell interactions associated with a true epithelium. With the mesenchymal to epithelial cell shape change, the somitic cells also become polarized. Five discrete stages of somite formation in the chick embryo have been described from the segmental plate, presomite or somitomere, to the distinct paired somite stage (Lash, 1985). The segmental plate cells appear homogeneous when viewed under the dissection microscope, although they already contain the eventual somite pattern, as repeating whorls of cells, i.e., the somitomeres (Meier, 1979). The

[1] To whom correspondence should be addressed at Department of Cell Biology, University of Medicine and Dentistry of New Jersey, 2 Medical Center Drive, Stratford, NJ 08084. Fax: (609) 566-6195. E-mail: linaskkk@umdnj.edu.

0012-1606/98 $25.00
Copyright © 1998 by Academic Press
All rights of reproduction in any form reserved.

presomitic cells then undergo compaction, which is thought to result from an increase in cell–cell adhesion in this region (Cheney and Lash, 1984; Lash, 1985). Subsequent stages include epithelialization of the future somite that delineates the anterior border of the somite. This is followed by the delineation of the lateral and posterior borders to separate the newly formed somite from the segmental plate.

The somite undergoes compartmentalization after its formation: the ventromedial portion forms the sclerotome, which gives rise to the vertebral cartilage; the dorsolateral region gives rise to the dermamyotome which maintains for a brief period the epithelial arrangement. Later the dermamyotome compartmentalizes further. Those cells localized immediately beneath the ectoderm comprise the dermatome which contributes to the dermis of the trunk and to some muscle cells (reviewed in Christ *et al.*, 1995). The cells that localize between the dermatome and the sclerotome remain associated closely with each other to form the myotome and eventually form the axial skeletal muscle (Christ *et al.*, 1978).

Important to our present study, Lipton and Jacobson (1974) suggested that the formation of the first six somite pairs may differ from that of the somites forming more posteriorly. When first forming, the anterior somites have a laterally, elongated shape. The first six somite pairs as they form appear to be two to three times wider than subsequent, more posterior somites. The reason for the rostral–caudal difference in segmental plate width is unknown. That rostral–caudal differences exist in somitogenesis is evident also in analyses of zebrafish somite mutants (van Eeden *et al.*, 1996).

Some of the regulatory factors controlling the process of somite formation are beginning to be determined (see Barnes *et al.*, 1997 and references cited). Evidence that local adhesive interactions, both cell–matrix and cell–cell, also are involved in regulating somitogenesis stems from the localization of adhesion molecules to the somite region and by the modulation of these molecules experimentally. It has been proposed that local adhesive interactions between cells within the somitomere may determine the final shape of the somites and their number (Bellairs *et al.*, 1977). Roles for the cell adhesion molecules as fibronectin (Ostrovsky *et al.*, 1983; Lash *et al.*, 1987; George *et al.*, 1993) and N-cadherin (Duband *et al.*, 1988; Hatta *et al.*, 1987; Takeichi, 1988) in somite formation have been suggested.

In vertebrates, axial skeletal muscle arises from the somites. There has been considerable interest recently in understanding how the skeletal muscle lineage is induced during vertebrate somitogenesis and which regulatory molecules mediate the induction of the myogenic pathway, including regulatory factors as paraxis, Pax3, MyoD, and Myf-5 (Burgess *et al.*, 1996; Maroto *et al.*, 1997; Tajbakhsh *et al.*, 1997). Expression of myogenic genes in the myotome seems to require a combination of *Wnts* and *Shh* (Stern and Hauschka, 1995; Yun and Wold, 1996; Rawls and Olson, 1997). How these regulatory molecules activate the myogenic pathway remains unclear. Cells from the newly formed somite initially appear to be multipotent and become committed to specific fates in response to signals in their environment. Cell adhesion and its signaling pathways also are involved. Recent *in vitro* studies suggest that N-cadherin-mediated cell–cell adhesion is involved in both the commitment of muscle precursors and their terminal differentiation (Redfield *et al.*, 1997; George-Weinstein *et al.*, 1997).

The cytoplasmic domain of cadherins interacts with β-catenin which in turn binds α-catenin. α-Catenin can interact with the actin cytoskeleton. Thus, the catenins serve to link the cadherins to the cytoskeleton (Wheelock and Knudsen, 1991). This intracellular link is necessary for cadherins' adhesive function. In addition to its involvement in cadherin adhesion, β-catenin is implicated in regulating transcription by its ability to bind and activate the LEF-1 transcription factor (Behrens *et al.*, 1996; Molenaar *et al.*, 1996). Thus, molecules that are involved in cell–cell adhesion also are shown to regulate transcription.

This study analyzes the spatiotemporal localization of N-cadherin and α- and β-catenin during morphoregulation of early somitogenesis. Subsequently N-cadherin-mediated adhesion in somitogenesis is analyzed by perturbation studies in chick embryos using function perturbing N-cadherin antibodies, and in mouse embryos using genetic manipulation of N-cadherin expression.

MATERIALS AND METHODS

Embryos

Fertile White Leghorn chick embryos for this study were supplied by Truslow Farms (Chestertown, MD). Stages of development are indicated according to the staging series of Hamburger and Hamilton (1951). The method of removal of embryos for analyses has been described in detail (Linask and Lash, 1986).

N-Cadherin-deficient mutant mouse embryos were removed on 8.5 days of gestation. The yolk sac was used to genotype the embryos as previously described (Radice *et al.*, 1997). Mouse embryos were placed in 4% *p*-formaldehyde in PBS for further processing for immunohistochemistry.

Whole Chick Embryo Culture Method: NCD-2 and LiCl Perturbation of Somite Development

The detailed methodology for culturing whole chick embryos has been described (Linask and Lash, 1988). Just before the beginning of incubation, each embryo was treated with 5 μl of functioning perturbing antibody placed gently on the ventral side of the embryo on the segmental plate regions. Both the rat monoclonal antibody NCD-2 (gift of Dr. M. Takeichi (Hatta *et al.*, 1985) and the mouse monoclonal antibody 6B3 (George-Weinstein *et al.*, 1997) were used for these studies. The effective concentration of antibody for whole embryo cultures was determined to be 100 μg/ml after incubating embryos in a series of different concentrations of antibody. Control embryos received similar concentrations of rat or mouse γ-globulin (Jackson ImmunoResearch, West Grove, PA). During these early embryonic stages, before a cardiovascular system is fully formed and functional, nutrients are taken up by

Copyright © 1998 by Academic Press. All rights of reproduction in any form reserved.

diffusion by the embryo and thus the germ layers of the embryo are accessible to the antibody. Antibody accessibility was confirmed by the application of a fluorescently labeled dextran of a similar molecular weight as that of IgG. After a 24-h incubation, the embryos were viewed under a Nikon stereomicroscope, photographed, and fixed in Histochoice (Amresco, Solon, OH) for further processing.

To perturb somitogenesis in older chick embryos (>10 somites), NCD-2 antibody was injected directly into the segmental plate region using a PLI-100 Pico-Injector (Medical Systems Corp., Greenvale, NY). This allows small liquid volumes to be delivered through a micropipet by applying a regulated pressure (with compressed gas N_2) for a digitally set period of time. Sharply tapered glass micropipets were pulled from a microcapillary (1 mm in diameter) using a Narishigi pipet puller. A pressure of 0.6 psi was used at 250 ms to deliver a small volume of NCD-2 antibody. Control injections of rat IgG produced no perturbing effects. The pressure and duration of injection had to be adjusted empirically for each new pulled micropipet to ensure delivery of approximately the same volume. To be able to visualize the region of injected antibody, 1 μl of the vital dye Nile green was added to 19 μl of antibody. Injections were made on either one or both sides of the neuraxis in the segmental plate region, as indicated under Results. The embryos were marked with carbon particles lateral to the area of injection.

LiCl (Sigma, St. Louis, MO) was used at concentrations of 2 mM, 1 mM, and 100 μM and was applied to whole embryos at the outset of incubation and 6 h later. Incubation of embryos continued for a total of 22–24 h. LiCl was not used for microinjections.

Antibodies

Mouse monoclonal antibodies against chick N-cadherin (13A9), α-catenin (1G5), and β-catenin (15B8; Johnson *et al.*, 1993) and the chick N-cadherin-perturbing mouse antibody 6B3 (George-Weinstein *et al.*, 1997) have been described previously. The hybridoma secreting the perturbing NCD-2 rat antibody (Hatta *et al.*, 1985) to chick N-cadherin was kindly supplied by Dr. M. Takeichi (Kyoto University, Japan). The polyclonal antibody to N-CAM was provided by Dr. S. Hoffman (Medical University of South Carolina, Charleston, SC).

Bromodeoxyuridine (BrdU) Labeling for Cell Proliferation

Stage 6 chick embryos were treated with function perturbing antibodies in F12 media for 6 h. From previous experiments 6 h is the time period when the first phenotypic differences due to antibody treatment begin to be apparent. The embryos were then transferred into 10 μM BrdU with antibody in F12 media for 80 min. Embryos were rinsed and immunostained using BrdU primary antibody followed by a Cy-3-conjugated secondary antibody. Each embryo also was counterstained using DAPI to count total number of cells. Sagittal sections were made through the somites and segmental plate regions. A representative section from each embryo was counted for the numbers of BrdU-labeled nuclei in the most recently formed two somites and the most anterior end of the segmental plate. Total number of cells apparent in each somite and in the anterior segmental plate was determined by counting DAPI-labeled cells.

High-Resolution Immunohistochemistry and Microscopy

After fixation in Histochoice (Amresco), the blastoderms were permeabilized in 100% cold methanol. The preembedding immunostaining and plastic embedding procedure in araldite have been described in detail (Linask, 1992). Sections were cut at 1 μm.

Observations of whole mount embryos, as well as of sections, were made with a Nikon Optiphot II microscope equipped for epifluorescence microscopy. Black and white photographs were taken using Kodak Tmax ASA 400 film.

RESULTS

To extend our previous studies on adhesion molecules during somitogenesis, we examined N-cadherin expression in spatiotemporal detail, in addition to documenting α- and β-catenin expression during somitogenesis. Whole embryos at different stages were immunostained with monoclonal antibodies to chick N-cadherin (13A9) and its associated intracellular proteins α-catenin (1G5) and β-catenin (15B8). Somites at different levels of the embryo, i.e., anterior, middle, or posterior, were analyzed in whole mounts or in transverse or sagittal sections of representative embryos cut through the somite regions. For each specific stage examined, the immunostaining pattern of N-cadherin, α-catenin, and β-catenin was identical to each other.

In describing temporal changes in the N-cadherin/catenin expression patterns, the stage of development of the somite and the axial level in relation to the embryonic cranial–caudal sequence is important for understanding the results of both the immunostaining and the N-cadherin perturbation experiments. For convenience somites are numbered in sequential order with the highest number reflecting the newest, i.e., the last somite to have formed. The cranial end of the segmental plate where the next somite will form is designated SP.

In Fig. 1 a schematic diagram contrasting somite development as based on N-cadherin/β-catenin localization in anterior and posterior somites is shown for orientation. In Fig. 1A the anterior or first six somite pairs are shown having a wider appearance than the more posterior somites, i.e., somite pairs 7 and beyond. This schematic is based on our data describing differences in anterior and posterior somite formation summarized in Fig. 1B. Beginning with the "younger" somite regions on both axial levels, N-cadherin/β-catenin localization at cell membranes within the segmental plate becomes detectable as pronounced foci of immunostaining. This is followed by a coalescence of these foci to form cell clusters. These cell clusters in turn coalesce to form somitic central regions of cells expressing high levels of N-cadherin/catenin. The presomitic cell clusters are more numerous and are spaced wider apart in the anterior segmental plate that gives rise to the first six somite pairs than in the posterior segmental plate.

Copyright © 1998 by Academic Press. All rights of reproduction in any form reserved.

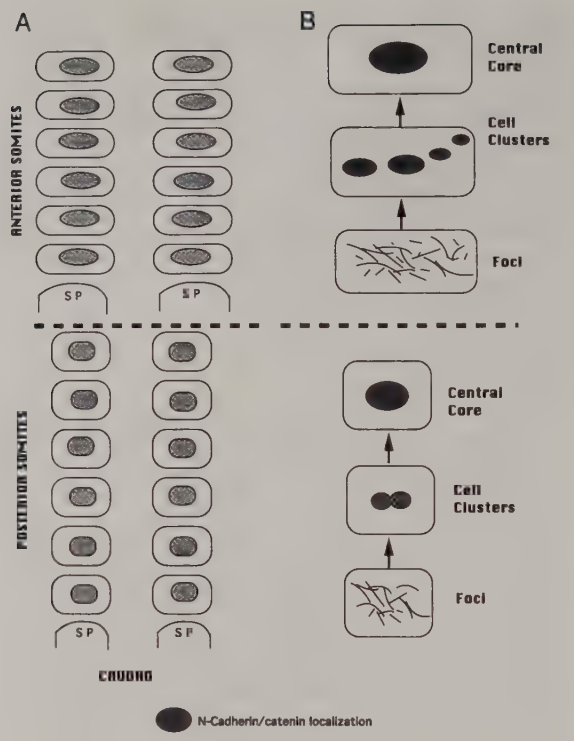

FIG. 1. A schematic diagram of somite development based on our results. Central region shown in gray depicts N-cadherin/catenin-expressing cells. In the left column (A) the anterior first six somites arising from a wide segmental plate are shown having a wider appearance than the more posterior somites. Based on cluster formation, approximate demarcation of anterior somites from posterior is shown by a discontinuous line. On the right-hand side of figure (B) cadherin/catenin adhesion-mediated steps during somitogenesis are depicted and contrasted for anterior (first 6 somite pairs) and posterior (somites 7 and beyond) regions. Beginning from the bottom of each section, or more earlier steps of somite development, foci of N-cadherin/β-catenin-expressing cells first appear. This is followed by a coalescence of these foci to form cell clusters, which in turn coalesce to form somitic core regions of cells expressing high levels of N-cadherin/catenins. In anterior segmental plate the cell clusters are more numerous and are spaced wider apart than posteriorly. SP, segmental plate or region where next somite will form.

N-Cadherin and Catenin Localization during Different Stages of Somitogenesis

In a stage 8+ embryo (26 h) immunostained for β-catenin and sectioned in a sagittal plane through the somite regions, five distinct somites are present (Fig. 2 montage). The fifth and newly formed somite (No. 5) shows a central core region expressing a high level of β-catenin. This somite, although distinct, is smaller than anterior somites 1–4. More posteriorly, in the adjacent, cephalic end of the segmental plate (SP), β-catenin localization is expressed ubiquitously with an apparent higher level on the more anterior side. A distinct, centrally localized region with an intense level of β-catenin expression is not detectable at this time in the segmental plate.

Whole mounts of different stage chick embryos immunostained for N-cadherin are shown in Figs. 3A through 3C. In the segmental plate region in an early stage 7 embryo (22 h of development), where the first two somites are forming (Fig. 3A), anterior and posterior somite boundaries are apparent as incomplete furrows. Both N-cadherin (shown here, arrows) and β-catenin (not shown) are discernible in the segmental plate mesoderm as small foci of staining. Cell membranes are beginning to localize these proteins along more extended lengths (marked by arrowhead) in the emerging somite regions. In Fig. 3B in a 6-somite embryo (25–26 h), the anterior somites, e.g., somite 3 (see arrow), now localize N-cadherin to a central region of cells which all express this adhesion molecule on their apical–lateral cell surfaces. This central region displays a characteristic oval or diamond-like shape. In Fig. 3C of a 16-somite embryo, posterior (caudal) somites are shown at the level of the last 5 somites that have formed, i.e., somites 12–16. In the segmental plate region of the next new somite pair to form (level shown by asterisks), expression of N-cadherin/β-catenin is already present in the segmental plate as small patches of immunostaining (see Fig. 5 for higher resolution of the segmental plate region). Cells beginning to show an increased expression of N-cadherin/β-catenin form small patch-like areas of immunostaining, as was seen earlier in the somites that were forming at stage 7 (see Fig. 3A).

As somitogenesis continues from the 2-somite stage, the segmental plate begins to display a definite clustering of N-cadherin staining cells in a central area within the segmental plate (Figs. 4A and 4B, see arrows). Multiple foci of N-cadherin expression are observed in the emerging anterior four somite regions (Fig. 4A, low magnification; Fig. 4B, high magnification). Specifically, multiple clusters are observed to occur often within the first six rows (see arrows in Figs. 4A). A similar pattern is evident for β-catenin. These initial clusters or foci of immunofluorescent staining appear to coalesce into a central region of N-cadherin/β-catenin-expressing cells. Somite 3 is numbered for orientation. In left somite 1 three clusters are apparent within this level. At the level of somites 2–4, distinct regions of N-cadherin foci and clusters (arrows) that are in the process of coalescing are apparent extending laterally from the neuraxis. In the somite 3 region of the embryonic left, the apparent coalescence process is seen to be spreading between the clusters. On the right side, also in somite 3 region, three separate clusters are apparent (see arrows on right side in Fig. 4A). By the 6-somite stage a central compact region of N-cadherin/β-catenin-expressing cells is discernible in all of the formed somites (compare with Fig. 3B). Thus, in the 2-somite embryo the initial, small, separated patches or foci of cells expressing N-cadherin/β-catenin appear to coalesce into several, larger clusters that are still apparent in a 4-somite embryo. These

Copyright © 1998 by Academic Press. All rights of reproduction in any form reserved.

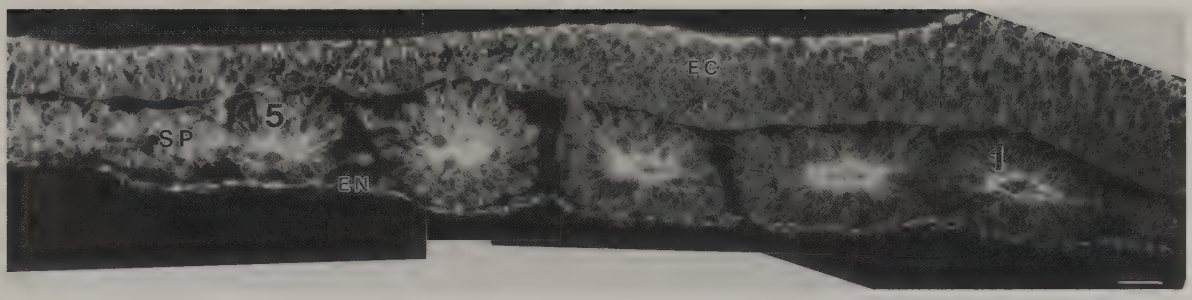

FIG. 2. β-Catenin immunostaining in a stage 8+ chick embryo that was sectioned in a sagittal plane through the somite regions. Five distinct somites are present in this montage. The anterior part of the embryo is to the right. Cells in central regions of all somites show a high level of β-catenin expression. The most mature somite (1) has a central core apparent with apical cell membranes expressing an apparent high level of β-catenin around the core. β-Catenin is also expressed at lower levels of intensity around cell membranes away from the core region. Level of expression in the central region appears to increase posteriorly. The newly emerging somite (5) is smaller than the more anterior somites. The segmental plate (SP) from which the next somite will emerge does not appear to express any specific high intensity of immunostaining, except possibly at its most anterior end. EC, ectoderm; EN, endoderm. Magnification bar, 50 μm.

multiple clusters in turn coalesce to form a single, wide central region of N-cadherin-expressing cells detectable at the 6-somite stage.

This sequential, multistep coalescence of N-cadherin-expressing cell clusters is seen with each new somite pair forming in the anterior segmental plate of younger embryos, specifically up to 6 pairs of somites. In older embryos with 7 or more somite pairs, this sequence of events is modified. For example, in a 16-somite embryo in Fig. 3C (N-cadherin) and Fig. 5A (N-cadherin) and Fig. 5B (β-catenin), all of the somites express β-catenin and N-cadherin in one central region of cells. In the newly formed somites 14 through 16 shown in Fig. 5, localized cell boundaries show an enhanced expression of N-cadherin (Fig. 5A) and β-catenin (Fig. 5B) in foci within a single central region. From the time they form in the stage 16 embryo, the posterior somites 12–16 tend to have a more finite boundary of N-cadherin/β-catenin expression from their first detection compared to the most anterior forming somites. Also, the cells closer to the neuraxis show a detectable, enhanced N-cadherin/β-catenin expression (see arrows in Fig. 3C and in Figs. 5A and 5B in a 16-somite embryo). The patterning of both N-cadherin and β-catenin is similar as the somite forms, i.e., beginning with small foci and leading to a central core region of expression.

α-Catenin expression during subdivisions of the somite. When the somite forms an epithelioid structure, α-catenin localized similarly as β-catenin and N-cadherin to the apical–lateral membranes of cells at the central region of the somite (arrows) and extended slightly laterally (Fig. 6). At the time the dermamyotome is formed, and sclerotome cells were seen migrating to the notochord where they will form the cartilage-producing cells of the developing vertebra, the sclerotome cells no longer expressed detectable α- or β-catenin, or detectable N-cadherin (Fig. 6B). α-Catenin (also β-catenin) remained strongly localized to the apical–lateral surfaces of the myotome cells (myo) forming a boundary between the ventral sclerotome (sl) population and the myotome population.

N-Cadherin Perturbation Experiments and Formation of Anomalous Somites

Antibody perturbation in chick embryos. When early stage 5–6 chick embryos were exposed to either of two N-cadherin-perturbing monoclonal antibodies (NCD-2 or 6B3) and were incubated for 22–24 h, anomalous somites often formed laterally in anterior regions. The anomalous somites were apparent for several rows rostral–caudad, predominantly within somite regions 1–6. Three representative patterns of anomalous somites are shown in Figs. 7A–7C. In Fig. 7A a whole embryo is shown with anomalous somites present in anterior regions (see arrow). This antibody-treated embryo also had characteristic heart region abnormalities and a nonextended neural tube. Many NCD-2-treated embryos were immunostained for β-catenin and two representative embryos are shown in Figs. 7B and 7C. Central clusters of cells express β-catenin in each somite. In Fig. 7B anomalous somites are present on one side only. In Fig. 7C multiple anomalous somites are present on both sides of the neuraxis extending laterally. Posterior to the antibody perturbed region the somites are present in pairs in the normal manner. When sectioned, the anomalous somites show a typical rosette configuration (not shown). Table 1 shows the number of embryos treated between stages 5 and 7 and the percentage of embryos showing multiple somite formation. The greatest percentage of anomalies was seen to occur in embryos treated at stage 6. This coincides with a period just preceding the appearance of the first somite pairs, at a period in which we would expect that the described adhesion-related processes are taking place. As a control for possible nonspecific effects due to an antibody binding to cell surface adhesion mol-

Copyright © 1998 by Academic Press. All rights of reproduction in any form reserved.

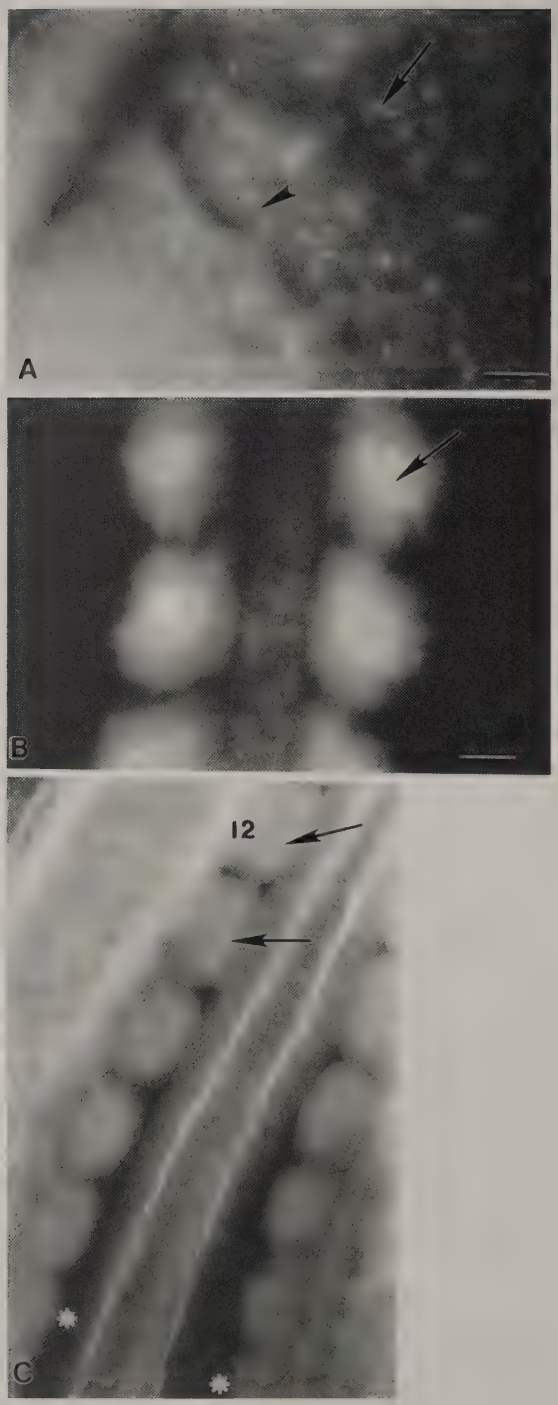

FIG. 3. Whole mounts of different stage chick embryos immunostained for N-cadherin. (A) Stage 7 embryo with two wide developing somite regions present. Within the first and second somite areas patches of N-cadherin are present (arrow). The arrowhead in somite 2 shows extended regions of cell membranes beginning to express N-cadherin. Similar patch-like staining regions are present in the segmental plate where the next somite will form. By the 6-somite stage shown in B these regions of localization (arrow) have coalesced into a central region of cells expressing N-cadherin. (C) By the 16-somite stage the patch-like expressing foci of N-cadherin are apparent in the central area of the somites that have formed within the last 6–7 h of incubation. A higher level of expression is noticeable on medial aspect of the somite closest to the neuraxis (arrow). This is specifically apparent in somites 12 (marked), 13, and 14. The high level of N-cadherin expression within the neural folds and at the neural plate/epithelial ectoderm border, which is apparent as two lines, also is specific. The anterior end of the segmental plate where the next somite will form is indicated by asterisks. Magnification bar: A, 10 μm; B and C, 60 μm.

ecules, a polyclonal antibody against N-CAM was also used for treatment of embryos. Normal somitogenesis resulted (see Fig. 8).

Evidence that anomalous somites do not arise from an increase in cell proliferation upon NCD-2 treatment of segmental plate cells is shown in Fig. 8. Embryos were treated with antibodies for 6 h and then transferred to BrdU-labeling media for 80 min to ascertain numbers of cells undergoing mitosis during during one somitic cell cycle. Figure 8A shows a control stage 6 embryo incubated in normal rat IgG and labeled for incorporated BrdU; Fig. 8B is a control embryo incubated in the presence of polyclonal rabbit anti-NCAM; and Fig. 8C is a NCD-2-treated embryo. Embryos were sectioned sagitally through the somite and segmental plate regions and proliferating, BrdU-labeled cells (shown in yellow) were counted in the last two somites that had formed and in the most anterior segmental plate region which gives rise to the next somite. At this period during one-cell cycle, no significant difference is apparent with the different antibody treatments in percentage of BrdU-labeled cells relative to DAPI-stained nuclei counted in the somitic regions (see Table 2). As shown in Figs. 8A–8C, all treated embryos show a similar pattern of cell proliferation. Similarly in the anterior part of the segmental plate, no significant difference in patterning or numbers of proliferative cells is detected. Thus, the formation of anomalous somites does not appear to be due to increased cell proliferation upon NCD-2 antibody treatment.

Microinjection of NCD-2 antibody into segmental plate of posterior regions of chick embryos. In the above experiments antibody was applied to embryos as soon as they were placed in culture, between stages 5 and 7 + (16–22 h). Additional antibody also was applied to posterior segmental plates later during the period of incubation to increase the possibility of perturbing somitogenesis in posterior regions. No effect was observed on posterior somitogenesis. Since somites posterior to the first six pairs appeared to develop normally in embryos that were incubated in the presence of the perturbing

Copyright © 1998 by Academic Press. All rights of reproduction in any form reserved.

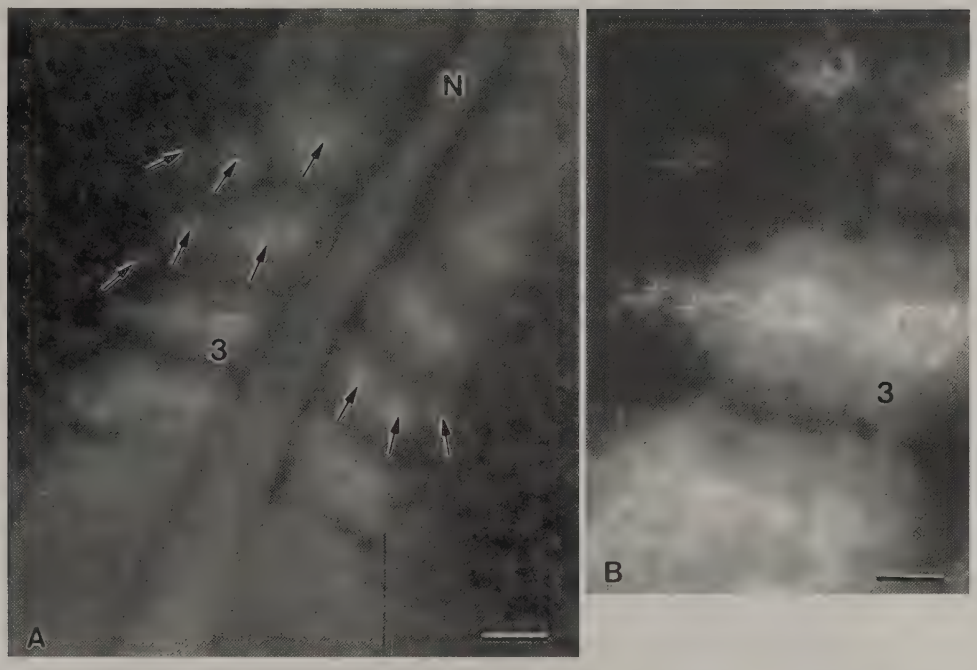

FIG. 4. N-cadherin localization in a normal stage 8 embryo with 4 somites. Somite 3 is marked. (A) Lower magnification showing all 4 somites (somite 4, newly emerging). Anterior is to the top. In left somite 1 multiple clusters of N-cadherin-expressing cells are still detectable. In somite area 3 on the right side of the neuraxis, three clusters of N-cadherin expression are apparent (see arrows). Within the embryonic left/right somite regions different degrees of coalescence of N-cadherin-expressing clusters (marked by small arrows) are apparent. The third somite region on left side of the same embryo is shown in B at higher magnification. In somite 3 it is apparent the N-cadherin-expressing clusters are coalescing into one. Magnification bar: A, 100 μm; B, 50 μm.

antibodies NCD-2 or 6B3, the possibilities existed that (1) somite formation occurred differently in more posterior regions, (2) presomite clusters were so close together that the antibody would not affect coalescence of closely spaced, adjacent small clusters, or (3) the antibody may not be able to diffuse into the segmental plate cell microenvironment in sufficient concentrations to perturb somitogenesis in posterior regions of older embryos.

To address the above possibilities, a series of experiments was carried out in which N-cadherin-perturbing antibody was microinjected directly into the segmental plate region from which the next somites will form. A carbon particle was placed laterally to the site of microinjection to mark the level of injection. The embryos were then incubated overnight, fixed and immunostained for β-catenin. A total of 14 embryos having at least 7 or more pairs of somites were microinjected with N-cadherin perturbing antibody. We observed two lateral somitic structures form on the anti-N-cadherin-injected side of the neuraxis. A total of 5 embryos showed the anomalous number of β-catenin-expressing foci in the somitic regions. Sites of injection are shown in Fig. 9A. The site of injection in this embryo is shown with the micropipet tip within the segmental plate just anterior to the Hensen's node region (large arrow). This is the most posterior site in which microinjections were done. The most anterior site of injection is shown with a small arrow pointing to the more anterior segmental plate region. Figure 9A was taken approximately 0.5 min after injection. The extent of diffusion during this time is seen by Nile Green localization (which appears darker in this image). The antibody being of much larger molecular weight than Nile Green most likely does not diffuse as far in 0.5 min. Control microinjections of diluted whole rat or mouse serum resulted in normal somitogenesis (Fig. 9B). In Fig. 9C one injection of NCD-2 antibody was made in the segmental plate on the embryonic left side of the neuraxis (viewed from the ventral side) of a 7-somite embryo. In Fig. 9D multiple injections of NCD-2 were made bilaterally in the segmental plate regions of a 9-somite embryo. Multiple cell clusters are apparent on both sides of the neuraxis (see arrows). These results indicate that anomalous somitic clusters, usually only two, can develop in the posterior regions after 22–24 h incubation, if antibody is injected directly into the segmental plate. Thus, the perturbation does not appear to be a mechanical perturbation or a dilution of local diffusible factors within the segmental plate.

Copyright © 1998 by Academic Press. All rights of reproduction in any form reserved.

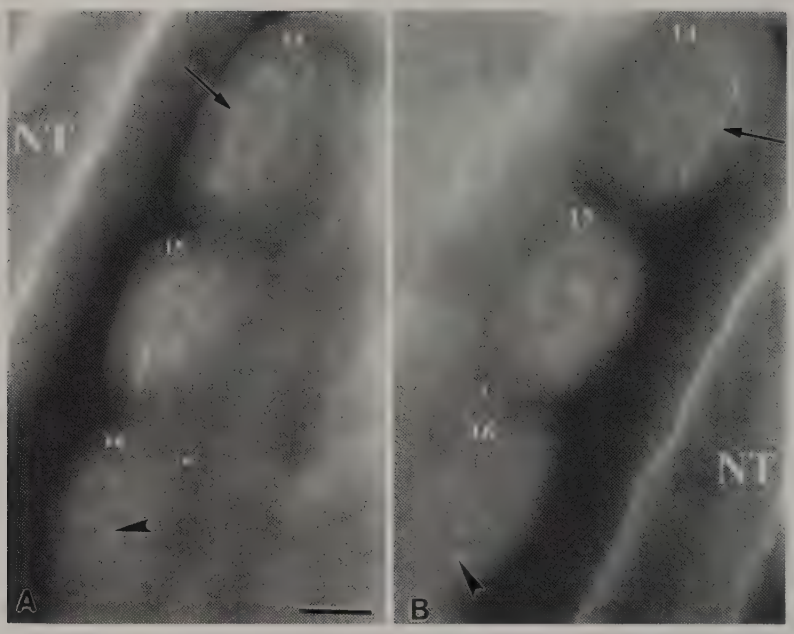

FIG. 5. Comparison of N-cadherin (A) and β-catenin (B) localization in somites 14–16 of a 16-somite embryo. Comparing these somitic regions, the localization and pattern of expression of both N-cadherin and β-catenin appear identical. In the newly emerging somite (16) patches of N-cadherin/β-catenin expression are seen. Arrowheads point to small patch-like foci of immunostaining that eventually will coalesce to form a central region of localization. In somite 14, N-cadherin/β-catenin show a defined pattern of expression in the central region with the highest level apparent on the side facing the neuraxis (see arrow). The localization of both N-cadherin and β-catenin during neural tube closure (N) within the folds is always discernible during these stages. Magnification bar: A and B, 50 μm.

LiCl treatment results in formation of anomalous somites. The results with N-cadherin/β-catenin localization and N-cadherin perturbation experiments suggest a possible involvement of β-catenin in initial stages of somitogenesis and in the formation of anomalous somites. This indicates the possibility of Wnt-mediated signaling in early steps of somitogenesis. LiCl has been described by several labs to mimic Wnt signaling (Klein and Melton, 1996; Stambolic *et al.*, 1996; Hedgepeth *et al.*, 1997). Thus, 53 chick embryos between stages 5 and 7 were exposed to reported, effective concentrations of LiCl of 0.1, 1.0, and 2 mM and assayed for somite formation. Anomalous somites similar to those in antibody-treated embryos formed at 1.0 and 2.0 mM concentrations with the same degree of variability seen with N-cadherin perturbation. Results indicated that 32% embryos treated with LiCl formed anomalous somites (17/53 embryos). The anomalous somites formed in two representative LiCl-treated stage 5 embryos are shown in Fig. 10. Embryos were immunostained for β-catenin after incubation for a 24-h period. Figure 10A shows anomalous somites that formed in the first 6 somite regions. The amnion was not removed in this embryo and is apparent covering part of the anterior somitic region. Figure 10B shows two small clusters of β-catenin-expressing cells in the posterior somitic regions, similar to our observations on NCD-2-microinjected embryos in the posterior part of the embryo and in the segmental plate regions. The anomalous somites, however, developed predominantly in the rostral 6 somitic regions, as with N-cadherin perturbation.

Perturbation of N-cadherin by genetic manipulation: Abnormal somitogenesis in* N-cadherin-null *mutant embryos. Within the somite region of *N-cadherin null* mouse embryos on day 8.5 of gestation, abnormal somite development also is apparent. Three *N-cadherin null* mouse embryos were immunostained for β-catenin and sectioned craniocaudad through the somite regions. Variability in perturbation of normal somite formation is apparent in the different *null* mutants, as was reported earlier (Radice *et al.*, 1997). Figure 11A shows somite development in normal littermates (+/+ or +/− for *N-cadherin*) at 8.5 days of gestation. In the *null* mutants shown in Figs. 11B, 11D, and 11E, several clusters of enhanced β-catenin expression in paraxial mesoderm regions are observed (arrows). It is apparent that the cells are clustering, but the clusters remain separate, have not formed normal somites in shape, and are small in size. These anomalous somitic clusters extended dorsal–ventrally near the neural tube and not laterally away from the neural tube as in the chick embryo (cf. Figs. 7 and 11). In some regions of cell clustering, β-catenin appears to be enriched cytoplasmically (see

Copyright © 1998 by Academic Press. All rights of reproduction in any form reserved.

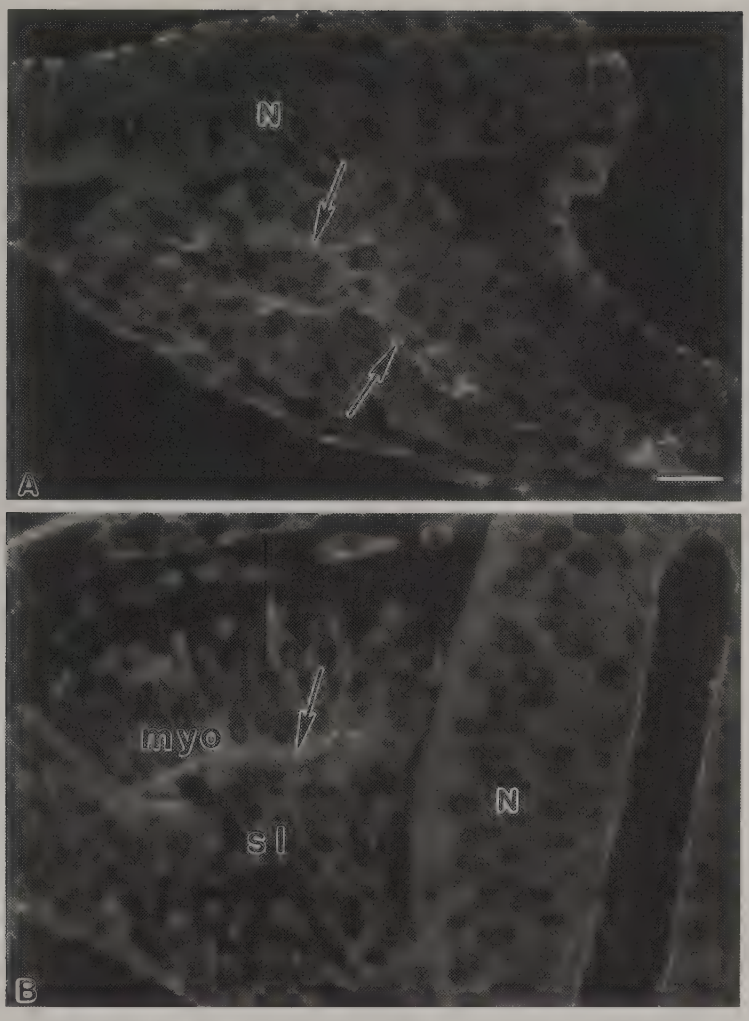

FIG. 6. Cross sections of stage 12 embryos (12–13 somites) sectioned transversely through the somite regions and stained for α-catenin. At this stage the localization is identical for N-cadherin and for β-catenin (not shown). (A) A formed somite is seen adjacent to the neural plate (N) on the right side of the embryo. α-Catenin is seen at the apices of the cells surrounding the central core. Cell processes extending between the cells at the core are discernible. In B, the sclerotome cells (sl) are seen. They will migrate toward the notochord and form the cartilage-producing cells of the developing vertebra. The sclerotome cells no longer express detectable α-catenin as they migrate. The α-catenin demarcates the boundary of the dermamyotome (myo; see arrow). The myotome population continues to express catenins and N-cadherin and remains associated with each other via adherens junctions. α- and β-catenin, as well as N-cadherin, also remain expressed at the junctions of the cells forming the neural plate and the cells which will line the lumen of the neural tube (N) after its closure. Magnification bar, 15 μm.

arrows in Figs. 11B and 11D). Some clusters shown in Fig. 11C from more posterior regions of the same embryo as in Fig. 11D are forming a single somitic structure, relatively normal in appearance, but smaller in size. Since these *N-cadherin null* embryos are embryonic lethals apparently due to poor cardiovascular development, compartmentalization of somites into dermamyotome and sclerotome could not be followed into later stages of gestation.

DISCUSSION

Somite Formation

Somites are the first obviously segmented structures to form in the embryo. They form in pairs, sequentially from the segmental plate in a rostral–caudal direction along the length of the embryo. As somites form, they undergo compaction to form a dense, cuboidal structure which then epithelializes. It

Copyright © 1998 by Academic Press. All rights of reproduction in any form reserved.

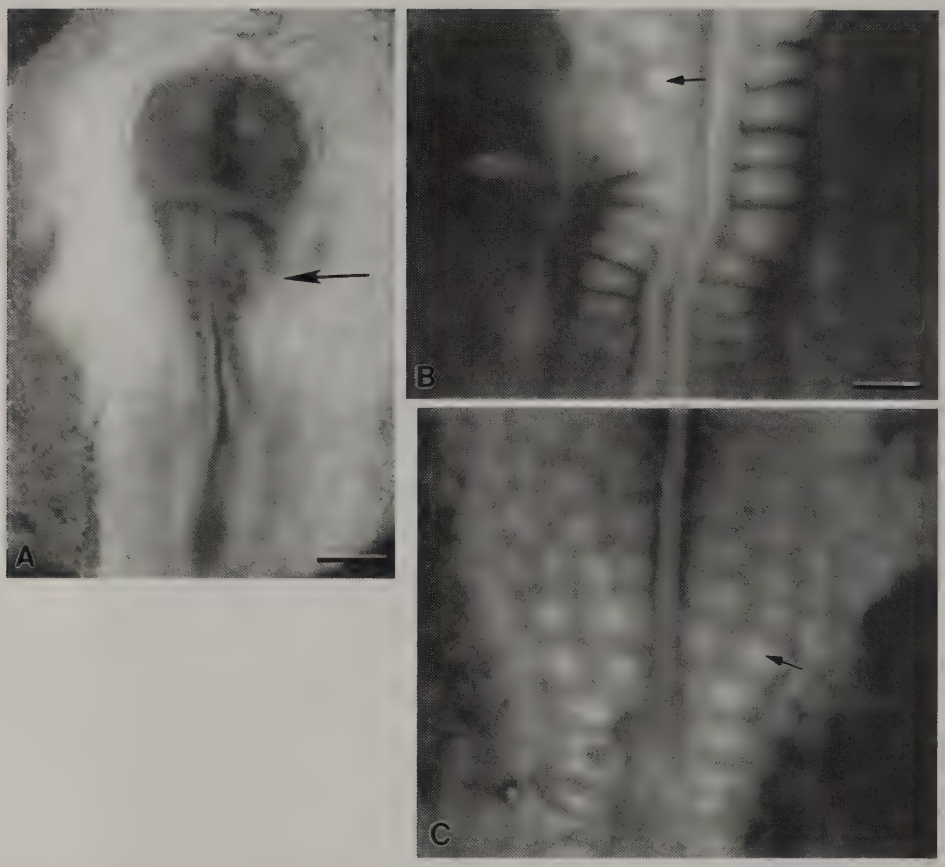

FIG. 7. Three representative patterns of anomalous somites are shown in A–C. In A a whole embryo is shown with anomalous somites present in anterior regions (see arrow). This antibody-treated embryo also had characteristic heart region abnormalities and a nonextended neural tube. Many NCD-2-treated embryos were immunostained for β-catenin and two representative embryos are shown in B and C. Central clusters of cells express β-catenin in each somite (see small arrow). In B anomalous somites are present on one side only. In C multiple anomalous somites are seen forming laterally away from the neural tube/notochord region, i.e., the neuraxis (N) region, during the formation of the first 3–6 somites. Posterior to the antibody-perturbed region, the somites are present in pairs in the normal manner. Anterior is to the top in both figures. Magnification bar: A, 400 μm; B and C, 100 μm.

has been shown that the transition to the compaction stage, prior to epithelialization, is correlated with the presence of fibronectin and that fibronectin appears to have a causal relationship in this process (Lash *et al.*, 1984, 1987; Lash, 1985). A spatiotemporal analysis of N-CAM during somitogenesis indicates that it also is involved (Duband *et al.*, 1987). Segmental plate cells weakly stain for N-CAM. During compaction, however, N-CAM expression is significantly increased. Isolated segmental plates are only weakly affected by N-CAM antibody, while those incubated in the presence of N-cadherin-perturbing antibody are dissociated (Duband *et al.*, 1987). Thus N-CAM appears less important in somitogenesis to a much lesser degree in contrast to N-cadherin and fibronectin.

TABLE 1
Perturbation with NCD-2 Antibody

Chick stages (HH)	Total No. embryos treated	No. embryos with anomalous somites	% Embryos with anomalous somites
Stage 5	41	14	34
Stage 6	16	12	75
Stage 7	7	1	14

It has been noted that N-cadherin is localized to the segmental plates and to apical–lateral cell membranes surrounding the central core region (Duband *et al.*, 1988; Hatta *et al.*, 1987). A causal role for N-cadherin has been sug-

Copyright © 1998 by Academic Press. All rights of reproduction in any form reserved.

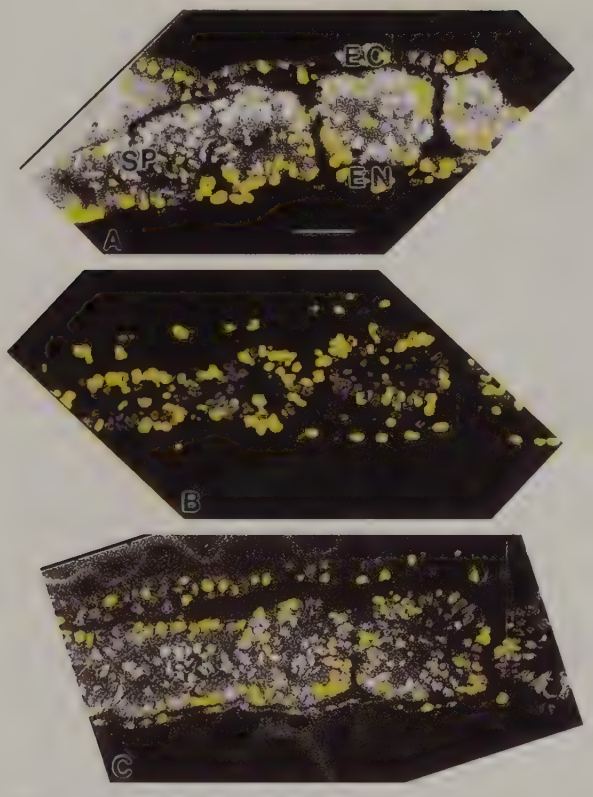

FIG. 8. Mitotic cells shown by bromodeoxyuridine (BrdU) labeling in antibody-perturbed embryos. Mitotic BrdU-labeled cells are seen in yellow. Anterior is to the right; segmental plate (SP) is on left. A shows a control stage 5 embryo incubated in normal rat IgG and labeled for BrdU; B is a control embryo incubated in the presence of polyclonal rabbit anti-NCAM; and C is an NCD-2-treated embryo. Embryos were sectioned sagitally through the somite and segmental plate regions and proliferating cells were counted in the last two somites that had formed and in the most anterior segmental plate region which gives rise to the next somite. At this period during the one-cell cycle, no significant difference is apparent in percentage of BrdU-labeled cells relative to DAPI-stained nuclei counted in these somitic regions (see Table 2). As shown in A–C, all treated embryos show a similar pattern of cell proliferation. Similarly, in the anterior part of the segmental plate, no significant difference in patterning or numbers of proliferative cells is detected. Thus, the formation of anomalous somites does not appear to be due to increased cell proliferation upon NCD-2 antibody treatment. EC, ectoderm; EN, endoderm Magnification bar, 50 μm.

gested previously (Duband *et al.*, 1987; Radice *et al.*, 1997). A stabilization of the cytoskeleton to this region is suggested by a concentration of filamentous actin and α-actinin to the apical regions of the somite cells surrounding the central core (see Lash and Ostrovsky, 1986; Ostrovsky *et al.*, 1988). The localization may be due to α-actinin and actin (Rimm *et al.*, 1995) binding to α-catenin (Knudsen *et al.*, 1995) which also is highly expressed in this same cellular region.

Several different models have been proposed to account for somite formation and have been reviewed by Keynes and Stern (1988). No single model, however, adequately explains somite development. In a "prepattern model" proposed by Bellairs (1985), it is suggested that there is a prepattern of somitogenic clusters in the posterior end of the segmental plate, to which new cells are added by cell division and by recruitment from the primitive streak. Each somite is directly related to a cell cluster and the size of the somite would depend upon the number of cells recruited into the cluster. Bellairs suggested that the number of "such tiny clusters may be much greater than the number of somites that will subsequently form . . ." The concept of multiple presomitic clusters of cells that form as a result of cadherin/β-catenin-mediated adhesion is strongly supported by our N-cadherin and LiCl perturbation experiments. Which cells initiate clustering is not known, but it may relate to Wnt signaling and β-catenin expression and subsequently the spread of N-cadherin expression among the cells to form a single cluster. That NCD-2 antibody does not appear to stimulate proliferation of segmental plate cells is indicated by similar numbers of randomly labeled BrdU-labeled cells in NCD-2-treated embryos, compared to control embryos receiving rat IgG or control embryos treated with N-CAM antibody.

Our analyses suggest that there are essentially three phases of somite development. First, foci of cells originate that begin to express β-catenin within the cytoplasm (phase 1) and in association with the cytoplasmic side of the cell membranes. N-cadherin associates with the β-catenin. Second, there is a coalescence of these N-cadherin/β-catenin-expressing cells into foci and clusters (phase 2). Subsequently, the cell clusters coalesce (phase 3) to form the central region of the somite. The recruitment or spread of adhesion among the cells appears to be mediated by N-cadherin. Cadherin-mediated cell-to-cell associations have been shown previously to trigger cell epithelialization (see also Wollner *et al.*, 1992; Marrs *et al.*, 1993; Linask *et al.*, 1997). Consequently, cadherin-mediated adhesion may trigger the epithelialization step. There is the possibility that other cadherins also are present, or up-regulated, that enable epithelialization to take place, even if N-cadherin is perturbed as in the *null* mutant embryos. N-cadherin, however, appears essential for the coalescence. These phases of somitogenesis are continuous and a dynamic sequence of events, rather than occurring as abrupt switches from one phase to another.

The N-cadherin/catenin-mediated events are coordinated with fibronectin-associated cell–substratum adhesion that also leads to compaction and segmentation of a population of cells within the segmental plate during somitogenesis (Lash *et al.*, 1984, 1985). Unpublished observations showing that soluble RGD peptides stimulate N-cadherin synthesis during somitogenesis (Yamada and Lash, personal commu-

Copyright © 1998 by Academic Press. All rights of reproduction in any form reserved

TABLE 2
Bromodeoxyuridine (BrdU) Labeling with Different Antibody Treatments

Antibody	No. BrdU-labeled cells	No. DAPI-labeled cells	% BrdU/DAPI
NCD-2	117	293	40
N-CAM	85	238	36
IgG	77	187	41

nication) suggest complementary function arising from an interaction between cell–cell and cell–matrix adhesion. Such cross-talk between members of the different families of adhesion molecules has been shown also for neural crest cells (Monier-Gavalle and Duband, 1997).

It can be argued that a static photograph cannot determine whether the N-cadherin/β-catenin-expressing clusters are coalescing or actually moving away from each other. Our interpretation of coalescence is based upon previous work addressing this issue. Upon injection of single segmental plate cells with a fluorescent tracer molecule, cells in the rostral two-thirds of the segmental plate contribute only to somite tissue and divide about every 10 h (Stern *et al.*, 1988). It is only in the most caudal portions of the segmental plate that cells contribute both to somites and to intermediate and lateral plate mesoderm derivatives. In our experiments anomalous somites occur in the most rostral regions.

Anomalous Somites

Our present analyses suggest that the formation of the anterior somites 1–6 differs in relation to the numbers of N-cadherin/β-catenin-expressing clusters from that observed in somites posterior to somite 6. As the first six pairs of somites form, the cells within the small N-cadherin/β-catenin-expressing foci coalesce to form multiple clusters of cells that continue to express N-cadherin and β-catenin. Anteriorly this coalescence of small foci occurs within the wide region of segmental plate and results in two to four apparently widely spaced large clusters extending lateral from the neuraxis in the chick embryo. In contrast, more caudal somites form from the coalescence of relatively more closely spaced, smaller foci within a much narrower segmental plate. It is only within this narrow developmental window, i.e., before coalescence of N-cadherin/catenin-expressing cell clusters, that the N-cadherin-perturbing antibodies have a dramatic effect on somitogenesis, resulting in multiple anomalous somites. Based upon our results, any possible perturbation of adhesion-mediated processes by temperature shock (e.g., Elsdale *et al.*, 1976; Primmett *et al.*, 1988) or by other disturbances (e.g., Stern and Bellairs, 1984) at this developmental time point of N-cadherin-mediated clustering of cells may result in the appearance of anomalous somites. If the developmental window for possible perturbation may be as short as 30 min or less (see Palmeirim *et al.*, 1997), for example, this can explain why the clusters do not always form and why one cannot obtain anomalous somites in the anterior regions in all treated embryos. The greatest percentage of anomalous somites occurs when embryos are at stage 6. This is a period during which the adhesion-mediated processes are most likely taking place in the embryo in the rostral most regions.

As indicated above, the phases of N-cadherin/β-catenin-mediated events are dynamic and occur in a continuum. As a consequence, the multiple epithelioid clusters resulting from modulation of adhesion by antibody treatment, LiCl treatment, or genetic mutation result in a great deal of variability in the numbers of anomalous somites that are obtained, if at all. Adhesion-related events may occur in approximately three phases as described above: appearance of individual foci of N-cadherin/β-catenin-expressing cells; coalescence of small foci into larger clusters of N-cadherin/β-catenin-expressing cells; and finally the coalescence of the larger clusters into one central N-cadherin/β-catenin-expressing region associated with the apical regions of cells. The number of initial foci that appear and numbers of clusters that form is variable. The duration of each phase is not known, but it appears to be short. There also appears to be a continuous flow from one phase to another. This pattern is repeated in the somites approximately in a 90-min cycle, as previously reported. This dynamic repetitive sequence occurs during the formation of every somite. The greater width or lateral distance involved in anterior segmental plate regions in contrast to narrower posterior segmental plates apparently affects the numbers of anomalous somites that can form. In addition, each chick embryo treated with NCD-2-perturbing antibody or LiCl will not be exactly at the same developmental window, even though the embryos may look phenotypically the same. Treatment within the different described phases of clustering within somitogenesis, distance between clusters and foci, diffusion gradients of antibody or LiCl, and accessibility to cell surfaces during clustering all will lead to variability in the observed results. In the mouse, compensatory pathways or other cadherins not being able to compensate for all of N-cadherin's function(s) can lead to variability in the transgenic knockout resulting from a chronic loss of N-cadherin.

The phases of N-cadherin/β-catenin-mediated events are similar to the dynamic continuum stages of expression described for the *c-hairy1* gene in presomitic mesoderm (Palmeirim *et al.*, 1997). The rhythmic *c-hairy* mRNA expression appears to be an autonomous property of the paraxial mesoderm and is linked to segmentation and

Copyright © 1998 by Academic Press. All rights of reproduction in any form reserved.

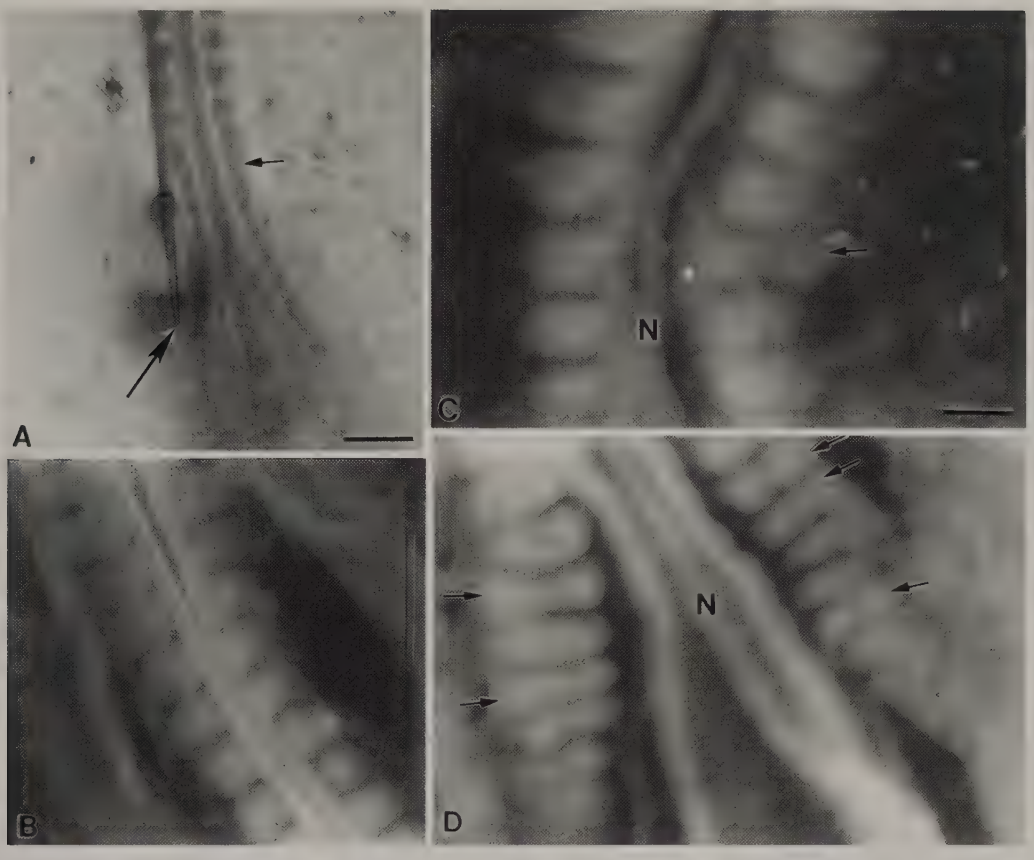

FIG. 9. Embryos in which N-cadherin-perturbing antibody was microinjected directly into the segmental plate regions of embryos with >7 somites and then incubated for a 24-h period. Embryos were immunostained for β-catenin which is seen only weakly in these images. Sites of injection are shown in A. The site of injection in this embryo is shown with the micropipet tip within the segmental plate just anterior to Hensen's node region. This is the most posterior site in which microinjections were done. The most anterior site of injection is shown with a small arrow pointing to the more anterior segmental plate region. A was taken approximately 0.5 min after injection. The extent of diffusion during this time is seen by Nile Green localization (which appears darker in this image). The antibody being of much larger molecular weight than Nile Green most likely does not diffuse as far in 0.5 min. B is a control rat IgG-microinjected embryo. Somitogenesis appeared normal. (C) This embryo was injected once in the anterior segmental plate on the right side of the neuraxis (N) of a 10-somite embryo. Arrow points to 2 somites that had formed after the incubation period on injected side of the neuraxis. These multiple somites did not form at the level of injection, but formed 2 somite lengths posterior to the site of injection. (D) In this embryo several injections were made bilaterally along the segmental plate region. Anomalous somites (arrows) are apparent in wider looking somites areas compared to control embryos. As can be seen, a longer area of the segmental plate was affected. N, neuraxis. Magnification bar: A, 200 μm; B, 100 μm; C and D, 40 μm.

somitogenesis of the paraxial mesoderm. During segmentation and somitogenesis *hairy* is expressed during a 90-min cycle in three continuous stages, each lasting approximately 30 min. The adhesion-mediated events described in this report and the rhythmicity of *c-hairy* expression may be linked. LiCl treatment which is reported to mimic Wnt signaling also resulted in anomalous somite formation. This supports the possibility of Wnt signal involvement in the paraxial mesoderm leading to modulation and possible stabilization of β-catenin in this region.

It is apparent that presomitic cell clusters are more closely spaced in caudal segmental plate regions. If one microinjects perturbing antibody directly into the segmental plate beyond the first six somite pairs, then two small β-catenin-expressing foci, instead of one, can develop on the injected side of the neuraxis. Double foci are detected with LiCl treatment. N-cadherin/catenin-expressing somite-nucleating centers may help explain experiments when the segmental plate on one side of the embryo is cut longitudinally into halves, two small longitudinal columns of

Copyright © 1998 by Academic Press. All rights of reproduction in any form reserved.

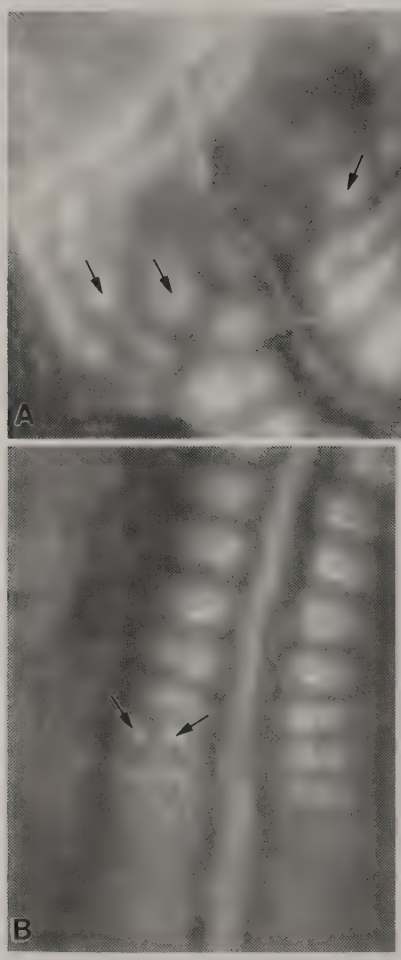

FIG. 10. Anomalous somites formed in LiCl-treated embryos. Embryos were immunostained for β-catenin after incubation for a 24-h period. (A) Anomalous somites (arrows) that formed in the first 6 somite regions. The amnion was not removed in this embryo and is apparent covering part of the anterior somitic region. (B) Two small clusters of β-catenin-expressing cells in one of the posterior somitic regions (arrows) of LiCl-treated embryos, similar to our observations on NCD-2-microinjected embryos in the posterior part of the embryo and in the segmental plate regions. Magnification bar, 100 μm.

somites formed which corresponded level for level with the single column of somites on the uncut control side of the embryo (Bellairs, 1985). In the latter experiments the N-cadherin/catenin-nucleating centers may have been physically separated into two clusters when the segmental plate was cut longitudinally. In our experiments the N-cadherin antibody may result in a similar molecular inhibition of the coalescence of closely spaced β-catenin-expressing foci, allowing multiple somites to form. The antibody cannot, however, inhibit the initial foci of N-cadherin/β-catenin-expressing cells from forming.

The notochord and neural tube are considered sources of signaling molecules for somitogenesis (Marcelle *et al.*, 1997; Stern and Hauschka, 1995; Buffinger and Stockdale, 1994). The appearance of multiple somites lateral to the axis suggests that diffusible signals from the neural tube/notochord region are not necessary for early somite formation. Thus, neighboring tissues may be required for the subcompartmentalization of the somite (see Marcelle *et al.*, 1997), but perhaps not for the initial formation. Autonomous signaling within the paraxial mesoderm resulting in segmentation has also been suggested by *c-hairy* expression (Palmeirim *et al.*, 1997) and also in the formation of anomalous somites with temperature shock (Primmett *et al.*, 1988). The role of neuraxial signaling in somitogenesis may be more downstream to the initial events described here.

Microinjection of nonimmune IgG indicates that dilution of diffusible factors probably does not occur since normal somites do form. The signal(s) initiating the cell clustering seen in association with β-catenin and N-cadherin appears to be a local one perhaps emanating from specific cells within the segmental plate that are sequestered by the extracellular matrix. Also based on our microinjection experiments, it would appear that N-cadherin/catenin-mediated events are in place and already stable within the segmental plate and extending over the distance of the next two to three somite pairs that will emerge. Perturbing antibodies injected into the most rostral area of the segmental plate have no effect on the immediate two to three somites to form, but only the subsequent third or fourth to form. Thus, in analyzing the "state" of differentiation or of adhesion of segmental plate cells, the exact rostral/caudal level of the segmental plate being viewed may provide different results and interpretations.

The initial, sparsely localized pattern of N-cadherin/catenin expression in the paraxial mesoderm suggests the existence of cells which may be involved in the initiation of the adhesion process. β-Catenin expression is an important component of early somitogenesis, possibly even being up-regulated before N-cadherin joins the complex. In the N-cadherin *null* mouse embryo, increased cytoplasmic β-catenin expression is observed in many of the cell clusters. β-Catenin expression has been involved with boundary formation in the chick embryo (Linask *et al.*, 1992, 1997), as well as segmentation in the *Drosophila* embryo (Peifer *et al.*, 1991). We suggest that the initial foci of β-catenin expression may represent activation by a *Wnt*-mediated signaling event. *Wnt* is the vertebrate homolog of *Drosophila wingless*. From our own observations and those reported (Eisenberg *et al.*, 1997), *Wnt-11* message localizes to somite regions in the chick embryo and may be involved in somitogenesis. Interestingly, *wingless* has been reported to be required for the formation of a subset of muscle founder cells during *Drosophila* embryogenesis (Baylies *et al.*, 1995). What activates *Wnt* signaling is not understood.

Copyright © 1998 by Academic Press. All rights of reproduction in any form reserved.

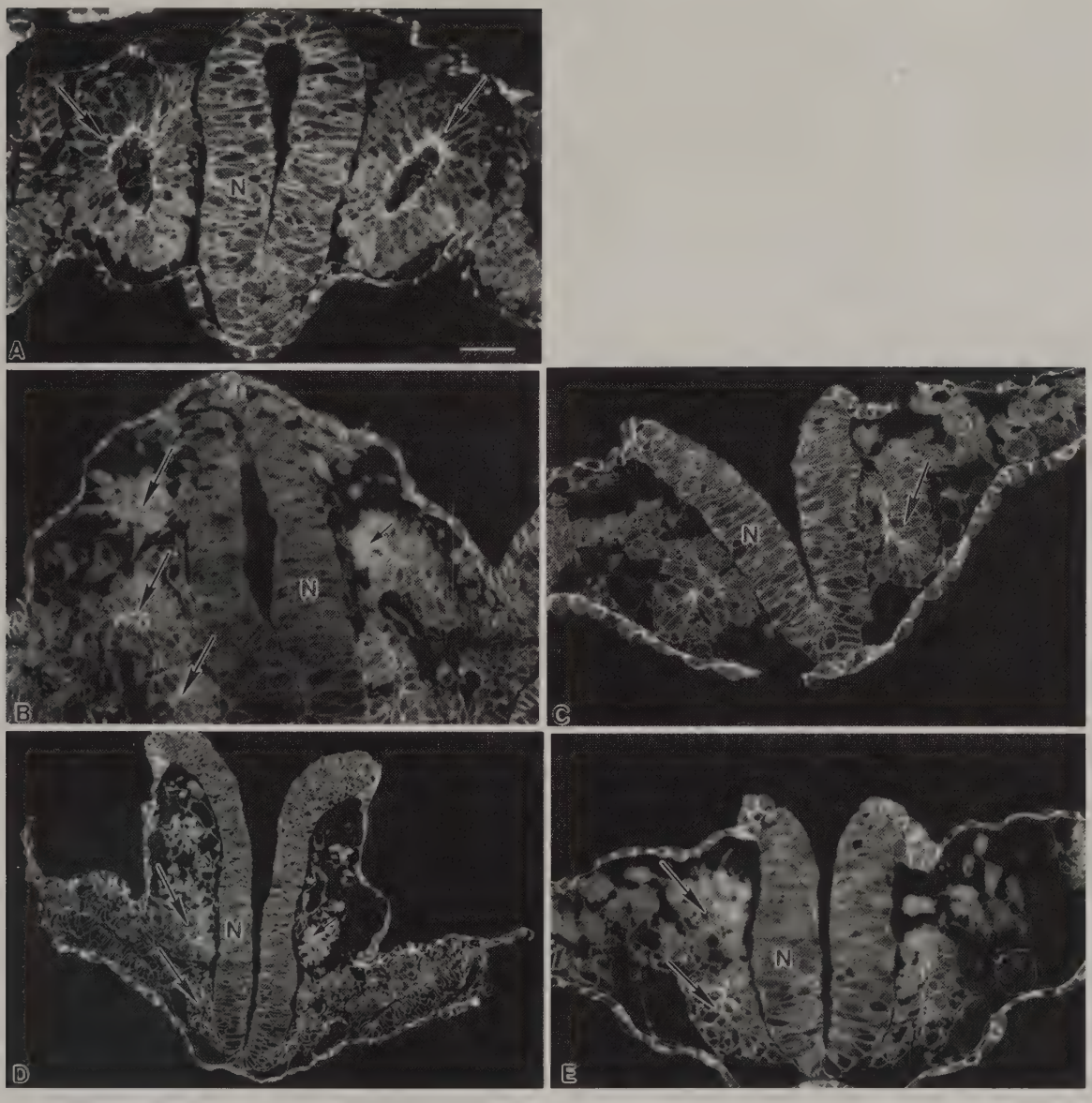

FIG. 11. Wild-type (A) and N-cadherin *null* (B–E) mouse embryos. The embryos were all immunostained for β-catenin. Variability in the phenotypes of *N-cadherin null* mutants within the somite regions is evident. (A) β-Catenin is seen at all cell membranes with a high level of expression at the core region of the two somites (arrows). Note size and typical organization of mouse somites. (B) Normal somites were not apparent in this mouse embryo. Multiple clusters of cells (see arrows) were apparent adjacent to the neural tube which also had an abnormal appearance with diminished β-catenin immunostaining. The more ventral clusters expressed more β-catenin within a central region. The more dorsal clusters show more cytoplasmic localization than apparent elsewhere. (B and C) Sections through the same embryo. In C the somites are relatively normal in appearance, although the central core region seen in the control embryo in A is not evident. In D the multiple clusters that were seen also in this embryo are shown (arrows). (E) In a third mutant embryo, multiple clusters in somite regions were again apparent (arrows). N, developing neural tube. Magnification bar in A and for B–E, 45 μm.

Somitogenesis in N-Cadherin Null *Mutant Embryos*

Antibody perturbation and genetic manipulation of N-cadherin result in similar abnormalities. Notably multiple cell clusters form in regions where normally there is only one somite. In the chick the anomalous somites form laterally; in the mouse anomalous somites form dorsoven-

Copyright © 1998 by Academic Press. All rights of reproduction in any form reserved.

trally, relative to the neural tube. That the somitogenic cluster localization is not identical in the two vertebrates may reflect differences in the embryonic organization. The chick embryo is flat at these stages, whereas the mouse embryo is curved with body folds tightly enclosing the somite region. Perturbation of N-cadherin adhesion by an antibody or by genetic manipulation cannot perturb β-catenin expression within cells in the clusters. This is apparent in the *N-cadherin null* mutant, where some cells continue to express β-catenin cytoplasmically and at cell membranes, and to show clustering. These small clusters, however, do not form normal epithelioid somitic structures. It is likely that another cadherin(s) may be present (Radice *et al.*, 1997). Based on our own immunohistochemical observations (unpublished) and those reported by others (Inuzuka *et al.*, 1991; Murphy-Erdosch *et al.*, 1994), R-cadherin and B-cadherin are not detectable at the early stages of somitogenesis reported here. The presence of cadherin-11 in somites during these stages has been shown on the mRNA level in the mouse (Kimura *et al.*, 1995). Thus, cadherin-11 may be able to compensate partially for N-cadherin during somitogenesis in the *null* mouse embryo and in our antibody perturbation experiments in the chick. That distinct cadherins may play different roles has been reported (Marrs *et al.*, 1993).

Adhesion-Related Similarities in Cardiac and Skeletal Myogenesis

Many adhesion-related developmental processes involved in somitogenesis and myotome formation are similar to those leading to heart development and the differentiation of the cardiomyocyte. The adhesion-mediated processes may serve as a common, evolutionarily conserved link in the myogenic pathways leading to cardiac and skeletal muscle phenotypes. Adhesion molecules, such as N-cadherin, are involved in coordinating the formation of the three-dimensional structure of somites, as well as in the specification of the skeletal myogenic cell population. A similar coordination of early heart cell compartmentalization *in vivo* and cardiac myogenesis by N-cadherin/β-catenin was reported (Linask *et al.*, 1997; Imanka-Yoshida *et al.*, 1998). It has also been shown that N-cadherin (A-CAM) is expressed during early somitogenesis and by myotome cells (Duband *et al.*, 1988; Hatta *et al.*, 1987), as well as by cardiac precursor cells and cardiomyocytes (Linask, 1992; Hatta *et al.*, 1987). Both cardiac precursors and myotome precursors within the somite undergo epithelialization events before the cells differentiate (Linask *et al.*, 1997; Linask and Lash, 1986). In addition, both somitogenesis and heart development, as well as specification of the different regions of the somite and of the heart, show a definite anterior to posterior progression of development, along with boundary development that is associated with N-cadherin/catenin expression. N-cadherin is expressed at high levels by the myotome cells in the somite and throughout skeletal muscle differentiation of the cells (George-Weinstein *et al.*, 1997; Redfield *et al.*, 1997). Both cardiac and skeletal myogenesis appear to depend upon cell–cell interactions occurring within a group of cells, called the *community effect* (Holt *et al.*, 1994; Gurdon *et al.*, 1992; Gurdon, 1988; Cossu *et al.*, 1995). Cell–cell interactions such as those mediated by N-cadherin are coordinated with cell–matrix adhesion and involving molecules such as fibronectin which have been shown to be important for both cardiomyogenesis and somitogenesis (George *et al.*, 1993; Lash *et al.*, 1984, 1987; Linask and Lash, 1986). It is highly likely that cross-talk between cadherin- and integrin-mediated events is essential for normal development of both the heart and skeletal muscle.

SUMMARY

In summary, N-cadherin/catenin complex expression and localization within the segmental plate apparently define and recruit a population of cells that are incorporated into one somitic structure. If the N-cadherin-mediated process of somitogenesis is perturbed before cells can form a central area of N-cadherin/catenin-expressing cells, then each cadherin/catenin-expressing cluster of cells by itself can form a somite. Our microinjection data would suggest that the adhesion process is stabilized already within the rostral end of the segmental plate extending across the next 2- to 3-somite-forming regions caudad. The initiator signal for each somite is not known, but may relate to *Wnt* signaling because β-catenin appears to be part of this process and lies in a *Wnt*-mediated pathway. Involvement of Wnt signaling is also suggested by the treatment of embryos with LiCl which is considered to mimic Wnt signaling. LiCl treatment also results in the formation of anomalous somites. Within each parasegment the spread or activation of N-cadherin adhesion among cells between foci and cell clusters results in the recruitment of cells eventually into a single compartment. The cells become associated with each other through cell junctions at their apical–lateral surfaces and with fibronectin and other extracellular matrix molecules at their basal surfaces with an apparent cross-talk between these adhesion systems. Concomitantly, the cells undergo a cell shape change facilitated by the apical–lateral expression of N-cadherin and possibly cadherin-11, to form the recognizable epithelioid somitic structure. Later, as the somite begins to undergo diversification, further modulation of cadherins occurs, as N-cadherin is down-regulated by the sclerotome cells and retained by the myotome population. How the events reported here may be coordinated with the expression of factors as, for example, c-hairy, paraxis, Pax-1, Pax-3, Pax-7, Myo D, and other regulatory factors remain to be determined. It is evident from our results that N-cadherin/β-catenin-mediated adhesion may be an important facet in the complex series of events that have been proposed for the initiation and formation of somites.

ACKNOWLEDGMENTS

This work was supported by NIH Grant HL48746 to K.K.L., the W.W. Smith Charitable Trust to K.A.K., and the American Heart

Copyright © 1998 by Academic Press. All rights of reproduction in any form reserved.

Association to G.L.R. The authors thank Dr. J.W. Lash for his critical review of the manuscript and useful suggestions. Many thanks also to Drs. M. Takeichi and M. George-Weinstein for their reading of the manuscript and their helpful comments.

REFERENCES

Barnes, G. L., Alexander, P. G., Hsu, C. W., Mariani, B. D., and Tuan, R. (1997). Cloning and characterization of chicken paraxis: A regulator of paraxial mesoderm development and somite formation. *Dev. Biol.* **189,** 95–111.

Baylies, M. K., Martinez Arias, A., and Bate, M. (1995). wingless is required for the formation of a subset of muscle founder cells during *Drosophila* embryogenesis. *Development* **121,** 3829–3837.

Behrens, J., von Kries, J. P., Kuhl, M., Bruhn, L., Wedlich, D., Grosschedl, R., and Birchmeier, W. (1996). Functional interaction of β-catenin with the transcription factor LEF-1. *Nature* **382,** 638–642.

Bellairs, R. (1985). A new theory about somite formation in the chick. *In* "Developmental Mechanisms: Normal and Abnormal," pp. 25–44. A. R. Liss, New York.

Bellairs, R., Curtis, A. S. G., and Sanders, E. J. (1977). Cell adhesiveness and embryonic differentiation. *J. Embryol. Exp. Morphol.* **46,** 207–213.

Buffinger, N., and Stockdale, F. E. (1995). Myogenic specification of somites is mediated by diffusible fuactors. *Dev. Biol.* **169,** 96–108.

Burgess, R., Rawls, A., Brown, D., Bradley, A., and Olson, E. N. (1996). Requirement of the paraxis gene for somite formation and musculoskeletal patterning. *Nature* **384,** 570–573.

Cheney, C. M., and Lash, J. W. (1984). An increase in cell–cell adhesion in the chick segmental plate results in a meristic pattern. *J. Embryol. Exp. Morphol.* **79,** 1–10.

Christ, B., Jacob, H. J., and Jacob, M. (1978). On the formation of myotomes in avian embryos. An experimental and scanning electon microscopic study. *Experientia* **34,** 514–516.

Christ, B., and Ordahl, C. P. (1995). Early stages of chick somite development. *Anat. Embryol.* **191,** 381–396.

Cossu, G., Kelly, R., DiDonna, S., Vivarelli, E., and Buckingham, M. (1995). Myoblast differentiation during mammalian somitogenesis is dependent upon a community effect. *Proc. Natl. Acad. Sci. USA* **92,** 2254–2258.

Duband, J. L., Dufour, S., Hatta, K., Takeichi, M., Edelman, G. M., and Thiery, J. P. (1987). Adhesion molecules during somitogenesis in the avian embryo. *J. Cell Biol.* **104,** 1361–1374.

Duband, J.-L., Volberg, T., Sabanay, I., Thiery, J. P., and Geiger, B. (1988). Spatial and temporal distribution of the adherens-junction-associated adhesion molecule A-CAM during avian embryogensis. *Development* **103,** 325–344.

Eisenberg, C. A., Gourdie, R. G., and Eisenberg, L. M. (1997). Wnt-11 is expresed in early avian mesoderm and required for the differentiation of the quail mesoderm cell line QCE-6. *Development* **124,** 525–536.

Elsdale, T. R., Pearson, J. J., and Whitehead, M. (1976). Abnormalities in somite segmentation following heat shock to *Xenopus* embryos. *J. Embryol. Exp. Morphol.* **35,** 625–636.

George-Weinstein, M., Gerhart, J., Blitz, J., Simak, E., and Knudsen, K. (1997). N-Cadherin promotes the commitment and differentiation of skeletal muscle precursor cells. *Dev. Biol.* **185,** 14–24.

Gurdon, J. B. (1988). A community effect in animal development. *Nature* **336,** 772–774.

Gurdon, J. B., Lemainre, P., and Kato, K. (1993). Community effects and related phenomena in development. *Cell* **75,** 831–834.

Hamburger, V., and Hamilton, H. L. (1951). A series of normal stages in the development of the chick embryo. *J. Morphol.* **88,** 49–92.

Hatta, K., Okada, T. S., and Takeichi, M. (1985). A monoclonal antibody disrupting calcium-dependent cell–cell adhesion of brain tissues: Possible role of its target antigen in animal pattern formation. *Proc. Natl. Acad. Sci. USA* **82,** 2789–2793.

Hatta, K., Takagi, S., Hajime, F., and Takeichi, M. (1987). Spatial and temporal expression pattern of n-cadherin cell adhesion molecules correlated with morphogenetic processes of chicken embryos. *Dev. Biol.* **120,** 215–227.

Hedgepeth, C. M., Conrad, L. J., Zhang, J., Huang, H. C., Lee, V. M. Y., and Klein, P. S. (1997). Activation of the Wnt signaling pathway: A molecular mechanism for lithium action. *Dev. Biol.* **185,** 82–91.

Holt, C. E., Lemaire, P., and Gurdon, J. B. (1994). Cadherin-mediated cell interactions are necessary for the activation of MyoD in *Xenopus* mesoderm. *Proc. Natl. Acad. Sci. USA* **91,** 10844–10848.

Inuzuka, H., Redies, C., and Takeichi, M. (1991). Differential expression of R- and N-cadherin in neural and mesodermal tissues during early chicken development. *Development* **113,** 959–967.

Johnson, K. R., Lewis, J. E., Li, D., Wahl, J., Soler, A. P., Knudsen, K. A., and Wheelock, M. J. (1993). P- and E-cadherin are in separate complexes in cells expressing both cadherins. *Exp. Cell Res.* **207,** 252–260.

Keynes, R. J., and Stern, C. D. (1988). Mechanisms of vertebrate segmentation. *Development* **103,** 413–429.

Kimura, Y., Matsunami, H., and Takeichi, M. (1996). Expression of cadherin-11 delineates boundaries, neuromeres, and nuclei in the developing mouse brain. *Dev. Dyn.* **206,** 455–462.

Klein, P. S., and Melton, D. A. (1996). A molecular mechanism for the effect of lithium on development. *Proc. Natl. Acad. Sci. USA* **93,** 8455–8459.

Knudsen, K. A., Peralta Soler, A., Johnson, K. R., and Wheelock, M. J. (1995). Interaction of α-actinin with the cadherin/catenin cell–cell adhesion complex via alpha-catenin. *J. Cell Biol.* **130,** 67–77.

Lash, J. W. (1985). Somitogenesis: Investigations on the mechanisms of compaction in the presomitic mass and a possible role for fibronectin. *In* "Developmental Mechanisms: Normal and Abnormal" (J. W. L. and L. Saxen, Eds.). A. R. Liss, New York.

Lash, J. W., Linask, K. K., and Yamada, K. M. (1987). Synthetic peptides that mimic the adhesive recognition signal of fibronectin: Differential effects on cell–cell and cell–substratum adhesion in embryonic chick cells. *Dev. Biol.* **123,** 411–420.

Lash, J. W., and Ostrovsky, D. (1986). On the formation of somites. *In* "Developmental Biology" (L. W. Browder, Ed.), Vol. 2, pp. 547–563. Plenum, New York.

Lash, J. W., Seitz, A. W., Cheny, C. M., and Ostrovsky, D. (1984). On the role of fibronectin during the compaction stage of somitogenesis in the chick embryo. *J. Exp. Zool.* **232,** 197–206.

Linask, K., Gui, Y. H., Rasheed, R., and Kwon, L. (1992). Pattern development during pericardial coelom formation and specification of the cardiomyocyte cell population by N-cadherin and the *Drosophila* armadillo protein homologue in the early chick embryo. *Mol. Biol. Cell* **3**(Suppl.), 206A.

Linask, K. K. (1992). N-cadherin localization in early heart development and polar expression of Na, K-ATPase, and integrin

Copyright © 1998 by Academic Press. All rights of reproduction in any form reserved.

during pericardial coelom formation and epithelialization of the differentiating myocardium. *Dev. Biol.* **151,** 213–224.

Linask, K. K., Knudsen, K. A., and Gui, Y. H. (1997). N-Cadherin–catenin interaction: Necessary component of cardiac cell compartmentalization during early vertebrate heart development. *Dev. Biol.* **185,** 148–164.

Linask, K. K., and Lash, J. W. (1986). Precardiac cell migration: Fibronectin localization at mesoderm–endoderm interface during directional movement. *Dev. Biol.* **114,** 87–101.

Linask, K. K., and Lash, J. W. (1988). A role for fibronectin in the migration of avian precardiac cells. I. Dose-dependent effects of fibronectin antibody. *Dev. Biol.* **129,** 315–323.

Lipton, B. H., and Jacobson, A. G. (1974). Analysis of normal somite development. *Dev. Biol.* **38,** 73–90.

Marcelle, C., Stark, M. R., and Bronner-Fraser, M. (1997). Coordinate actions of BMPs, Wnts, Shh and Noggin mediate patterning of the dorsal somite. *Development* **124,** 3955–3963.

Maroto, M., Reshef, R., Munsterberg, A. E., Koester, S., Goulding, M., and Lassar, A. B. (1997). Ectopic Pax-3 activates MyoD and Myf-5 expression in embryonic mesoderm and neural tissue. *Cell* **89,** 139–148.

Marrs, J. A., Napolitano, E. W., Murphy-Erdosh, C., Mays, R. W., Reichardt, L. F., and Nelson, W. J. (1993). Distinguishing roles of the membrane-cytoskeleton and cadherin mediated cell–cell adhesion in generating different Na, K-ATPase distributions in polarized epithelia. *J. Cell Biol.* **123,** 149–164.

Meier, S. (1979). Development of the chick embryo mesoblast: Formation of the embryonic axis and establishment of the metameric pattern. *Dev. Biol.* **73,** 25–45.

Molenaar, M., van de Wetering, M., Oosterwegel, M., Peterson-Maduro, J., Godsave, S., Korinek, V., Roose, J., Destree, O., and Clevers, H. (1996). XTcf-3 transcription factor mediates catenin-induced axis formation in *Xenopus* embryos. *Cell* **86,** 391–399.

Monier-Gavalle, F., and Duband, J. L. (1997). Cross talk between adhesion molecules: Control of N-cadherin acitvity by intracellular signals elicited by β1 and β3 integrins in migrating neural crest cells. *J. Cell Biol.* **137,** 1663–1681.

Murphy-Erdosh, C., Napolitano, E. W., and Reichardt, L. F. (1994). The expression of B-cadherin during embryonic chick development. *Dev. Biol.* **161,** 107–125.

Palmeirim, I., Henrique, D., Horowicz, D., and Pourquie, O. (1997). Avian *hairy* gene expression identifies a molecular clock linked to vertebrate segmentation and somitogenesis. *Cell* **91,** 639–648.

Peifer, M., Rauskolb, C., Williams, M., Riggleman, B., and Wieschaus, E. (1991). The segment polarity gene armadillo interacts with the wingless signaling pathway in both embryonic and adult pattern formation. *Development* **111,** 1029–1043.

Primmett, D. R. N., Stern, C. D., and Keynes, R. J. (1988). Heat shock causes repeated segmental anomalies in the chick embryo. *Development* **104,** 331–338.

Ostrovsky, D., Cheney, C. M., Seitz, A. W., and Lash, J. W. (1983). Fibronectin distribution during somitogenesis in the chick embryo. *Cell Differ.* **13,** 217–223.

Ostrovsky, D., Sanger, J. W., and Lash, J. W. (1988). Somitogenesis in the mouse embryo. *Cell Differ.* **23,** 17–26.

Radice, G. L., Rayburn, H., Matsunami, H., Knudsen, K. A., Takeichi, M., and Hynes, R. O. (1997). Developmental defects in mouse embryos lacking N-cadherin. *Dev. Biol.* **181,** 64–78.

Rawls, A., and Olson, E. N. (1997). MyoD meets its maker. *Cell* **89,** 5–8.

Redfield, A., Nieman, M. T., and Knudsen, K. A. (1997). Cadherins promote skeletal muscle differentiation in three-dimensional cultures. *J. Cell Biol.* **138,** 1323–1331.

Rimm, D. L., Koslov, E. R., Kebriaei, P., Cianci, C. D., and Morrow, J. S. (1995). Alpha 1 (E)-catenin is an actin-binding and -bundling protein mediating the attachment of F-actin to the membrane adhesion complex. *Proc. Natl. Acad. Sci. USA* **92,** 8813–8817.

Stambolic, V., Ruel, L., and Woodgett, J. R. (1996). Lithium inhibits glycogen synthase kinase-3 activity and mimics wingless signalling in intact cells. *Curr. Biol.* **6,** 1664–1668.

Stern, C. D., and Bellairs, R. (1984). The roles of node regression and elongation of the *area pellucida* in the formation of somites in avian embryos. *J. Embryol. Exp. Morphol.* **81,** 75–92.

Stern, C. D., Fraser, S. E., Keynes, R. J., and Primmett, D. R. N. (1988). A cell lineage analysis of segmentation in the chick embryo. *Development* **104**(Suppl.), 231–244.

Stern, H. M., and Hauschka, S. D. (1995). Neural tube and notochord promote *in vitro* myogenesis in single somite explants. *Dev. Biol.* **167,** 87–103.

Tajbakhsh, S., Rocancourt, D., Cossu, G., and Buckingham, M. (1997). Redefining the genetic hierarchies controlling skeletal myogenesis: Pax-3 and Myf-5 act upstream of MyoD. *Cell* **89,** 127–138.

Takeichi, M. (1988). The cadherins: Cell–cell adhesion molecules controlling animal morphogenesis. *Development* **102,** 639–655.

van Eeden, F. J. M., Granato, M., Schach, U., Brand, M., Furutani-Seiki, M., P., J., Hammerschmidt, M., Heisenberg, C. P., Jiang, Y. J., Kane, D. A., Kelsh, R. N., Mullins, M. C., Odenthal, J., Warga, R. M., Allende, M. L., Weinberg, E. S., and Nusslein-Volhard, C. (1996). Mutations affecting somite formation and patterning in the zebrafish, *Danio rerio*. *Development* **123,** 153–164.

Wheelock, M. J., and Knudsen, K. A. (1991). N-cadherin-associated proteins in chicken muscle. *Differentiation* **46,** 35–42.

Wollner, D. A., Krzeminski, K. A., and Nelson, W. J. (1992). Remodeling the cell surface distribution of membrane proteins during the development of epithelial cell polarity. *J. Cell Biol.* **116,** 889–899.

Yun, K. S., and Wold, B. (1996). Skeletal muscle determination and differentiation—Story of a core regulatory network and its context. *Curr. Opin. Cell Biol.* **8,** 877–889.

Received for publication January 2, 1998
Revised July 16, 1998
Accepted July 16, 1998

Copyright © 1998 by Academic Press. All rights of reproduction in any form reserved.

DEVELOPMENTAL BIOLOGY **202**, 103–112 (1998)
ARTICLE NO. DB988989

Precocious Expression of the Wilms' Tumor Gene *xWT1* Inhibits Embryonic Kidney Development in *Xenopus laevis*

John B. Wallingford, Thomas J. Carroll, and Peter D. Vize[1]
Center for Developmental Biology, Department of Zoology, University of Texas, Austin, Texas 78712

The tumor suppressor WT1 has been demonstrated to have a wide variety of activities *in vitro* and is required for metanephric development *in vivo*. In the experiments presented here, the *Xenopus* pronephros was used as a simple model system to examine the activity of *Xenopus WT1* (*xWT1*) during kidney development. *xWT1* was ectopically expressed in *Xenopus* embryos by mRNA injection and found to inhibit pronephric tubule development. Confocal microscopy confirmed this observation and revealed that the inhibition was the result of a failure to form a pronephric anlage of appropriate size rather than a defect in epithelialization. Examination of *Xlim-1* expression, an early molecular marker of pronephric specification, in tailbud embryos indicated that injected *xWT1* mRNA inhibited pronephric specification prior to any overt sign of morphogenesis (*Xenopus* stage 21). These results suggest that xWT1 may act to repress tubule-specific gene expression in the portion of the pronephros fated to form its vascular structure, the glomus. © 1998 Academic Press

Key Words: **pronephros; organogenesis; WT1; glomus; pronephric tubules.**

INTRODUCTION

Embryos form and utilize different kidney types at different stages of development. In the higher vertebrates, a pair of embryonic mesonephroi control water and salt balance during early development, and this function is later relinquished to a pair of metanephroi, the adult kidneys. In lower vertebrates, such as fish and amphibians, the mesonephroi are in fact the adult kidneys, and embryonic water balance is maintained by a pair of much simpler organs, the pronephroi (Müller, 1829; Burns, 1955; Saxén, 1987; Vize *et al.*, 1997). Each pronephros is organized in a manner similar to that of a single metanephric nephron, with a filtration apparatus (the glomus), a simple set of tubules for the collection of filtrate and resorption of nutrients (the pronephric tubules), and an excretory duct (pronephric or Wolffian duct) for the disposal of wastes (Field, 1891; Fox, 1963; Balinsky, 1970; Vize *et al.*, 1995; Carroll and Vize, 1996). The simple architecture of the pronephroi, as well as their amenability to experimental manipulation and observation, make the amphibian embryo an excellent system in which to study organogenesis of the kidney. Interestingly, several recent experiments demonstrate that many of the same genes are expressed during organogenesis of pro-, meso-, and metanephroi, suggesting that conserved genetic pathways may be used in the development of all three forms of this organ (reviewed by Vize *et al.*, 1997).

The tumor suppressor gene *WT1* is expressed in the developing mammalian nephric system (Pelletier *et al.*, 1991a; Armstrong *et al.*, 1992; Mundlos *et al.*, 1993), and in mice lacking *WT1*, the metanephric blastema degenerates early in development, and kidneys do not form (Kreidberg *et al.*, 1993). These results suggest a critical role for *WT1* in the development of the metanephric tubules. In the later stages of nephrogenesis, *WT1* expression is restricted to the podocytes of the Bowman's capsule, the vascularized component of mammalian nephrons (Pelletier *et al.*, 1991a; Armstrong *et al.*, 1992; Mundlos *et al.*, 1993), and humans with mutations in *WT1* often suffer from glomerular nephropathy, a failure of kidney vascular development (Pelletier *et al.*, 1991b). These results suggest a role for WT1 in the development of the vascular component of the kidney in addition to the early role in mesenchymal condensation. Such a role in the development of the vascular component of the kidney is supported by the observation that expres-

[1] To whom correspondence should be addressed. Fax: (512) 471-1188. E-mail: peter@pvize.zo.utexas.edu.

0012-1606/98 $25.00
Copyright © 1998 by Academic Press
All rights of reproduction in any form reserved.

sion of the *Xenopus* ortholog of *WT1* (*xWT1*) is restricted to the vascularized glomus throughout pronephric development (Carroll and Vize, 1996).

WT1 encodes a zinc-finger type transcription factor, and mutations in *WT1* have been identified in Wilms' tumors, pediatric tumors of the kidney (reviewed by Coppes *et al.*, 1995). *In vitro*, WT1 is a powerful suppressor of transcription from several promoters, including *Pax2*, *IGF* II, the *EGF* receptor, and the *PDGF* a-chain, genes that have been implicated in the regulation of kidney development (Madden *et al.*, 1991; Ryan *et al.*, 1995; Drummond *et al.*, 1992; Englert *et al.*, 1995; Wang *et al.*, 1995). WT1 also contains an RNA recognition motif and may regulate gene activity posttranscriptionally by binding mRNA (Kennedy *et al.*, 1996; Caricasole *et al.*, 1996; Larsson *et al.*, 1995). Despite of the wealth of data concerning WT1 activity, its precise role in the development of the kidney has yet to be determined.

In this report, the *Xenopus* pronephros was utilized as a simple kidney model system in which to examine the activity of xWT1 *in vivo*. *xWT1* was ectopically expressed in *Xenopus* embryos by mRNA injection and found to inhibit pronephric development prior to the first signs of morphogenesis at stage 21 (Nieuwkoop and Faber, 1994). The inhibitory action of xWT1 on pronephric tubule development suggests a role for *WT1* genes in the downregulation of the response to inductive signals during nephrogenesis. This activity and the expression patterns of *WT1* and *xWT1* further suggest that this gene plays a similar role in the development of the vascular components of both pronephroi and metanephroi: inhibiting the expression of tubule-specific genes in cells which will form the vascular component of the kidney.

MATERIALS AND METHODS

DNA constructs. The xWT1-KTS coding region was released from pGEMxWT1 (Carroll and Vize, 1996) with *Bam*H1 and subcloned into the *Bgl*II site of pSP64TS to generate p64TSxWT1-KTS. pSP64TS is a modified form of pSP64T (Krieg and Melton, 1984) and contains a polylinker with two additional cloning sites (*Eco*RV and *Spe*I) following the existing *Bgl*II site, followed by translation termination codons in all three reading frames. pSP64TS provides *in vitro* transcribed mRNAs with *Xenopus* globin 5′ and 3′ untranslated regions and greatly increases the amount of protein translated (Krieg and Melton, 1984). To construct the +KTS expression plasmid, the coding region of xWT23 (Carroll and Vize, 1996) was amplified by PCR using primers with *Bam*HI ends and cloned into the *Bgl*II site of pSP64TS. The resulting intermediate clone was digested with *Apo*I to release the 3′ half of xWT1 + KTS as well as about 300 bp of pSP64TS 3′ to the xWT1 insert. p64TSxWT1-KTS was similarly digested with *Apo*I, and the +KTS 3′ half of xWT1 from the intermediate plasmid was inserted, producing p64TSxWT1 + KTS.

Embryos and microinjection. Female adult *Xenopus* were induced to ovulate with human chorionic gonadotropin, and eggs were fertilized *in vitro* according to Peng *et al.* (1991). Embryos were dejellied in 3% cysteine solution and washed in 0.2× MMR. Embryos were then reared at 13–18°C in 0.2× MMR. Microinjections were performed as previously described (Vize *et al.*, 1991). Capped mRNA was produced by *in vitro* transcription (Krieg and Melton, 1984). To minimize nonspecific toxicity effects, mRNA was purified using a Sephadex G-50 column. *In vitro* transcriptions were also treated with DNaseI prior to mRNA Sephadex purification to minimize the amount of DNA injected. Purified mRNAs were resuspended in sterile water for injections. All mRNAs were translated *in vitro* and generated proteins of appropriate size, indicating that all mRNAs were functional.

The volume of each injection was 5 nl, and the dosage was varied by altering the concentration of the mRNA injected. Injections were made at the 16- to 64-cell stages into the presumptive pronephric region (blastomeres C3 and D3 at the 32-cell stage) or the presumptive somite (blastomeres C2 and C3 at the 32-cell stage) according to the fate map of Dale and Slack (1987). In all cases 0.25 ng of β-galactosidase mRNA was co-injected as a lineage tracer for the injected *xWT1* mRNA (Vize *et al.*, 1991).

RT-PCR. Embryos were injected at the 32-cell stage, and their development was stopped at stages noted in the text and figure legends. RNA was purified from these staged samples. To ensure that this analysis detected only the injected mRNA and not injected plasmid DNA, all samples were treated with DNaseI prior to RT–PCR. RT–PCR was performed according to Carroll and Vize (1996). cDNA was synthesized using two primers: oligo(dT) and a primer homologous to the extreme 3′ end of the *Xenopus* β-globin 3′ untranslated region (5′ GGAGCAGATACGAAT 3′). The second primer was included in case the short poly(A) tail contained within the transcribed region was insufficient for priming by oligo(dT) (Krieg and Melton, 1984). Two primer sets were used for PCR amplification of this cDNA. The first amplified the injected xWT1 mRNA specifically by using a 5′ primer (5′ CACACSCACGGGGTCT 3′) homologous to *xWT1* and a 3′ primer homologous to the *Xenopus* β-globin 3′ untranslated region (5′ GACTCCATTCGGGTG 3′). The second set amplified endogenous EF-1α mRNA as a control for RNA recovery and RT–PCR efficacy (5′ CAGATTGGTGCTGGATATGC 3′ and 5′ ACTGCCTTGATGACTCCTAG 3′). Negative control reactions omitting reverse transcriptase were performed on the first and last samples in the series; positive controls were performed using 1 ng of pSP64TSxWT1-KTS plasmid DNA. Twenty-five cycles of amplification of injected xWT1-β-globin fusion mRNA and 19 cycles of amplification of endogenous EF-1α mRNA were performed using 0.5 embryo equivalents of cDNA.

Immunohistochemistry. Embryos were fixed in MEMFA for 30 min and then washed in 1× PBS. β-Galactosidase activity was detected according to Vize *et al.* (1991), and embryos were then washed in PBS, refixed for 30 min in MEMFA, washed in TBST, dehydrated overnight in methanol at 4°C, rehydrated in TBST, and blocked with 20% horse serum, 0.1 mg/ml BSA, and TBST. Embryos were incubated in primary antibody overnight at 4°C and then washed 6 × 1 h in TBST, blocked again, incubated in alkaline phosphatase-conjugated secondary antibody overnight, washed 6 × 1 h in TBST, and stained for alkaline phosphatase using NBT/BCIP (Boehringer-Mannheim) or Histomark Red (Kirkegard and Perry) (see Vize *et al.*, 1995). Antibody 3G8 was used to detect pronephric tubules (Vize *et al.*, 1995); antibody 12/101 was used to detect somite (Kintner and Brockes, 1984).

In situ hybridization. Embryos were fixed, stained for β-galactosidase, and refixed as described above. *In situ* hybridization was then carried out according to the procedure of Harland (1991).

Copyright © 1998 by Academic Press. All rights of reproduction in any form reserved.

Confocal microscopy. Embryos were fixed in MEMFA for 1 h and washed in TBST, dehydrated overnight in methanol at 4°C, and rehydrated in TBST. Antibody 3G8 and a rhodamine-coupled secondary were applied as described above except that after washing out excess secondary antibody, embryos were dehydrated in an ethanol series and cleared for confocal viewing in 2:1 benzyl benzoate:benzyl alcohol. Embryos were viewed using a rhodamine GHS filter set, and images were collected using a Bio-Rad MRC-500 confocal scanning laser microscope. For nuclear staining, embryos were rehydrated in TBST and incubated in 5 μg/ml propidium iodide for 1 h, washed in TBST, and prepared for confocal viewing as above.

RESULTS

The Pronephric Index (PNI)

In order to facilitate studies of early kidney development, a simple index (defined in the legend to Fig. 1) was designed to quantify the extent of pronephric tubule development. The pronephros is a dynamic structure in the developing tadpole, so slight differences between the two pronephroi within an embryo are not uncommon; however, significant differences are very rare (Vize *et al.*, 1995; Fox, 1963). After observing hundreds of uninjected control embryos, a PNI of greater than 2 (for calculation, see Fig. 1) was determined to indicate a disparity in pronephric development not attributable to normal variation. Indeed, less than 1% of uninjected embryos display such differences between the two pronephroi (Table 1). Therefore, experimental perturbations can be made on one side of the embryo and the opposite side can act as an internal control for the degree of pronephric development in each embryo examined.

Injection of mRNA into *Xenopus* embryos has been demonstrated to be a very effective method for analyzing gene function (Vize *et al.*, 1991). β-Galactosidase mRNA was injected at a range of concentrations to control for the possibility that any observed pronephric phenotype following mRNA injection may be the result of injection trauma or nonspecific mRNA toxicity. Injections were made into the C3 and D3 blastomeres on one side of 32-cell stage embryos, as these blastomeres are fated to contribute to the pronephros (Dale and Slack, 1987). Detection of β-galactosidase activity indicated that injections into these blastomeres targeted the mRNA to the pronephric region of the tadpole (Fig. 1B). Analysis of pronephric tubule development with the pronephric tubule-specific antibody 3G8 (Vize *et al.*, 1995) demonstrated that injection of doses ranging from 0.25 to 2 ng of β-galactosidase mRNA consistently had no effect on pronephric development (Table 1, Fig. 1, and data not shown).

Overexpression of xWT1 Inhibits Pronephric Tubule Development

In order to examine the activity of the *xWT1* gene *in vivo*, mRNA encoding xWT1 (Carroll and Vize, 1996) was microinjected into *Xenopus* embryos which were then reared to tadpole stages and analyzed for pronephric development by immunohistochemistry with the pronephric tubule-specific antibody 3G8. Injections were made on one side at the 32-cell stage into the C3 and D3 blastomeres, which are fated to contribute to the pronephros (Fig. 1; Dale and Slack, 1987). All embryos were co-injected with *xWT1* mRNA as well as 0.25 ng of β-galactosidase mRNA as a lineage tracer in order to ensure that all analyzed embryos did express exogenous *xWT1* mRNA in the pronephros. Only embryos in which β-galactosidase activity was detected in the region of the pronephros were scored for pronephric phenotypes.

TABLE 1
Frequency of xWT1-Induced Inhibition of Pronephric Tubule Development

Injected RNA	% Embryos PNI > 2	N
None	0.7	2/270
β-Galactosidase	1.5	1/66
xWT1-KTS	34.0	36/106
xWT1+KTS	21.0	8/38

Note. Embryos were injected on one side at the 32-cell stage with the mRNA's as indicated, reared to tadpole stages, fixed, analyzed for β-galactosidase expression, and assayed for pronephric tubule development with antibody 3G8. Only embryos with β-galactosidase expression in the pronephric region were scored. Pronephric tubule development was quantified according to the pronephric index defined in the text and in the legend to Fig. 1. A portion of the embryos were injected independently in another lab and scored blind in our lab.

While pronephroi developed normally on the uninjected sides of experimental embryos in all cases (Figs. 2A and 2C), injection of xWT1 mRNA strongly suppressed pronephric tubule development on the injected side (Figs. 2B and 2D). In mild cases, tubules formed in injected pronephroi, but the tubule diameter and length were noticeably reduced (Fig. 2B). In many instances, the distal branches of the collecting tubules were absent (Figs. 2B and 2b'). In more severe cases, only a single, small, unbranched tubule was present on the injected side (Figs. 2D and 2d'). In extreme cases, there was no sign of tubule staining whatsoever on the injected side of the embryo (not shown). Ectopic expression of either splice form of xWT1 elicited identical phenotypes, although xWT1 + KTS (Carroll and Vize, 1996) did so at a slightly lower frequency (Table 1 and data not shown).

Several other mRNAs were injected into the presumptive pronephric region as controls to ensure that the small pronephroi were not due to a general mRNA toxicity problem. As mentioned above, injection of β-galactosidase mRNA had no effect on the development of the pronephros (Fig. 1, Table 1). Several genes involved in kidney development were also overexpressed by mRNA injection, including *Xlim-1* (Taira *et al.*, 1995), *xHGF* (Nakamura *et al.*, 1995), and *XPax-2* (Heller and Brandli, 1997); none of these injections inhibited pronephric development (data not shown).

Copyright © 1998 by Academic Press. All rights of reproduction in any form reserved.

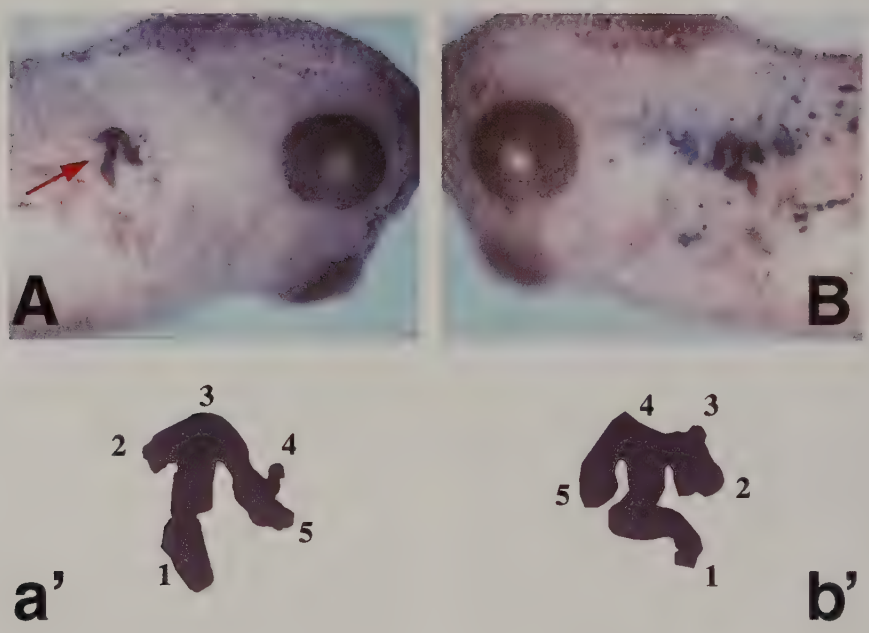

FIG. 1. The pronephric index. The index quantifies the extent of pronephric development by comparing the left and right pronephroi within an embryo (based upon the pattern of antibody 3G8 staining at stage 37/38). (A and B) Opposite sides of an embryo injected on one side with 1 ng of β-galactosidase mRNA and stained with antibody 3G8 to detect pronephric tubules (arrow in A indicates staining). Staining for β-galactosidase activity (light blue/green in B) indicates that injection into the C3 and D3 blastomeres has targeted mRNA to the pronephric region of the injected side (B). (a' and b'). Enlarged, diagrammatic representation of the pronephroi in A and B. For quantification of pronephric development, each pronephros in an embryo is scored by assigning one point for each of the numbered tubule components in the figure (a' and b'). A normal *Xenopus* pronephros has five components: one vertical tube, one horizontal tube, and three attached branches (see Vize *et al.*, 1995), so a score of 5 is assigned to a normal pronephros; 0 indicates no pronephros. The pronephric index (PNI) is then expressed as the difference between the two sides. PNI = 0 indicates two identical pronephroi; PNI = 5 indicates a normal pronephros on one side and no pronephros on the other. The embryo shown in A and B has a pronephric index of 0, indicating that injection of β-galactosidase mRNA has no effect on pronephric development.

It was possible that xWT1 was acting as a nonspecific inhibitor of differentiation. To address this issue, xWT1-KTS mRNA was injected into cells fated to contribute the somites (blastomere C2; Dale and Slack, 1987). Expression of *xWT1* resulted in no significant increase in somite defects over controls when assayed by immunohistochemistry with somite-specific antibodies (data not shown), indicating that xWT1 is not a general inhibitor of differentiation.

Confocal Microscopic Analysis of xWT1 Overexpression Phenotype

The pronephric anlage is first morphologically recognizable at around stage 23 as a distortion of the intermediate mesoderm as cells change shape, becoming more columnar. These condensed cells distend the overlying epidermis, forming the pronephric swelling. Cells within this condensation later epithelialize and form the pronephric tubules (Goodrich, 1930; Armstrong, 1932; Vize *et al.*, 1995, 1997). The reduced pronephroi of xWT1-injected embryos could arise from a smaller than normal pronephric anlage, or they could result from a failure of tubule morphogenesis within a normal anlage. Because antibody 3G8 stains only the lumenal surface of the pronephric tubules (Vize *et al.*, 1995), the phenotype observed in whole-mount could represent a simple failure to epithelialize and form a lumen within an otherwise normal pronephric anlage.

In order to explore the morphology of the phenotype resulting from *xWT1* overexpression, injected embryos were examined using confocal scanning laser microscopy. Optical sagittal (Figs. 3A and 3B) and transverse (Figs. 3C and 3D) sections revealed a normal tubular epithelium surrounding the pronephric tubule complex in these embryos. However, the volume of 3G8 stained tubules was significantly reduced on injected sides (Figs. 3B and 3D) compared to uninjected sides (Figs. 3A and 3C). The optical

Copyright © 1998 by Academic Press. All rights of reproduction in any form reserved.

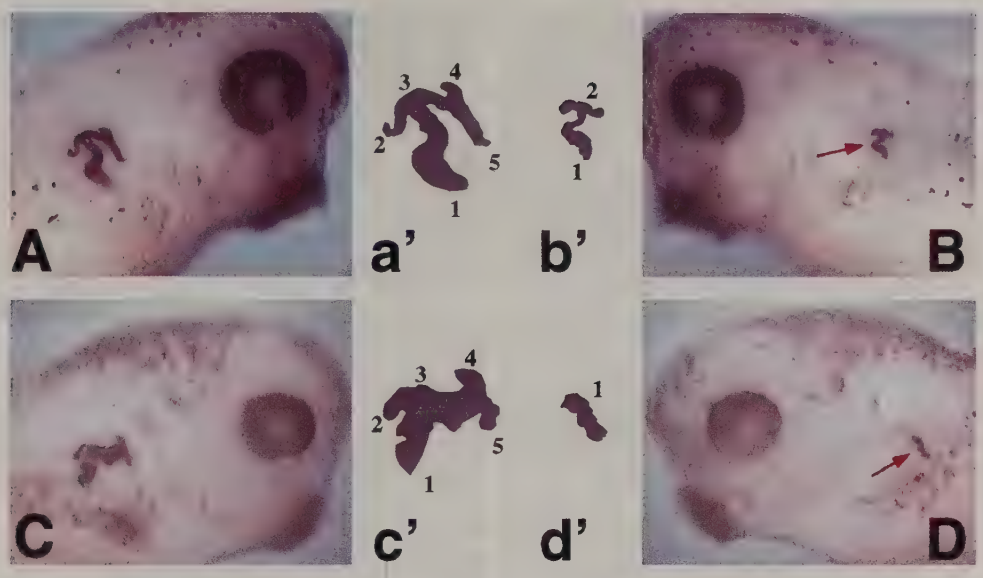

FIG. 2. Injection of xWT1-KTS mRNA inhibits the development of the pronephric tubules. Antibody 3G8 was used to detect the pronephric tubules (dark purple in all panels), and X-Gal was used to detect the β-galactosidase (light blue/green in B and D). (A and B) Opposite sides of an experimental embryo injected with 1 ng of xWT1-KTS mRNA (+0.25 ng of β-galactosidase mRNA). The uninjected side (A) is normal, while all distal branches of the collecting tubule are absent on the injected side (B). The diameter and length of the remaining common tubule and collecting tubule are also reduced on the injected side (B) compared to the uninjected side (A). The control, uninjected pronephros (diagrammed in a') is normal and is assigned 5 points; the pronephros on the injected side of the same embryo (diagrammed in b') is lacking all distal branches of the connecting tubule and is assigned only 2 points. The resulting PNI for this embryo is 3, indicating a significant inhibition of pronephric development (see Table 1). (C and D) Opposite sides of a different embryo injected with 1 ng of xWT1-KTS mRNA (+0.25 ng of β-galactosidase mRNA) displaying a more severe phenotype. The uninjected pronephros (C) is normal and is assigned 5 points (c'). However, the pronephros on the injected side (D) consists only of a single unbranched tubule and is assigned only 1 point (d'). The PNI for this embryo is 4, again indicating inhibition of pronephric development. While the morphology of the uninjected pronephros is normal (c'), note that it is somewhat swollen compared to normal, likely the result of hypertrophy in order to compensate for loss of pronephric function on the injected side (Fox, 1956; Howland, 1921). The reduction in the amount of β-galactosidase staining in injected embryos (B and D) compared to the embryo shown in Fig. 1 is consistent with the amount of β-galactosidase mRNA injected: 0.25 ng co-injected with xWT1 in this figure compared to 1 ng when β-galactosidase was injected alone in Fig. 1.

transverse sections also revealed considerably reduced pronephric swellings on injected sides, as judged by a less obvious bulge in overlying epidermis and reduced compression of the underlying splanchnic lateral plate and endodermal mass, compared to uninjected sides of the same embryos (Figs. 3C and 3D).

In order to better characterize the pronephric tubule epithelia of experimental embryos, injected embryos were stained with propidium iodide and confocal microscopy was used to visualize nuclei. This analysis revealed fewer cells within xWT1 mRNA-injected pronephroi compared to uninjected controls (Figs. 3E and 3F). This observation suggests that the reduction in size of the pronephric tubules results from a failure to specify an anlage of appropriate size, rather than a failure of epithelialization within a properly developed anlage.

Overexpression of xWT1 Disrupts Very Early Stages of Pronephric Specification

Endogenous *xWT1* expression commences around stage 20, shortly before the pronephric tubule anlage segregates from the intermediate mesoderm (Carroll and Vize, 1996; Nieuwkoop and Faber, 1994). To determine if the injected *xWT1* message was present during the developmental period when the pronephros is patterned and begins to differentiate, the stability of injected *xWT1* mRNA was examined. RNA was injected into blastomeres C3 and D3 of 32-cell stage embryos as described above. Subsequent RT–PCR using primers specific for the injected message revealed that the *xWT1* mRNA was present in injected embryos until at least stage 30 (Fig. 4), indicating that the injected *xWT1* message is stable throughout pronephric patterning and differentiation (Vize *et al.*, 1995; Nieuwkoop

Copyright © 1998 by Academic Press. All rights of reproduction in any form reserved.

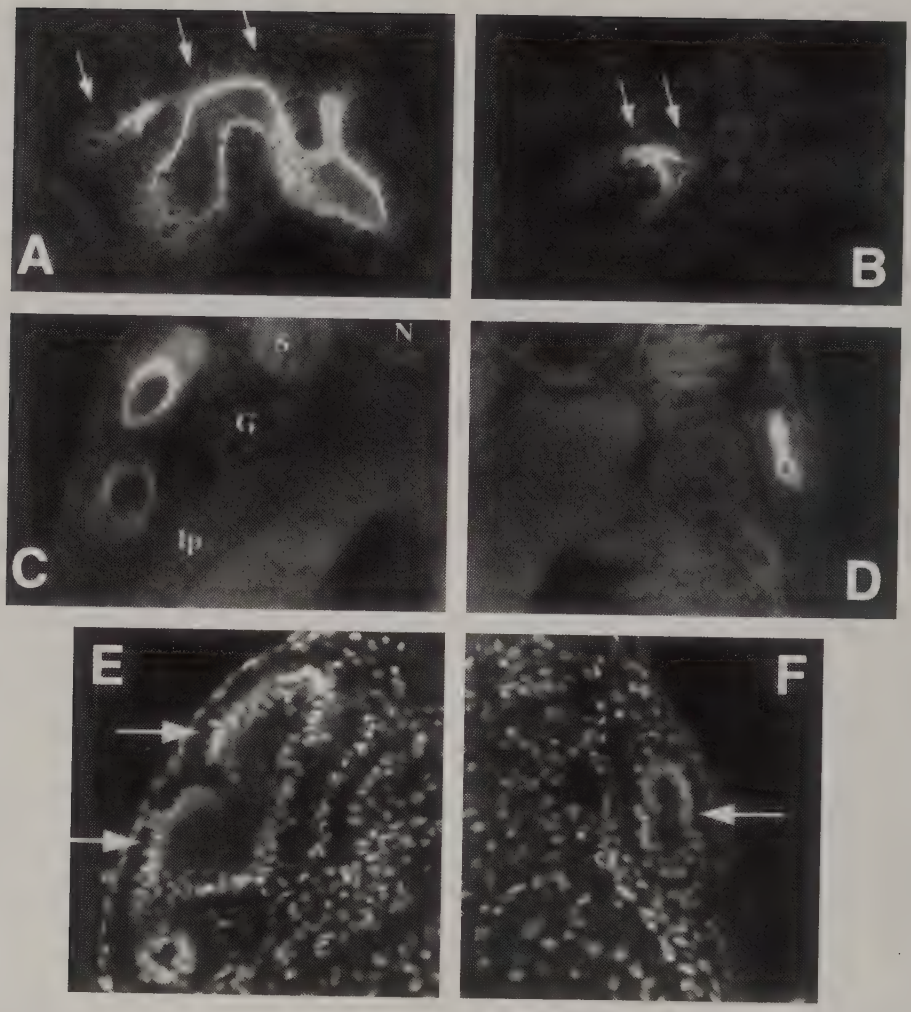

FIG. 3. Confocal microscopic analysis of the xWT1 overexpression phenotype. (A and B) High-magnification confocal optical sagittal sections through the pronephroi of an embryo injected on one side with xWT1-KTS mRNA. The embryo is stained with 3G8 using a rhodamine-conjugated secondary antibody, and the cell boundaries of tubular epithelial cells (indicated by arrows) are visible due to autofluorescence of yolk platelets (see Wallingford *et al.*, 1997). A single layer of pronephric epithelial cells surrounds the pronephric lumen on both uninjected (A) and injected (B) sides of the embryos. However, the pronephric tubule epithelial complex on the injected side (B) is significantly smaller than that on the uninjected side (A). (C and D) Confocal optical transverse sections of an embryo injected with xWT1-KTS mRNA. The pronephros on the injected side (D) is significantly reduced compared to that on the uninjected side (C). The ventral portion of the somite (S), the notochord (N), and the lateral plate (lp) are normal on both sides. The glomus (G) appears to be highly disorganized on the injected side of the embryo (D), consistent with the hypothesis that signals from the tubules are required for the formation of the glomus (Fales, 1935). (E and F) Confocal optical transverse sections of an embryo injected on one side with xWT1-KTS mRNA and stained with propidium iodide to visualize nuclei. The pronephric tubule epithelium on the uninjected side (E, arrows) is normal, while the tubule epithelium on the injected side (F, arrow) is significantly smaller and contains fewer cells.

and Faber, 1994). As such, it was possible that exogenous xWT1 inhibited pronephric tubule development at very early stages. It was also possible that exogenous xWT1 was acting much later, at a time when endogenous *xWT1* is also expressed. In order to address this issue, we examined xWT1-injected embryos for expression of a very early molecular marker for the developing pronephros, *Xlim-1* (Taira *et al.*, 1994).

Embryos were injected at the 32-cell stage with either xWT1-KTS mRNA (plus β-galactosidase) or with β-galact-

Copyright © 1998 by Academic Press. All rights of reproduction in any form reserved.

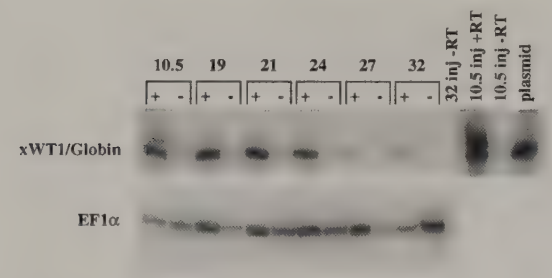

FIG. 4. Injected xWT1 message persists throughout pronephric development. RT–PCR using primers which specifically amplify the injected message indicates that the injected xWT1 mRNA remains stable until at least stage 30, by which time the pronephros is well differentiated. EF1α was also amplified as a loading control. Numbers at the top of the figure indicate developmental stages; +, injected embryos; −, uninjected embryos; −RT, no reverse transcriptase; plasmid, PCR performed on 1 ng of xWT1 plasmid as a positive control. The small amount of signal in the stage 10.5 uninjected sample is probably due to spillage during gel loading.

osidase mRNA alone. Injected embryos were then reared to tailbud stages (stage 20), and *in situ* hybridization was used to examine expression of *Xlim-1*. Injection of 1.25 ng of β-galactosidase had no effect on the expression pattern of *Xlim-1* (Figs. 5A and 5B). On the other hand, injection of 1 ng of xWT1 mRNA resulted in dramatic reduction in *Xlim-1* expression on the injected sides of experimental embryos (Figs. 5C and 5D). This result suggests that precocious expression of xWT1 inhibits the early stages of pronephric patterning, acting well before the onset of endogenous xWT1 expression.

DISCUSSION

The manipulability of the *Xenopus* embryo and the simplicity of its pronephroi make this system very appealing for the study of early events in kidney development (Vize *et al.*, 1997). The first experiments described here define the consistency with which *Xenopus* pronephroi develop and a simple index has been generated by which the extent of pronephric development following experimental manipulation can be quantified. This system has then been used to examine the activity of xWT1 in pronephric development. The results presented indicate a role for *WT1* genes in the downregulation of tubule-specific gene expression and highlight interesting similarities and differences between pronephric and metanephric development.

Mode of Action of Ectopic xWT1

When *xWT1* was ectopically expressed in the pronephric tubule primordia, it acted at a very early stage to inhibit tubule specification (Figs. 2 and 5). WT1 is a powerful transcriptional repressor (Madden *et al.*, 1991), and as WT1 inhibits the expression of *Pax-2* (Ryan *et al.*, 1995), *Pax-2* inhibition could in theory be responsible for the *xWT1* overexpression phenotype. However, this cannot be the case, as pronephric expression of *Xenopus Pax-2* does not commence until stage 21 (Heller and Brandli *et al.*, 1997), and *xWT1*-injected embryos display marked defects in pronephric development prior to stage 20 (Fig. 5).

It is nonetheless quite likely that ectopic xWT1 acts as a transcriptional repressor of target genes other than *Pax-2*, and the repression of genes required for tubule development results in the formation of a smaller pronephric anlage and in turn a smaller pronephric tubule complex. The finding that both xWT1 + KTS and xWT1 − KTS inhibit tubule development (Table 1) is consistent with this hypothesis, as both splice forms can act as transcriptional repressors *in vitro* (Ryan *et al.*, 1995; Wang *et al.*, 1995). On the other hand, WT1 has also been shown to bind mRNA and may downregulate gene expression posttranscriptionally (Kennedy *et al.*, 1996; Caricasole *et al.*, 1996; Larsson *et al.*, 1995), so it is also possible that this activity, rather than direct transcriptional regulation, is responsible for the observed phenotype.

A Role for WT1 in the Inhibition of Tubule-Specific Gene Expression

Ectopic expression of *xWT1* in the tubule primordia restricted the formation of the pronephric tubule anlage, resulting in a smaller anlage, and thus a reduction in tubule size and complexity compared to control pronephroi. This result introduces the intriguing possibility that the role of endogenous WT1 may be to inhibit expression of genes involved in the response to kidney inducing signals. Consistent with this hypothesis is the finding that murine WT1 binds to and represses the *Pax-2* promoter, and the onset of *WT1* expression in the metanephros correlates well with the downregulation of *Pax-2* expression (Ryan *et al.*, 1995). Such downregulation is essential to proper metanephric tubule development as continued expression of *Pax-2* results in severe defects in metanephric tubule development (Dressler *et al.*, 1993).

A Role for WT1 in the Development of the Vascular Component of the Kidney

In mammals, *WT1* is expressed in the condensed metanephric mesenchyme during the early stages of kidney development, and this expression is required for metanephric tubule differentiation (Kreidberg *et al.*, 1993). At later stages, mammalian *WT1* expression is restricted solely to the developing glomeruli (Mundlos *et al.*, 1993; Armstrong *et al.*, 1992), suggesting an additional role for this gene in the development of the vascular component of the nephron. Consistent with this hypothesis, many humans with mutations in *WT1* exhibit defective vascu-

Copyright © 1998 by Academic Press. All rights of reproduction in any form reserved.

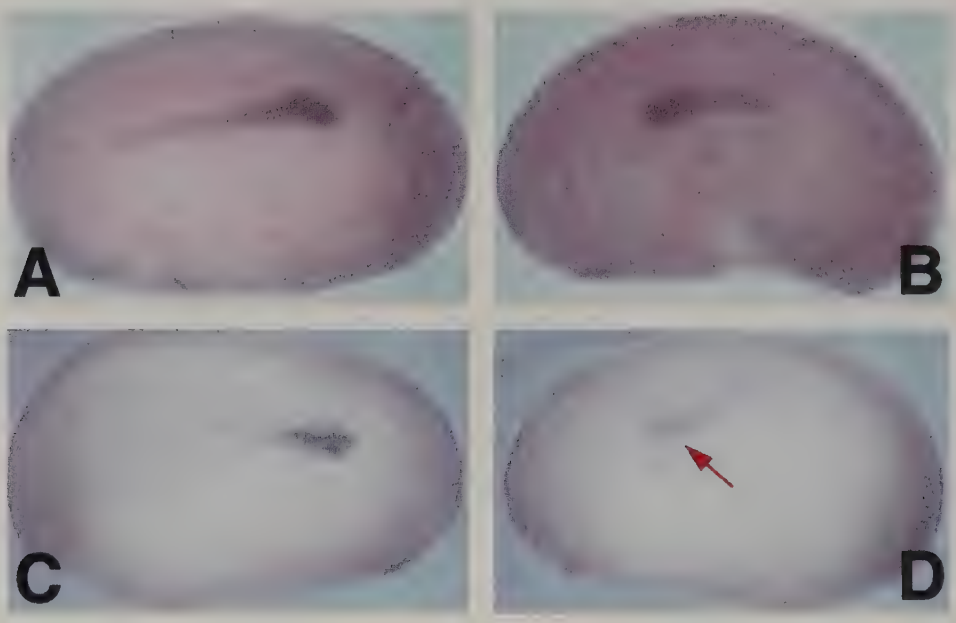

FIG. 5. xWT1 expression disrupts early events in pronephric specification. Expression of *Xlim-1*, an early molecular marker for the pronephros, was detected at stage 20 by *in situ* hybridization (dark purple in all panels) and β-galactosidase was detected with X-Gal (light blue/green in B and D). (A and B) Opposite sides of an embryo injected on one side with of β-galactosidase mRNA. *Xlim-1* expression is strong on both the uninjected (A) and injected (B) sides. (C and D) Opposite sides of an embryo injected on one side with xWT1-KTS (+β-galactosidase mRNA). *Xlim-1* expression is normal on the uninjected side (C), while expression is dramatically reduced on the injected side (D). The result indicates that ectopic xWT1 mRNA expression inhibits pronephric development at a very early stage.

lar development in the glomeruli (Pelletier *et al.*, 1991; Denys *et al.*, 1967; Drash *et al.*, 1970). Interestingly, the expression of *xWT1* is restricted to the vascular component of the kidney throughout pronephric development; it is never expressed at detectable levels in the pronephric tubules (Carroll and Vize, 1996).

In light of the *xWT1* expression pattern, the finding that *xWT1* expression inhibits pronephric tubule development suggests that the normal role of xWT1 in the developing pronephros may be to restrict the fate of these cells, preventing *Pax*-2 expression and thus tubule specification, reserving them for the later formation of the glomus. The timing of xWT1 expression is consistent with this hypothesis. xWT1 transcription commences in the cells of the presumptive glomus concomitant with the onset of tubule differentiation in adjacent cells (about stage 20). However, the glomus will not differentiate until much later (about stage 27). xWT1 may be necessary to inhibit tubule differentiation in the pool of cells which are reserved for the later formation of the glomus over this time period. The fact that WT1 inhibits the expression of several genes involved in tubule development (discussed above) is also consistent with this hypothesis.

The Pronephros and the Metanephros: Similarities and Differences

The results presented here underscore both important differences and similarities between pronephric development and metanephric development. For example, the finding that endogenous *xWT1* is not expressed in pronephric tubules (Carroll and Vize, 1996) strongly argues that WT1 is dispensable for pronephric tubule differentiation; and consistent with this hypothesis, the more cranial (pronephros-like) mesonephric tubules of mice develop normally in the absence of functional WT1 (Sainio *et al.*, 1997). However, WT1 activity is clearly required for the development of the caudal mesonephric and metanephric tubules (Kreidberg *et al.*, 1993). These results may highlight an important difference in how pronephric and metanephric tubules develop. During metanephric development, mesenchymal cells of the nephrogenic cord proliferate to form the metanephric blastema, which then condenses and epithelializes to form tubules (Saxen, 1987), and WT1 is required for this process (Kreidberg *et al.*, 1993). During pronephric development, on the other hand, the pronephric anlage forms as cells in the intermediate mesoderm segregate by cell shape changes, and this anlage then epithelializes to

Copyright © 1998 by Academic Press. All rights of reproduction in any form reserved.

form tubules (Vize *et al.*, 1997), a process which does not appear to require WT1 expression.

On the other hand, the vascular components of both pronephroi and metanephroi apparently utilize very similar genetic pathways to restrict cell fate during development despite their vastly different architecture. Furthermore, although the requirements for WT1 are different in the development of different kidney forms, it appears that the activity of this protein as a negative regulator of tubule-specific gene expression is the same in all cases, downregulating expression of specific genes in the tubules in order to allow differentiation to proceed and downregulating expression of specific genes in the vascular components in order to restrict their fate.

ACKNOWLEDGMENTS

The authors thank Douglas Melton for encouragement and support throughout the course of this work and for performing the independent microinjection experiments. We thank Michael Danilchik for the use of the confocal microscope (supported by NSF IBN 9396063) and for invaluable technical advice. We thank Matthew Grow and Eric Small for critical reading of the manuscript. This research was supported by Texas ARP Grant 187 (P.V.), NSF IBN9630621 (P.V.), and NIH Training Grant T-32 HD07296-GT (T.C.).

REFERENCES

Armstrong, P. B. (1932). The embryonic origin of function in the pronephros through differentiation and parencyma–vascular association. *Am. J. Anat.* **51,** 157–188.

Armstrong, J. F., Pritchard-Jones, K., Bickmore, W. A., Hastie, N. D., and Bard, J. B. L. (1992). The expression of the Wilms' tumor gene WT1 in the developing mammalian embryo. *Mech. Dev.* **40,** 85–97.

Balinsky, B. I. (1970). "An Introduction to Embryology." Saunders, Philadelphia.

Burns, R. K. (1955). Urogenital system. In "Analysis of Development" B. H. Willier, P. A. Weiss, and V. Hamburger, Eds.). Saunders, Philadelphia.

Caricasole, A., Duarte, A., Larsson, A., Hastie, N., Little, M., Holmes, G., Todorov, I., and Ward, A. (1996). RNA binding by the Wilms' tumor suppressor zinc finger proteins. *Proc. Natl. Acad. Sci. USA* **93,** 7562–7566.

Carroll, T. J., and Vize, P. D. (1996). The Wilms' tumor suppressor gene is involved in the development of disparate kidney forms: Evidence from expression in the *Xenopus* pronephros. *Dev. Dyn.* **206,** 131–138.

Coppes, M. J., Campbell, C. E., and Williams, B. R. G. (1995). "Wilms' Tumor: Clinical and Molecular Characterization." Landes, Austin, TX.

Dale, L., and Slack, J. M. W. (1987). Fate map of the 32-cell stage of *Xenopus*. *Development* **99,** 527–551.

Denys, P., Malvaux, P., van den Berghe, H., Tanghe, W., and Proesmans, W. (1967). Association d'un syndrome anatomopathologique de pseudohermaphrodisme masculin, d'un tumeur de Wilms, d'une nephropathie parenchymateuse et d'une mosaicisme XX/XY. *Arch. Fr. Pediatr.* **24,** 729–739.

Drash, A., Sherman, F., Hartman, W. H., and Blizzard, R. M. (1970). A syndrome of pseudohermaphrodism, Wilms' tumor, hypertension, and degenerative renal disease. *J. Pediatr.* **76,** 585–593.

Dressler, G. R., Wilkinson, J. E., Rothenpieler, U. W., Patterson, L. T., William-Simons, L., and Westhal, H. (1993). Deregulation of Pax-2 expression in transgenic mice generates severe kidney abnormalities. *Nature* **362,** 65–67.

Drummond, I., Madden, S., Rohwer-Nutter, P., Bell, G. I., Sukhatme, V. P., and Rauscher, F. J. (1992). Repression of the insulin-like growth factor II gene by the Wilms' tumor suppressor WT1. *Science* **257,** 674–678.

Englert, C., Hou, X., Maheswaran, S., Bennett, P., Ngwu, C., Re, G., Garvin, A., Rosner, M., and Haber, D. (1995). WT1 suppresses synthesis of the epidermal growth factor receptor. *EMBO J.* **14,** 4462–4675.

Fales, D. E. (1935). Experiments on the development of the pronephros of *Ambystoma punctatum*. *J. Exp. Zool.* **72,** 147–173.

Field, H. H. (1891). The development of the pronephros and the segmental duct in Amphibia. *Bull. Mus. Comp. Zool. Harv.* **21,** 201–240.

Fox, H. (1963). The amphibian pronephros. *Quart. Rev. Biol.* **38,** 1–25.

Fox, H. (1956). Compensation in the remaining pronephros of *Triturus* after unilateral preonephrectomy. *J. Embryol. Exp. Morph.* **4,** 139–151.

Goodrich, E. S. (1930). "Studies on the Structure and Development of Vertebrates." Macmillan, London. [Reprinted by the University of Chicago Press, Chicago, 1986]

Harland, R. (1991). *In situ* hybridization: An improved method for *Xenopus* embryos. In "Methods in Cell Biology" (B. K. Kay and H. B. Peng, Eds.), Vol. 36, pp. 685–695. Academic Press, San Diego.

Heller, N., and Brandli, A. W. (1997). *Xenopus Pax*-2 displays multiple splice forms during embryogenesis and pronephric kidney development. *Mech. Dev.* **69,** 83–104.

Howland, R. B. (1921). Experiments of the effects of removal of the pronephros of amphibian embryos. *J. Exp. Zool.* **32,** 355–395.

Kennedy, D., Ramsdale, T., Mattick, J., and Little, M. (1996). An RNA recognition motif in Wilms' tumour protein (WT1) revealed by structural modelling. *Nat. Genet.* **12,** 329–331.

Kintner, C., and Brockes, J. P. (1984). Monoclonal antibodies identify blastemal cells derived from differentiating muscle in newt limb regeneration. *Nature* **308,** 67–69.

Kreidberg, J. A., Sariola, H., Loring, J. M., Maeda, M., Pelletier, J., and Jaenisch, R. (1993). WT-1 is required for early kidney development. *Cell* **74,** 679–691.

Krieg, P. A., and Melton, D. A. (1984). Functional messenger RNAs are produced by SP6 *in vitro* transcription of cloned cDNAs. *Nucleic Acids Res.* **12,** 7057–7070.

Larsson, S. H., Charlieu, J. P., Miyagawa, K., Engelkamp, D., Rassoulzadegan, M., Ross, A., Cuzin, F., van Heyningen, V., and Hastie, N. D. (1995). Subnuclear localization of WT1 in splicing or transcription factor domains is regulated by alternative splicing. *Cell* **81,** 391–401.

Madden, S., Cook, D. M., Morris, J., Gashler, A., Sukhatme, V. P., and Rauscher, F. J. (1991). Transcription repression mediated by the WT1 Wilms tumor gene product. *Science* **253,** 1550–1553.

Müller, J. (1829). Uber die Wolffschen körper bei den embryonen der frösche und kröten. *Arch. Anat. Phys. Jhrg.*, 65–70. [Translation in Adelman, H. B. (1966), "Marcello Malpighi and the Evolution of Embryology." Cornell Univ. Press, Ithaca, NY]

Copyright © 1998 by Academic Press. All rights of reproduction in any form reserved.

Mundlos, S., Pelletiaer, J., Darveau, A., Bachmann, M., Winterspacht, A., and Zabel, B. (1993). Nuclear localization of the protein encoded by the Wilms' tumor gene WT1 in embryonic and adult tissues. *Development* **119,** 1329–1341.

Nakamura, H., Tashiro, K., Nakamura, T., and Shiokawa, K. (1995). Molecular cloning of *Xenopus* HGF cDNA and its expression studies in *Xenopus* early embryogenesis. *Mech. Devel.* **49,** 123–131.

Nieuwkoop, P. D., and Faber, J. (1994). "Normal Table of *Xenopus laevis* (Daudin)," 3rd ed. Garland, New York.

Pelletier, J., Schalling, M., Buckler, A. J., Rogers, A., Haber, D. A., and Housman, D. (1991a). Expression of the Wilms' tumor gene WT1 in the murine urogenital system. *Genet. Dev.* **5,** 1345–1356.

Pelletier, J., Bruening, W., Kashtan, C., Mauer, S., Manivel, J., Striegel, J., Houghton, D., Junien, C., Habib, R., Fouser, L., Fine, R., Silvermn, B., Haber, D., and Housman, D. (1991b). Germiline mutations in teh Wilms' tumor suppressor gene are associated with abnormal urogenital development in Denys–Drash syndrome. *Cell* **67,** 437–447.

Peng, H. B. (1991). Solutions and protocols. In "Methods in Cell Biology" (B. K. Kay and H. B. Peng, Eds.), Vol. 36, pp. 657–662. Academic Press, San Diego.

Ryan, G., Steele-Perkins, V., Morris, J., Rauscher, F., and Dressler, G. R. (1995). Repression of *Pax*-2 by WT1 during normal kidney development. *Development* **121,** 867–875.

Sanio, K., Hellstedt, P., Kreidberg, J. A., Saxen, L., and Sariola, H. (1997). Differential regulation of two sets of mesonephric tubules by WT1. *Development* **124,** 1293–1299.

Saxén, L. (1987). "Organogenesis of the Kidney." Cambridge Univ. Press, Cambridge.

Taira, M., Otani, H., Jamrich, M., and Dawid, I. (1994). Expression of the Lim class homeobox gene *Xlim-1* in the pronephros and CNS cell linages of *Xenopus* embryos is affected by retinoic acidand exogastrulation. *Development* **120,** 1525–1536.

Vize, P., Melton, D., Hemmati-Brivanlou, A., and Harland, R. (1991). Assays for gene function in developing *Xenopus* embryos. *Methods Cell Biol.* **36,** 367–387.

Vize, P., Jones, E., and Pfister, R. (1995). Development of the *Xenopus* pronephros. *Dev. Biol.* **171,** 531–540.

Vize, P., Seufert, D. W., Carroll, T. J., and Wallingford, J. B. (1997). Model systems for the study of kidney development: Use of the pronephros in the analysis of organ induction and patterning. *Dev. Biol.* **188,** 189–204.

Wallingford, J., Sater, A., Uzman, J. A., and Danilchik, M. (1997). Inhibition of morphogenetic movement during *Xenopus* gastrulation by injected sulfatase: Implications for anteroposterior and dorsoventral axis formation. *Dev. Biol.* **187,** 224–235.

Wang, Z-Y., Qiu, Q-Q., Huang, J., Gurrieri, M., and Deuel, T. (1995). Products of alternatively spliced transcripts of the Wilms' tumor suppressor gene WT1 have altered DNA binding specificity and regulate transcription in different ways. *Oncogene* **10,** 415–122.

Received for publication May 15, 1998
Accepted June 17, 1998

Copyright © 1998 by Academic Press. All rights of reproduction in any form reserved.

DEVELOPMENTAL BIOLOGY 202, 113–124 (1998)
ARTICLE NO. DB988982

Voltage-Dependent Activation of Frog Eggs by a Sperm Surface Disintegrin Peptide

Fraser M. Shilling,[1] Craig R. Magie,[2] and Richard Nuccitelli[3]
Section of Molecular and Cellular Biology, University of California at Davis, Davis, California 95616

Fertilin, a sperm protein of the metalloprotease/disintegrin/cysteine-rich (MDC) family, plays a critical role in sperm–egg binding in mammals. Peptides corresponding to the disintegrin domain of fertilin and antibodies against fertilin have been shown to inhibit mammalian sperm–egg binding and fusion. A protein from the same family, xMDC16, was recently cloned from frog (*Xenopus laevis*) testis and was found to be involved in frog sperm–egg binding. Here we report that xMDC16 is localized predominantly on the posterior surface of egg jelly-activated sperm, and peptides from the disintegrin domain of this protein activate eggs when applied near the egg surface. Egg activation was dependent on (1) specific amino acid residues (KTX); (2) the presence of divalent cations, but not external Ca^{2+} alone; and (3) voltage across the egg plasma membrane. This is the first demonstration of egg activation in vertebrates by the surface application of a peptide derived from a sperm surface protein, supporting a model for egg activation that involves a signal transducing receptor for sperm in the egg's plasma membrane. © 1998 Academic Press

Key Words: **fertilization; disintegrin; integrin; frog; egg activation.**

INTRODUCTION

Our current understanding of fertilization in vertebrates is based largely on data from amphibians and mammals. In both of these classes, the hydrolysis of a minor plasma membrane lipid, phosphatidylinositol-4,5-bisphosphate (PIP_2), is required for sperm-induced egg activation, but the mechanism used by the sperm to trigger this hydrolysis is unknown (Miyazaki *et al.*, 1992; Nuccitelli *et al.*, 1993). The two most popular hypotheses currently being tested are the diffusible sperm factor hypothesis and the sperm receptor hypothesis. The former proposes that a sperm factor diffuses into the egg following sperm–egg fusion, and this factor initiates calcium oscillations in the egg (Parrington *et al.*, 1996), presumably in response to PIP_2 hydrolysis. The latter hypothesis proposes that the sperm binds to a receptor in the egg's plasma membrane and that binding leads to the stimulation of a signal transduction cascade that initiates PIP_2 hydrolysis (Jaffe, 1990; Foltz and Shilling, 1993). Here we provide support for this sperm receptor hypothesis by identifying a sperm surface disintegrin peptide that can activate frog eggs upon external application near the egg's surface. The term disintegrin refers to soluble peptides from snake venom and domains of metalloprotease/disintegrin/cysteine-rich (MDC) proteins that bind to integrins (Bigler *et al.*, 1997). MDC proteins play a role in binding sperm to eggs in several mammalian species (Wolfsberg and White, 1996). The β subunit of the surface protein, fertilin, from mammalian sperm has a disintegrin-like domain that may function in binding the sperm to the egg's plasma membrane (Primakoff *et al.*, 1987; Blobel *et al.*, 1992; Myles *et al.*, 1994; Wolfsberg *et al.*, 1995). Peptides corresponding to the disintegrin domain of fertilin and antibodies against fertilin inhibited sperm binding and fusion to the egg. More recently, a fertilin fusion protein has been shown to bind specifically to a β_1-containing integrin in the mouse egg's plasma membrane (Evans *et al.*, 1997).

The frog sperm surface protein studied here was discovered by probing frog testis cDNA for conserved sequences from the disintegrin domain of known MDC genes, such as the mammalian sperm fertilin (Weskamp and Blobel, 1994). Five MDC genes were identified in this way and have been cloned from frog testis (Shilling *et al.*, 1997). Peptides derived from the disintegrin domains of three of these MDCs were found to inhibit fertilization. The mRNA of one of these genes, xMDC16, was found only in the testis, suggesting a potential role for it in fertilization. A peptide (CRMPKTEC) derived from xMDC16 and corresponding to the putative integrin-binding sequence in other MDCs (Blobel *et al.*, 1992; Wolfs-

[1] Present address: Center for Water and Wildland Resources, University of California, Davis, CA 95616.
[2] Present address: Department of Zoology, University of Washington, Seattle, WA 98195.
[3] To whom correspondence should be addressed.

0012-1606/98 $25.00
Copyright © 1998 by Academic Press
All rights of reproduction in any form reserved.

berg *et al.*, 1995) was used in the present study to investigate the role of this protein in egg activation.

The involvement of a receptor–ligand type of interaction in sperm-induced egg activation has been proposed previously (Jaffe, 1990; Foltz and Shilling, 1993). Evidence for this model in animal eggs includes egg activation in the marine worm, *Urechis caupo*, by a sperm acrosomal protein and a peptide derived from it (Gould *et al.*, 1987) and the ability of heterologously expressed neurotransmitter and growth factor receptors to activate eggs [starfish (Shilling *et al.*, 1994); frog (Kline *et al.*, 1988; Yim *et al.*, 1994), and mouse (Moore *et al.*, 1993)]. In addition, Iwao and Fujimura (1996) have recently found that a commonly used integrin-binding consensus sequence, RGDS, is capable of activating *Xenopus* eggs in a voltage-independent manner.

In the present study, we tested the possible role of xMDC16 in such a receptor–ligand system in frog egg activation. We used antibodies to a fusion protein containing xMDC16 domains to demonstrate its localization on live, egg jelly-activated sperm. In addition, a peptide (CRMPKTEC) derived from xMDC16, corresponding to the putative integrin-binding sequence in other MDCs, induced egg activation in a manner similar to that caused by sperm. These results strongly suggest a role for this sperm surface protein in signal transduction events at fertilization.

MATERIAL AND METHODS

Frog egg preparation and activation. Adult wild-type and albino, female adults of *Xenopus laevis* were injected with human chorionic gonadotropin (300 to 400 U) 12 h prior to obtaining eggs. Eggs were dejellied by gentle swirling for <1 min in 0.3% β-mercaptoethanol in 1/3 modified Ringers (MR), pH 8.8, followed by washing with MR, pH 6.5, and MR and F1, pH 7.8 [F1 composition (mM): NaCl, 41.25; KCl, 1.75; Na_2HPO_4, 0.5; NaOH, 1.9; Hepes, 2.5; $CaCl_2$, 0.25; $MgCl_2$, 0.063; and MR composition (mM): NaCl, 100; KCl, 1.8; $MgCl_2$, 1.0; $CaCl_2$, 2.0; Hepes, 5.0]. Eggs for all experiments were used within an hour of release from the female. Egg activation was scored as (1) vitelline envelope elevation and (2) contraction of the animal (pigmented) half of the egg. Dejellied eggs were fertilized with egg jelly water-treated sperm in agarose-coated dishes. The egg jelly water was isolated by gently washing eggs in 1/3 MR and separating loosened jelly coats by passing the eggs over a nylon mesh. A final concentration of 10% Ficoll was added and the mixture frozen. Vitelline coats were removed from eggs by using fine forceps to grasp the coat and manually strip it from the egg. This was done in agarose-coated dishes, and the eggs were allowed to sit for ~10 min before use to ensure that the removal of the vitelline coat did not cause activation.

Immunofluorescent labeling of live sperm. An antiserum was developed in rabbits against a fusion protein of the cysteine-rich region and the disintegrin domain (aa 320 to aa 642) of xMDC16 and glutathione *S*-transferase (pGEX, Pharmacia). This rabbit antiserum was a kind gift from Dr. Carl Blobel (Memorial Sloan-Kettering Cancer Center, NY). Sperm were obtained by squeezing a testis gently in F1 and were incubated in egg jelly water for 10 min to make them fertilization-competent. These sperm have a 2-μm-long acrosomal granule at their anterior tip (Bernardini *et al.*, 1986), but thus far no one has developed a technique that allows detection of the acrosome reaction. Twenty-microliter drops of sperm were put onto glass coverslips coated with polylysine (Sigma Co., St. Louis, MO) and the sperm allowed to settle and stick to the glass. The F1 was replaced with F1/0.1% bovine serum albumin (BSA) in three successive washes and incubated at either room temperature or on ice for at least 30 min. Antiserum at 1:250 dilution in F1/BSA was applied to the sperm and incubated for at least 1 h. The sperm were washed six times with F1/BSA in two successive series of three washes, over a 1-h period. Secondary antibodies (goat anti-rabbit from Sigma Co.) conjugated to FITC were applied at a 1:100 dilution and incubated for 1 h. The sperm were washed six times again and used for confocal fluorescence microscopy (LSM 410, Zeiss Instruments Co., 63×, 1.25 N.A.). Individual images were collected of between 1 and 10 sperm for each of the different treatments, with the pinhole at the maximum opening.

The distribution of label on sperm was determined for each image area by counting the number obviously fluorescent on a confocal microscope and noting where on the sperm head labeling occurred, with the same gain and black level settings for all treatments (e.g., preimmune vs immune serum). Intensity of labeling was also determined for each sperm in images collected at the emission wavelength for FITC (520 nm). The labeled region of the sperm, or the area usually found to be fluorescent if no labeling was observed, was selected for post hoc intensity measurements. Background intensity was measured adjacent to each sperm and subtracted from the total intensity. The region of the sperm of interest was encircled using a freehand mode provided by the Zeiss imaging software, and the light intensity in that area was measured. Comparisons were made among different batches of sperm (five males) by comparing the labeling to that of the immune serum-treated sperm within each batch and expressing the intensity relative to that for immune serum-labeled sperm. Western blots of sperm membrane preparations using the rabbit antibody were also conducted.

Western blotting of sperm membrane proteins. Sperm were obtained by gently squeezing a testis to obtain as pure a sperm sample as possible. They were boiled for 10 min in sample buffer containing 0.1 M dithiothreitol and separated by SDS–PAGE. Proteins were transferred to nitrocellulose and blotted with the rabbit sera (1/250 dilution). Horse radish peroxidase-conjugated secondary antibody and enhanced chemiluminescence were used for detection. The blots were blocked and washed in Tris-buffered saline (0.5% Tween 20) containing nonfat milk (2%). In some experiments (Fig. 3B), the immune serum was incubated with the xMDC16 fusion protein (1 mg/ml) for 2–12 h prior to applying to the nitrocellulose.

Calcium imaging and peptide treatment. Injection, calcium imaging, and image processing procedures were identical to those described by Nuccitelli *et al.* (1993). The software used was "ml12" written by Roger Tsien. For the fluorescence ratio-imaging studies, dejellied eggs were injected with fura-2–dextran (50 to 100 μM final concentration) in Ca^{2+}-free OR-2 containing 5 mM chlorobutanol (Ca^{2+}-free OR-2 is NaCl, 82 mM; KCl, 2 mM; $MgCl_2$, 20 mM; Hepes, 5 mM; EGTA, 0.1 mM), washed in F1, and incubated for 20 min to allow dispersal of the dye. The egg was placed into a chamber with a glass coverslip as a base, containing 400 μl of F1, and held in position with a gold wire glued to the bottom of the chamber. Changes in intracellular free calcium within the egg were measured as described previously (Nuccitelli *et al.*, 1993) using fluorescence ratio imaging (alternating excitation at 350 and 385 nm), by monitoring with an intensified CCD video camera. Recording was conducted prior to and during exposure to the peptide or sperm. The peptide, dissolved in F1 or Ca^{2+}-free F1, was added, using a pipetor, as a single aliquot (1 or 2 μl of 20 mM peptide) within a few millimeters of the egg. For experiments where Ca^{2+} was not present in the external medium, EGTA (2 or 5 mM, final concentration) was added to the peptide in solution prior to treatment of the egg.

Copyright © 1998 by Academic Press. All rights of reproduction in any form reserved.

Peptides were obtained from three different sources; Memorial Sloan-Kettering Cancer Center Peptide Synthesis Lab (New York, NY), Chiron (St. Louis, MO), and SynPep (Dublin, CA). Each peptide used was HPLC purified to 98.5–99.8% purity and the molecular weight was confirmed by mass spectroscopy.

For addition of small volumes of the peptide solution (<1 μl), a microsyringe mounted on a micromanipulator was used. A glass micropipet was ground down to give a 5- to 10-μm opening at the tip. The volume of peptide solution added was calibrated by ejecting the same size bolus into silicon oil (Fluorinert FC-70, Sigma) and measuring the diameter. The micropipet was brought within 100 μm of the egg surface and the peptide solution ejected slowly (100 to 180 s interval). Eggs with the vitelline coat intact and without the vitelline coat were both used for these experiments. The vitelline coat was manually removed using finely tipped watchmaker forceps.

Immobilizing the peptides. We attached peptides to beads using three different linkages to immobilize them for local application studies. Six-micrometer aliphatic amine latex beads (Interfacial Dynamics Corp., Portland, OR) were coupled to the cyclic 8-mer peptide, H_2N-CRMPKTEC-COOH, at the carboxy terminal of the peptide. Thirty-four-micrometer NHS-activated Sepharose beads bound to amino groups on the cyclic 8-mer peptide (Pharmacia Biotech, Washington, DC). In addition, a biotinylated 13-mer of xMDC-16 (H_2N-CRMPKTECDLAEY-6-aminohexonoic acid-Lys(biotin)-COOH) was bound to the streptavidin- or neutravidin-conjugated to three brands of beads (Paramagnetic beads, Polysciences Inc., Warrington, PA; BioMag beads Perseptive Diagnostics Inc., Cambridge, MA; and Ultralink Neutravidin beads, Pierce, Rockford, IL). The coupling of peptide was conducted following the manufacturer's specifications. Various peptides derived from xMDC-16 were also immobilized on cellulose using the carboxy terminus of the peptide to covalently bind to derivatized cellulose using the SPOTs peptide synthesis technique (Genosys Biotechnologies, The Woodlands, TX). The following peptide sequences were used: (1) native peptide, CRMPKTECDLAEY; (2) alanine substituted, CRMPAAACDLAEY; (3) scrambled version 1, CEADREPCYTMKL; and (4) scrambled version 2, CKPREMTCDLAEY. The two scrambled controls retain the cysteines at positions 1 and 8. These SPOTs were about 4 mm in diameter and contained 5–10 nmol of peptide per spot.

Electrophysiology. For voltage clamp studies, two microelectrodes (resistance = 3–20 MΩ, filled with 3 M KCl) were inserted into dejellied eggs (in F1) while monitoring voltage. The 3 MΩ electrode was used to pass current to clamp the egg's potential at the desired level using a two-electrode voltage clamp system (GeneClamp 500; Axon Instruments Inc., Foster City, CA). The current injected was recorded as an unfiltered signal with both a chart recorder and computer data acquisition program (PCLAMP6, Axon Instruments Inc.). The reference electrodes (Ag/AgCl) were embedded in agarose/0.15 M NaCl and immersed in the chamber containing the eggs. Eggs were placed in wells in the agarose that covered the bottom of the chamber. xMDC16 peptide (1 or 2 μl of 20 mM solution) or egg jelly-treated sperm was added near eggs using a micropipetor, and the eggs were observed periodically for morphological signs of activation.

RESULTS

Recognition of an Antigen on the Surface of Live Sperm by Antiserum to an xMDC16 Fusion Protein

An antiserum was developed in rabbits against a portion of xMDC16 containing the disintegrin and cysteine-rich regions as part of a fusion protein. Live sperm squeezed from whole testes (Fig. 1a) were treated with this immune serum (fig. 1 and Table 1). We failed to observe antibody labeling on fixed sperm and assume the fixation cross-linking destroys the antigenic site on the sperm. An antigen was recognized by the rabbit antiserum on the surface of live sperm more often (53/68 sperm, Fig. 1b) if the sperm were first treated with egg jelly–water than if they were not treated (15/47, Fig. 1c). Egg jelly–water treatment of frog sperm allows them to bind and fuse to jelly-free eggs, which is thought to be due to the

FIG. 1. Labeling of live *Xenopus laevis* sperm with a rabbit antibody generated against a fusion protein containing the disintegrin and cysteine-rich portions of xMDC16 (secondary antibody coupled to FITC). (a) A differential interference contrast image of a single sperm showing the head region (10 μm long); the posterior end of the head is indicated, as is the tail. (b) Live sperm were labeled with immune serum following activation by egg jelly–water. The label was found predominantly on the posterior region of the helical sperm head. (c) Sperm without egg jelly treatment, exposed to the xMDC16 antiserum, showed no labeling. (d) Sperm labeling was eliminated by previous incubation of the antiserum with a fusion protein containing the disintegrin and cysteine-rich domains of xMDC16. (e) Preincubation of the antiserum with MBP alone had no effect on antibody labeling of the sperm. Scale bar (10 μm) applies to all confocal fluorescent images.

Copyright © 1998 by Academic Press. All rights of reproduction in any form reserved.

TABLE 1
Summary of Live Sperm Surface Labeling by Antibody on Sperm Treated with Egg Jelly–Water

Source of antibody	No. labeling (%)	Labeling localization
Preimmune rabbit serum	12/78 (15%)	—
Immune rabbit serum	71/106 (67%)	Anterior head: 9/71 (13%) Posterior head: 52/71 (73%) Midsection: 10/71 (14%)
Secondary antibody alone	2/37 (5%)	—

activation of sperm by a factor in the jelly–water that may trigger an acrosome reaction (Reed and Stanley, 1972; Bernardini *et al.*, 1986). However, we have been unable to develop a method for detecting the acrosome reaction in frog sperm. Although preimmune serum labeled a small fraction of the sperm (12/78), this low proportion was similar to that observed with secondary antibody alone (2/37) (also see Fig. 2). Labeling of the sperm by rabbit immune serum occurred primarily on the posterior end of the head (73%, $n = 52$, five males), although labeling was also observed on the midsection alone (14%, $n = 10$) and anterior (13%, $n = 9$) segments of the sperm head (Table 1).

Keeping the sperm on ice, to reduce lateral diffusion of membrane proteins, during the incubation with primary and secondary antibodies did not change the binding pattern. The apparent variability in the expression of the protein on the sperm head may be due to the fact that the labeling procedure was done on live sperm and takes as long as 5 h, allowing variation in responses of the sperm to the egg jelly–water treatment and lateral diffusion of xMDC16 in the sperm plasma membrane. However, experiments conducted on ice, which should be below the membrane liquid–crystalline phase transition temperature (Noiles *et al.*, 1995), gave the same protein distribution and argue against lateral diffusion as the explanation.

In order to control for nonspecific antibody binding, the rabbit serum was first incubated with a fusion protein containing the disintegrin and cysteine-rich regions of xMDC16 joined to maltose-binding protein (MBP). This preincubation reduced the intensity of staining of the sperm (Fig. 1d) in a concentration-dependent manner (Fig. 2). Preincubation with the fusion protein reduced labeling to an intensity similar to that seen with preimmune serum, whereas preincubation with the MBP component of the fusion protein alone did not significantly reduce staining intensity (Fig. 1e and Fig. 2). This control for specificity is commonly used (Bruckner *et al.*, 1997). We conclude that xMDC16 is expressed on the surface of mature sperm, after egg jelly–water treatment.

Western Blotting of Sperm Protein

Total dithiothreitol-reduced sperm protein was separated by SDS–PAGE, transferred to nitrocellulose, and treated with the same antibody preparation as was used in the immunocytochemistry studies. A 56-kDa band was recognized by the antibody, but this band was not recognized by preimmune preparation (Fig. 3A). We checked for the specificity of labeling by preexposing the immune serum with the fusion protein and then applying it to the blot (Fig. 3B). The 56-kDa band did not label well under these conditions in four different blots. Nonreduced sperm protein was not immunoreactive, suggesting the presence of disulfide bonds in the recognized protein (data not shown). These data reinforce the results of the surface labeling, which indicated that xMDC16 is present in the sperm.

Disintegrin Domain Peptides Trigger Fertilization Envelope Elevation and Cortical Contraction

Cyclized peptides of eight amino acids containing the disintegrin region of xMDC16 were applied to groups ($n =$

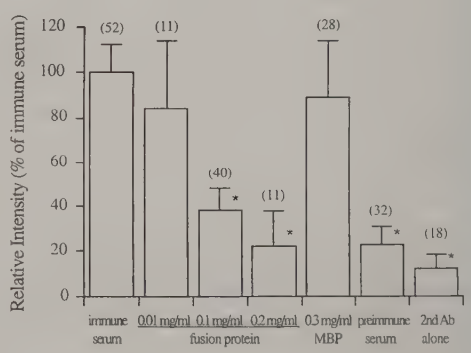

FIG. 2. Quantitation of the immunofluorescence labeling accomplished by measuring the summed labeling intensity within the labeled sperm as the amount of competing fusion protein was varied. The error bars are equal to the 95% confidence intervals around the mean; n is indicated in parentheses above each bar. Sperm from five males were used. The asterisk refers to a statistically significant difference from the immune serum value ($P < 0.05$, analysis of variance). These data suggest that the antibodies to xMDC16 recognize a protein on the surface of live, egg jelly-activated sperm and support the specificity of labeling by the rabbit immune serum since the label intensity on the sperm is reduced when the serum is preexposed to the indicated amount of xMDC16 fusion protein, but not with exposure to MBP alone.

Copyright © 1998 by Academic Press. All rights of reproduction in any form reserved.

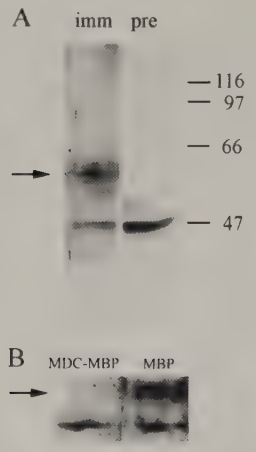

FIG. 3. Western blot of *Xenopus laevis* sperm proteins separated by PAGE and blotted onto nitrocellulose. Sperm protein was boiled in reducing sample buffer for 10 min (0.1 M DTT). The numbers next to blot indicate the molecular weights in kDa of standards run on the blot. (A) Blot was treated with immune and preimmune sera from rabbits injected with a fusion protein containing the cysteine-rich and disintegrin domains of xMDC16 (the rabbit serum was a kind gift from Dr. Carl Blobel). Arrow indicates a band around 56 kDa that labels in the immune but not preimmune blot. (B) When the immune serum is pretreated with the xMDC16 fusion protein (1 mg/ml) and applied to the blot, the 56-kDa band no longer labels, compared to pretreatment with the same amount of maltose-binding protein (MBP) alone. This result was observed in four separate Western blots.

8) of jelly-free eggs in agarose wells. Cyclized peptides were used in an attempt to mimic the three-dimensional structure of the native protein in which the disintegrin domain has been shown to reside on a loop (Adler *et al.*, 1991). Two and a half to 10 μl of a 20 mM stock solution was applied about 100 μm from the surface of individual or groups of eggs (Table 2). Activation was scored as the elevation of the fertilization envelope which usually occurred within 3 to 5 min of peptide treatment. Cortical contraction followed the onset of envelope elevation by 1 to 2 min. The peptides most effective at activating eggs contained the KTX sequence found in the disintegrin domain of xMDC16. KTA-containing peptide was as effective as the peptide with KTE at activating eggs. Both of these peptides activated 93–100% of the eggs to which they were applied in both Ca^{2+}-containing and Ca^{2+}-free media (Table 2). We used four different control peptides for comparison. When the KTE was replaced by AAA or ATA, no significant egg activation was observed using the same 20 mM stock concentration under identical application conditions. Thus, the lysine on the peptide appears to be critical for the activating ability. Next we synthesized two different scrambled forms of the peptide. We found that both activated eggs quite well in Ca^{2+}-containing media but activated less well in Ca^{2+}-free media (39 and 29%, respectively, Table 2). One interpretation of this is that the presence of the lysine residue anywhere in the eight-amino acid peptide conveys activating ability, at least in the presence of Ca^{2+} (but also see immobilized peptide data below). To test for a possible role for the lysine residue (K) alone, eggs were treated with a 20 mM lysine solution. Lysine did not activate any eggs (0%, $n = 20$, two females), compared to activation of sibling eggs by the KTE-containing peptide (88%, $n = 16$). To further test for the role of lysine, another control peptide was tested, calmodulin kinase II substrate (CKII, Calbiochem). This is a 10-mer with several residues in common with the wild-type xMDC16 disintegrin peptide, including lysine (CKII: H-MHRNETVDCLK-NH_2). None of the 50 eggs treated with this peptide in the same manner as the xMDC16 disintegrin peptide activated (10 μl of 20 mM stock was added to 200 μl containing eggs). Also, eggs dropped into a 10 mM solution of this peptide did not activate (0/24). These results suggest that the presence of lysine in a short peptide is alone not sufficient to activate eggs, adding support to the specific nature of the action of KTE-containing xMDC16 disintegrin peptide.

Although the final concentration of uniformly dispersed peptide would have been 1 mM in the above experiments, the concentration around the egg could have been higher during the application of the 20 mM bolus. In order to determine the effective uniform dose, we tested eggs with between 1 and 10 mM solutions of peptide. When eggs were added to 1 mM xMDC16 peptide (KTE or AAA) in F1, no eggs activated (Fig. 4a). However, when eggs were added to F1 containing 10 mM peptide, all eggs activated for the peptide containing KTE (22/22, five females), but not AAA (2/22, Fig. 4a). No obvious morphological abnormalities were visible under these treatment conditions (such as pigment aberrations or lysis).

Local Application of Peptide

In order to mimic the effects of a sperm binding to the egg surface, small volumes of peptide solution (20 mM) were added locally to eggs using a micropipet. External application of as little as 0.2 nmol (10 nl bolus of 20 mM stock) of peptide to eggs caused a small dark spot to form on the egg's surface near the application point, lasting up to 2 min, which developed into the cortical contraction and was accompanied by fertilization envelope elevation (Fig. 4b). The small amounts (10 to 100 nl) of peptide were applied over a 100- to 180-s interval in order to achieve activation. Shorter application times resulted in no activation for volumes <100 nl, possibly due to rapid dispersion of the activating signal. Manual removal of the vitelline coat slightly decreased the sensitivity of eggs to the peptide (Fig. 4b), suggesting the loss of part of the responding mechanism with removal of this extracellular investment. This could be due to pulling off some of the egg's microvilli closely associated with the vitelline envelope when the vitelline envelope was removed. For eggs that did not activate, there was often a slight darkening of the pigment immediately adjacent to the pipet tip within 2 min after the beginning of

Copyright © 1998 by Academic Press. All rights of reproduction in any form reserved.

TABLE 2
Peptide-Induced Egg Activation in *Xenopus laevis*

Peptide	μl of 20 mM stock added (final μM)	% VE elevation, normal Ca^{2+} (No. activated/*n*)	% VE elevation, Ca^{2+}-free F1[a] (No. activated/*n*)
Cyclic CRMP**KTE**C	2.5 (250)	56 (10/18)	56% (23/41)
	5 (500)	100 (19/19)	67% (38/57)
	10 (1000)	93 (26/28)	95% (21/22)
Cyclic CRMP**KTA**C	2.5 (250)	7 (1/15)	40% (6/15)
	5 (500)	60 (12/20)	90% (9/10)
	10 (1000)	100 (17/17)	90% (9/10)
Cyclic CRMP**ATA**C	2.5 (250)	0 (0/6)	—
	5 (500)	0 (0/6)	—
	10 (1000)	0 (0/30)	—
Cyclic CRMP**AAA**C	2.5 (250)	0 (0/10)	0% (0/20)
	5 (500)	0 (0/18)	8% (2/25)
	10 (1000)	0 (0/19)	0% (0/12)
Scrambled #1 C**TMPERK**C	2.5 (250)	12 (3/25)	30% (9/30)
	5 (500)	55 (11/20)	40% (14/35)
	10 (1000)	95 (20/21)	39% (11/28)
Scrambled #2 C**KPREMT**C	10 (1000)	100 (10/10)	29% (5/17)
Cellulose-bound CRMP**KTE**CDLAEY	—	48 (14/29)[b]	—
Cellulose-bound CRMP**AAA**CDLAEY	—	0 (0/18)[b]	—
Cellulose-bound scrambled No. 3: C**EADREPCYTMKL**	—	5 (1/19)[b]	—
Cellulose-bound scrambled No. 4: C**KPREMT**CDLAEY	—	6 (1/18)[b]	—
RGDS	10 (1000)	24 (10/42)	—
RFDS	10 (1000)	0 (0/40)	—
Lysine	10 (1000)	0 (0/20)	—
MHRNETVDCLK	10 (1000)	0 (0/50)	—

[a] The calcium chelator, EGTA, was present at a concentration of 2.5 or 5 mM and no Ca^{2+} was added in the experiments conducted in Ca^{2+}-free F1. The number of adult females used ranged from 2 to 10 per condition employed.
[b] Vitelline envelopes were removed in these eggs so cortical contraction was used to score for egg activation.

peptide addition, which faded within 1 to 2 min. Eggs previously treated with peptide (0.6 to 2 nmol) that did not activate could be subsequently activated with sperm (8/8 eggs). In eggs that activated following peptide application, the cortical contraction invariably began at the place where the peptide was added and commenced within 3 to 5 min after beginning addition. Because it was possible that the peptide was entering the eggs and having an effect from within, peptide was injected into eggs; however, injection of the peptide (8 nl of 20 mM = 2% egg volume) did not cause activation (0/14 eggs, two females).

To confirm the results of a previous report where integrin-binding peptides were used to activate frog eggs (Iwao and Fujimura, 1996), we also treated eggs with the commercially available peptide RGDS (Arg-Gly-Asp-Ser, Sigma Co.). Peptides containing this sequence bind to integrins in other systems (Saudek *et al.*, 1991; Adler *et al.*, 1991). RGDS was added to eggs as 10 μl of a 20 mM solution, at a final concentration of 1 mM. Eggs (10/42, four females) underwent cortical contraction and fertilization envelope elevation in response to this peptide, whereas 0/40 sibling eggs activated in response to a similar peptide, RFDS (Arg-Phe-Asp-Ser, Sigma Co.; Table 1). The proportion of eggs activated by RGDS was lower than that previously reported (40/40, 1 mM final concentration) by Iwao and Fujimura (1996).

Immobilized Peptide also Activates Eggs

In order to better mimic the sperm–egg interaction, we immobilized the peptide on several different substrates. We used both latex and agarose beads 6, 34, and 60 μm in diameter coupled to the peptide by either amine linkages activated by NHS (Pharmacia, Washington, DC) or streptavidin- or neutravidin–biotin linkages (Pierce). Eggs did not significantly activate in response to contact with any of these bead preparations, with or without the vitelline coat. Because of the short length of the peptides, it is possible that they did not extend sufficiently beyond the bead

Copyright © 1998 by Academic Press. All rights of reproduction in any form reserved.

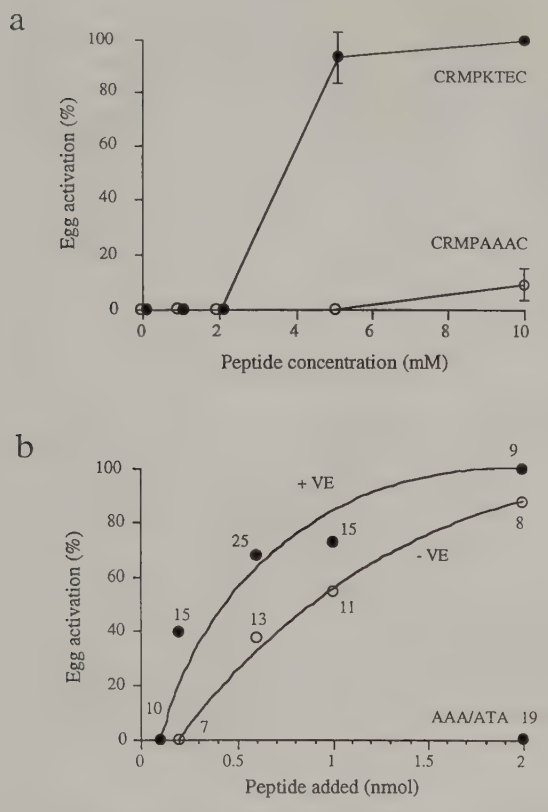

FIG. 4. Peptide-induced activation of *X. laevis* eggs. (a) Activation of dejellied eggs by increasing concentrations of xMDC16 peptide, with KTE or AAA sequences. The eggs were placed into wells containing the indicated concentration of each peptide. The vertical bars indicate the 95% confidence intervals. (b) Activation of vitelline envelope-intact (+VE) and vitelline envelope-free eggs (−VE) after local application of peptide containing the KTE sequence or the AAA and ATA substitution. Replacement of the KTE region by either AAA or ATA resulted in loss of the ability to activate eggs. The number of eggs treated is indicated beside each point.

surface to interact with a component of the egg's plasma membrane.

In contrast to the negative results with the beads, the peptide-bound cellulose was capable of activating eggs (assayed by cortical contraction) after vitelline coat removal. Vitelline coats were manually removed from eggs with forceps and the eggs placed onto the cellulose. We tried to arrange it so that most eggs landed on their equator to expose both animal and vegetal plasma membrane to the peptide. For the wild-type peptide, 14 of 29 eggs activated, whereas for the alanine-substituted peptide 0 of 18 activated. In contrast to the results with the scrambled peptides in solution, the two scrambled peptides immobilized to cellulose did not significantly activate eggs (1/19 for version 3 and 1/18 for version 4). When eggs activated, it was within 2.5 to 5 min of being placed on the cellulose. All experiments were in the presence of calcium and magnesium, using eggs from four females and three different SPOT preparations of the peptide.

Rise in Intracellular Calcium in Response to Peptide Treatment

The xMDC16 disintegrin peptide induced an increase in intracellular free calcium ($[Ca^{2+}]_i$) that began at the point of peptide addition and spread as a wave across the egg (Fig. 5a). The change in $[Ca^{2+}]_i$ began approximately 2 to 4 min after exposure to the peptide. Typically, the Ca^{2+} wave took 3 to 4 min to traverse the egg. Peak $[Ca^{2+}]_i$ was as high as 2 μM. The mean $[Ca^{2+}]_i$ rise was 0.74 ± 0.07 μM (standard error of the mean (SEM), n = 10), in response to peptide, similar to that observed at fertilization (Fig. 5b and Nuccitelli *et al.*, 1993). We never observed more than one initiation site for the calcium wave. The kinetics and amplitude of the calcium wave were independent of the presence of external calcium (Fig. 5), suggesting that the source of calcium for the wave was from internal stores. For example, the mean calcium change in the presence of external calcium was 0.75 ± 0.12 μM (SEM, n = 4) and in the absence of external calcium was 0.73 ± 0.09 μM (SEM, n = 6).

The Ca^{2+} wave velocity was measured near the center of the egg image, where there is the least curvature and was 7.05 ± 0.83 $\mu m\ s^{-1}$ (SEM, n = 6). This is comparable to the velocity previously measured for sperm-induced Ca^{2+} waves in albino frog eggs (7.5 ± 0.5 $\mu m\ s^{-1}$, SEM, n = 8) (Nuccitelli *et al.*, 1993).

Requirement for Divalent Cations

Integrin–ligand interactions are thought to require divalent cations (D'Souza *et al.*, 1994), so we examined the divalent cation dependence of egg activation by peptide. In the presence of EDTA (5 mM), which chelates both Mg^{2+} and Ca^{2+}, 3 of 58 eggs (three females) were activated by peptide application, compared to 28 of 28 eggs in calcium-free F1 containing 5 mM EGTA (10 μl of 20 mM peptide in a 200-μl total volume). Of the eggs in the EDTA–F1, 26 of 28 activated in response to reapplication of peptide upon return to calcium-free F1 (i.e., containing Mg^{2+}). This suggests that the presence of Mg^{2+} is required for peptide-induced activation and supports a possible role for integrins in this activation.

Voltage Sensitivity of Peptide-Induced Egg Activation

We used a two-electrode voltage clamp system (GeneClamp, Axon Instruments) to study the voltage sensitivity of peptide-induced egg activation. When eggs were clamped at negative voltages, the addition of 20 or 40 nmol of xMDC16 peptide (1 or 2 μl of 20 mM stock) induced an "activation current" (top trace, Fig. 6) that varied in peak amplitude with

Copyright © 1998 by Academic Press. All rights of reproduction in any form reserved.

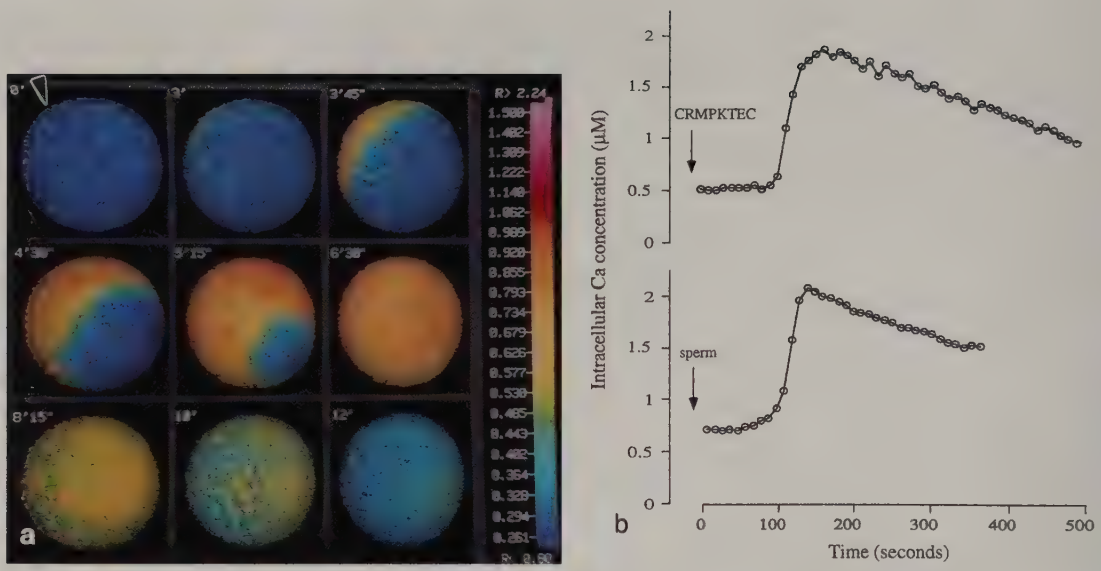

FIG. 5. Peptide-induced changes in $[Ca^{2+}]_i$ in the *Xenopus* egg. (a) Peptide-induced changes in $[Ca^{2+}]_i$ in a dejellied, albino egg injected with fura-2–dextran (50–100 μM final concentration) in Ca^{2+}-free F1 medium detected by ratio imaging. Response to soluble xMDC16 peptide (20 nmol) added from direction indicated (arrowhead). The fluorescence emitted was calibrated as described previously (Nuccitelli *et al.*, 1993) and converted into a pseudocolor representation of the calcium concentration. Egg diameter, 1.2 mm. (b) Comparison of intracellular calcium levels in dejellied albino eggs treated with xMDC16 (upper trace, no external Ca^{2+}) or sperm (lower trace, normal Ca^{2+}). The interval between data points is 10 s, and the time of sperm or peptide addition is indicated. Intracellular free calcium in eggs is elevated in response to xMDC16 peptide in a manner identical to that at fertilization.

initial membrane potential. The kinetics of the rise and duration of the current were similar to those for activation with sperm (bottom trace, Fig. 6) as was the total charge translocated (data not shown). The peak current reached was 351 nA for one egg activated by sperm and 355 nA for a sibling egg activated by peptide treatment, when the membrane was voltage-clamped at −30 mV. The voltage across the egg plasma membrane was clamped over a range of −30 to +20

FIG. 6. Two-electrode voltage clamp study of peptide-induced egg activation. Activation current across the plasma membrane in eggs clamped at −20 mV. The traces were copied from a chart recording and correspond to the current passed to keep the voltage constant. The times of addition of peptide or sperm are indicated with an arrow. (Upper trace) Egg clamped at −20 mV and treated with 20 nmol of xMDC16 (1 μl of 20 mM stock). (Lower trace) An egg clamped at −20 mV and treated with sperm. Asterisk (*) indicates initial rapid inward current.

Copyright © 1998 by Academic Press. All rights of reproduction in any form reserved.

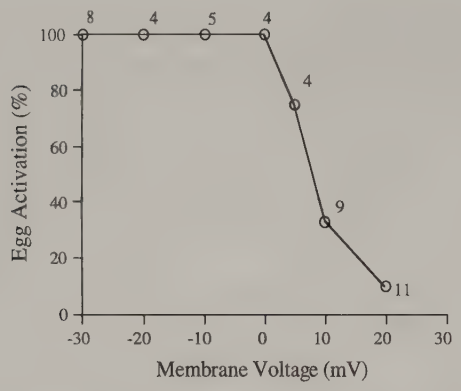

FIG. 7. Percentage of egg activation by xMDC16 disintegrin peptide in eggs voltage clamped at different membrane potentials. The number of eggs per data point is indicated. Activation was scored by the elicitation of an activation current, vitelline envelope elevation, and cortical contraction. Peptide-induced egg activation includes an inward activation current similar to that observed at fertilization and the ability of the peptide to activate is dependent on the voltage across the egg's plasma membrane.

mV and activation was determined by the initiation of a large activation current and vitelline envelope elevation. For eggs clamped at potentials between −30 and 0 mV, activation was not affected by the potential (9/9, Fig. 7). At potentials of +5 and +10 mV activation was partially inhibited (6/13). At +20 mV, activation was effectively blocked (1/11, Fig. 7). Eggs that did not activate in response to peptide while voltage clamped at ≥+5 mV could all be subsequently activated by sperm or further peptide treatment when the clamp potential was reduced to ≤−10 mV.

DISCUSSION

New Findings

We have found that mature eggs of *Xenopus laevis* can be activated by the external application of a peptide derived from the disintegrin domain of a sperm surface MDC protein in a voltage-dependent manner. This peptide did not activate eggs when it was injected into them. This activation is accompanied by a wave of $[Ca^{2+}]_i$ increase that is independent of extracellular Ca^{2+}. Extracellular Mg^{2+} is required for peptide-induced activation. A rabbit antibody generated against a fusion protein containing the disintegrin and cysteine-rich regions of xMDC16 labels the surface of fertilization-competent sperm and recognizes a 56-kDa sperm membrane protein band by Western blot. These results support a role for the sperm protein, xMDC16, in egg activation. Substitutions with alanine for certain amino acids within the peptide result in the elimination of the effectiveness of the peptide. These results suggest the involvement of this sperm surface protein in sperm binding and egg activation, possibly through a signal-transducing receptor in the egg's plasma membrane that recognizes a disintegrin-containing protein. This is the first indication that an MDC protein may play a role in fertilization besides the binding or fusion of the sperm to the egg (Myles *et al.*, 1994; Shilling *et al.*, 1997) and is also the first report of a peptide derived from a sperm-surface protein activating vertebrate eggs. The only other similar report in the literature is for the invertebrate, *Urechis caupo*, the eggs of which can be activated by an acrosomal peptide (Gould and Stephano, 1991). However, in that species a voltage-sensitive Ca^{2+} channel in the egg's plasma membrane opens to increase $[Ca^{2+}]_i$ via Ca^{2+} influx in contrast to the $[Ca^{2+}]_o$-independent intracellular Ca^{2+} increase that we observe in *X. laevis*.

Surface Expression on Sperm of xMDC16

Live sperm were labeled by antisera against a fusion protein containing the disintegrin and cysteine-rich regions of xMDC16. The labeling by the antisera was primarily in the posterior portion of the sperm head and occurred less frequently in the anterior head or midregion. As an interesting comparison we should point out that the distribution of fertilin on guinea pig sperm is initially found over the entire head on testicular sperm and redistributes to reside exclusively on the posterior head upon passing through the epididymis (Hunnicutt *et al.*, 1997). The presence of xMDC16 on the sperm surface makes it available for interaction with proteins in the egg's plasma membrane. This interaction may be purely for binding or may have a role in signal transduction at egg activation.

Western Blot of Sperm Membrane Protein

The protein recognized in Western blotting is smaller (56 kDa) than the calculated molecular weight for xMDC16 (73 kDa; Shilling *et al.*, 1997). This may be due to posttranslational processing, which has been observed for other MDCs in vertebrate sperm (Blobel *et al.*, 1990). In the absence of glycosylation, a size of 56 kDa would result if the sperm xMDC16 were cleaved in the pro-domain, leaving the metalloprotease domain intact. The specificity of this 56-kDa band was checked by preincubating the antiserum with xMDC16 fusion protein. This antiserum no longer recognized the band, offering further support that this band is indeed the xMDC16 protein.

Peptide-Induced Egg Activation

Eggs respond to local peptide addition by forming a dark spot (pigment contraction) at the point of the addition. This spot persists for 30 s to 2 min before the contraction wave is initiated from that region as a ring of concentrated pigment enlarging and spreading across the egg. In eggs for which the amount of peptide was insufficient to activate eggs, the dark spot would still sometimes form but would not enlarge, suggesting that some cortical process had been

Copyright © 1998 by Academic Press. All rights of reproduction in any form reserved.

initiated, but was terminated due to a lack of a persistent stimulus.

Activation by the peptide required the presence of Mg^{2+} but not Ca^{2+}. This is similar to the requirement of integrin ligands (such as disintegrin peptides) for divalent cations in order to bind to integrins. The ligand binding site in integrins from mammalian cells is near a divalent cation binding site which may keep the conformation of the integrins open to ligand binding (D'Souza *et al.*, 1994; Pasqualini *et al.*, 1995). These data support the role of external divalent cations in sperm–egg binding, but not in the subsequent calcium rise, which must come from intracellular stores.

The control peptides tested failed to activate eggs when the KTE was replaced by ATA or AAA, suggesting that lysine is an important component of this disintegrin domain. It is apparently not all that is needed, since neither pure lysine nor an 10-mer containing lysine would activate eggs. We are puzzled by the ability of two soluble scrambled control peptides to activate eggs in the presence of extracellular Ca^{2+}, but feel that the more physiological controls are those in which the peptides were immobilized on cellulose. Under those conditions, the native disintegrin domain sequence exhibited significant egg-activating ability, while the two scrambled sequences failed to activate significantly. Therefore, we feel confident that this activation response can be attributed to the KTE domain of the xMDC disintegrin peptide.

Intracellular Calcium Release in Response to Peptide Addition

Treatment of eggs with peptide in this study caused an increase in $[Ca^{2+}]_i$ with kinetics very similar to the increase at fertilization. This increase occurred in response to the addition of the peptide containing KTE in the putative binding domain, but not in response to the presence of a similar peptide, where KTE was replaced by AAA or ATA. This suggests that the KTE region is responsible for the ability of the peptide to induce a rise in $[Ca^{2+}]_i$. It is also conceivable that this region is the part of xMDC16 (when it resides on the sperm surface) responsible for initiating the cascade of cellular events at fertilization.

Peptide-Induced Activation Is Voltage-Sensitive

When the voltage across the plasma membrane of the frog egg was clamped at $\leq +10$ mV, the application of peptide (20 to 40 nmol) caused egg activation (fertilization envelope elevation and cortical contraction, 15 of 22 eggs). At a voltage of +20 mV, on the other hand, the peptide caused egg activation in only 1 of 11 eggs. Yet all of these eggs activated when the voltage was subsequently changed to a permissive level of ≤ -10 mV. A similar voltage dependence for fertilization has been previously reported for *X. laevis* (Jaffe *et al.*, 1983), *Bufo Japonicus* (Iwao and Jaffe, 1989), and *Rana pipiens* (Cross and Elinson, 1980). For these species, voltage clamping of the eggs above +10 to +20 mV effectively eliminated sperm-induced egg activation (0 to 10% fertilized). Experiments with heterologous crosses with voltage-clamped eggs showed that the potential at which sperm-induced activation occurred was determined by the voltage sensitivity within the species contributing the sperm (Jaffe *et al.*, 1982, 1983; Iwao and Jaffe, 1989). Our experiments provide a candidate voltage sensor for the sperm–egg interaction, namely, the sperm surface protein, xMDC16, identified in the present study.

Signaling through Integrins, Similarity to Fertilization

Integrins can act as signal-transducing receptors in cell–extracellular matrix and cell–cell interactions (Richardson and Parsons, 1995), stimulating protein tyrosine kinase activity (Vuori and Ruoslahti, 1993; Shattil *et al.*, 1994), phosphoinositide metabolism through phosphorylation of PLC-γ (Kanner *et al.*, 1993; Cybulsky *et al.*, 1993), and the release of intracellular free calcium (Ng-Sikorski *et al.*, 1991; Kanner *et al.*, 1993). To date the integrins that are presumably bound by the disintegrin domain-containing proteins in frog have not been identified. MDC sperm surface proteins have been reported to bind to the $\alpha_6\beta_1$ integrin in mouse (Almeida *et al.*, 1995); however, there is some uncertainty about the role of α_6 (Evans *et al.*, 1997). Integrins have been found in frog eggs and embryos (Gawantka *et al.*, 1994; Alfandari *et al.*, 1995) and oocytes and eggs of echinoderms and mammals (Tarone *et al.*, 1993; Almeida *et al.*, 1995; de Nadai *et al.*, 1996).

Model for Fertilization in Animals

Previous research has lead to two major models for the mechanism of egg activation by sperm in vertebrates, the diffusible sperm factor model and the signal-transducing sperm receptor model. A cytosolic factor in sperm may diffuse into the egg after fusion causing intracellular calcium elevation (Lawrence *et al.*, 1997). Although this factor has not been definitively identified, some evidence in the mouse egg points toward an enzyme similar to the bacterial protein, hexose phosphate isomerase (Parrington *et al.*, 1996). One appealing aspect of this model is that activation and the fast block to polyspermy could not occur until a sperm has fused with the egg since it requires diffusion of molecules from the sperm into the egg. Another model posits a surface receptor on the egg being stimulated upon sperm binding and transducing the signal to the cytoplasmic face of the plasma membrane (Jaffe, 1990; Foltz and Shilling, 1993). No receptor has been identified in this process and it is certainly possible that this receptor-mediated signal transduction may happen in concert with a diffusible factor from sperm.

There are two surface receptor types that are candidates for receiving the signal from sperm. The evidence for integrins comes from studies of mammalian eggs and includes inhibition of sperm-binding by a function-blocking monoclonal antibody (GoH3) to the α_6 integrin (Almeida *et*

Copyright © 1998 by Academic Press. All rights of reproduction in any form reserved.

al., 1995) and disintegrin peptides, presumed to bind to integrins (Shilling *et al.*, 1997). A sperm-binding protein has also been identified in sea urchin eggs (Foltz *et al.*, 1993; Giusti *et al.*, 1997), but it is not clear that sperm-binding is its only function (Mauk *et al.*, 1997). This membrane-associated molecule binds bindin, a peptide on the surface of acrosome-reacted sea urchin sperm (Foltz and Lennarz, 1993), and soluble bindin can inhibit fertilization in a concentration-dependent manner (Minor *et al.*, 1993). Similar receptor/ligand systems have not been identified in vertebrate eggs and sperm. However, a conservative model for a sperm receptor in vertebrates must include the possibility of a similar receptor being involved in sperm binding. We suggest a system for sperm binding and egg activation that includes an integrin as an integral part of a cluster of molecules that are responsible for sperm binding, signal transduction, and possibly fusion.

ACKNOWLEDGMENTS

We thank Drs. Diana Myles and Carl Blobel for their suggestions during this project. This work was supported by the NIH (HD19966) and in part by a training grant for Nonlinear Dynamics from the NSF (DBI-96-02226).

REFERENCES

Adler, M., Lazarus, R. A., Dennis, M. S., and Wagner, G. (1991). Solution structure of kistrin, a potent platelet aggregation inhibitor and GP IIb-IIIa antagonist. *Science* **253,** 445–448.

Alfandari, D., Whittaker, C. A., DeSimone, D. W., and Darribere, T. (1995). Integrin alpha v subunit is expressed on mesodermal cell surfaces during amphibian gastrulation. *Dev. Biol.* **170,** 249–261.

Almeida, E. A. C., Huovila, A.-P. J., Sutherland, A. E., Stephens, L. E., Calarco, P. G., Shaw, L. M., Mercurio, A. M., Sonnenberg, A., Primakoff, P., Myles, D. G., and White, J. M. (1995). Mouse egg integrin $\alpha_6\beta_1$ functions as a sperm receptor. *Cell* **81,** 1095–1104.

Bernardini, G., Stipani, R., and Melone, G. (1986). The ultrastructure of *Xenopus* spermatozoon. *J. Ultrastruct. Mol. Struct. Res.* **94,** 188–194.

Bigler, D., Chen, M., Waters, S., and White, J. M. (1997). A model for sperm–egg binding and fusion based on ADAMS and integrins. *Trends Cell. Biol.* **7,** 220–225.

Blobel, C. P., Myles, D. G., Primakoff, P., and White, J. M. (1990). Proteolytic processing of a protein involved in sperm-egg fusion correlates with acquisition of fertilization competence. *J. Cell Biol.* **111,** 69–78.

Blobel, C. P., Wolfsberg, T. G., Turck, C. W., Myles, D. G., Primakoff, P., and White, J. M. (1992). A potential fusion peptide and an integrin ligand domain in a protein active in sperm–egg fusion. *Nature* **356,** 248–252.

Bruckner, K., Pasquale, E. B., and Klein, R. (1997). Tyrosine phosphorylation of transmembrane ligands for Eph receptors. *Science* **275,** 1640–1643.

Cross, N. L., and Elinson, R. P. (1980). A fast block to polyspermy in frogs is mediated by changes in the membrane potential. *Dev. Biol.* **75,** 187–198.

Cybulsky, A. V., Carbonetto, S., Cyr, M. D., McTavish, A. J., and Huang, Q. (1993). Extracellular matrix-stimulated phospholipase activation is mediated by beta 1-integrin. *Am. J. Physiol.* **264,** C323–C332.

D'Souza, S. E., Haas, T. A., Piotrowicz, R. S., Byers-Ward, V., McGrath, D. E., Soule, H. R., Cierniewski, C., Plow, E. F., and Smith, J. W. (1994). Ligand and cation binding are dual functions of a discrete segment of the integrin beta 3 subunit: Cation displacement is involved in ligand binding. *Cell* **79,** 659–667.

de Nadai, C., Fenichel, P., Donzeau, M., Epel, D., and Ciapa, B. (1996). Characterisation and role of integrins during gametic interaction and egg activation. *Zygote* **4,** 31–40.

Evans, J. P., Kopf, G. S., and Schultz, R. M. (1997). Characterization of the binding of recombinant mouse sperm fertilin beta subunit to mouse eggs: Evidence for adhesive activity via an egg beta 1 integrin-mediated interaction. *Dev. Biol.* **187,** 79–93.

Foltz, K. R., and Lennarz, W. J. (1993). The molecular basis of sea urchin gamete interactions at the egg plasma membrane. *Dev. Biol.* **158,** 46–61.

Foltz, K. R., Partin, J. S., and Lennarz, W. J. (1993). Sea urchin egg receptor for sperm: Sequence similarity of binding domain and hsp70. *Science* **259,** 1421–1425.

Foltz, K. R., and Shilling, F. M. (1993). Receptor-mediated signal transduction and egg activation. *Zygote* **1,** 276–279.

Gawantka, V., Joos, T. O., and Hausen, P. (1994). A beta 1-integrin associated alpha-chain is differentially expressed during *Xenopus* embryogenesis. *Mech. Dev.* **47,** 199–211.

Giusti, A. F., Hoang, K. M., and Foltz, K. R. (1997). Surface localization of the sea urchin egg receptor for sperm. *Dev. Biol.* **184,** 10–24.

Gould, M., and Stephano, J. L. (1987). Electrical responses of eggs to acrosomal protein similar to those induced by sperm. *Science* **235,** 1654–1656.

Gould, M. C., and Stephano, J. L. (1991). Peptides from sperm acrosomal protein that initiate egg development. *Dev. Biol.* **146,** 509–518.

Hunnicutt, G. R., Koppel, D. E., and Myles, D. G. (1997). Analysis of the process of localization of fertilin to the sperm posterior head plasma membrane domain during sperm maturation in the epididymis. *Dev. Biol.* **191,** 146–159.

Iwao, Y., and Fujimura, T. (1996). Activation of *Xenopus* eggs by RGD-containing peptides accompanied by intracellular Ca^{2+} release. *Dev. Biol.* **177,** 558–567.

Iwao, Y., and Jaffe, L. A. (1989). Evidence that the voltage-dependent component in the fertilization process is contributed by the sperm. *Dev. Biol.* **134,** 446–451.

Jaffe, L. A. (1990). First messengers at fertilization. *J. Reprod. Fertil.* **42,** 107–116.

Jaffe, L. A., Cross, N. S., and Picheral, B. (1983). Studies of the voltage-dependent polyspermy block using cross-species fertilization of amphibians. *Dev. Biol.* **98,** 319–326.

Jaffe, L. A., Gould-Somero, M., and Holland, L. Z. (1982). Studies of the mechanism of the electrical polyspermy block using voltage clamp during cross-species fertilization. *J. Cell Biol.* **92,** 616–621.

Kanner, S. B., Grosmaire, L. S., Ledbetter, J. A., and Damle, N. K. (1993). Beta 2-integrin LFA-1 signaling through phospholipase C-gamma 1 activation. *Proc. Natl. Acad. Sci. USA* **90,** 7099–7103.

Kline, D., Simoncini, L., Mandel, G., Maue, R. A., Kado, R. T., and Jaffe, L. A. (1988). Fertilization events induced by neurotransmitters after injection of mRNA in *Xenopus* eggs. *Science* **241,** 464–467.

Copyright © 1998 by Academic Press. All rights of reproduction in any form reserved.

Lawrence, Y. M., Whitaker, M., and Swann, K. (1997). Sperm–egg fusion is the prelude to the initial Ca^{2+} increase at fertilization in the mouse. *Development* **124,** 233–241.

Mauk, R., Jaworski, D., Kamei, N., and Glabe, C. G. (1997). Identification of a 97-kDa heat shock protein from *S. franciscanus* ovaries with 94% amino acid identity to the *S. purpuratus* egg surface receptor for sperm. *Dev. Biol.* **184,** 31–37.

Minor, J. E., Britten, R. J., and Davidson, E. H. (1993). Species-specific inhibition of fertilization by a peptide derived from the sperm protein bindin. *Mol. Biol. Cell.* **4,** 375–387.

Miyazaki, S., Yuzaki, M., Nakada, K., Shirakawa, H., Nakanishi, S., Nakede, S., and Mikoshiba, K. (1992). Block of Ca^{2+} wave and Ca^{2+} oscillation by antibody to the inositol 1,4,5-trisphosphate receptor in fertilized hamster eggs. *Science* **257,** 251–255.

Moore, G. D., Kopf, G. S., and Schultz, R. M. (1993). Complete mouse egg activation in the absence of sperm by stimulation of an exogenous G protein-coupled receptor. *Dev. Biol.* **159,** 669–678.

Myles, D. G., Kimmel, L. H., Blobel, C. P., White, J. M., and Primakoff, P. (1994). Identification of a binding site in the disintegrin domain of fertilin required for sperm–egg fusion. *Proc. Natl. Acad. Sci. USA* **91,** 4195–4198.

Ng-Sikorski, J., Andersson, R., Patarroyo, M., and Andersson, T. (1991). Calcium signaling capacity of the CD11b/CD18 integrin on human neutrophils. *Exp. Cell Res.* **195,** 504–508.

Noiles, E. E., Bailey, J. L., and Storey, B. T. (1995). The temperature dependence in the hydraulic conductivity, Lp, of the mouse sperm plasma membrane shows a discontinuity between 4 and 0 degrees C. *Cryobiology* **32,** 220–238.

Nuccitelli, R., Yim, D. L., and Smart, T. (1993). The sperm-induced Ca^{2+} wave following fertilization of the *Xenopus* egg requires the production of $Ins(1,4,5)P_3$. *Dev. Biol.* **158,** 200–212.

Parrington, J., Swann, K., Shevchenko, V. I., Sesay, A. K., and Lai, F. A. (1996). Calcium oscillations in mammalian eggs triggered by a soluble sperm protein. *Nature* **379,** 364–368.

Pasqualini, R., Koivunen, E., and Ruoslahti, E. (1995). A peptide isolated from phage display libraries is a structural and functional mimic of an RGD-binding site on integrins. *J. Cell Biol.* **130,** 1189–1196.

Primakoff, P., Hyatt, H., and Tredick-Kline, J. (1987). Identification and purification of a sperm surface protein with a potential role in sperm-egg membrane fusion. *J. Cell Biol.* **104,** 141–149.

Reed, S. C., and Stanley, H. P. (1972). Fine structure of spermatogenesis in the South African clawed toad *Xenopus laevis* Daudin. *J. Ultrastruct. Res.* **41,** 277–295.

Richardson, A., and Parsons, J. T. (1995). Signal transduction through integrins: A central role for focal adhesion kinase? *BioEssays* **17,** 229–236.

Sato, K., Iwasaki, T., Tamaki, I., Aoto, M., Tokmakov, A. A., and Fukami, Y. (1998). Involvement of protein-tyrosine phosphorylation and dephosphorylation in sperm-induced *Xenopus* egg activation. *FEBS Lett.* **424,** 113–118.

Saudek, V., Atkinson, R. A., and Pelton, J. T. (1991). Three-dimensional structure of echistatin, the smallest active RGD protein. *Biochemistry* **30,** 7369–7372.

Shattil, S. J., Haimovich, B., Cunningham, M., Lipfert, L., Parsons, J. T., Ginsberg, M. H., and Brugge, J. S. (1994). Tyrosine phosphorylation of pp125FAK in platelets requires coordinated signaling through integrin and agonist receptors. *J. Biol. Chem.* **269,** 14738–14745.

Shilling, F. M., Carroll, D. J., Muslin, A. J., Escobedo, J. A., Williams, L. T., and Jaffe, L. A. (1994). Evidence for both tyrosine kinase and G-protein-coupled pathways leading to starfish egg activation. *Dev. Biol.* **162,** 590–599.

Shilling, F. M., Kratzschmar, J., Cai, H., Weskamp, G., Gayko, U., Leibow, J., Myles, D. G., Nuccitelli, R., and Blobel, C. P. (1997). Identification of metalloprotease/disintegrins in *Xenopus laevis* testis with a potential role in fertilization. *Dev. Biol.* **186,** 155–164.

Tarone, G., Russo, M. A., Hirsch, E., Odorisio, T., Altruda, F., Silengo, L., and Siracusa, G. (1993). Expression of $\beta 1$ integrin complexes on the surface of unfertilized mouse oocyte. *Development* **117,** 1369–1375.

Vuori, K., and Ruoslahti, E. (1993). Activation of protein kinase C precedes alpha 5 beta 1 integrin-mediated cell spreading on fibronectin. *J. Biol. Chem.* **268,** 21459–21462.

Weskamp, G., and Blobel, C. P. (1994). A family of cellular proteins related to snake venom disintegrins. *Proc. Natl. Acad. Sci. USA* **91,** 2748–2751.

Wolfsberg, T. G., Straight, P. D., Gerena, R. L., Huovila, A. P., Primakoff, P., Myles, D. G., and White, J. M. (1995). ADAM, a widely distributed and developmentally regulated gene family encoding membrane proteins with a disintegrin and metalloprotease domain. *Dev. Biol.* **169,** 378–383.

Wolfsberg, T. G., and White, J. M. (1996). ADAMs in fertilization and development. *Dev. Biol.* **180,** 389–401.

Yim, D. L., Opresko, L. K., Wiley, H. S., and Nuccitelli, R. (1994). Highly polarized EGF receptor tyrosine kinase activity initiates egg activation in *Xenopus*. *Dev. Biol.* **162,** 41–55.

Received for publication December 30, 1997
Revised June 9, 1998
Accepted June 15, 1998

Copyright © 1998 by Academic Press. All rights of reproduction in any form reserved.

DEVELOPMENTAL BIOLOGY 202, 125–135 (1998)
ARTICLE NO. DB988997

A Novel Alternative Spliced Variant of the Transcription Factor AP2α Is Expressed in the Murine Ocular Lens

Chiaki Ohtaka-Maruyama,*,† Fumio Hanaoka,* and Ana B. Chepelinsky†,[1]

**Cellular Physiology Laboratory, the Institute for Chemical and Physical Science (RIKEN), 2-1 Hirosawa, Wako, Saitama 351-01, Japan; and †Laboratory of Molecular and Developmental Biology, National Eye Institute, National Institutes of Health, Bethesda, Maryland 20892*

The AP2α gene encodes a transcription factor containing a basic, helix–span–helix DNA-binding/dimerization domain, which is developmentally regulated and retinoic acid inducible. Recent reports about AP2α null mice indicate that AP2α plays an important role in embryogenesis, especially in craniofacial development and midline fusion. Ocular development is also affected in these null mice. As AP2α may be involved in transcriptional regulation in the lens, it was important to examine the expression of the AP2α gene in the lens. Four AP2α mRNA variants have been previously isolated from whole mouse embryos. Variants 1, 3, and 4 are transcriptional activators that are transcribed from different promoters and variant 2 is a repressor lacking the activation domain encoded by exon 2. Using *in situ*-PCR, we found that AP2α is expressed in the lens epithelia but not in the lens fibers. RT-PCR analysis of lens mRNA with amplimers specific for each variant revealed that AP2α variants 1, 2, and 3 are expressed in newborn mouse lenses. However, variant 4 is not expressed in the lens. In this report we characterized a novel isoform, which we named variant 5, expressed in the lens and kidney. Variant 5, which is generated by alternative splicing, may function as a repressor due to the partial deletion of the proline-rich transactivation domain encoded by exon 2. This is the first molecular characterization of AP2α gene expression in the lens. Our results indicate that two activator and two repressor AP2α isoforms may play a role in regulating gene expression in the lens. © 1998 Academic Press

INTRODUCTION

Transcriptional regulation plays a central role in the cell differentiation program during development. Tissue-specific gene expression requires precise temporal and spatial regulation during embryogenesis. To elucidate the mechanisms involved in tissue-specific expression, many transcription factors which interact with specific DNA sequences have been characterized. Published data reveal that not only tissue-specific factors but also general or tissue-preferred factors including positive and negative transcriptional regulators are involved in the precise regulation of cell-type-restricted gene expression (Mendel and Crabtree, 1991; Snape *et al.*, 1991; Zhang *et al.*, 1994; Ho *et al.*, 1996). Either many transcription factors belong to protein families with conserved DNA-binding domains or multiple isoforms lacking either the activation or the DNA-binding domains arise from a single gene by alternative splicing, generating activators or repressors (Kingsley and Winoto, 1992; Buettner *et al.*, 1993; Grove and Plumb, 1993; Meier *et al.*, 1995; Oyake *et al.*, 1996; Skerjanc *et al.*, 1996). Their DNA and protein/protein interaction domains function as modules, allowing modulation of their regulatory functions depending on their cellular environment.

The transcription factor AP2 is a retinoic acid-inducible factor that was initially isolated from HeLa cells (Williams *et al.*, 1988; Luscher *et al.*, 1989). The mouse and *Xenopus* orthologous genes were subsequently characterized (Winning *et al.*, 1991; Moser *et al.*, 1993). During mouse embryogenesis, AP2 is expressed in neural crest cells and in restricted parts of the nervous system, face, limbs, nephric system, and epidermis (Mitchell *et al.*, 1991). The expression pattern of AP2 during *Xenopus* development is similar to the one in the mouse (Winning *et al.*, 1991). AP2 is

[1] To whom correspondence should be addressed at National Institutes of Health, 6 Center Drive MSC 2730, Building 6, Room 211, Bethesda, MD 20892-2730. Fax: (301) 480 7933. E-mail: abc@helix.nih.gov.

0012-1606/98 $25.00
Copyright © 1998 by Academic Press
All rights of reproduction in any form reserved.

essential for epidermis-specific keratin gene expression in human and *Xenopus* (Leask *et al.*, 1991; Snape *et al.*, 1991; Winning *et al.*, 1991; Byrne *et al.*, 1994). Two recent reports of AP2 null mutant mice indicate that AP2 plays a key role in early embryogenesis, especially in cranial development. The null mice fail to close the cranial neural tube and have severe dismorphogenesis of the skull, eyes, sensory organs, and cranial ganglia (Schorle *et al.*, 1996; Zhang *et al.*, 1996).

Two additional AP2-related genes were later characterized, AP2β and AP2γ (Moser *et al.*, 1995; Oulad-Abdelghani *et al.*, 1996). The basic DNA-binding domain which overlaps with a helix–span–helix (HSH) dimerization domain is highly conserved in the three members of the AP2 family (Williams and Tjian, 1991a,b; Moser *et al.*, 1995; Oulad-Abdelghani *et al.*, 1996). Therefore, AP2, which encodes four mRNA variants produced by alternative splicing in the embryonic mouse (Meier *et al.*, 1995), was later renamed AP2α. The four mRNA variants share the DNA binding/dimerization domain. Variants 3 and 4 differ from variants 1 and 2 in their exon 1, due to the usage of different promoters. Variant 2 differs from variant 1 in the absence of exon 2, which encodes the transactivation domain, as a result of alternative splicing.

The precise spatial and temporal regulation of gene expression in the ocular lens provides a useful model for studying transcriptional regulation during development. We have been studying the transcriptional regulation of the MIP gene which is specifically expressed in the lens fiber cells. Purified human AP2α interacts with a domain of the human MIP gene required for promoter activity in lens cells (Ohtaka-Maruyama *et al.*, 1998). The eye phenotype of the AP2α null mice is similar to the mutant phenotype of Pax6, which was identified as a master control gene for eye development (Halder *et al.*, 1995; Morris-Kay, 1996; Schorle *et al.*, 1996; Zhang *et al.*, 1996), suggesting that AP2α may also play an important role in ocular development. To examine the role of AP2α in lens differentiation and in the regulation of lens-specific gene expression, we studied the spatial localization of AP2α in the lens and the expression of each of the four AP2α isoforms in the lens. We found expression of the AP2α gene in the lens epithelia but not in the lens fibers. Our results show that three of the four isoforms which had been reported and one novel AP2α isoform which lacks part of the proline-rich transactivation domain are expressed in the lens. The ratio of negative and positive regulatory AP2α isoforms may play a role in the precise regulation of gene expression in the lens.

MATERIALS AND METHODS

Oligonucleotides. Oligonucleotides were synthesized either in an Applied Biosystems synthesizer or in a Perspective Biosystems Expedite nucleic acid synthesis system followed by purification in G-25 Sephadex columns.

RT-PCR analysis of AP2 transcripts in various tissues. Total RNA was isolated from various tissues of 5-day-old mice by the guanidinium thiocyanate/phenol chloroform single-step extraction method. Poly(A) RNA was isolated with oligo(dT)-Dynabeads (Dynal As, Oslo, Norway). One microgram of poly(A) RNA was reversed transcribed using the first-strand synthesis kit (Clontech) with random primers. Five microliters of first-strand reaction was amplified by PCR using amplimers corresponding to AP2α cDNA sequences (Meier *et al.*, 1995), as indicated in Fig. 1. The oligonucleotide sequence for primers A through H, indicated in Fig. 1 are: A, 5′-ACTTTGCGCTAACCCAGAGA-3′, and B, 5′-GAGGGGCAAATCCGATCACG-3′ (exon 1a, sense primer); C, 5′-CTGGGAGGATAGAGATCGTG-3′, and D, 5′-GTTACCCCAGACTCTTCGCA-3′ (exon 1b, sense primer); E, 5′-GCCTGCTTCACTTCTTGGGT-3′,and F, 5′-GTTGATACCCCCTACTTCGG-3′ (exon 1c, sense primer); G, 5′-CGTGAGGAGAGTAACGTTG-3′,and H, 5′-CCCTGCTGGCAGATTCA-3′ (exon 5, antisense primer); I, 5′-ATCTGCCAGCAGGGAGACGTAAAGCTGCCA-3′ (exon 5, sense primer); and J, 5′-GGCCT CGGTGAGATAGTTCTGCAGGGCCGT-3′ (exon 7, antisense primer).

As a positive control, an equal amount of first-strand reaction was amplified with primers corresponding to G3PDH, 0.45-kb control amplimer set (Clontech). The PCR conditions were 30 cycles at 94°C, 1 min for denaturation; 60°C, 1 min for hybridization; and 72°C, 2 min for extension. The PCR products were analyzed by polyacrylamide gel electrophoresis.

To specifically amplify transcripts from the AP2β gene, the following oligonucleotides were designed and synthesized: 5′-CACACGCCATCATCGGACTT-3′ (exon 2, sense) and 5′-GGGAGGGACAGGAACTTTTT-3′ (exon 3, antisense), at positions 355/374 and 776/795, respectively (Moser *et al.*, 1995). To specifically amplify transcripts from the AP2γ gene the oligonucleotides 5′-CCTGGATTTAACTGGCGACT-3′ (noncoding exon 1, sense) and 5′-CCTCCAGCCCTGAAATATGG-3′ (exon 2, antisense), at positions 180/199 and 599/618, respectively (Oulad-Abdelghani *et al.*, 1996) were designed and synthesized. The RT-PCR conditions were similar to the ones for AP2α, except that the hybridization step was at 63°C.

PCR products were analyzed in 6% polyacrylamide electrophoresis.

Cloning and sequencing of RT-PCR products. The RT-PCR products obtained with each amplimer were cloned into the pCR-Script Amp SK(+) vector, using the PCR-Script cloning kit (Stratagene). Five microliters of each PCR reaction mixture was ligated to the SfI-linearized vector with T4 DNA ligase at room temperature for 1 h and transformed into *Escherichia coli* strain XL1-blue. Plasmids were isolated from positive white colonies. Both strands of each inserted DNA fragment were sequenced using the dideoxy method with fluorescein-labeled single primers in the ALF express automated sequencing system (Pharmacia).

In situ RT-PCR. Heads isolated from embryonic day 14 mice were fixed in 4% paraformaldehyde and paraffin embedded and eye sections containing the lens in the anterior/posterior orientation were obtained. Pretreatment of the sections was as follows: deparaffination with xylene (twice, 10 min each); ethanol series (twice 100, 95, 75, 50, and 30%), 1 min each; PBS for 2 min; 4% PFA/PBS for 20 min; 20 μg/ml proteinase K in 50 mM Tris–HCl, pH 8.0, 5mM EDTA for 7.5 min; PBS for 2 min; 4% PFA/PBS for 5 min; PBS for 2 min; water quick dip; 0.1 M TEA–0.4% acetic anhydride for 10 min; PBS for 2 min; EtOH series (30, 50, 75, 95, and 100%); and air drying for 30 min. For the reverse transcription (RT) reactions, 65 μl of water and 5 μl of oligo(dT) primer (0.5 μg/μl) were added to the tissue sections and covered with Parafilm. Slides were incubated at 70°C for 10 min followed by cooling on ice for 1 min. Slides were incubated with SuperScript II reverse transcriptase (Gibco-

Copyright © 1998 by Academic Press. All rights of reproduction in any form reserved.

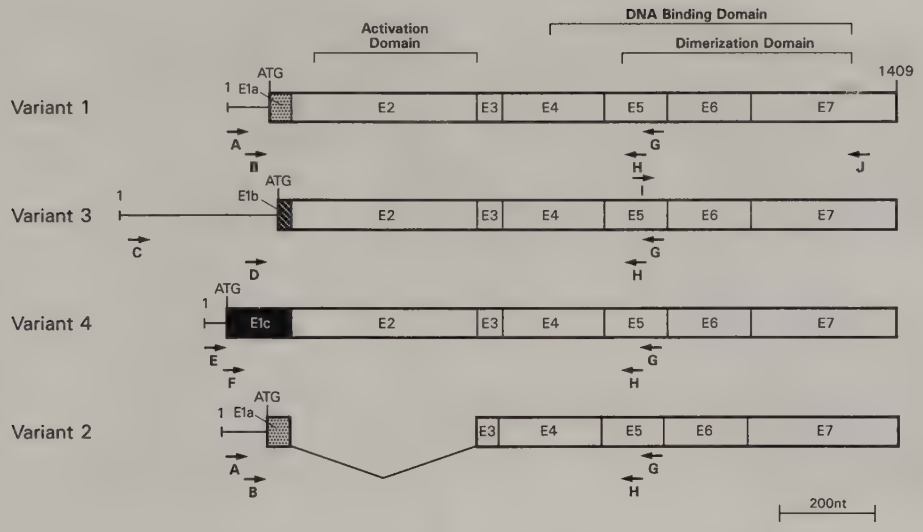

FIG. 1. Diagram of AP2α variants. Exon 1 to 3 boundaries in variants 1 to 4 are based on Meier *et al.*, 1995; exon 5 to 7 boundaries are based on the human AP2α gene (Bauer *et al.*, 1994). (1) indicates initiation of exon 1; line indicates exon 1 untranslated sequence; dotted bar, coding exon 1a (E1a); hatched bar, coding exon 1b (E1b); solid bar, coding exon 1c (E1c). Arrows indicate the location and orientation of primers designed for RT-PCR experiments. Exons 2 to 7 are indicated as E2–E7, respectively. The location of the activation, DNA-binding and dimerization domains is indicated with brackets (Williams and Tjian, 1991a,b; Bauer *et al.*, 1994).

BRL) as indicated by the manufacturer. After the RT reaction, slides were rinsed twice with PBS. The sections were covered with the PCR reaction mixture and sealed with a SlideSeal (Hybaid, England). The PCR reaction mixture contained primers I and J, 1 ng each, in a 100-μl PCR reaction mixture containing digoxigenin-dUTP, *Taq* polymerase, and *Taq* Start antibody from the Expand high-amplification system kit (Boehringer Mannheim). PCR reactions were performed in a OmniSlide thermal cycler (Hybaid); amplification conditions were 20 cycles at 94°C for 15 s, 55°C for 15 s, and 72°C for 1 min and one cycle of 72°C for 5 min. Negative controls either without the addition of RT or without amplimers were performed at the same time. After the PCR reaction, the slides were washed with 0.1× SSC at 45°C for 20 min and rinsed in DIG system buffer 1 (Boehringer Mannheim) at room temperature for 10 min. The color reaction with antidigoxigenin and NBT-BCIP was performed according to the nonradioactive DIG detection kit from Boehringer Mannheim. The slides were then mounted with Crystalmount and Permount (Fischer).

RESULTS

The AP2 Gene Is Expressed in the Lens

Poly(A) RNA was isolated from the ocular lens and eight additional tissues were dissected from 5-day-old mice. In order to examine the expression of the AP2α gene in the lens, we performed RT-PCR analysis with primers I and J, corresponding to exons 5 and 7, respectively (Fig. 1). This amplimer amplifies a region present in the four AP2α mRNA variants which encodes the DNA-binding/dimerization domain. As shown in Fig. 2, an expected band of approximately 392 bp was detected in the lens, kidney, and cerebellum. Weak bands were detected in brain, thymus, lung, and heart, but no bands were observed in liver and spleen. These data indicate that the AP2α gene is expressed in the ocular lens.

Spatial Localization of AP2α mRNA in the Lens

To determine the localization of AP2α expression in the lens, we analyzed the spatial localization of AP2α mRNA in paraffin embedded eye sections from E14 mouse embryos. We initially performed *in situ* hybridization with the digoxigenin-labeled AP2α antisense riboprobe from plasmid pB240 (Mitchell *et al.*, 1991), but no positive signal was detected. Therefore, we performed *in situ* PCR using the I/J amplimers which amplify exon 5 to exon 7 (Fig. 1). We detected a strong signal in lens epithelial cells but not in the fiber cells of 14-day-old mouse embryo (Fig. 3A). Two negative controls were performed, one without the incubation step with reverse transcriptase and another one without the addition of PCR primers to the PCR reaction (Fig. 3B). No NBT-BCIP hybridization signal was observed in the absence of RT or primers. These results show that the gene encoding the transcription factor AP2α is expressed in the whole anterior lens epithelia region and stops being expressed as soon as the epithelial cells start elongating in the equatorial region.

Copyright © 1998 by Academic Press. All rights of reproduction in any form reserved.

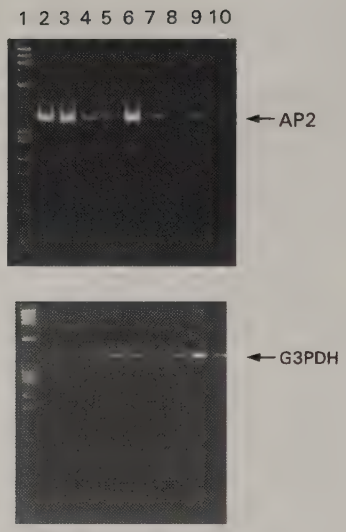

FIG. 2. Analysis of AP2α gene expression in various mouse tissues by RT-PCR. Poly(A) RNA was isolated from various mouse tissues and analyzed by RT-PCR as indicated under Materials and Methods. (Top) Polyacrylamide gel electrophoresis using the amplimers I/J (exons 5 and 7, respectively (see Fig. 1). (Bottom) Polyacrylamide gel electrophoresis using amplimers corresponding to G3PDH. Lane 1, DNA size markers (ϕX174 *Hae*III digested fragments); lane 2, lens RNA; lane 3, kidney RNA; lane 4, brain (cerebrum) RNA; lane 5, thymus RNA; lane 6, cerebellum RNA; lane 7, lung RNA; lane 8, liver RNA; lane 9, heart RNA; lane 10, spleen RNA. Arrows indicate the expected amplified band with the AP2α I/J amplimers, 392bp (top), and with G3PDH amplimers, 452bp (bottom).

AP2α mRNA Variants Expressed in the Lens

Meier *et al.* (1995) characterized four mRNA variants derived from the AP2α gene in embryonic mice. Variants 1, 3, and 4 arise from the usage of three different promoters; variants 1 and 2 are transcribed from the same promoter but variant 2 lacks the activation domain encoded in exon 2 due to alternative splicing (see Fig. 1). As the amplimers used in the previous experiment (Fig. 2) amplify the four isoforms, additional experiments are required to determine which isoforms are expressed in the lens. To address this question, we performed RT-PCR using variant-specific primers. Figure 4 shows the results obtained with the lens and eight additional tissues. Variants 1 and 2 were analyzed using the primers A and G, corresponding to exon 1a and 5, respectively (see Fig. 1) and the results obtained are shown in Fig. 4A. When we used the amplimer A/G, a 949-bp band derived from variant 1 was detected in the lens, kidney, and cerebellum; faint bands were also detected in brain and lung. As exon 2 is deleted in variant 2, a 514-bp RT-PCR product would be expected from this variant. As shown in Fig. 4A, the band corresponding to variant 2 was also detected in the lens, kidney, and cerebellum. We consistently noticed an additional band migrating with a mobility between the amplified products of variants 1 and 2; this band was detected in the lens and kidney but not in other tissues. To confirm this result we designed two additional primers for exons 1a and 5, primers B and H respectively (see Fig. 1). The additional band was also detected with the amplimer B/H (see Fig. 5B).

To detect variant 3, we designed two primers specific to exon 1b. Figure 4B shows the results obtained with the amplimer C/G. The expected 1.1-kb band derived from variant 3 was observed in kidney and cerebellum. A weaker band was detected in the lens, brain, and lung (Fig. 4B). A band with the expected size for variant 3 was also detected in the lens using another amplimer for exons 1b and 5 (primers D/H, Fig. 1) (data not shown).

To detect variant 4, we used primers E and G, corresponding to exons 1c and 5, respectively. As shown in Fig. 4C, the corresponding band of 987 bp was detected only in the cerebellum but not in other analyzed tissues. This result was reproducible when we used the amplimer F/H (data not shown).

Variant 5 Is a Novel AP2α mRNA Variant Produced by Alternative Splicing

To verify that the RT-PCR products obtained with lens RNA correspond to the predicted AP2α mRNA variants, the PCR products were cloned and sequenced. Cloning and sequencing of the RT-PCR products obtained with amplimers A/G (949- and 514-bp bands) and C/G (1148-bp band), corresponding to variants 1, 2, and 3, respectively, were 100% identical to the sequences that had been reported by Meier *et al.* (1995). Sequencing of the 784-bp band obtained with lens RNA using amplimer A/G revealed the presence of a novel AP2 mRNA variant containing a 165-bp deletion in exon 2 (Fig. 6). We named this new isoform variant 5. Our data show that the lens expresses AP2α variants 1, 2, 3, and 5; variant 4 is not expressed in the lens (Figs. 5A and 5B). Variants 1, 2, and 3 are also expressed in the kidney and cerebellum (weak expression was observed in brain and lung). Variant 4 is expressed only in the cerebellum. Besides being expressed in the lens, variant 5 is also expressed in the kidney. Our data also confirmed previous observations by others (Mitchell *et al.*, 1991; Meier *et al.*, 1995; Moser *et al.*, 1995, 1997b) that the AP2α gene is expressed in some selected tissues; no AP2α variant was observed in thymus, spleen, heart, and liver (see Fig. 4).

Nucleotide sequence analysis of the 165-bp deleted in variant 5 indicates the presence of splicing signals in this DNA fragment. The sequences GT and AG, which are present at the 5′- and 3′-end, respectively, of this DNA fragment, are highly conserved in the 5′- and 3′-ends of introns (Balvay *et al.*, 1993). Furthermore, the sequences flanking the 5′- and 3′-ends of this deletion show similarities to the 5′-splice site AG/GT [A/G]AGT and 3′ splice site CAG/G consensus sequence, respectively. In the deleted

Copyright © 1998 by Academic Press. All rights of reproduction in any form reserved.

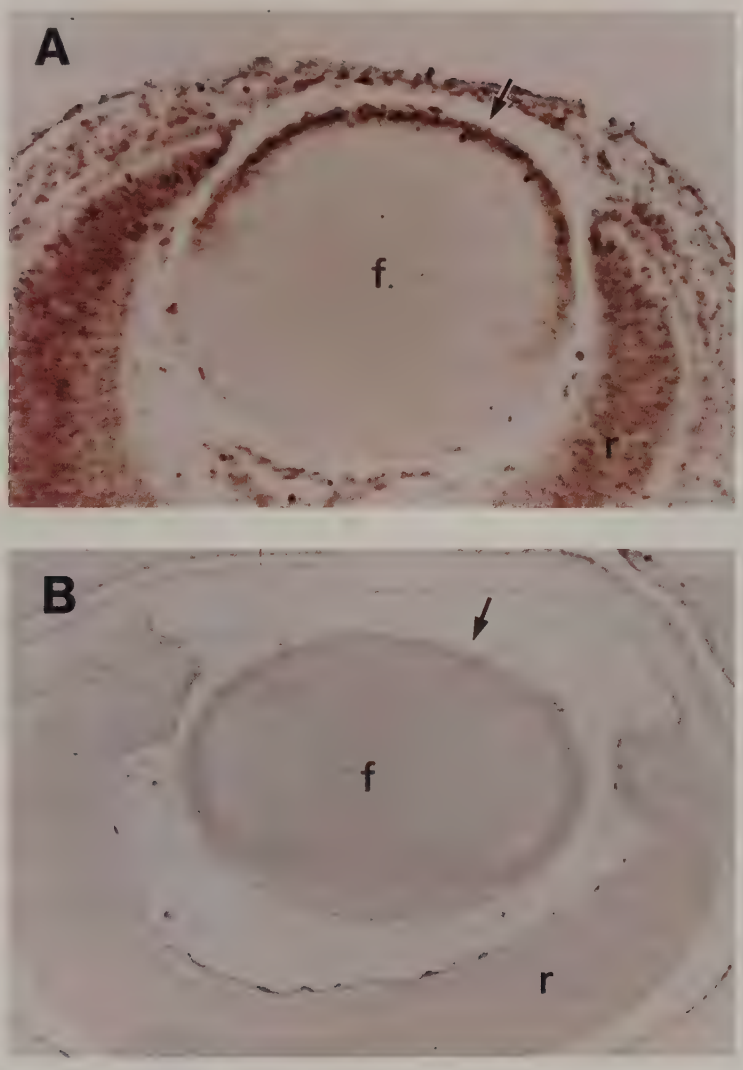

FIG. 3. Localization of AP2α transcripts in the lens by *in situ* PCR. Paraffin head sections of 14-day-old mouse embryo were deparaffinized and fixed as indicated under Materials and Methods. The RT reaction, *in situ* PCR reaction and color development were performed as described under Materials and Methods. (A) *In situ* PCR was performed with amplimers I/J. (B) Negative control without the addition of amplimers I/J to the PCR reaction (similar results were obtained without the incubation with reverse transcriptase in the RT step). f, lens fibers; arrow indicates lens epithelia; r, retina. Magnification, 100×.

sequence there is an adenine positioned 18 nucleotides from the 3′-junction, followed by a pyrimidine-enriched region (Figs. 6 and 7B). This adenine correlates well with the branch point, which is the site of lariat formation, generally found 15 to 40 nucleotides upstream of the 3′-splice site, followed by a stretch of pyrimidines. Thus, the 165-bp deleted in AP2α variant 5 contains the conserved consensus splicing signals characteristic of an intron. Therefore, the 165-bp deletion in variant 5 may be considered an intron, intron 2ab, spliced out by alternative splicing, generating the novel exons 2a and 2b (see Figs. 7A and 7B). The stretch of pyrimidines between the lariat and the 3′-splice site in intron 2ab contains some purine insertions, the 3′-end of exon 2a and the 5′-end of exon 2b differ from the consensus 5′- and 3′-splice signals. As these features probably result in a weaker signal for splicing intron 2ab, retention of this intron to form exon E2 may be the preferred alternative splicing event.

Copyright © 1998 by Academic Press. All rights of reproduction in any form reserved.

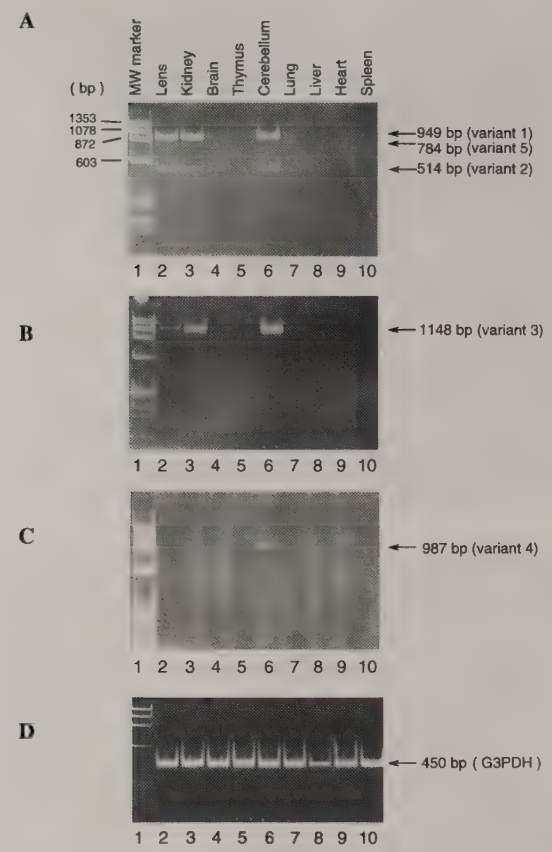

FIG. 4. AP2α isoforms analysis in various tissues by RT-PCR. Polyacrylamide gel electrophoresis of RT-PCR products using poly(A) RNA isolated from various tissues, performed with AP2α variant specific primers. (A) Amplimer A/G (exons 1a and 5); (B) amplimer C/G (exons 1b and 5); (C) amplimer E/G (exons 1c and 5); (D) G3PDH amplimers. Size markers are indicated to the left. Sizes of the expected RT-PCR products for each variant are indicated with an arrow to the right.

The 165-bp in-frame-deletion in variant 5 encodes a proline-rich region 55 amino acids long, part of the AP2α transactivation domain (Fig. 7C) (Williams and Tjian, 1991b). Therefore, variant 5 may function as a repressor.

The AP2β and AP2γ Genes Are Not Expressed in the Lens

Two other members of the AP2 family, AP2β and AP2γ, with an expression pattern different from AP2α, have been isolated (Moser *et al.*, 1995, 1997b; Oulad-Abdelghani *et al.*, 1996). The DNA-binding domain is highly conserved in the three members of the AP2 family but the dimerization and activation domains are less conserved (Oulad-Abdelghani *et al.*, 1996). When we aligned the amino acid sequence encoded by exon 2, we found that the 55 amino acid domain deleted in AP2α variant 5 was highly conserved in the three members of the family (see Fig. 8). Therefore, it was important to determine whether the AP2β and AP2γ genes are also expressed in the lens to contribute to the regulation of gene expression in this tissue. To this end, we performed RT-PCR with primers specific for each gene. AP2β was expressed in the kidney, brain, and cerebellum. APγ was expressed in the brain, cerebellum, and lung as shown by others (Moser *et al.*, 1995, 1997b; Oulad-Abdelghani *et al.*, 1996). However, neither AP2β nor AP2γ was expressed in the lens (Fig. 9).

DISCUSSION

AP2α Gene Expression in the Lens

We report in this study the finding of a novel splicing variant of the AP2α gene in the lens which shows tissue selectivity and which may have implications in regulating gene expression in the lens.

The ocular lens develops from the surface ectoderm by induction of the optic pit in the region of the future forebrain during embryogenesis. After the lens vesicle detaches from the surface ectoderm, epithelial cells in the equatorial zone start differentiating into primary fibers filling the whole lens vesicle. Several lens-specific genes, including crystallins and MIP, start being expressed at this differentiation stage. Transcription factors that interact with promoter elements of several crystallin genes have been characterized, δEF-1 (Funahashi *et al.*, 1993), Sox-2 (Kamachi *et al.*, 1995), several zinc finger proteins (Liu *et*

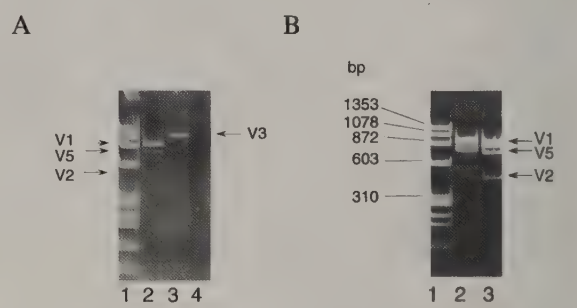

FIG. 5. RT-PCR analysis of AP2α variants expressed in lens. Polyacrylamide gel electrophoresis of PCR products. (A) Lane 1, DNA size marker (ϕX174 *Hae*III digestion fragments). Lens RNA RT-PCR with amplimers A/G (lane 2), C/G (lane 3), and E/G (lane 4). Arrows to the left indicate the PCR products of expected size for variants 1, 5, 2, and 3 with amplimers A/G; arrow to the left indicates variant 3 expected size with amplimer C/G. (B). Lane 1, DNA size marker (ϕX174 *Hae*III digestion fragments). Lens RNA RT-PCR with primers A/G (lane 2) and B/H (lane 3). Arrows to the right indicate variants 1, 5, and 2 expected length with amplimer B/H.

Copyright © 1998 by Academic Press. All rights of reproduction in any form reserved.

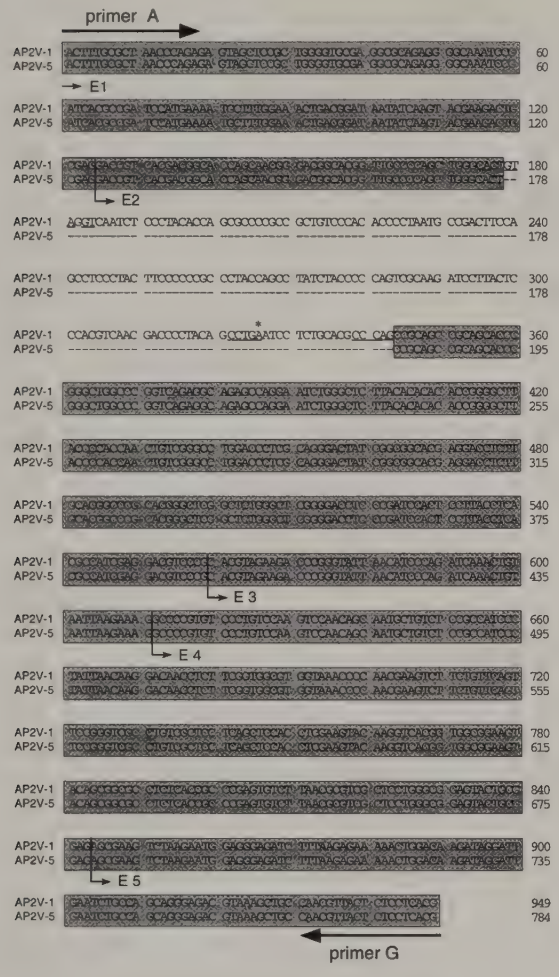

FIG. 6. Nucleotide sequence of AP2α variant 5. Alignment of mouse AP2α variant 1 and variant 5 DNA sequences. Bold arrows indicate the location of primers A and G. Position number 1 corresponds to bp number 23 in AP2α variant 1. Identical sequences are shown in shaded boxes. 5′-end of exons 2 to 5 are indicated with arrows. (—) Nucleotides deleted in variant 5, corresponding to variant 1 nucleotides 178/343 . Splicing signal sequences are underlined. (*)Adenine at the putative branch site of the splicing signal.

al., 1994; Brady *et al.*, 1995), members of the Maf gene family (Ogino and Yasuda, 1998; Sharon-Friling *et al.*, 1998) and Pax6 (Cvekl *et al.*, 1995a,b; Richardson *et al.*, 1995; Sharon-Friling *et al.*, 1998). However, these factors are not lens specific, being also expressed in other tissues. This suggests that interaction of non-lens-specific transcription factors may be important for determining lens-specific gene expression.

We found that the AP2α gene, which is preferentially expressed in some tissues (Mitchell *et al.*, 1991; Meier *et al.*, 1995; Moser *et al.*, 1995, 1997b), is also expressed in the lens and retina. In the lens, AP2α gene expression localizes to the central and equatorial lens epithelia but not to the lens fibers. AP2α pattern of expression in the lens is similar to the one displayed by Pax6 (Richardson *et al.*, 1995). Pax6 is a paired- and homeodomain-containing protein which is considered to be a master control gene for eye development (Halder *et al.*, 1995). The eyes of AP2α-null embryos resemble those of Pax6 mutant embryos in the deep-set optic cups and absence of lenses (Grindley *et al.*, 1995; Schorle *et al.*, 1996; Zhang *et al.*, 1996). However, a lens rudiment was occasionally observed in the AP2α-null embryos, suggesting that temporary inductive contact between the optic epithelium and lens ectoderm had been made (Schorle *et al.*, 1996; Morris-Kay, 1996). Therefore, AP2α may also be involved in regulating early lens differentiation.

AP2α Variants Expressed in the Lens

We found that the transcripts of the AP2α gene in the lens code for two activator forms (variants 1 and 3) and two potential repressor forms (variants 2 and 5). The promoters for variant 1 and 3 are functional in the lens; however, the promoter for variant 4 is not active in the lens and appears to have a more restricted tissue specificity. The whole exon 2 is deleted in variant 2, whereas the transactivation domain is only partially deleted in variant 5. Whether the two different repressor forms are expressed in the same or different lens epithelia cells remains to be elucidated. It is possible that exons 2a and 2b, which contains regions of the transactivation domain may be responsible for interaction with other proteins, different from the ones which interact with variant 2 or variant 3. As a result, variant 5 may regulate target genes differently from variant 2. Different amino acids in the N-terminal region of the transactivation domain of variants 1 and 3 may also modulate the activator activity of these two isoforms.

The Novel AP2α Variant Is Produced by Alternative Splicing

The novel AP2α variant 5 has a 165-bp in-frame deletion within exon 2 which corresponds to a 55 amino acid deletion in the proline-rich transactivation domain. The presence of splicing signals inside this deletion suggests it is an intron spliced out by alternative splicing. mRNA splicing usually involves excision of intron sequences and ligation of the exon sequences. Alternative splicing usually involves skipping exons; however, partial splicing of exons has also been observed in several genes, such as the human caldesmon, the bovine growth hormone, and Pax6 genes (Humphrey *et al.*, 1995; Dirksen *et al.*, 1995; Richardson *et al.*, 1995; Jaworski *et al.*, 1997). Splicing signals inside exons have been characterized in several genes (Conboy *et*

Copyright © 1998 by Academic Press. All rights of reproduction in any form reserved.

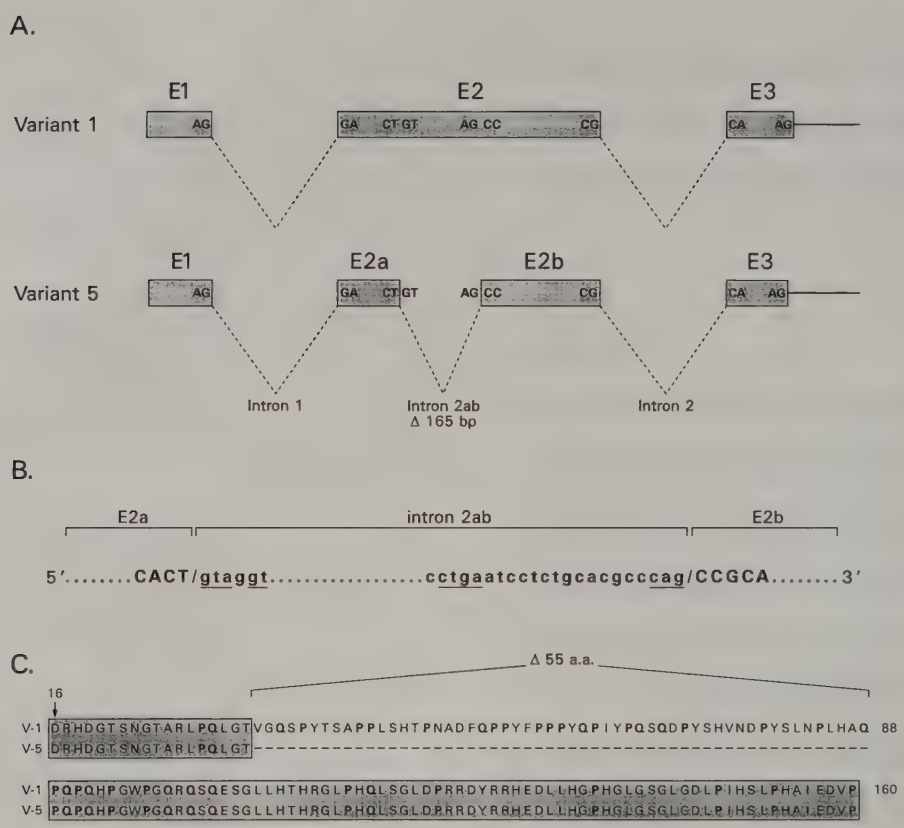

FIG. 7. Variant 5 is produced by alternative splicing. (A) Diagram showing alignment of exons 1 to 3 in variants 1 and 5. 5′- and 3′-end exon sequences are indicated. Sequence at 3′- and 5′-end of the 165-bp deletion in variant 5 exon 2 may be considered a new intron (2ab), which is spliced out in variant 5, creating exons 2a and 2b. Exons are indicated as shaded boxes; introns are indicated with broken lines. (B) Diagram indicate the splicing signals present in intron 2ab, that may be responsible for this alternative splicing event. (C) Comparison of deduced amino acid sequence encoded by AP2α exon 2 between variant 1 and variant 5. Conserved amino acids are shown in shaded boxes. (—) The deleted region in variant 5. Shaded box at the N-terminal side of the deletion corresponds to exon 2a and at the C-terminal side of the deletion corresponds to exon 2b. (P) Prolines and (Q) glutamines present in exon 2 . Numbers refer to the amino acid sequence of AP2α variant 1 (Meier *et al.*, 1995).

al., 1991; Humphrey *et al.*, 1995; Kornblihtt *et al.*, 1996). Tissue- and development-specific RNA splicing results in multiple heterogeneity of the erythroid membrane protein 4.1 (Conboy *et al.*, 1991). Secondary splicing from pre-mRNA is also proposed as a mechanism to create in-frame internal deletions in the transcription factor LSF (Shirra *et al.*, 1994). In these cases, a tissue- or development-specific splicing factor could bind with different affinity to each splice site. Exon-splicing enhancer sequences (ESE) located in downstream exons have been characterized in immunoglobulin, growth hormone, and fibronectin primary transcripts to facilitate splicing of weak splicing signals (Watakabe *et al.*, 1993; Dirksen *et al.*, 1995; Kornblihtt, 1996). Their interaction with *trans*-acting factors may facilitate the splicing process. Additional splicing factor(s) may be required when weak splicing signals are present (Watakabe *et al.*, 1993; Berget, 1995; Kornblihtt *et al.*, 1996). As splicing signals in AP2α intron 2ab shows some deviations from the consensus sequences, it could be considered a weak splicing site. Therefore, ESE may be present in exon E2b or intron 2. As we have observed splicing of intron 2ab in AP2α variant 5 in lens and kidney but not in other tissues, it may very well be that this factor(s) may be selectively expressed in these two tissues. Similarities in gene regulation in lens and kidney have been observed; BMP7 null mutant mice show developmental defects in kidney and lens (Dudley *et al.*, 1995; Luo *et al.*, 1995; Jena *et al.*, 1997). Therefore, the presence of this AP2α splice variant in lens and kidney may be due to the presence of the factor(s) required for this splicing event in these two tissues.

Copyright © 1998 by Academic Press. All rights of reproduction in any form reserved.

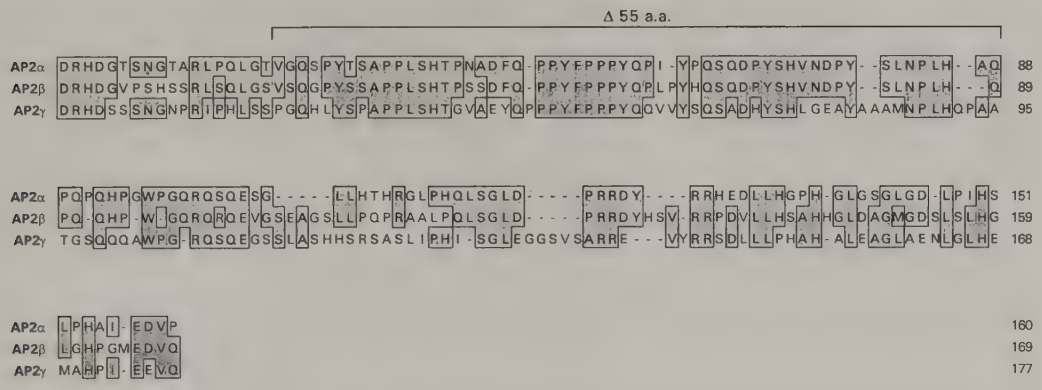

FIG. 8. Exon 2 amino acid sequence encoded by AP2α, AP2β, and AP2γ mouse genes. Conserved amino acids are shown in shaded boxes. Bracket shows amino acids deleted in AP2α variant 5. Δ55 a.a., 55 amino acid deletion in AP2α variant 5. Alignment of mouse AP2α amino acids 16 to 160 (Moser *et al.*, 1993), AP2β amino acids 17 to 169 (Moser *et al.*,1995), and AP2γ amino acids 17 to 177 (Oulad-Abdelghani *et al.*, 1996).

Possible Role of AP2α in Transcriptional Regulation in the Lens

The AP2 family of transcription factors may play a role in regulating apoptosis. AP2α knockout mice show apoptosis of midbrain (Schorle *et al.*, 1996; Zhang *et al.*, 1996) and AP2α may play a role in remodeling of limb buds during chicken embryonic development (Shen *et al.*, 1997). AP2β knockout mice show apoptotic cell death of collecting duct and distal tubular epithelia. AP2α and AP2β repress apoptosis induced by c-*myc*, suggesting that they may play a role in programming cell survival during embryogenesis (Moser *et al.*, 1997a). As loss of cell nuclei during lens fiber differentiation has some characteristics of apoptosis (Bassnett and Mataic, 1997; Zelenka *et al.*, 1997), the absence of AP2α gene expression in the lens fibers may play a role in activation of the denucleation process in the lens fibers.

We observed AP2α expression in the lens equatorial region, where lens epithelia cells withdraw from the cell cycle and start differentiating. AP2α has been shown to inhibit cell cycle progression and activation of an AP2-responsive promoter element of the p21 gene, which encodes a cdk inhibitor, in cancer cells (Zeng *et al.*, 1997). Therefore, AP2α activator variant/s may play a role in withdrawal from the cell cycle by activating transcription of p21 or other cell cycle regulators in the lens (Fromm and Overbeek, 1997; Zelenka *et al.*, 1997).

Putative AP2-binding sites are present in the promoter region of several lens-specific crystallin genes (Piatigorsky and Zelenka, 1992). Therefore, AP2α activator variants may activate expression of genes expressed in lens epithelia whereas repressor variants may repress expression in epithelia of genes specifically expressed in the lens fibers (i.e., γ-crystallins and MIP).

We previously characterized a promoter element of the human MIP gene containing overlapping binding sites for

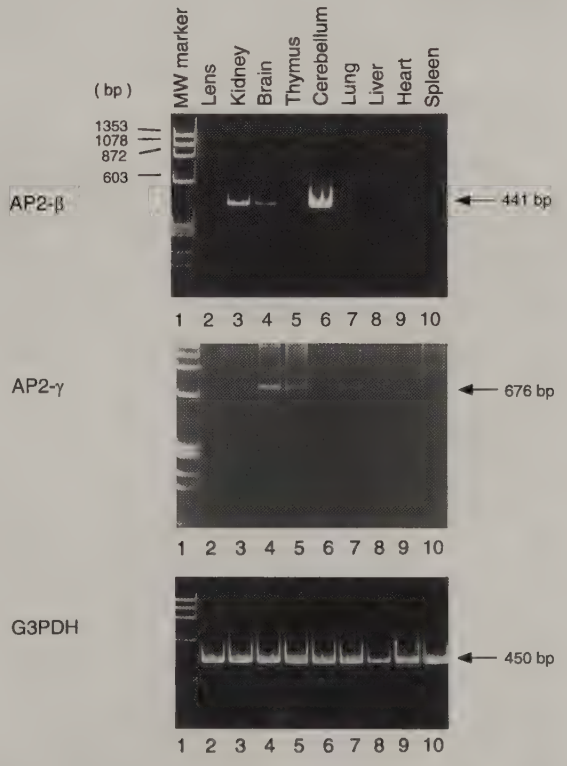

FIG. 9. Analysis of AP2β and AP2γ gene expression in various mouse tissues. Poly(A) RNA isolated from various mouse tissues were used for RT-PCR with specific primers of AP2β, AP2γ, and G3PDH as indicated under Materials and Methods. Polyacrylamide gel electrophoresis of PCR products of AP2β (top), AP2γ (middle), and G3PDH as a positive control (bottom). Lane 1, DNA size markers; lanes 2 to 10, RT-PCR with RNA from tissues indicated above the top panel. Arrows to the right indicate the expected size for the RT-PCR product with each amplimer.

Copyright © 1998 by Academic Press. All rights of reproduction in any form reserved

the transcription factors Sp1 and AP2α (Ohtaka-Maruyama *et al.*, 1998). This regulatory element is conserved in the human and mouse MIP gene (Ohtaka-Maruyama and Chepelinsky, unpublished). As the MIP gene is specifically expressed in the lens fibers, AP2α variants 2 and 5 may function as repressors of MIP expression in lens epithelia. However, as we found AP2α expression in the lens equatorial region where lens cells begin differentiating, AP2α variants 1 and 3 may be involved in activating MIP transcription, if expressed in those cells. Therefore, it will be important to determine which activator and repressor AP2α variants are expressed in the central lens epithelia and in the equatorial region and whether activator and repressor AP2α variants are coexpressed in the same cell or in different lens cells.

Further studies will allow us to elucidate whether AP2α variant 5 functions as a repressor by interacting with the AP2-binding regulatory element, through its DNA-binding domain, but unable to interact with coactivators or as a modulator by having a different protein–protein interaction domain or different affinity with coactivator/s.

ACKNOWLEDGMENTS

We thank Dr. Graeme Wistow for stimulating discussions and the critical reading of the manuscript, Dr. Hiroshi Sasaki for technical advice on *in situ* hybridization, Dr. Pamela Mitchell for the plasmid pB240, and Nicole Neuman for preparing the paraffin sections. This work was supported in part by grants to F. H. and C.O.-M. from the Ministry of Education, Science, Sports and Culture of Japan and a special grant for the promotion of Research from the Institute of Physical and Chemical Research (RIKEN) and the RIKEN Biodesign Research Program to C.O.-M., who is presently a special postdoctoral researcher at RIKEN.

REFERENCES

Balvay, L., Libri, D. and Fiszman, M. Y. (1993). Pre-mRNA secondary structure and the regulation of splicing. *BioEssays* **15,** 165–169.

Bassnett, S., and Mataic, D. (1997). Chromatin degradation in differentiating fiber cells of the eye lens. *J. Cell Biol.* **137,** 37–49.

Bauer, R., Imhof, A., Pscherer, A., Kopp, H., Moser, M., Seegers, S., Kerscher, M., Tainsky, M. A., Hofstaedter, F., and Buettner, R. (1994). The genomic structure of the human AP-2 transcription factor. *Nucleic Acids Res.* **22,** 1413–1420.

Berget, S. M. (1995). Exon recognition in vertebrate splicing. *J. Biol. Chem.* **270,** 2411–2414.

Brady, J. P., Kantorow, M., Sax, C. M., Donovan, D. M., and Piatigorsky, J. (1995). Murine transcription factor alpha A-crystallin binding protein I: Complete sequence, gene structure, expression, and functional inhibition via antisense RNA. *J. Biol. Chem.* **270,** 1221–1229.

Buettner, R., Kannan, P., Imhof, A., Bauer, R., Yim, S. O., Glockshuber, R., Vandyke, M. W., and Tainsky, M. (1993). An alternatively spliced mRNA from the AP-2 gene encodes a negative regulator of transcriptional activation by AP-2. *Mol. Cell. Biol.* **13,** 4174–4185.

Byrne, C., Tainsky, M., and Fuchs E. (1994). Programming gene expression in developing epidermis. *Development* **120,** 2369–2383.

Conboy, J. G., Chan, J. Y., Chasis, J. A., Kan, Y. W., and Mohandas, N. (1991). Tissue- and development-specific alternative RNA splicing regulates expression of multiple isoforms of erythroid membrane protein 4.1. *J. Biol. Chem.* **266,** 8273–8280.

Cvekl, A., Kashanchi, F., Sax, C. M., Brady, J. N., and Piatigorsky, J. (1995a). Transcriptional regulation of the mouse alpha A-crystallin gene: Activation dependent on a cyclic AMP-responsive element (DE1/CRE) and a Pax-6-binding site. *Mol. Cell. Biol.* **15,** 653–660.

Cvekl, A., Sax, C. M., Li, X., McDermott, J. B., and Piatigorsky, J. (1995b). Pax-6 and lens-specific transcription of the chicken delta 1-crystallin gene. *Proc. Natl. Acad. Sci. USA* **92,** 4681–4685.

Dirksen, W. P., Sun, Q., and Rottman, F. M. (1995). Multiple splicing signals control alternative intron retention of bovine growth hormone pre-mRNA. *J. Biol. Chem.* **270,** 5346–5352.

Dudley, A. T., Lyons, K. M., and Robertson, E. J. (1995). A requirement for bone morphogenetic protein-7 during development of the mammalian kidney and eye. *Genes Dev.* **9,** 2795–2807.

Fromm, L., and Overbeek, P. A. (1997). Inhibition of cell death by lens-specific overexpression of bcl-2 in transgenic mice. *Dev. Genet.* **20,** 276–287.

Funahashi, J., Sekido, R., Murai, K., Kamachi, Y., and Kondoh, H. (1993). Delta-crystallin enhancer binding protein delta EF1 is a zinc finger-homeodomain protein implicated in postgastrulation embryogenesis. *Development* **119,** 433–446.

Grindley, J. C., Davidson, D. R., and Hill, R. E. (1995). The role of Pax-6 in eye and nasal development. *Development* **121,** 1433–1442.

Grove, M., and Plumb, M. (1993). C/EBP, NF-kappa B, and c-Ets family members and transcriptional regulation of the cell-specific and inducible macrophage inflammatory protein 1 alpha immediate-early gene. *Mol. Cell. Biol.* **13,** 5276–5289.

Halder, G., Callaerts, P., and Gehring, W. J. (1995). Induction of ectopic eyes by targeted expression of the *eyeless* gene in *Drosophila*. *Science* **267,** 1788–1792.

Ho, I.-C., Hodge, M. R., Rooney, J. W., and Glimcher, L. H. (1996). The proto-oncogene *c-maf* is responsible for tissue-specific expression of interleukin-4. *Cell* **85,** 973–983.

Humphrey, M. B., Bryan, J., Cooper, T. A., and Berget, S. M. (1995). A 32-nucleotide exon-splicing enhancer regulates usage of competing 5′ splice sites in a differential internal exon. *Mol. Cell. Biol.* **15,** 3979–3988.

Jaworski, C., Sperbeck, S., Graham, C., and Wistow, G. (1997). Alternative splicing of *Pax6* in bovine eye and evolutionary conservation of intron sequences. *Biochem. Biophys. Res. Commun.* **240,** 196–202.

Jena, N., Martin-Seisdedos, C., McCue, P., and Croce, C. M. (1997). BMP7 null mutant in mice: developmental defects in skeleton, kidneys, and eye. *Exp. Cell Res.* **230,** 28–37.

Kamachi, Y., Sockanathan, S., Liu, Q., Breitman, M., Lovell, B. R., and Kondoh, H. (1995). Involvement of SOX proteins in lens-specific activation of crystallin genes. *EMBO J.* **14,** 3510–3519.

Kingsley, C., and Winoto, A. (1992). Cloning of GT box-binding proteins: a novel Sp1 multigene family regulating T-cell receptor gene expression. *Mol. Cell. Biol.* **12,** 4251–4261.

Kornblihtt, A. R., Pesce, C. G., Alonso, C. R., Cramer, P., Srebrow, A., Werbajh, S., and Muro, A. F. (1996). The fibronectin gene as a model for splicing and transcription studies. *FASEB J.* **10,** 248–257.

Copyright © 1998 by Academic Press. All rights of reproduction in any form reserved.

Leask, A., Byrne C., and Fuchs, E. (1991). Transcription factor AP2 and its role in epidermal-specific gene expression. *Proc. Natl. Acad. Sci. USA* **88,** 7948–7952.

Liu, Q., Shalaby, F., Puri, M. C., Tang, S., and Breitman, M. L. (1994). Novel zinc finger proteins that interact with the mouse gamma F-crystallin promoter and are expressed in the sclerotome during early somitogenesis. *Dev. Biol.* **165,** 165–177.

Luo, G., Hofman, C., Bronckers, A. L. J. J., Sohocki, M., Bradley, A., and Karsenty G. (1995). BMP-7 is an inducer of nephrogenesis, and is also required for eye development and skeletal patterning. *Genes Dev.***9,** 2808–2820.

Luscher, B., Mitchell, P. J., Williams, T., and Tjian, R. (1989). Regulation of transcription factor AP-2 by the morphogen retinoic acid and by second messengers. *Genes Dev.* **3,** 1507–1517.

Meier, P., Koedood, M., Philipp, J., Fontana, A., and Mitchell, P. J. (1995). Alternative mRNAs encode multiple isoforms of transcription factor AP-2 during murine embryogenesis. *Dev. Biol.* **169,** 1–14.

Mendel, D. B., and Crabtree, G. R. (1991). HNF-1, a member of a novel class of dimerizing homeodomain proteins. *J. Biol. Chem.* **266,** 677–680.

Mitchell, P. J., Timmons, P. M., Hebert, J. M., Rigby, P. W. J., and Tjian, R. (1991). Transcription factor AP-2 is expressed in neural crest lineages during mouse embryogenesis. *Genes Dev.* **5,** 105–119.

Morris-Kay, G. M. (1996). Craniofacial defects in AP-2 null mutant mice. *BioEssays* **18,** 785–788.

Moser, M., Pscherer, A., Bauer, R., Imhof, A., Seegers, S., Kerscher, M., and Buettner, R. (1993). The complete murine cDNA sequence of the transcription factor AP-2. *Nucleic Acids Res.* **21,** 4844.

Moser, M., Imhof, A., Pscherer, A., Bauer, R., Amselgruber, W., Sinowats, F., Hofstadter, F., Shule, R., and Buettner, R. (1995). Cloning and characterization of a second AP-2 transcription Factor: AP-2β. *Development* **121,** 2779–2788.

Moser, M., Pscherer, A., Roth, C., Becker, J., Nucher, G., Zerres, K., Dixkens, C., Weis, J., Guay-Woodford, L., Buettner, R., and Fassler, R. (1997a). Enhanced apoptotic cell death of renal epithelial cells in mice lacking transcription factor AP-2β. *Genes Dev.* **11,** 1938–1948.

Moser, M., Ruschoff, J., and Buettner, R. (1997b). Comparative analysis of AP-2α and AP-2β gene expression during murine embryogenesis. *Dev. Dynam.* **208,** 115–124.

Ogino, H., and Yasuda, K. (1998). Induction of lens differentiation by activation of a bZIP transcription factor, L-Maf. *Science* **280,** 115–118.

Ohtaka-Maruyama, C., Wang, X., Ge, H., and Chepelinsky, A. B. (1998). Overlapping Sp1 and AP2 binding sites in a promoter element of the lens specific MIP gene. *Nucleic Acids Res.* **26,** 407–414.

Oulad-Abdelghani, M., Bouillet, P., Chazaud, C., Dolle, P., and Chambon, P. (1996). AP-2.2: A novel AP-2-related transcription factor induced by retinoic acid during differentiation of P19 embryonal carcinoma cells. *Exp. Cell Res.* **225,** 338–347.

Oyake, T., Itoh, K., Motohashi, H., Hayashi, N., Hoshino, H., Nishizawa, M., Yamamoto, M., and Igarashi, K. (1996). Bach proteins belong to a novel family of BTB-basic leucine zipper transcription factors that interact with MafK and regulate transcription through the NF-E2 site. *Mol. Cell. Biol.* **16,** 6083–6095.

Piatigorsky, J., and Zelenka, P. S. (1992). Transcriptional regulation of crystallin genes: *cis* elements, *trans*-factors, and signal transduction system in the lens. *Adv . Dev. Biochem.* **1,** 211–256.

Richardson, J., Cvekl, A., and Wistow, G. (1995). Pax-6 is essential for lens-specific expression of zeta-crystallin. *Proc. Natl. Acad. Sci. USA* **92,** 4676–4680.

Schorle, H., Meier, P., Buchert, M., Jaenisch, R., and Mitchell, P. J. (1996). Transcription factor AP-2 essential for cranial closure and craniofacial development. *Nature* **381,** 235–238.

Sharon-Friling, R., Richardson, J., Sperbeck, S., Lee, D., Rauchman, M., Maas, R., Swaroop, A., and Wistow, G. (1998). Lens-specific recruitment of zeta-crystallin through Pax6, Nrl-Maf, and brain suppressor sites. *Mol. Cell. Biol.* **18,** 2067–2076.

Shen, H., Wilke, T., Ashique, A. M., Narvey, M., Zerucha, T., Savino, E., Williams, T., and Richman, J. M. (1997) Chicken transcription factor AP-2: Cloning, expression and its role in outgrowth of facial prominences and limb buds. *Dev. Biol.* **188,** 248–266.

Shirra, M. K., Zhu, Q., Huang, H. C., Pallas, D., and Hansen, U. (1994). One exon of the human LSF gene includes conserved regions involved in novel DNA-binding and dimerization motifs. *Mol. Cell. Biol.* **14,** 5076–5087.

Skerjanc, I. S., Truong, J., Filion, P., and McBurney, M. W. (1996). A splice variant of the ITF-2 transcript encodes a transcription factor that inhibits MyoD activity. *J. Biol. Chem.* **271,** 3555–3561.

Snape, A. M., Winning, R., and Sargent, T. D. (1991). Transcription factor AP-2 is tissue-specific in *Xenopus* and is closely related or identical to keratin transcription factor 1 (KTF-1). *Development* **113,** 283–293.

Watakabe, A., Tanaka, K., and Shimura, Y. (1993). The role of exon sequences in splice site selection. *Genes Dev.* **7,** 407–418.

Williams, T., Admon, A., Luscher, B., and Tjian, R. (1988). Cloning and expression of AP-2, a cell-type-specific transcription factor that activates inducible enhancer elements. *Genes Dev.* **2,** 1557–1569.

Williams, T., and Tjian, R. (1991a). Characterization of a dimerization motif in AP-2 and its function in heterologous DNA-binding proteins. *Science* **251,** 1067–1071.

Williams, T., and Tjian, R. (1991b). Analysis of the DNA-binding and activation properties of the human transcription factor AP-2. *Genes Dev.* **5,** 670–682.

Winning, R. S., Shea, L. J., Marcus, S. J., and Sargent, T. D. (1991). Developmental regulation of transcription factor AP-2 during *Xenopus laevis* embryogenesis. *Nucleic Acids Res.* **19,** 3709–3714.

Zelenka, P. S., Gao, C-Y., Rampalli, A., Arora, J., Chauthaiwale, V., and He, H-Y. (1997). Cell cycle regulation in the lens: Proliferation, quiescence, apoptosis and differentiation. *Prog. Ret. Eye Res.* **16,** 303–322.

Zeng, Y-X., Somasundaram, K., and El-Deiry, W. S. (1997). AP2 inhibits cancer cell growth and activates $p21^{WAF1/CIP1}$ expression. *Nature Genet.* **15,** 78–82.

Zhang, D., Hetherington, C. J., Tan, S., Dziennis, S. E., Gonzalez, D. A., Chen, H., and Tenen, D. G. (1994). Sp1 is a critical factor for the monocyte specific expression of human CD14. *J. Biol. Chem.* **269,** 11425–11434.

Zhang, J., Hagopian-Donaldson, S., Serbedzija, G., Elsemore, J., Plehn-Dujowich, D., McMahon, A. P., Flavell, R. A., and Williams, T. (1996). Neural tube, skeletal and body wall defects in mice lacking transcription factor AP-2. *Nature* **381,** 238–241.

Received for publication April 9, 1998
Accepted June 18, 1998

Copyright © 1998 by Academic Press. All rights of reproduction in any form reserved.

DEVELOPMENTAL BIOLOGY 202, 136–151 (1998)
ARTICLE NO. DB988980

Identification of Gametophytic Mutations Affecting Female Gametophyte Development in *Arabidopsis*

Cory A. Christensen, Santhi Subramanian, and Gary N. Drews[1]
Department of Biology, University of Utah, 257 South 1400 E, Salt Lake City, Utah 84112-0840

The female gametophyte (embryo sac or megagametophyte) plays a critical role in sexual reproduction of angiosperms. It is the structure that produces the egg cell and central cell which, following fertilization, give rise to the seed's embryo and endosperm, respectively. In addition, the female gametophyte mediates a host of reproductive processes including pollen tube guidance, fertilization, and the induction of seed development. Several major events occur during megagametogenesis, including syncitial nuclear divisions, cellularization, nuclear migration and fusion, and cell death. While these events have been described morphologically, the molecules regulating them in the female gametophyte are largely unknown. We discuss a genetic screen based on reduced seed set and segregation distortion to identify mutations affecting megagametogenesis and female gametophyte function. We report on the isolation of four mutants (*fem1, fem2, fem3,* and *fem4*) and show that the four mutations map to different locations within the genome. Additionally, we show that the *fem1* and *fem2* mutations affect only the female gametophyte, while the *fem3* and *fem4* mutations affect both the female and male gametophyte. We analyzed female gametophyte development in these four mutants as well as in the *gfa2, gfa3, gfa4, gfa5,* and *gfa7* mutants. We found that the *fem2, fem3, gfa4,* and *gfa5* mutants abort development at the one-nucleate stage, while the *fem1, fem4, gfa2, gfa3,* and *gfa7* mutants are affected in processes later in development such as polar nuclei fusion and cellularization. The establishment of a genetic screen to identify mutants and the development of a rapid procedure for analyzing mutant phenotypes represent a first step in the isolation of molecules that regulate female gametophyte development and function. © 1998 Academic Press

Key Words: **female gametophyte development; *Arabidopsis;* nuclear fusion; cellularization; plant reproduction; embryo sac.**

INTRODUCTION

Plants have a two-staged life cycle in which a haploid gametophyte generation alternates with a diploid sporophyte generation. Angiosperms are heterosporous and have male and female gametophytes. The male gametophyte (pollen grain) develops within the stamen's anther and consists of two sperm cells encased within a vegetative cell. The female gametophyte (embryo sac or megagametophyte) develops within the carpel's ovary and exhibits a variety of forms. The most common form, which is found in approximately 70% of the species examined, is referred to as the *Polygonum* type (Maheshwari, 1950; Willemse and van Went, 1984; Reiser and Fischer, 1993). As shown in Fig. 1, the *Polygonum*-type female gametophyte is a seven-cell structure consisting of one egg cell, two synergid cells, three antipodal cells, and one central cell.

The female gametophyte plays a central role in sexual reproduction in angiosperms. During sexual reproduction, the male gametophyte is transferred from the anther to the carpel's stigma, where it forms a pollen tube that grows through the carpel to deliver its two sperm cells to the female gametophyte. Following fertilization, the female gametophyte's egg cell and central cell give rise to the seed's embryo and endosperm, respectively. The female gametophyte plays a role in several steps of this reproductive processes including pollen tube guidance (Hulskamp *et al.*, 1995; Ray *et al.*, 1997), fertilization (van Went and Willemse, 1984; Russell, 1993), the induction of seed development (Ohad *et al.*, 1996; Chaudhury *et al.*, 1997), and gametophytic maternal control (Ray, 1997; Drews *et al.*, 1998).

Female gametophyte development consists of two phases referred to as megasporogenesis and megagametogenesis.

[1] To whom correspondence should be addressed. Fax: (801) 581-4668. E-mail: drews@bioscience.utah.edu.

0012-1606/98 $25.00
Copyright © 1998 by Academic Press
All rights of reproduction in any form reserved.

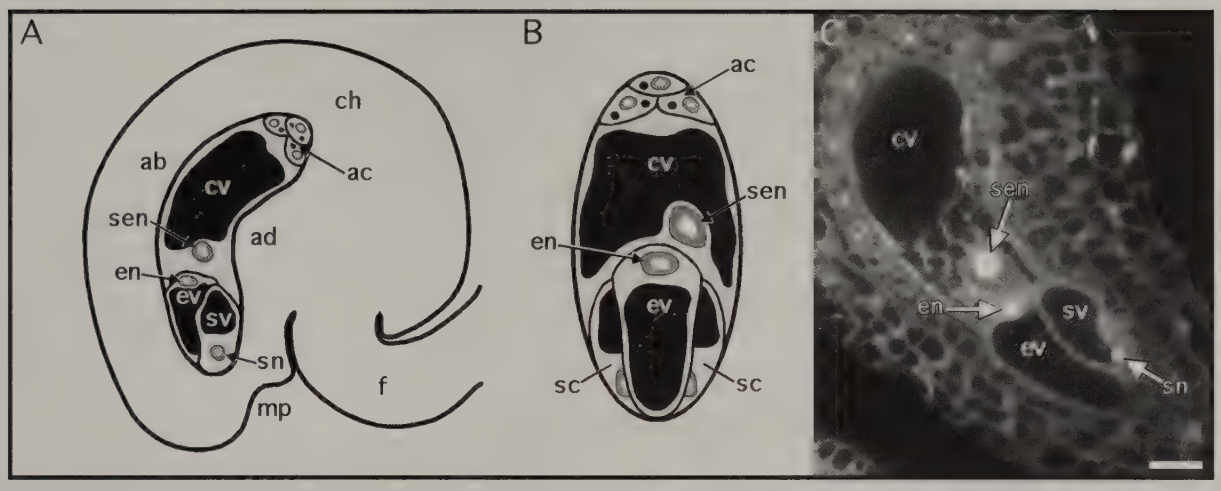

FIG. 1. The *Arabidopsis* female gametophyte. (A,B) Depictions of a wild-type female gametophyte at the seven-cell stage (stage FG6). Depicted are cytoplasm (light gray areas), vacuoles (black areas), nuclei (dark gray areas), and nucleoli (white areas within the nuclei). The female gametophyte in A is shown in longitudinal view; it is oriented with its adaxial surface (adjacent to the funiculus; ad) to the right, its abaxial surface (opposite the funiculus; ab) to the left. The female gametophyte in B is viewed from the abaxial direction. (C) CLSM image of a wild-type female gametophyte at the terminal stage (stage FG7). The second synergid cell was present but not included in this image. This image consists of a single 1.5-μm optical section. All female gametophytes are oriented with their chalazal poles up and their micropylar poles down. Abbreviations: ab, abaxial surface; ac, antipodal cells; ad, adaxial surface; ch, chalazal pole; cv, central cell vacuole; en, egg cell nucleus; ev, egg cell vacuole; f, funiculus; mp, micropylar pole; sen, secondary endosperm nucleus; sn, synergid cell nucleus; sv, synergid cell vacuole. Scale bar, 10 μm.

During megasporogenesis, a diploid megaspore mother cell undergoes meiosis and gives rise to four haploid megaspores, three of which undergo cell death. During megagametogenesis, the surviving megaspore undergoes three rounds of mitosis without cytokinesis, producing an eight-nucleate cell. Nuclear migrations, nuclear fusion, and cellularization then result in the seven-cell structure depicted in Fig. 1.

Little is known about the haploid-expressed genes that regulate and mediate the major events in megagametogenesis (mitosis, polarity establishment, nuclear migration, nuclear fusion, cellularization, and cell specification) and female gametophyte function (pollen tube guidance, fertilization, induction of seed development, and gametophytic maternal control). A number of female gametophyte mutants have been identified in both *Arabidopsis* (Redei, 1965; Castle *et al.*, 1993; Kieber *et al.*, 1993; Niyogi *et al.*, 1993; Springer *et al.*, 1995; Moore *et al.*, 1997) and maize (Singleton and Mangelsdorf, 1940; Nelson and Clary, 1952; Kermicle, 1971), indicating a requirement for haploid-expressed genes in megagametogenesis and female gametophyte function (Drews *et al.*, 1998). However, a specific function is known only for the *PRL* gene, which encodes a protein required in DNA replication and cell division (Springer *et al.*, 1995).

We have been using *Arabidopsis* as a system to identify and study haploid-expressed genes regulating and mediating female gametophyte development and function. Extensive descriptive studies of *Arabidopsis* female gametophyte structure and development have been carried out and have shown that *Arabidopsis* has a *Polygonum*-type female gametophyte (Misra, 1962; Poliakova, 1964; Webb and Gunning, 1990; Mansfield and Briarty, 1991; Mansfield *et al.*, 1991; Murgia *et al.*, 1993; Webb and Gunning, 1994; Schneitz *et al.*, 1995; Christensen *et al.*, 1997). Phenotypic analysis of female gametophyte mutants in *Arabidopsis* is facilitated by the fact that an *Arabidopsis* pistil contains a large number of ovules (50 to 60) and that the female gametophytes within these ovules develop synchronously (Christensen *et al.*, 1997). Additionally, confocal laser scanning microscopy procedures have been developed that allow for the rapid characterization of mutant phenotypes, making large-scale genetic screens practical (Christensen *et al.*, 1997).

In this paper we describe a procedure to identify female gametophyte mutants and report the isolation of four mutants, *female gametophyte1* (*fem1*), *fem2*, *fem3*, and *fem4*. We show that all of the *fem* mutations exhibit reduced transmission through the female gametophyte and that the *fem3* and *fem4* mutations also affect the male gametophyte. We also report the phenotypic characterization of these four mutants, as well as the *gfa2*, *gfa3*, *gfa4*, *gfa5*, and *gfa7* mutants (Feldmann *et al.*, 1997).

Copyright © 1998 by Academic Press. All rights of reproduction in any form reserved

MATERIALS AND METHODS

Plant growth and kanamycin selection. Plant growth conditions and kanamycin selection (50 μg/ml) were performed as previously described (Christensen *et al.*, 1997; Feldmann *et al.*, 1997).

Mutant isolation. The *fem1* mutant was isolated in a screen of ethyl methanesulfonate (EMS)-mutagenized lines. Landsberg *erecta* seed was soaked in 0.1% EMS for 14 h, washed for 3 h in water, and then sown. On each of 1000 M1 plants, the M2 seed from a single silique was collected. Five M2 seeds from each M1 silique were planted and grown until at least 15 flowers had been self-pollinated. With each M2 plant, at least three siliques were cut open and scored for the 50% desiccated ovules phenotype. The *fem1* mutant was backcrossed five generations before genetic and morphological analysis was carried out.

The *fem2*, *fem3*, and *fem4* mutants were isolated in a screen of T-DNA-mutagenized lines as described under Results. The *fem2* and *fem3* mutants were isolated from lines generated by Ken Feldmann and obtained from the *Arabidopsis* Biological Resource Center in pools of 20. For these lines, we screened an average of 53 plants in each of 57 pools (pools CS2361–CS2365, CS2461–CS2494, CS2497–CS2501, CS2505, CS2507, CS2509–CS2515, CS2520, CS2522, CS2523, and CS2534). We isolated *fem4* from a screen of 195 lines generated and provided by Tom Jack.

Genetic mapping. We used simple sequence length polymorphisms (Bell and Ecker, 1994) and cleaved amplified polymorphic sequences (Konieczny and Ausubel, 1993) to map the mutations within the *Arabidopsis* genome. *fem1*, in the Landsberg *erecta* background, and *fem2* and *fem3*, in the Wassilewskija (Ws) background, were crossed to Columbia (Col) ecotype females. *fem4* in the Col background was crossed to a Ws female. For the *fem2*, *fem3* and *fem4* mutants, one KanR F1 plant from each cross was selected and again crossed to a Col female (*fem2* and *fem3*) or a Ws female (*fem4*). For the *fem1* mutant one F1 plant exhibiting the 50% desiccated ovules phenotype was selected and again crossed to a Col female. In all cases, the progeny resulting from the second cross constituted our mapping population.

DNA was extracted from either KanR plants (*fem2*, *fem3*, and *fem4*) or plants exhibiting the 50% seed set phenotype (*fem1*) in the mapping populations as described by Murray and Thompson (1980). Twenty-microliter polymerase chain reaction (PCR) reactions were done using 1.6 μl of template (concentration not determined), 10 pmol of each primer (Research Genetics, Huntsville, AL), 4 μmol each dNTP, 30 μmol $MgCl_2$, 0.5–1 unit of Biolase polymerase (ISC BioExpress, Kaysville, UT), 1× Biolase reaction buffer (ISC BioExpress), and either 1× tartrazine/Ficoll or 1× sucrose/creosol red (Idaho Technologies, Idaho Falls, ID). PCR cycling parameters were an initial denaturation step at 94°C for 4 min and then 40 cycles of denaturation at 94°C for 15 s, annealing at 55°C for 15 s, extension at 72°C for 30 s, and then a final extension at 72°C for 4 min on an MJ Research, Inc., PTC-100 Programmable Thermal Controller.

At least 52 individuals from each mapping population were tested against each marker for linkage. In all cases, the most closely linked markers had recombination frequencies that were significantly different than 0.5 by χ^2 analysis ($P < 0.025$). Recombination frequencies were calculated and converted to genetic map distances according to Koornneef and Stam (1992) and Kosambi (1944). *fem1* mapped between nga76 and LFY3 on chromosome 5. *fem1* and nga76 had a recombination frequency of 33.3 ± 7.8 (map distance = 40.2 cM, $n = 54$) and *fem1* and LFY3 had a recombination frequency of 25.0 ± 6.0 (map distance = 27.5 cM, $n = 52$). *fem2* and nga8 on the top of chromosome 2 had a recombination frequency of 9.6 ± 4.1 (map distance = 9.7 cM, $n = 52$). *fem3* and nga280 on chromosome 1 showed no recombination (LOD score = 16.3, $n = 54$). Finally, *fem4* mapped between nga280 and AthATPASE on chromosome 1. *fem4* and nga280 had a recombination frequency of 33.3 ± 7.8 (map distance = 40.2 cM, $n = 54$) and *fem4* and AthATPASE had a recombination frequency of 24.1 ± 5.8 (map distance = 26.3 cM, $n = 54$).

Confocal laser scanning microscopy. Tissue preparation, microscopy, image capture, and figure preparation were performed as previously described (Christensen *et al.*, 1997) with the following modifications. For female gametophyte analysis, carpel walls were separated from the septum prior to fixation by slicing along both sides of the pistil's replum with a 30-gauge syringe needle. After clearing, each placenta was dissected by removing the pedicel, style, and carpel walls. For male gametophyte analysis, anthers were fixed just prior to dehiscence and whole mounted.

Assignment of a female gametophyte stage to a pistil. We previously showed that female gametophyte development within a pistil is fairly synchronous (Christensen *et al.*, 1997). In most cases, a single female gametophyte stage predominates (≥75%) within a pistil. Under this circumstance, we assign one female gametophyte stage to a pistil. In some cases, a single stage does not predominate because the pistil is at a transition between two stages. Under this circumstance, we assign the pistil the two stages that together constitute ≥75% of the female gametophytes.

Reciprocal crosses. To prevent the possibility of inadvertent self-pollination or cross-contamination, single female parents were isolated in 2-liter soda bottles, all flowers on the primary inflorescence were emasculated daily before dehiscence and pollinated the following day, and secondary inflorescences were removed. In crosses between mutant males and wild-type females, the female parent was *male sterile1-1* (van der Veen and Wirtz, 1968).

RESULTS

Isolation of Female Gametophyte Mutants

We screened for lines containing female gametophyte lethal mutations. Our screen consisted of two steps. As a primary screen, we opened siliques and screened for plants with reduced seed set. On a plant heterozygous for a female gametophyte mutation, about 50% of its female gametophytes are wild type and functional, and approximately 50% are mutant and nonfunctional. Following fertilization, functional ovules develop into seeds. By contrast, ovules harboring defective female gametophytes fail to undergo seed development and desiccate instead. Thus, siliques from heterozygous female gametophyte mutants contain approximately 50% normal seeds and 50% desiccated ovules.

The secondary screen was based on the concept that female gametophyte mutants exhibit altered segregation patterns. For example, self-pollination of a heterozygous female gametophyte mutant produces heterozygous and wild-type progeny in a 1:1 ratio (if the mutation is fully penetrant and does not affect the male gametophyte). The lines we screened were mutagenized with a T-DNA containing the chimeric *nptII* gene which confers kanamycin resistance (Feldmann *et al.*, 1997). Thus, self-pollination of

Copyright © 1998 by Academic Press. All rights of reproduction in any form reserved.

TABLE 1
Mutants Discussed in This Paper

Mutant	Isolate no.	Mutagen	Mutant class[a]	Source
female gametophyte1 (fem1)	864	EMS	FGS	This paper
female gametophyte2 (fem2)	2462-5	T-DNA	FGS	This paper
female gametophyte3 (fem3)	2465-35	T-DNA	GG	This paper
female gametophyte4 (fem4)	TJ160	T-DNA	GG	This paper
gametophytic factor2 (gfa2)	102	T-DNA	GG	(Feldmann *et al.*, 1997)
gametophytic factor3 (gfa3)	13	T-DNA	GG	(Feldmann *et al.*, 1997)
gametophytic factor4 (gfa4)	84	T-DNA	GG	(Feldmann *et al.*, 1997)
gametophytic factor5 (gfa5)	114	T-DNA	GG	(Feldmann *et al.*, 1997)
gametophytic factor7 (gfa7)	21	T-DNA	GG	(Feldmann *et al.*, 1997)

[a] FGS, female gametophyte-specific; GG, general gametophytic.

a heterozygous female gametophyte mutant produces kanamycin resistant (KanR) and kanamycin sensitive (KanS) progeny in a 1:1 ratio (if the mutation is fully penetrant and does not affect the male gametophyte). By contrast, self-pollination of a heterozygous sporophytic mutant (e.g., a mutant defective in flower development) produces KanR and KanS progeny in a 3:1 ratio.

All potential mutants identified in the primary screen were allowed to self-pollinate, 100–200 progeny seeds were germinated in the presence of Kan, and Kan resistance ratios (KanR/KanS) were scored. Although we were primarily interested in lines in which KanR/KanS was 1.0, we also examined lines in which KanR/KanS was slightly higher or lower than 1.0 because, as discussed below, female gametophyte mutations can be partially penetrant and can also affect the male gametophyte.

Three lines, *fem2*, *fem3*, and *fem4*, were identified that exhibited reduced seed set and in which KanR/KanS was less than 1.5. We also identified one female gametophyte mutant (*fem1*) in an EMS screen (see Materials and Methods) and obtained five additional female gametophyte mutants (*gfa2*, *gfa3*, *gfa4*, *gfa5*, and *gfa7*) from other sources, as listed in Table 1.

Linkage Analysis

To determine whether the *fem2–fem4* mutations were linked to the *nptII* gene, we crossed heterozygous female gametophyte mutants with wild type, germinated the F1 progeny in the presence of Kan, transferred 100 KanR F1 progeny to dirt, and scored these plants for reduced seed set. With the *fem2–fem4* mutants, all 100 of the F1 progeny scored exhibited reduced seed set, indicating that in each of these lines, the *nptII* gene was linked to the female gametophyte mutation within 3.7 cM at the 95% confidence level. The tight linkage between the *nptII* gene and the female gametophyte mutations allowed us, in subsequent experiments, to use the KanR trait as a marker for the presence of the mutations.

We determined the genetic map positions of the *fem* mutations. All four mutations mapped to locations in the genome that were different from each other and from the *gfa1–gfa7* mutations (Feldmann *et al.*, 1997), indicating that they are not allelic (see Materials and Methods). Of the other mutants discussed in this paper, only *gfa3* and *gfa7* map to similar positions (Feldmann *et al.*, 1997).

Penetrance in the Female Gametophyte

To determine the penetrance of the *fem* mutations in the female gametophyte, we crossed heterozygous mutant plants as female parents with wild-type males and scored the number of F1 progeny that were heterozygous (KanR or exhibited 50% seed set) and homozygous wild type (KanS or exhibited 100% seed set). The data from these crosses are summarized in Table 2. With all mutants tested, the ratio of heterozygous to homozygous wild-type (KanR/KanS) progeny was <1.0, indicating that these mutations exhibited reduced transmission through the female gametophyte and thus affected the female gametophyte. With the *fem1* and *fem4* mutants, no transmission of the mutation was observed, indicating that the *fem1* and *fem4* mutations were 100% penetrant in the female gametophyte. By contrast,

TABLE 2
Results from Crosses of Heterozygous Female Gametophyte Mutants as Female Parents with Wild-Type Males

Mutant	No. of progeny		Het/Homo[a]	Penetrance in FG
	Heterozygous	Homozygous		
fem1	0	206	0	100
fem2	273	486	0.56	44
fem3	225	388	0.58	42
fem4	0	111	0	100

[a] Ratio of heterozygous to homozygous progeny.

Copyright © 1998 by Academic Press. All rights of reproduction in any form reserved.

TABLE 3
Results from Crosses of Heterozygous Female Gametophyte Mutants as Male Parents with Wild-Type Females

Mutant	No. of progeny		Het/Homo[a]	Penetrance in MG
	Heterozygous	Homozygous		
fem1	219	221	0.99	1[b]
fem2	342	303	1.13	0
fem3	340	606	0.56	44
fem4	238	412	0.58	42

[a] Ratio of heterozygous to homozygous progeny.
[b] Not significantly different than 0%.

with the *fem2* and *fem3* mutants, at least 56% transmission of the mutation through the female gametophyte was observed, indicating that the corresponding mutations were partially penetrant in the female gametophyte. We, in addition, carried out crosses with the *gfa2, gfa3, gfa4, gfa5,* and *gfa7* mutants and obtained penetrance values similar to those reported previously (Feldmann *et al.,* 1997).

Female Gametophyte Specificity

To determine whether the *fem* mutations also affect the male gametophyte, we crossed heterozygous mutant plants as male parents with wild-type females and scored the number of F1 progeny that were heterozygous (KanR or exhibited 50% seed set) and homozygous wild type (KanS or exhibited 100% seed set). The data from these crosses are summarized in Table 3. With the *fem1* and *fem2* mutants, heterozygous and homozygous wild-type progeny were present in approximately equal proportions in the F1 generation, indicating that the *fem1* and *fem2* mutations do not affect the male gametophyte. By contrast, with the *fem3* and *fem4* mutants, the ratio of heterozygous to homozygous wild-type (KanR/KanS) progeny was <0.6, indicating that the corresponding mutations exhibited reduced transmission through the male gametophyte and thus affected the male gametophyte.

In summary, we have identified two classes of female gametophyte mutations. One class affects the female gametophyte but not the male gametophyte and the second class affects both gametophytes. We refer to these two classes as female gametophyte-specific mutations and general gametophytic mutations, respectively. The class that each of the female gametophyte mutations falls within is listed in Table 1.

Megagametogenesis in the fem and gfa Mutants

Female gametophyte mutations could affect the female gametophyte either by disrupting megagametogenesis or by interfering with one of the female gametophyte's functions. To distinguish between these possibilities, we analyzed the terminal phenotypes of the female gametophyte mutants. To do this, we allowed the female gametophytes within heterozygous pistils to progress to the terminal developmental stage (stage FG7, Fig. 2A) and examined at least 80 female gametophytes for each mutant. The *fem1, fem2, fem3, fem4, gfa2, gfa3, gfa4, gfa5,* and *gfa7* mutants had morphologically abnormal female gametophytes at the terminal developmental stage, indicating that the mutations in these lines affect megagametogenesis. The terminal phenotypes of the female gametophyte mutants are summarized in Table 4 and are discussed in detail below.

To determine the developmental stage at which megagametogenesis departs from wild type in the *fem* and *gfa* mutants, we analyzed megagametogenesis at all developmental stages in heterozygous pistils. We previously showed that female gametophyte development within a pistil is synchronous (Christensen *et al.,* 1997), which allowed us to use wild-type female gametophytes to determine the developmental stage of mutant female gametophytes within the same pistil. Each developmental stage was analyzed by confocal laser scanning microscopy (CLSM). Using this procedure, nucleoli appear white, cytoplasm appears gray, and vacuoles appear black (Figs. 1C, 3, and 4) (Christensen *et al.,* 1997). The results of this analysis are summarized in Table 5. CLSM images of mutant female gametophytes are shown in Figs. 3 and 4.

Megagametogenesis in wild type. Megagametogenesis in wild-type *Arabidopsis* has been described (Misra, 1962; Poliakova, 1964; Webb and Gunning, 1990; Mansfield *et al.,* 1991; Murgia *et al.,* 1993; Webb and Gunning, 1994; Schneitz *et al.,* 1995; Christensen *et al.,* 1997) and has been divided into seven morphologically distinct stages that are depicted in Fig. 2A (Christensen *et al.,* 1997). First, the surviving megaspore (stage FG1) undergoes mitosis to produce a two-nucleate cell (stage FG2). Shortly thereafter, the two nuclei separate to the chalazal and micropylar poles and a vacuole forms in the center (stage FG3). The developing female gametophyte then undergoes second (stage FG4) and third rounds of mitosis. This results in an eight-nucleate cell with four nuclei at each of two poles separated by a large central vacuole (beginning of stage FG5). Next, one nucleus from each pole (the polar nuclei) migrates toward the female gametophyte's center and the embryo sac becomes cellularized. The polar nuclei eventually fuse and the female gametophyte consists of seven cells and seven nuclei (stage FG6; Figs. 1A and 1B). As a final developmental step, the three antipodal cells undergo cell death. Thus, the mature *Arabidopsis* female gametophyte (stage FG7) consists of one haploid egg cell, two haploid synergid cells, and one diploid central cell (Figs. 1C and 2B). Megagametogenesis in *Arabidopsis* occurs over a period of approximately 3.5 days (C. A. Christensen and G. N. Drews, unpublished results).

To determine the extent to which abnormal female gametophyte development occurs in wild type, we analyzed >1000 wild-type female gametophytes encompassing all developmental stages. Under our growth conditions (Chris-

Copyright © 1998 by Academic Press. All rights of reproduction in any form reserved.

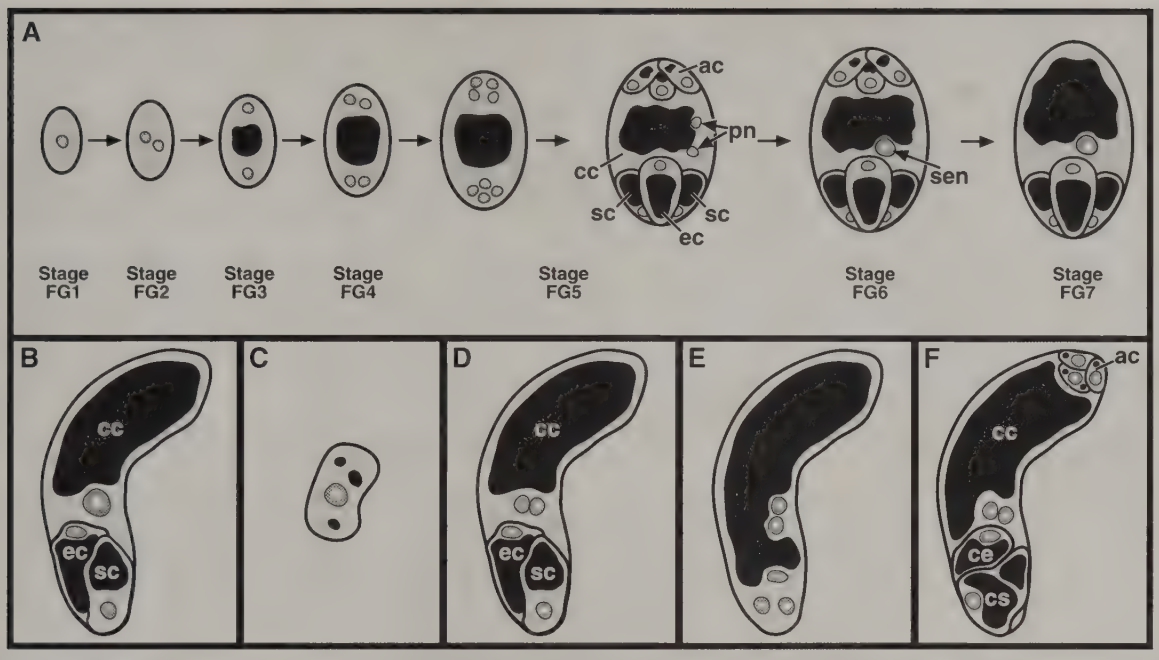

FIG. 2. Depictions of megagametogenesis in wild-type (A,B) and female gametophyte mutant phenotypes at the terminal stage (C–F). (A) Megagametogenesis stages (Christensen *et al.*, 1997). (B) Longitudinal view of a wild-type female gametophyte at the terminal stage (stage FG7). (C) Terminal phenotype of *fem2, fem3, gfa4,* and *gfa5* female gametophytes. (D) Terminal phenotype of *gfa2, gfa3,* and *gfa7* female gametophytes. (E) Terminal phenotype of *gfa3* and *gfa7* female gametophytes. (F) Terminal phenotype of the *fem4* mutant. Depicted are cytoplasm (light gray areas), vacuoles (black areas), nuclei (dark gray areas), and nucleoli (white areas within the nuclei). All female gametophytes are oriented with their chalazal poles up and their micropylar poles down. Abbreviations: ac, antipodal cells; cc, central cell; ce, cell in similar position and polarity to egg cell; cs, cell in similar position and polarity to synergid cell; ec, egg cell; pn, polar nucleus; sc, synergid cell; sen, secondary endosperm nucleus.

tensen *et al.*, 1997), less than 1% of the ovules we observed contained a female gametophtye that had undergone abnormal development. Of those that developed abnormally, all aborted at the one-nucleate stage and none had a defect in a later developmental step (i.e., polar nuclei migration, cellularization, polar nuclei fusion, or antipodal cell death).

gfa2. At the terminal developmental stage (stage FG7) approximately half of the embryo sacs in *gfa2/GFA2* pistils were phenotypically mutant (Table 5), consistent with the 100% penetrance of the *gfa2* mutation in the female gametophyte (Feldmann *et al.*, 1997). The terminal phenotype of *gfa2* female gametophytes is shown in Fig. 3B and depicted in Fig. 2D. In mature *gfa2* female gametophytes, the overall morphology of the egg cell, central cell, and synergid cells was normal (Fig. 3B and data not shown). However, in contrast to wild-type female gametophytes at stage FG7, the nucleoli of the two polar nuclei were unfused (Fig. 3B). Because Fig. 3B is a projection of several CLSM optical sections, the nuclear membrane boundary was not distinguishable. Figures 3C and 3D are single optical sections of mature *gfa2* female gametophytes showing that the two polar nuclei, as well as the nucleoli, were separate. Thus, the *gfa2* mutation appears to specifically affect fusion of the polar nuclei.

To determine the stage in which female gametophyte development departs from wild type, we analyzed *gfa2/GFA2* pistils containing female gametophytes between stages FG1 and FG7. In *gfa2/GFA2* pistils containing female gametophytes between stages FG6 and FG7 (pistil stages FG6/7 and FG7), approximately half (109/207) of the female gametophytes observed were abnormal (Table 5). By contrast, in *gfa2/GFA2* pistils containing female gametophytes at stage FG5 and earlier (pistil stages FG1-FG5/6), essentially all (283/291) female gametophytes observed were morphologically wild type (Table 5). We therefore conclude that *gfa2* female gametophytes begin to develop abnormally beginning at the transition from stage FG5 to stage FG6, which is the time when the polar nuclei fuse (Fig. 2A).

In our analysis of developing female gametophytes, the major defect observed was a failure of the polar nuclei to fuse. In wild-type female gametophytes, antipodal cell degeneration occurs subsequent to polar nuclei fusion. In *gfa2*

Copyright © 1998 by Academic Press. All rights of reproduction in any form reserved

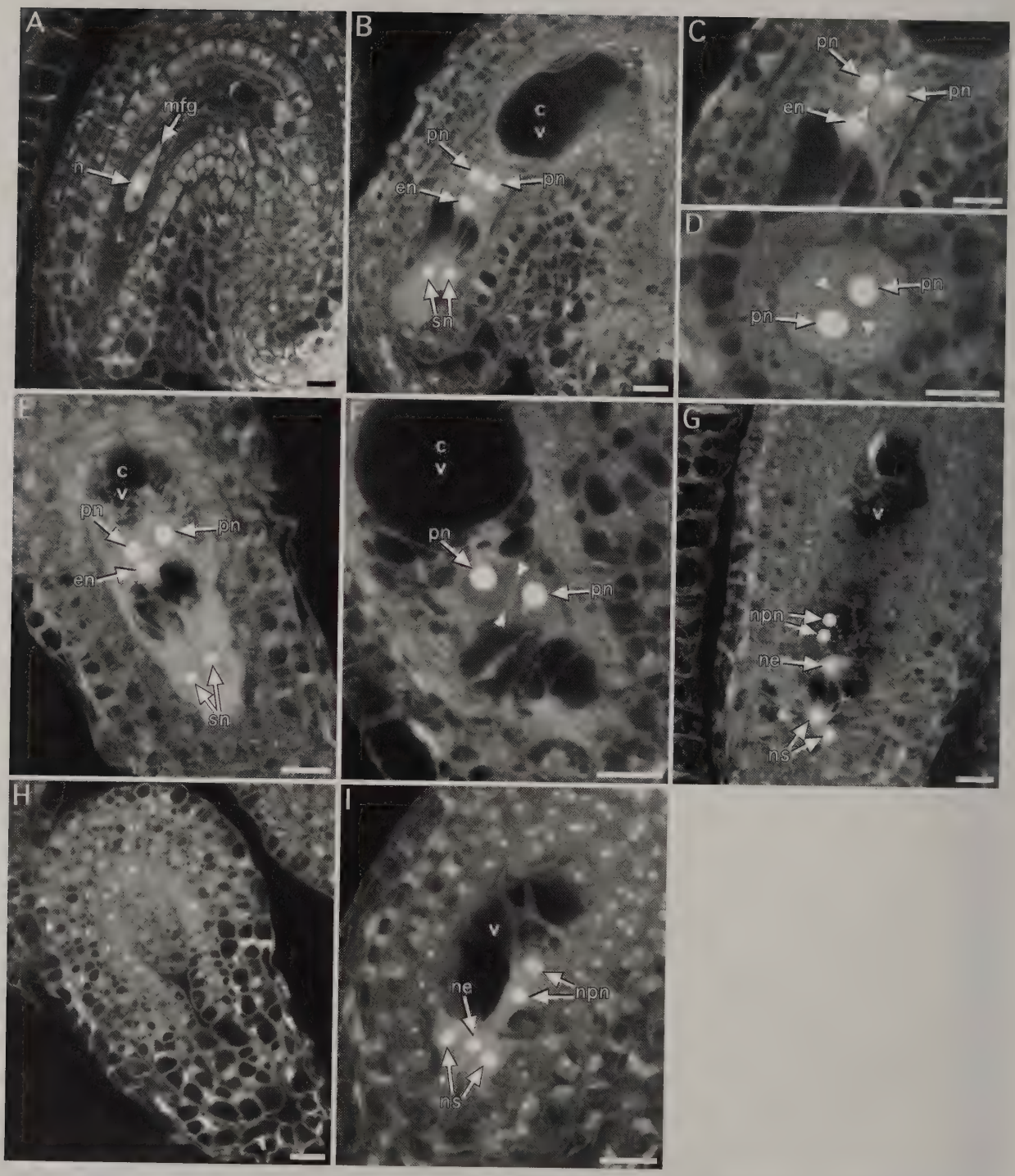

FIG. 3. CLSM images of *fem3*, *gfa2*, and *gfa3* female gametophytes. (A) Terminal phenotype of a *fem3* female gametophyte. This image is a projection of two 1.5-μm optical sections. (B) Terminal phenotype of a *gfa2* female gametophyte. This image is a projection of four 1.5-μm optical sections. (C,D) Single optical sections showing a magnified view of the unfused polar nuclei in two *gfa2* female gametophytes. The image in C is a single optical section of the projection shown in B. Arrowheads show the position of the nuclear

Copyright © 1998 by Academic Press. All rights of reproduction in any form reserved.

TABLE 4
Terminal Phenotypes of Female Gametophyte Mutants

Mutant	Phenotype
fem1	Female gametophyte absent. Embryo sac cavity filled with highly autofluorescent material.
fem2	One-nucleate female gametophyte.
fem3	One-nucleate female gametophyte.
fem4	At the micropylar pole, cell morphology, including nuclear positioning, vacuolar and cellular shape, and vacuole number was irregular. Nuclear and cell numbers correspond to those of stages FG5, FG6, or FG7.
gfa2	Polar nuclei fail to fuse.
gfa3	In most (59%), the polar nuclei fail to fuse. In some (22%), the embryo sac has five nuclei in approximately the correct positions (to be the egg, synergid and unfused polar nuclei), but appears to be uncellularized. In some (19%), the ovules lacked female gametophytes.
gfa4	One-nucleate female gametophyte.
gfa5	One-nucleate female gametophyte.
gfa7	In most (58%), the polar nuclei fail to fuse. In some (28%), the embryo sac has five nuclei in approximately the correct positions (to be the egg, synergid and unfused polar nuclei), but appears to be uncellularized. In some (14%), the ovules lacked female gametophytes.

female gametophytes, antipodal cell degeneration also occurs, although it appeared to occur more slowly than in wild type (data not shown).

gfa3. Under our growth conditions, the penetrance of the *gfa3* mutation in the female gametophyte was 82%; thus, the expected frequency of phenotypically mutant embryo sacs in *gfa3/GFA3* pistils was 41%. However, at the terminal developmental stage (stage FG7), approximately 30% of the female gametophytes in *gfa3/GFA3* pistils were phenotypically mutant (Table 5), suggesting that some nonfunctional *gfa3* female gametophytes were morphologically normal at the resolution of CLSM.

The phenotypes exhibited by *gfa3* female gametophytes at the terminal developmental stage are shown in Figs. 3E–3H and depicted in Figs. 2D and 2E. The predominant (54/92) defect observed was failure of the polar nuclei to fuse (Figs. 2D and 3E). As with *gfa2* mutants, individual optical sections showed that the polar nuclei were adjacent to one another but remained separate (Fig. 3F). Two less frequent terminal phenotypes were also observed at the terminal stage (Table 4). The first was female gametophytes that were uncellularized but contained five nuclei that were in approximately the correct positions to be the egg nucleus, synergid nuclei, and unfused polar nuclei (Figs. 2E and 3G). The second was an ovule lacking a female gametophyte (Fig. 3H).

The defects exhibited by developing *gfa3* female gametophytes are summarized in Table 6. The major defect observed occurred during stage FG6. During stage FG6 in wild type, the polar nuclei are fused and the antipodal cells are undergoing cell death. By stage FG7, the antipodal cells are completely degenerated (Fig. 2A). In *gfa3/GFA3* pistils at stage FG7, 304 female gametophytes were observed that lacked antipodal cells, and of these 54 had unfused polar nuclei ("unfused polar nuclei" column in Table 6, Fig. 3E). Prior to stage FG6, two less frequent defects were observed. The first was compressed embryo sacs at the four-nucleate stage ("Four nuclei and compressed" column in Table 6) and the second was uncellularized female gametophytes at late stage FG5 ("Uncellularized" column in Table 6, Fig. 3I). Based on frequency and developmental progression, these two defects probably gave rise to the ovules lacking female gametophytes ("No FG" column in Table 6, Fig. 3H) and the uncellularized female gametophytes observed at the terminal stage ("Uncellularized" column in Table 6, Fig. 3G), respectively.

gfa7. The *gfa7* mutant exhibited the same three terminal phenotypes that were exhibited by the *gfa3* mutant in

boundaries. (E) Terminal phenotype of a *gfa3* female gametophyte. This image is a projection of five 1.5-μm optical sections. (F) Single optical section showing a magnified view of the unfused polar nuclei in a *gfa3* female gametophyte. Arrowheads show the position of the nuclear boundaries. (G) Terminal phenotype of a *gfa3* female gametophyte. This image is a projection of eight 1.5-μm optical sections. (H) Terminal phenotype of a *gfa3* female gametophyte. This image consists of a single optical section. (I) Phenotype of a *gfa3* female gametophyte at pistil stage FG5. This image is a projection of eight 1.5-μm optical sections. All female gametophytes are oriented with their chalazal poles up and micropylar poles down and their abaxial surface to the left and adaxial surface to the right. Abbreviations: en, egg cell nucleus; cv, central cell vacuole; mfg, mutant female gametophyte; n, nucleus; ne, nucleus in similar position to egg nucleus; npn, nucleus in similar position to polar nucleus; ns, nucleus in similar position to synergid nucleus; pn, polar nucleus; sn, synergid cell nucleus; v, vacuole. Scale bars, 10 μm.

Copyright © 1998 by Academic Press. All rights of reproduction in any form reserved.

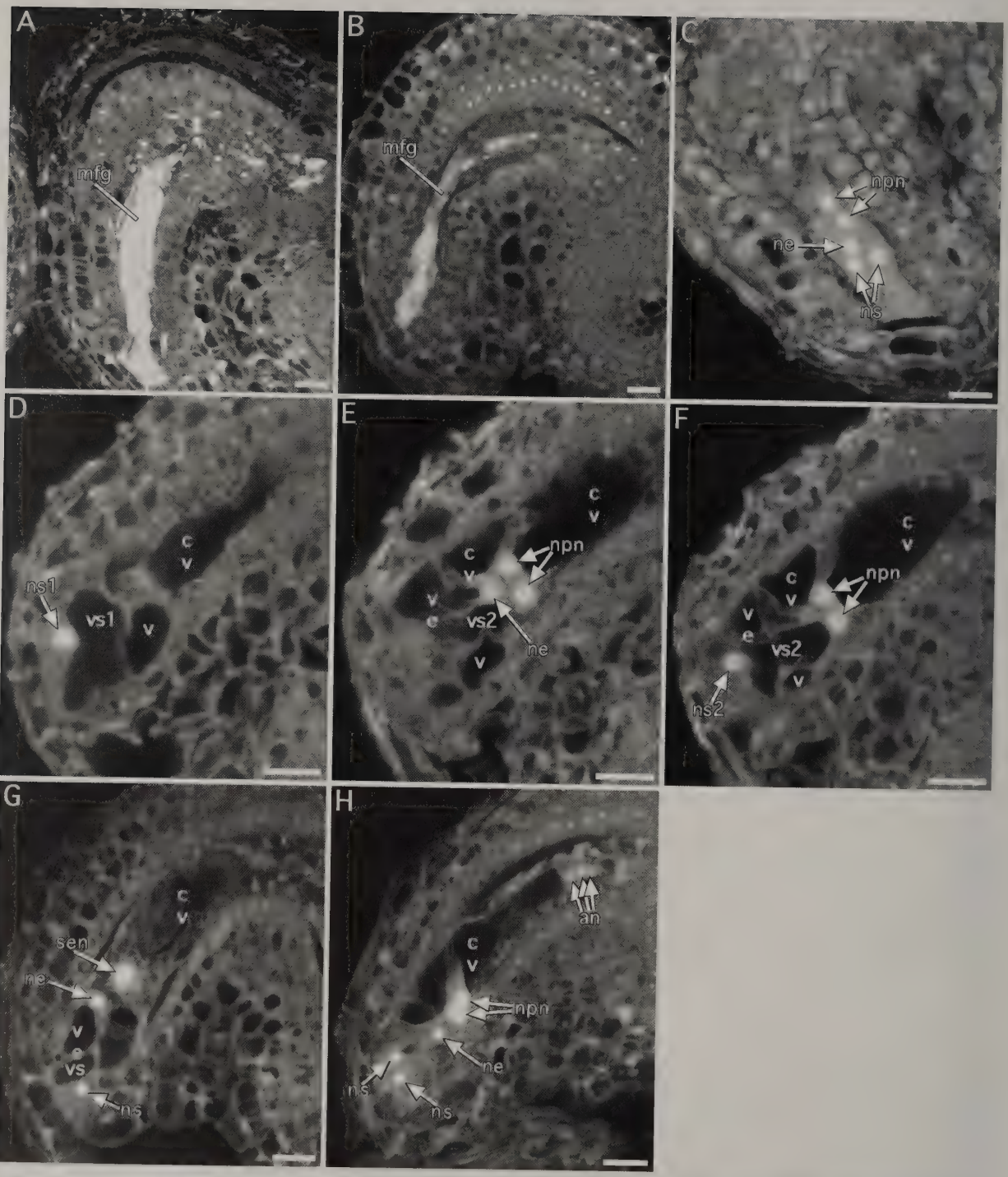

FIG. 4. CLSM images of *fem1* and *fem4* female gametophytes. (A) Terminal phenotype of a *fem1* female gametophyte. This image is a projection of six 1.5-μm optical sections. (B,C) Phenotypes of two *fem1* female gametophytes at pistil stage FG5/6. Each image is a projection of four 1.5 μm optical sections. (D–H) Phenotypes of *fem4* female gametophytes at the terminal stage. Due to abnormal cellular morphologies, distinct cellular identities could not be assigned. The position and overall polarity of cell e are similar to those of the egg cell.

Copyright © 1998 by Academic Press. All rights of reproduction in any form reserved.

TABLE 5
Summary of CLSM Analysis of Female Gametophyte Mutants

Mutant	Pistil stage[a]	No. of pistils analyzed	No. of normal FGs observed	No. of abnormal FGs observed	% Abnormal
fem1	FG3–FG4/5	9	108	2	2
	FG5	4	60	0	0
	FG5/6	4	41	33	45
	FG6/7	9	74	77	51
	FG7	5	38	42	53
fem4	FG1–FG3/4	11	158	1	< 1
	FG4	4	51	4	7
	FG4/5	4	37	7	16
	FG5	5	45	13	22
	FG5/6	2	19	13	41
	FG6	2	11	10	48
	FG6/7	4	18	17	49
	FG7	10	86	86	50
gfa2	FG1–FG4/5	15	197	3	2
	FG5	6	60	1	2
	FG5/6	2	26	5	16
	FG6/7	3	21	19	48
	FG7	11	77	90	54
gfa3	FG1–FG4	7	83	0	0
	FG4/5	4	77	3	4
	FG5	5	44	10	19
	FG5/6	7	66	12	15
	FG7	18	212	92	30

[a] Assignment of a pistil stage is described under Materials and Methods.

approximately the same frequencies (Table 4). Since the *gfa3* and *gfa7* mutants have an identical terminal phenotype (Table 4) and also have the same map position (Feldmann *et al.*, 1997), they most likely harbor mutations in the same gene. For this reason, we examined earlier developmental stages only in the *gfa3* mutant.

fem1. At the terminal developmental stage (stage FG7), approximately half of the female gametophytes in *fem1/FEM1* pistils were phenotypically mutant (Table 5), consistent with the 100% penetrance of the *fem1* mutation. As shown in Fig. 4A, *fem1* female gametophytes at the terminal stage were completely degenerated and their embryo sac cavities were filled with autofluorescent material.

As shown in Table 5, *fem1* female gametophytes begin to develop abnormally at approximately late stage FG5 or stage FG6, which is about the time when the polar nuclei fuse (Fig. 2A). The most commonly observed (27/33) phenotype at this developmental time is shown in Fig. 4B. As with later stages (Fig. 4A), the female gametophyte was completely degenerated and the embryo sac cavity was

The positions and overall polarities of cells s1 and s2 are similar to those of the synergids. (D–F) Serial optical sections of the micropylar half of one *fem4* female gametophyte. (D) A single optical section showing cell s1 (ns1 and vs1). (E) A projection of two 1.5-μm optical sections showing cell e (ne and ve). (F) A projection of two 1.5-μm optical sections showing cell s2 (ns2 and vs2). The vacuole labeled v was in addition to the three vacuoles normally seen in the egg apparatus. The two vacuoles labeled cv were connected (not shown). (G) In this *fem4* female gametophyte, the polar nuclei have fused (sen) and the antipodal cells have degenerated. This image is a projection of three 1.5-μm optical sections. An additional synergid cell was present but not included in the projection. (H) In this *fem4* female gametophyte, the polar nuclei (npn) were unfused and the antipodal cells (an) were present. This image is a projection of five 1.5-μm optical sections. All female gametophytes are oriented with their chalazal poles up and micropylar poles down and their abaxial surface to the left and adaxial surface to the right. Abbreviations: an, antipodal cell nucleus; cv, central cell vacuole; mfg, mutant female gametophyte; ne, nucleus in similar position to egg nucleus; npn, nucleus in similar position to polar nucleus; ns, nucleus in similar position to synergid nucleus; ns1, nucleus of cell s1; ns2, nucleus of cell s2; sen, secondary endosperm nucleus; v, vacuole; ve, vacuole in similar position to egg cell vacuole; vs, vacuole in similar position to synergid cell vacuole; vs1, vacuole of cell s1; vs2, vacuole of cell s2. Scale bars, 10 μm.

Copyright © 1998 by Academic Press. All rights of reproduction in any form reserved.

TABLE 6
Summary of Defects Observed in Developing *gfa3* Female Gametophytes

Pistil stage[a]	No. of pistils analyzed	No. of FGs analyzed	No. of abnormal female gametophytes observed				
			Four nuclei and compressed	No FG	Uncellularized	Unfused polar nuclei	Total
FG4/5	4	80	1	0	2	0	3
FG5	5	54	5	1	3	1	10
FG5/6	7	78	2	6	3	1	12
FG7	18	304	0	18	20	54	92

[a] Assignment of a pistil stage is described under Materials and Methods.

filled with autofluorescent material. Occasionally (6/33) the less severe phenotype shown in Fig. 4C was observed. In such female gametophytes, the nuclei were present in the correct numbers and at the appropriate positions to be the polar nuclei, egg nucleus, and synergid nuclei, but a prominent central vacuole was absent (compare Fig. 4C with Fig. 1C). In some (3/6) of these, the "polar nuclei" were adjacent to each other but were unfused (e.g., the female gametophyte shown in Fig. 4C). Generally, one or more of the nuclei had an irregular shape and thus was probably in the process of degeneration (data not shown). Taken together, these data suggest that development of *fem1* female gametophytes begins to depart from wild type just before polar nuclei fusion (late stage FG5) and that an early event appears to be degeneration of the central vacuole.

fem4. At the terminal developmental stage (stage FG7), 50% of embryo sacs in *fem4/FEM4* pistils were abnormal (Table 5), corresponding to the 100% penetrance of the *fem4* mutation (Table 2). The terminal phenotype of *fem4* female gametophytes is shown in Figs. 4D–4H and depicted in Fig. 2F. Essentially all (85/86) of the *fem4* female gametophytes we observed at the terminal developmental stage had defects in cellular morphology in the cells at the embryo sac's micropylar pole (Table 7). In wild type, the egg cell has a distinctive pear shape and a highly polarized cytoplasm; its nucleus and most of its cytoplasm are at its chalazal end and a large vacuole occupies the remaining three-fourths of the cell (Fig. 1). Likewise, wild-type synergid cells have a distinctive shape and a highly polarized cytoplasm, which has the opposite polarity of the egg cell cytoplasm (Fig. 1). As with wild type, *fem4* female gametophytes at the terminal developmental stage had three cells at the micropylar pole. However, in contrast to wild type, these cells had irregular shapes and polarities. An example of a *fem4* female gametophyte at the terminal developmental stage is shown in Figs. 4D–4F. In this example, the egg cell is not pear shaped and is tilted relative to the female gametophyte's long axis (Fig. 4E), and the synergid cells were abnormally shaped and their nuclei occupied positions more chalazal and abaxial than those of wild type (Figs. 4D and 4F).

In addition to the cellular morphology defects exhibited by all *fem4* female gametophytes, some mature *fem4* fe-

TABLE 7
Summary of Defects Observed in Developing *fem4* Female Gametophytes

Pistil stage[a]	No. of pistils analyzed	No. of FGs analyzed	No. of abnormal female gametophytes observed					
			Abnormal nuclear position at stage FG4	Developmental delay	Abnormal cellular morphology at stage FG5	Abnormal cellular morphology at stage FG6	Abnormal cellular morphology at stage FG7	Total
FG4	4	55	2	0	1	1	0	4
FG4/5	4	44	4	0	2	1	0	7
FG5	5	58	3	3[b]	7	0	0	13
FG5/6	2	32	4	0	9	0	0	13
FG6	2	21	0	10	0	0	0	10
FG6/7	4	35	0	0	15	2	0	17
FG7	10	172	0	1	35	23	27	86

[a] Assignment of a pistil stage is described under Materials and Methods.
[b] One of these female gametophytes was at stage FG3, and the others were at stage FG4.

Copyright © 1998 by Academic Press. All rights of reproduction in any form reserved.

male gametophytes also exhibited defects in polar nuclei fusion and antipodal cell degeneration, which are developmental steps that follow cellularization (Fig. 2A). Of the 86 abnormal female gametophytes observed at the terminal developmental stage, 27% had intact antipodal cells and 41% had unfused polar nuclei and intact antipodal cells (Fig. 4H, Table 7).

To determine the developmental stage at which cellular morphology becomes abnormal, we analyzed female gametophyte development in *fem4/FEM4* pistils at all developmental stages. These data are summarized in Table 7. In wild type, cellularization begins immediately following the third mitosis (early stage FG5) and by late stage FG5, the egg and synergid cells have distinct polarities and morphologies as described above (Fig. 2A; Christensen *et al.*, 1997). In *fem4* female gametophytes at late stage FG5, the egg and synergid cells already exhibited defects in cell shape, vacuolar shape, and cell position, indicating that cellular morphology was abnormal as soon as these cells were formed (Table 7).

Analysis of female gametophyte development in the *fem4* mutant also revealed two subtle defects that occurred before stage FG5 and were not manifested at the terminal developmental stage (Table 7). The first was abnormal nuclear position at stage FG4 ("Abnormal nuclear position at stage FG4" column in Table 7). In *fem4/FEM4* pistils, some four-nucleate embryo sacs were observed in which one of the two nuclei at each pole was closer to the center of the embryo sac than in wild type (data not shown). The second defect was apparent developmental asynchrony ("Developmental delay" column in Table 7). We previously showed that megagametogenesis in wild type is fairly synchronous and that female gametophytes at stage FG4 are not present in pistils containing female gametophytes at stage FG6 (Christensen *et al.*, 1997). However, some *fem4/FEM4* pistils contained both stage FG4 and stage FG6 female gametophytes (Table 7). Nevertheless, *fem4* female gametophytes do progress beyond stage FG4 because by the terminal stage nearly all (85/86) *fem4* female gametophytes observed had undergone the third mitosis and had become cellularized (Table 7).

fem2, fem3, gfa4, and gfa5. The phenotype of the *fem2, fem3, gfa4,* and *gfa5* mutants is depicted in Fig. 2C. In this group, megametogenesis did not progress beyond stage FG1 (one-nucleate stage; Fig. 2A). As shown in Fig. 3A, ovule morphology (integument length and ovule shape) was similar to ovules containing mature, wild-type female gametophytes. However, female gametophyte morphology was similar to female gametophytes at stage FG1 [tear drop shape, one nucleus, and small vacuoles (Webb and Gunning, 1990; Christensen *et al.*, 1997)]. We did not examine earlier developmental stages in this group.

Within *fem2/FEM2, fem3/FEM3, gfa4/GFA4,* and *gfa5/GFA5* pistils, the frequencies of morphologically abnormal female gametophytes were 51, 47, 10, and 18%, respectively. The fact that the these frequencies were higher than expected for the *fem2* and *fem3* mutants (based on the genetic transmission data in Table 2) suggests that these mutations may be linked to chromosomal rearrangements (Ray *et al.*, 1997). The fact that these frequencies were higher than expected for the *gfa4* and *gfa5* mutants [based on the 42% penetrance of the *gfa4* mutation and the 79% penetrance of the *gfa5* mutation reported by Feldmann *et al.* (1997)] may suggest that some morphologically normal female gametophytes were nonfunctional.

Microgametogenesis in the fem and gfa Mutants

As shown in Table 1, the *fem3, fem4, gfa2, gfa3, gfa4, gfa5,* and *gfa7* mutations also affect the male gametophyte. To determine whether they affect microgametogenesis, we analyzed the terminal phenotypes of these mutants. To do this, we used CLSM to analyze the male gametophytes within anthers from late stage 12 (just prior to dehiscence) flowers (Smyth *et al.*, 1990). The results of this analysis are shown in Fig. 5. Within *fem3/FEM3, gfa3/GFA3, gfa4/GFA4,* and *gfa5/GFA5* anthers, morphologically abnormal pollen grains were observed (Figs. 5B–5E). With these mutants, abnormal pollen grains were collapsed (arrows) or highly vacuolate (arrowheads). These data indicate that the *fem3, gfa3, gfa4,* and *gfa5* mutations affect microgametogenesis. By contrast, only morphologically normal pollen grains (over 75 pollen grains scored) were observed in *fem4/FEM4* and *gfa2/GFA2* anthers (Figs. 5F and 5G), suggesting that the *fem4* and *gfa2* mutations may affect some aspect of male gametophyte function.

DISCUSSION

Isolation of Female Gametophyte Mutants

Molecules mediating and regulating the major events of megagametogenesis (mitosis, polarity establishment, vacuole formation, nuclear migration, cellularization, cell specification and differentiation, nuclear fusion, and cell death) and female gametophyte function (pollen tube guidance, fertilization, induction of seed development, and gametophytic maternal control) have not been identified. To begin to identify these molecules, we have initiated a genetic screen for female gametophyte mutants that is based on two criteria, seed set and segregation distortion. Each of these criteria alone is ineffective in definitively identifying female gametophyte mutants. Reduced seed set screens are limited because this phenotype also can be caused by a variety of other factors including adverse environmental conditions (e.g., high growth temperature or water stress), chromosomal rearrangements (e.g., reciprocal translocations and large inversions), and sporophytic mutations (e.g., a female-sterile mutation with partial penetrance). Segregation distortion screens are limited because they identify both female gametophyte and male gametophyte mutations. However, when combined, these two criteria are effective in identifying female gametophyte mutants. Using

Copyright © 1998 by Academic Press. All rights of reproduction in any form reserved.

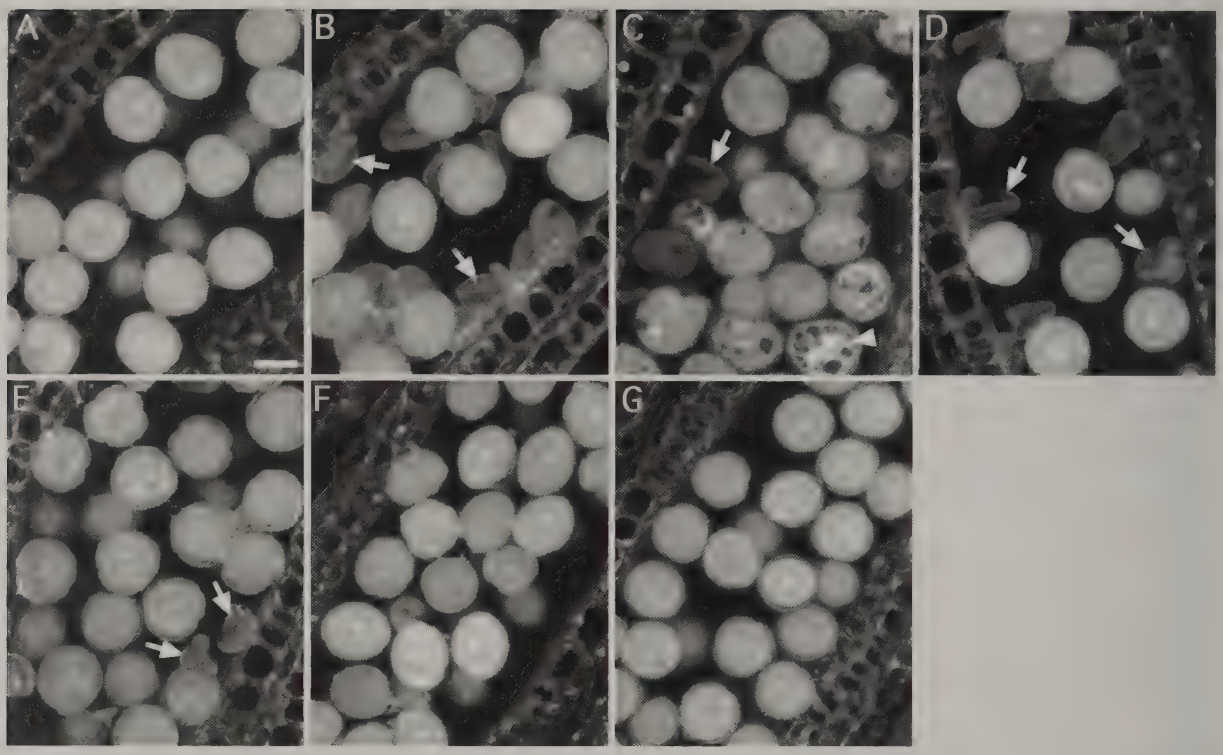

FIG. 5. CLSM images of mature pollen grains from wild type and the *fem3, fem4, gfa2, gfa3, gfa4,* and *gfa5* mutants. (A) Wild type. (B) *fem3.* (C) *gfa3.* (D) *gfa4.* (E) *gfa5.* (F) *fem4.* (G) *gfa2.* Arrows show collapsed pollen grains; arrowhead shows hypervacuolate pollen grain. All images are single 1.5-μm optical sections. Scale bar, 10 μm.

this screening procedure, we identified four lines (*fem1, fem2, fem3,* and *fem4*) containing female gametophyte mutations. Several female gametophyte mutants were previously identified based on reduced seed set or segregation distortion including the *Arabidopsis ctr1, emb173, Gf, gfa1 – gfa7, hdd, prl,* and *trp1;trp4* mutants (Redei, 1965; Castle *et al.,* 1993; Kieber *et al.,* 1993; Niyogi *et al.,* 1993; Springer *et al.,* 1995; Feldmann *et al.,* 1997; Moore *et al.,* 1997) and the maize *ig, lo1, lo2, sp1,* and *sp2* mutants (Manglesdorf, 1931; Singleton, 1932; Rhoades and Rhoades, 1939; Singleton, 1940; Singleton and Mangelsdorf, 1940; Nelson and Clary, 1952; Kermicle, 1971). The isolation of these mutants, as well as the mutants described in this paper, demonstrates that the criteria of reduced seed set and segregation distortion should be effective in large-scale screens for female gametophyte mutants.

Female Gametophyte-Specific and General Gametophytic Mutations

The mutants discussed in this paper fall into two classes. The *fem1* and *fem2* mutations affect the female gametophyte but not the male gametophyte and, thus, fall into the female gametophyte-specific class. The *fem3, fem4, gfa2, gfa3, gfa4, gfa5,* and *gfa7* mutations affect both the female and male gametophyte and, therefore, are general gametophytic (Feldmann *et al.,* 1997). Female gametophyte-specific mutations are important because the affected genes encode functions required by the female gametophyte but not the male gametophyte including the establishment of female gametophyte polarity, specification and differentiation of the female gametophyte cells, controlled cell death of the antipodal and synergid cells, central vacuole formation and maintenance, pollen tube guidance, induction of seed development, and gametophytic maternal control (Drews *et al.,* 1998). General gametophytic mutations are also an important mutation class because many important cellular processes are required in both gametophytes including mitosis, vacuole formation, cell expansion, subcellular migration, nuclear migration and fusion, and cellularization. Thus, mutations affecting some of the major events of megagametogenesis are likely to fall into the general gametophytic class (Drews *et al.,* 1998). With all of the mutants described in this paper, we do not yet know

Copyright © 1998 by Academic Press. All rights of reproduction in any form reserved

whether the corresponding mutations also affect the sporophyte.

The fem1, fem2, fem3, fem4, gfa2, gfa3, gfa4, gfa5, and gfa7 Mutations Affect Megagametogenesis

All of the female gametophyte mutations we analyzed affect megagametogenesis. These nine mutations affect a range of steps. In the *fem2, fem3, gfa4,* and *gfa5* mutants, megagametogenesis does not progress beyond the one-nucleate stage (stage FG1; Figs. 2C and 3A). Developmental arrest at the one-nucleate stage could result from defects in a variety of processes including mitosis, cell cycle regulation, cellular metabolism, or developmental control. From the genetic and morphological data presented here, there is no way to determine which of these processes is affected by the *fem2, fem3, gfa4,* and *gfa5* mutations.

The *gfa2* mutation affects fusion of the polar nuclei (Figs. 2D and 3B–3D). In this mutant, the polar nuclei migrate together, come to lie side-by-side, but fail to fuse. Polar nuclei fusion has been described in plants and has been shown to consist of two steps. In the first step, the endoplasmic reticulum (ER) membranes that are continuous with the outer nuclear membranes of the two nuclei fuse, resulting in a continuous outer membrane surrounding unfused inner nuclear membranes; and in the second step, the inner nuclear membranes come in contact and merge to complete the fusion process (Jensen, 1964). We do not yet know which of these steps is affected by the *gfa2* mutation. Nuclear fusion has also been studied in yeast and has been found to occur via a process similar to that in plants (Kurihara *et al.*, 1994). Yeast nuclear fusion mutants have been identified and some of the affected genes encode components of the translocon, which is a protein complex embedded in the ER membrane that is responsible for protein translocation into the ER (Marsh and Rose, 1997).

Polar nuclei fusion is also affected by the *gfa3* and *gfa7* mutations (Figs. 2D, 3E, and 3F). However, unlike the *gfa2* mutation, the *gfa3* and *gfa7* mutations are pleiotropic and also result in uncellularized female gametophytes (Figs. 2E, 3G, and 3I). Pleiotropy of mutations affecting polar nuclei fusion is not surprising because, in yeast, some of the molecules required for nuclear fusion are also required for other cellular processes and, as a consequence, some of the yeast nuclear fusion mutations are pleiotropic (Marsh and Rose, 1997). For example, the yeast Sec63 protein is required for both nuclear fusion and protein translocation into the ER lumen (Ng and Walter, 1996). Thus, by analogy, the pleiotropy exhibited by the *gfa3* and *gfa7* mutations could reflect additional functions of the *GFA3* and *GFA7* gene products.

fem1 female gametophytes develop normally until late during stage FG5 (Table 5), which is just before polar nuclei fusion but after three rounds of mitosis and cellularization. Thus, the *fem1* mutation does not affect many fundamental cellular processes such as mitosis, vacuole formation, nuclear migration, and cellularization. In some (6/33, Table 5) *fem1* embryo sacs, most aspects of morphology are normal except that the central vacuole is not present (Fig. 4C). Thus, FEM1 may be required for maintenance of the central vacuole and the *fem1* mutation may cause disintegration of this vacuole. If this is true, then the more severe phenotype observed (Figs. 4A and 4B) could be caused by the release of vacuolar contents. Additional analysis using transmission electron microscopy is required to determine if that is the case.

fem4 female gametophytes exhibit defects in cellular morphology (Figs. 2F and 4D–4H). The mechanism of cellularization during megagametogenesis is not well understood (Russell, 1993). One model is that following the third mitosis, microtubules emanate radially from individual nuclei, phragmoplasts form where the microtubules meet, and cell plates form at the equator of the phragmoplasts (Brown and Lemmon, 1991; Russell, 1993). In support of this model, phragmoplasts have been observed in *Arabidopsis* female gametophytes between sister and nonsister nuclei following the third mitosis (Webb and Gunning, 1994). In this model, the location of the cell walls is ultimately determined both by the position of the nuclei and the organization of the cytoskeleton. If this model is correct, then the *fem4* mutation could affect cellular morphology by disrupting nuclear position or the organization or function of the cytoskeleton. Cytoskeletal organization defects also could explain the aberrant nuclear position and apparent developmental delay observed in *fem4* female gametophytes at stage FG4 (Table 7). Further analysis of cellularization and cytoskeletal organization in *fem4* female gametophytes is required to address these issues. Some *fem4* embryo sacs also exhibit defects in polar nuclei fusion and antipodal cell degeneration (Table 7); however, because these developmental steps occur after cellularization, these defects probably occur as a secondary consequence of the earlier cellularization defect.

Of the previously identified female gametophyte mutants, morphological analysis throughout megagametogenesis has been carried out only with the *Gf* (Redei, 1965), *hdd* (Moore *et al.*, 1997), *ig* (Kermicle, 1971), *lo2* (Nelson and Clary, 1952), and *prl* (Springer *et al.*, 1995) mutations. The *Gf* mutation causes a phenotype identical to that of the *fem2, fem3, gfa4,* and *gfa5* mutants, developmental arrest at the one nucleate stage (stage FG1). By contrast, the phenotypes of the *hdd, ig, lo2,* and *prl* mutants do not resemble those of the mutants presented here. The *hdd, lo2,* and *prl* mutations cause developmental arrest at the one-, two-, four-, or eight-nucleate stage (Moore *et al.*, 1997; Sheridan and Huang, 1997), and the *ig* mutation causes extra cycles of nuclear divisions to occur (Kermicle, 1971; Lin, 1978; Lin, 1981; Huang and Sheridan, 1996). In addition, the *hdd* and *ig* mutations cause asynchrony of nuclear divisions at the micropylar and chalazal poles (Huang and Sheridan, 1996; Moore *et al.*, 1997). These data suggest that the *HDD, IG, LO2,* and *PRL* genes may play a role in controlling nuclear division. Consistent with this idea, the *PRL* gene

Copyright © 1998 by Academic Press. All rights of reproduction in any form reserved.

is related to the yeast MCM2-3-5 genes that are required for initiation of DNA replication (Springer *et al.*, 1995).

The fem3, gfa3, gfa4, and gfa5 Mutations Affect Microgametogenesis

As discussed above, the *fem3, fem4, gfa2, gfa3, gfa4, gfa5,* and *gfa7* mutations affect both the female and male gametophyte. Thus, information about the pollen defects caused by these mutations may help to understand the functions of the corresponding genes during megagametogenesis. As a first step in this direction, we analyzed the terminal pollen phenotypes of these mutants. We found that *fem3, gfa3* (and presumably also *gfa7*), *gfa4,* and *gfa5* affect microgametogenesis. Further analysis is required to determine the specific steps of microgametogenesis affected. By contrast, the *gfa2* and *fem4* mutations do not appear to affect microgametogenesis and may instead affect some aspect of pollen function such as pollen germination, pollen tube growth, or pollen tube guidance.

ACKNOWLEDGMENTS

We thank Ken Feldmann for providing the *gfa2, gfa3, gfa4, gfa5* and *gfa7* mutants, Tom Jack for providing T-DNA mutagenized lines, and the *Arabidopsis* Biological Resource Center for making available the Ken Feldmann collection and *ms1-1.* We also thank Diana Lee for helpful comments on the manuscript. This work was supported by National Science Foundation Grant IBN-9630371.

REFERENCES

Bell, C. J., and Ecker, J. R. (1994). Assignment of 30 microsatellite loci to the linkage map of *Arabidopsis. Genomics* **19,** 137–144.

Brown, R. C., and Lemmon, B. E. (1991). Pollen development in orchids. 1. Cytoskeleton and the control of division plane in irregular patterns of cytokinesis. *Protoplasma* **163,** 9–18.

Castle, L. A., Errampalli, D., Atherton, T. L., Franzmann, L. H., Yoon, E. S., and Meinke, D. W. (1993). Genetic and molecular characterization of embryonic mutants identified following seed transformation in *Arabidopsis. Mol. Gen. Genet.* **241,** 504–514.

Chaudhury, A. M., Ming, L., Miller, C., Craig, S., Dennis, E. S., and Peacock, W. J. (1997). Fertilization-independent seed development in *Arabidopsis thaliana. Proc. Natl. Acad. Sci. USA* **94,** 4223–4228.

Christensen, C. A., King, E. J., Jordan, J. R., and Drews, G. N. (1997). Megagametogenesis in *Arabidopsis* wild type and the *Gf* mutant. *Sex. Plant Reprod.* **10,** 49–64.

Drews, G. N., Lee, D., and Christensen, C. A. (1998). Genetic control of female gametophye development and function. *Plant Cell* **10,** 1–15.

Feldmann, K. A., Coury, D. A., and Christianson, M. L. (1997). Exceptional segregation of a selectable marker (KanR) in *Arabidopsis* identifies genes important for gametophytic growth and development. *Genetics* **147,** 1411–1422.

Huang, B.-Q., and Sheridan, W. F. (1996). Embryo sac development in the maize *indeterminate gametophyte1* mutant: Abnormal nuclear behavior and defective microtubule organization. *Plant Cell* **8,** 1391–1407.

Hulskamp, M., Schneitz, K., and Pruitt, R. E. (1995). Genetic evidence for a long-range activity that directs pollen tube guidance in *Arabidopsis. Plant Cell* **7,** 57–64.

Jensen, W. A. (1964). Observations on the fusion of nuclei in plants. *J. Cell Biol.* **23,** 669–672.

Kermicle, J. L. (1971). Pleiotropic effects on seed development of the indeterminate gametophyte gene in maize. *Am. J. Bot.* **58,** 1–7.

Kieber, J. J., Rothenberg, M., Roman, G., Feldman, K. A., and Ecker, J. R. (1993). *CTR1,* a negative regulator of the ethylene response pathway in *Arabidopsis,* encodes a member of the Raf family of protein kinases. *Cell* **72,** 427–441.

Konieczny, A., and Ausubel, F. M. (1993). A procedure for maping *Arabidopsis* mutations using co-dominant ecotype-specific PCR-based markers. *Plant J.* **4,** 403–410.

Koornneef, M., and Stam, P. (1992). Genetic analysis. In "Methods in *Arabidopsis* Research" (C. Koncz, N.-H. Chua, and J. Schell, Eds.), pp. 83–99. World Scientific Publishing, Singapore.

Kosambi, D. D. (1944). The estimation of map distances from recombination values. *Ann. Eugen.* **12,** 172–175.

Kurihara, L. J., Beh, C. T., Latterich, M., Schekman, R., and Rose, M. D. (1994). Nuclear congression and membrane fusion: Two distinct events in the yeast karyogamy pathway. *J. Cell Biol.* **126,** 911–923.

Lin, B.-Y. (1978). Structural modifications of the female gametophyte associated with the *indeterminate gametophyte* (*ig*) mutant in maize. *Can. J. Genet. Cytol.* **20,** 249–257.

Lin, B.-Y. (1981). Megagametogenetic alterations associated with the indeterminate gametophyte (*ig*) mutation in maize. *Rev. Brasil Biol.* **41,** 557–563.

Maheshwari, P. (1950). "An Introduction to the Embryology of Angiosperms." McGraw-Hill, New York.

Manglesdorf, P. C. (1931). Modification of mendelian ratios in maize by mechanical separation of gametes. *Proc. Natl. Acad. Sci. USA* **17,** 698–700.

Mansfield, S. G., and Briarty, L. G. (1991). Early embryogenesis in Arabidopsis thaliana. II. The developing embryo. *Can. J. Bot.* **69,** 461–476.

Mansfield, S. G., Briarty, L. G., and Erni, S. (1991). Early embryogenesis in *Arabidopsis thaliana.* I. The mature embryo sac. *Can. J. Bot.* **69,** 447–460.

Marsh, L., and Rose, M. D. (1997). The pathway of cell and nuclear fusion during mating in *S. cerevisiae.* In "The Molecular and Cellular Biology of the Yeast *Saccharomyces*" (J. R. Pringle, J. R. Broach, and E. W. Jones, Eds.), pp. 827–888. Cold Spring Harbor Laboratory Press, Cold Spring Harbor, NY.

Misra, R. C. (1962). Contribution to the embryology of *Arabidopsis thaliana* (Gay and Monn.). *Agra Univ. J. Res. Sci.* **11,** 191–199.

Moore, J. M., Calzada, J.-P. V., Gagliano, W., and Grossniklaus, U. (1997). Genetic characterization of *hadad,* a mutant disrupting female gametogenesis in *Arabidopsis thaliana. Cold Spring Harbor Symp. in Quant. Biol.,* in press.

Murgia, M., Huang, B.-Q., Tucker, S. C., and Musgrave, M. E. (1993). Embryo sac lacking antipodal cells in *Arabidopsis thaliana* (Brassicaceae). *Am. J. Bot.* **80,** 824–838.

Murray, M. G., and Thompson, W. F. (1980). Rapid isolation of high molecular weight plant DNA. *Nucleic Acids Res.* **8,** 4321–4325.

Nelson, O. E., and Clary, G. B. (1952). Genetic control of semi-sterility in maize. *J. Hered.* **43,** 205–210.

Ng, D. T. W., and Walter, P. (1996). ER membrane protein complex required for nuclear fusion. *J. Cell Biol.* **132,** 499–509.

Copyright © 1998 by Academic Press. All rights of reproduction in any form reserved.

Niyogi, K. K., Last, R. L., Fink, G. R., and Keith, B. (1993). Suppressors of *trp1* fluorescence identify a new *Arabidopsis* gene, *TRP4*, encoding the anthranilate synthase beta subunit. *Plant Cell* **5,** 1011–1027.

Ohad, N., Margossian, L., Hsu, Y.-C., Williams, C., Repetti, P., and Fischer, R. L. (1996). A mutation that allows endosperm development without fertilization. *Proc. Natl. Acad. Sci. USA* **93,** 5319–5324.

Poliakova, T. F. (1964). Development of the male and female gametophytes of *Arabidopsis thaliana* (L) Heynh. *Issledov Genet. USSR* **2,** 125–133.

Ray, A. (1997). Three's company: Regulatory cross-talk during seed development. *Plant Cell* **9,** 665–667.

Ray, S., Park, S.-S., and Ray, A. (1997). Pollen tube guidance by the female gametophyte. *Development* **124,** 2489–2498.

Redei, G. P. (1965). Non-mendelian megagametogenesis in *Arabidopsis*. *Genetics* **51,** 857–872.

Reiser, L., and Fischer, R. L. (1993). The ovule and the embryo sac. *Plant J.* **5,** 1291–1301.

Rhoades, M. M., and Rhoades, V. H. (1939). Genetic studies with factors in the tenth chromosome in maize. *Genetics* **24,** 302–314.

Russell, S. D. (1993). The egg cell: Development and role in fertilization and early embryogenesis. *Plant Cell* **5,** 1349–1359.

Schneitz, K., Hulskamp, M., and Pruitt, R. E. (1995). Wild-type ovule development in *Arabidopsis thaliana:* A light microscope study of cleared whole-mount tissue. *Plant J.* **7,** 731–749.

Sheridan, W. F., and Huang, B.-Q. (1997). Nuclear behavior is defective in the maize (Zea mays L.) *lethal ovule2* female gametophyte. *Plant J.* **11,** 1029–1041.

Singleton, W. R. (1932). Complete elimination of certain classes of gametes in *Zea*. *Proc. Sixth Int. Cong. Genet.* **2,** 182–184.

Singleton, W. R. (1940). Influence of female stock on the functioning of small pollen male gametes. *Proc. Natl. Acad. Sci. USA* **26,** 102–104.

Singleton, W. R., and Mangelsdorf, P. C. (1940). Gametic lethals on the fourth chromosome of maize. *Genetics* **25,** 366–389.

Smyth, D. R., Bowman, J. L., and Meyerowitz, E. M. (1990). Early flower development in *Arabidopsis*. *Plant Cell* **2,** 755–767.

Springer, P. S., McCombie, W. R., Sundaresan, V., and Martienssen, R. A. (1995). Gene trap tagging of *PROLIFERA*, an essential *MCM2-3-5*-like gene in *Arabidopsis*. *Science* **268,** 877–880.

van der Veen, J. H., and Wirtz, P. (1968). EMS induced genic male sterility in *Arabidopsis thaliana:* A model selection experiment. *Euphytica* **17,** 371–377.

van Went, J. L., and Willemse, M. T. M. (1984). Fertilization. In "Embryology of Angiosperms" (B. M. Johri, Ed.), pp. 273–317. Springer-Verlag, Berlin.

Webb, M. C., and Gunning, B. E. S. (1990). Embryo sac development in *Arabidopsis thaliana*. I. Megasporogenesis, including the microtubular cytoskeleton. *Sex. Plant Reprod.* **3,** 244–256.

Webb, M. C., and Gunning, B. E. S. (1994). Embryo sac development in *Arabidopsis thaliana*. II. The cytoskeleton during megagametogenesis. *Sex. Plant Reprod.* **7,** 153–163.

Willemse, M. T. M., and van Went, J. L. (1984). The female gametophyte. In "Embryology of Angiosperms" (B. M. Johri, Ed.), pp. 159–196. Springer-Verlag, Berlin.

Received for publication April 20, 1998
Revised June 10, 1998
Accepted June 10, 1998

Copyright © 1998 by Academic Press. All rights of reproduction in any form reserved.

ERRATUM

Volume **192,** Number 2 (1997), in Article No. DB978773, "Localized Maternal Proteins in *Xenopus* Revealed by Subtractive Immunization," by James M. Denegre, Erich R. Ludwig, and Kimberly L. Mowry, pages 446–454: On page 452, Fig. 4, the labels above Figs. 4A and 4B and above Figs. 4E and 4F were inadvertently switched. The legend was correct as printed. For the reader's convenience, the correct Fig. 4 and its legend are printed here.

This erratum is Article No. DB988957.

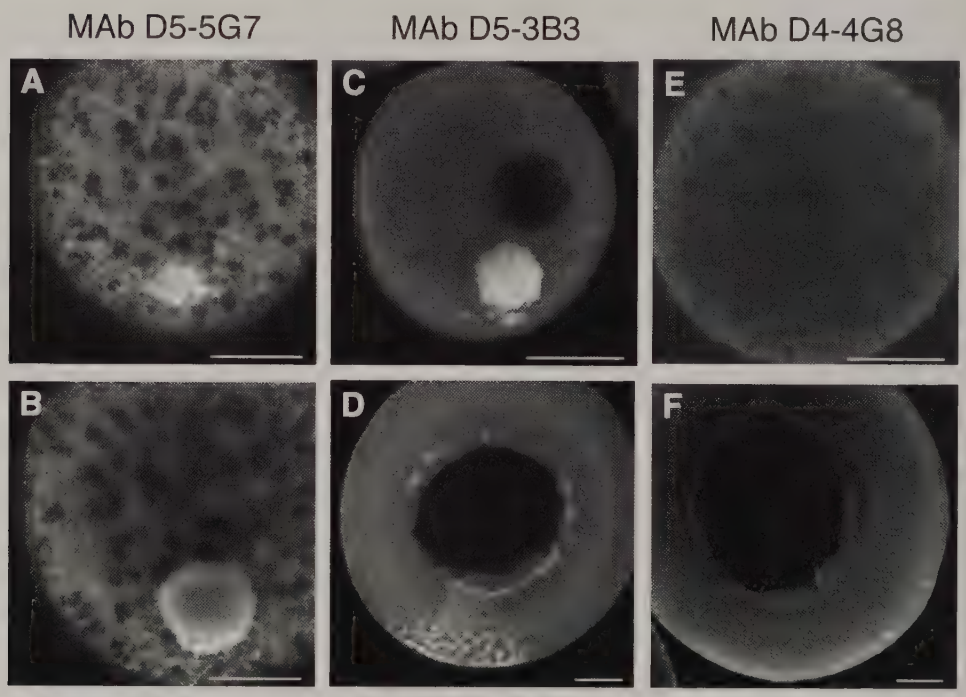

FIG. 4. Two distinct patterns of biogenesis during early oogenesis. Oocytes were stained with the indicated MAbs and imaged using a Zeiss confocal microscope. Scale bars for all panels represent 50 μm. (A, B) Serial sections of a stage I oocyte, stained with D5-5G7. (C) Stage I oocyte stained with D5-3B3. (D) Stage II oocyte stained with D5-3B3. (E) Stage I oocyte stained with D4-4G8. (F) Stage III oocyte stained with D4-4G8.

Copyright © 1998 by Academic Press
All rights of reproduction in any form reserved.

DEVELOPMENTAL BIOLOGY

Information for Authors

Home page: http://www.academicpress.com/db

Developmental Biology publishes papers containing new and significant information bearing on developmental mechanisms of general interest. Descriptive studies will not be published unless they lead to new insights into developmental processes. Submission of a manuscript implies the authors' assurance that the work has not been published nor is under consideration for publication elsewhere and that its submission for publication has been approved by all of the authors. Authors submitting a manuscript do so on the understanding that if it is accepted for publication, copyright in the article, including the right to reproduce the article in all forms and media, shall be assigned exclusively to the Publisher. The Copyright Transfer Agreement, which may be copied from the pages following the Information for Authors or found on the journal home page listed here, should be signed by the appropriate person(s) and should accompany the original submission of a manuscript to this journal. The transfer of copyright does not take effect until the manuscript is accepted for publication.

Submit 4 copies, including illustrations, to:

Developmental Biology, Editorial Office
525 B Street, Suite 1900
San Diego, CA 92101-4495
Phone: 619-699-6325 Fax: 619-699-6211
E-mail: db@acad.com

Authors may also submit their papers directly to an Editor. Addresses for the Editors appear on the following page.

Manuscripts Guidelines

Original papers usually do not exceed 15,000 words and must be preceded by an abstract of about 200 words. Manuscripts should be double-spaced throughout on one side of 8 1/2 × 11-inch or A4 paper. Pages should be numbered consecutively and organized as follows: title page (page 1), containing the article title, authors' names and complete affiliations, footnotes to the title, a running title of fewer than 50 characters, and the address for correspondence (including telephone and fax numbers and an e-mail address); abstract and key words (page 2); introduction; material and methods; results; discussion (results and discussion may be combined); acknowledgments; references; footnotes; tables; and figure legends.

Review Articles

Review articles are solicited; however, the Editor-in-Chief and Reviews Editor invite inquiries and suggestions. Review articles are subject to the same review process as original papers, but receive priority publication.

References

References should be cited in the text by name and date. Only articles that have been published or are in press should be included in the references. Unpublished results or personal communications should be cited as such in the text. Please use the following styles:

Arcaro, K. F., and Lnenicka, G. A. (1995). Intrinsic differences in axonal growth from crayfish fast and slow motoneurons. *Dev. Biol.* **168,** 272–283.

Girard, S., and Clapham, D. E. (1994). Simultaneous near ultraviolet and visible excitation confocal microscopy of calcium transients in *Xenopus* oocytes. In "Methods in Cell Biology" (R. Nuccitelli, Ed.), Vol. 40, pp. 263–283. Academic Press, San Diego.

Figures

Figures should be in a finished form suitable for publication and must be large enough to withstand appropriate reduction for publication. **Two color figures** will be published free of charge in each article. **Additional color figures** will be published free of charge at the discretion of the Editors. Color figures *must* be submitted on flexible board due to the nature of the reproduction process. Tooling: White space between panels of a figure should be no more than 1/16 of an inch.

Cover Submissions

Authors are encouraged to submit figures that come from the manuscript or relate to it in some way. Authors may submit cover figure possibilities as electronic files with the following parameters: $8\frac{1}{2} \times 11$-in., 300 dpi resolution, TIFF or EPS format, and CMYK color mode. Included should be an $8\frac{1}{2} \times 11$-in., hard-copy print. Files may be sent on 3.5-in. floppy disk, 44, 88, or 200 MB Syquest disk, 100 MB Zip disk, 1 GB Jaz disk or via FTP. FTP instructions can be found on the home page. We also accept color slides with an $8\frac{1}{2} \times 11$-in. hard-copy print of the figure or a hard-copy print only. A short (one-line) legend should accompany each photograph. If the cover artwork is related to an article in the issue, 100 reprints with covers will be provided *free of charge* to the author.

Electronic Submission

Manuscripts may be submitted electronically to *Developmental Biology* after all revisions have been incorporated and the manuscript has been accepted for publication. A hard-copy printout of the manuscript that exactly matches the electronic file must be supplied. The manuscript will be edited according to the style of the journal, and the proofs must be read carefully by the author. Complete instructions for electronic submission can be found on the *Developmental Biology* home page.

Proofs and Reprints

Proofs will be sent to the authors with reprint order forms. Fifty reprints of each article are provided free of charge. Additional reprints may be ordered using the form provided.

Distribution of Material

Authors who publish a research article in *Developmental Biology* must be prepared to freely distribute to academic researchers for their own use any cell lines, DNA clones, monoclonal antibodies, or genetically engineered mice described in the article. All genetic sequence information published in *Developmental Biology* must also be deposited with GenBank.

For information about advertising in *Developmental Biology*, please contact the Advertising Coordinator, Academic Press, 525 B Street, Suite 1900, San Diego, California 92101-4495 (telephone: 619-699-6825, fax: 619-699-6390).

Editor-in-Chief

Eric N. Olson
Department of Molecular Biology and Oncology
University of Texas
Southwestern Medical Center at Dallas
6000 Harry Hines Blvd., Rm. NA8.602
Dallas, TX 75235-9148 USA
phone: (214) 648-1187
fax: (214) 648-1140
email: eolson@hamon.swmed.edu

Editors

Marianne Bronner-Fraser
Division of Biology, 139-74
California Institute of Technology
1200 E. California Blvd.
Pasadena, CA 91125 USA
phone: (626) 395-3356
fax: (626) 395-7717
email: mbronner@caltech.edu

Eric H. Davidson
Division of Biology, 156-29
California Institute of Technology
1200 E. California Blvd.
Pasadena, CA 91125 USA
phone: (626) 395-4937
fax: (626) 564-9571
email: davidson@mirsky.caltech.edu

Scott E. Fraser
Beckman Institute, 139-74
California Institute of Technology
1200 E. California Blvd.
Pasadena, CA 91125 USA
phone: (626) 395-2790
fax: (626) 395-7717
email: sefraser@caltech.edu

Richard Harland
Department of Molecular and Cell Biology
401 Barker Hall, #3204
University of California
Berkeley, CA 94720-3204 USA
phone: (510) 643-6003
fax: (510) 643-1729
email: harland@socrates.berkeley.edu

Philip Ingham
Developmental Genetics Programme
Krebs Institute
University of Sheffield
Firth Court, Western Bank
Sheffield S10 2TN UK
phone: 44-114-222-2803
fax: 44-114-222-2788
email: p.w.ingham@sheffield.ac.uk

Laurinda A. Jaffe
Department of Physiology, L5004
University of Connecticut Health Center
263 Farmington Ave.
Farmington, CT 06030-3503 USA
phone: (860) 679-2661
fax: (860) 679-1661
email: ljaffe@cortex.uchc.edu

Robb Krumlauf
Laboratory of Developmental Neurobiology
National Institute for Medical Research
The Ridgeway, Mill Hill
London NW7 1AA UK
phone: 44-181-913-8530
fax: 44-181-913-8658
email: r-krumla@nimr.mrc.ac.uk

Gail Martin
Department of Anatomy
University of California, San Francisco
Rm. S-1457, 513 Parnassus Ave.
San Francisco, CA 94143-0452 USA
phone: (415) 476-2441
fax: (415) 476-3493
email: gmartin@itsa.ucsf.edu

Gary Ruvkun
Department of Molecular Biology
Wellman 8
Massachusetts General Hospital
Boston, MA 02114 USA
phone: (617) 726-5959
fax: (617) 726-6893
email: ruvkun@molbio.mgh.harvard.edu

Matthew P. Scott
Departments of Developmental Biology and Genetics
Howard Hughes Medical Institute
Stanford University School of Medicine
279 Campus Dr., Beckman Ctr. B300
Stanford, CA 94305-5329 USA
phone: (650) 725-7680
fax: (650) 725-7739
email: scott@cmgm.stanford.edu

Gary M. Wessel
Department of Molecular and Cell Biology and Biochemistry
Brown University
69 Brown Street
Providence, RI 02912 USA
phone: (401) 863-1051
fax: (401) 863-1182
email: rhet@brown.edu

NOTICE

Under the terms of the U.S. copyright law effective January 1, 1978, and the copyright laws of many other countries, journal publishers are required to obtain written confirmation from authors to acquire copyright rights for papers published in their journals. We ask your cooperation because it is of vital importance for the widest possible dissemination of your paper. We must have your written confirmation to authorize libraries and other information centers to use this material and to perform other appropriate publishing functions. We are therefore asking you to sign and return the form accompanying this notice. PLEASE SIGN ONLY THE APPLICABLE SECTION.

Which section of the form should you sign? If you and your co-authors, if any, own rights in your paper as individuals (for example, you are working at a university or research institute, even if you are supported by a government grant), please sign **Section A** of the attached form. If you work for a corporation that owns the rights in the paper, please have an authorized officer of the corporation sign **Section B**. If the paper is in the public domain because you and all your co-authors created it within the scope of your employment with the U.S. government, please sign **Section C**. If the paper is subject to Crown copyright because you and all your co-authors are employees of the British or Canadian government, please sign **Section C**. If not all authors are government employees, then one of the nongovernment employees should sign **Section A**. If any governmental entity other than the U.S., British, or Canadian government owns copyright, please call Academic Press at the number below. No manuscript will be processed until the appropriate form has been returned.

If your manuscript is not published within a reasonable period of time after acceptance, upon written request, AP will promptly return the rights to the manuscript to the author(s).

General Terms of Publication in Academic Press Journals

1. Author Warranties

1.1. The work submitted for review is new and has been written by the stated authors and has not been published elsewhere.
1.2. The work submitted is not currently under review for another journal and will not be submitted to another journal while under review for the present journal.
1.3. Submission of the work has been approved by all the authors and by the institutions where the work was carried out. Written authorization may be required at the Editor's discretion. For works with multiple authors, all the authors participated meaningfully in the work and agree on the submitted version of the work.
1.4. Any person cited in the work as a source of personal communications has approved such citation.
1.5. Submitted paper and electronic versions of the work are identical, except for elements that cannot be represented on paper.
1.6. All necessary permissions for the reproduction or excerpting of the work of others have been obtained.

2. Understandings

2.1. All works submitted to Academic Press journals are subject to peer review, a process that is the responsibility of the Editors.
2.2. The authors agree that, if the work is accepted for publication, they will transfer the copyright in it exclusively to Academic Press, including the right of reproduction in all forms and media, whether now known or hereafter developed, and the right to include it in collections and databases.

3. Personal Servers

3.1. Upon submitting an article to an Academic Press journal for review and possible publication, authors are requested to add the following notice to the first screen of any posted electronic preprint versions of the paper: *This work has been submitted to Academic Press for possible publication. Copyright may be transferred without notice, after which this version may no longer be accessible.* Authors should note that posting the entire work may be regarded as prior publication by some journal editors (see Information for Authors of the specific journal).
3.2. When an Academic Press journal accepts the work for publication, the authors may post it, in its final accepted form, on their personal servers (but not on any organized preprint server) with a notice *Accepted for publication in* <name of journal> *as of* <date>, until it is published by Academic Press in print or electronic form.
3.3. After publication, authors may post their Academic Press copyrighted material on their own servers without permission, provided that the server displays as the first line of the HTML page the following notice alerting readers to their obligations with respect to copyrighted material: *This material has been published in* <name of journal, issue number and date, page numbers>, *the only definitive repository of the content that has been certified and accepted after peer review. Copyright and all rights therein are retained by Academic Press. This material may not be copied or reposted without explicit permission.* The posted work must also include the Academic Press copyright notice (*Copyright © 199x by Academic Press*) and a link to IDEAL (International Digital Electronic Access Library) at http://www.idealibrary.com or http://www.europe.idealibrary.com.

IMPORTANT: Note that Academic Press may choose to publish an abstract or portions of the paper prior to publishing the paper in the journal. Please contact Academic Press immediately if you would like Academic Press to refrain from such prior publication for any reason, including disclosure of a patentable invention.

If you have any questions about the procedures, call Academic Press at (619) 699-6413.
Please **return the form** to *Developmental Biology,* Academic Press, 525 B Street, Suite 1900, San Diego, CA 92101-4495.
Thank you.

Copyright Transfer Agreement

ATTENTION AUTHORS: PLEASE SIGN IN APPROPRIATE SECTION **ONLY**.

Journal: *Developmental Biology*

Tentative Manuscript Title: _____

_____

Authors: _____

A. University/research institute employees and others who own rights as individuals. You hereby confirm the assignment to Academic Press (AP) of the entire copyright in and to the manuscript named above (the Work) throughout the world in all forms and media, whether now known or hereafter developed, and in all languages effective if and when it is accepted for publication by AP. You agree to abide by the terms of publication stated on the accompanying notice. You also warrant that the Work has not been published before and contains no materials the publication of which would violate any copyright or other personal or proprietary right of any person or entity, and you acknowledge that AP is relying on this document in publishing this Work. Notwithstanding the assignment of copyright to AP, you:

1. Retain patent rights, if any.
2. May make photocopies of all or part of the Work for use in your classroom teaching.
3. May use your original figures/tables/illustrations/photographs from the Work in future works of your own.
4. May include the Work as part of your dissertation, for noncommercial distribution only.

You agree that all copies and inclusions made under the above conditions will carry a notice of copyright and a citation to the journal article.

To be signed by all the authors (**or** by an author who has obtained the written assent of the nonsigning authors).

Signed: _____ Date: _____

B. Corporate employees. The Work was written as part of the duties of the author as an employee of the company signing below or otherwise as a "work made for hire" (as defined in the relevant copyright law) for such company. As the authorized representative of such company, you hereby confirm the assignment to AP of the entire copyright in and to the Work throughout the world in all forms and media, whether now known or hereafter developed, and in all languages effective if and when it is accepted for publication by AP. You agree to abide by the terms of publication stated on the accompanying notice. You also warrant that the Work has not been published before and contains no materials the publication of which would violate any copyright or other personal or proprietary right of any person or entity, and you acknowledge that AP is relying on this document in publishing this Work. Notwithstanding the assignment of copyright to AP, you:

1. Retain patent rights, if any.
2. May prepare derivative works based on the Work, with proper acknowledgment.
3. May reproduce the Work in reasonable quantities for internal use, with proper acknowledgment. However, copies of the Work may not be used for resale or in any way that implies that AP, the journal, or the editorial board endorses any procedures or products of your company.

Signed: _____ Date: _____

Title: _____

C. Government employees. You certify that the Work has been written as part of your official duties either as (a) an employee of the U.S. government or another government whose works are not subject to copyright protection, and as such there is no copyright to transfer; or as (b) an employee of the British, Canadian, or other government whose works are subject to Crown copyright, and via the authorized signature of the relevant government entity below, AP is hereby obtaining a nonexclusive license to publish (and to authorize others to publish) the Work in all forms and media, whether now known or hereafter developed, and in all languages effective if and when it is accepted for publication. If not all of the authors are government employees, one of the nongovernment employees should sign Section A. You also warrant that the Work has not been published before and contains no materials the publication of which would violate any copyright or other personal or proprietary right of any person or entity, and you acknowledge that AP is relying on this document in publishing this Work.

To be signed by all the authors (**or** by an author who has obtained the written assent of the nonsigning authors).

Signed: _____ Date: _____

Government authorization (if needed): _____ Date: _____

Research Made Easy

Guide to Human Genome Computing

SECOND EDITION

Completely updated!

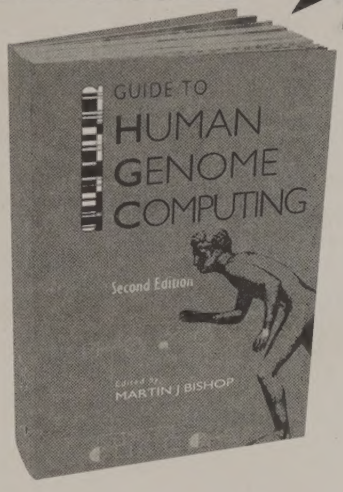

Edited by

Martin Bishop
HGMP Resource Centre, Hinxton, Cambridgeshire, U.K.

Computing resources are fully explained, including:

- Internet resources, i.e. databases
- Genetic analysis
- Sib pair studies
- Comparative mapping
- Radiation hybrids
- Sequence ready clone maps
- Human genome sequencing
- ESTs
- Gene prediction
- Gene expression

The **Guide to Human Genome Computing** is invaluable to scientists who wish to make use of the powerful computing tools now available to assist them in the field of human genome analysis. This book clearly explains access and use of sequence databases, and presents the various computer packages used to analyze DNA sequences, measure linkage analysis, compare and align DNA sequences from different genes or organisms, and infer structural and functional information about proteins from sequence data.

The Second Edition contains completely updated material. Essentially a new book, based on the subjects which will be of interest over the coming years, this book is truly international, both in scope and authorship.

April 1998, 306 pp., $69.95/£45.00
ISBN: 0-12-102051-7

CONTENTS:

L. Stein, Introduction to Human Genome Computing via the World Wide Web
M. Rhodes and R. Elaswarapu, Biological Materials and Services
S. Bryant, Managing Pedigree and Genotype Data
P. Sham and J. Zhao, Linkage Analysis Using Affected Sib-Pairs
M. Bishop, Comparative Mapping in Man and Vertebrates
L. McCarthy and C. Soderland, Radiation Hybrid Mapping
C. Soderland, S. Gregory, and I. Dunham Sequence Ready Clone Maps
S. Dear, Software for Human Genome Sequencing
G. Slater, Human EST Sequences
L. Milanesi and I. Rogozin, Prediction of Human Gene Structure
A. Krogh, Gene Finding: Putting the Parts Together
D. Davidson and C. Dubreuil, Gene Expression Databases

Order from your local bookseller or directly from:

ACADEMIC PRESS
Order Fulfillment Dept. DM27103
6277 Sea Harbor Drive, Orlando, FL 32887
Call Toll Free **1-800-321-5068**
Fax **1-800-874-6418**
E-mail **ap@acad.com**

ACADEMIC PRESS
HARCOURT BRACE & CO.
Customer Services Dept.
Foots Cray High Street
Sidcup, Kent DA14 5HP, U.K.
Tel: **+44 (0)181 308 5700**
Fax: **+44 (0)181 309 0807**

Find us on the Web! www.academicpress.com

Prices subject to change without notice. ©1998 by Academic Press.
All Rights Reserved. LB/CG/LBS-34058A-6/98

ACADEMIC PRESS

SCIENCE

Start Your Day with inScight

Science and ***Academic Press*** invite you to start your day with **inScight,** the online information service devoted specifically to late-breaking science news.

Located at **www.apnet.com/inscight,** the site is a free service featuring daily topical news items of interest to researchers, practitioners, students, and anyone with an interest in current science issues. The experienced and preeminent news team of the weekly ***Science*** compiles and provides **inScight** with the day's primary science news stories which are then formatted and maintained online through the Academic Press electronic production services department.

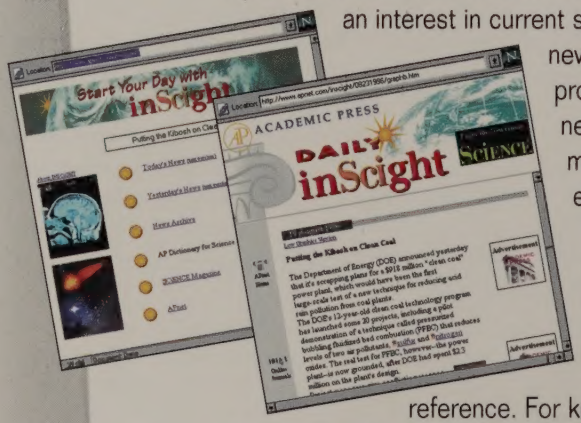

In addition to providing daily science news, **inScight** features a daily-updated network of links to related newsmakers, associations, and appropriate science subjects. Stories are archived for easy searchable reference. For key word descriptions, the service incorporates the **Academic Press Dictionary of Science and Technology,** a comprehensive reference of more than 130,000 entries.

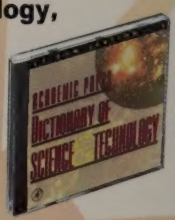

Start your day off right, with inScight!

inScight–
www.apnet.com/inscight

Science–www.sciencemag.org

Academic Press–www.apnet.com/ or
www.europe.apnet.com/

LK/KJ/FF 18116